ISSN 0386-0744

ENVIRONMENTAL RESEARCH IN THE ARCTIC 2000

NATIONAL INSTITUTE OF POLAR RESEARCH
TOKYO MARCH 2001

This document is provided by JAXA.

Editorial Board
Editor-in-Chief: Okitsugu Watanabe, *National Institute of Polar Research (NIPR)*
Editors: Takehiko Aso, *NIPR*
Masaki Ejiri, *NIPR*
Ryoichi Fujii, *Nagoya University*
Yoshiyuki Fujii, *NIPR*
Mitsuo Fukuchi, *NIPR*
Yoshikuni Hiroi, *Chiba University*
Hiroshi Kanda, *NIPR*
Shun'ichi Kobayashi, *Niigata University*
Satoru Kojima, *Tokyo Woman's Christian University*
Shinji Mae, *Hokkaido University*
Masamichi Miyamoto, *University of Tokyo*
Yasuhiko Naito, *NIPR*
Hiroshi Sasaki, *Senshu University of Ishinomaki*
Kazuo Shibasaki, *Kokugakuin University*
Kazuo Shibuya, *NIPR*
Kazuyuki Shiraishi, *NIPR*
Masashi Takada, *Nara Women's University*
Hideki Wada, *Shizuoka University*
Takashi Yamanouchi, *NIPR*

This document is provided by JAXA.

MEMOIRS OF NATIONAL INSTITUTE OF POLAR RESEARCH
SPECIAL ISSUE No. 54

ENVIRONMENTAL RESEARCH IN THE ARCTIC 2000

Proceedings of the Second International Symposium on Environmental Research in the Arctic and Fifth Ny-Ålesund Scientific Seminar, 23-25 February 2000, NIPR, Tokyo

Edited by
Okitsugu Watanabe and Takashi Yamanouchi

PUBLISHED BY NATIONAL INSTITUTE OF POLAR RESEARCH

TOKYO MARCH 2001

This document is provided by JAXA.

Memoirs of National Institute of Polar Research
Special Issue, No. 54

ENVIRONMENTAL RESEARCH IN THE ARCTIC 2000

Proceedings of the Second International Symposium on Environmental Research in the Arctic and Fifth Ny-Ålesund Scientific Seminar, 23–25 February 2000, NIPR, Tokyo

Editorial board of this volume
Editor-in-chief: Okitsugu Watanabe *(NIPR)*
Executive editor: Takashi Yamanouchi *(NIPR)*
Editors:

Takehiko Aso *(NIPR)*
Kaoru Sato *(NIPR)*
Masataka Shiobara *(NIPR)*
Yoshiyuki Fujii *(NIPR)*
Kokichi Kamiyama *(NIPR)*
Tsuneo Odate *(NIPR)*
Hiroshi Kanda *(NIPR)*
Satoru Kojima *(TWCU)*
Tadahiro Sato *(NAO)*
Hajime Ito *(NIPR)*

Chris Hall *(Univ. Tromsø)*
Hartwig Gernandt *(AWI)*
Elisabeth Isaksson *(NP)*
Louis Legendre *(Univ. Laval)*
Ulf Molau *(Göteborg Univ.)*
Kim Holmén *(Stockholm Univ.)*

Copyright 2001 by the National Institute of Polar Research
9–10, Kaga 1-chome, Itabashi-ku, Tokyo 173-8515

Printed by Yoshimi Kohsan Corporation

This document is provided by JAXA.

PREFACE

The Second International Symposium on Environmental Research in the Arctic and Fifth Ny-Ålesund Scientific Seminar were held jointly at the National Institute of Polar Research, 23-25 February 2000. The symposium provided a platform to discuss Arctic research based on recent results.

National Institute of Polar Research (NIPR) started activities in the Arctic in 1990, when the Arctic Environment Research Center was established in NIPR. The first International Symposium was held in 1995 with the particular goal to promote Arctic research in terms of the global environment. Since 1995, NIPR has conducted major research activities in the Arctic as the "International Cooperative Research Project on Arctic Environment (1995-1998)" according to International Arctic Science Committee (IASC) initiatives. The symposium served as the final report of this International Cooperative Project.

The purpose of the annual Ny-Ålesund Scientific Seminars is to promote scientific exchange to stimulate interaction and further cooperation among all scientists active in Ny-Ålesund. This seminar is jointly organized by the Ny-Ålesund Science Managers Committee and EU-sponsored Large Scale Facility "Ny-Ålesund Arctic Environmental Research Facility".

The Symposium and Seminar were jointly organized in order to provide a unique opportunity for exchange among scientists active in Ny-Ålesund and those working in other geographical areas of the Arctic. A total of 129 papers were presented at the symposium under six major topics: (1) overview of Arctic environmental research, (2) atmospheric environment in the Arctic, (3) glaciological environments in the Arctic, (4) change in Arctic marine environment, (5) Arctic terrestrial ecosystems and (6) Arctic upper atmosphere environment. The present volume contains 51 full-length papers, submitted under four categories: scientific original papers, scientific notes, review papers and reports. The scientific papers were refereed by two reviewers each, and the others by one reviewer each.

It is hoped that this volume will contribute to the progress of research on the Arctic environment and international cooperation. Our sincere thanks are due to all of the contributors and referees who have readily cooperated to bring about this volume. We also thank Ms. M. Sakai and the publication officers at the Library of the National Institure of Polar Research for the publication of the proceedings.

December 2000
Okitsugu Watanabe and Takashi Yamanouchi

This document is provided by JAXA.

This document is provided by JAXA.

CONTENTS

Preface. . . . . Okitsugu Watanabe and Takashi Yamanouchi. . . i

I: Arctic upper atmosphere environment

Observations of the Arctic troposphere and lower stratosphere with the SOUSY Svalbard Radar *(scientific note)*
. . . . . Jürgen Röttger. . . 1

Observations of the polar *D*-region and the mesosphere with the EISCAT Svalbard Radar and the SOUSY Svalbard Radar *(scientific paper)*
. . . . . Jürgen Röttger. . . 9

Climatic mesospheric cooling: Employing the long time-series of ionospheric soundings from Norwegian stations *(scientific note)*
. . . . . C. M. Hall. . . 21

Conjugate imaging riometer observations at polar cusp/cap stations: A daytime absorption event for a specific change of solar wind conditions *(scientific paper)*
. . . . . Masanori Nishino, Hisao Yamagishi, Natsuo Sato, Yozo Murata, Ruiyuan Liu, Peter Stauning and Jan A. Holtet. . . 29

A study on the Arctic upper-atmosphere tide by EISCAT radar —Recent results and prospects— *(scientific note)*
. . . . . Takehiko Aso. . . 43

II: Atmospheric environment in the Arctic

Recent contributions to long-term atmospheric studies at Koldewey-Station *(review)*
. . . . . H. Gernandt, R. Neuber and P. von der Gathen. . . 49

An intercomparison campaign of ozone and temperature measurements in the Arctic (NAOMI-98, Ny-Ålesund/Spitsbergen) *(scientific note)*
. . . . . R. Neuber, G. Beyerle, P. von der Gathen, P. Wahl, A. Dahl, M. Gross, Th. McGee, U. Klein and W. Steinbrecht. . . 65

Temporal variations of atmospheric CO_2 concentration and carborn isotope ratio in Ny-Ålesund, Svalbard *(scientific paper)*
. . . . . Shinji Morimoto, Shuhji Aoki and Takashi Yamanouchi. . . 71

Global quality control for long-lived trace gas measurements *(review)*
. . . . . Roger Francey, Manfred Groening, Kim Holmén, Krung-Ryul Kim, John Miller, Pieter Tans and Neil Trivett. . . 81

Black carbon and ionic species in the Arctic aerosol *(scientific paper)*
. . . . . K. Eleftheriadis, S. Nyeki, K. Tørseth and I. Colbeck. . . 91

Arctic study of tropospheric aerosol and radiation, ASTAR 2000-field plan *(report)*
. . . . . Takashi Yamanouchi and Andreas Herber. . . 101

Radiative forcing due to anthropogenic activities *(scientific note)*
. . . . . F. Stordal and G. Myhre. . . 107

This document is provided by JAXA.

Three years spectral resolved UV-measurements at Koldewey-Station (1997–1999) *(scientific paper)*
..... Christian Groß, Helmut Tüg and Otto Schrems... 113
Radiation and turbulence parameterizations at Ny-Ålesund, Svalbard Islands *(scientific note)*
.. Teodoro Georgiadis, Marianna Nardino, Francescopiero Calzolari, Vincenzo Levizzani, Jon Børre Ørbæk, Stefan Claes and Roberta Pirazzini... 125
Feasibility study on scientific balloon experiment at Ny-Ålesund *(scientific paper)*
..... Hideyuki Honda, Naoki Izutsu and Nobuyuki Yajima... 133
Climate change and its impacts on the arctic environment *(scientific paper)*
..... Gunter Weller... 143
Summit Greenland environment observatory *(report)*
..... Atsumu Ohmura... 153

III: Glaciological environment in the Arctic

Atmospheric teleconnection between Japan and the Saint Elias Moutains, Yukon *(scientific paper)*
..... Gerald Holdsworth... 161
Stable oxygen isotope ratio observed in the precipitation at Ny-Ålesund, Svalbard *(scientific note)*
..... Makoto Igarashi, Kokichi Kamiyama and Okitsugu Watanabe... 169
Northern Eurasia glacier response to global climate change *(scientific note)*
..... Yuriy Kononov, Maria Ananicheva and Natalia Davidovich... 183
Effects on spectral reflectance from snow ageing *(scientific note)*
.... J-G. Winther, S. Gerland, J. B. Ørbæk, B. Ivanov, A. S. Zachek and A. M. Bezgreshnov... 193
Sudden climatic change *(scientific note)*
..... Roy M. Koerner... 203
210-year ice core records of dust storms, volcanic eruptions and acidification at Site-J, Greenland *(scientific note)*
.. Yoshiyuki Fujii, Kokichi Kamiyama, Hitoshi Shoji, Hideki Narita, Fumihiko Nishio, Takao Kameda and Okitsugu Watanabe... 209
Japanese glaciological study efforts in the North Greenland Ice Core Project (NGRIP) *(report)*
..... Hitoshi Shoji and Okitsugu Watanabe... 221
Studies on climatic and environmental changes during the last few hundred years using ice cores from various sites in Nordaustlandet, Svalbard *(scientific paper)*
..... Okitsugu Watanabe, Hideaki Motoyama, Makoto Igarashi, Kokichi Kamiyama, Sumito Matoba, Kumiko Goto-Azuma, Hideki Narita and Takao Kameda... 227

This document is provided by JAXA.

Field observations of the Japanese Arctic Glaciological Expeditions in Svalbard from 1993 to 1995 *(report)*
..... Kokichi Kamiyama, Hideaki Motoyama and Okitsugu Watanabe... 243
Activities of the Japanese Arctic Glaciological Expedetion in 1999 (JAGE 1999) *(report)*
.... Hideaki Motoyama, Okitsugu Watanabe, Kumiko Goto-Azuma, Makoto Igarashi, Morihiro Miyahara, Tomoharu Nagasaki, Lars Karlöf and Elisabeth Isaksson... 253
In-situ snow temperature monitoring at an Arctic tundra site: A comparison of manual and automatic measurements *(scientific note)*
..... Sebastian Gerland, Jan-Gunnar Winther and Knut Sand... 261
The geochemical phenomenon—Local geochemical fields in a glacier *(scientific note)*
..... V. N. Makarov... 271
Determination of ice flow velocity in Svalbard from ERS-1 interferometric observations *(scientific paper)*
..... Bernard Lefauconnier, Didier Massonnet and Geir Anker... 279
Ocean tides and loading in the Nordic Seas *(scientific note)*
..... M. S. Bos and T. F. Baker... 291
Inversion of global tide gauge data for present-day ice load changes *(scientific paper)*
..... Hans-Peter Plag and Hans-Ulrich Jüttner... 301
The determination of the reference point of the VLBI antenna in Ny-Ålesund *(scientific note)*
..... Paolo Tomasi, Pierguido Sarti and Maria Rioja... 319

IV: Change in Arctic marine environment
Scientific achievements in the First Chinese Expedition to the Arctic Ocean *(report)*
..... Zhaoqian Dong and Weijia Qin... 331
Greenland Sea in winter *(report)*
..... Hajime Ito... 337
The International North Water Polynya Study (NOW): A progress report *(scientific note)*
..... L. Fortier, M. Fortier, M. Fukuchi, D. Barber, Y. Gratton, L. Legendre, T. Odate and B. Hargrave... 343
Persistent organic pollutants in Arctic animals in the Barents Sea area and at Svalbard: Levels and effects *(review)*
..... Geir Wing Gabrielsen and Espen O. Henriksen... 349
Arctic Ocean change and consequences to biodiversity: A perspective on linkage and scale *(scientific note)*
..... Eddy Carmack and Fiona McLaughlin... 365

This document is provided by JAXA.

Vernal export and retention of biogenic matter in the north-eastern North Atlantic and adjacent Arctic Ocean: The role of the Norwegian Atlantic Current and topography *(review)*
..... Paul Wassmann... 377
The upper layer circulation in Kongsfjorden and Krossfjorden—A complex fjord system on the west coast of Spitsbergen *(scientific paper)*
.. Randi Ingvaldsen, Marit Bø Reitan, Harald Svendsen and Lars Asplin... 393
The Arctic sea ice biological communities in recent environmental changes *(scientific note)*
..... Igor A. Melnikov, Ludmila S. Zhitina and Helena G. Kolosova... 409
Laboratory experiments on the frazil ice formation with application to the Arctic marine environment *(scientific note)*
..... Andrei G. Zatsepin and Pavel N. Golovin... 417
Stable isotope compositions of arctic copepods in the Greenland Sea in winter *(scientific note)*
..... Hiroshi Sasaki, Daisuke Kawai and Megumi Sato... 423

V: Arctic terrestrial ecosystems

Personal ultraviolet-B dosimetry at Koldewey-Station by using an electronic dosimeter ELUV-14 *(scientific note)*
..... Saad El Naggar, Hartwig Gernandt, Nicole Spelten and Andrew Klaas... 429
Arctic hot and CO_2 springs: Natural models of impact of climate change on terrestrial ecosystems *(scientific paper)*
..... Dmitri G. Zamolodchikov and Dmitri V. Karelin... 437
Tundra plant responses to experimental and natural temperature changes *(scientific paper)*
..... Ulf Molau... 445
Pattern of seedling emergence of alpine plants: Comparisons between fellfield and snowbed habitats *(scientific note)*
..... Yoshiko Shimono and Gaku Kudo... 467
Ecological notes on the heath community on Mt. Ebeko, Paramushir Island, northern Kuriles *(scientific paper)*
..... Susumu Okitsu, Yoshinori Minami and Sergei Yu. Grishin... 479
Occurrence of bryophytes in Paramushir Island, northern Kuriles, Far East Russia *(scientific paper)*
..... Yoshinori Minami, Susumu Okitsu, Hiroshi Kanda, Valentina Ya. Cherdantseva and Sergei Yu. Grishin... 487
Biological characteristics of dark colored material (cryoconite) on Canadian Arctic glaciers (Devon and Penny ice caps) *(scientific paper)*
..... Nozomu Takeuchi, Shiro Kohshima, Kumiko Goto-Azuma and Roy M. Koerner... 495

This document is provided by JAXA.

Ecological role of fungal infections of moss carpet in Svalbard *(scientific paper)* ..... Tamotsu Hoshino, Motoaki Tojo, Hiroshi Kanda and Anne Marte Tronsmo... 507

Program of Second International Symposium on Environmental Research in the Arctic and Fifth Ny-Ålesund Scientific Seminar, 23–25 February 2000, Tokyo..... 515

Author index..... 519

This document is provided by JAXA.

Mem. Natl Inst. Polar Res., Spec. Issue, 54, 1–8, 2001

Scientific note

Observations of the Arctic troposphere and lower stratosphere with the SOUSY Svalbard Radar

Jürgen Röttger

Max-Planck-Institut für Aeronomie, D-37191 Katlenburg-Lindau, Germany
(roettger@linmpi.mpg.de)

Abstract: The SOUSY Svalbard Radar was operated in the ST (stratosphere-troposphere) mode during tests and several campaigns since September 1998. Here we describe the configuration used for this purpose. We present results of wind and reflectivity profiles, showing layered structures during passage of synoptic-scale disturbances and tropopause variations. It is also reported that lee wave activity is frequently quite pronounced over Svalbard.

1. Introduction

Continuous observations of the structure and dynamics of the Arctic troposphere and stratosphere are of particular interest to obtain information on the climatology of atmospheric waves and turbulence in the high latitudes. Investigations of the variability of the polar vortex and the propagation of synoptic scale disturbances into high latitudes are also essential phenomena of polar meteorology, which require continuous observations. Stratosphere-troposphere (ST) wind profiler radars are proper tools for such studies, although they cover only one location and are limited to altitudes up to about 20–25 km. Measurements with these radars can also provide estimates on transport by turbulence or mean velocity. Röttger and Larsen (1990) have described these systems and summarized their capabilities, and Röttger and Tsuda (1995) have presented particular suggestions for radar studies of the polar middle and lower atmosphere.

The SOUSY Svalbard Radar is a mesosphere-stratosphere-troposphere (MST) radar operated for studies of Polar Mesosphere Summer Echoes (Czechowsky *et al.*, 1998; Röttger, 2001), of coupling processes in the middle and the lower atmosphere and the structure and dynamics of the troposphere and lower stratosphere (Röttger, 2000a). We introduce here first results of observations of small-scale gravity waves, mountain lee waves, and passages of synoptic- and meso-scale disturbances as well as the structure of the tropopause over Svalbard at the high latitude of 78°N.

2. The SOUSY Svalbard Radar

In the year 1998 the Max-Planck-Institut für Aeronomie has constructed the SOUSY Svalbard Radar (SSR (Czechowsky *et al.*, 1998)) near Longyearbyen (78°N, 16°E) on the island Spitzbergen, which is part of the archipelago of Svalbard. The SSR is an MST VHF

This document is provided by JAXA.



Fig. 1. Part of the phased-array antenna of the SOUSY Svalbard Radar located near Longyearbyen (78°N, 16°E), which consists of 356 four-element Yagis in total (July 1999).

radar and operates on 53.5 MHz with 70 kW peak power, applying a hybrid modulation of single and complementary pulse coding for ST applications, and a phased antenna array of 356 Yagis (Fig. 1). The antenna has a beam width of 4 degrees and is steerable into the zenith direction, and at 5 degrees zenith angle in four azimuths NE, SE, SW and NW. It is being separated into four receiving sub-arrays (4×36 Yagis) for spaced antenna and interferometer measurements. These sub-arrays are indicated by gray shading in Fig. 2. In the initial troposphere and lower stratosphere observations, which are briefly described here, only a sub-module of 4 Yagis was used for reception to allow recording of signals from lower tropospheric heights down to about 1 km. Since the beam width of the receiving modules (with vertical pointing direction) is wider than the steering angle of the full array antenna, the vertical pointing receiving beams need not to be steered.

3. Observations

It is common to display height-time-intensity plots of the measured parameters, such as the received power, and the wind velocity components in horizontal and vertical direction etc. The received power is a measure of the reflectivity of layers in the atmosphere and in particular indicates vertical humidity gradients in the lower troposphere and temperature gradients in the upper troposphere and stratosphere. The reflectivity of such layers is also affected by turbulence, which can be deduced from measured velocity fluctuations.

In Figs. 3 and 4 we present such typical plots obtained from measurements between

This document is provided by JAXA.

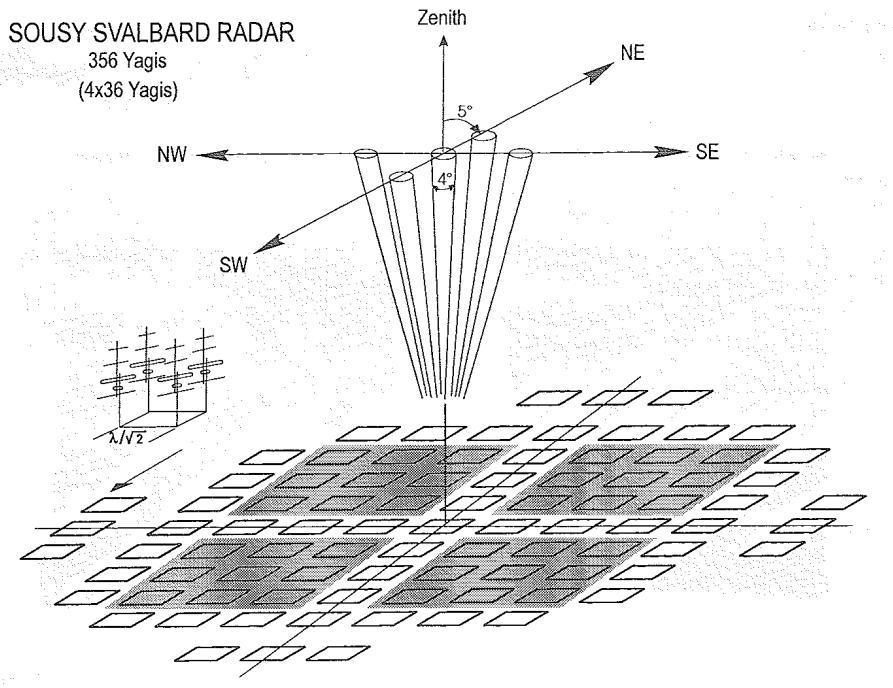


Fig. 2. Layout of the antenna array of the SOUSY Svalbard Radar, showing the five possible beam directions. Each small square represents a subset of 4 Yagis. The four shaded areas comprise the modules taken out by passive transmit-receive switches for spaced-antenna reception.

13 and 15 November 1999. The lower panels show the power variation, and the upper panels the variation of velocity as function of height and time. These observations were during a passage of a warm front over Svalbard, which is clearly seen in the downward sloping structure in the lower left-hand panel of Fig. 3. These detach from a strong structure around 10 km, which is an indicator of the tropopause. Larsen and Röttger (1985) have shown the relevance of ST radar investigations of frontal zone and tropopause structures. Downward slopes of radar-detected structures, as seen in Fig. 3, correspond to warm front passages. The lower right-hand side plot of Fig. 3 shows the power received in the NE beam at 5 degrees angle off-zenith. The power level 0 dB (light-yellow color) corresponds to the noise level. The reduced power at this angle, as compared to those measured with the vertical beam (lower left-hand panel of Fig. 3) determines the aspect sensitivity of the atmospheric structures detected by VHF radars. The aspect sensitivity is a measure for the stability of the atmospheric region in which this structure is embedded. The frontal structure is separated into 3–4 meso-scale substructures. The high power received from the altitudes below 4–6 km is likely due to increased humidity. Following the detachment of the frontal structure the tropopause is lifted significantly and also separates into a multiple tropopause. Following the warm front we find the increase of velocity in the altitudes between 6 and 10 km, which is the jet stream concurring with the frontal passage. The zonal (u) and meridional (v) velocities are shown in the upper panels of Fig. 3. The blank parts in these

This document is provided by JAXA.

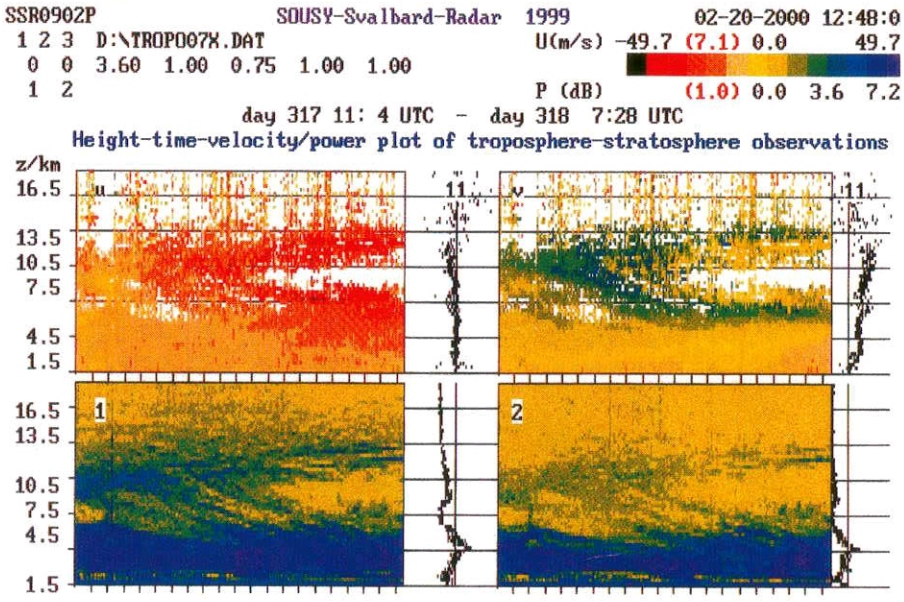


Fig. 3. Height-time-intensity plots of eastward velocity u (upper left panel), northward velocity v (upper right), power received in the vertical beam (lower left) and in the NE beam (lower right), recorded between 1104 UT on 13 November 1999 and 0728 UT on 14 November 1999 (day 318). The color scales define ± 49.7 m s^{-1} for velocities and 0 dB to 7.2 dB in the relative power scales. The scatter profiles in the center and the right margin are the corresponding velocity components of 11–12 UT on 13 November (upper plots) and the averages of the radar power in the lower panels.

velocity plots result from lacking signal in this region.

These observations are basically equivalent to the observations with radiosondes performed every day at 11 UT at Ny-Ålesund (operated by the Alfred Wegener Institut für Polar und Meeresforschung), which is about 100 km north of the SSR. The surface weather maps (Fig. 4) show the warm front passage at Svalbard around 18 UT on 14 November, which is a few hours later than we extrapolate from the latter down-sloping structure detected by the SSR in Longyearbyen (Fig. 3).

In the following period, 15–16 November 1999, relatively extreme variations of the quasi-vertical velocity were observed with the SOUSY Svalbard Radar. These are presented in Fig. 5, where we show, in addition to the height-time-intensity plot of the power, the velocities deduced from the Doppler shift of the signals received in the vertical beam and in the opposite NE and SW field beams (*e.g.* Röttger and Larsen, 1990). The latter can be combined to yield an additional estimate of the quasi-vertical velocity. In homogeneous and horizontally stratified reflectivity and velocity fields these two velocity estimates should be equal, yielding the correct vertical velocity component. We notice some equivalence of these two velocity estimates in the beginning of this period whereas they deviate significantly in the latter part of this period. We also see a change of direction of these velocities with height and with time. These are clear signs of a non-homogeneous wind

This document is provided by JAXA.

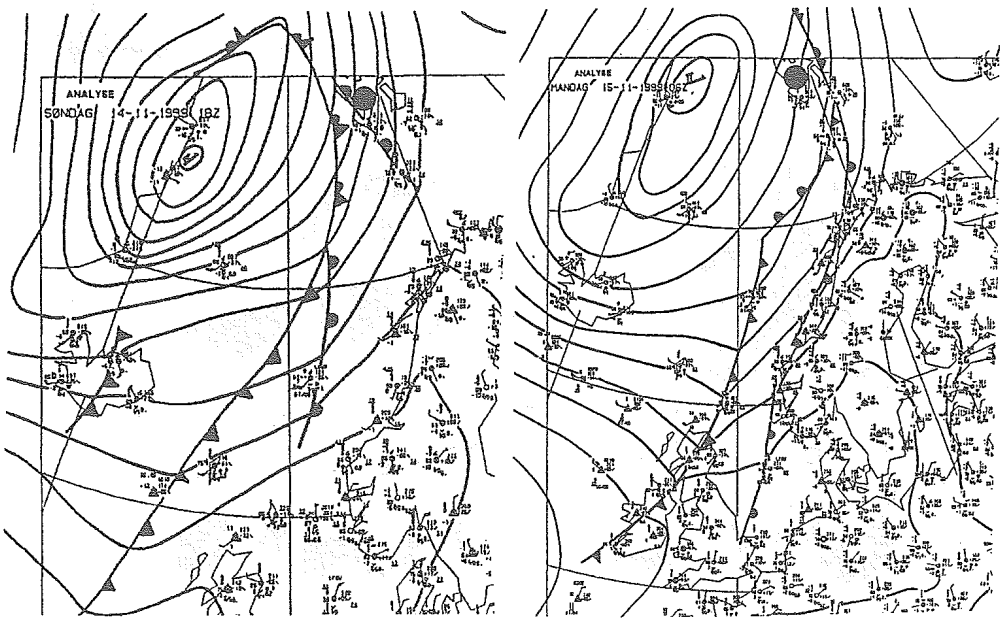


Fig. 4. Weather maps (sea level) of 14 November (18 UT) and 15 November 1999 (06 UT). The location of Longyearbyen, Svalbard, is marked by the filled circle in the upper part of the maps (provided by courtesy of Longyearbyen airport).

field. The periodicity at vertical scales of a few kilometers and time scales of hours, which are observed after about 12 UT point to quasi-stationary mountain lee waves. In the beginning of the period some shorter period oscillations at some 10 to 20 min are noted, which are likely due to small-scale gravity waves. These long- and short-period wave disturbances are superimposed on the mean background wind field.

It is apparent from the shown combination of the vertical beam and the NE and SW beams, that the horizontal wavelength of the lee waves, observed after about 18 UT, is much less than a few kilometers, resulting from the separation of the radar beam pointing directions. This has a non-negligible effect on the determination of mean vertical and horizontal winds, and requires a very careful consideration. This potential effect can be ameliorated by including the spatial interferometer technique (*e.g.,* Röttger *et al.*, 1990). The SOUSY Svalbard Radar is, thus, being extended to allow such interferometer measurements with the spaced antenna configuration (see Fig. 2).

Svalbard is an archipelago with high mountains, steeply extending from the ocean surface. Strong surface winds can, thus, easily generate mountain lee waves, which propagate into the lower atmosphere. Our observations with the SSR show that these wave disturbances are frequently occurring in the troposphere over Svalbard. Their amplitudes can be up to 2–3 m s^{-1}. This corresponds to high tubulence intensity, if encountered by aircraft. When these waves break, also smaller scale turbulence is created, which we may see in the highly variable power received from the middle and lower troposphere (Fig. 5). We

This document is provided by JAXA.

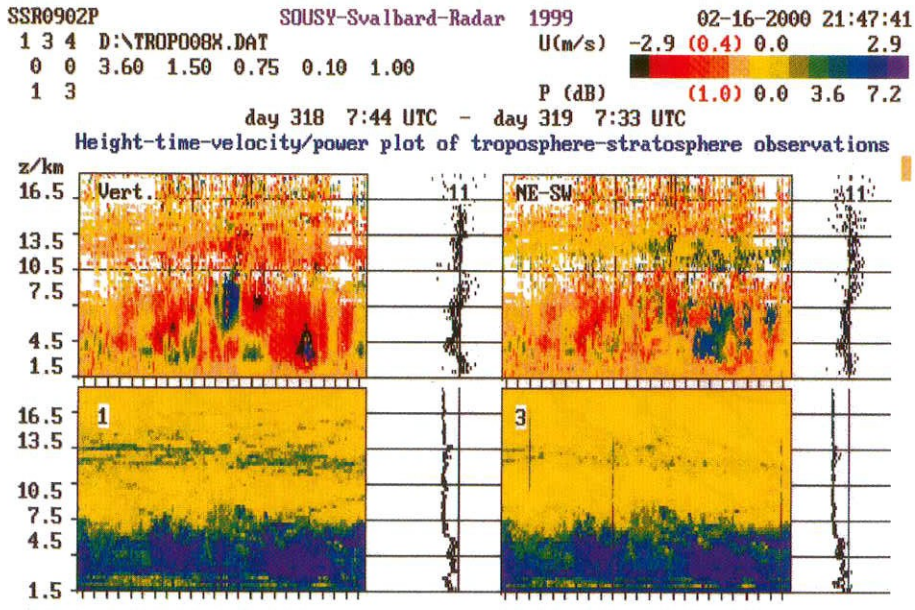


Fig. 5. Same as Fig. 3 but for the following time period 0744 UT on 14 November to 0733 UT on 15 November 1999 (day 319). The right-hand lower plot shows the power in the SE beam. The upper plots show the velocity in the vertical beam (left panel) and the quasi-vertical velocity composed from the NE and SW beam (right). The scatter plots in the center and the right are displaying averages of the corresponding parameters on their left between 11 UT and 12 UT. The color scales cover ±2.9 m s^{-1} for the velocity and 0 dB to 7.2 dB in the relative power scales.

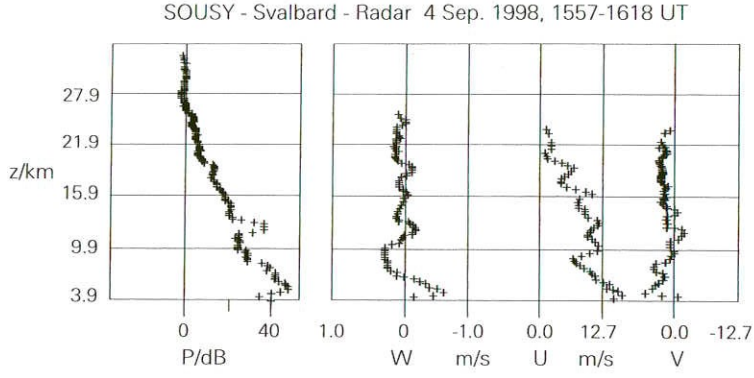


Fig. 6. Profiles of relative power P, quasi-vertical velocity w, zonal velocity u and meridional velocity v, measured during test-operation on 4 September 1998, using the full antenna array for transmission and reception as well.

also notice in Fig. 5 that the quasi-vertical velocities occasionally change direction within short time periods. This can only be explained by either changes in the source activity, or

This document is provided by JAXA.

by variations of the wind and/or temperature profiles aloft. In Fig. 6 mean profiles (average over 20 min) of power and the three wind velocity components, *u*, *v*, and *w*, are shown. We note the periodic variations of the velocity components with height. The horizontal velocity components are significantly out of phase by 180 degrees, which supports the view that these variations are due to a lee wave.

Röttger (2000b) has reviewed the VHF radar investigations of atmospheric waves over mountainous areas. It appears to us that the intensity of lee wave activity over Svalbard is very pronounced as compared to other sites. We need to analyze these mountain wave effects over Svalbard quite carefully and more intensely in future investigations.

4. Conclusion

Initial results of troposphere and stratosphere observations with the SOUSY Svalbard Radar (SSR) have been presented. These show that this radar can substantially contribute to the investigations of high polar latitude meteorology by observing tropospheric and lower stratospheric structures and wind fields, including strong lee wave activity. The SSR has subsequently been operated in a continuous mode during the ASTAR-2000 campaign in March and April 2000. Figure 7 shows a copy of a real-time plot of three main measurement parameters, namely the zonal (u) and the meridional (v) wind components, and the power (P_t), which is a measure of the radar reflectivity and shows the layered structure of the troposphere and the tropopause. The presented display shows the passage of an occlusion, combined with a tropopause folding event between 20 UT and 24 UT on

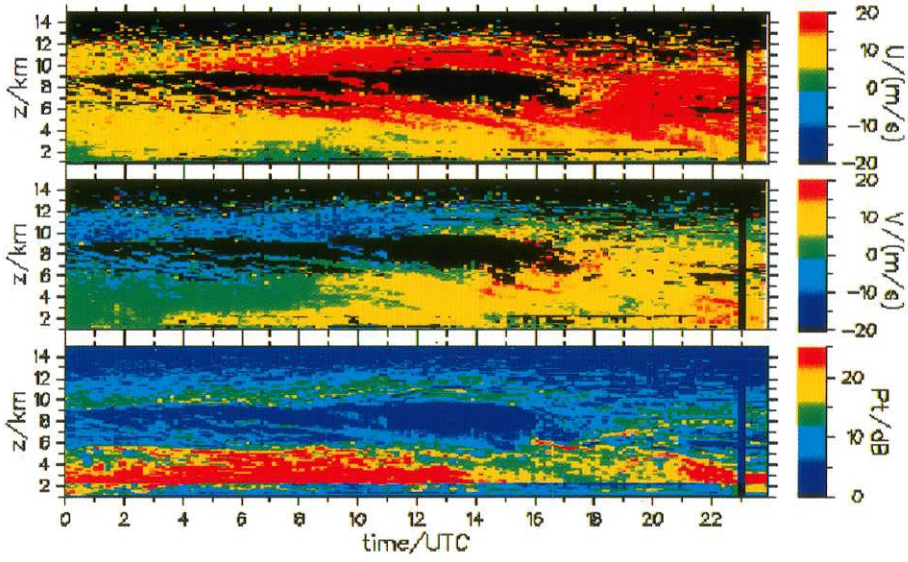


Fig. 7. Height-time-intensity plots of provisional real-time estimates of zonal velocity u, meridional velocity v and relative total power P_t (noise + signal) recorded over a 24-hour period on 8 April 2000 during the ASTAR-2000 campaign.

This document is provided by JAXA.

8 April 2000. These plots are available in real time on the home page of the MPAe. We expect the SOUSY Svalbard Radar to attend several future campaigns of this kind.

Acknowledgments

I thank my colleagues at MPAe for their appreciated collaboration in establishing and running the SOUSY Svalbard Radar. My particular thanks are directed to R. Rüster and H. Bruns for preparing the software for the real-time data plots used during the ASTAR-2000 campaign.

References

Czechowsky, P., Klostermeyer, J., Röttger, J., Rüster, R. and Schmidt, G. (1998): The SOUSY Svalbard Radar for middle and lower atmosphere research in the polar region. Proc. 8th Workshop Tech. Sci. Aspects MST Radar, SCOSTEP, 318-321.

Larsen, M.F. and Röttger, J. (1985): Observations of frontal zone and tropopause structures with VHF Doppler radar and radiosondes. Radio Sci., **20**, 1223-1232.

Röttger, J. (2000a): Radar investigations of the mesosphere, stratosphere and the troposphere in Svalbard. Adv. Polar Upper Atmos. Res., **14**, 202-220.

Röttger, J. (2000b): ST radar observations of atmospheric waves over mountainous areas: A review. Ann. Geophys., **18**, 750-765.

Röttger, J. (2001): Observations of the polar *D*-region and the mesosphere with the EISCAT Svalbard Radar and the SOUSY Svalbard Radar. Mem. Natl Inst. Polar Res., Spec. Issue, **54**, 9-20.

Röttger, J. and Larsen, M.F. (1990): UHF/VHF radar techniques for atmospheric research and wind profiler applications. Radar in Meteorology, Am. Meteorol. Soc., 235-281.

Röttger, J. and Tsuda, T. (1995): Studies of the polar middle and lower atmosphere by an MST radar on Svalbard. J. Geomagn. Geoelectr., **47**, 929-942.

Röttger, J., Liu, C.H., Chao, J.K., Chen, A.J., Pan, C.J. and Fu, I.J. (1990): Spatial interferometer measurements with the Chung-Li VHF radar. Radio Sci., **25**, 503-515.

(Received June 21, 2000; Revised manuscript accepted October 2, 2000)

This document is provided by JAXA.

Mem. Natl Inst. Polar Res., Spec. Issue, 54, 9–20, 2001

Scientific paper

Observations of the polar *D*-region and the mesosphere with the EISCAT Svalbard Radar and the SOUSY Svalbard Radar

Jürgen Röttger

Max-Planck-Institut für Aeronomie, D-37191 Katlenburg-Lindau, Germany
(roettger@linmpi.mpg.de)

Abstract: Two new radars are operated at high polar latitudes on Svalbard, the EISCAT Svalbard Radar (ESR) and the SOUSY Svalbard Radar (SSR). The application of these systems for studies of Polar Mesosphere Summer Echoes (PMSE) is described. The ESR is also used for studies of the *D*-region using the incoherent scatter method. Combined observations with these two radars yield insight into the wavenumber dependence of the scatter cross section, which in turn leads to indications on the diffusion of electrons in the presence of heavy ions.

1. Introduction

The polar middle atmosphere is of unique nature, since in that region processes from above (solar wind–magnetosphere–ionosphere–thermosphere) and from below (troposphere–stratosphere–mesosphere–lower thermosphere) merge. Röttger (1994a) and Röttger and Tsuda (1995) have summarized the contributions of incoherent scatter and MST radars to study these processes. In particular the effects of Joule heating and high energetic particles on the lower thermosphere and upper mesosphere wind and temperature fields, the interaction of the neutral and ionized middle atmosphere during particle precipitation and the presence of aerosols, cluster ions and ice particles in the cold polar mesopause in summer are of special interest. The effect of planetary waves, tides, gravity waves and turbulence on the polar middle atmosphere at not very well known either. The archipelago of Svalbard at high polar latitudes close to 80°N is a unique location to study many of these processes.

Of great importance are the Polar Mesosphere Summer Echoes (see Cho and Röttger, 1997, for a review), which had not been studied at the high latitudes of Svalbard. Besides their relation to electron density, the Polar Mesosphere Summer Echoes (PMSE) are strongly dependent on temperature and water vapor mixing ratio. These parameters vary with latitude. Hemispheric differences of PMSE are also reported (Balsley *et al.*, 1995), which may indicate temperature differences between the Arctic and the Antarctic mesopause. Comparisons of PMSE observations on Svalbard with those at lower latitudes and in the southern hemisphere will consequently be very valuable. The PMSE distinctly depend on the wavenumber of the probing radar. Combined observations with radars on different frequencies, such as the EISCAT Svalbard Radar (Wannberg *et al.*, 1997; Röttger *et al.*, 1998) and the SOUSY Svalbard Radar (Czechowsky *et al.*, 1998; Röttger, 2000), are mandatory to understand the scattering mechanism and the governing spatial irregularity

This document is provided by JAXA.

structure causing PMSE. The fairly continuous appearance of the PMSE can properly be used to study dynamic processes, such as long period waves, tides, gravity waves and turbulence, which occur in the high latitude mesopause region.

In this paper early observations of the *D*-region and mesopause region with the ESR and the SSR are described. Observations of the lower stratosphere and the troposphere are presented in the companion paper (Röttger, 2001).

2. The EISCAT Svalbard Radar

During our initial *D*-region experiments in 1998 and 1999 the EISCAT Svalbard Radar (ESR), which is an incoherent scatter radar operated on 500 MHz, a peak power between 500 kW or 1000 kW was transmitted using the 32 m parabolic dish antenna. It is estimated that in this particular experiment configuration the smallest detectable electron density is close to 3×10^{8} m^{-3} for maximum integration times in the order of minutes. This would be decreased by about a factor of two with the second antenna, which is now available at the EISCAT Svalbard Radar (Fig. 1).

Due to longer coherence time of echoes from the lower ionosphere the pulse-to-pulse modulation has to be applied (Röttger, 1997). It is suitable to implement the complementary code to increase the average transmitted power and thus the significance of the result estimates. Röttger *et al.* (1998) have described the operational mode of the ESR for these observations. The technical details of the whole ESR system have been published by Wannberg *et al.* (1997).

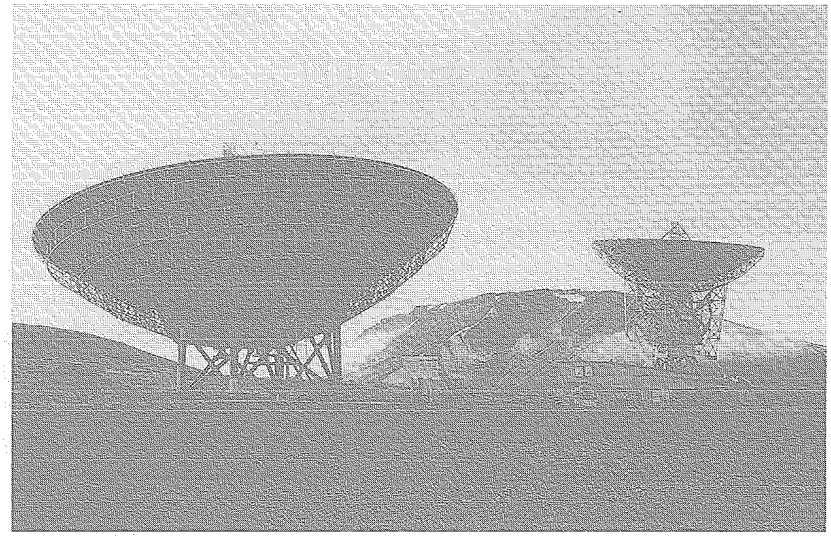


Fig. 1. The EISCAT Svalbard Radar (ESR) with the 32-m steerable dish in the background and the 42-m fixed dish in the foreground (September 1999).

This document is provided by JAXA.

3. The SOUSY Svalbard Radar

The SOUSY Svalbard Radar (SSR) is an MST radar and was particularly conceived for the studies of Polar Mesosphere Summer Echoes (Czechowsky *et al.*, 1998). This radar uses the main basic components of the mobile SOUSY VHF radar, combined with a new phased-antenna array of 356 Yagis (Fig. 2). The antenna can be steered to five beam directions: the zenith, and to 5 degrees zenith angle in NE, SE, SW, and NW azimuths. The SSR operates at 53.5 MHz and was run at a peak power around 70 kW during several campaigns in 1999, applying the complementary code. Röttger (2000) has preliminarily summarized the basic results of these first operations, which consisted of PMSE, meteor and stratosphere-troposphere programs, and Rüster *et al.* (2001) have described some typical features of PMSE, such as their double layer structure and the wind field in the mesopause region.

The SOUSY Svalbard Radar (SSR) is located in very close vicinity of the EISCAT Svalbard Radar (ESR), which allows well coordinated experiment operations for observations of the mesosphere, and the *D*- and *E*-region, which are of great importance to understand the aeronomy and dynamics of the upper middle atmosphere (say, 50 km to 100 km altitude) at high polar latitudes.

A summary of the system parameters of the SSR and ESR, relevant for these particular studies, is given in Table 1. Both these radars are located at 78°N, 16°E.

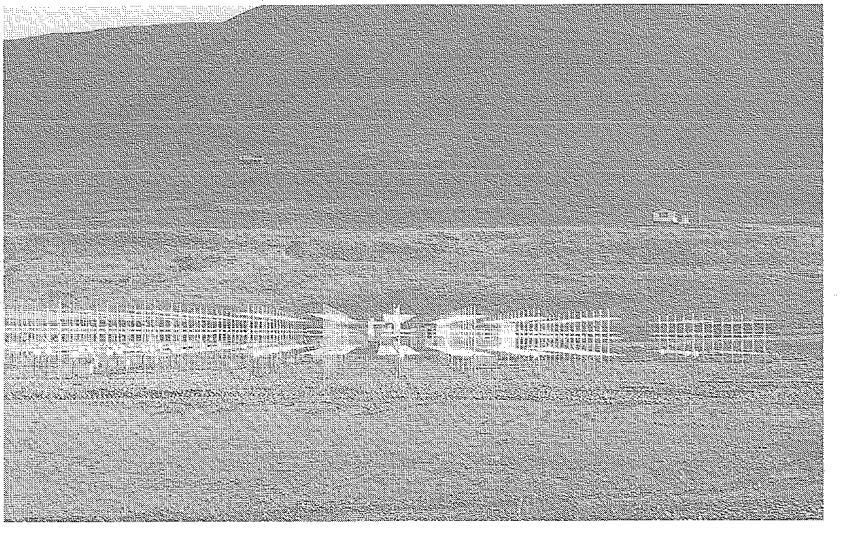


Fig. 2. The SOUSY Svalbard Radar (SSR) with the phased array consisting of a total of 356 Yagi antennas (September 1998).

This document is provided by JAXA.

Table 1. System parameters of the EISCAT Svalbard Radar (ESR) and the SOUSY Svalbard Radar (SSR).

System parameters	ESR	SSR
Antenna gain G in dBi	42.5	33.0
Half power beam width Θ	1.23°	4.0°
Frequency f in MHz	500	53.5
Wavelength λ in m	0.60	5.61
Peak power P_p in MW	0.8	0.07
Duty cycle d	0.14	0.04
Average power P_a in kW	115	2.8
Number n_b of code bauds	32	20
Effective power $2 \cdot P_p \cdot n_b$ in MW	51.2	2.4
System efficiency (assumed)	0.8	0.8
Pulse (baud) length τ in μs	6	2
System temperature T_s in K	70	3000
Number coherent integrations n_{coh}	2	4×21
Detection bandwidth f_b in kHz	83.3	2.98
System figure of merit F_m	$1 \cdot 10^{23}$	$6 \cdot 10^{22}$
Minimum detectable radar reflectivity η in m^{-1}	$2.6 \cdot 10^{-19}$	$7.5 \cdot 10^{-19}$

4. Observations of incoherent scatter from the lower ionosphere with the ESR

Incoherent scatter from the lower ionosphere (mesosphere) is collision dominated. This means that the spectra are approaching Lorentzian shape, rather than displaying the double-hump shape of the spectra from the E- and F-region. The spectrum width in the collision-dominated regime is a measure of temperature and density of the neutral atmosphere, and the Doppler shift is a direct measure of the neutral air velocity. The scattered power is in the first order proportional to the electron density. Since this is usually fairly low in the D- and lower E-region, the scattered signal is very weak. This means that either long integration times have to be applied to obtain significant estimates of the given parameters or ionization increases need to occur during ionospheric disturbances. In the polar cap (Svalbard is located in the polar cap) usually energetic particle precipitation during solar proton events enhance the D-region density, which allow integration times of less than one minute.

The first tests of D-region observations with the ESR (Röttger *et al.*, 1998) were during the declining phase of a solar proton event and signals could be detected at significant levels. Figure 3 shows examples of dynamic spectra (left-hand panels) of echoes from the lower D-region at altitudes between 54 km and 64 km, which were detected on 24 April 1998. The right-hand side displays the corresponding scatter plots of the spectra. The peak signal power is in the order of the variance of the background noise and the signal-to-noise ratio is a few percent only. To obtain reasonable estimates of electron density and velocity, thus, requires a few minutes of post-integration of the spectra. This allows to studying short-term variations of the D-region, for instance during solar proton events. Indications of such variations are seen in the development of the dynamic spectra as function of height and time. We note some quasi-periodic variation of the spectral power, *i.e.* electron density,

This document is provided by JAXA.

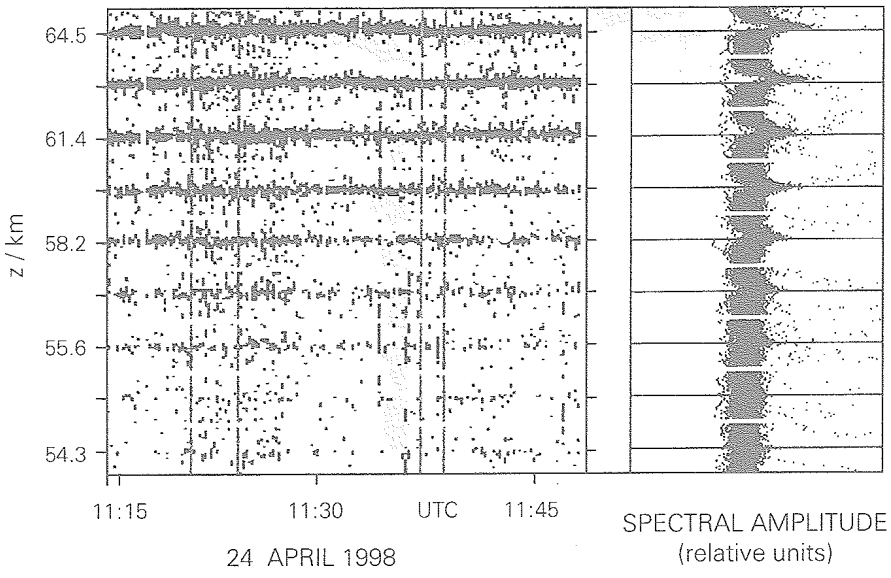


Fig. 3. Dynamic spectra (left-hand panels) of incoherent scatter signals from the lower D-region detected by the ESR on 24 April 1998 during the decaying phase of a solar proton event. On the right hand-panels the scatter plots of the spectra for the total time period are shown. The Doppler velocity limits of the spectra are $\pm 111\ m\,s^{-1}$.

below about 60 km in Fig. 3 with maxima around 1125 UT and 1140 UT.

At higher altitudes the signal-to-noise ratio improves, which can be seen in another example (Fig. 4), where data taken with the ESR on 15 July 1999 are presented. This operation was during a campaign to search for PMSE. The upper panel shows the height-time-intensity plot and the scatter profile of the raw power estimate between 78 and 101 km altitude, which was recorded between 1315 and 1325 UT. The raw power estimate represents a first-order estimate of the yet uncalibrated electron density profile. A gradual weak increase of the raw power is noticed to occur above about 85 km. The raw power then increases significantly above 90 km, which comprises the lower *E*-region. There is even an indication of a sporadic-*E* or ion layer around 95 km. Due to the applied pulse-to-pulse modulation using the complementary code (optimized for PMSE detection), the incoherent scatter signals from heights above about 88 km are aliased. Thus, full spectra cannot be obtained, but the power is a proper first-order estimate of the electron density, since coherent integration was not applied in our experiments.

Particular narrow lines occur in the spectra at altitudes 88–89 km in Fig. 4. These are features of Polar Mesosphere Summer Echoes, which will be discussed further in the following chapter. Röttger (2000) has described more details of these first PMSE observations with the ESR, and Hall and Röttger (2001) discussed their occurrence frequency and further principle features. In the following we present and discuss scatter cross section comparisons of common PMSE observations with the ESR and the SSR, which will provide an indication on the presence of aerosols and ice particles.

This document is provided by JAXA.

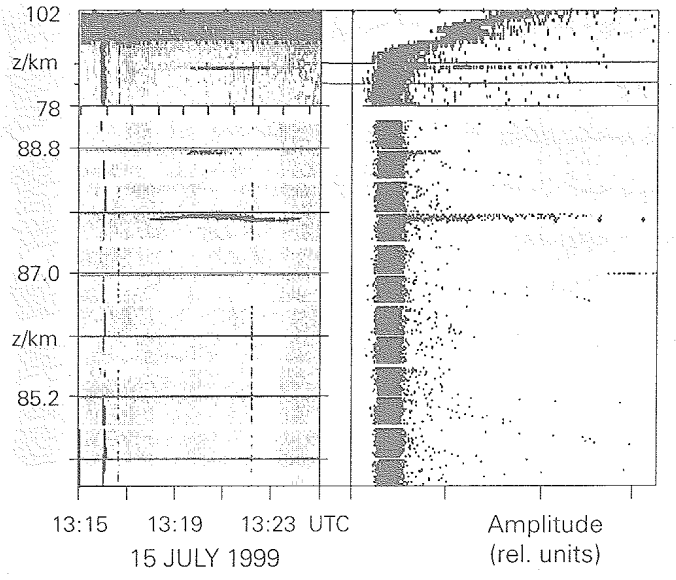


Fig. 4. Left-hand panels: Height-time intensity plot of signals from the D-region and lower E-region (upper plot), and six dynamic spectra of signals from the height ranges embraced by the tick marks/lines the upper diagrams. The straight lines in the dynamic spectra indicate zero velocity. The velocity limits are $\pm 111\ m\,s^{-1}$.
Right-hand panels: Scatter plots of the parameters in the left-hand panels.

5. Observations of Polar Mesosphere Summer Echoes with the ESR and SSR

Whereas incoherent scatter results from electrons in thermal equilibrium (thermal scatter), in particular conditions, such as large cluster ions and other particles in the mesopause region, the incoherent scatter process is changed substantially. This process can be called non-thermal scatter. The scattered signal exhibits a highly coherent nature and its amplitude exceeds the common incoherent and turbulence scatter level by many orders of magnitude. This is seen in the narrow spectral lines, occurring in narrow height slices, as displayed in Fig. 4. These echoes, called Polar Mesosphere Summer Echoes (PMSE), occur in the very cold high-latitude mesopause and are related to the formation of ion clusters and ice particles. They should not be confused with the common coherent scatter echoes, which are detected by MST radars, and which result from neutral-turbulence induced irregularities in the *D*-region/mesosphere. Although the difference between the scatter causing the PMSE and the conventional incoherent and turbulence scatter from the mesosphere is generally agreed upon, the scattering process occurring during the PMSE conditions is not fully explained yet (*e.g.,* Cho and Röttger, 1997; Klostermeyer, 1999).

PMSE had been observed over a wide range of frequencies (Röttger, 1994b), corresponding to radar wavelengths of 100 m to 0.25 m. Some comparisons of the phenomenology of PMSE had been done using data obtained with collocated radars (*e.g.,*

This document is provided by JAXA.

Röttger *et al.*, 1990; Bremer *et al.*, 1996), but finally robust estimates of scatter cross sections during concurrent observations and comparisons with model results were not yet done. This was first performed using data acquired in 1999 with the SOUSY Svalbard Radar and the EISCAT Svalbard Radar, and is briefly described here.

In July 1999 these two radars were partly operated simultaneously to search for events when PMSE occurred on the frequencies 53.5 MHz (SSR) and 500 MHz (ESR). Such a comparison should allow indications about the scattering process, *i.e.* whether the 500 MHz scatter would be enhanced Thomson scatter by dressed particles, enhancement of the particle line of modified Thomson scatter or enhancement due to an increase of the Schmidt number (for references see Röttger, 1994b; Cho and Röttger, 1997; Klostermeyer, 1999). A conclusion in turn would allow indications on the microphysics of the scattering medium, for instance whether there are multiply charged aerosols, reduced electron diffusion in the presence of heavy ions, or just enhanced neutral turbulence. The latter, however, is believed to be excluded since neutral turbulence in the mesopause region does not extend to short scales matching the Bragg wavelengths of these two radars.

The decrease of the scatter cross section of PMSE as function of the spatial wave number, given by the conventionally applied spectrum, dictates that there should be a several orders of magnitude smaller cross section on 500 MHz than on 53.5 MHz (Kelley *et al.*, 1987). To estimate whether such a search for PMSE on 500 MHz would be successful we first need to compare the corresponding system parameters of the SSR and the ESR. This comparison is shown in Table 1. Röttger (in preparation) has described the given parameters in more detail. We note that the ESR and SSR have fairly equal system figures of merit. This results from the facts that the ESR has a more than one order of magnitude wider detection bandwidth to match the broader signal spectrum on 500 MHz (resulting in higher noise power), and from about ten times larger antenna aperture of the SSR (yielding higher signal levels). These counter-balance the higher system temperature and lower average power of the SSR as compared to the ESR. Since the signal-to-noise ratio of PMSE observed with the SSR can be to about 50 dB, we assumed that chances would exist to detect PMSE also with the ESR. This was proved by the first detection of PMSE with the ESR in July 1999.

In Fig. 5 height-time intensity plots (upper plots in the upper (ESR) and lower (SSR) panels) of a typical PMSE event are presented. The lower six/seven plots of the two panels show the dynamic spectra of the signals in the height ranges limited by the tick-marks on the left-hand side of the height-time-intensity plots. After about 1001 UT an enhancement was detected by the ESR with fairly wide spectra around 87–88 km and a much narrower spectra lower down at 86–87 km. The corresponding dynamic spectra of the SSR are shown in the lower panel of Fig. 5. We note some similarity in the occurrence of echoes of the SSR and the ESR. Closer inspection of temporal and spatial variations of the echoes (the SSR scans through five directions, which cover the one direction of the ESR beam) that these echoes, detected by the ESR and the SSR, result from the same irregularity structure, which was drifting horizontally through the observation area.

In Fig. 6 the spectra of the ESR signals are shown, which demonstrates the occurrence of broad and narrow spectrum widths. This means that there are two different irregularity structures, one is strongly turbulent (termed case 1 in Table 2, corresponding to the broad spectra in Fig. 6) and the other quite stable (which we annotate as non-turbulent; case 2 in

This document is provided by JAXA.

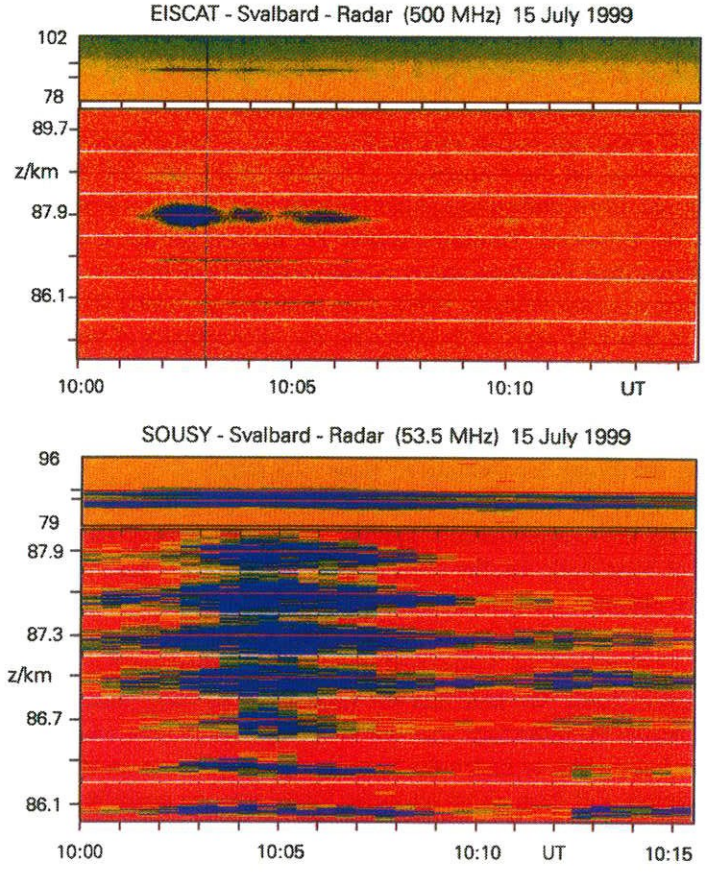


Fig. 5. Height-time-intensity plots and dynamic spectra of Polar Mesosphere Summer Echoes recorded with the EISCAT Svalbard Radar (upper panel) and the SOUSY Svalbard Radar (lower panel); from Röttger (2000).

Table 2, corresponding to the narrow spectra in Fig. 6), respectively. The ESR signal-to-noise ratio of the wide spectrum event is about 20%, and that of the narrow spectrum event is about 2%. Using proper system and noise calibration (Röttger, in preparation) we can estimate the received absolute signal power and convert that into radar reflectivity. This has been done for the given two events detected simultaneously by the ESR and the SSR. From the spectrum widths of the ESR we can also estimate the turbulence dissipation rate ε for an assumed reasonable Brunt-Väisälä frequency at these altitudes. The spectrum width is a measure for the turbulence energy dissipation rate, provided that antenna beam width and shear broadening is negligible. Since the beam width of the ESR of 1.23° is much narrower than that of the SSR (4°), we use the ESR spectrum widths to obtain the turbulence estimate. The electron density estimate N_e can be obtained from the background incoherent scatter signal as detected by the ESR (*e.g.*, Fig. 4). All these parameters are determining the radar reflectivity. Using the measured parameters (Table 2) and the system parameters

This document is provided by JAXA.

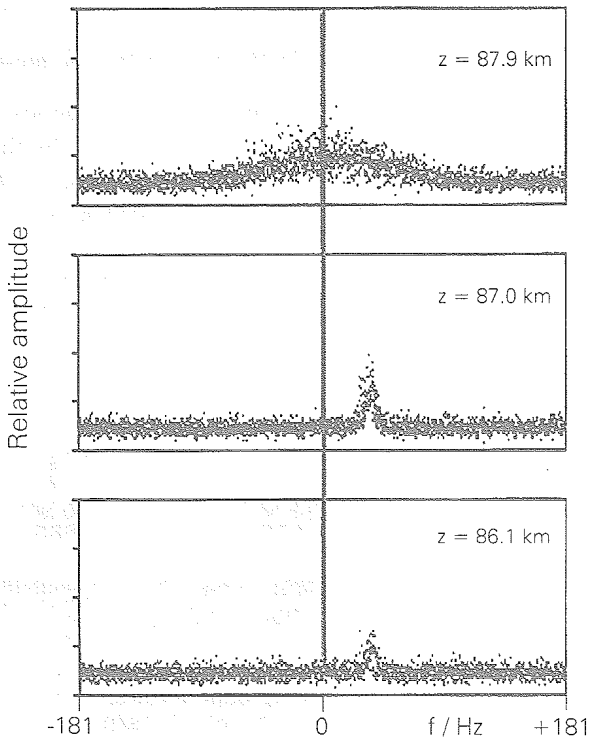


Fig. 6. Scatter plots of spectra of PMSE observed with the ESR, averaged over 90 s. Each single data point results from one 512-point spectrum taken over 1.4 s.

Table 2. Parameters deduced from radar observations during PMSE conditions.

	ESR	SSR		ESR	SSR
Case 1 (broad spectra, 87.9 km)			Case 2 (narrow spectra, 87.0 km)		
Received power in W	$1.6 \cdot 10^{-16}$	$1.2 \cdot 10^{-12}$		$1.0 \cdot 10^{-17}$	$1.0 \cdot 10^{-13}$
Radar reflectivity in m^{-1}	$5.3 \cdot 10^{-19}$	$2.2 \cdot 10^{-14}$		$3.3 \cdot 10^{-20}$	$1.8 \cdot 10^{-15}$
Turbulence energy dissipation rate ϵ in W kg^{-1}	0.26	(0.56)		0.01	(0.05)
Background electron density in m^{-3}	$5 \cdot 10^{8}$	-		$5 \cdot 10^{8}$	-

PMSE at 87–88 km height. Longyearbyen, 15 July 1999, 1002–1006 UT.

(Table 1), we can apply the technique of Hocking (1995) to deduce the radar volume reflectivity, which is the scatter cross section per unit volume, for the two cases of wide (case 1) and narrow (case 2) spectra.

This document is provided by JAXA.

6. Conclusion on ice particles in the polar summer mesopause

The spectral density of neutral turbulence need not to be identical with the spectrum of a passive scalar, such as free electrons in the D-region, mixed by this turbulence. The resulting deviations are determined by the Schmidt number $S_c = \nu/D$, where ν is the molecular viscosity of the neutral gas and D the diffusion coefficient of the electrons. The diffusion of the electrons is ambipolar and is controlled by the ions. Since massive ions are existent in the cold summer mesopause, it is expected that S_c can get much larger than one, which was suggested by Kelley *et al.* (1987) to be the cause for PMSE. Cho (1993) had

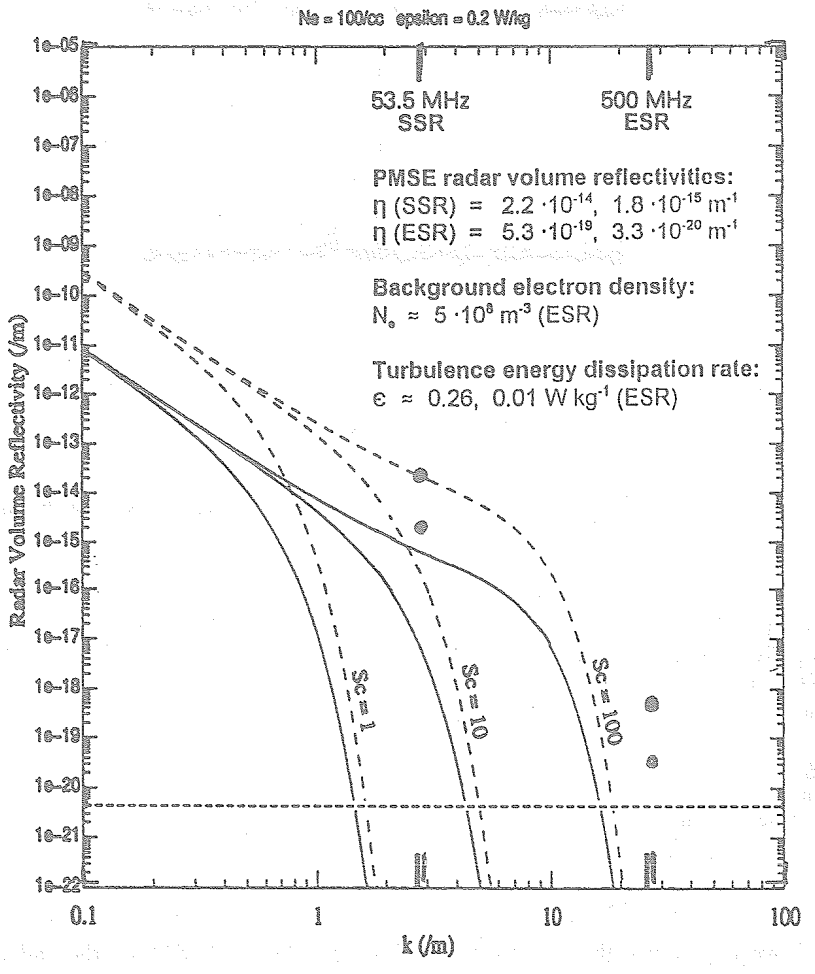


Fig. 7. Radar volume reflectivity of PMSE as function of wavenumber k for different Schmidt numbers S_c, calculated by Cho (1993). Included are the observed radar volume reflectivities η (for case 1 and case 2, see Table 2), and estimates of electron density N_e and turbulence energy dissipation rate ε deduced from the radar observations.

This document is provided by JAXA.

derived the radar volume reflectivity for different Schmidt numbers including the other controlling parameters, such as turbulence energy dissipation rate and the electron density. An example of Cho's diagrams is given in Fig. 7, which shows the radar volume reflectivity as function of wavenumber k. We have indicated here the Bragg wavenumbers of the SSR and the ESR. The radar volume reflectivities of the ESR and the SSR for the turbulent and non-turbulent echoes are shown by the full circles in Fig. 7. We note that the values deduced by our observations fit quite well into the calculations of Cho (1993) for the smaller wavenumber of the SSR. However, we need Schmidt numbers in excess of 100 to explain the relatively high volume reflectivities observed by the ESR.

The effective diffusion coefficient depends on the size and the charge number density of heavy ions or charged aerosol particles (*e.g.,* Hill, 1978). Cho (1993) had calculated the reduction of electron diffusion as function of aerosol or ice particles to electron density. We conclude from those calculations that particle radii would be in the order of a few tens of nanometers for Schmidt numbers larger than 100. The radii of ice particles, which are observed as Noctilucent Clouds and are considered essential for the creation of PMSE, are a few tens of nanometers (Klostermeyer, 1999). The results of our radar observations are compatible with these size distributions of ice particles in the high latitude summer mesopause. The intermittency of the PMSE layers observed in height and time (see Figs. 4 and 5) lets us assume that the ice particles, which are a prime reason for these echoes, occur in inhomogeneous layered structures, which are temporally intermittent and drift over the radars.

We have shown that the combination of two collocated and calibrated radars, operating at different frequencies, can provide significant proof that the electron diffusion in the polar summer mesopause is substantially reduced. This gives rise to enhancements of backscatter cross sections of PMSE. We also conjecture that the results of our two-radar observations are consistent with the presence of ice particle layers in the polar summer mesopause.

Acknowledgments

The author is indebted to his colleagues of the SOUSY project group collaborating in the SOUSY Svalbard Radar project. The EISCAT Svalbard Radar is funded by CNRS (France), MPG (Germany), NFR (Norway), NFR (Sweden), NIPR (Japan), PPARC (UK) and SA (Finland).

References

Balsley, B.B., Woodman, R.F., Sarango, M., Rodrigues, R., Urbina, J., Ragaini, E., Carey, J., Huaman, M. and Giraldez, A. (1995): On the lack of southern hemisphere polar mesosphere summer echoes. J. Geophys. Res., **100**, 11685–11693.

Bremer, J., Hoffmann, P., Manson, A.H., Meek, C.E., Rüster, R. and Singer, W. (1996): PMSE observations at three different frequencies in northern Europe during summer 1994. Ann. Geophys., **14**, 1317–1327.

Cho, J.Y.N. (1993): Radar scattering from the summer polar mesosphere: Theory and observations. Ph. D. dissertation, Cornell University, Ithaca, NY, USA, 181 p.

Cho, J.Y.N. and Röttger, J. (1997): An updated review of polar mesosphere summer echoes: Observations, theory, and their relations to noctilucent clouds and subvisible aerosols. J. Geophys. Res.,

This document is provided by JAXA.

102, 2001–2020.
Czechowsky, P., Klostermeyer, J., Röttger, J., Rüster, R. and Schmidt, G. (1988): The SOUSY Svalbard Radar for middle and lower atmosphere research in the polar region. Proc. 8th Workshop Techn. Sci. Aspects MST Radar, SCOSTEP, 318–321.
Hall, C.M. and Röttger, J. (2001): Initial observations of Polar Mesospheric Summer Echoes using the EISCAT Svalbard Radar. Geophys. Res. Lett., **28**, 131–134.
Hill, R.J. (1978): Nonneutral and quasi-neutral diffusion of weakly ionized miulti-constituent plasma. J. Geophys. Res., **83**, 989–998.
Hocking, W.K. (1995): Measurement of turbulent energy dissipation rates in the midle atmosphere by radar techniques: a review. Radio Sci., **20**, 1403–1422.
Kelley, M.C., Farley, D.T. and Röttger, J. (1987): The effect of cluster ions on anomalous VHF backscatter from the summer polar mesosphere. Geophys. Res. Lett., **14**, 1031–1034.
Klostermeyer, J. (1999): Physics of Polar Mesosphere Summer Echoes. Proc. 14th ESA Symposium on European Rocket and Balloon Programmes and Related Research, ESA SP-437, ESTEC, The Netherlands, 293–298.
Röttger, J. (1994a): Middle atmosphere and lower thermosphere processes at high latitudes studied with the EISCAT radars. J. Atmos. Terr. Phys., **56**, 1173–1195.
Röttger, J. (1994b): Polar Mesosphere Summer Echoes: Dynamics and Aeronomie of the Middle Atmosphere. Adv. Space Res., **14**(9), 123–138.
Röttger, J. (1997): Radar observations of the middle and lower atmosphere. Incoherent Scatter Theory, Practice and Science, ed. by D. Alcayde. EISCAT, 263–314 (Techn. Rep. **97/53**).
Röttger, J. (2000): Radar investigations of the mesosphere, stratosphere and the troposphere in Svalbard. Adv. Polar Upper Atmos. Res., **14**, 202–220.
Röttger, J. (2001): Observations of the Arctic troposphere and lower stratosphere with the SOUSY Svalbard Radar. Mem. Natl Inst. Polar Res., Spec. Issue, **54**, 1–8.
Röttger, J. and Tsuda, T. (1995): Studies of the polar middle and lower atmosphere by an MST radar on Svalbard. J. Geomagn. Geoelectr., **47**, 929–942.
Röttger, J., Rietveld, M.T., LaHoz, C., Hall, T., Kelley, M.C. and Swartz, W.E. (1990): Polar mesosphere summer echoes observed with the EISCAT 933-MHz radar and the CUPRI 46.9-MHz radar, their similarity to 224-MHz radar echoes and their relation to turbulence and electron density profiles. Radio Sci., **25**, 671–687.
Röttger, J., Markannen, J. and Wannberg, U.G. (1998): The EISCAT Svalbard Radar—Its potential for middle atmosphere studies. Proc. 8th Workshop Techn. Sci. Aspects MST Radar, SCOSTEP, 314–317.
Rüster, R., Röttger, J., Schmidt, G., Czechowsky, P. and Klostermeyer, J. (2001): Observations of Mesospheric Summer Echoes at VHF in the polar cap region. Geophys. Res. Lett., **28**, 1471–1474.
Wannberg, U.G., Wolf, I., Vanhainen, L.G., Koskeniemi, K., Röttger, J., Postila, M., Markannen, J., Jacobsen, R., Stenberg, A., Larsen, R., Eliassen, S., Heck, S. and Huuskonen, A. (1997): The EISCAT Svalbard Radar: A case study in modern incoherent scatter radar design. Radio Sci., **32**, 2283–2307.

(Received June 12, 2000; Revised manuscript accepted October 2, 2000)

This document is provided by JAXA.

Mem. Natl Inst. Polar Res., Spec. Issue, 54, 21-28, 2001

Scientific note

Climatic mesospheric cooling: Employing the long time-series of ionospheric soundings from Norwegian stations

C. M. Hall

Tromsø Geophysical Observatory, Faculty of Science, University of Tromsø, 9037 Tromsø, Norway

Abstract: While so-called greenhouse gases are responsible for global warming in the lower atmosphere, they can also cause cooling in the middle atmosphere. Cooling of the middle atmosphere in turn causes shrinking. One consequence of this is that the ionosphere occurs at lower altitude. Observations at several global locations have indicated that the ionospheric F2 layer, at least, is sinking. Here, these phenomena and observations will be briefly reviewed. At Tromsø (69°N), ionosonde observations exist since 1935 and a *précis* history will be given. Furthermore, similar datasets, albeit rather less extensive, exist for other Norwegian stations, notably Svalbard (≈80°N). In the light of work in other countries, we shall examine the potenial of the Norwegian data for studying climatic change in the arctic and sub-arctic. The importance of such archives and also future maintenance of ionospheric observations cannot be overstated.

1. The shrinking atmosphere

The so-called greenhouse gases, primarily carbon dioxide (CO_2) and methane (CH_4) with sources at the earth's surface emit efficiently in the infrared. In the troposphere, this infrared radiation is trapped as in a greenhouse and thus the equilibrium temperature is higher for correspondingly higher greenhouse gas concentration. In the middle atmosphere, these greenhouse gases are still present, and heat is similarly dissipated by long-wave radiation. However, the middle atmosphere is largely outside the "roof" of the "greenhouse" such that the re-emitted radiation is free to escape into space. In this way, CO_2 and CH_4 effectively remove heat from the middle atmosphere —in fact from any part of the atmosphere above the cloud layers— and cool it. Roble and Dickinson (1989) describe the process in detail. To summarise, one thinks of "greenhouse warming" in the troposphere, but of "greenhouse cooling" in the middle and upper atmosphere. The pertinent regions of the atmosphere are sketched in Fig. 1, although for a fuller description, the reader should refer to a text such as Hargreaves (1992).

As the atmosphere cools it occupies less space: it shrinks. Obviously, lower air densities will occur at lower altitudes as a consequence, and it may be deduced that ionisation similarly occurs at lower altitude. This cooling effect and its consequences for the heights of the ionospheric layers have been derived elsewhere: Rishbeth and Roble (1992) model the effect in detail; the effect on the ionospheric layers is summarised by Rishbeth (1990);

This document is provided by JAXA.

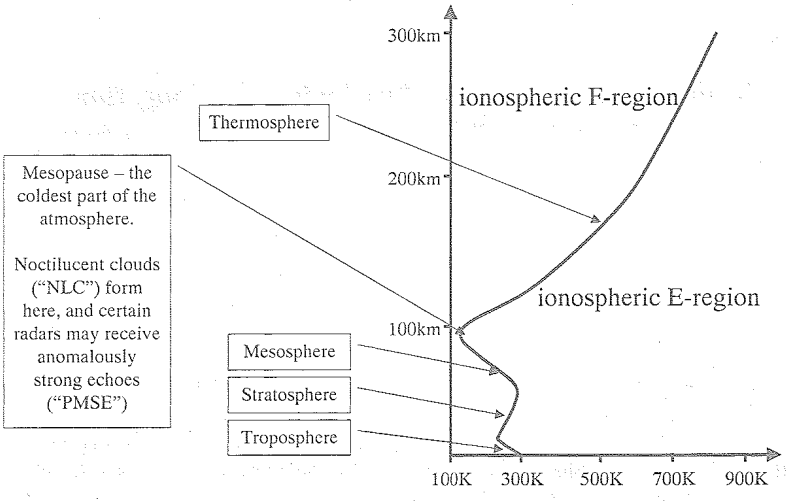


Fig. 1. Schematic of the atmosphere showing, in an extremely simplified fashion, the ionospheric F2 and E layers and their relation to the neutral regions characterised by their temperature behaviour.

an excellent review containing many references may be found in Rishbeth and Clilverd (1999). Increasing frequency of noctilucent cloud (NLC) occurrence is attributable to a combination of increasing water vapour concentration due to oxidisation of methane and also due to lowering of the mesopause temperature (Thomas *et al.*, 1989). Thomas (*e.g.* 1996) has explicitly identified the increase in NLC occurrence with climatic cooling of the middle atmosphere. Changes in solar flux could conceivably be responsible for such changes also; however, since sunspot number and 10 cm flux measurements exist as long time-series, it is easy to rule out such effects, and we a faced with the conclusion that the cause lies in the biosphere.

There is observational evidence of this cooling from ionospheric soundings also, as proposed by Bremer (1992). At high latitude (67°N), Ulich and Turunen (1997) have identified a systematic decrease in the height of the ionospheric F2 layer using a sequence of observations from 1958. At mid-latitude, similarly unambiguous results have been reported by Bremer (1998). The above references are not intended to be exhaustive; nevertheless, many references to the phenomena described here can be found therein. While ionosondes measure only the virtual heights of the atmospheric layers (due to group delay of the radio wave in the underlying ionosphere), the studies mentioned here employ a different (frequency-related) parameter combined with models to estimate the true F2 layer height.

The important result of Ulich and Turunen (1997) for Sodankylä in northern Finland is reproduced in Fig. 2. Despite seasonal and solar-cycle fluctuations, these authors found a trend of around 14 km reduction in F2 layer height over a 40 year period. At mid-latitude (55°N) Bremer (1998) reports 8 km for the same time period. This leads us to wonder whether the sub-arctic station at Tromsø (69°N) yields similar results to that at Sodankylä. Perhaps even more importantly, is the effect more pronounced nearer the poles? (Upwelling

This document is provided by JAXA.

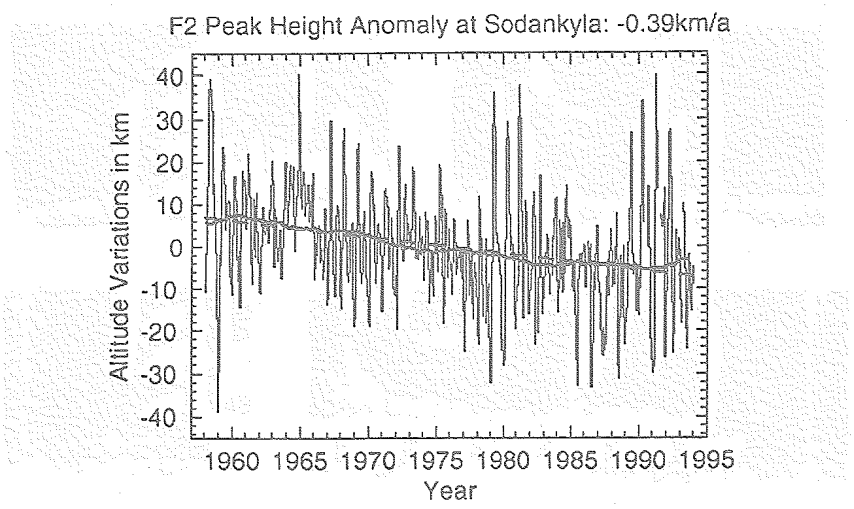


Fig. 2. The results of Ulich and Turunen (1997) showing the sinking of the F2 layer and here over the 41-year period from 1958–1999 (courtesy of Thomas Ulich). Despite the seasonal and solar-cycle fluctuations, the trend is undeniable.

near the poles transports greenhouse gases into the mesosphere at high latitude.) In the next section, we shall examine the data availability for potentially useful Norwegian stations.

Focus hitherto has been on the *F*-region. This is because the height changes are expected to be greater for these layers than for the *E*-region. While doubling of CO_2 and CH_4 are predicted to cause the F2 layer to cool by 30–40 K and fall by 17–20 km, the corresponding figures for the *E*-region are 10 K and 3–4 km respectively; the timescale for this change being around 50 years from present. It would be challenging to look for the predicted changes in the *E*-region also but a longer time-series will be desirable if the result is to be unambiguous.

2. Norwegian ionospheric observations at Tromsø

Ionospheric soundings at the Auroral Observatory in Tromsø were first performed during the Second Polar Year, 1932–33 by British expedition under the direction of Sir Edward Appleton, and simultaneously by a German expedition from Berlin. Soundings of the ionosphere on a regular basis in Tromsø commenced in April 1935 as described by Harang (1937). The British Radio Research Station in Slough, England allowed their ionosonde to be copied, the construction of the instrument being financed by the (then) Norwegian Scientific Research Fund (now Norges Forskningsråd) and The Norwegian Broadcasting Company (now Norsk Rikskringkasting), apparently to a total sum of 11000 Norwegian Crowns. The instrument featured two CRTs, one for visual observation, and the other for photographic recording. Figure 3 shows a page from Harang (1937) illustrating the photographic records of the time. The frequency was adjusted by hand, usually from 1 to 12 MHz. While one operator tuned to progressively higher transmission frequency, the critical frequencies of the ionospheric layers were noted by a second operator (O. Harang,

This document is provided by JAXA.

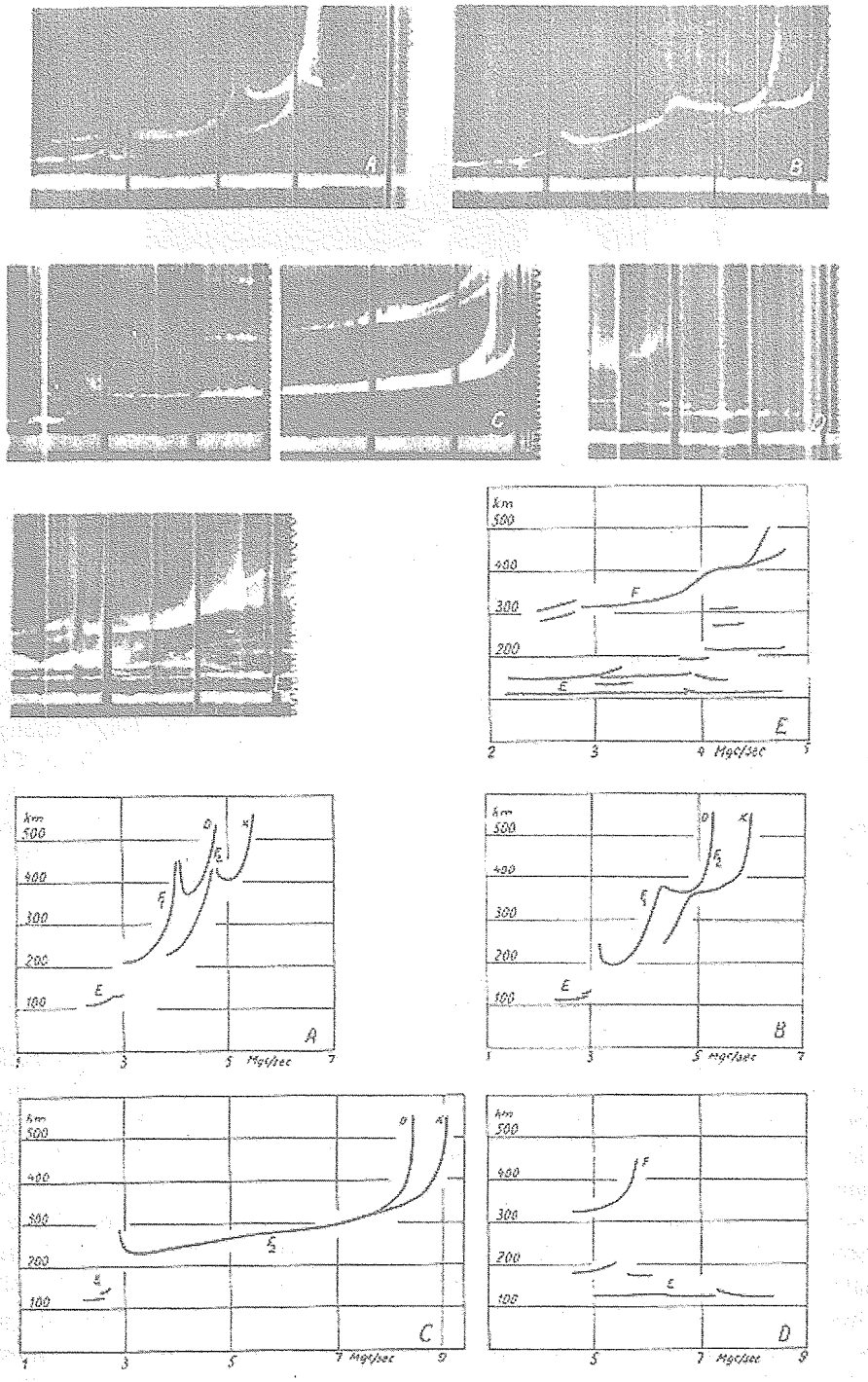


Fig. 3. A page from Harang (1937), the first of a series of annual reports summarising ionosonde observations at Tromsø. The page contains both examples of photographic ionograms from the instrument installed in 1935 and the operators' interpretation of the signal.

This document is provided by JAXA.



Fig. 4. The 1935 instrument was upgraded to this semi-automatic version in 1950.

private communication). During the first years, only the critical frequencies were noted and not the echo height, and observations were only made at 09, 11 and 13 UT. Observations were somewhat erratic during the war years 1939–45, but became regular from 1951. Hourly measurements were made by virtue of a more automatic instrument, installed in 1950 (Fig. 4), and heights were also recorded. These results were assembled in regular reports until 1972. Today, scaling (extraction of critical frequencies and reflection heights) is performed by computer, sadly, because pattern recognition by the human eye is still more reliable than that by computer, at least for ionogram analysis. The original raw data recording onto photographic paper was superseded by film recording in 1968. In the early 80s, a new film format was introduced which operated in parallel with recording to magnetic tape. The digital recording proved itself reliable and photographic recording was phased out in 1983.

The period from 1972 until 1992, while yielding much data of good quality was devoid of scaling; the published reports were apparently discontinued in 1972 with the exception of an isolated report in 1978. Nevertheless, the photographic data remain, and the digitally recorded data are also being preserved, and thus it will be possible to scale these data with appropriate resources.

The present instrument, located at Ramfjordmoen, a few kilometres to the east of the site of the original 1935 installation, is a University of Massachusetts Lowell DPS-4 digisonde, owned and operated jointly by the Defence Evaluation and Research Agency of the UK and the University of Tromsø. Details of this instrument may be found at http://ulcar.uml.edu/.

This document is provided by JAXA.

3. Data coverage

The Sodankylä dataset used by Ulich and Turunen (1997) is probably unique in that not only have the data been regularly scaled since inception of the instrument in 1958, but also the scaling has been performed by the same person. For long time series in which one is to look for climatic change, particularly in the E-region height, such luxury is unattainable since measurements must be made over duration longer than that of an observer's career. In Table 1, the time series for the various Norwegian stations are compared, along with that for Sodankylä. The geographic locations of these stations are illustrated by Fig. 5. The observations for Kjeller (near Oslo) and Longyearbyen (Svalbard) are erratic. A new instrument (University of Leicester, England) is currently operating on Svalbard. Some data gaps exist for the Tromsø dataset, but the real challenge will be in scaling these ionograms while at the same time ensuring that no systematic change is introduced.

Table 1. Ionosonde data availability.

Station	Latitude	Earliest year
Sodankylä	67°	1958
Kjeller (Oslo)	60°	1952
Tromsø	69°	1935
Longyearbyen (Svalbard)	79°	1956

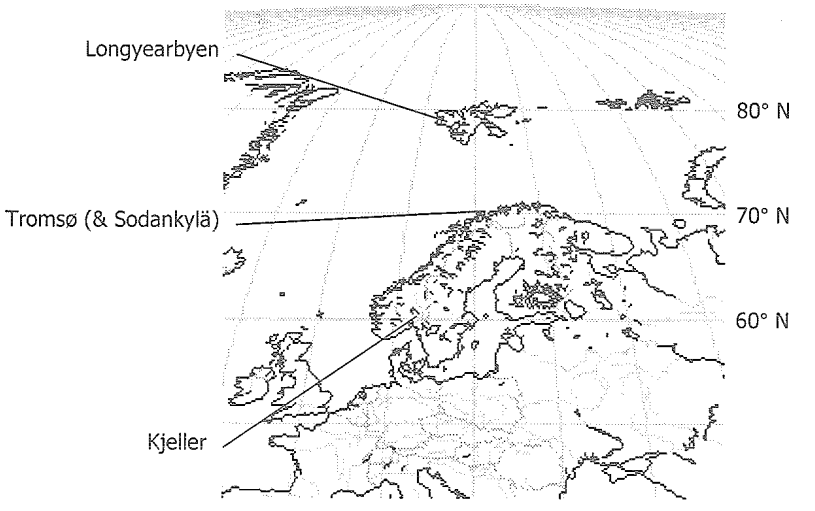


Fig. 5. Geographic locations of the Norwegian stations. The Finnish station, Sodankylä, is at almost the same latitude as Tromsø.

This document is provided by JAXA.

4. Conclusions

First, it should be reiterated that a climatic cooling is indeed occurring in the mesosphere. Although this report has focussed on the response of the height of the ionosphere to this cooling, and the detection of the cooling by ionospheric observation, this is by no means the sole evidence. Changing H_2O concentrations combined with lowering of the mesopause temperature are the only viable explanation of the increasing NLC occurrence, not only with time, but also by equatorward spreading (Thomas, 1996). Temperature data from lidar and satellite (*e.g.* Aikin *et al.*, 1991) and sodium layer height (Clemesha *et al.*, 1992) all support the indication of climatic change.

In turn, this cooling can affect the atmosphere in many ways. Increasing NLC coverage will, principle, increase the planetary albedo, although this will be a marginal effect due to the tenuous nature of the clouds. Perhaps more importantly, if the temperature structure changes such that atmospheric stability is affected, the spatial destribution of gravity wave energy dissipation will change. Such factors give feedback into the overall energy budget in a way that predictions become non-trivial. In an attempt to investigate these climatic changes, the heights of the ionospheric layers can and should be monitored. One must recall that originally, ionosondes were constructed to study radio wave propagation; little thought was given to the possibility that they could yield information on climate. With this thought in mind, the importance of maintaining measurements over extended periods of time cannot be overstressed, even though the exact future use of the data may not be evident *a priori*. One can also understand that it is desirable to establish two or more independent means of monitoring temperature (for example by the means mentioned earlier) and then maintain these observations. All efforts will be made to analyse the existing data from Norwegian stations, and furthermore efforts must be made to ensure that such observations continue indefinitely.

References

Aikin, A.C., Chanin, M.L., Nash, J. and Kendig, D.J. (1991): Temperature trends in the lower mesosphere. Geophys. Res. Lett., **18**, 416–419.

Bremer, J. (1992): Ionospheric trends in mid-latitudes as a possible indicator of the atmospheric greenhouse effect. J. Atmos. Terr. Phys., **54**, 1505–1511.

Bremer, J. (1998): Trends in the ionospheric *E* and *F* regions over Europe. Ann. Geophys., **16**, 986–996.

Clemesha, B.R., Simonich, D.M. and Batista, P.P. (1992): A long-term trend in the height of the atmospheric sodium layer: possible evidence for global change. Geophys. Res. Lett., **19**, 457–460.

Harang, L. (1937): The Auroral Observatory at Tromsø—Results of radio echo observations for the years 1935 and 1936. Publikasjoner fra det norske Institutt for kosmisk fysikk **11**, 24 p., A.S. John Greig, Bergen, Norway. (English)

Hargreaves, J.K. (1992): The Solar-terrestrial Environment: An Introduction to Geospace. Cambridge, Cambridge University Press, 420 p.

Rishbeth, H. (1990): A greenhouse effect in the ionosphere? Planet. Space Sci., **38**, 945–948.

Rishbeth, H. and Roble, R.G. (1992): Cooling of the upper atmosphere by enhanced greenhouse gases—modelling of thermospheric and ionospheric effects. Planet. Space Sci., **40**, 1011–1026.

Rishbeth, H. and Clilverd, M. (1999): Long-term change in the upper atmosphere. Astron. Geophys., **40**, 3.26–3.28.

This document is provided by JAXA.

Roble, R.G. and Dickinson R.E. (1989): How will changes in carbon-dioxide and methane modify the mean structure of the mesosphere and thermosphere? Geophys. Res. Lett., **16**, 1441–1444.
Thomas, G.E. (1996): Global change in the mesosphere-lower thermosphere region: has it already arrived? J. Atmos. Terr. Phys., **58**, 1629–1656.
Thomas, G.E., Olivero, J.J., Jensen, E.J., Schroeder, W. and Toon, O.B. (1989): Relation between increasing methane and the presence of ice clouds at the mesopause. Nature, **338**, 490–492.
Ulich, Th. and Turunen, E. (1997): Evidence for long-term cooling of the upper atmosphere. Geophys. Res. Lett., **24**, 1103–1106.

(Received March 28, 2000; Revised manuscript accepted August 1, 2000)

This document is provided by JAXA.

Mem. Natl Inst. Polar Res., Spec. Issue, 54, 29–41, 2001

Scientific paper

Conjugate imaging riometer observations at polar cusp/cap stations: A daytime absorption event for a specific change of solar wind conditions

Masanori Nishino[1], Hisao Yamagishi[2], Natsuo Sato[3], Yozo Murata[3], Ruiyuan Liu[4], Peter Stauning[5] and Jan A. Holtet[6]

[1]*Solar-Terrestrial Environment Laboratory, Nagoya University, Honohara, Toyokawa 442-8507*
[2]*National Institute of Polar Research, Kaga 1-chome, Itabashi-ku, Tokyo 173-8515*
[3]*Department of Polar Science, the Graduate University for Advanced Studies, Kaga 1-chome, Itabashi-ku, Tokyo 173-8515*
[4]*Polar Research Institute of China, 451 Shang Chuan Road, Shanghai, 200129, China*
[5]*Danish Meteorological Institute, Lyngbyvej 100, Copenhagen, Denmark*
[6]*Department of Physics, University of Oslo, Oslo, Norway*

Abstract: Using the imaging riometers at Ny-Ålesund and Danmarkshavn in the Arctic region, and Zhongshan in Antarctica, a daytime absorption spike event was observed at both hemispheric stations in the post-noon (13–15 h MLT) on August 3, 1997. The conjugate absorption spikes with a quasi-periodic feature were associated with the sequence of solar wind dynamic pressure pulses during northward interplanetary magnetic field (IMF). In particular, the absorption spike associatied with the steep pressure increase and the synchronous short-period southward IMF change exhibited a time difference (~1 min) between the occurrences in the two hemispheres. From comparison between the absorption images and simultaneous aurora all-sky images at Zhongshan, it is recognized that the absorption spike shows a feature of small-scale enhancement with fast eastward motion in the large-scale absorption extending by about 1000 km in longitude and about 50 km in latitude. Ground geomagnetic variations at the high-latitude stations in the both hemispheres showed good response to the solar wind pressure pulse sequence. These observational results indicate that magnetic compressional waves driven by the solar wind pressure pulses could stimulate energetic electrons populating in the outer magnetosphere and thus the electrons could precipitate into the polar cleft ionosphere in both hemispheres due to intensification of upward region-1 field aligned currents near the duskside magnetopause.

1. Introduction

The solar wind flow around the Earth's magnetosphere is by no means in a steady state but is characterized by major changes of the interplanetary magnetic field (IMF) and its plasma velocity as well as its plasma density. The response of the dayside magnetosphere to sudden changes of solar wind conditions is a major dynamic feature of the solar wind interaction with the Earth's magnetosphere.

Glassmeier and Heppner (1992) illustrated schematically magnetopause current layer

This document is provided by JAXA.

perturbations associated with solar wind pressure pulses and magnetic merging (reconnection). Pressure enhancement and magnetic merging events result in localized increases of the local magnetopause current density. From current continuity at the boundary, field-aligned currents (FACs) flow out of the auroral ionosphere, carrying magnetospheric electrons into the dayside ionosphere. Therefore, ground-based auroral observation in the polar cusp/cleft region is a significant remote sensing technique for studying transfer of momentum and energy from the solar wind to the magnetosphere and the polar ionosphere.

Sandholt *et al.* (1994) revealed that strong, isolated enhancements in solar wind dynamic pressure gave rise to equatorward shifts of the cusp/cleft aurora at Ny-Ålesund (geomag. lat., 76°) during southward ($B_z<0$) and westward ($B_y<0$) IMF. Farrugia *et al.* (1995) demonstrated a series of transient auroral emissions in the 1300–1600 MLT sector using the daytime auroral observations at Ny-Ålesund. The IMF showed a strong westward ($B_y\ll0$) and a small northward or zero B_z. They interpreted the emissions in terms of modulations in the reconnection rate at the dayside magnetopause, stimulated by the arrival at Earth of upstream dynamic pressure pulses of the solar wind. Sandholt *et al.* (1996) demonstrated impulsive auroral emissions associated with the arrival of the interplanetary shock and with an IMF directional discontinuity during northward B_z. The transient form with strong green-line emissions at the equatorward boundary of the preexisting aurora showed an equatorward shift of about 100 km south of the zenith over Ny-Ålesund. Thus, as a next step of the dayside aurora studies, the topology of the magnetosphere when the reconnection region maps to the ionospheric projection of the boundary between open and close magnetic field-lines is required. This suggests a necessity of conjugate observations between high-latitude stations in the northern and southern hemispheres.

However, optical observations of auroral particle precipitation have limitations due to climate and sunlit conditions, in particular, simultaneous optical observations between high-latitude stations in the both hemispheres are nearly impossible. By contrast, measurement of ionospheric absorption of cosmic radio signals using a riometer (Relative Ionospheric Opacity meter) is always useful for detecting auroral particle precipitation without these limitations.

An imaging riometer for ionospheric study (IRIS) which is capable of measuring the spatial scale, shape and movement of absorption events, was initially deployed at South Pole station, Antarctica (invariant latitude −74°) in January 1988 (Detrick and Rosenberg, 1990), and since then multiple IRIS instruments have been installed in the Arctic region (*e.g.,* Stauning *et al.*, 1992; Nishino *et al.*, 1993) and in Antarctica (*e.g.,* Nishino *et al.*, 1998). Using the IRISs at Ny-Ålesund/Longyearbyen in Svalbard and Zhongshan station in Antarctica, a conjugate relationship of nighttime absorption events has been discussed in terms of the east-west component (B_y) of the IMF (Nishino *et al.*, 1998).

This paper presents in turn a daytime absorption event observed by the IRISs at the hemispheric high-latitude stations. The IRIS data used are from Ny-Ålesund in Svalbard, Danmarkshavn in Greenland and at Zhongshan station in Antarctica. A characteristic feature of the event is an association with a specific change of solar wind dynamic pressure and IMF. Solar wind parameters from the WIND satellite, aurora all-sky camera data at Zhongshan and ground geomagnetic data at high-latitude stations are used for examination of the conjugate relationship and for discussion of aurora particle precipitations, as a case study.

This document is provided by JAXA.

Table 1. Geographical coordinates of Danmarkshavn (DMH), Ny-Ålesund (NYA) and Zhongshan (ZHS) and their corrected geomagnetic latitudes, approximate magnetic-noon and total magnetic field according to the IGRF model.

Stations	Geographical coordinates	Corrected geomag. latitude	Eccentric dipole magnetic noon	Total magnetic field
Danmarkshavn(DMH)	76.77N, 18.66W	77.26	1036 UT	53660 nT
Ny-Ålesund (NYA)	78.92N, 11.92E	76.05	0847 UT	53959 nT
Zhongshan (ZHS)	69.37S, 76.38E	−74.52	1015 UT	53733 nT

Table 1 gives the geographical coordinates of Danmarkshavn (DMH), Ny-Ålesund (NYA) and Zhongshan (ZHS) and their corrected geomagnetic latitudes, approximate magnetic noon and the total intensity of the magnetic field according to the IGRF model.

2. Imaging riometers

The IRIS instruments at the three stations have almost the similar antenna configurations: a two-dimensional array of 8 by 8 dipole-elements with spacing of a half-wavelength at 38.2 MHz for ZHS/DMH, and with spacing of 0.65-wavelength at 30.0 MHz for NYA. Figure 1 shows the projection of half-power width patterns of 64 antenna-beams on an ionospheric absorption layer at 90 km altitude. The IRIS field-of-view (FOV) is a square of approximately 400 km side and 200 km side for DMH/ZHS and NYA, respectively (Yamagishi *et al.*, 1992).

Figure 2 shows the locations of DMH and NYA and their IRIS FOVs on the European arctic map with invariant latitude contours for 70°and 80°. The north-south direction at DMH, NYA and ZHS IRIS antennas points to the north magnetic pole,

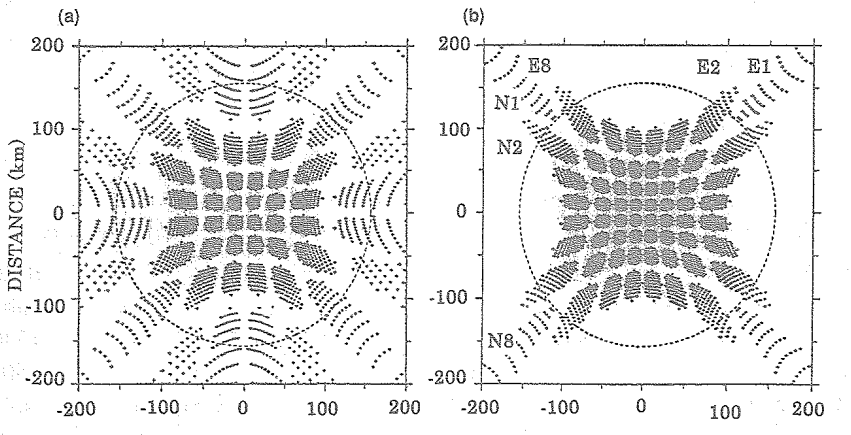


Fig. 1. The projection of a half-power width of 64 antenna-beams on an ionospheric absorption layer at 90 km altitude. The patterns are shown for (a) 0.5-wavelength spacing (Zhongshan/Danmarkshavn IRISs) and (b) 0.65-wavelength spacing (Ny-Ålesund IRIS) (after Yamagishi et al., 1992). The beam numbers noted in the pattern (b) are assigned for north-south and east-west directions.

This document is provided by JAXA.

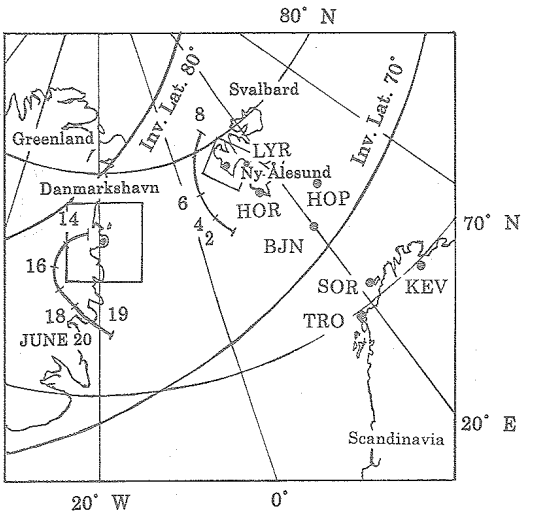


Fig. 2. The IRIS FOVs at Danmarkshavn and at Ny-Ålesund with the invariant latitude contours for 70° and 80° on the European arctic map. Contours giving conjugate locations of Zhongshan are displayed for the morning and afternoon sectors for northern summer solstice (June 20), based on the calculations using the Tsyganenko 1996 model (modified after Yamagishi et al., 1998). The IMAGE magnetometer chain stations extending from Svalbard to northern Scandinavia are also noted by acronyms.

invariant magnetic pole and the south magnetic pole, respectively. Contours giving conjugate locations of ZHS, calculated using the Tsyganenko 1996 model (Tsyganenko and Stern, 1996) under the IMF condition $B_y=B_z=0$ are also displayed for the morning and afternoon sectors at the northern summer solstice (June 20) (Yamagishi *et al.*, 1998). No conjugate location is obtained between 8 h UT and 14 h UT in the noon sector and between 19 h and 2 h UT in the night sector because of open magnetic field-lines. The locations of IMAGE magnetometer chain stations used in this study are also shown in this figure (Lühr *et al.*, 1998).

3. The daytime absorption event of August 3, 1997

Figure 3 shows time variations of the B_x-, B_y- and B_z-components of the IMF, and ion density (N) and ion dynamic pressure (P_{dyn}) of solar wind from the WIND satellite for the 1030–1400 UT interval of August 3, 1997 in the upper panel, together with absorption variation in the east-west direction near the zenith (S4) at ZHS during 1100–1330 UT in the lower panel. During this interval, the WIND satellite was located at $R_x \sim +80\ R_e$, $R_y \sim -60\ R_e$ and $R_z \sim +15\ R_e$ (in GSE) in the solar wind. The variation of the solar wind dynamic pressure ($P_{dyn}=mNv^2$) arises almost solely from the ion density. The solar wind dynamic pressure increased from a quiet state (~2 nPa) to ~6 nPa at 1005 UT, remained at 6–8 nPa (not shown in the panel), and decreased to 6 nPa at about 1100 UT. Thereafter the pressure showed a positive swing ($\Delta P/P$ ~0.6) which started at 1132 UT, a gradual step-like increase ($\Delta P/P$ ~0.8) which started at 1150 UT, and a subsequent steep increase

This document is provided by JAXA.

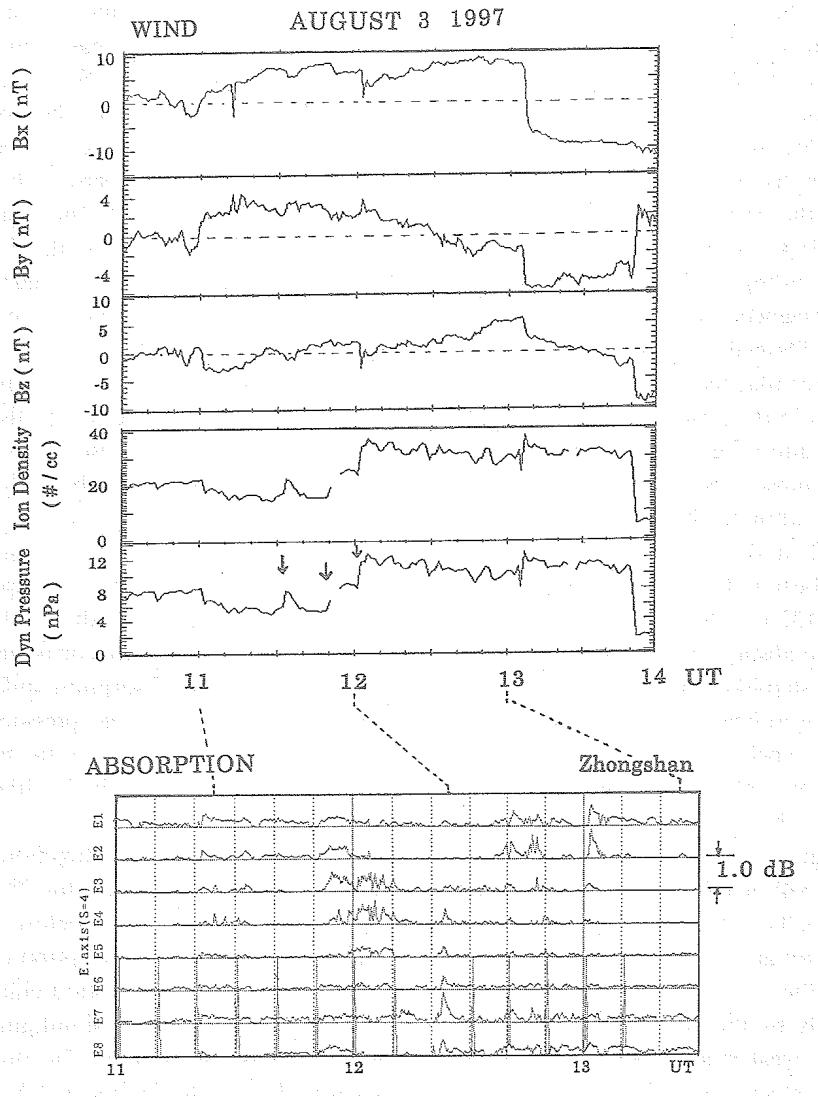


Fig. 3. Time variations of B_x-, B_y- and B_z-components of the IMF, ion density (N) and ion dynamic pressure (P_{dyn}) of solar wind from WIND satellite during 1030–1400 UT on August 3, 1997 (upper panel) together with absorption variation in the east-west direction (E1–E8) near the zenith (S4) during 1100–1330 UT at ZHS (lower panel). Absorption unit is 1.0 dB/div. Dashed lines between the upper and lower panels show the 25-min delay.

($\Delta P/P \sim 1.6$) which started at 1201 UT, followed by a quasi-periodic fluctuation (repetition of ~8 min). Between 11 h–13 h UT, B_x was positive with a negative spike at 1201 UT, and B_y was positive with a positive spike at 1201 UT and a gradual negative change at about 1230 UT. B_z gradually changed from negative to positive with a sharp negative spike (peak, −4 nT) at 1201 UT.

This document is provided by JAXA.

To show the relationship between the solar wind conditions and the absorption variation, we estimate a total time delay of 22 min to account for propagation from the satellite to the bow shock (~12 R_e) at an average solar wind velocity of 450 km/s, from the bow shock to the magnetopause (~9 R_e) and from the magnetopause to the polar ionosphere (Stauning *et al.*, 1995). However, this time delay may be erroneous because the discontinuity in solar wind is not necessarily perpendicular to the sun-earth line. Then we refer to the ground magnetometer data at the low-latitude station Hermanus (geographic lat., −34.4°, long., 19.2°), located on the day side during the present daytime event. Corresponding to the steep pressure increase at 1201 UT, sudden commencement (SC) of the geomagnetic variation started at 1226 UT at Hermanus, which indicates a time delay of 25 min. Dashed lines connecting the panels show the 25-min delay.

Since magnetic noon is approximately 1015 UT at ZHS, the absorption spike event occurred in the post-noon sector (1300–1500 MLT). Unfortunately, strong impulses caused by the calibration signals in the riometer receivers contaminated the absorption variation on the most western beam (E8) every 10 min. Here, we note the absorption spikes corresponding to the solar wind dynamic pressure pulses which started at about 1132 UT, 1150 UT, and 1201 UT, marked by downward arrows. The absorption spikes seen in the eastern beams (E1–E4) around 1152 UT likely correspond to the positive swing pressure of about 1132 UT, followed by fluctuating absorption spikes (E3 and E4) during 1200–1210 UT. The absorption seen only in beam E7 during 1212–1216 UT may correspond to the gradual step-like pressure increase at 1150 UT. The pronounced absorption spike seen in the east-west beams (E3–E8) near 1223 UT clearly corresponds to the steep pressure increase and the synchronous short-period southward IMF change at 1201 UT. The succeeding absorption spikes with a quasi-periodic (QP) feature seen best on beam E7 likely correspond to the pressure oscillation after the steep increase.

Figure 4 shows time variations of the absorption in the east-west direction near the zenith (N4) at DMH and NYA together with those near the zenith (S4) for ZHS shown in Fig. 3. The intensity of absorption spikes at all three stations is mostly below 1 dB. The absorption around 1153 UT at ZHS likely corresponds to very weak absorption (<0.2 dB) seen in the E2–E6 beams at DMH (shown by broken lines). The absorption enhancement seen only by the E7 beam at ZHS during 1212–1216 UT is probably simultaneous with gradual, weaker absorption in the E2–E6 beams at NYA. By contrast, the pronounced absorption spike seen near 1223 UT at ZHS is clearly identical to the one at NYA (shown by broken lines). The absorption spike at ZHS appears one minute earlier than the one at NYA, and shows eastward motion. The succeeding QP absorption spikes seen best by beam E7 at ZHS are also clearly identical to the spikes for beam E5 or E6 at NYA.

Since during the whole study interval the sun was well below the horizon at Zhongshan, optical aurora observations could be made by all-sky camera. Figure 5 shows a time series of IRIS images of the pronounced absorption spike around 1223 UT (lower panel) and approximately simultaneous aurora all-sky images observed at ZHS (upper panel). Each absorption image shows the average during 32 s. The all-sky camera has panchromatic performance centred at 520 nm wavelength, and thus is most sensitive to green-line emissions produced at about 100 km altitude.

It is quite clear from the absorption images that a small-scale (~100 km) absorption enhancement is evident on the western side of the IRIS FOV from 1222:20 UT to 1222:52

This document is provided by JAXA.

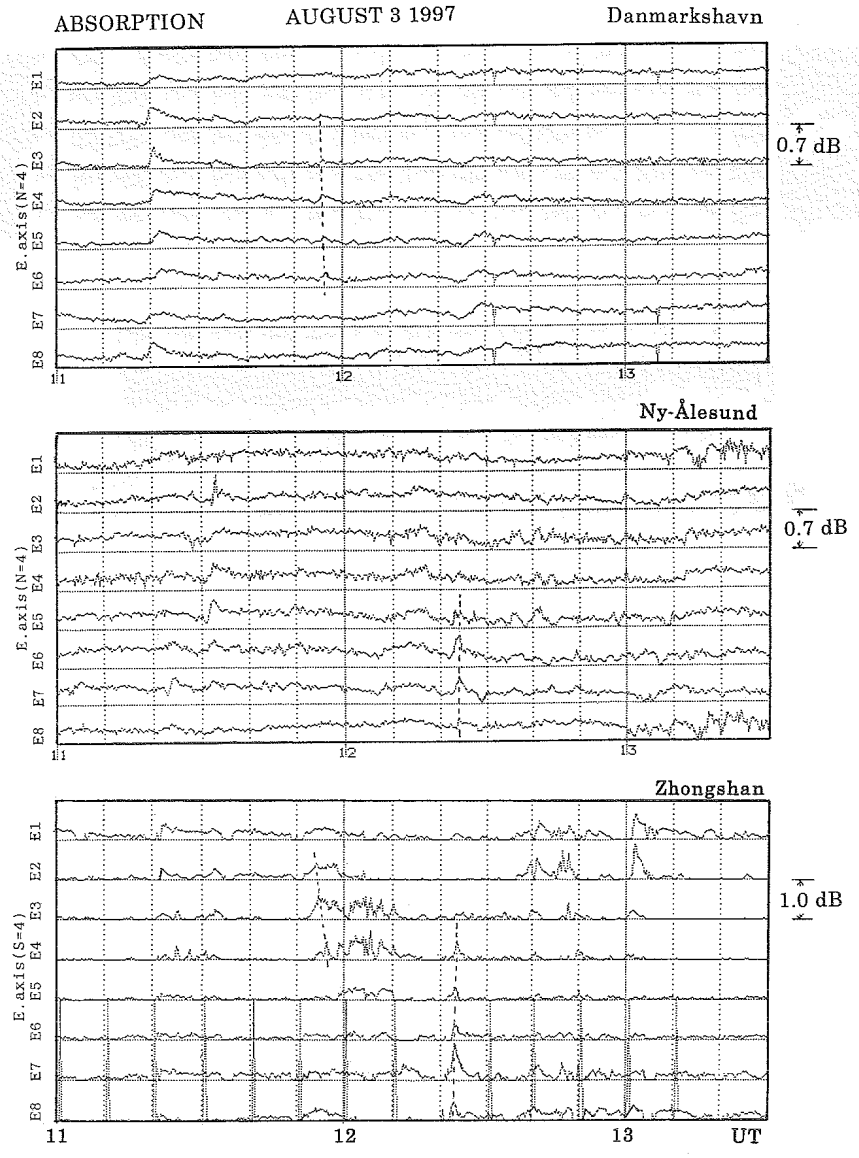


Fig. 4. Time variations of the absorption in the east-west direction near the zenith at DMH, NYA and ZHS during 1100–1330 UT on August 3, 1997. The absorption unit is noted at the right side of the absorption variation, respectively.

UT. Subsequently, the enhancement part moves eastward with a motion of about 3.7 km/s in the large-scale absorption extending exceeding 400 km in longitude and about 50 km in latitude. Maximum absorption (~0.9 dB) is found at the western part and near the zenith at 1223:24 UT. Thereafter the absorption activity decreases everywhere. This dynamic behavior is very similar to an auroral arc both in shape and motion (upper panel). However, since the auroral arc is extended in longitude in the whole all-sky FOV, it is

This document is provided by JAXA.

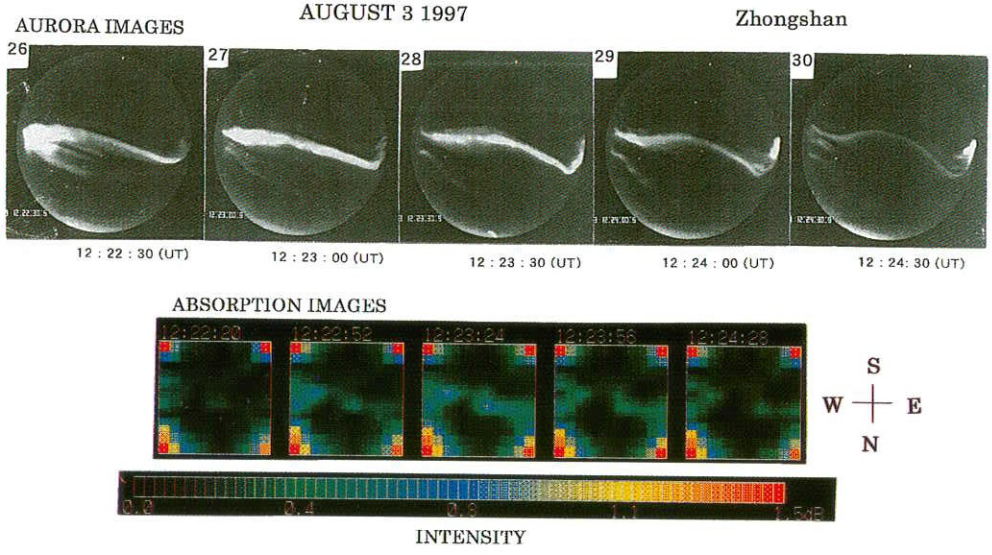


Fig. 5. A time series of images of the absorption spike (lower figure) and the corresponding aurora all-sky images (upper figure) at Zhongshan. Top is magnetic south (high-latitude), left is magnetic west. Each absorption image is the average during 32 s. The absorption intensity is color coded up to 1.5 dB. The bright color spots seen at four corners in the absorption images are contaminated by strong radio wave interferences.

estimated that the large-scale absorption is extended by about 1000 km in longitude.

4. Discussion

With regards to ionospheric signatures in high-latitudes to solar wind conditions, Mende *et al.* (1990) presented five magnetic impulse events observed at South Pole station and in the magnetically conjugate area at Iqualuit in Canada. The magnetic events appeared to be possible ionospheric signatures of sporadic dayside magnetic reconnection via flux transfer processes. Coordinated ground-based image-intensified all-sky camera data signified the event initiation on closed magnetic field-lines. Sibeck *et al.* (1989a) have revealed that some transient ground events with bipolar north-south magnetic field deflections at South Pole station are related to impulse variations in solar wind dynamic pressure and not necessarily to magnetic merging (reconnection) at the dayside magnetopause. Sibeck *et al.* (1989b) demonstrated a quasi-periodic feature of riometer absorption, geomagnetic perturbations and ELF/VLF radio emissions at South Pole station associated with oscillations of solar wind dynamic pressure. The good correlation between the riometer absorptions and ELF/VLF pulses has indicated that the precipitation mechanism involves a wave-particle interaction between the magnetospheric electrons and ELF/VLF waves. Farrugia *et al.* (1989) demonstrated ground magnetic deflections associated with sudden changes in solar wind dynamic pressure during northward IMF. Some magnetic deflections showed a "ringing" of the magnetospheric cavity, while others showed

This document is provided by JAXA.

evident deflections for only the initial pressure pulse. Prikryl *et al.* (1998) showed a good correlation between quasi-periodic fluctuations in the solar wind pressure and quasi-periodic convection flow bursts observed by the Iceland HF radars, and also Prikryl *et al.* (1999) showed a good correlation between the riometer absorption fluctuations at Gillam (~68°N) in Canada and the 3-4 min oscillations of the B_y-component during southward IMF. As described above, sudden and fluctuating changes in solar wind dynamic pressure and IMF variation do influence the dynamics of the dayside magnetosphere and thus the high-latitude ionosphere, signifying plasma convection flow bursts, ionospheric current perturbations, and ionospheric absorption increases, as well as aurora activations.

First we discuss a conjugate feature of the absorption spike at about 1223 UT (~14 MLT at ZHS) associated with the steep solar wind pressure increase at 1201 UT. Nishino *et al.* (2000) discussed the conjugate relationship between the two hemispheric stations for the same absorption with the one presented in this paper. They have revealed that the conjugate location of ZHS cannot be near 12 h UT under the quiet IMF condition (IMF $B_y=B_z=0$) due to open magnetic field-lines, as shown in Fig. 2, but could be at the lower-latitude side with eastward displacement under solar wind pressure increase and positive (eastward) IMF-B_y conditions. Here we discuss the time difference of about 1 min between the ZHS and NYA on the absorption spike occurrence near 1223 UT. The IMF B_z changed steeply southward (peak value, -4 nT) with a short period (~2 min) at 1201 UT. This IMF change suggests a possibility of transient magnetic reconnection in the lower latitude boundary layer (LLBL) at the duskside magnetopause. Associated with reconnection enhancement, magnetic compressional waves may stimulate magnetospheric electrons on the magnetic shells (Prikryl *et al.*, 1998). If the reconnection occurs in the southern hemisphere, magnetospheric electrons stimulated by the compressional waves may precipitate earlier into the southern hemisphere ionosphere than into the northern hemisphere ionosphere: the absorption spike would appear earlier at the southern hemisphere station (Hargreaves and Chivers, 1965). However, since the B_y orientation is eastward (duskward), it is unreasonable to predict magnetic reconnection in the southern hemisphere. Rather, it may be reasonable to consider that the absorption located in the western region out of the NYA FOV could propagate eastward and reach the NYA station.

Next we discuss plasma sources of the daytime absorption and the mechanism of auroral particle precipitation from the dayside magnetosphere. Nishino *et al.* (2000) found absorption enhancement (~1 dB) from the CANOPUS riometer chain in Canada which occurred preceding about one hour from the present absorption spike, and inferred that a population of ample energetic electrons drifting eastward from substorm injection into the nightside magnetosphere would be plasma sources. Another bit of evidence is found from the energy-time spectrogram of electrons (32 eV-32 keV) on the low-altitude DMSP satellite (~800 km) (Newell and Meng, 1988). The DMSP satellite passed over the northern part (~78°N) in Greenland at about 1220 UT through the northern area (~78°N) outside Svalbard, and observed precipitations of energetic electron fluxes with a uniform structure in the range above 2 keV during about 1220-1224 UT (not shown here). Thus these observations confirm that plasma sources of the present daytime absorption spikes are high-energy magnetospheric electrons populated in the lower latitude boundary layer (LLBL) at the duskside magnetopause.

In order to examine the magnetic signature for the solar wind pressure variation, we

This document is provided by JAXA.

show the variance of the solar wind pressure exceeding 4 nPa during 1140–1340 UT (upper panel) and the geomagnetic X-components at the IMAGE magnetometer chain stations and at Zhongshan station in Antarctica during 12–14 h UT (lower panel) in Fig. 6. The solar wind pressure variation is shifted by 25 min delay for the ground geomagnetic variation. It is found that the geomagnetic amplitude variation at ZHS is roughly similar to the solar wind pressure variation. It is also found that the geomagnetic amplitude variations are better correlated between ZHS and HOP (or BJN) than between ZHS and NYA (or LYR). These indicate that the conjugate magnetic signature to the solar wind pressure is most evident between ZHS and HOP (or BJN) in both hemispheres, which is consistent with the calculation that the conjugate point of ZHS would be located at lower-latitude than NYA under the solar wind pressure increase and eastward IMF-B_y.

Figure 6 also shows that the geomagnetic amplitude peaks at higher-latitude stations than BJN show a poleward progressing phase with a speed of about 2 km/s, as shown by

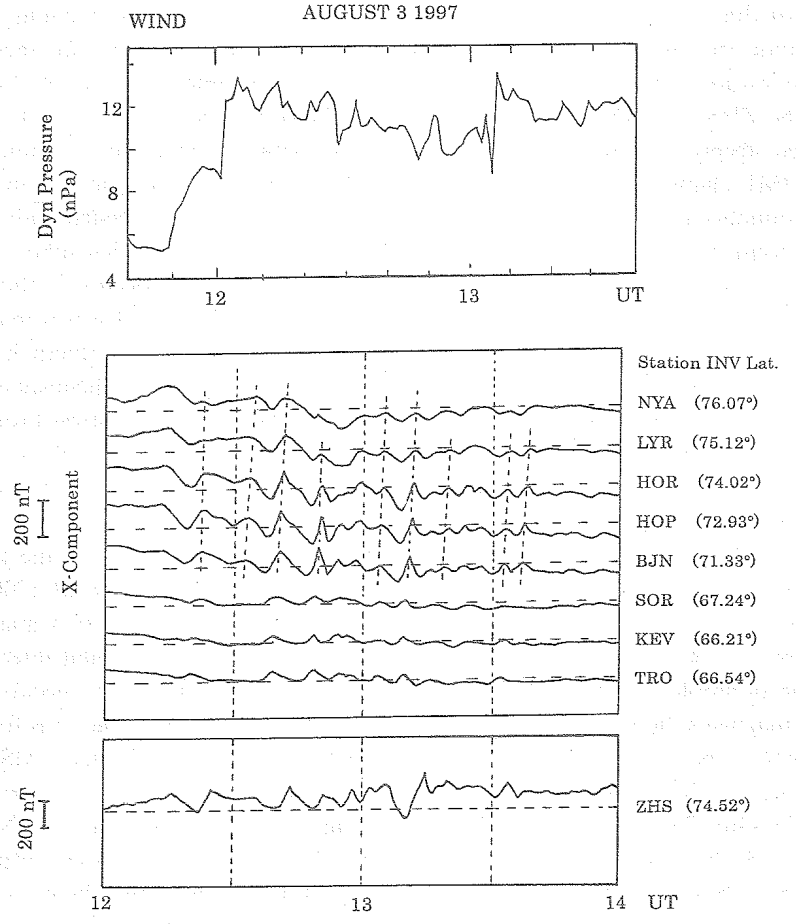


Fig. 6. The variance exceeding 4 nPa of the solar wind dynamic pressure from the WIND satellite (upper panel) and geomagnetic north-south (X) components at the IMAGE magnetometer chain stations and at Zhongshan with invariant latitudes (lower panel). The pressure variation is displayed by 25-min delay for the geomagnetic variation.

This document is provided by JAXA.

some of the broken lines. This feature is in agreement with the variation of the geomagnetic X-components from five high-latitude stations (68.1°–75.2°), which was indicated as a magnetic signature due to the magnetopause motion associated with the solar wind ram pressure (Farrugia *et al.*, 1989). Prikryl *et al.* (1998) also showed a poleward progressing phase of the geomagnetic X-components from the magnetometer chain on the west coast of Greenland, which was associated with the sudden southward IMF change. They have revealed that the poleward progressing is typical of field line resonance (FLR) in the outer magnetosphere. Although the phase relation between the X-components at ZHS and HOP shows a 2–3 min delay in Fig. 6, it shows near phase agreement between the Y-components at both stations (not shown here). This indicates that the FLR is not determined for the fundamental mode (odd mode) or for the even mode; that is, the two phase relations may be a complicated combination of the FLR effect with the inductive effect of the ionospheric current caused by the enhanced conductivity due to auroral particle precipitations. Further detailed analysis of the phase relation is required.

From the Polar Patrol Balloon experiments near Syowa Station (L~6), Antarctica, Hirashima *et al.* (1999) have revealed that compressional MHD waves can produce whistler waves in the outer magnetosphere through electron cyclotron resonance, and result in the identification of pulsating X-rays, Pc5 range ULF pulsations and VLF emissions. The simultaneous identification between riometer absorption and ELF/VLF waves at South Pole station associated with oscillations of the solar wind pressure may indicate that the compressional mode waves would scatter magnetospheric electrons populating in the outer magnetosphere (Sibeck *et al.*, 1989b). Since we have no VLF emission or X-ray data at either hemispheric station, we cannot definitely rule out the mechanism of pitch angle diffusion through electron cyclotron resonance.

However, from statistical analysis of the ground IRIS observations at Sondre Stromfjord (73.7° inv. lat.) in Greenland, Stauning and Rosenberg (1996) have revealed that the high-latitude daytime absorption spikes, typically 0.2–0.3 dB at 38 MHz with spatial extent of 50–100 km, are related to the sudden precipitation of high-energy (30–300 keV) magnetospheric electrons, and may be generated at or a few degrees equatorward of the convection reversal boundary, due to upward region-1 FAC intensification in the afternoon convection cell, although they could not determine a definite relationship between the daytime absorption spike events and the solar wind conditions. Sandholt *et al.* (1996) have revealed that the transient form with strong green-line emissions at the equatorward boundary of the preexisting aurora may be explained by the generation of strong, localized field-aligned currents associated with the conversion of a compressional wave into the Alfvén mode at the location of a gradient in the plasma density at the inner edge of the LLBL. Thus it is reasonable to consider that the small-scale enhancement of the absorption showing eastward travel in the large-scale absorption shown in Fig. 5 would be caused by localized energetic electron precipitation due to the formation of field-aligned potential drop between the outer magnetosphere and polar cleft ionosphere.

5. Concluding remarks

We present a post-noon absorption spike event observed by the high-latitude IRIS stations in both the northern and southern hemispheres. Particularly, we examined the

This document is provided by JAXA.

conjugate feature of the absorption spike associated with the steep increase of solar wind pressure and the synchronous southward IMF change, and discussed the mechanism of the energetic particle precipitations including plasma sources. The following concluding remarks emerged from this case study.

1) The post-noon absorption spikes with a quasi-periodic feature observed between the conjugate IRIS stations in both the northern and southern hemispheres showed the conjugate ionospheric signature on closed magnetic field-lines.
2) The absorption spike showed the small-scale feature with the fast eastward motion in the large-scale absorption extending by about 1000 km in longitude and about 50 km in latitude.
3) Magnetic compressional waves driven by the solar wind pressure pulses could stimulate magnetospheric electrons populating in the outer magnetosphere, and the electrons could be precipitated into the cleft ionosphere due to intensification of the strong, localized upward region-1 FAC.

Acknowledgments

We are pleased to acknowledge the encouragement of A. Egeland, University of Oslo. We gratefully acknowledge the Norwegian Polar Research Institute and Chinese Antarctic Expedition for incessant observations at Ny-Ålesund and Zhongshan, respectively, and we greatly appreciate the careful operation of the imaging riometer at Danmarkshavn. We also gratefully acknowledge Ron Lepping, and K. Ogilvie, NASA Goddard Flight Center for supplying the WIND satellite data, P.T. Newell, Johns Hopkins University for supplying the DMSP data. The geomagnetic data at the IMAGE magnetometer stations and at Hermanus station were provided through Web services.

References

Detrick, D. and Rosenberg, T.J. (1990): A phased-array radio wave imager for studies of cosmic noise absorption. Radio Sci., **25**, 325–338.

Farrugia, C.J., Freeman, M.P., Cowley, S.W.H., Southwood, D.J., Lockwood, M. and Etemadi, A. (1989): Pressure-driven magnetopause motions and attendant response on the ground. Planet. Space Sci., **37**, 589–607

Farrugia, C.J., Sandholt, P.E., Cowley, S.W.H., Southwood, D.J., Egeland, A., Stauning, P., Lepping, R.P., Lazarus, A.J., Hansen, T. and Friis-Christensen, E. (1995): Reconnection-associated auroral activity stimulated by two types of upstream dynamic pressure variations: Interplanetary magnetic field $B_z \sim 0$, $B_y \ll 0$ case. J. Geophys. Res., **100**, 21753–21772.

Glassmeier, K.H. and Heppner, C. (1992): Traveling magnetospheric convection twin vortices: Another case study, global characteristics, and a model. J. Geophys. Res., **97**, 3977–3992.

Hirashima, Y., Simobayashi, H., Yamagishi, H., Suzuki, H., Murakami, H., Yamada, A., Yamagami, T., Namiki, M. and Kodama, M. (1999): MHD wave characteristics inferred from correlations between X-ray, VLF, and ULF's at Syowa Station, Antarctica and Tjörnes, Iceland ($L \sim 6$). Earth Planet. Sci., **51**, 33–41.

Hargreaves, J.K. and Chivers, H.J.A. (1965): A study of auroral absorption events at the South Pole, 2. Conjugate properties. J. Geophys. Res., **70**, 1093–1102.

Lühr, H., Aylward, A., Bucher, S.C., Pajunpaa, K., Holmboe. T. and Zalewski, S.M. (1998): Westward moving dynamic substorm features observed with the IMAGE magnetometer network and the ground-based instruments. Ann. Geophys., **16**, 425–440.

Mende, S.B., Rairden, R.L., Lanzerotti, L.J. and Maclenman, C.G. (1990): Magnetic impulses and

This document is provided by JAXA.

associated optical signatures in the dayside aurora. Geophys. Res. Lett., **17**, 131–134.
Newell, P.T. and Meng, C.-I. (1988): The cusp and the cleft/boundary layer: Low altitude identification and statistical local time variation. J. Geophys. Res., **93**, 14549–14556.
Nishino, M., Tanaka, Y., Oguti, T., Yamagishi, H. and Holtet, J.A. (1993): Initial observation results with imaging riometer at Ny-Ålesund ($L=16$). Proc. NIPR Symp. Upper Atmos. Phys., **6**, 47–61.
Nishino, M., Yamagishi, H., Sato, N., Sanoo, Y., Ruiyuan, L., Honquao, H. and Stauning, P. (1998): Initial results of imaging riometer observations at polar cap conjugate stations. Proc. NIPR Symp. Upper Atmos. Phys., **12**, 58–72.
Nishino, M., Yamagishi, H., Sato, N., Liu, R., Hongquao, Hu., Stauning, P. and Holtet, J.A. (2000): Conjugate features of daytime absorption associated with specific changes in the solar wind observed by inter-hemispheric high-latitude imaging riometers. Adv. Polar Upper Atmos. Res., **14**, 76–92.
Prikryl, P., Greenwald, R.A., Sofko, G.J., Villain, J.P., Ziesolleck, C.W.S. and Friis-Chistensen, E. (1998): Solar-wind-driven pulsed magnetic reconnection at the dayside magnetopause, Pc5 compressional oscillations, and field line resonances. J. Geophys. Res., **103**, 17307–17322.
Prikryle, P., Macdougall, J.W., Grant, I.F., Steele, D.P., Sofko, G.J. and Greenwald, R.A. (1999): Observations of polar patches generated by solar wind Alfvén wave coupling to the dayside magnetosphere. Ann. Geophys., **17**, 463–489.
Sandholt, P.E., Farrugia, C.J., Burlaga, L.F., Holtet, J.A., Moen, J., Lybekk, B., Jacobsen, B., Opsvic, D., Egeland, A., Lepping, R., Lazarus, A.J., Hansen, T., Brekke, A. and Friis-Christensen, E. (1994): Cusp/cleft aurora activity in relation to solar wind dynamic pressure, interplanetary magnetic field B_z and B_y. J. Geophys. Res., **99**, 17323–17342.
Sandholt, P.E., Farrugia, C.J., Stauning, P., Cowley, S.W.H. and Hansen, T. (1996): Cusp/cleft auroral forms and activities in relation to ionospheric convection: Responses to specific changes in solar wind and interplanetary magnetic field conditions. J. Geophys. Res., **101**, 5003–5020.
Sibeck, D.G., Baumjohann, W. and Lopez, R.E. (1989a): Solar wind dynamic pressure variations and transient magnetospheric signatures. Geophys. Res. Lett., **16**, 13–16.
Sibeck, D.G., Baumjohann, W., Elphic, R.C., Fairfield, D.H., Fennel, J.F., Gail, W.B, Lanzerotti, L.I., Lopez, R.E., Luehr, H., Lui, T.Y., Maclennan, C.G., McEntire, R.W., Potemra, T.A., Rosenberg, T.J. and Takahashi, K. (1989b): The magnetospheric response to 8-minute period strong-amplitude upstream pressure variations. J. Geophys. Res., **94**, 2505–2519.
Stauning, P. and Rosenberg, T.J. (1996): High-latitude daytime absorption spike events. J. Geophys. Res., **101**, 2377–2396.
Stauning, P., Henriksen, S. and Yamagishi, Y. (1992): Imaging riometer installation in Danmarkshavn, Greenland. Danish Meteorological Institute, Technical Report, **92-4**, 1–25.
Stauning, P., Clauer, C.R., Rosenberg, T.J., Friis-Christensen, E. and Sitar, R. (1995): Observations of solar-wind-driven progression of interplanetary magnetic field B_y-related dayside ionospheric disturbances. J. Geophys. Res., **100**, 7567–7585.
Tsyganenko, N.A. and Stern, D.P. (1996): Modeling the global magnetic field of the large-scale Birkeland current systems. J. Geophys. Res., **101**, 27187–27198.
Yamagishi, H., Nishino, M., Sato, M., Kato, Y., Kojima, M., Sato, N. and Kikuchi, T. (1992): Development of imaging riometers. Nankyoku Shiryô (Antarct. Rec.), **36**, 227–250 (in Japanese with English abstract).
Yamagishi, H., Fujita, Y., Sato, N., Stauning, P., Nishino, M. and Makita, K. (1998): Conjugate features of auroras observed by TV cameras and imaging riometers at auroral and polar cap conjugate-pair stations. Polar Cap Boundary Phenomena, ed. by J. Moen *et al.* Doerdrecht, Kluwer Academic Publ., 289–300 (NATO ASI Ser.; Ser. C 509).

(Received June 2, 2000; Revised manuscript accepted November 6, 2000)

This document is provided by JAXA.

This document is provided by JAXA.

Mem. Natl Inst. Polar Res., Spec. Issue, 54, 43-48, 2001

Scientific note

A study on the Arctic upper-atmospheric tide by EISCAT radar —Recent results and prospects—

Takehiko Aso

Arctic Environment Research Center, National Institute of Polar Research, Kaga 1-chome, Itabashi-ku, Tokyo 173-8515 (aso@nipr.ac.jp)

Abstract: The polar middle and upper atmospheric tide can be affected by both electromagnetic disturbances from above due to ion drag or Juole coupling and by the various interactions due to polar vortex and wave dynamics in the denser lower atmosphere. The EISCAT radar system now includes mono-static UHF radar in Svalbard (ESR, 78°N) in the polar cap region, which complements the mainland KST system of both tri-static UHF and mono-static VHF radars in the auroral region of northern Scandinavia (67–69°N). It is expected that this radar system will play more important role in studying the Arctic upper and middle atmosphere dynamics. Here, a brief description of recent EISCAT tidal observations by the new ESR (EISCAT Svalbard Radar) is given.

1. Introduction

Four years have elapsed since the National Institute of Polar Research, Japan joined the EISCAT Scientific Association. During this period, research activities in the Arctic upper atmosphere have widely expanded in the vast disciplines of the solar-terrestrial environment from the mesosphere to the thermosphere, ionosphere, and magnetosphere. Especially, conjunctive and global multi-instrumental observations with satellites, ground-based radar and optical platforms are intensive by on-going and planned. EISCAT mainland radar comprises two radars, a tri-static UHF (931 MHz) system in Tromsø (69 °N, Norway), Sodankyla (67°N, Finland) and Kiruna (68°N, Sweden), and a VHF (224 MHz) mono-static radar in Tromsø. In 1997, a new EISCAT UHF (500 MHz) radar system was built in Svalbard, (78°N, referred to as EISCAT Svalbard Radar ESR) which can explore the polar cap ionosphere where solar wind flows directly into the earth's upper atmosphere through the cusp/cleft region. In autumn 1999, a fixed Cassegrain antenna was added to the ESR system, and observation of higher temporal and spatial resolutions has become possible.

We are working on the observation of polar upper-atmospheric dynamics by the EISCAT radar and associated radars and optics to study the dynamical coupling of the polar middle atmosphere and lower thermosphere. Specifically, observations of atmospheric tides have ever been done in Tromsø. The ESR radar further north is expected to reveal latitudinal differences in tidal signatures and also involved dynamical features influenced from above via particles and fields driven by geomagnetic disturbances, and from below via

This document is provided by JAXA.

wave and mean flow coupling in the polar middle atmosphere. Here emphasis is placed on the recent results and prospect of a study on atmospheric tides by the EISCAT radar.

2. Observations

In August 1998, ground clutter, which precludes the lower altitude sounding without going to low antenna elevation was fairly well eliminated by adopting the appropriate gup3 coding (Turunen, 1999), and the ESR radar detected echo returns from ranges down to 90 km in the field-aligned beam pointing direction. It must be added that Röttger *et al.* (1998) had also previously done a *D*-region sounding experiment with the ESR by using a complementary code. Collaborative data analysis of the first ESR upper-mesosphere-lower thermosphere dynamics test run on August 11–14 and the following CP (common program) run on August 17–19, 1998, have been reported by Van Eyken *et al.* (2000) and Aso *et al.* (1999). Then, the ionosphere *D* and *E* layer observation on October 5, 1998 (interrupted by the power failure) and 2-component (zonal/meridional) phase quadrature observation on March 17–18, 1999 were carried out by us in collaboration with the University of Tromsø. The March run was a 24 hr short observation by switching the antenna beam direction between south and west at elevation angle 45°. Hence, the neutral wind inference is limited to the lower altitudes in this run. In July 1999, a fairly long period of observation of tides and gravity waves was proposed by UK scientists and participated in by all the associated countries. Radar runs were carried out in CP2 mode by KST radar (99/07/01 1500–99/07/03 0000 and 99/07/03 1200–99/07/09 1500) and in gup3 mode by ESR (99/07/01 0900–99/07/09 1500) over 9 days in July 1999 with some interruptions. A series of these observations is planned to study problems of the arctic polar atmospheric tide, including climatology of the diurnal tidal component, penetration of non-migrating tide to polar latitudes, the erratic appearance and temporal variabilities of zonal wavenumber 1 semidiurnal component which was first detected by the meteor radar observation at the South Pole (Forbes *et al.*, 1995; Portnyagin *et al.*, 1998), other tidal variabilities associated with mode coupling and non-linear coupling with planetary and gravity waves (*e.g.,* Beard *et al.*, 1999), behavior and variabilities of the ter-diurnal component, the effect of hydromagnetic tides and ionosphere-magnetosphere disturbances from above and the effect of wave and mean flow interactions in the lower atmosphere (Aso *et al.*, 1987). EISCAT Tromsø data in summer 1998 show enhanced equatorward flow of ions associated with strong particle precipitation above 120 km. Moreover, the energy dissipation rate of the gravity wave in the high latitude region has been estimated from spectrum analysis of wind-velocity data down to 85 km based on our October observation (Hall and Aso, 1999). In the next section, a brief description on the tidal analysis of recent EISCAT observations and comparison with the ATM2 modeling (Aso *et al.*, 1987) is given.

3. Results and discussion

Figure 1 shows the results of analysis of the diurnal component of magnetically northward (almost meridional) wind for the radar runs mentioned above. Amplitudes (solid lines) are converted from the measured field-aligned to horizontal velocities by multiplying with $1/\sin 8^\circ = 7.2$ for ESR and $1/\sin 12^\circ = 4.8$ for Tromsø where 8° and 12°

This document is provided by JAXA.

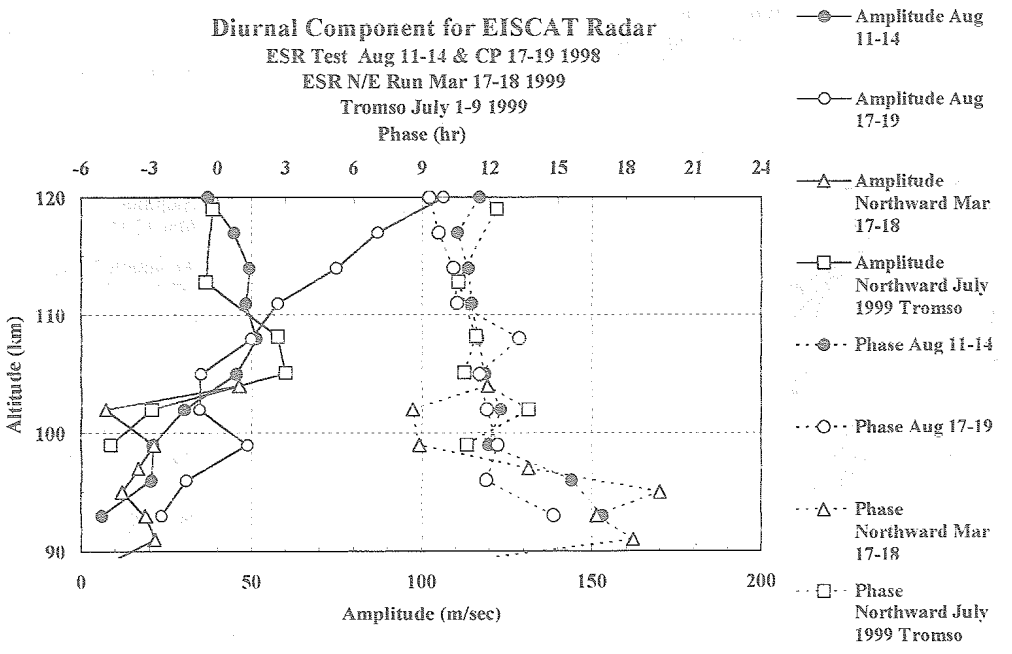


Fig. 1. Amplitude and phase of diurnal component observed by EISCAT radar.

are the magnetic field inclination, respectively. Phase (dashed lines) refers to the time of northward maximum in UT (local time −1 hour). Solid and open circles refer to ESR runs in August 1998, triangles to observations by ESR on March 17, 1999, and squares to the Tromsø long run in July. The March run was only for 24 hr, and data quantity at night was low. A study of possible ion-drag induced neutral instability has also been made based on this experiment (Hall and Aso, 2000). For summer-time observations latitudinal difference is not obvious.

Horizontal amplitude lies between 20–70 m/s and is larger than is obtained from the ATM2 model without thermospheric *in-situ* forcing (Aso *et al.*, 1987). Amplitude increase and constant phase above 100 km might suggest *in-situ* forcing in this altitude region and above (Miyahara and Miyoshi, 1997). Phase is consistent with the dominating evanescent (1, −2) mode at high latitudes with its phase staying around 1100 UT. Furthermore, superposition of some phase gradient or propagating characteristic is envisaged. In winter-time, penetration of a non-migrating diurnal component to higher latitude is indicated by ATM2 modeling (Ekanayake *et al.*, 1997; Aso, 2000). The electron density in winter is fairly low, and observation at this altitude around 100 km is not easy. A meteor radar, if it exists, can complement this high-powered incoherent scatter radar in its continuous operation. Williams *et al.* (1994) have given the Tromsø tidal result averaged over 11 days during August to October in 1987 to 1988. Amplitude and phase there are, by and large, consistent with the present results.

Altitude profiles of amplitude and phase for the semidiurnal component are shown in Fig. 2. Details are the same as in Fig. 1. Also, ATM2 modeling profiles of the northerly

This document is provided by JAXA.

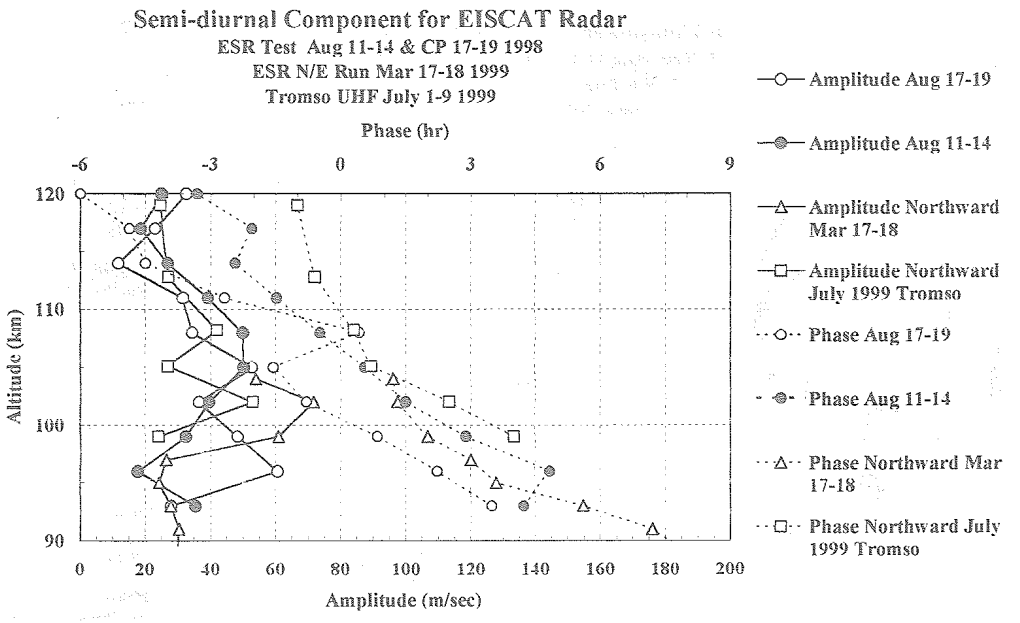


Fig. 2. Amplitude and phase of semi-diurnal component observed by EISCAT radar.

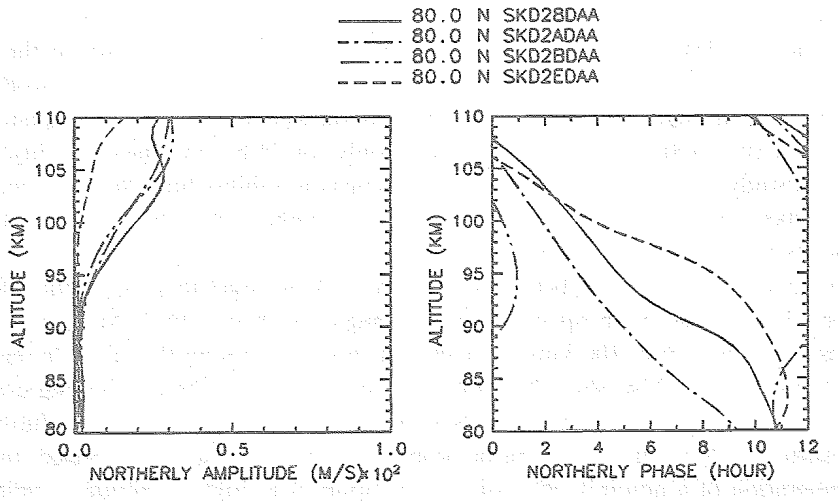


Fig. 3. Numerical profiles of the northerly amplitude (left) and phase (right) of the semi-diurnal tides at 80°N for August (solid), October (dashed-dot), November (dashed-double-dot) and equinox (dashed) wind conditions by the ATM2 modeling.

amplitude (left) and phase (right) of the semi-diurnal tide at 80°N are indicated in Fig. 3 for August (solid), October (dashed-dot), November (dashed-double-dot) and equinox (dashed) background wind conditions. The amplitude of the semidiurnal tide in Fig. 2 lies

This document is provided by JAXA.

around 40–70 m/s; the ATM2 modeling result is by and large smaller. This might be due to the possible mixture of non-migrating s=1 semidiurnal component also at summer polar mesosphere and to *in-situ* forcing or caused by an influence of $E \times B$ ion drift above 110 km. The slope of a phase is steep corresponding to both prevailing higher order modes at high latitudes and the non-migrating mode (not shown here), and vertical wavelength is about 30 km, consistent with the ATM2 model calculation at high latitudes. The observed phase is −2~0 UT 110 km, 0–3 at 100 km, 5–7 at 90 km and a deviation is seen with the ATM2 model. Apart from a small phase lag, the result by Williams *et al.* (1994) shows similar features to those in Fig. 2. The result of the GSWM (Global Scale Wave Model) model based on the formulation by Forbes (1982) is also similar to our ATM2 result. In doing observations and analyzing the semidiurnal component data, we must take into account the diminishing migrating component at the pole, dominant summer time zonal wavenumber 1 component, and other complications such as inertial oscillations and pseudo-tide observed in temperature variations (Walterscheid *et al.*, 1986). At present, numerical modeling by Miyahara (Personal communication, 2000) suggests that the wavenumber 1 semidiurnal component is evidently dominating the migrating component at higher latitudes and might presumably be due to the nonlinear interaction of semidiurnal tide and zonal wavenumber 1 stationary planetary waves in the lower atmosphere, as suggested by Forbes *et al.* (1995). Our ATM2 modeling assuming hypothetical forcing in the winter strato-mesosphere also supports the dominance of nonmigrating semidiurnal tide in the opposite hemisphere. In addition, the 3-hour phase difference of semidiurnal component is clearly found in the beam-switching experiment between south and west in March.

Strong $E \times B$ ion drift is imparted to the neutral motion daring the disturbed condition. Comparison of magnetogram and ion drift suggests that this hydromagnetic effect is less obvious below ~110 km. Though some works have dealt with this issue (*e.g.,* Johnson and Luhmann, 1985), this should, however, still be pursued from both theoretical and observational points of view by relying on the vectorially derived EISCAT radar velocity data.

4. Conclusion

Analyses of the EISCAT 9 days continuous observations in July 1999 are now on-going. In order to clarify the tidal climatology in the polar region, long-term and global observations with respect to longitude, latitude and conjugate chain are essential. To this end, we are planning to install a meteor radar and the airglow spectrometer in Longyearbyen, Svalbard to participate in the comprehensive analysis with radar and optical instruments such as the SOUSY radar which detects PMSE echo, Esrad in Kiruna, MF radars in Tromsø and Poker Flat, a meteor radar in Dixon Island, and also the MF/meteor radar in Antarctica.

References

Aso, T. (2000): Penetration of the non-migrating atmospheric diurnal tide into polar latitudes. Adv. Polar Upper Atmos. Res., **14**, 138–145.

This document is provided by JAXA.

Aso, T., Ito, S. and Kato, S. (1987): Background wind effect on the diurnal tide in the middle atmosphere. J. Geomagn. Geoelectr., **39**, 297–305.

Aso, T., Van Eyken, A. and Williams, P.J.S. (1999): EISCAT Svalbard radar-derived tidal features in the lower thermosphere as compared with the numerical modeling ATM2. Adv. Polar Upper Atmos. Res., **13**, 48–56.

Beard, A.G., Mitchell, N.J., Williams, P.J.S. and Kunitake, M. (1999): Non-linear interactions between tides and planetary waves resulting in the periodic tidal variability. J. Atmos. Terr. Phys., **61**, 363–76.

Ekanayake, E.M.P., Aso, T. and Miyahara, S. (1997): Background wind effect on propagation of nonmigrating diurnal tides in the middle atmosphere. J. Atmos. Solar-Terr. Phys., **59**, 401–429.

Forbes, J.M. (1982): Atmospheric tides, 1, model description and results for solar diurnal component. J. Geophys. Res., **87**, 5222–5240.

Forbes, J.M., Makarov, N.A. and Portnyagin, Yu.I. (1995): First results from the meteor radar at South Pole: A large 12-hour oscillation with zonal wavenumber one. Geophys. Res. Lett., **22**, 3247–3250.

Hall, C. and Aso, T. (1999): Mesospheric velocities and buoyancy subrange spectral slopes determined over Svalbard by ESR. Geophys. Res. Lett., **26**, 1685–1688.

Hall, C.M. and Aso, T. (2000): Identification of possible ion-drag induced neutral instability in the lower thermosphere over Svalbard. to appear in Earth Planets Space.

Johnson, R.M. and Luhmann, J.G. (1985): High-latitude mesopause neutral winds and geomagnetic activity: A cross-correlation analysis. J. Geophys. Res., **90**, 8501–8506.

Miyahara, S. and Miyoshi, Y. (1997): Migrating and non-migrating atmospheric tide simulated by a middle atmosphere general circulation model. Adv. Space Res., **20**(6), 1201–1207.

Portnyagin, Yu.I., Forbes, J.M., Makarov, N.A., Merzlyakov, E G. and Palo, S. (1998): The summertime 12-h wind oscillation with zonal wavenumber s=1 in the lower thermosphere over the South Pole. Ann. Geophys., **16**, 828–837.

Röttger, J., Markannenn, J. and Wannberg, U. G. (1988): The EISCAT Svalbard Radar—Its potential for middle atmosphere studies. Proc. 8th Workshop on Techn. Sci. Aspects of MST Radar, SCOSTEP, 314–317.

Turunen, T. (1999): New experiments for the EISCAT Svalbard radar. Abstract for 9th International EISCAT Workshop, Wernigerode, 48.

Van Eyken, A.P., Williams, P.J.S., Buchert, S.C. and Kunitake, M. (2000): First measurements of tidal modes in the lower thermosphere by the EISCAT Svalbard Radar. Geophys. Res. Lett., **27**, 931–934.

Walterscheid, R.L., Sivjee, G.G., Schubert, G. and Hamwey, R.M. (1986): Large-amplitude semidiurnal temperature variations in the polar mesopause: evidence of a pseudotide. Nature, **324**, 347–349.

Williams, P.J.S., Virdi, T.S., Jones, G.O.L. and Huuskonen, A. (1994): A comparison of three methods of measuring tidal oscillations in the lower thermosphere using EISCAT common programmes. J. Atmos. Terr. Phys., **56**, 1347–1359.

(Received July 28, 2000; Revised manuscript accepted September 22, 2000)

This document is provided by JAXA.

Mem. Natl Inst. Polar Res., Spec. Issue, 54, 49–63, 2001

Review

Recent contributions to long-term atmospheric studies at Koldewey-Station

H. Gernandt[1], R. Neuber[2] and P. von der Gathen[2]

Alfred Wegener Institute for Polar and Marine Research, Germany
[1]Columbusstrasse, D-27568 Bremerhaven,
[2]Telegrafenberg A43, D-14473 Potsdam

Abstract: The Koldewey-Station at Ny-Ålesund/Spitsbergen is the German Arctic research station, which has two main tasks. It serves as a platform for research campaigns in many different scientific fields carried out by German scientists in the Kongsfjord area. It also serves as an observatory for long term measurements, mainly for atmospheric research. Herewith the station contributes to several global observing networks like NDSC, BSRN and GAW and others. Validation of the resulting data sets is a regular topic in order to achieve a constant high quality level. This in turn makes data from the Koldewey-Station attractive to others for the validation of remote sensing instrumentation *e.g.* on satellites or airborne platforms.

A brief overview is given on current atmospheric measurement capabilities at the station. Secondly recent crucial results of long-term measurements and campaigns are summarised, and their contributions to regional and bi-polar investigations are briefly discussed. Observations are focussed to measurements of aerosols and trace gases and the climate effect of their long-term development. Regional investigations are for example related to the stratospheric ozone loss, which is studied with a "Match" technique. The comparison with Antarctic observations reveals the different pattern in long-term development. Validation efforts and campaigns are summarised, which contribute to satellite experiments as well as to large international campaigns.

1. Introduction to facilities and research programmes

The Koldewey-Station at Ny-Ålesund/Spitsbergen is the German Arctic research station. It serves as a platform for a wide range of atmospheric, marine biological and geophysical investigations. It also serves as an observatory for long-term measurements, particularly for climate and atmospheric research. Balloon-borne observations and ground-based remote sensing techniques are applied to study dynamical and chemical processes. Because of its location, appropriate scientific equipment, and data quality, the station contributes as a Primary Arctic Site to the global Network for Detection of Stratospheric Change (NDSC). Meteorological and radiation programmes are run similarly to those at Neumayer-Station in the Antarctic. Data are also fed to networks of WMO like the Baseline Surface Radiation Network (BSRN) or the Global Atmosphere Watch (GAW). An automatic seismological station completes long-term observations.

This document is provided by JAXA.

Validation of the resulting data sets is a regular topic in order to achieve a constant high quality level. This in turn makes data from the Koldewey-Station attractive to others for the validation of remote sensing instrumentation *e.g.* on satellites or airborne platforms. Data from the station have contributed *e.g.* to the validation of satellite experiments like the Global Ozone Monitoring Experiment GOME or have provided auxiliary data like for the Improved Limb Atmospheric Spectrometer (ILAS) on board of the Advanced Earth Observing Satellite (ADEOS). The Koldewey-Station also participated in several major international campaigns investigating the Arctic ozone layer. This includes participation in the ozone campaigns European Arctic Stratospheric Ozone Experiment (EASOE), the Second European Stratospheric Arctic and Mid latitude Experiment (SESAME), and the Third European Stratospheric Experiment on Ozone (THESEO). Recently, the NASA Validation Team for the third Stratospheric Aerosol and Gas Experiment (SAGE III) included the contributions of the Koldewey-Station for the SAGE III validation as one of two "anchor sites" globally. Also for the 1999/2000 campaign SOLVE/THESEO 2000, which was organised by NASA and the European Union (EU) the Koldewey-Station was integrated (SOLVE=SAGE III and Ozone Loss Validation Experiment).

Key wintering staff consists of a scientific station leader and an engineer, who are running the meteorological and stratospheric observatories. They are also responsible for on-site station management. Beside atmospheric studies an increasing number of projects were dedicated to marine biology and geophysics. About 80 scientists and technicians work here with 1125 man days each year. The Koldewey station is also part of the Ny-Ålesund Large Scale Facility (LSF) funded by EU. Access is offered to researchers from EU member states. A major complement to the station in 1999 was the construction of a balloon preparation and launching house which improves the handling of meteorological balloons by making them less wind-dependent. A general description of the Koldewey-Station and it's facilities can be found on the WWW (http://www.awi-potsdam.de/www-pot/koldewey/kolnav.html).

2. Atmospheric sciences

The scientific programmes running at the Koldewey-Station are mainly related to climate research, focusing on meteorology and tropospheric and stratospheric investigations. Instrumentation used comprises ground based remote sensing instruments like multi wavelength lidar, Fourier Transform Spectrometer (FTS), spectrometers sensitive in the UV and visible spectral range, multi spectral photometers using sun and star light, and microwave radiometers. In situ sondes to measure meteorological parameters, ozone, and aerosol properties are launched regularly by rubber or plastic balloons from the dedicated balloon launch facility.

Stratospheric ozone, aerosol, temperature, and tropospheric aerosols are observed by a multi wavelength lidar facility, comprising two lasers, three telescopes and three detection systems. The investigations cover Polar Stratospheric Clouds (PSCs), volcanic aerosols and the tropospheric aerosol burden. Above the aerosol layers, *i.e.* above 30 km, the backscatter signal is used to derive temperature profiles. The Differential Absorption ozone Lidar (DIAL) uses the output from an XeCl Excimer laser at 308 nm which is partly Raman shifted to 353 nm. A multi channel detector records all signals simultaneously. The lidar

This document is provided by JAXA.

system participated successfully in NDSC related validation activities for ozone and aerosol measurements (Godin *et al.*, 1999; Steinbrecht *et al.*,1999; Neuber *et al.*, 2001). Main results of the stratospheric aerosol investigations revealed the occurrence of liquid and solid PSC particles, which sometimes can co-exist in the same air volume (Biele *et al.*, 2000), while some types of PSC, which have been found above northern Scandinavia, are only rarely observed above Spitsbergen.

The FTS measurements at Koldewey-Station are performed using a commercial Bruker 120 HR Fourier transform spectrometer with maximum spectral resolution of 0.0025 cm^{-1} and spectral coverage between 600 and 33000 cm^{-1}. In order to overcome the lack of measurements during polar night, the system and the observational procedures were tuned to use the moon as light source. Due to the low IR intensity of moon light, spectra have to be recorded at low resolution (typically 0.02 cm^{-1}). Nevertheless, up to 20 trace gases from the tropo- and stratosphere are retrievable from the lunar observations (Notholt, 1994). The multi year observations allow to establish the annual course of the various trace gases, which allows *e.g.* to validate chemical transport models for the ozone depletion reactions and which also allows the comparison of their development in both polar regions (Notholt *et al.*, 1997).

Quasi-continuous observations of several atmospheric species are performed by measuring the absorption of visible and near ultraviolet sunlight scattered from the zenith sky or that from direct moonlight. Vertical column abundances of molecules such as ozone, NO_2, OClO, BrO and IO are derived by means of a Differential Optical Absorption (DOAS) algorithm and a radiative transfer model. These activities contribute to the calibration and validation studies of data from the GOME instrument on the ERS-II satellite and from future ENVISAT instruments (Wittrock *et al.*, 1999; Richter *et al.*, 1998).

Monitoring of the strength of solar radiation is performed in the wavelength ranges 280–320 nm (UV-B) and 320–400 nm (UV-A) by two non-scanning spectrophotometers installed on top of the observatory building. As complete spectra are taken each second, short time variations, which regularly are produced by the variable cloud cover, can be resolved (Groß *et al.*, 2001).

Since March 1991 regular measurements of the spectral optical depth of aerosols have been performed using sun photometers. Since January 1996 measurements during the polar night have been firstly possible using a star pointing photometer, which was developed by AWI. Significant features of the annual aerosol variations could be detected, like spectral characteristics of Arctic Haze aerosols and formation of ice crystals in the lower troposphere (Herber *et al.*, 2000a, b).

The Radiometer for Atmospheric Measurements (RAM) has been developed by the Institute of Environmental Physics of the University of Bremen as an instrument for ground-based millimeter-wave observations of the trace gases like ozone, ClO, and water vapour in the stratosphere and lower mesosphere. These data sets allowed a close investigation of the relation between atmospheric motions and the ozone content (*e.g.* Sinnhuber *et al.*, 1999).

A rather important tool for frequent ozone observations is the balloon-borne ozonesonde. At the Koldewey-Station, ozone soundings are performed at least once per week, and during winter times normally three times per week. An electrochemical ozone

This document is provided by JAXA.

sonde of type ECC 6A is used together with radiosondes RS 80. Major achievements resulting from these long term measurements are related to tropospheric as well as stratospheric results (Gernandt *et al.*, 1997; Rex *et al.*, 2000).

Sampling of airborne aerosols by filter automated instruments, as well as deposition sampling in flasks is used to observe the chemical composition of particulate matter transported to the polar regions. GC-MS coupled analyses of the probes are performed at the home institute (Kriews *et al.*, 2000a,b).

Table 1. Instrumentation for long-term atmospheric observations at Koldewey-Station (79°N, 12°E) and Neumayer station (70°S, 8°W) operated by AWI, University Bremen[1] and University Heidelberg[2].

Parameter	Koldewey-Station	Neumayer station
Meteorology		
ground p, T, u, wind,	weather mast	yes
profiles of p, T, u, wind	balloon-borne sondes	yes
Radiation		
IR–vis balance	BSRN station	yes
UV	UV-A, UV-B spectral rediometer	yes
Air chemistry		
trace gases	-	sampling
heavy metals	deposition and filter samplers	filter samplers
Aerosols		
aerosol optical depth	sun photometer	yes
	star photometer	-
extinction profiles	tropospheric lidar (extinction)	-
backscatter profiles	stratospheric multi λ lidar	-
backscatter & number		
density profiles	balloon borne sondes	-
surface aerosol	filter sampler	yes
Ozone		
concentration profiles	balloon-borne sondes (ECC)	yes
	ozone lidar	-
mixing ratio profiles	microwave radiometer RAM[1]	-
column density	FTIR-spectroscopy	-
	UV-vis. spectroscopy-DOAS[1]	DOAS[2]
surface ozone	(by NILU, NIPR)	KJ cell
		UV-absorption cell
Trace gases		
column densities	FTIR-spectroscopy	-
	UV-vis. spectroscopy-DOAS[1]	DOAS[2]
Surface processes		
transport and energy flux	two instrumented field sites	-

3. Climate research and bi-polar approach

Long-term observations provide a reliable data record for climate studies. The combination of different methods provides an appropriate tool to study physical and chemical processes as well. At Koldewey-Station both objectives have been part of the comprehensive

This document is provided by JAXA.

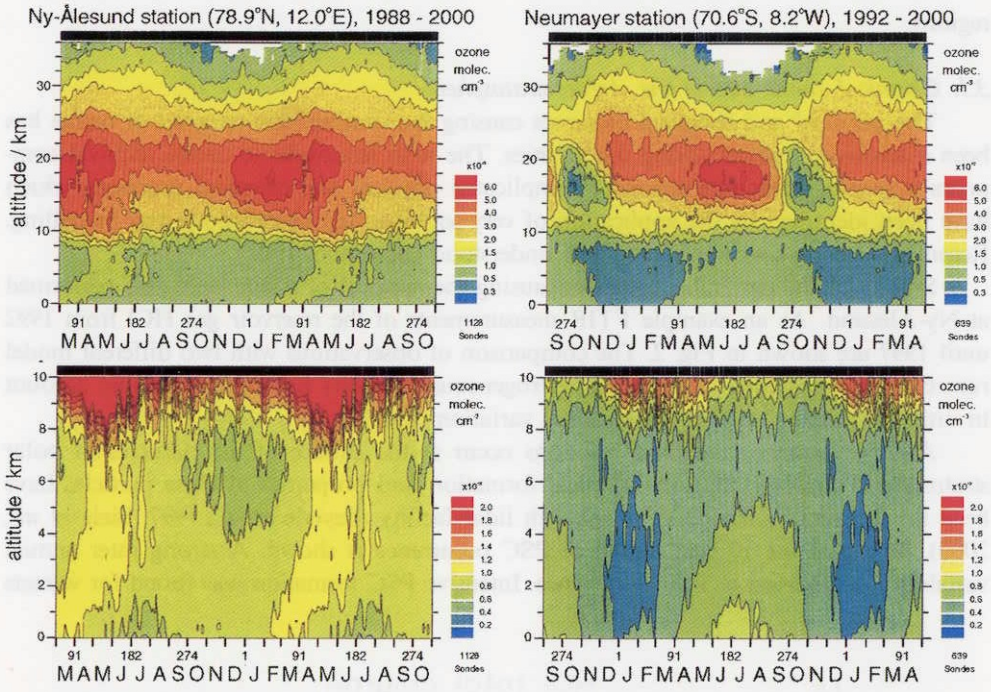


Fig. 1. Mean annual variation of ozone concentration recorded by balloon-borne sondes at Ny-Ålesund (79° N, 12° E) and Neumayer (71° S, 08° W); upper panels show the totally covered altitude range of observation; lower panels show tropospheric altitudes; ozone concentration is colour coded ($\times 10^{12}$ molecules/cm^3); time is scaled by days and months over 20 months period.

activities since its very beginning in 1988. In order to assess certain physical and chemical processes as well as long-term changes in the Arctic atmosphere, it is reasonable to include Antarctic observations for those studies (Gernandt *et al.*, 1998). Consequently certain observations and methods are additionally applied in a bi-polar approach, *i.e.* some instruments are also run at the German Neumayer station in the Antarctic. Atmospheric parameters recorded at Ny-Ålesund as well as the complement in the Antarctic are summarised in Table 1. These data records can be easily compared because identical instruments are used and attention is drawn to keep all procedures and evaluation algorithms at the same standard.

During the nineties for almost one decade a bi-polar record of vertical ozone distributions was obtained by regular balloon-borne observations in the Arctic and Antarctic. Altogether 1200 launches at Ny-Ålesund from 1989 until 2000 and about 640 launches at Neumayer from 1992 until 2000 have been performed. The updated mean annual variation of ozone concentration is shown in Fig. 1. The mean patterns show significant differences in the stratosphere as well as in the troposphere. The well known ozone depletion significantly and strongly appears in the Antarctic stratosphere. In the troposphere the mean annual variations also show an opposite seasonal course for both

This document is provided by JAXA.

regions.

3.1. Chemical ozone loss in the Arctic stratosphere

The physical and chemical processes causing the stratospheric removal of ozone has been extensively studied during the nineties. The term stratospheric ozone removal comprises a very complex interaction of complicated physical and chemical processes, which have been identified by the application of very sophisticated observations and modelling. Recently these processes are fairly well understood (Solomon, 1999).

Studies of the particular processes causing the removal of ozone were also performed at Ny-Ålesund. As an example FTIR measurements of the reservoir gas HCl from 1992 until 1997 are shown in Fig. 2. The comparison of observations with two different model runs clearly shows, that the so called heterogeneous chemistry has to be taken into account in order to model the observed seasonal variation of HCl.

As heterogeneous chemical reactions occur at the surface of the particles of polar stratospheric clouds (PSC), the physical formation and properties of these particles have been investigated by the multi wavelength lidar facility (Beyerle *et al.*, 1997; Biele *et al.*, 2000). In Fig. 3 the 10 year record of PSC occurrence is shown. A strong inter annual variability is observed in PSC occurrence. Intensive PSC formation was found for winters

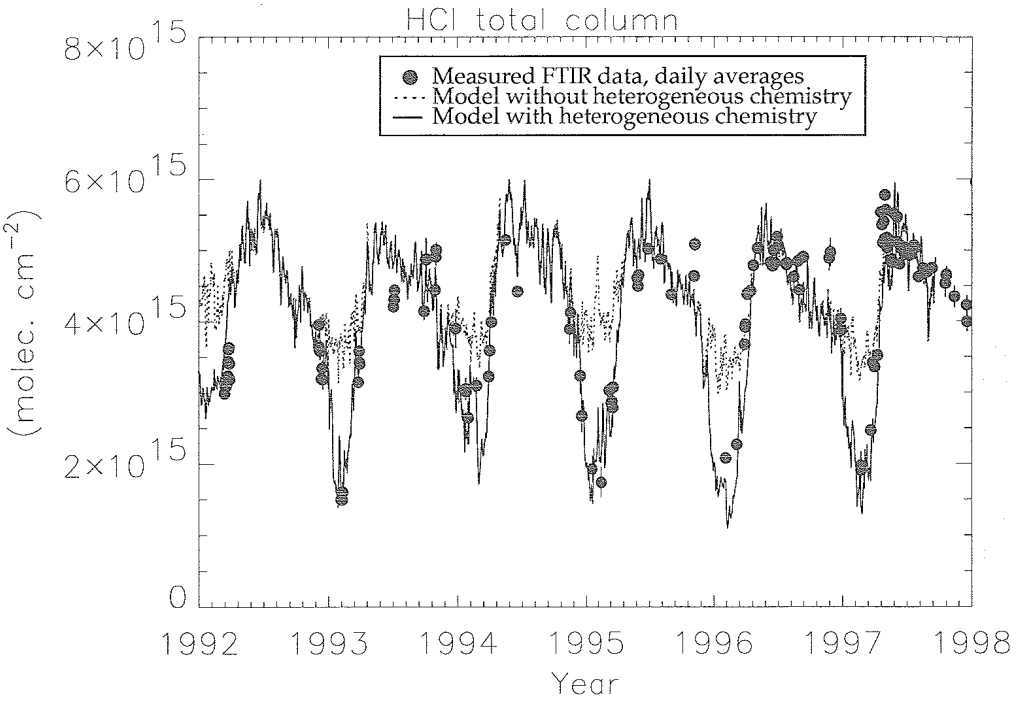


Fig. 2. Annual variation of HCl column densities recorded at Ny-Ålesund from 1992 until 1998 compared with runs of a three dimensional chemical transport model (SLIMCAT); broken line without heterogeneous chemistry; black line with heterogeneous chemistry (private communications by J. Notholt and M. Chipperfield, 1999).

This document is provided by JAXA.

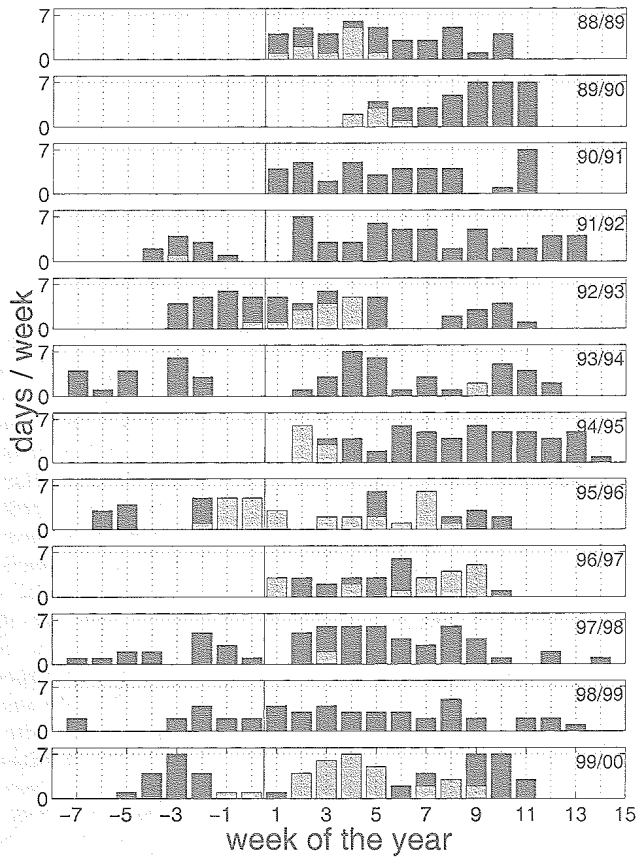


Fig. 3. Record of PSC observations by multi wavelength lidar at Ny-Ålesund for 12 winters from 1989 until 2000; dark columns indicate the total number of measurement days per week; light columns indicate observations of Polar Stratospheric Clouds (PSCs).

in 1992/93, and the winters following 1994/95 until 1996/97. As the existence of PSCs forces heterogeneous reactions at the particles' surfaces, strong removals of HCl into reactive chlorine were recorded for the respective winters (Fig. 2).

Although the preconditions to remove stratospheric ozone were observed in Ny-Ålesund, the ozone data do not show a corresponding decrease of ozone in the lower stratosphere (Fig. 1). The large dynamic variability in the Arctic stratosphere makes it more difficult to directly detect chemical ozone loss in comparison to Antarctic conditions. Thus, a much greater effort has been necessary to identify PSC related ozone losses in the Arctic stratosphere. Ozone loss rates can be directly measured by the so called Match technique (Von der Gathen *et al.,* 1995). A match is defined as a pair of ozonesonde measurements where sondes are launched from different stations and at different times but probe the same air parcel as it passes by. To identify the matches, calculated air parcel trajectories are used to track the motion of the air parcel between the measurements (Rex *et al.*, 1997).

Figure 4 shows an overview of the chemical ozone loss rates measured by Match

This document is provided by JAXA.

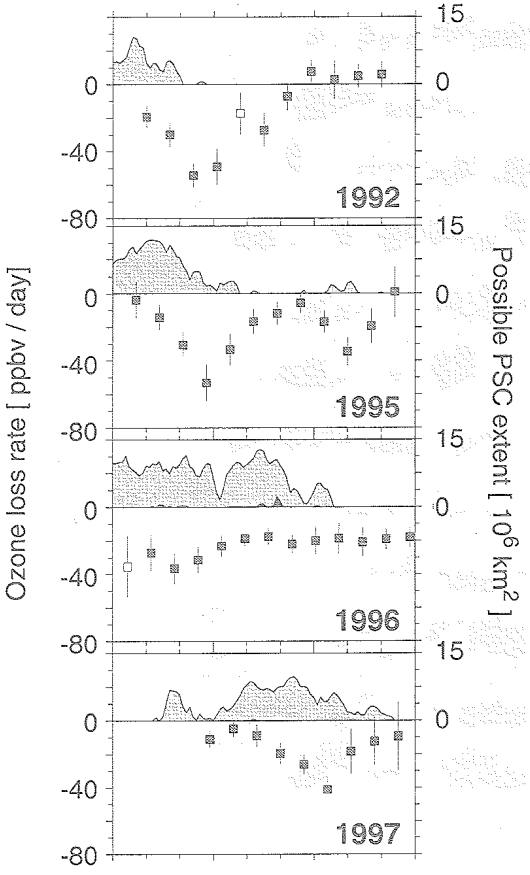


Fig. 4. Match results for 4 Arctic winters; points give the variation of ozone loss rates per day through the winter as retrieved for an isentropic level of 475 K potential temperature (approx. 20 km altitude); each point (square) is the result of a linear regression over a subset of matches which occurred during a period of 7 days before and after the date of the point; filled squares indicate that the subset comprises 10 or more matches; the shaded curves in the upper parts give the area of the northern hemisphere where temperatures have been below the temperature threshold to form Polar Stratospheric Cloud (PSC) particles (Rex et al., 2000).

technique during the covered winters. Chemical ozone loss was detected except for winters 1998 and 1999. The years with strongest loss rates coincide well with the above mentioned local observations of PSC occurrence (Fig. 3) and HCl reduction (Fig. 2) in Ny-Ålesund. In winter 1995 maximum local loss of approximately 60% occurred in about 20 km altitude. The accumulated loss in the ozone column reached 127 DU, *i.e.* approximately 30% (Rex *et al.*, 1997). That is significantly less than observed above Neumayer station, where it comes to 90% ozone loss every year.

Summarising the Match observations since 1992 and from 1995–1999 stratospheric ozone loss rates show a strong inter-annual variability in the Arctic stratosphere (Fig. 4). But the inter-annual variability is less pronounced in the Antarctic. Here the spring ozone loss is strong in every year. The interaction between dynamics and subsequent chemical processes is different in both polar regions mainly because of the different dynamical constraints in the Arctic and Antarctic (Rex *et al.*, 2000).

3.2. Tropospheric ozone in both polar regions

The mean annual courses of ozone concentration in the troposphere are strikingly different for the Arctic and Antarctic (Fig. 1). The records of both stations show how

This document is provided by JAXA.

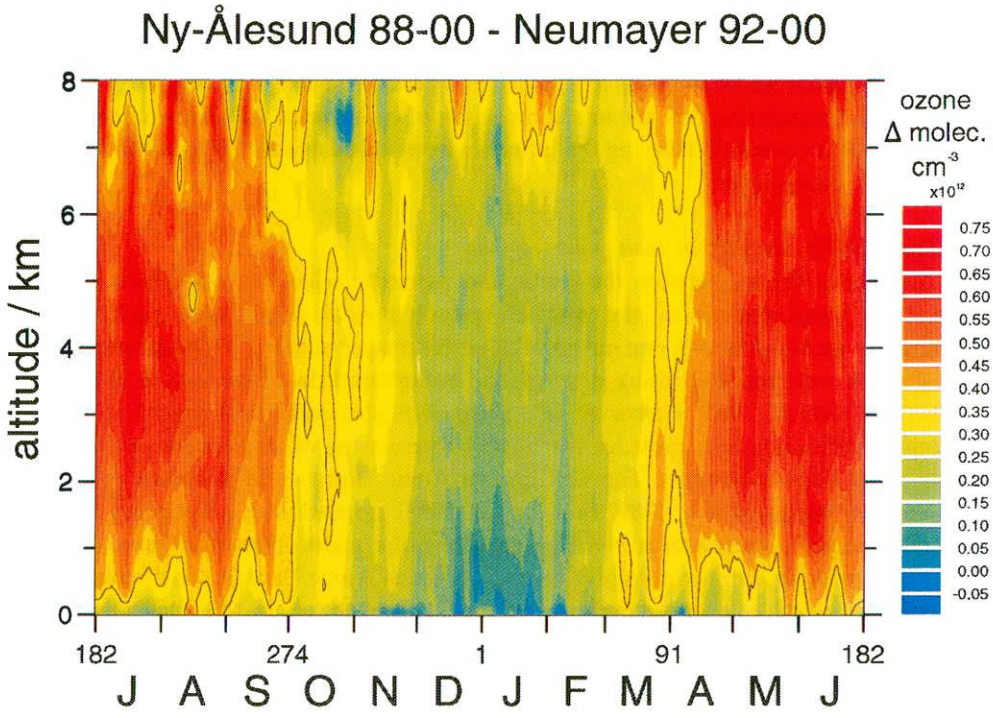


Fig. 5. Difference of mean tropospheric ozone concentration between Ny-Ålesund (1988–2000) and Neumayer (1992–2000) for corresponding seasons (e.g. Arctic spring–Antarctic spring) obtained by exactly left panel minus right panel of both bottom panels of Fig. 1; time scale indicates days and months for the Northern hemisphere.

differently tropospheric ozone appears in the remote and pristine Antarctic troposphere on the one hand and in the probably more perturbed Arctic troposphere on the other hand. The differences of ozone concentrations between the Arctic and Antarctic measurements for corresponding seasons clearly indicates the deviations in the Arctic with respect to the reference pattern of the pristine Antarctic region (Fig. 5).

In the Arctic tropospheric ozone concentrations are higher up to 0.60 molecules/cm^3 from April until September. Smallest differences are obtained for the winter season, *i.e.* for the polar night. But there is also an altitude dependence. In the boundary layer differences are smallest up to about 0.20 molecules/cm^3. That roughly corresponds to the mean difference of about 10 ppb less ozone in Antarctic regions as retrieved from surface ozone measurements (Oltmans *et al.*, 1998). However, as the ozone sonde observations show, these differences are three times greater, up to 0.60×10^{12} molecules/cm^3, above 1 km altitude in the whole troposphere.

The tropospheric ozone content is controlled by downward transport of ozone rich air from the stratosphere and additionally by *in-situ* photochemical production or reduction of ozone depending on certain levels of nitrogen oxid concentrations in the troposphere (Crutzen, 1970). The higher ozone content in the Arctic troposphere with respect to the

This document is provided by JAXA.

Antarctic reference might be mainly due to a net photochemical production of ozone because of sufficient high concentrations of nitrogen oxides. The transport of mid-latitude air masses towards Arctic latitudes is regarded as a possible source of those species (Solberg *et al.*, 1997). Considering this, the intercomparison of ozonesonde data shown here may be understood as an example showing the influence from northern mid-latitudes to the Arctic tropospheric ozone layer.

3.3. Tropospheric aerosols in both polar regions

Another difference between the Arctic and Antarctic refers to tropospheric aerosols. Since 1991 measurements of the spectral aerosol optical depth were performed by photometers in Ny-Ålesund and in parallel at Neumayer station. Tropospheric aerosol optical depth were retrieved using stratospheric background data from SAGE II measurements (McCormick, 1987; Herber *et al.*, 1993). The successful deployment of the star photometer technique now provides year round observations of atmospheric aerosols even during polar night conditions. The well known Arctic Haze, so far discussed as a spring phenomenon (Heintzenberg, 1989; Shaw *et al.*, 1993), appears with a frequency of about 40% in the lower troposphere at Ny-Ålesund. The polar night observation provided some new information on the climatology of the occurrence of Arctic Haze. It was discovered that the aerosol clouds even occur in February with a frequency of about 17% during late winter twilight conditions. But low optical depths comparable to those for summer conditions are also observed in spring (Herber *et al.*, 2000a).

The Arctic Haze causes a strong seasonal variability of aerosol burden in the Arctic troposphere. During late winter and spring high aerosol concentrations occur, but in summer and fall they are as low as for the clean air background levels recorded in the Antarctic during all seasons (Herber *et al.*, 1993; Gernandt *et al.*, 1997). The appearance of those aerosol clouds is also explained by long-range transport of air masses carrying species for the formation of aerosols from lower latitudes (Iverson, 1989). As the Arctic Haze frequently occurs even from February until the beginning of summer season, these elevated concentrations of aerosols may have some impact on radiative forcing in the Arctic troposphere (Wendling *et al.*, 1985). The impact of aerosols on Arctic climate recently became a major topic of atmospheric research. Preliminary model studies considering the existence of very simplified haze layers reveal a possible warming up to 2 K in the aerosol layer and a response in surface temperatures between ± 2 K depending on further conditions (Shaw *et al.*, 1993). More sophisticated model studies need appropriate input of optical properties, *e.g.* absorption and scattering coefficients, as well as temporal and spatial distributions of tropospheric aerosols. Such extended studies took place in spring 2000 in a co-operation between NIPR and AWI called the Arctic Study of Tropospheric Aerosol and Radiation (ASTAR). The joint ASTAR 2000 campaign comprises aircraft measurements above the Svalbard region and ground-based observations at Ny-Ålesund as well as SAGE II satellite data (Yamanouchi *et al.*, 2001).

3.4. Long-term ozone layer changes in both polar regions

Having performed regular ozone sonde launches at Ny-Ålesund and at Neumayer for a period of 8 years from 1992 until 1999, a simple estimate of long-term changes in the ozone layer has been made for both the Arctic and the Antarctic. Mean annual variations

This document is provided by JAXA.

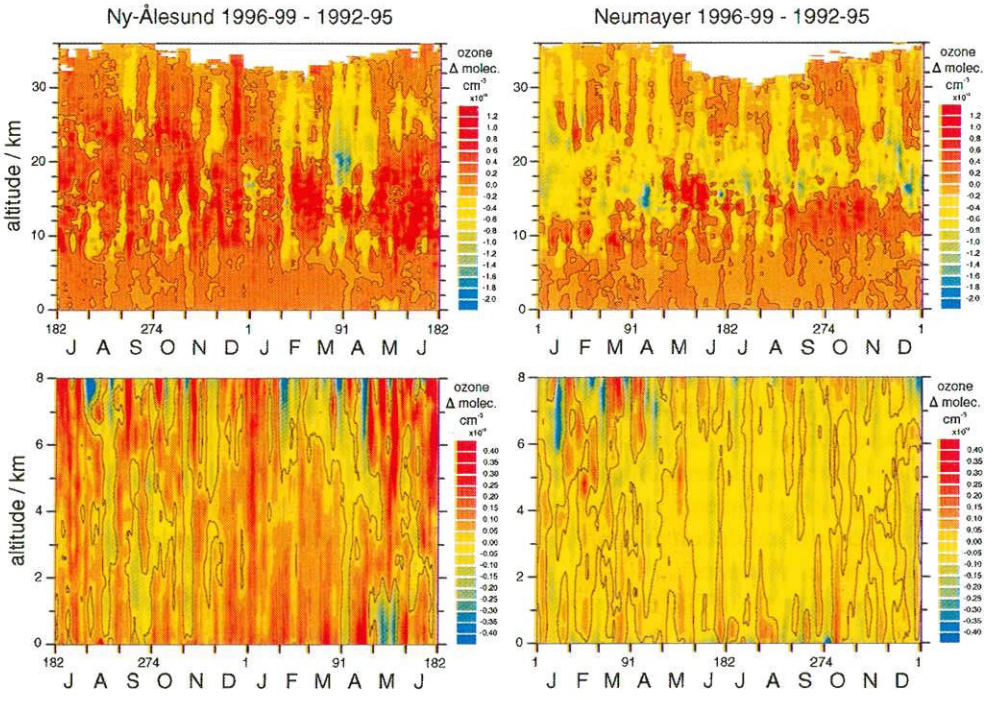


Fig. 6. Differences of mean ozone concentrations calculated for the period 1996/99 minus period 1992/95 for Ny-Ålesund and Neumayer; upper panels show the totally covered altitude range of observation; lower panels show tropospheric altitudes; differences of ozone concentration are colour coded ($\times 10^{12}$ molecules/cm^3); time is scaled by days and months related to the seasons of hemisphere.

were calculated for two subsections of 4 years time each, from 1992 to 1995 and for 1996 to 1999, respectively. The change of ozone is obtained by calculating the difference between these mean patterns as "mean 1996/99" minus "mean 1992/95". Results are shown in Fig. 6. The obtained changes of ozone concentration are colour coded.

The upper panels (Fig. 6) show the recorded changes in the stratosphere, which seem to be different for both polar regions during the considered period of time. In the Arctic stratosphere (upper left panel) a significant decreasing trend of stratospheric ozone can be identified between 16 km and 26 km altitude in March and April during spring season. Simultaneously even higher ozone concentration is recorded between 10 km and 20 km altitude in February as well as in May and June. Except for these limited changes the mean distribution of ozone did not significantly change during the considered period of years. A surprisingly different result was obtained for the Antarctic stratosphere. Since 1992 ozone concentration has decreased between roughly 14 km and 24 km altitude for all seasons of the year.

The lower panels (Fig. 6) show the same results in more detail for tropospheric altitudes. In the Antarctic (lower right panel) ozone concentrations have not significantly changed. But for the Arctic a slight increase of tropospheric ozone concentrations can be

This document is provided by JAXA.

stated from the ground up to about 5 km from December until March during the winter season.

This bi-polar assessment is very preliminary because of the temporally limited data records. But it shows a surprising result on a possible different long-term development of the ozone layer in both polar regions. Because records are getting continuously longer in time, those analyses might be more reliable and expressive in the future. Recently it can only be stated that balloon-borne observations show those changes from 1992 until 1999. To explain possible physical or chemical causes these observations need further confirmation.

4. Validation experiments

In order to fulfil the quality assurance requirements within global and regional networks, the data sets from individual stations have to be validated. Within the Network for the Detection of Stratospheric Change (NDSC) detailed rules have been established for the various instruments describing in detail the validation procedures. The FTIR, microwave, and lidar instruments and the balloon borne ozone sondes have been subject to individual, on site validation efforts, in addition to efforts aiming at the homogenisation of the data retrieval processes.

The results of the FTIR on site instrument intercomparison, which was the first in a series of on site comparisons conducted in recent years, have provided the basis for a study of the most significant sources of uncertainty in ground-based FTIR measurements (Paton-Walsh *et al.*, 1997). Overall uncertainties for the column densities of the most important species were found to vary from 6% for N_2O over less than 10% for HCl and HF to 14% for HNO_3.

An international microwave intercomparison campaign was conducted at Ny-Ålesund in February to March of 1997 with four participating instruments from CRL (Tokyo), FZK (Karlsruhe), SUNY (New York), and IUP (Bremen). It was mainly focussed to measure chlorine monoxide in the stratosphere by ground-based microwave instruments and to compare the retrieval algorithms. Those measurements from the ground remain a great challenge and further improvement of instrumentation and applied retrieval algorithms is necessary (Neuber, 1999).

The Ny-Ålesund Aerosol and Ozone Measurement Intercomparison campaign in winter 1998 (NAOMI-98) was a major effort to validate all instruments making ozone profile measurements in Ny-Ålesund (Neuber *et al.*, 2001). The travelling NDSC standard instrument, the mobile ozone lidar system from the NASA Goddard Space Flight Center, was installed at the Koldewey-Station. In addition to AWI's ozone and aerosol multi wavelength lidar, the balloon borne ECC sondes and the microwave radiometer RAM, were included in the comparison. The results reveal a strong altitude dependence of the quality of the retrieved ozone profiles. While for the main body of the ozone layer the difference of the methods is less than 5% for the average profiles, altitude range, resolution and error decrease differently for higher altitudes. While the microwave system shows the largest altitude range and best temporal coverage and resolution, the singular balloon borne measurements have the finest altitude resolution. The strength of the lidar instruments, which had an excellent agreement of less than 5% between 15 and 32 km altitude, relies on their capability to reveal short term variability in the ozone layer. Their data revealed *e.g.*

This document is provided by JAXA.

a stable wave pattern in the 17–22 km altitude range during the course of the campaign from mid-January to mid-February 1998 (Steinbrecht *et al.*, 1999).

The proven high quality of the data sets collected at Koldewey-Station in Ny-Ålesund qualify the station for satellite validation efforts. The GOME instrument onboard the ERSII satellite was validated with Spitsbergen trace gas columns, like bromine monoxide (Richter *et al.*, 1998), as will its follow-up instruments, the SCIAMACHY and MIPAS experiments onboard ENVISAT. The SAGE III instrument, scheduled for launch in 2001, will be mainly validated globally by two so called "anchor sites", namely Lauder, New Zealand and Ny-Ålesund, Spitsbergen. In addition to the validation efforts, ozone and aerosol data from Koldewey-Station were used as correlative data sets for the ILAS instrument onboard ADEOS and shall be used for the ADEOS II mission as well.

5. Conclusion

It could be shown that the atmospheric observations contribute to climate and process studies for the Arctic region. An important complement are the observations in the Antarctic to understand changes in a climatological scale as well as to identify the importance of different physical and chemical processes.

On the other hand local observations have to be connected with satellite measurements in order to study atmospheric phenomena in their regional and global scale. The ground-truth validations, which have been performed already, form the foundation for such upcoming investigations.

The analysis of the bi-polar ozone record presented in this paper revealed not only the differences in the stratospheric ozone loss processes, but gives evidence of chemical processes in the polar tropospheres, which become more and more important.

The long-term activities at the Koldewey-Station in Ny-Ålesund will be continued in the future in order to help answering the questions raised when considering the changes in both polar regions.

Acknowledgments

We gratefully acknowledge the contributions by our colleagues at AWI, Univ. Bremen and elsewhere, in particular by Klaus Dethloff, Dörte Handorf, Andreas Herber, Michael Eisinger, Ulf Klein, Jens Langer, Justus Notholt, Markus Rex, Andreas Richter, Annette Rinke, Rolf Weller, Folkard Wittrock, and others. We also appreciate the kind hospitality provided by the Norwegian Polar Institute and by the Kings Bay AS in Ny-Ålesund.

References

Beyerle, G., Luo, B.P., Neuber, R., Peter, Th. and McDermid, I.St. (1997): Temperature dependence of ternary solution particle volumes as observed by lidar in the Arctic stratosphere during winter 1992/93. J. Geophys. Res., **102**, 3603–3609.

Biele, J., Tsias, A., Carslaw, K.S., Peter, Th. and Neuber, R. (2000): Coexistence of solid and liquid particles in Arctic stratospheric clouds studied by Lidar in Winters 94/95 to 96/97. submitted to J. Geophys. Res.

Crutzen, P.J. (1970): The influence of nitrogen oxides on atmospheric ozone content. Quart. J. R.

This document is provided by JAXA.

Meteorol. Soc., **96**, 320–325.
Gernandt, H., Von der Gathen, P. and Herber, A. (1997): Ozone change in the polar atmosphere. Ground Level and Satellite Ozone Observations: Changes in the Mediterranean Region, NATO, 73–100 (NATO ASI Series I, **53**).
Gernandt, H., Herber, A., Von der Gathen, P. and Kaneto, S. (1998): Ozone variation in the southern polar stratosphere. Mem. Natl Inst. Polar Res., Spec. Issue, **52**, 68–88.
Godin, S. and 13 colleagues (1999): Ozone differential absorption lidar algorithm intercomparison. Appl. Opt., **38**, 6225–6236.
Groß, C., Tüg, H. and Schrems, O. (2001): Three years spectral resolved UV-measurements at Koldewey-Station (1997–1999). Mem. Natl Inst. Polar Res., Spec. Issue, **54**, 113–123.
Heintzenberg, J. (1989): Arctic Haze: Air pollution in the polar regions. Ambio, **18**, 50–55.
Herber, L., Thomason, W., Radionov, V.F. and Leiterer, U. (1993): Comparison of Trends in the tropospheric and stratospheric optical depths in the Antarctic. J. Geophys. Res. **98**, 18441–18447.
Herber, A., Leiterer, U., Nagel, D., Thomason, L.W., Albrecht, T., Kaptur, J., Lamakin, M., Schulz, K. H., Notholt, J. and Gernandt, H. (2000a): Sun and Star photometer Measurements in the Arctic. submitted to J. Geophys. Res.
Herber, A. and 12 colleagues (2000b): Aerosol measurements at Ny-Ålesund/Spitsbergen and its possible climate impact. Second International Symposium on Environmental Research in the Arctic and Fifth Ny-Ålesund Scientific Seminary, 23–25 February 2000, Program and Abstract. Tokyo, Natl Inst. Polar Res., 28.
Iverson, T. (1989): Numerical modelling of the long range atmospheric transport of sulphurdioxide and particulate sulfate to the Arctic. Atmos. Env., **23**, 2571–2595.
Kriews M., Stölting, I. and Schrems, O. (2000a): Chemical composition of total deposition samples from Spitsbergen. Second International Symposium on Environmental Research in the Arctic and Fifth Ny-Ålesund Scientific Seminar, 23–25 February 2000, Program and Abstract. Tokyo, Natl Inst. Polar Res., 30.
Kriews M., Stölting, I. and Schrems, O. (2000b): Event-induced aerosol sampling at Spitsbergen. Second International Symposium on Environmental Research in the Arctic and Fifth Ny-Ålesund Scientific Seminar, 23–25 February 2000, Program and Abstract. Tokyo, Natl Inst. Polar Res., 207.
McCormick, M.P (1987): SAGE II: An overview. Adv. Space Rev., **7**, 319–326.
Neuber, R. ed. (1999): ESMOS/Arctic II Final Report. available via www.awi-potsdam.de
Neuber, R., Beyerle, G., Von der Gathen, P., Wahl, P., Dahl, A., Gross, M., McGee, Th., Klein, U. and Steinbrecht, W. (2001): An intercomparison campaign of ozone and temperature measurements in the Arctic (NAOMI-98, Ny-Ålesund/Spitsbergen). Mem. Natl Inst. Polar Res., Spec. Issue, **54**, 65–70.
Notholt, J. (1994): The moon as light source for FTIR measurements of stratospheric trace gases during the polar night: Application for HNO_3 in the Arctic. J. Geophys. Res., **99**, 3607–3614.
Notholt, J., Toon, G.C., Lehmann, R., Sen, B. and Blavier, J.-F. (1997): Comparison of Arctic and Antarctic trace gas column abundances from ground-based FTIR spectrometry. J. Geophys. Res., **102**, 12863–12869.
Oltmans, S.J. and 17 colleagues (1998): Trends of ozone in the troposphere. Geophys. Res. Lett., **25**, 139–142.
Paton-Walsh, C., Bell, W., Gardiner, T., Swann, N., Woods, P., Notholt, J., Schütt, H., Galle, B., Arlander, W. and Mellqvist, J. (1997): An uncertainty budget for ground-based Fourier transform infrared column measurements of HCl, HF, N_2O, and HNO_3 deduced from results of side-by-side instrument intercomparisons. J. Geophys. Res., **102**, 8867–8873.
Rex, M. and 23 colleagues (1997): Prolonged stratospheric ozone loss in the 1995/96 Arctic winter. Nature, **389**, 835–838.
Rex, M., Dethloff, K., Handorf, D., Herber, A., Lehmann, R., Neuber, R., Notholt, J., Rinke, A., Von der Gathen, P., Weisheimer; A. and Gernandt, H. (2000): Arctic and Antarctic ozone layer observations. to be published in Polar Res.
Richter, A., Wittrock, F., Eisinger, M. and Burrows, J.P. (1998): GOME observations of tropospheric

This document is provided by JAXA.

BrO in Northern Hemispheric spring and summer 1997. Geophys. Res. Lett., **25**, 2683–2686.
Shaw, G.E., Stamnes, K. and Hu, Y.X. (1993): Arctic haze: Perturbation to the radiation field. Meteorol. Atmos. Phys., **51**, 227–235.
Sinnhuber, B.-M. *et al.* (1999): Interpretation of mid-stratospheric Arctic ozone measurements using a photochemical box-model. J. Atmos. Chem., **34**, 281–290.
Solberg, S., Stordal, F. and Hov, O. (1997): Tropospheric ozone at high Latitudes in clean and polluted airmasses, a climatological study. J. Atmos. Chem., **28**, 111–123.
Solomon, S. (1999): Stratospheric ozone depletion: A review of concepts and history. Rev. Geophys., **37**, 275–316
Steinbrecht, W., Gross, M.R., McGee, T.J., Neuber, R., Von der Gathen, P., Wahl, P., Klein, U. and Langer, J. (1999): Results of the 1998 Ny-Ålesund ozone measurements intercomparison NAOMI. J. Geophys. Res., **104**, 30515–30523.
Von der Gathen and 14 colleagues (1995): Observational evidence for chemical ozone depletion over the Arctic in winter 1991–92. Nature, **375**, 131–134.
Wendling, P., Wendling, R., Renger, W., Covert, D.S., Heintzenberg, J. and Moerl, P. (1985): Calculated radiative effects of Arctic haze during a pollution episode in spring 1983 based on ground-based and airborne measurements. Atmos. Env., **19**, 2181–2193.
Wittrock, F., Altmeyer, H., Bruns, M., Laue, M., Munderloh, K., Richter, A., Schlieter, S. and Burrows, J. P. (1999): Observations of O_3, NO_2, BrO and OClO at different latitudes. Fifth Europ. Workshop on Stratosph. Ozone, St. Jean de Luz, France.
Yamanouchi, T. and Herber, A. (2001): Arctic study of tropospheric aerosol and radiation, ASTAR 2000-field plan. Mem. Natl Inst. Polar Res., Spec. Issue, **54**, 101–106.

(Received April 28, 2000; Revised manuscript accepted June 8, 2000)

This document is provided by JAXA.

This document is provided by JAXA.

Mem. Natl Inst. Polar Res., Spec. Issue, 54, 65–70, 2001

Scientific note

An intercomparison campaign of ozone and temperature measurements in the Arctic (NAOMI-98, Ny-Ålesund/Spitsbergen)

R. Neuber[1], G. Beyerle[1,6], P. von der Gathen[1], P. Wahl[1], A. Dahl[2], M. Gross[3], Th. McGee[3], U. Klein[4] and W. Steinbrecht[5]

[1]*Alfred Wegener Institute for Polar and Marine Research, Telegrafenberg A43, D-14473 Potsdam, Germany*
[2]*University of Trondheim, N-7000 Trondheim, Norway*
[3]*Goddard Space Flight Center, Code 910, Greenbelt, Maryland 20771, U.S.A.*
[4]*University of Bremen, Institute of Environmental Physics, Kufsteiner Str. NW1, D-28359 Bremen, Germany*
[5]*Deutscher Wetterdienst, Meteorological Observatory Hohenpeißenberg, D-82383 Hohenpeißenberg, Germany*
[6]*now at GeoForschungsZentrum Potsdam, Telegrafenberg, D-14473 Potsdam, Germany*

Abstract: The Ny-Ålesund Ozone Measurements Intercomparison (NAOMI) campaign for measurements of stratospheric ozone and temperature was conducted at the Primary Station of the NDSC in Ny-Ålesund/Spitsbergen during January–February 1998. Local instrumentation (ozone and aerosol lidar, microwave radiometer RAM, ECC-type ozone sondes) was complemented with the NDSC mobile ozone lidar from NASA/GSFC. The aim was the validation of stratospheric ozone and temperature profiles according to NDSC guidelines. The blind intercomparison of ozone profiles revealed good agreement ($<\pm 5\%$) up to 31 km. At higher altitudes the different altitude ranges and resolutions of the instruments, as well as effects of retrieval algorithms have to be considered. Temperature data of the two lidar systems agreed well and revealed the stratospheric warming, which occurred in early February 1998. NCEP temperature analyses for Spitsbergen agreed very well with lidar data before, but not during this warming event.

1. Experimental procedures

At Ny-Ålesund/Spitsbergen (79°N, 12°E), a primary site within the Network for the Detection of Stratospheric Change (NDSC), observations of the stratospheric ozone profile are performed with lidar, microwave radiometer and balloon borne sondes, with temperature data also recorded by lidar. For the intercomparison the NDSC travelling ozone lidar maintained by NASA's Goddard Space Flight Center (GSFC) was deployed to Ny-Ålesund in winter 1997/98. The intensive measurement period for the campaign started on 19 January and ended on 10 February 1998. Weather conditions have been extremely favourable, with cloud cover never preventing measurements for more than 24 h. Accordingly lidar measurements could be taken on every day. As the ozone microwave radiometer is practically insensitive to clouds, this instrument has the best overall measurement statistics.

This document is provided by JAXA.

Due to optical interference problems, the two ozone lidars had to operate alternately on interleaving times. Due to high background levels of the approaching daylight, measurements were prevented around local noon.

Lidar raw data were integrated over 2–6 hours and the retrieved ozone profiles transferred via internet to the referee, as were the quasi automatically retrieved microwave ozone profiles (12 min data on every hour). The intercomparison of the ozone profiles was conducted blindly. Data from ozone sondes, however, which were performed almost daily during the intensive measurement period, were publicly available and accessible to the participants.

Although usually in January and February Polar Stratospheric Clouds (PSCs) occur above Spitsbergen, only one minor PSC event was observed during the intercomparison period. The lack of stratospheric aerosols prevented the originally planned intercomparison of aerosol profiles. However, the absence of large aerosol signals improves the ozone lidar data and allows to derive good atmospheric temperature data by lidar from elastically scattered laser lines *e.g.* at 353 nm in addition to the temperature data collected by Raman channels.

2. Instrumentation for the intercomparisons

2.1. The Ny-Ålesund Multiwavelength Lidar facility

The combined ozone- and aerosol-lidar instrument at Ny-Ålesund utilises a XeCl-Excimer laser for UV-wavelengths, running at 90 Hz and a Nd: YAG-laser for near IR- and visible wavelengths running at 30 Hz pulse repetition. Aerosol data is obtained at the wavelengths 353 nm, and 532 nm (including depolarisation at 532 nm, see Beyerle *et al.*, 1994), the 353 nm and the 532 nm data is used for temperature retrievals, and the ozone measurements are performed using the DIAL principle and employing the signals at 308 and 353 nm. All signals are collected by a telescope of 60 cm diameter and are guided into a detector system, which records up to eight wavelength channels simultaneously. A mechanical chopper suppresses high intensity signals from the troposphere, so that the photomultiplier tubes (Thorn EMI types) can be used in photon counting mode. Their dynamic range allows to cover the altitude range from 14 to 65 km. Data acquisition is done with eight multi channel scalers from EG&G ORTEC ("Turbo-MCS") which collect a preset number of laser pulses corresponding to an original time resolution of *ca.* 1 min. Data is then collected from each MCS individually by a PC and stored on hard disc within the local computer network of the Koldewey-Station, which in turn is connected to the internet.

2.2. The Ny-Ålesund Microwave Radiometer

The Radiometer for Atmospheric Measurements (RAM), developed by the Institute of Environmental Physics of the University of Bremen operates in the frequency range from 100–300 GHz. As part of the German ozone research program (OFP) and the European Stratospheric Monitoring Stations projects (ESMOS/Arctic I & II) this instrument is operated continuously according to the requirements for a primary NDSC station. The RAM is a heterodyne receiver consisting of two front-ends for the observation of ozone at 142 GHz and chlorine monoxide (ClO) at 204 GHz, which are operated in a time-sharing

This document is provided by JAXA.

mode. Both front-ends consist of a rotatable mirror for calibration, a quasi-optics and a mixer-HEMT preamplifier stage which is cryogenically cooled to about 12 K. The back-end consists of a 2048 channel acousto-optical spectrometer (AOS) with a centre frequency of 2.1 GHz, a bandwidth of 945 MHz and a frequency resolution of ~1.3 MHz. This allows to retrieve trace gas volume mixing ratio profiles in the altitude range from 15 to 60 km from the shape of the observed signal. The whole system is computer controlled and can operate automatically (Langer *et al.*, 1996).

2.3. The Ny-Ålesund ozone sonde facility

At Ny-Ålesund ECC ozone sondes of type 6A from Science Pump Corp. are launched with RS80 radiosondes from VAISALA. The sondes are flown with Totex rubber balloons, which are pre-treated during periods of low stratospheric temperatures resulting in burst altitudes usually above 30 km. Altitude resolution of the data transmittance is approximately 50 m depending on the balloon ascent rate. The altitude resolution, however, is reduced to about 300 m due to the response time of the sensor, which is filled with 3 cm^3 of 1% KI solution. The ECC data is treated according to the manufacturer's instructions, which follow those given by Komhyr (1986), including the tabled pump correction factors given there (that is *e.g.* 1.054 at 10 hPa). Due to polar night conditions for about half of the year total ozone correction by a Dobson spectrometer is never performed.

2.4. The NASA/GSFC lidar

The Goddard Space Flight Center mobile Stratospheric Ozone Lidar in Trailer Experiment (STROZ-LITE) was developed under the auspices of the Network for the Detection of Stratospheric Change as its travelling standard lidar instrument. It is a DIAL set up capable of making measurements of the vertical profiles of temperature, ozone and aerosols simultaneously (McGee *et al.*, 1995). The lidar instrument uses excimer lasers with 200 Hz pulse repetition rate to generate the two wavelengths (308 and 351 nm) which are transmitted into the atmosphere. A 30″ Dall-Kirkham telescope collects the backscattered radiation, and a series of beamsplitters spectrally separate the light into four wavelengths; the elastically backscattered signal from each of the transmitted laser beams, and the N_2 Raman shifted wavelengths for each laser wavelength.

3. Results

3.1. Ozone measurements

The ozone measurements have been extensively analysed by Steinbrecht *et al.* (1999). Altitude resolutions vary from 0.3 to more than 14 km between balloon borne sondes, lidars and the microwave RAM, with lidar resolutions from 1 to 6 km, depending on altitude. Temporal resolution is less than 1 hour for the RAM, several hours for the lidars and days for the balloon launches. For this intercomparison, only temporally averaged profiles are considered. The results are summarised in Fig. 1a and 1b. They display the relative difference with respect to the average of the travelling standard, the GSFC lidar, for the period 26 January to 9 February 1998. Figure 1a reveals, that the lidars and ECC sondes agree to better than 5% up to the balloon burst height. The lidars agree to better than 5% in this altitude range, and within 12% up to 42 km, with rapidly increasing error bars with

This document is provided by JAXA.

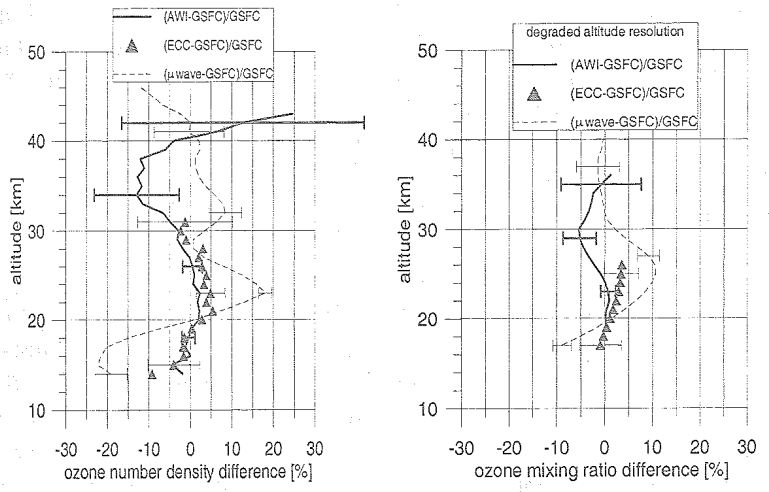


Fig. 1. Relative differences of the average ozone profiles: 1a (left) number densities with full altitude resolution, 1b (right) mixing ratios with reduced altitude resolution (see text), 2σ error bars. Figure taken from Steinbrecht et al. (1999).

increasing height. The comparison with the microwave radiometer looks worse, which is an effect of its much coarser altitude resolution. The agreement improves, when the lidar and sonde altitude resolution is reduced according to the retrieval kernels of the microwave analysis, as seen in Fig. 1b (for details of the procedure see Steinbrecht *et al.*, 1999). Now differences are less than 5% below 22 km and above 28 km altitude. The difference peaks with 10% at 25 km. At this altitude, the average ozone mixing ratio profile (not shown here) features an unusual plateau. As the apriori profile used for the microwave retrieval increases steadily here and is about 40% higher, it could be a reason for this bias, which was not found in earlier comparisons between ECC sondes and RAM.

3.2. Temperature measurements

Temperature data has been derived from the Rayleigh backscattered signals of the AWI and GSFC lidars, as well as from the N_2 Raman channel of the GSFC system for lower altitudes. In Fig. 2 the temporal development of the stratospheric temperature above Ny-Ålesund for the winter 1997/98 is displayed, using the AWI lidar data set. The figure reveals the strong warming pulse, which appeared above Spitsbergen in February, just towards the end of the NAOMI measurement phase. Both lidar systems covered this period very well and detected the warming. In Fig. 3 we compare temperature profiles retrieved by both instruments with the NCEP analysis temperatures before and during this warming event. Figure 3a displays an example of the derived temperature profiles together with the local radio sonde profile and the analysis of NCEP for Ny-Ålesund at 30 January. For the GSFC data set also the error is displayed as two additional curves at $T \pm \Delta T$. At *ca.* 28 km the shift between the low altitude Raman data and the high altitude Rayleigh data of the GSFC system is visible as a reduction in the error. The altitude range covered by the balloon borne radiosonde, the low and high altitude GSFC-Lidar channels and of the

This document is provided by JAXA.

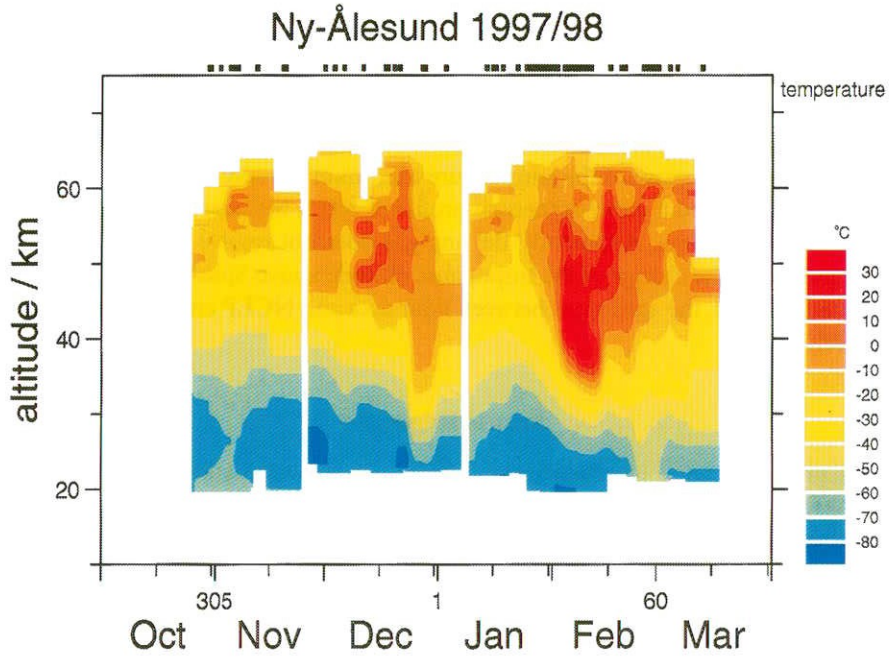


Fig. 2. Temperature development above Ny-Ålesund during winter 1997/98 as measured by the AWI backscatter lidar. The bars above the figure indicate the measurement periods. The x-axis denotes the number of the days in 1997 and 1998, 1 corresponds to 1.1.1998.

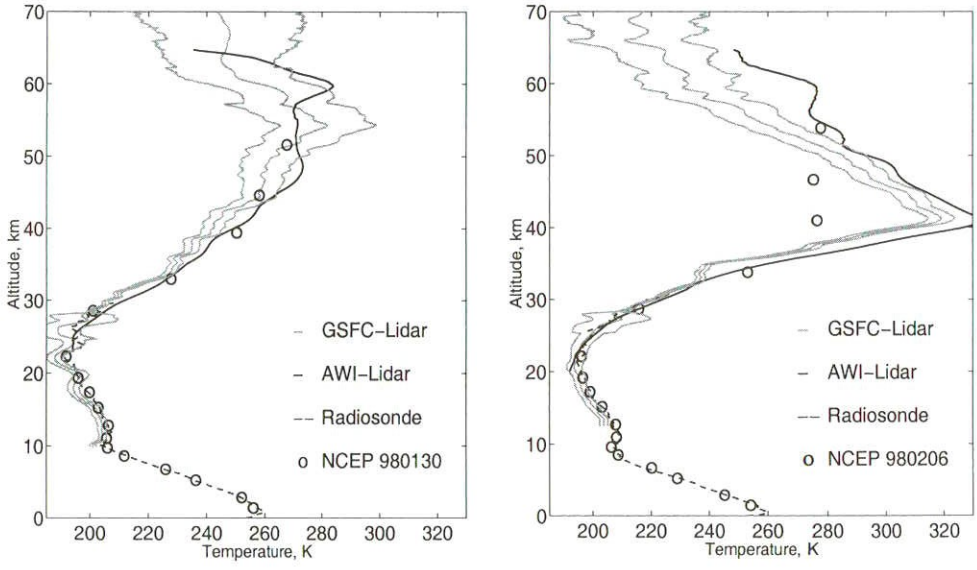


Fig. 3. Temperature profiles and NCEP analysis for 30 January 98 (3a, left) and 6 February 98 (3b, right). Light grey: GSFC lidar, black: AWI lidar, dashed: radio sonde, circles: NCEP analysis.

This document is provided by JAXA.

AWI lidar vary considerably. Their altitude resolution is much finer than that of the NCEP analysis. In the common altitude range the agreement between the different data sets is very good up to more than 55 km on this day. This is a typical result for a normal mid-winter situation. Figure 3b displays the same data sets for a day one week later, during the stratospheric warming. Both lidar data sets reveal a large descend of the stratopause from 55 to 40 km and an increase of the temperature maximum to more than 310 K. The NCEP analysis, however, found a more isothermal profile of 280 K between 35 and 55 km altitude, persisting for several days. Apparently the analysis does not resolve the full extend of the warming pulse and the change of the tropopause altitude above Spitsbergen. Lateron, when the warming decayed, the agreement between lidar data and NCEP analysis improved again considerably.

Acknowledgments

This project received excellent support by the Koldewey-Station personnel T. Weinzierl, B. Wichura, I. Beninga and D. Römermann, and by Kings Bay AS, Ny-Ålesund. It was partly funded by the European Commission (project ESMOS/Arctic II) within the 4th Framework Programme, and performed as a NDSC activity. The NCEP data was provided by NOAA through NDSC.

References

Beyerle, G. *et al.* (1994): Multiwavelength lidar measurements of stratospheric aerosols above Spitsbergen during winter 1992/93. Geophys. Res. Lett., **21**, 57–60.

Komhyr, W. (1986): Operations Handbook-Ozone Measurements to 40 km Altitude with 4A Electrochemical Concentration Cell (ECC) Ozonesondes. NOAA Technical Memo. ERL ARL-149.

Langer, J. *et al.* (1996): A versatile millimeter wave radiometer for spectroscopic measurements of atmospheric trace gases. Atmospheric Ozone: Proceedings of the XVIII Quadrennial Ozone Symp. L'Aquilla, Italy, ed. by R.D. Bojkov and G. Visconti.

McGee, T.J. *et al.* (1995): Improved stratospheric ozone lidar. Opt. Eng., **34**, 1421–1430.

Steinbrecht, W. *et al.* (1999): Results of the Ny-Ålesund ozone measurements intercomparison NAOMI. J. Geophys. Res., **104**, 30515–30523.

(Received May 31, 2000; Revised manuscript accepted July 6, 2000)

This document is provided by JAXA.

Mem. Natl Inst. Polar Res., Spec. Issue, 54, 71–79, 2001

Scientific paper

Temporal variations of atmospheric CO_2 concentration and carbon isotope ratio in Ny-Ålesund, Svalbard

Shinji Morimoto[1], Shuhji Aoki[1,2] and Takashi Yamanouchi[1]

[1]*National Institute of Polar Research, Kaga 1-chome, Itabashi-ku, Tokyo 173-8515*
[2]*Center for Atmospheric and Oceanic Studies, Graduate School of Science, Tohoku University, Sendai 980-8578*

Abstract: Ground based observation of the atmospheric CO_2 concentration and its carbon isotope, $\delta^{13}C$, have been performed in Ny-Ålesund, Svalbard since 1991. The CO_2 concentration and $\delta^{13}C$ observed in 1991–1999 showed clear seasonal cycles with peak-to-peak amplitudes of 16.5‰ ppmv and 0.8, respectively. From comparison of the seasonal cycles, it was found that the seasonal CO_2 cycle in Ny-Ålesund is mainly caused by seasonal change of biospheric activities. Interannual variations of the CO_2 concentration and $\delta^{13}C$ superimposed on their secular trends were also observed. Comparing both of the interannual variations revealed that the cause was primarily ascribed to the imbalance of the CO_2 exchange between the atmosphere and the terrestrial biosphere.

1. Introduction

For better understanding of the global carbon cycle on the earth's surface, it is necessary to obtain a precise and long-term data set of the background CO_2 concentration in the atmosphere over geographically wide areas. For this purpose, many monitoring programs have been initiated around the world and the data obtained by these measurements provide us with global pictures of the distribution of the atmospheric CO_2 concentration (*e.g.* Conway *et al.*, 1994). Based on the present understanding, about half of the industrially released CO_2 remains in the atmosphere and the rest is absorbed by the surface ocean and the terrestrial biosphere (Keeling *et al.*, 1989b). However, individual roles of the surface ocean and the terrestrial biosphere in the global carbon cycle are not well understood (Francey *et al.*, 1995; Keeling *et al.*, 1995; Morimoto *et al.*, 2000).

Carbon isotopic ratio, $\delta^{13}C$, of atmospheric CO_2, defined as:

$$\delta^{13}C=\left(\frac{(^{13}CO_2/^{12}CO_2)_{sample}}{(^{13}CO_2/^{12}CO_2)_{standard}}-1\right)10^3, \quad (1)$$

has been used as an effective tool for separating the net air-sea fluxes of CO_2 from those between the atmosphere and the terrestrial biosphere, since the degree of isotopic fractionation effect is different between these exchange processes. When a net CO_2 exchange occurs between the atmosphere and the terrestrial biosphere, $\delta^{13}C$ of the atmospheric CO_2 varies at a rate of -0.05‰/ppmv (Keeling *et al.*, 1989b). On the other hand, the net CO_2 exchange

This document is provided by JAXA.

between the atmosphere and the ocean causes only about −0.005‰/ppmv change in $\delta^{13}C$ (Siegenthaler and Münnich, 1981).

We have maintained a systematic air sampling program at ground level in Ny-Ålesund, Svalbard (78°55′N, 11°56′E) since 1991 for measuring the atmospheric CO_2 concentration and carbon isotope ratio, $\delta^{13}C$, of CO_2 (Yamanouchi *et al.*, 1996). In this paper, we will present temporal variations of the atmospheric CO_2 concentration and $\delta^{13}C$ for 1991–1999 and 1996–1999, respectively. The $\delta^{13}C$ data before 1995 were removed from the analyses since there were some experimental and sample quality problems. Using the available data, seasonal and secular variations of the atmospheric CO_2 concentration and their causes will be discussed.

2. Experimental procedures

Air samples analyzed in this study were collected at the Japanese Observatory, called "Rabben", in Ny-Ålesund, Svalbard (78°55′N, 11°56′E) during the period from August 1991 to October 1999. Figure 1 shows the location of Ny-Ålesund. An air sample was pumped from an air intake mounted on the roof of Rabben and pressurized up to 9.9×10^5 Pa into an 0.800×10^{-3} m^3 stainless-steel flask with stop-valves at both ends. The air sampling was performed once a week by the staff of the Norwegian Polar Institute without any sampling criterion, *e.g.,* wind direction or wind speed. The flasks filled with air samples were returned to the National Institute of Polar Research (NIPR) once per two months and

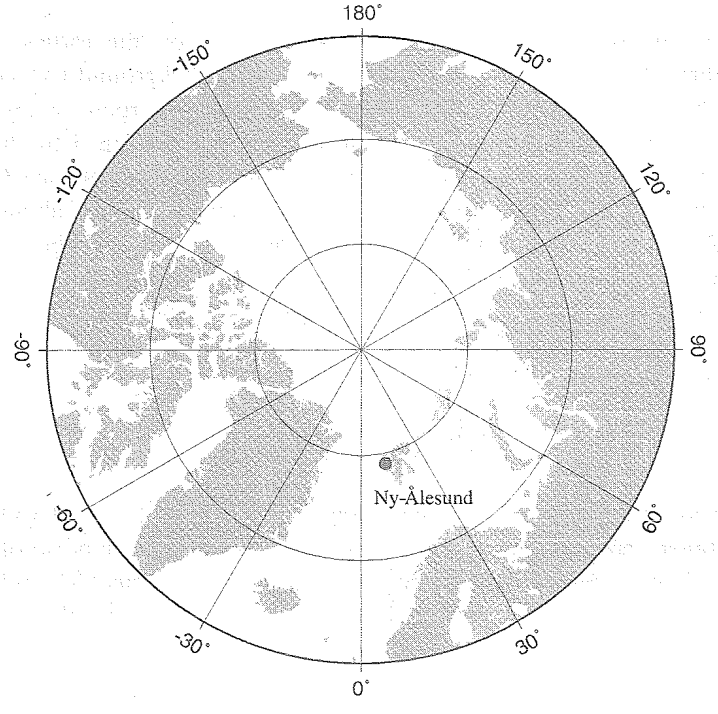


Fig. 1. Location of Ny-Ålesund, Svalbard.

This document is provided by JAXA.

subsequent analyses were performed. The time between air sampling and concentration analysis is ordinarily about 2.5-3 months.

The CO_2 concentrations of the air samples were determined against our CO_2-in-air standard gases using a non-dispersive infrared (NDIR) analyzer (Tanaka *et al.*, 1983) with a precision of 0.1 and 0.02 ppmv before and after August 1996, respectively, when our NDIR analyzer was exchanged. After the CO_2 concentration analysis, part of the air sample was used for determining CH_4 concentration by a gas chromatograph with a flame ionization detector (GC/FID) (Aoki *et al.*, 1992). The CO_2 sample used for $\delta^{13}C$ measurement was cryogenically extracted from the remaining air sample in the flask using an automatic extraction system at NIPR.

The automatic CO_2 extraction system consists of a mass flow controller, pneumatic valves, H_2O trap, temperature controlled CO_2 trap, turbo molecular pump and oil rotary pump. A computer automates the CO_2 extraction procedure, described below. After the system was sufficiently evacuated to lower than 1.3×10^{-4} Pa, H_2O and CO_2 traps were cooled at about -80 and -197℃, respectively. The air sample was pumped through the traps at a constant flow rate of 50×10^{-6} m^3/min (50 cc/min). The extracted CO_2 was sublimed by increasing the temperature of the CO_2 trap and transferred into a sample tube cooled at -197℃. When the transfer of CO_2 was finished, the tube was flamed off by a gas burner. The reliability of the NIPR extraction system was confirmed by comparing $\delta^{13}C$ values of the extracted CO_2 samples with those extracted at Tohoku University (Nakazawa *et al.*, 1993, 1997a). A typical amount of a CO_2 sample was about 0.280×10^{-6} m^3_{STP} (280 μl_{STP}). The $\delta^{13}C$ values of the CO_2 samples were analyzed by a mass spectrometer, Finnigan MAT-δS at Tohoku University. The instrumental reproducibility for the $\delta^{13}C$ analysis was within 0.02‰ (Nakazawa *et al.*, 1997a).

3. Results and discussions

From August 1991 to October 1999, about 370 air samples were collected at Ny-Ålesund and analyzed in Japan. Figures 2a and b show the observed CO_2 concentrations and $\delta^{13}C$ values, respectively, together with their best fit curves to the data, long-term trends and annual increase rates. These fitted curves were calculated by a digital filtering technique including Fourier harmonics, linear interpolations, Reinsch-type splines and a Butterworth filter. Details of the curve fitting procedures were presented in Nakazawa *et al.* (1997b). In the curve fitting procedures, data lying more than 3 standard deviations from the best fit curve were regarded as 'non-baseline data', mainly due to local human activities, and were eliminated from the data set. The $\delta^{13}C$ data obtained before 1996 had problems in their quality, since some of the air samples were stored in the flasks for more than one year, and/or there might have been problems in the mass spectrometer analyses. Therefore, we did not include the $\delta^{13}C$ data obtained before 1995 in the present study.

As seen in Fig. 2, the CO_2 concentration and $\delta^{13}C$ show secular increase and decrease, respectively, due mainly to fossil fuel combustion, as well as seasonal cycles and interannual variation. The seasonal cycles of $\delta^{13}C$ are quite similar to those of CO_2 concentration, but they are 180° out of phase. The average seasonal amplitudes of CO_2 concentration and $\delta^{13}C$ are about 16.5 ppmv and 0.8‰ peak-to-peak, respectively. These values are almost the same as those obtained for 40°-55°N in the western Pacific during 1984-1991 (Nakazawa *et al.*,

This document is provided by JAXA.

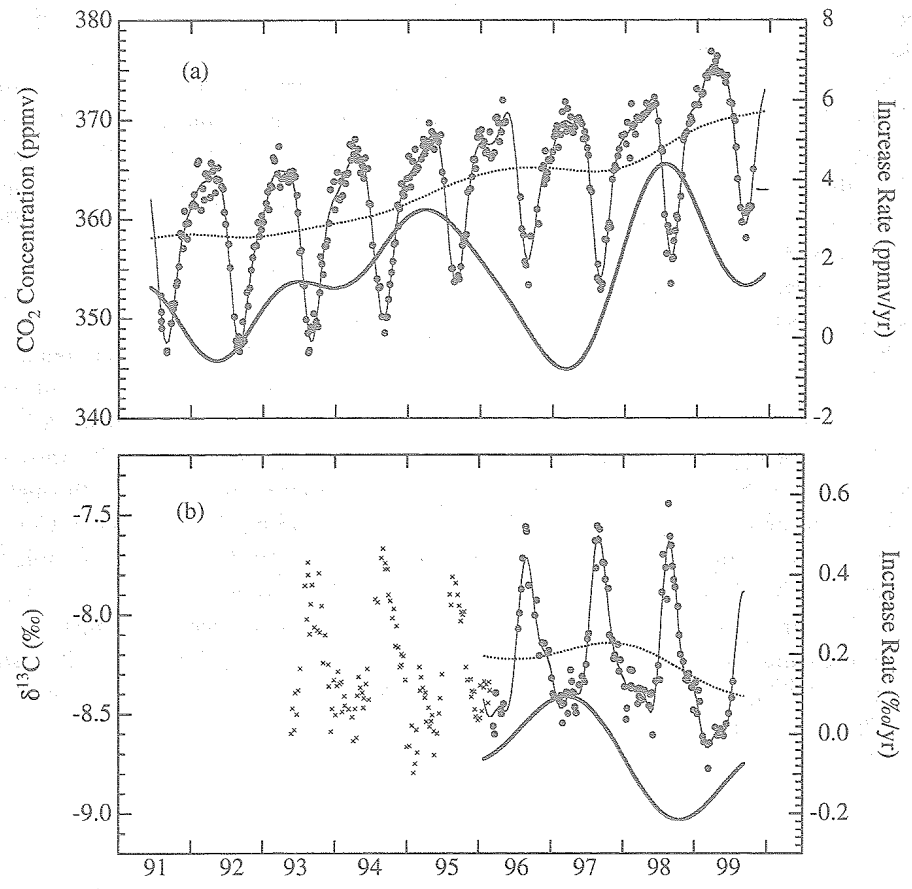


Fig. 2a. The CO_2 concentration observed at Ny-Ålesund from 1991 to 1999. Closed circles, thin and broken lines represent observed data, best fit curve to the data and long-term trend, respectively (left axis). Thick line shows the increase rate of the CO_2 concentration (right axis).

b. Same as (a), but for $\delta^{13}C$ data from 1996 to 1999. Crosses are data that were not included in this study.

Table 1. Annual mean values of the CO_2 concentration and $\delta^{13}C$ observed in Ny-Ålesund, Svalbard.

	1991	1992	1993	1994	1995	1996	1997	1998	1999
CO_2 (ppmv)	358.15	358.34	358.95	360.45	363.16	365.04	364.95	367.13	370.18
$\delta^{13}C$ (‰)	-	-	-	-	-	−8.216	−8.162	−8.217	−8.386

1997a). Annual mean values of the CO_2 concentration and $\delta^{13}C$ observed in Ny-Ålesund are listed in Table 1.

To investigate causes of the seasonal CO_2 cycles, the observed CO_2 concentration and

This document is provided by JAXA.

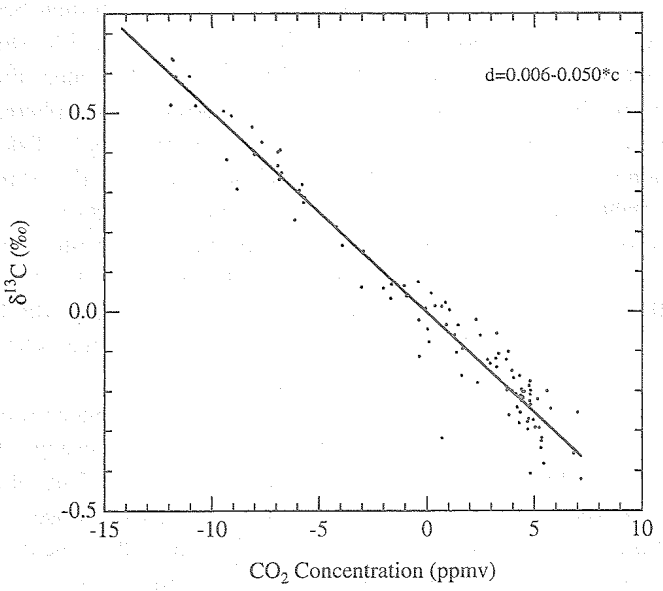


Fig. 3. Relationship between the seasonal cycles of the CO_2 concentration and $\delta^{13}C$ observed at Ny-Ålesund during the period from 1996 to 1999. Closed circles represent the observed data and the thin line is the fitted line.

$\delta^{13}C$ from 1996 to 1999 were compared after their long-term trends had been subtracted. The relationship of the seasonal component between the CO_2 concentration and $\delta^{13}C$ is plotted in Fig. 3. It is clearly seen in this figure that the relationship is almost linear. The change rate of $\delta^{13}C$ with respect to the CO_2 concentration was calculated by a least square method to be around -0.05‰/ppmv. This result suggests that the seasonal variation of the CO_2 exchange between the atmosphere and the terrestrial biosphere is responsible for the observed CO_2 seasonal cycles in Ny-Ålesund. Aoki *et al.* (1996) observed extremely low partial pressure of CO_2 (pCO_2) in Greenland Sea surface water in summer and speculated that the Greenland Sea acted as a strong sink for atmospheric CO_2 in summer. However, the relationship between CO_2 concentration and $\delta^{13}C$ shown in Fig. 3 demonstrates that the seasonal change of the terrestrial biospheric activity caused the observed variations of the CO_2 concentration in Ny-Ålesund on the seasonal time scale.

Engardt *et al.* (1996) analyzed their CO_2 concentration and $\delta^{13}C$ data observed in Ny-Ålesund and concluded that, on time scales of a few days in spring and early summer when phytoplankton blooms occurred in Greenland Sea, an oceanic air mass depleted in CO_2 by oceanic uptake produced dips of 2–4 ppmv in the CO_2 concentration in Ny-Ålesund.

As shown in Fig. 2, short-term variations of CO_2 concentration and $\delta^{13}C$ are more prominent in winter than in other seasons. Similar phenomena have also been reported by Engardt and Holmén (1999) in Ny-Ålesund and at other Arctic stations such as Alert (Trivett *et al.*, 1996; Yuen *et al.*, 1996) and Point Barrow (Conway *et al.*, 1994). To obtain information on the source of the short-term variations observed in Ny-Ålesund, we

This document is provided by JAXA.

compared deviations of the CO_2 concentration and $\delta^{13}C$ data from their best-fit curves. The relationship between the deviations of the CO_2 concentration and $\delta^{13}C$ showed a negative correlation, of which the slope was -0.047 ± 0.008‰/ppmv. As stated above, when a net CO_2 exchange occurs between the atmosphere and the terrestrial biosphere, the change rate of $\delta^{13}C$ with respect to the CO_2 concentration is about -0.05‰/ppmv. Taking into account that the $\delta^{13}C$ signature of the fossil fuel CO_2 is close to that of the terrestrial biosphere (Andres *et al.*, 1999), the source of the short-term variations observed in Ny-Ålesund was ascribed to the biospheric and/or fossil fuel CO_2 in origin. This result is in agreement with the 3-dimensional model analysis by Brandefelt and Holmén (2001). They showed that the cause of sporadic high CO_2 concentrations observed in Ny-Ålesund is ascribed to advection of an air mass from Europe, where both biospheric and fossil fuel CO_2 are released in winter.

It has been pointed out that the increase rate of the CO_2 concentration fluctuates in association with El Niño and Southern Oscillation (ENSO) events (Bacastow, 1976; Keeling *et al.*, 1989a). As shown in Fig. 2a, such interannual variations of the CO_2 increase rate have been observed in Ny-Ålesund; rapid increase of the CO_2 concentration in relation to the occurrence of ENSO events was found in 1995 and 1998. It is also noticeable that the CO_2 increase almost stopped in 1997. The long-term trend of $\delta^{13}C$ data in Fig. 2b shows rapid increase and decrease in the beginning of 1997 and 1998, respectively, which correspond well to variations of CO_2 concentration but for the opposite sign.

In order to compare more quantitatively the magnitude of the interannual variations in the CO_2 concentration and $\delta^{13}C$, we first extracted the interannual components from the long-term trends by the following procedures. It should be noted that the following analyses were performed during the period from 1996 to 1999, during which our $\delta^{13}C$ data were available. (1) Assuming that the year-to-year change of the fossil fuel combustion rate is small, the contribution of the fossil fuel CO_2 was approximated by a linear fit to the long-term CO_2 trend. (2) The fitted line, thus obtained, was subtracted from the observed long-term trend of the CO_2 concentration and the residual was regarded as the interannual component of the CO_2 concentration. (3) Similarly, the contribution of the fossil fuel combustion and isotopic disequilibrium flux (Tans *et al.*, 1993) to the $\delta^{13}C$ trend was approximated by a linear fit to the long-term $\delta^{13}C$ trend and was subtracted from it. (4) The residual, thus obtained, was regarded as the interannual component of $\delta^{13}C$. Figure 4a shows the interannual component of the CO_2 concentration in Ny-Ålesund from 1996 to 1999. We then calculated the $\delta^{13}C$ variations expected when only the oceanic CO_2 produced the interannual CO_2 variation and when only the terrestrial biospheric CO_2 did, respectively, by multiplying the respective values of -0.005‰/ppmv and -0.05‰/ppmv by the interannual variation of the CO_2 concentration shown in Fig. 4a. The rate of change of $\delta^{13}C$ with respect to the CO_2 concentration is calculated to be from -0.054 to -0.050‰/ppmv for the terrestrial biospheric CO_2 when using the annual average values of the CO_2 concentration and $\delta^{13}C$ from 1996 to 1999, and -27 and -28‰ as the $\delta^{13}C$ value of the biospheric CO_2, respectively. Similarly, the change rates of $\delta^{13}C$ range from -0.0048 to -0.0079‰/ppmv for the oceanic CO_2. In this case, we assume sea surface temperature and $\delta^{13}C$ values of the dissolved inorganic carbon in the Greenland Sea to be 2.4℃ and 1.2–1.36‰, respectively (our unpublished data, 2000). These calculations show that the respective change rate in $\delta^{13}C$ is not so sensitive to the long-term change in the atmospheric CO_2 concentration and

This document is provided by JAXA.

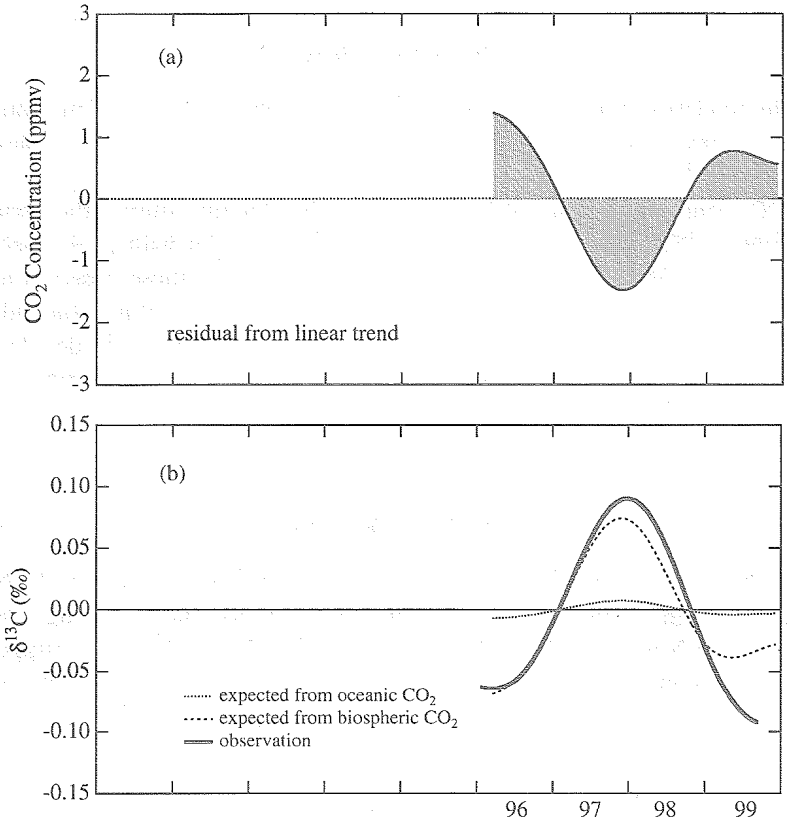


Fig. 4a. Interannual variation of the CO_2 concentration at Ny-Ålesund from 1996 to 1999.
b. Comparison of observed interannual variation of $\delta^{13}C$ (thick line) with those calculated on the basis of biospheric CO_2 (broken line) and oceanic CO_2 (dotted line) at Ny-Ålesund.

$\delta^{13}C$ and uncertainties in the estimated $\delta^{13}C$ values of the biospheric and oceanic CO_2.

The results are shown in Fig. 4b. It is obvious from this figure that the observed $\delta^{13}C$ variations are well reproduced by those calculated based on the terrestrial biospheric CO_2. From this examination, it is suggested that the cause of the interannual variations of the CO_2 concentration observed in Ny-Ålesund from 1996 to 1999 were produced by an imbalance of the net CO_2 exchange between the atmosphere and the terrestrial biosphere. This finding will be further studied with the aid of global data sets of CO_2 concentration and $\delta^{13}C$. A recent phenomenological model study (Ito and Oikawa, 2000) showed that the terrestrial biosphere released excess CO_2 of 2.7 PgC/year (GtC/yr), which is equivalent to 1.26 ppmv CO_2 in the atmosphere, in 1998. Ito and Oikawa (2000) used a climate data set and their biosphere model, and concluded that higher temperatures and excess precipitation during the 1998 ENSO event accelerated plant respiration and soil decomposition. Their results are consistent with our findings obtained by atmospheric CO_2 concentration and $\delta^{13}C$ observations.

This document is provided by JAXA.

4. Conclusions

In order to clarify temporal variations of the atmospheric CO_2 concentration and $\delta^{13}C$, we have continued a systematic air sampling in Ny-Ålesund with cooperation of the Norwegian Polar Institute since 1991.

The CO_2 concentration and $\delta^{13}C$ observed in Ny-Ålesund during the periods 1991–1999 and 1996–1999, respectively, showed clear seasonal cycles with peak-to-peak amplitudes of 16.5 ppmv and 0.8‰. The amplitudes were similar to those observed at latitudes 40°–55°N in our previous study. It was also found that the CO_2 concentration and $\delta^{13}C$ data showed interannual variations in association with an ENSO event. From detailed comparisons of the CO_2 concentration and $\delta^{13}C$ data, it was found that the variations in the CO_2 exchange between the atmosphere and the terrestrial biosphere were responsible for the CO_2 variations on both seasonal and interannual time scales.

Acknowledgments

The authors wish to express their sincere thanks to the staff members of the Norwegian Polar Institute for their support in our air sampling at Ny-Ålesund for a long time. We also thank Ms. Hiroko Nagamoto, National Institute of Polar Research, for her support in flask preparations and concentration analyses. This work was supported by Grants-in-Aid Nos. 09740369 and 10144103 from the Ministry of Education, Science, Sports and Culture of Japan.

References

Andres, R.J., Marland, G., Boden, T. and Bishoff, S. (1999): Carbon dioxide emissions from fossil fuel combustion and cement manufacture 1751–1991 and an estimate of their isotopic composition and latitudinal distribution. Stanford, Cambridge University Press, 53–62.

Aoki, S., Nakazawa, T., Murayama, S. and Kawaguchi, S. (1992): Measurements of atmospheric methane at Japanese Antarctic Station, Syowa. Tellus, **44B**, 273–281.

Aoki, S., Morimoto, S., Ushio, S., Itoh, H., Nakazawa, T., Yamanouchi, T., Ono, N. and Vinje, T. (1996): Carbon dioxide variations in the Greenland Sea. Mem. Natl Inst. Polar Res., Spec. Issue, **51**, 299–306.

Bacastow, R.B. (1976): Modulation of atmospheric carbon dioxide by the Southern Oscillation. Nature, **261**, 116–118.

Brandefelt, J. and Holmén, K. (2001): Anthropogenic and biogenic winter sources of Arctic CO_2—a model study. Tellus, **53B**, 10–21.

Conway, T.J., Tans, P.P., Waterman, L.S., Thoning, K.W., Kitzis, D.R., Masarie, K.A. and Zhang, N. (1994): Evidence for interannual variability of the carbon cycle from the National Oceanic and Atmospheric Administration/Climate Monitoring and Diagnostic Laboratory Global Air Sampling Network. J. Geophys. Res., **99**, 22831–22855.

Engardt, M. and Holmén, K. (1999): Model simulations of anthropogenic-CO_2 transport to an Arctic monitoring station during winter. Tellus, **51B**, 194–209.

Engardt, M., Holmén, K. and Heintzenberg, J. (1996): Short-term variations in atmospheric CO_2 at Ny-Ålesund, Spitsbergen, during spring and summer. Tellus, **48B**, 33–43.

Francey, R.J., Tans, P.P., Allison, C.E., Enting, I.G., White, J.W.C. and Trolier, M. (1995): Changes in oceanic and terrestrial carbon uptake since 1982. Nature, **373**, 326–330.

Ito, A. and Oikawa, T. (2000): The large carbon emission from terrestrial ecosystem in 1998: A model

This document is provided by JAXA.

simulation. J. Meteorol. Soc. Jpn., **78**, 103–110.
Keeling, C.D., Bacastow, R.B., Carter, A.F., Piper, S.C., Whorf, T.P., Heimann, M., Mook, W.G. and Roeloffzen, H. (1989a): A three-dimensional model of atmospheric CO_2 transport based on observed winds: 1. Analysis of observed data. Aspects of Climate Variability in the Pacific and Western Americas. Washington, D.C., Am. Geophys. Union, 165–236.
Keeling, C.D., Piper, S.C. and Heimann, M. (1989b): A three-dimensional model of atmospheric CO_2 transport based on observed winds: 4. mean annual gradients and interannual variations. Aspects of Climate Variability in the Pacific and Western Americas. Washington, D.C., Am. Geophys. Union, 305–362.
Keeling, C.D., Wholf, T.P., Wahlen, M. and Van der Plicht, J. (1995): Interannual extremes in the rate of rise of atmospheric carbon dioxide since 1980. Nature, **375**, 666–670.
Morimoto, S., Nakazawa, T., Higuchi, K. and Aoki, S. (2000): Latitudinal distributions of atmospheric CO_2 sources and sinks inferred by $\delta^{13}C$ measurements. J. Geophys. Res., **105**, 24315–24326.
Nakazawa, T., Morimoto, S., Aoki, S. and Tanaka, M. (1993): Time and space variations of the carbon isotopic ratio of the tropospheric carbon dioxide over Japan. Tellus, **45B**, 258–274.
Nakazawa, T., Morimoto, S., Aoki, S. and Tanaka, M. (1997a): Temporal and spatial variations of the carbon isotopic ratio of atmospheric carbon dioxide in the western Pacific region. J. Geophys. Res., **102**, 1271–1285.
Nakazawa, T., Ishizawa, M., Higuchi, K. and Trivett, N.B.A. (1997b): Two curve fitting methods applied to CO_2 flask data. Environmetrics, **8**, 197–218.
Siegenthaler, U. and Münnich, K.O. (1981): $^{13}C/^{12}C$ fractionation during CO_2 transfer from air to sea. Carbon Cycle Modeling, ed. by B. Bolin. Chichester, J. Wiley, 246–257.
Tanaka, M., Nakazawa, T. and Aoki, S. (1983): High quality measurements of the concentration of atmospheric carbon dioxide. J. Meteorol. Soc. Jpn., **61**, 678–685.
Tans, P.P., Berry, J.A. and Keeling, R.F. (1993): Oceanic $^{13}C/^{12}C$ observations: A new window on ocean CO_2 uptake. Global Biogeochem. Cycles, **7**, 353–368.
Trivett, N.B.A., Higuchi, K., Yuen, C.W. and Worthy, D.E.J. (1996): The impact of Arctic circulation on trace gas measurements at Alert, Canada. Mem. Natl Inst. Polar Res., Spec. Issue, **51**, 165–176.
Yamanouchi, T., Aoki, S., Morimoto, S. and Wada, M. (1996): Report on atmospheric science observations at Ny-Ålesund, Svalbard. Mem. Natl Inst. Polar Res., Spec. Issue, **51**, 153–164.
Yuen, C.W., Higuchi, K., Trivett, N.B.A. and Cho, H.-R. (1996): A simulation of a large positive CO_2 anomaly over the Canadian Arctic archipelago. J. Meteorol. Soc. Jpn., **74**, 781–795.

(Received May 30, 2000; Revised manuscript accepted October 30, 2000)

This document is provided by JAXA.

This document is provided by JAXA.

Mem. Natl Inst. Polar Res., Spec. Issue, 54, 81–90, 2001

Review

Global quality control for long-lived trace gas measurements

Roger Francey[1], Manfred Groening[2], Kim Holmén[3], Krung-Ryul Kim[4], John Miller[5], Pieter Tans[6] and Neil Trivett[7]

[1]*Commonwealth Scientific and Industrial Research Organization, Aspendale, VIC, Australia*
[2]*International Atomic Agency, Vienna, Austria*
[3]*Department of Meteorology, Stockholm University, Stockholm, Sweden*
[4]*Seoul National University, Seoul, Korea*
[5]*World Meteorological Agency, Geneva, Switzerland*
[6]*NOAA-CMDL, Boulder, CO, U.S.A.*
[7]*Environmental Systems Research, Burlington, ON, Canada*

Abstract: This report arose from the 10th World Meteorological Organization's (WMO) meeting of Experts on Carbon Dioxide Concentration and Related Tracer Measurement Techniques, Stockholm, 23–26 August 1999, at which a proposal was put forward to address some of the known problems associated with quality control of global trace gas measurements, in particular, carbon dioxide, methane and their respective isotopes, and proposes some changes to significantly improve on current situation. The meeting was also attended by a member of the Research Co-ordination Meeting of the International Atomic Energy Agency's (IAEA) Co-ordinated Research Project on Isotope-aided studies of atmospheric carbon dioxide and other greenhouse gases. The aim of this proposal is greatly improved inter-laboratory comparability for measurement of long-lived atmospheric trace gas species, resulting in improved derivation of source/sink fluxes from spatial and temporal atmospheric composition changes. A network with regional "hubs" responsible for maintaining an efficient means of inter-comparing all laboratories with a much higher frequency than what has been practiced to date is proposed. Mayor needs and components of such a network will be presented. This proposal is supported, in principle, by both WMO and IAEA, and has implications for all scientific groups involved in trace gas measurements.

1. Introduction

There is abundant recent evidence, some examples of which are referred to below, that the differences between laboratory measurements of atmospheric composition often exceed the quoted precision of measurement. This is also true with a given laboratory's programs when several analysis methods (non dispersive infra red [NDIR] *vs.* gas chromatography [GC]) and/or *in situ vs.* grab sampling techniques are used. This limits our confidence in the accuracy of regional sources and sinks that are being derived from the observed spatial and temporal patterns of a trace gas with the help of atmospheric chemical transport models. It also limits the usefulness of individual programs in expanding the global coverage of measurements sorely needed by the models. About 10 years ago a target precision for large-scale spatial and temporal differences was set by WMO to 0.1 μmol per

This document is provided by JAXA.

mol for CO_2 in the northern hemisphere, and 0.05 μmol per mol in the southern hemisphere; 0.01 per mil was set for $d^{13}C$ in IAEA/WMO forums. These targets have never been consistently achieved. Secondly, the ongoing process of international negotiations about limiting trace gas emissions in order to avoid or minimize man-made climate change has made the issue more urgent. A third motivation relates to on-going improvements in technology, which are expected to make it easier to achieve the target for the complete measurement system, including methods and procedures, standard reference gases, calibration transfers, and field sampling and measurement systems.

Some of the well documented systematic problems that still require explanation, and remedy or effective allowance are given below:

- Systematic CO_2 discrepancies at the 0.2 μmol per mol level when flask air samples are operated next to a continuously monitoring instrument.
- Similar differences between laboratories at the same site.
- Large and variable CO_2 discrepancies between up to 24 laboratories in the 1991–93 and 1994–97 WMO Round Robin comparisons.
- Clear indication of non-linearity in CO_2 measurement, involving most laboratories reporting to the 1994–97 WMO Round Robin.
- $\delta^{13}C$ differences 10 times target inter-comparability in the 1996–98 IAEA CLASSIC circulation between 4 major network laboratories with clear evidence of non-linearity.
- Documented evidence of subtle systematic CO_2 and $\delta^{13}C$ offsets caused by high pressure regulators.
- Mounting evidence for pressure dependence in CO_2 from high pressure aluminium containers.
- Flask air-sharing comparisons showing CO_2 differences up to 10 times the differences measured in high pressure cylinders.
- Flask air-sharing comparisons of real samples revealing and documenting both step changes ($\delta^{13}C$, $\delta^{18}O$) and long term drifts (CO, H_2) between two laboratories , not detected by conventional intercalibration activities.
- (Note: while these examples are mainly focussed on CO_2, the most studied trace gas, it is expected that similar problems will influence other trace gas measurements).

2. Historical links

WMO has been a strong supporter of the global measurement programs which are now incorporated into the Global Atmosphere Watch program and has sponsored 10 "Experts" meetings since their inception. Initially, these meetings were held approximately every 4 years and focussed on problems of measurement, comparability of scales and interpretation of the data collected in the global networks. While scale and measurement problems remained, the frequency increased to every 2 years and the focus gradually shifted to understanding the problems associated with the use of the global data in inversion models to infer regional sources and sinks in the global carbon cycle. Recognizing that there were on-going problems in merging data sets from different measurement programs, a number of inter-comparison programs were started including the WMO Round Robin set of CO_2-in-Air tanks which were sent to each laboratory, several flask sample inter-comparison projects, such as, the one at Alert, NWT, (WMO, 2001) and another between two of the

This document is provided by JAXA.

major labs (NOAA-CMDL and CSIRO) at Cape Grim, Tasmania (Masarie *et al.*, 1999), and the data integration project called GLOBALVIEW initiated by the NOAA-CMDL labs (Masarie *et al.*, 1995). Unfortunately, these are still considered insufficient to bring closure to the integration of the data sets into a common one suitable for inversion modelling on shorter time and space scales than is currently possible.

The proposal presented here is an integration of elements of the IAEA carbon isotope "CLASSIC-AL" inter-comparisons (Collin Allison, an unpublished manuscript), the WMO CO_2 "Round Robin" inter-comparisons (Peterson *et al.*, 1999), the CMDL-CSIRO flask air-sharing inter-comparison (ICP), and culminating in enhanced GLOBALVIEW data assimilations by the Cooperative Atmospheric Data Integration Project.

(Possible interaction with GAW QA/SAC (Quality Assurance/Science Activity Centres) with similar objectives, have not yet been explored).

3. General approach

The essence of quality control is redundancy and frequent scrutiny of the data. Ideally, all reference gases need to be unambiguously traceable to a single common calibration scale. The reference gases may be drifting, however, or a mistake may have been made, and therefore all reference gases need to be checked regularly in an independent way. During the use of reference gases in calibrating measurements systematic errors may be introduced due to procedures and materials. Linearity of measurement instrumentation is often overlooked as a source of inter-calibration error. Finally, errors will be introduced by the measurement or sampling procedures themselves, independent of any calibration problems. Inter-comparisons between different methods and between laboratories are necessary as a means of detecting and addressing such problems. All of these controls need to be exercised on a continuing basis because the experience of many decades shows that unacceptable discrepancies tend to develop over time.

Secondly, too little thought has been given to data management by many laboratories, often resulting in difficult access even to their own data. Improved and transparent access to data is an integral part of this plan.

Thirdly, because of the global nature of many environmental problems, it is essential that access to first-rate quality control needs to be made both easier and affordable for many laboratories.

Note that the plan below does not provide, and should not be used to provide, a link to an international calibration scale! Instead, it is aimed at providing a dynamic monitoring of inter-comparability between measurement laboratories. In so far as the major interpretative studies involve conversion of trace gas composition differences into fluxes, there is an immediate application for improved inter-comparability results. This plan anticipates such application by automatic inclusion of results in enhanced GLOBALVIEW data assimilations.

Also intrinsic to this plan is a two-year international review process that assesses all inter-comparison information and makes recommendations for ongoing operation. These reviews will examine performance in the light of contemporary scientific requirements. Initially, the plan is expected to elucidate many of the systematic errors that have largely prevented merging of past data sets. In the longer term, the plan is expected to be of use in

This document is provided by JAXA.

establishing and maintaining globally accessible calibration scales.

The initial focus is on the urgent problems of measuring CO_2 and CO_2 isotopes, but this does not exclude other trace gases that can be measured without compromising cylinder lifetime or circulation frequency (*e.g.* CH_4, CO, N_2O, H_2, $\delta^{13}CH_4$, etc.).

4. The GLOBALHUBS plan

Four globally distributed and tightly linked 'HUB' laboratories that are a source of well-characterised air for laboratories in their region. Two HUB laboratories are identified for special duties, a PREPARATION HUB (nominally GASLAB in CSIRO Atmospheric Research, Australia), and a CALIBRATION HUB associated with the WMO Central CO_2 Laboratory at CMDL, NOAA, USA (Fig. 1).

5. Quality control of calibrations

A key new element, essential for the PREP. HUB, but also arguably for each HUB, is improved NDIR techniques (DaCosta and Steele, 1999; WMO-TD No. 952). The new low-flow system is expected to permit routine quality-assessment of regulators and standards for CO_2 to a precision of around 0.002 μmol per mol (*e.g.* regulators assessed in hours, cylinder drifts detected in weeks/months rather than years, decanting accurately and monitored, etc.). If necessary, cylinder drifts in CO_2 can be accurately and economically tracked over the cylinder lifetime. As the program moves into other trace gas species, modern up-to-date GC systems will also be required.

(1) Annual circulation between the four HUBS of 5 high pressure cylinders ("circulators")
 a) Aluminium cylinders (~5 litres @ 150 bar=800 litres).
 b) Estimated circulator tank lifetime ~10 years.
 c) filled with clean dry Southern Hemisphere air, but with composition of target gases modified to bracket anticipated atmospheric values (*e.g.* for CO_2, 350, 375, 385, 400, 430 μmol per mol; $\delta^{13}C$, 0 to -45‰, etc.)
 d) dedicated high-quality high-pressure regulators, and uniform high-pressure cylinder sampling protocols (addressing identified systematic problems with previous round-robin methods)
 e) A back/up set of 5 cylinders will be prepared, for emergency/redundancy, in addition to the IAEA CLASSIC cylinders.

(2) A new set of non-circulating "primary" high-pressure cylinder air standards (with dedicated regulators) to join the suite of primaries at the Central CO_2 Laboratory.
 a) Aluminium cylinders (~30 litres @ 150 bar=6000 litres).
 b) Estimated lifetime $>$25 years.
 c) Have particular relevance to CO_2 isotope measurement scales (*e.g.* for CO_2 [μmol per mol], $\delta^{13}C$ (‰): 360, 0; 375, -7.5; 390, -8.5; 405, -9.5; 420, -45). Measure the isotopic composition of the current CCL primaries.
 d) dedicated high-quality high-pressure regulators

(3) Frequent (four times per year) high-precision monitoring of the relative measurement between each of three HUBS and the PREP. HUB ("oscillators") using low pressure 'ambient' air standards in large volume containers (34L stainless steel containers) at <4

This document is provided by JAXA.

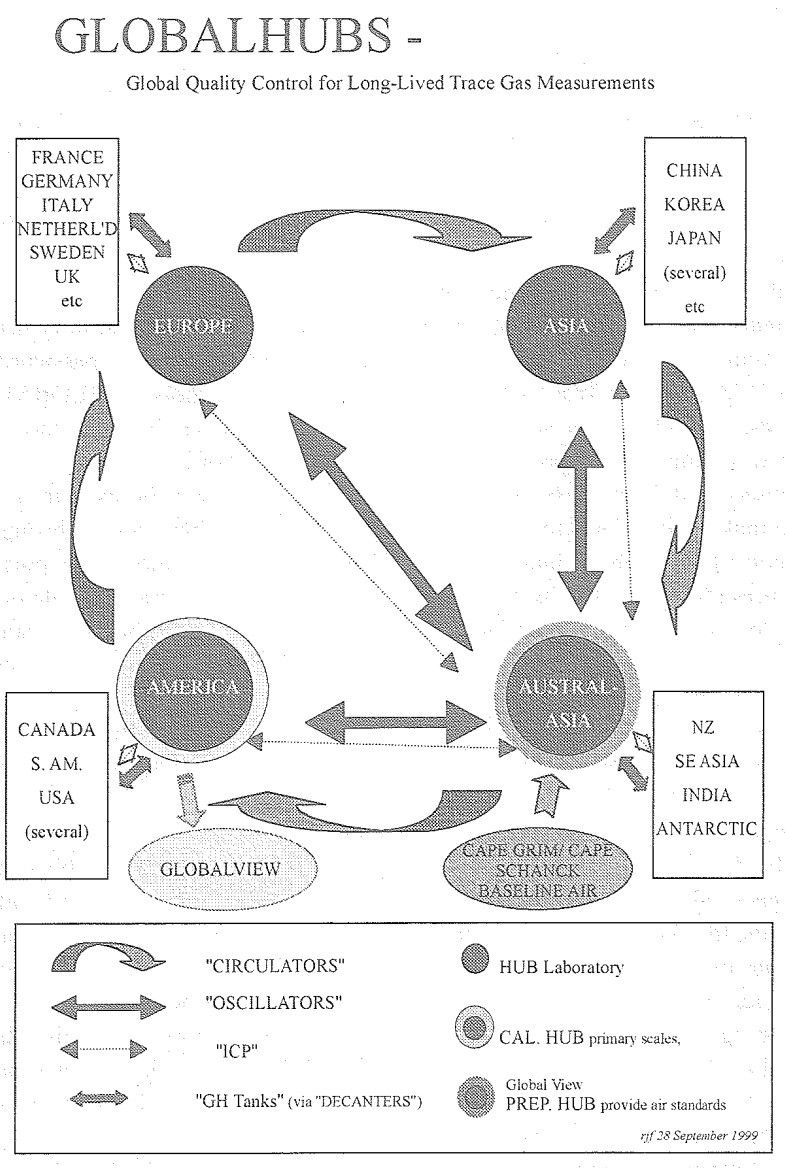


Fig. 1. A schematic outlining the exchange of gases in flasks, low-pressure cylinders and high-pressure tanks between hubs is shown above. A similar pattern of exchange could be developed between the hubs and the client laboratories in their respective regions.

bar.

a) Sufficient air for many repeat measurements, but ~1 year lifetime.
b) Avoids systematic effects often observed with high pressure regulators. These comparisons are half-way between standards and actual samples.
c) Non-hazardous goods, implying reduced freight costs.

This document is provided by JAXA.

6. Quality control of sample measurements

(1) Weekly low-precision monitoring of the relative measurement by the four HUBS on routine sampling network flask samples collected at two sites for all four hub laboratories.

a) This is designed to catch any systematic differences due to sample flask filling/storage/analysis

b) also carries biogeochemical information

(2) Automated and up-to-date logging and presentation of HUB laboratory activities and results (circulators, oscillators, and HUB-ICP comparisons) on a password protected World Wide Web (WWW) site open only to all contributors to GLOBALVIEW.

a) Near real-time electronic access to assigned values and calibration status of the air standard for individual species for participating laboratories.

b) The observed differences between the HUB laboratories will be used in a transparent way to make adjustments to contributed laboratory data when they are brought together into consistent global data sets (GLOBALVIEW) for modeling purposes. The differences are NOT used by any laboratory to adjust its calibration scale or change its data because that would sacrifice the traceability of the calibration scale. When a problem becomes apparent, the laboratory should fix the problem itself, either in its standard reference gases or in its procedures.

(3) Customer service involves a HUB laboratory responding to requests from regional laboratories, (on a cost recovery basis), for regular and ongoing access to characterised air in GLOBALHUBS (GH) tanks. HUB laboratories are expected to stimulate the exchange of melons with regional laboratories.

a) Each HUB will be provided by a SUPERHUB with a maintained supply of aluminium cylinders (~30 litres @ 150 bar=6000 litres, "decanters") filled with ambient whole air standards, for decanting into GH tanks (provided on short-term loan to a laboratory).

b) Activities over and above basic HUB commitments to be negotiated on a commercial basis? (*e.g.* acquisition of more melons, or more frequent access?)

(4) Continuing inter-comparison of actual flask samples between regional laboratories (including their HUB), or between regional laboratories linked to a separate HUB (more expensive), are a final essential part of the integrated quality control of sampling and measurement procedures.

(Note: Automated software for transferring data between CMDL and CSIRO and updating statistical comparisons and plots has been operating for several years, and is being implemented at other sites).

7. Summary of suggested HUB and SUPERHUB commitments

(1) HUB Commitments (not necessarily all in one laboratory).

a) Minimum 5 year institutional commitment?

b) Maintain circulation of HUB circulators, oscillators and ICP comparisons.

c) Ensure prompt registration of results on WWW (software recommendations to be developed/might include assistance).

This document is provided by JAXA.

d) Only adjust internal calibration scales in response to independently identified and quantified systematic error.
e) Ensure and encourage the provision of standard air in GH Tanks (specify maximum frequency) to SUITABLE laboratories in their region.
f) Record transactions and results.
g) Play a key role in the 2-yearly GLOBALHUBS assessment meetings.

(2) PREPARATION HUB Commitments (over and above routine HUB operation) include:

a) Provision of primary, circulator, and decanter air standards in high pressure cylinders.
b) The acquisition and quality assessment of HUB hardware (high pressure and low pressure cylinders, regulators)
c) Filling of high pressure cylinders at a clean-air site (also involves spiking and stripping whole air for specified span ranges).
d) Develop and document decanting from decanters into GH Tanks.
e) Monitor decanting (from high pressure cylinders to GH Tanks) protocols and effectiveness.

(3) CALIBRATION HUB Commitments (over and above routine HUB operation) include:

a) Link GLOBALHUBS primaries to manometric/gravimetric standards at regular intervals.
b) Design and implement consistent software for managing and reporting of results, including graphical presentations, on the WWW.

8. Funding strategy

At this stage we are suggesting a coordinated approach to the three regional networks APN (Asia Pacific Network), ENRICH (Europe Network for Research in Global Change)), IAI (Inter-America Institute for Global Change Research), three funding organisations with a charter to develop regional cooperation on global change research. For example APN supports "global environmental change research projects which cannot be conducted on a national basis and require regional cooperation". Alternatively, part funding might be sought from GEF (Global Environmental Facility) or similar agencies.

Request SUPERHUB and HUB set up costs, and HUB/SUPERHUB basic operating costs over three years.

International set up funding directed at core activities only. Regional funding then requested regionally. After set up, the whole exercise might be best operated on a user pays basis (with developing countries continuing to seek funding aid.

9. Training strategy

The human resources required to operate the GLOBALHUBS program can be partly addressed by the HUBS acting as training and development centres for scientific/technical people from developing laboratories. In addition we should develop a course in high-accuracy trace gas monitoring.

This document is provided by JAXA.

10. Implementation strategy

The initial hurdle is obtaining funding for a SUPERHUB so that preparation of a suitable number and quality of HUB standards can commence. Initial container storage tests will occupy a minimum of 3-6 months. It is expected that different HUBS might take different times to become fully operational (depending also on the availability of HUB establishment costs).

There will clearly be regional politics involved in identifying a HUB and hopefully these can be largely sorted out within each region. The initial criteria for being a HUB will demand a considerable degree of experience and competence. Sharing arrangements might be considered, but would have to demonstrate that they do not compromise the basic integrity, dispatch and lifetime of the circulating and oscillating standards. Some sort of phased implementation needs to be developed once HUBS are identified and committed?

Table 1. GLOBALHUBS Setup Hardware.
A draft estimate of setup costs to be revised when the plan is finally implemented.

	Container volume (L)	Full Pressure/ volume (bar/ L STP)	Lifetime (years)	Number of containers	Number of regulators	Span CO_2 (μmol per mol) $\delta^{13}C$ (‰)	Circulation ($year^{-1}$)
HUB							
PRIMARIES	30	150/6000	>25	5	5	350 to 430 0 to -45	(CAR to CMDL)
CIRCULATORS	5	150/800	~10		2x5	350 to 430 0 to -45	1
OSCILLATORS	34	4/140	~1	2x3	2x3	ambient	4
FLASC/ICP	0.5-2	2/(1-4)	~0.1	-	-	sample	>20
Customer				Per HUB	Per HUB	Per HUB	Per HUB
DECANTERS	30	150/6000	~1 ~5?	3 2	5	~ambient lo&hi	0.5
GH Tanks	34	4/140	~2*	5	-	~ambient lo&hi	~1-4
FLASC/ICP	0.5-2	2/(1-4)	~0.1	-	-	sample	>20

*@300 L per decant/DECANTER Cylinder

Hardware	approximate	costing:	Containers (@$1000)	Regulators (@1500)	Cost
Aluminium	8000L	Primaries	5	5	$12,500 AU
		Decanters	5x4=20	20	$50,000
Aluminium	800 L	Circulators	2x5	10	$25,000
Stainless	Steel 34L	Oscillators	2x3	-	$ 6,000
		GH Tanks	4x5	-	$20,000
					$113,500
					~ $75,000 US

This document is provided by JAXA.

11. Australian SUPERHUB?

As a stimulus for further discussion, here are preliminary considerations of the required support to establish an Australian SUPERHUB (Table 1)

In addition to cylinder hardware in Table 1, an Australasian HUB/SUPERHUB would require: a back-up RIX compressor system, money to construct a dedicated LO FLOW HIGH PRECISION CO_2 analyser, at least one full time technical officer (including overheads) for set up (2 years), at a technical officer position for ongoing HUB commitments (training positions). We would also be seeking all freight and consumable costs for SUPERHUB and HUB activities.

References

DaCosta and Steele (1999): WMO-TD No. 952

Masarie, K.A. and Tans, P.P (1995): Extension and Integration of Atmospheric Carbon Dioxide Data into a Globally Consistent Measurement Record. J. Geophys. Res., **100**, 11593-11610.

Masarie, K.A., Conway, T., Dlugokencky, E., Novelli, P., Tans, P., Vaughn, B., White, J., Trolier, M., Francey, R., Langenfelds, R., Steele, P. and Allison, C. (1999): An update on the ongoing Flask-Air Intercomparison program between the NOAA CMDL Carbon Cycle Group and the CSIRO DAR Global Atmospheric Sampling Laboratory. Report of the 9th WMO Meeting of Experts on Carbon Dioxide Concentration and Related Tracer Measurement Techniques, Aspendale, Vic. Australia, 1-4 September 1997, ed. by R. Francey. Geneva, World Meteorological Organization.

Peterson, J., Tans, P. and Kitzis, D. (1999): CO_2 Round-Robin Reference Gas Intercomparison. Report of the Ninth WMO Meeting of Experts on Carbon Dioxide Concentration and Related Tracer Measurement Techniques, Aspendale, Vic. Australia, 1-4 September 1997, ed. by R. Francey. Geneva, World Meteorological Organization.

WMO (2001): Report of the 10th WMO Meeting of Experts on Carbon Dioxide Concentration and Related Tracer Measurement Techniques, Stockholm, Sweden, 23 August 1999, ed. by Kim Holmen (in press).

(Received February 21, 2000; Revised manuscript accepted July 11, 2000)

This document is provided by JAXA.

Appendix A - DRAFT RECOMMENDATIONS BY WMO (and IAEA) EXPERTS related to the GLOBALHUBS proposal, Stockholm, August 26, 1999.

1. The meeting unanimously endorsed the proposal as one that:

   a) Recognised the need for this measurement community to react to new demands, particularly in relation to improved estimates of regional trace gas fluxes deduced from measured changes in atmospheric composition.
   b) Identified serious systematic error in current CO_2 and CO_2 tracer measurement both within and across programs that are not adequately addressed with existing calibration and inter-comparison strategies.
   c) Outlined a strategy which would significantly reduce these errors by:

      i. improved access to precisely-characterized standard air for laboratory inter-comparison. (The improvement pertains to existing highly-developed laboratories but is particularly relevant for developing laboratories)
      ii. providing a motivation and framework for rapid integration of the improved inter-comparison information into existing international data repositories (particularly enhancing the value of the output of smaller/regional laboratories)
      iii. providing greatly improved access for the user (modelling) community to globally consistent data sets
      iv. providing greater transparency of methodologies leading to global data assimilations.

2. The meeting agreed with a suggestion that a small working group be formed to further develop the GLOBALHUBS proposal. The responsibilities of the group include:

   a) Survey the expectations of participating (customer) measurement laboratories
   b) Define the interaction with existing inter-comparison activities, e.g. WMO Round Robins, IAEA CLASSIC)
   c) Explore interactive relationships with major clients such as the carbon budget modelling community (TRANSCOM), other international data repositories, in particular GAW QA/SAC, the WMO and CDIAC.
   d) Explore interactions with major science planning groups (IGAC, etc.?)
   e) Define the responsibilities of SUPERHUB and HUB laboratories
   f) Estimate the setup, operating costs and possible implementation schedule
   g) Explore possible funding agencies
   h) Prepare a funding strategy
   i) Prepare appropriate funding proposals
   j) Provide a full on-going record of actions to WMO (Dr John Miller) and IAEA (Dr Manfred Groening).
   k) Provide a full summary to the Experts community and invite comment, prior to implementation of any action with future policy implications.
   l) Aim for a 6-month timeframe to complete these tasks, subject to the availability of a consultant to assist with data collection and summaries.

Roger Francey offered to form a working group and/or co-opt experts, and approach WMO/IAEA with the view of acquiring the services of Dr Neil Trivett as an independent consultant. This offer was accepted by the meeting.

This document is provided by JAXA.

Mem. Natl Inst. Polar Res., Spec. Issue, 54, 91-99, 2001

Scientific paper

Black carbon and ionic species in the Arctic aerosol

K. Eleftheriadis[1], S. Nyeki[2,3], K. Tørseth[4] and I. Colbeck[2]

[1]*Institute of Nuclear Techn.- Radiation. Protection, National Center for Scientific Research "Demokritos", 15310 Agia Paraskevi Attikis, Greece*
[2]*Institute for Environmetal Research, University of Essex, Colchester/Essex, England*
[3]*Paul Scherrer Institute, CH-5232 Villigen PSI, Switzerland*
[4]*NILU, P.O. Box 100, N-2007 Kjeller, Norway*

Abstract: Previous studies on Arctic aerosol characteristics have shown a pronounced winter-spring maximum and summer-autumn minimum in aerosol concentration. Measurements of black carbon concentration in the atmospheric aerosol were obtained by means of an aethalometer at the Zeppelinfjellet station Ny-Ålesund, Svalbard. Simultaneous 24 hour measurements of the concentration of key aerosol species like sulphate, ammonium and nitrate together with sulphur dioxide, conducted by NILU are presented and discussed in order to evaluate the transport processes governing their presence in the High Arctic. Large variations are seen to be superimposed on an overall trend that apparently exhibits higher values in winter than in late summer. Back trajectory analysis of the airmasses arriving at Zeppelin station, reveals that enhanced concentrations observed for black carbon and sulphate are associated with long range transport of polluted air from Eurasia. Black carbon, sulphur dioxide and sulphate concentrations are correlated well. Nitrate and ammonium display a rather poor association with the above species and between each other.

1. Introduction

The term Black Carbon (BC) is commonly used in the literature to describe the optically absorbing part of carbonaceous aerosols. It is produced during the incomplete combustion of fossil and other fuels as well as biomass burning. In remote regions the concentration of BC in the air is an excellent tracer of aerosol derived from anthropogenic emissions. Fossil fuel and biomass combustion is the only source of BC in the atmosphere and its concentration is dependent on transport and physical removal processes (see *e.g.* Penner and Eddleman, 1993). Its lifetime in the atmosphere is variable depending on its ability to: 1) mix with other aerosols (coagulation), 2) interact chemically with gaseous species and 3) become hygroscopic and absorb water. These processes are not yet fully understood but it is recognized that freshly emitted BC aerosol is a reducing agent in the atmosphere. Freshly emitted BC particles play an important role in heterogeneous chemical reactions due to its large surface area and the formation of functional groups (*e.g.* carboxylic) on its surface (Lary *et al.*, 1999). During its lifetime in the atmosphere, BC surface is chemically modified, it becomes hygroscopic and can be activated as CCN (Chughtai *et al.*, 1996). It gradually becomes "inert" as the aerosol ages in the atmosphere. Previous

This document is provided by JAXA.

studies on Arctic aerosol characteristics have shown a pronounced winter-spring maximum and summer-autumn minimum in aerosol concentration as a result of long-range transport from industrial regions and relatively inefficient atmospheric removal processes. The present work aims to comment on the transport and evolution processes of atmospheric aerosol in the Arctic, by studying the variation in concentration of key aerosol species. In the case of black carbon its mass is chemically conserved (affected only by physical removal processes) while other species namely SO_2 and SO_4, have their concentration governed by chemistry through gas to particle conversion as well as the physical removal processes. Apart from the fact that such measurements in the Arctic are lacking, they facilitate the study of aged aerosol properties by allowing the investigation of these species after long range transport in the absence of intermediate range sources.

2. Experimental

Measurements of BC concentration in the atmospheric aerosol were obtained by means of an aethalometer (Magee AE-9) at the Zeppelinfjellet station (474 m asl; 78°54′N, 11°53′E), Ny-Ålesund, Svalbard. Two intensive field campaigns were conducted in August 1998 and May 1999, and continuous measurements of BC occurred from the first campaign to June 1999. The aethalometer continuously monitors the attenuation of light through an aerosol loaded filter in comparison to a reference value from a particle-free section of the filter. The instrument is calibrated so that the BC mass is calculated from the relationship:

$$\text{BC mass/filter unit area: } BC_m = ATN/\alpha_{API},$$

where $ATN = -100 \ln(I/I_0)$, I_0=transmitted light intensity through a blank portion of filter material, I=transmitted light intensity through a portion of aerosol loaded filter material, and α_{API} is the absorption efficiency of BC aerosol on the filter.

The value for α_{API} provided by the manufacturer is 19 $m^2\ g^{-1}$. The data reported here are based on this value. However, it has been recognized that these settings are specific for a given sampling site and aerosol type. In remote areas this value is expected to be lower resulting in higher BC mass concentrations from those reported here for Ny-Ålesund (Petzold and Niessner, 1995). Thermal analyses of the filter samples are currently being performed, so that in future work a correction factor can be applied to presented data. The concentration of inorganic aerosol species and their gaseous precursors were obtained by measurements performed at Ny-Ålesund by NILU. Details about the methodology used, are found in Tørseth *et al.* (2000). Air is sampled on a 24 hour basis by a low volume sampler utilising a three stage filter pack. A teflon filter on the first stage collects the aerosol while the second and third stage consist of Whatman 40 filters impregnated with potassium hydroxide for acidic gas collection and oxalic acid for alkaline gas collection, respectively. Samples are analysed by Ion Chromatography for sulphate, nitrate and ammonium. Results allow the concentrations of particulate sulphate and gaseous sulphur dioxide to be determined. The sampler's configuration does not permit distinction between nitric acid and particulate nitrate or ammonia and particulate ammonium. The results for these species are expressed as total nitrate and total ammonium. Meteorological parameters like temperature, pressure and relative humidity are also monitored by NILU at Ny-Ålesund and are utilized in the present work. Back trajectory analysis was also performed on selected periods of

This document is provided by JAXA.

frequent pollution episodes identified by high BC concentrations (January to March). Back trajectories for Ny-Ålesund were calculated by means of the NOAA developed model (HYSPLIT4 model, 1997). The model can be used for trajectory and concentration calculations. It employs a hybrid method between Eulerian and Langrangian approaches, in that advection and diffusion are calculated in a Langrangian framework, whereas concentrations are calculated on a fixed grid. Advection and diffusion are modeled so that "particle" dispersion is employed in the vertical direction and puff dispersion in the horizontal. The model requires gridded meteorological data as input, which are mapped on an internally defined grid system. Map projections such as mercator or polar stereographic are employed. In the vertical, a terrain-following co-ordinate system is used. A library, containing gridded land use and roughness length data for the whole globe with a resolution of 1×1 degree, is incorporated in the calculations. The model also calculates vertical mixing and stability. The calculations performed here used the NFL meteorological data, available at the NOAA web site, which cover the whole globe and are interpolated from global measurements. The model was run for the Zeppelin station altitude (475 m a.s.l.) and for at least a 5 days period in time.

3. Results

The results for BC, sulphate, sulphur dioxide, nitrate and ammonium are presented in Fig. 1. Sulphate and sulphur dioxide are presented as sulphur mass concentration while nitrate and ammonium are expressed as the sum of gaseous (HNO_3 and NH_3) and aerosol ionic component concentrations, respectively. The winter period of measurements between October and June is presented here in order to evaluate long range transport events. Large variations are seen to be superimposed on an overall trend of increasing concentrations from October to March, and decreasing from April to June. The mass concentration levels for BC and inorganic species are comparable to those reported by Worthy *et al.* (1994) and Jaeschke *et al.* (1999), respectively. Some distinct features for the presented aerosol species can be derived from Fig. 2 where 30-day running mean values of the concentrations are displayed together with the water-mixing ratio. It is observed that changes in the general trends of the concentrations of ammonium, sulphate and SO_2 occur when sunlight returns to the Arctic. Higher photochemical conversion rates of SO_2 to sulphate lead to the latter becoming the dominant sulphur component during spring in contrast to the dark period of the year. This is a general feature in the Arctic also observed at Alert (Sirois and Barrie, 1999). It has to be noted that the other oxidation path of SO_2 to sulphate through diffusion of SO_2 in aerosol droplets is continuously contributing to sulphate conversion to a certain extent. It is not clear how the increased ammonia/ammonium values during the same period are associated to the sulphur compounds. However, high ammonium concentrations associated with sulphate were linked by Jaeschke *et al.* (1999) to long range transported pollutants from Siberia. The water-mixing ratio was calculated from meteorological parameters. It is evident that low values of the examined species are associated with humid airmasses indicating increased aerosol washout. It has to be noted that aerosol in-cloud scavenging was observed at the measuring site on Zeppelin mountain to have the strongest effect on aerosol number concentration and BC mass concentration. Table 1 displays the correlation coefficients between the examined species. BC and sulphate concentrations are

This document is provided by JAXA.

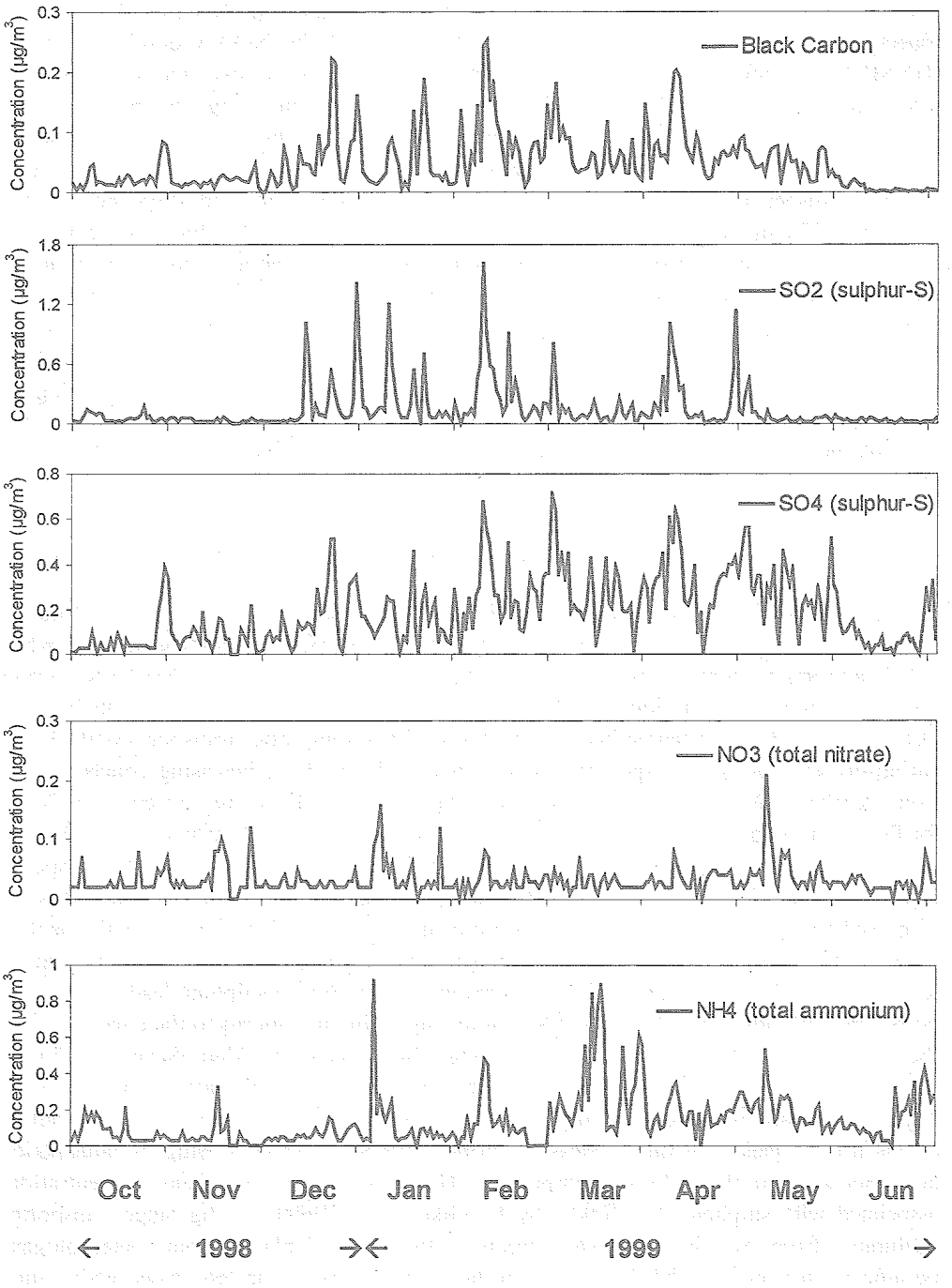


Fig. 1. Time series of Black Carbon, sulphur dioxide, sulphate, total nitrate and total ammonium 24 hour mass concentration ($\mu g\ m^{-3}$) from October to June at Zeppelin station, Ny-Ålesund.

This document is provided by JAXA.

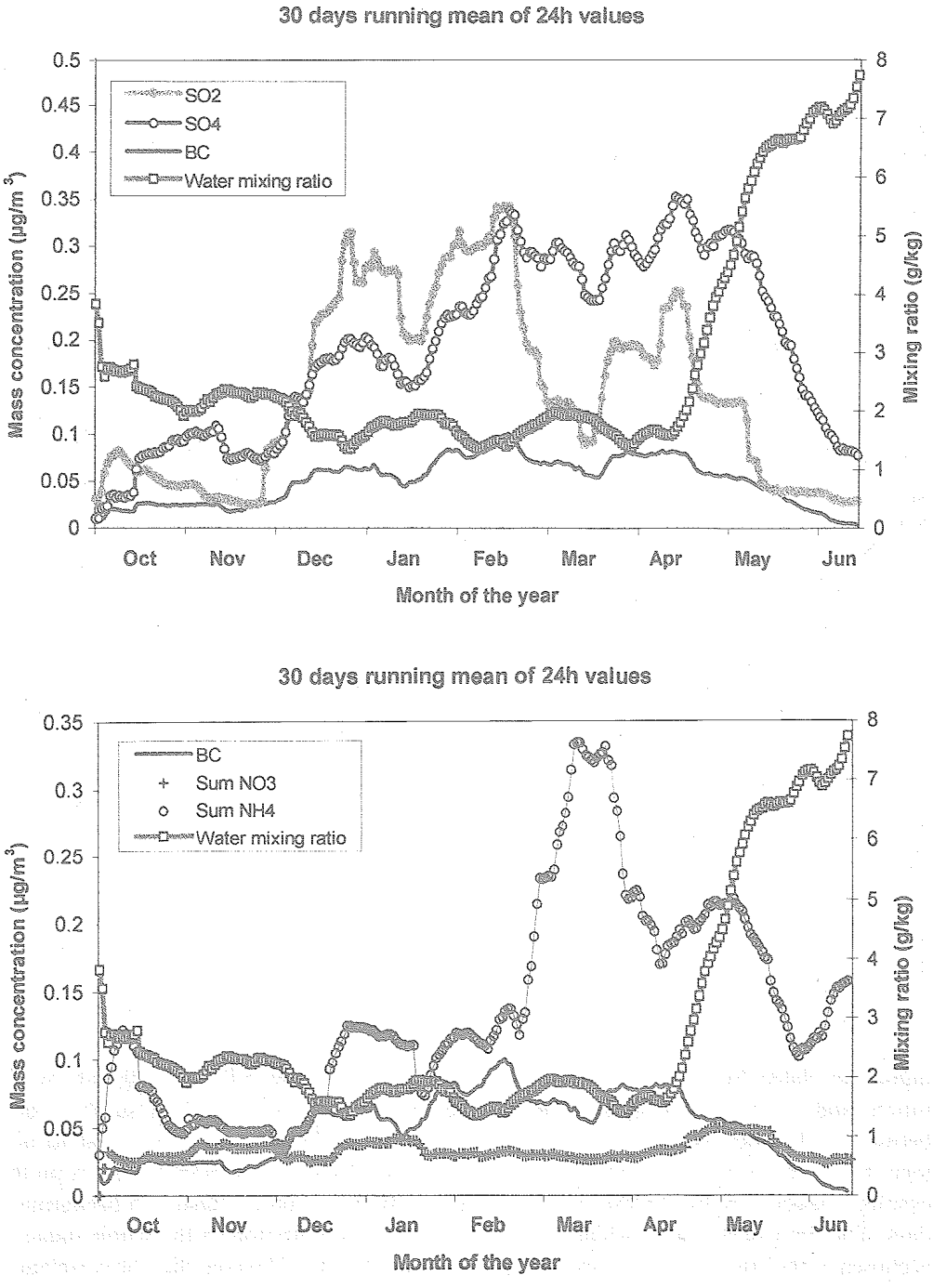


Fig. 2. Black Carbon, sulphur dioxide, sulphate, total nitrate and total ammonium running mean mass concentration ($\mu g\ m^{-3}$) for a 30 days time window, from October to June at Zeppelin station, Ny-Ålesund.

This document is provided by JAXA.

Table 1. Correlation coefficients among the 24 h concentrations of aerosol and gaseous species measured at Ny-Ålesund from October to June.

Correlation coefficient	SO_2	SO_4	Sum NO_3	Sum NH_4	BC	H_2O Mixing ratio
SO_2	1.00					
SO_4	0.54	1.00				
Sum NO_3	0.11	0.26	1.00			
Sum NH_4	0.16	0.38	0.30	1.00		
BC	0.63	0.76	0.15	0.28	1.00	
H_2O Mixing ratio	−0.30	−0.15	0.12	−0.01	−0.29	1.00

Table 2. Correlation coefficients among the 24 h concentrations of aerosol and gaseous species measured at Ny-Ålesund from October to June for the cases with BC concentrations above 50 ng/m³.

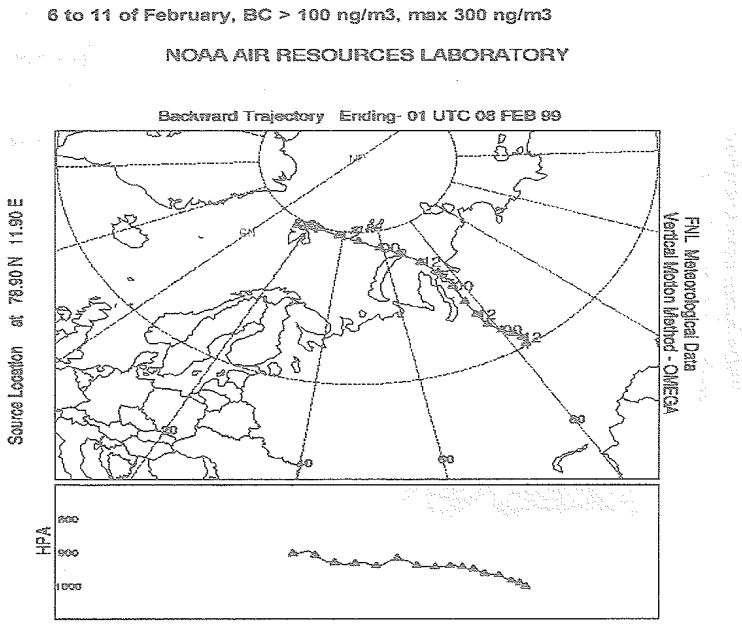
Correlation coefficient	SO_2	SO_4	Sum NO_3	Sum NH_4	BC	H_2O Mixing ratio
SO_2	1.00					
SO_4	0.48	1.00				
Sum NO_3	0.02	0.15	1.00			
Sum NH_4	0.12	0.37	0.40	1.00		
BC	0.58	0.61	0.04	0.24	1.00	
H_2O Mixing ratio	−0.28	−0.20	0.27	0.07	−0.26	1.00

Table 3. Correlation coefficients among the 24 h concentrations of aerosol and gaseous species measured at Ny-Ålesund from October to June for the cases with BC concentrations below 50 ng/m³.

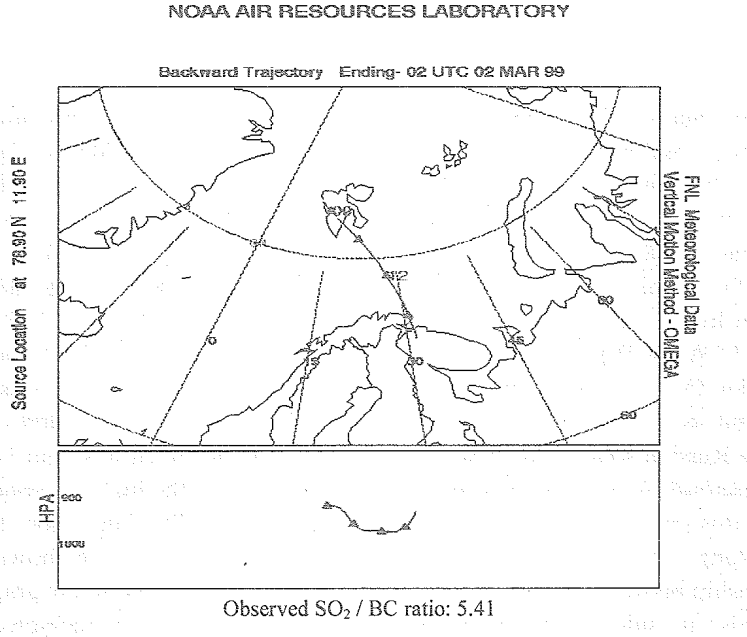
Correlation coefficient	SO_2	SO_4	Sum NO_3	Sum NH_4	BC	H_2O Mixing ratio
SO_2	1.00					
SO_4	0.08	1.00				
Sum NO_3	0.06	0.21	1.00			
Sum NH_4	−0.01	0.27	0.16	1.00		
BC	0.31	0.59	0.15	0.23	1.00	
H_2O Mixing ratio	−0.12	0.15	−0.07	−0.02	−0.26	1.00

highly correlated. Sulphur dioxide shows a weaker correlation with BC and sulphate, while nitrate and ammonium display a rather poor association with BC and sulphate and between each other. Nitrate is the only component, which cannot be associated to any identified event of pollutant long-range transport. The effects of long range transport on the examined species are further explored by the correlation tests on polluted and background days. The limit of 50 ng/m³ which is the average BC concentration of the whole data-set, is chosen as the criterion for this exercise (Tables 2 and 3). It is observed that the correlation coefficients calculated for the polluted days are very similar to those observed for the complete data-set. On the other hand, for the periods with background BC values they appear low for all species with the exception of the pair BC-SO_4. This indicates that the lifetime of these species is governed by the same atmospheric processes. Airmass back

This document is provided by JAXA.



Observed SO_2 / BC ratio: 6.69



Observed SO_2 / BC ratio: 5.41

Fig. 3. Examples of airmass back trajectories associated with high BC concentrations at Ny-Ålesund, coinciding with the two main air pollution sources for the High Arctic, the industrial complexes at Norilsk and Kola peninsula of Russia. Back trajectories performed by means of the NOAA Hysplit model through their network service.

This document is provided by JAXA.

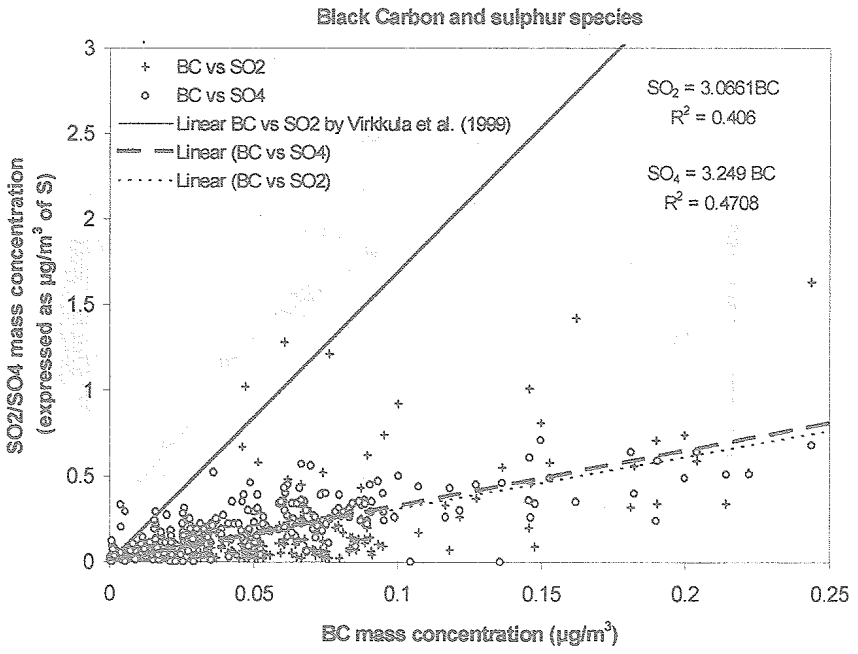


Fig. 4. Linear regression results for the pairs BC-SO_2 and BC-SO_4. The relationship between BC-SO_2 based on the measured BC data and the SO_2 calculated from their ratio observed near the emission sources at the Kola peninsula is also presented.

trajectory analysis for Zeppelin station, reveals the expected association of enhanced concentrations observed for BC and sulphate with long range transport of polluted air from Eurasia. A simplified approach for estimation of air mass origin was followed for the months with highest BC concentrations observed (December–April). The origin of an air mass was classified according to major geographical sectors, when 75% of the trajectory points fall within a sector. These sectors were selected as follows (defined by the region between longitude intervals): Russian (30°E–130°E), North Pacific (130°E–130°W), American (130°W–60°W), Atlantic (60°W–5°W), European (5°W–30°E). An additional sector, the Polar Oceanic region, was defined as the area north of 80°. It was found that the dominant sectors was the Polar Oceanic region which accounted for 40% of the trajectories and the Russian sector with 31%. All other sectors contributed less than 12%, while 18% of the trajectories were of mixed origin. It is concluded that the high BC concentration events during this period originate almost exclusively from the Russian sector. Two examples of major long range transport events identified during this study are shown in Fig. 3. The relationship between the two sulphur species and BC is explored in the graph of Fig. 4. The graph also includes the estimated BC mass concentration for the measured SO_2 concentrations when the ratio SO_2/BC, reported by Virkkula *et al.* (1999) and found equal to 16 at Sevettijarvi near the industrialised Kola peninsula, is utilised. There is lack of other such measurements near the Russian pollution source areas. Penner and Eddleman (1993), have constructed a model for BC global concentration estimates based on the BC/SO_2 ratio. For

This document is provided by JAXA.

the whole of Russia they assume this ratio to be equal to 3. The average SO_2/BC ratio derived from Fig. 4 is very close to this figure. Long term measurements of BC concentration along with that of the sulphur species at Ny-Ålesund are needed in order to explore the significance of this ratio as a characteristic feature of the arctic aerosol.

Acknowledgments

Our thanks are extended to the staff at the Norwegian Polar Institute and NILU. The financial support of the EU funded Ny-Ålesund LSF project is greatly acknowledged.

References

Chughtai, A.R., Brooks, M.E. and Smith, D.M. (1996): Hydration of black carbon. J. Geophys. Res., **101**, 19505–19514.

Jaeschke, W., Salkowski, T., Dierssen, J.P., Trumbach, J.V., Krischke, U. and Gunther, A. (1999): Measurements of trace substances in the Arctic troposphere as potential precursors and constituents of Arctic Haze. J. Atmos. Chem., **34**, 291–319.

HYSPLIT4 (HYbrid Single-Particle Lagrangian Integrated Trajectory) Model (1997): Web address: http://www.arl.noaa.gov/ready/hysplit4.html, NOAA Air Resources Laboratory, Silver Spring, MD.

Lary, D.J., Shallcross, D.E. and Toumi, R. (1999): Carbonaceous aerosols and their potential role in atmospheric chemistry. J. Geophys. Res., **104**, 15929–15940.

Penner, J.E. and Eddleman, H. (1993): Towards the development of a global inventory for Black Carbon emissions. Atmos. Environ., **27A**, 1277–1295.

Petzold, A. and Niessner, R. (1995): Method Comparison study on soot-selective techniques. Microchim. Acta, **117**, 215–237.

Sirois, A. and Barrie, L.A. (1999): Arctic lower tropospheric aerosol trends and composition at alert, Canada: 1980–1995. J. Geophys. Res., **104**, 11599–11618.

Tørseth, K., Semb, A., Schaug, J., Hanssen, J.E. and Aamlid, D. (2000): Proceses affecting deposition of oxidised nitrogen and associated species in the coastal areas of Norway. Atmos. Environ., **34**, 207–217.

Virkkula, A., Aurela, M. Hillamo, R., Makela, T., Pakkanen, T., Kerminen, V., Maenhaut, W., Francois, F. and Cafmayer, J. (1999): Chemical composition of atmospheric aerosol in the European subarctic. J. Geophys. Res., **104**, 23681–23696.

Worthy, D.E.J., Trivett, N.B.A., Hopper, J.F., Bottenheim, J.W. and Levin, I. (1994): Analysis of long range transport events at Alert, Northwest territories during the Polar Sunrise Experiment. J. Geophys. Res., **99**, 25329–25344.

(Received April 10, 2000; Revised manuscript accepted November 13, 2000)

This document is provided by JAXA.

This document is provided by JAXA.

Mem. Natl Inst. Polar Res., Spec. Issue, 54, 101-106, 2001

Report

Arctic study of tropospheric aerosol and radiation, ASTAR 2000-field plan

Takashi Yamanouchi[1] and Andreas Herber[2]

[1]*National Institute of Polar Research, Kaga 1-chome, Itabashi-ku, Tokyo 173-8515 (yamanou@pmg.nipr.ac.jp)*
[2]*Alfred-Wegener Institute for Polar and Marine Research, Am Handelshafen 12, 27570 Bremerhaven, Germany (aherber@awi-bremerhaven.de)*

Abstract: A new German-Japanese cooperative project on aerosols in the Arctic, ASTAR 2000 (Arctic Study of Tropospheric Aerosol and Radiation) is to be carried out in March and April 2000 in the high Arctic region (vicinity of Svalbard). The goal of the project is to investigate the behavior, properties and radiative forcing of tropospheric aerosols in the Arctic with special focus on the "Arctic Haze".

Airborne observations of vertical distribution of physical, chemical and optical properties of aerosols will be performed using Dornier 228 aircraft of Alfred-Wegener Institute for Polar and Marine Research. Extinction coefficients will be measured by sunphotometer. *In-situ* measurements and sampling of aerosols will also be made. Fifteen flights with about 75 flight hours are planned to be conducted based at Longyearbyen airport (78°N, 15°E) during March 15 and April 25, 2000.

Coordinated remote sensing by lidar and photometers, *in situ* measurements and sampling of aerosols will be done at the surface at Ny-Ålesund Scientific Station (78°55′N, 11°56′E), Svalbard. Also, balloon-borne aerosol sondes will be launched. Data are compared with the SAGE II (Stratospheric Aerosol and Gas Experiment) satellite measurements. These data will be used as input parameters for an Arctic regional climate model to calculate the radiative forcing of aerosols and to subsequently study their climatic impact.

1. Introduction

The polar regions are receiving increased attention in climate change scenarios obtained from climate models. This attention arises from the "polar amplification" of the surface warming in simulations with increased concentrations of greenhouse gases. The zonally averaged warming in the Arctic is two or three times larger than the global warming for a doubling of CO_2 (Randall *et al.*, 1998; IPCC, 1996). The enhanced warming in high latitudes is partly attributable to the retreat of sea ice, which is accelerated by the positive feedback between temperature and surface albedo (Walsh and Chapman, 1998). Recently, large variations in many climate parameters have been found in the "Changing Arctic" (Morison *et al.*, 1998; Heintzenberg, 1989). Warming of the air temperature near the surface is clearly observed, especially over the continent (Chapman and Walsh, 1993), and thinning of sea ice in the 1990s is reported for a wide area of the Arctic Ocean (Rothrock *et al.*,

This document is provided by JAXA.

1999).

Aerosols, together with clouds, are believed to have a strong impact on climate through the radiative effect with a large spatial variability; however, their 3-D distribution and interactions are still uncertain, especially in the polar regions. In the Arctic, concentrations of normal background aerosols are very low and optical thickness in the 500 nm range is in the range 0.03 to 0.05 (Herber *et al.*, 1996). However, strong seasonal variations in aerosol optical depth are known and the large spring increase is due to high concentrated layered aerosols called "Arctic Haze" (Shaw, 1995; Herber *et al.*, 1996). This large spring maximum of aerosol loading is originated from anthropogenic sources surrounding the Arctic, and trapped a long time in the strong inversion layer over the Arctic Ocean without any effective removal process (Shaw, 1995). Though this is only a seasonal phenomenon, its radiative effect is not negligible, because solar radiation becomes effective just in this season after the long polar night and a large influence might be expected related to the melting and decay of sea ice. Many observational studies have been devoted to the Arctic Haze (Bodhaine and Dutton, 1993; Jaeschke *et al.*, 1999); however, not so much has been done concerning the radiative effect yet.

Radiative forcing of atmospheric aerosols has been investigated by using very simplified models of aerosol optical properties. In this stage, the aerosol data used have been based on the Global Aerosol Data Set (GADS), see Koepke *et al.* (1997), which only considered the total aerosol optical depths and a homogeneous distribution of aerosols for the whole Arctic region. Simplified studies of radiative forcing for the Arctic Haze periods have provided a qualitative evidence of aerosol impact. Nevertheless these results have already shown that aerosols might have a significant impact on radiative forcing processes in the troposphere. Unfortunately, consistent data records are not yet available for all regions and areas of interest.

A new cooperative project on aerosols in the Arctic, ASTAR 2000 (Arctic Study of Tropospheric Aerosol and Radiation) is planned for March and April 2000 in and around Svalbard to investigate the 3-D behavior and radiative effects of tropospheric aerosols in the Arctic and their impact on climate. Airborne observations of vertical distributions of physical, chemical and optical properties of aerosols will be made around Svalbard using a Dornier 228 aircraft (Polar 4) of Alfred-Wegener Institute for Polar and Marine Research operated from Longyearbyen airport. Also, coordinated remote sensing of aerosols, *in-situ* measurements and sampling of aerosols will be done at the international research site, Ny-Ålesund, Svalbard (Fig. 1). At this site, scientists from several countries including German and Japanese scientists have already conducted ground based atmospheric science observations for about 10 years (Gernandt *et al.*, 2001; Yamanouchi *et al.*, 1996). Satellite measurements of SAGE-II (Stratospheric Aerosol and Gas Experiment) are also included as part of the ASTAR 2000 campaign. Finally, data will be used as input for regional climate model studies (HIRHAM) to estimate radiative forcing and discuss the climatic impact of aerosols in the Arctic atmosphere.

The project is co-organized by the National Institute of Polar Research (NIPR) and Alfred-Wegener Institute for Polar and Marine Research (AWI), with participants from Hokkaido University, Nagoya University, NASA Langley Research Center, Norwegian Institute for Air Research (NILU), Meteorological Institute of Stockholm University (MISU), Norwegian Polar Institute (NP), National Oceanic and Atmospheric Administra-

This document is provided by JAXA.

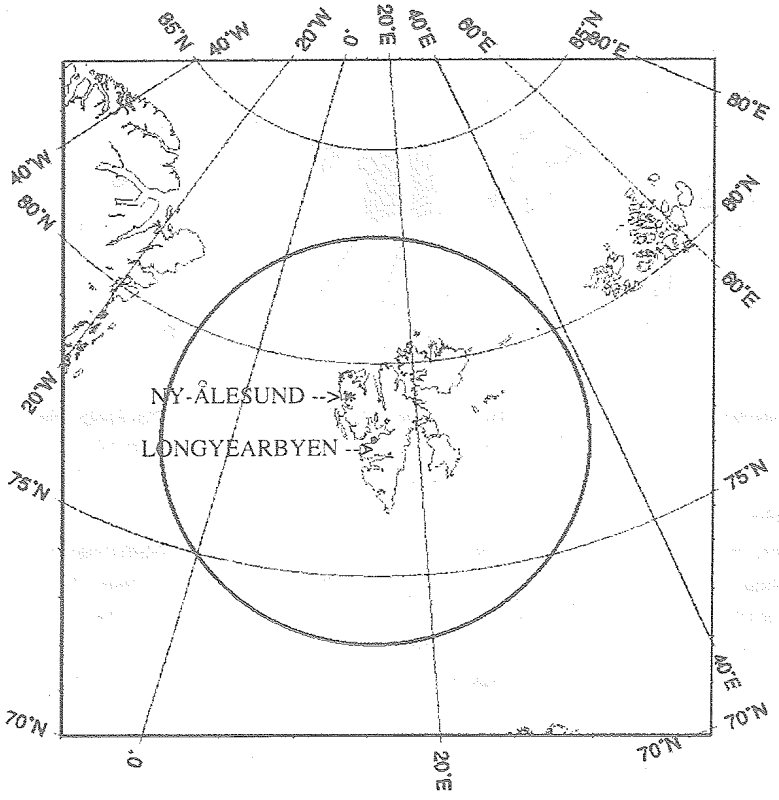


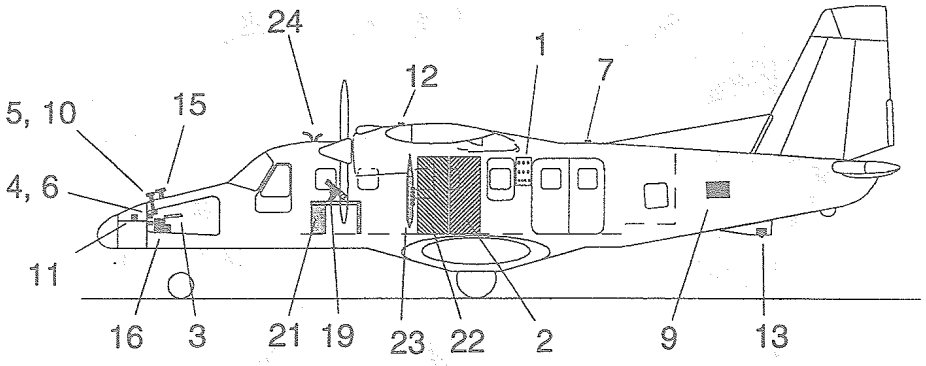
Fig. 1. Map showing the ground-based observation site, Ny-Ålesund, and base of airborne observation, Longyearbyen. Also shown is a circle with maximum flight radius.

tion (NOAA), Max Planck Institute for Aeronomie (MPAe) and with contributions from German Aerospace (DLR) and Aerodata Braunschweig (AD).

2. Airborne observations

Airborne observations using Dornier 228 aircraft of Alfred-Wegener Institute for Polar and Marine Research (AWI) are to be the crucial experimental part of the project. A sunphotometer will be used for the measurement of solar radiance to derive optical depth and extinction coefficients, and also for the measurement of sky brightness in the almucanter plane to derive the scattering phase function. The sunphotometer will be installed in the plane on a solar tracker behind a quartz window, which was prepared specially for optical measurements. The sunphotometer is to be adjusted to the direction of the sun, 80 degrees apart from the plane heading and the solar height should be between 15° to 7° for the extinction measurement. By rotating the heading of the air plane 180 degrees, horizontal scan for brightness measurement in the same zenith angle will be made. Downward and upward shortwave and longwave radiation fluxes will be measured by broad band radiometers settled on the roof and bottom of the plane. *In-situ* measurements of aerosols

This document is provided by JAXA.



Basic Equipment:
1 Central Data Interface
2 Rack
3 Pitot Tube
4 Pressure Transducer
5 Temperature Sensor
6 Electrical Distribution
7 GPS Antenna
9 INS

Humidity Sensor System:
10 Humidity Sensor
11 Signal Amplifier

Radiation Sensors:
12 Pyranometer and Pyrgeometer Top
13 Pyranometer and Pyrgeometer Bottom

Dew Point Mirror:
15 Sensor
16 Power Supply and Control Units

Sun Photometer:
19 Photometer Unit
21 Photometer Desk

NIPR Systems:
22 Rack with instruments
23 Diffuser
24 Air Inlet

Fig. 2. Instrumentation of Polar 4 for ASTAR 2000 campaign.

are to be made; particle size distribution, absorption and scattering coefficients will be measured by optical particle counters (OPCs), a particle soot absorption photometer (PSAP) and an integrating nephelometer (IN), respectively. Aerosols will also be sampled with a low volume filter sampler and aerosol impactor to conduct chemical analyses and electron microscope analyses. As shown in Fig. 2, air is introduced to the diffuser from the intake settled at the roof of the plane, and then guided to each instrument. Data from all the instruments are to be recorded in a central data recorder together with flight information and basic meteorological parameters such as pressure, temperature, relative humidity, dew point and wind velocity.

Using Longyearbyen airport (78°N, 15°E) as the operational base, 16 flights with about 80 flight hours were scheduled for the period from March 15 until April 25, 2000. The aircraft observations consist of three phases: phase I for special closure observations with ground based observations at Ny-Ålesund, phase II for the haze observations and phase III for comparison with SAGE II satellite observations. Those flights will be made in small target areas depending on the objective within about 500 km from Longyearbyen, as shown in Fig. 1. In the target area, a vertical profile from near the surface up to 8 km is to be measured with the level flight at 1 km altitude intervals.

This document is provided by JAXA.

3. Ground-based and *in-situ* observation

The airborne measurements are complemented by comprehensive ground-based measurements, providing such crucial aerosol parameters as phase fuction and absorption coefficients as a function of height. Coordinated ground-based remote sensing, *in-situ* measurements, sampling and balloon-borne observations of aerosols will be performed at the surface, at the international research site, Ny-Ålesund (78.95°N, 11.93°E; Fig. 1).

In 1991, regular measurements of aerosols commenced at Ny-Ålesund. Since then observations have been improved and extended by newly developed instruments, such as sun and star photometers, to retrieve the aerosol optical depth and phase function in the visible and near infrared spectral range, the tropospheric Raman-lidar to measure extinction coefficients and depolarization as a function of altitude, and the Fourier transformed infrared spectrometer (FTIR) to calculate the aerosol optical depth in the IR spectral range by measuring emission spectra. Additional new systems are a micropulse lidar for backscatter measurement and sky radiometers for extinction and phase function measurements.

In-situ measurements will be made by optical particle counters (OPCs), integrating nephelometer and particle mobility analyzer. Ground sampling of aerosols will be done by high volume and low volume samplers and an aerosol impactor. Balloon-borne aerosol sondes with OPC will be launched and a tethered balloon with OPC will be used to obtain the vertical distribution of aerosol particle concentration in the atmosphere close to the surface. Supporting data will be include surface ozone measured by Dasibi ozone meter, precipitable water amount and liquid water content by microwave radiometer, precipitation by POSS, surface radiaitive fluxes by BSRN (Baseline Surface Radiation Network) radiometers and aerological soundings. At the Zepelin mountain station (470 m a.s.l.), *in-situ* measurements and samplings of aerosols will also be made.

4. Satellite observations and model studies

SAGE-II (Stratospheric Aerosol and Gas Experiment) satellite observations of stratospheric aerosols are used to separate the tropospheric contribution from total atmospheric aerosol burden and provide information on spatial distributions in the Arctic region (McCormick, 1987). Also, satellite extinction measurement will be validated from airborne measurement data. A combination of all of these methods is recently used to obtain as much information as possible on temporal and vertical distributions of atmospheric aerosols and their optical properties.

For detailed model studies it is necessary to provide data on the temporal and spatial—in particular—vertical distribution of aerosols. Furthermore, optical parameters such as spectral optical depth, extinction coefficient, absorption coefficient, and phase function have to be measured. For all of these parameters a large number of different methods and instruments are used, including satellite information, like SAGE-II. There is not yet a clear understanding of the impact of tropospheric aerosols on radiative forcing processes in the Arctic. All these aerosol data will then be incorporated in to the HIRHAM Arctic regional climate model (Dethloff *et al.*, 1996) for detailed model studies on the direct radiative forcing of Arctic tropospheric aerosols.

This document is provided by JAXA.

Acknowledgments

This work is to be supported by Special Scientific Research Program (No. 11208201) and Grant-in-Aid (No. 10144103) from the Ministry of Education, Science, Sports and Culture of Japan.

References

Bodhaine, B.A. and Dutton, E.G. (1993): A long-term decrease in Arctic-Haze at Barrow, Alaska. Geophys. Res. Lett., **20**, 947–950.

Chapman, W.L. and Walsh, J.E. (1993): Recent variations of sea ice and air temperature in high latitudes. Bull. Am. Meteorol. Soc., **74**, 33–47.

Dethloff, K., Rinke, A., Lehmann, R., Christensen, J.H., Botzet, M. and Machenhauer, B. (1996): Regional climate model of the Arctic atmoshere. J. Geophys. Res., **101**, 23401–23422.

Gernandt, H., Neuber, R. and Von der Gathen, P. (2001): Recent contributions to long-term atmospheric studies at Koldewey-Station. Mem. Natl Inst. Polar Res., Spec. Issue, **54**, 49–63.

Herber, A., Thomason, L.W., Dethloff, K., Viterbo, P., Radionov, V.F. and Leiterer, U. (1996): Volcanic perturbation of the atmosphere in both polar regions: 1991–1994. J. Geophys. Res., **101**, 3921–3928.

Heintzenberg, J. (1989): Arctic Haze: Air pollution in the polar region. AMBIO, **18**, 50–55.

IPCC (1996): Climate Change 1995: The Scince of Climate Change. Cambridge University Press, 572 p.

Jaeschke, W., Salkowski, T., Dierssen, J.P., Trumbach, J.V., Krischke, U. and Gunther, A. (1999): Measurements of trace substances in the Arctic troposphere as potential precursors and constituents of Arctic haze. J. Atmos. Chem., **34**, 291–319.

Koepke, M., Heß, M., Schult, I. and Shettle, E.P. (1997): Global Aerosol Data Set. MPI Rep., **243**, 75 p.

McCormick, M.P (1987): SAGE II: An overview. Adv. Space Rev., **7**, 319–326.

Morison, J., Aagaard, K. and Steele, M. (1998): Report on Study of the Arctic Change Workshop held November 10–12, 1997, University of Washington, Seattle, Washington. Report No. 8, Polar Science Center, Applied Physics Laboratory, University of Washington, 34 p.

Randall, D., Curry, J., Battisti, D., Flato, G., Grumbine, R., Hakkinen, S., Martinson, D., Preller, R., Walsh, J. and Weatherly, J. (1998): Status and outlook for large scale modeling of atmosphere-ice-ocean interactions in the Arctic. Bull. Am. Meteorol. Soc., **79**, 197–219.

Rothrock, D.A., Yu, Y. and Maykut, G.A. (1999): Thinning of the Arctic sea-ice cover. Geophys. Res. Lett., **26**, 3469–3472.

Shaw, G.E. (1988): Antarctic aerosols: A review. Rev. Geophys., **26**, 89–112.

Shaw, G.E. (1995): The Arctic haze phenomenon. Bull. Am. Meteorol. Soc., **76**, 2403–2413.

Walsh, J.E. and Chapman, W.L. (1998): Arctic cloud-radiation-temperature associations in observational data and atmospheric reanalyses. J. Clim., **11**, 3030–3045.

Yamanouchi, T., Aoki, S., Morimoto, S. and Wada, M. (1996): Report of atmospheric science observations at Ny-Ålesund, Svalbard. Mem. Natl Inst. Polar Res., Spec. Issue, **51**, 153–163.

(Received April 28, 2000; Revised manuscript accepted June 8, 2000)

This document is provided by JAXA.

Mem. Natl Inst. Polar Res., Spec. Issue, 54, 107–111, 2001

Scientific note

Radiative forcing due to anthropogenic activities

F. Stordal[1,2] and G. Myhre[2,1]

[1]*Norwegian Institute for Air Research (NILU), P.O. Box 100, N-2007 Kjeller, Norway*
[2]*Institute for Geophysics, University of Oslo, P.O. Box 1022, Blindern N-0314 Oslo, Norway*

Abstract: A wide range of anthropogenic as well as natural forcing mechanisms may lead to climate change. We present calculations of the radiative forcing due to anthropogenic emissions leading to changes in the concentrations of several trace gases and aerosols. Increase in all major well mixed greenhouse gases are included as well as changes in tropospheric and stratospheric ozone. The radiative forcing due to certain aerosols is also estimated. The calculations have been performed for the Northern Hemisphere, and the main focus in this scientific note is on high latitudes.

1. Introduction

Several climate forcing mechanisms may lead to climate change (IPCC, 1996; Hansen *et al.*, 1998; Shine and Forster, 1999). At present the known anthropogenic forcing mechanisms include well mixed greenhouse gases, ozone, aerosols (direct and indirect effects), and land surface albedo. In this scientific note we point to work that we have already published on the radiative forcing due to several forcing mechanisms. We include also a short description of the radiative transfer models which we have used, in Section 2.

Our results have previously mainly been seen in a global context, whereas we here briefly discuss matters of particular interest for high latitudes in the Northern Hemisphere. Results for each of the individual contributions to the radiative forcing are discussed in Section 3.

2. Radiative transfer models

The radiative forcing is calculated using radiative transfer models. We use an emissivity/absorptivity broad band model for thermal infrared radiation (Myhre and Stordal, 1997). The model includes about 50 absorption bands including all the major greenhouse gases. Clouds are included in the model. For solar radiation a multi-stream model using the discrete ordinate method (Stamnes *et al.*, 1988) is used. Absorption by O_2, O_3, CO_2, and H_2O, Rayleigh scattering, aerosols, and clouds are taken into account. The spectral resolution varies from 1 nm to dividing the spectral interval into 70 regions (see Berntsen *et al.*, 1997; Myhre *et al.*, 1998b for more details).

This document is provided by JAXA.

3. Radiative forcing due to anthropogenic forcing mechanisms

In Table 1 we show estimates of all near present (1995) radiative forcings since industrialization (1750). The numbers are global and seasonal averages. The global distribution of the radiative forcing due to all the anthropogenic contributions discussed in the following is shown in Fig. 1 for seasonally averaged conditions.

3.1. Well mixed greenhouse gases

We have previously established formulas for global radiative forcing as a function of

Table 1. Global-mean radiative forcing in 1995 since industrialization.

Species	Radiative forcing (Wm^{-2})
CO_2	+1.38
CH_4	+0.47
N_2O	+0.12
CFCs	+0.33
Total for well mixed greenhouse gases	+2.30
Stratospheric ozone	−0.15
Tropospheric ozone	+0.38
Total for ozone	+0.23
Sulfate	−0.36
Soot	+0.14
Total for sulfate and soot aerosols (external mixing)	−0.22

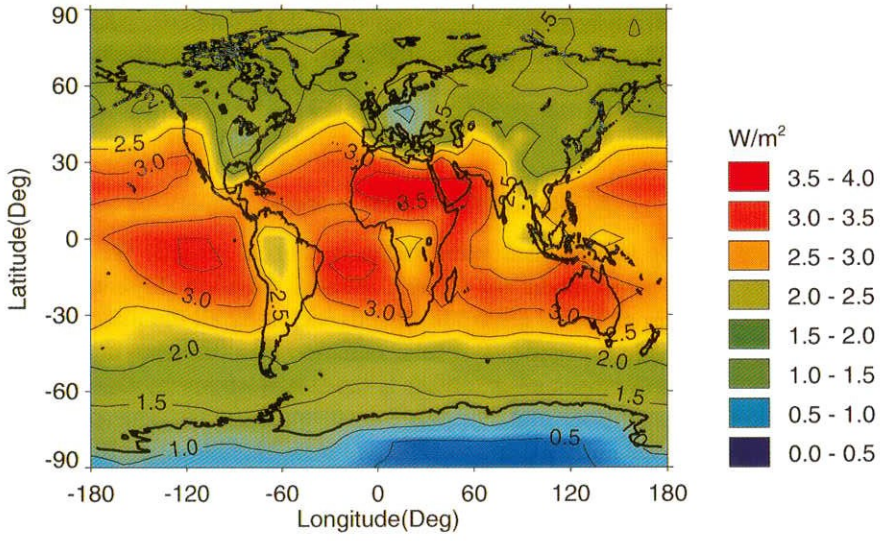


Fig. 1. Radiative forcing due to anthropogenic activity (in Wm^{-2}). The results are for changes in well mixed greenhouse gases, tropospheric and stratospheric ozone, sulfate and soot aerosols from pre-industrial to 1995 conditions.

This document is provided by JAXA.

atmospheric concentrations for the well mixed greenhouse gases (Myhre *et al.*, 1998a) based on calculations with models described in Section 2. We have applied these functions along with changes in the concentrations of well mixed greenhouse gases specified in Hansen *et al.* (1998) to establish the radiative forcing in 1995. CO_2, CH_4, N_2O and a group of halocarbons yield a forcing of 2.30 Wm^{-2}, out of which CO_2 contributes with 1.38 Wm^{-2}. There is a marked latitudinal gradient in the forcing, with largest values in the tropics, due to the large temperature between the warm surface and the cold tropopause region (Myhre and Stordal, 1997). This pattern can clearly be seen in Fig. 1. The forcing at high latitudes in the Northern Hemisphere is about 70% of the global average.

3.2. Ozone

In a recent study we have investigated the evolution of tropospheric ozone and its radiative forcing from 1850 to 1990, due to emissions of ozone precursors (Berntsen *et al.*, 2000), based on the same models as in Berntsen *et al.* (1997). Regional differences in the radiative forcing due to tropospheric ozone are marked, with maxima at longitudes near the regions of maximum emissions of the ozone precursors. The maxima in radiative forcing, which are displaced towards lower latitudes, *e.g.* due to the larger difference in the vertical temperature gradient, as for the well mixed greenhouse gases, can also be seen in Fig. 1. Consequently, the radiative forcing is weak at high northern latitudes. The global radiative forcing is 0.38 Wm^{-2}.

In a recent calculation of the radiative forcing due to change in stratospheric ozone (Myhre *et al.*, 2000), we have adopted the ozone data from the work of Randel and Wu (1999); who developed zonal mean stratospheric ozone changes based on satellite observations and ozone sonde measurements in the polar regions. Long wave and short wave calculations are performed with the models described in Section 2. Strong radiative forcing is found at northern high latitudes, with values between -0.3 Wm^{-2} and -0.4 Wm^{-2}. In the tropical region the radiative forcing is close to zero. The global and annual mean radiative forcing due to change in stratospheric ozone is calculated to -0.15 Wm^{-2}.

3.3. Direct effect of aerosols

Several different aerosol components are of climatic importance, and we have included the direct effect of two types of aerosols in this scientific note, namely sulfate and soot. These are important components of the Arctic ambient particulate matter, e.g. in Arctic haze (see *e.g.* Shaw *et al.*, 1993).

We have previously calculated the value -0.36 Wm^{-2} for the present (1995) forcing due to sulfate (Myhre *et al.*, 1998b). Several recent estimates of the forcing due to sulfate are performed, some in line with this estimate (see discussion in Myhre *et al.*, 1998b) and some with stronger radiative forcing (Haywood and Ramaswamy, 1998; Penner *et al.*, 1998). Uncertainties in representation of hygroscopic effects of the sulfate aerosols and forcing in cloudy areas are major reasons for the large differences found. Likewise, a soot forcing of 0.14 Wm^{-2} based on Myhre *et al.* (1998b) was estimated. This estimate is slightly lower than other estimates (Haywood *et al.*, 1997; Haywood and Ramaswamy, 1998; Penner *et al.*, 1998). Large uncertainties for this aerosol component also exists, mostly related to the mass and the distribution of the soot, optical properties, and mixing with other types of aerosols (Haywood *et al.*, 1997; Myhre *et al.*, 1998b).

This document is provided by JAXA.

Thus, large uncertainties also exist for the forcing at high northern latitudes. In general, the radiative forcing due to the largely scattering sulfate aerosol is reduced at very high latitudes due to the high surface albedo in the areas covered with ice and snow. Conversely, the radiative forcing due to the absorbing soot aerosols is enhanced in the same region.

4. Discussion

There are several features which make radiative forcing values at high northern latitudes deviate from the global averages. The well mixed greenhouse gases are of somewhat less importance due to the lower vertical gradient between the surface and the tropopause. This is the case also for tropospheric ozone, in this case also because of the distance to the regions of emissions of ozone precursors.

Stratospheric ozone changes, on the other hand, maximize at high latitudes and in particular in the Arctic, so the radiative forcing due to depletion of the ozone layer is largest there. Whereas the well mixed greenhouse gases have increased in atmospheric burden since the time of industrialization, the most significant ozone depletion has taken place over only about two decades. Consequently, at high northern latitudes, the heating due to well mixed greenhouse gases has been nearly been balanced by the cooling due to reductions in stratospheric ozone over the last two decades.

Aerosols also play a role in the radiative balance at high northern latitudes, in the so-called Arctic haze events. The uncertainties in the radiative forcing estimates are large, but it is clear that the effect of scattering sulfate aerosols is reduced and the effect of the absorbing soot aerosol is enhanced relative to the globally averaged conditions due to the high local surface albedo.

In the Arctic there is a large seasonal variation in the radiative forcing. This is most noticeable for the forcing due to Arctic haze and changes in stratospheric ozone. The Arctic haze maximizes during the winter and spring. The radiative effect is largest in the visible wavelengths. Consequently it peaks during spring after the winter time polar night (Shaw *et al.*, 1993). Likewise, the radiative effects of changes in stratospheric ozone maximize during spring, which is the time of the strongest ozone depletion, which also depends on solar radiation (see WMO, 1999 and references therein).

Acknowledgments

This work was partly financed by the project PVC funded by the European Commission, and by RegClim, funded by the Norwegian Research Council.

References

Berntsen, T.K., Isaksen, I.S.A., Myhre, G., Fuglestvedt, J.S., Stordal, F., Alsvik Larsen, T., Freckleton, R.S. and Shine, K.P. (1997): Effects of anthropogenic emissions on tropospheric ozone and its radiative forcing. J. Geophys. Res., **102**, 28101–28126.

Berntsen, T.K., Myhre, G., Stordal, F. and Isaksen, I.S.A. (2000): Time evolution of tropospheric ozone and its radiative forcing. J. Geophys. Res., **105**, 8915–8930.

Hansen, J., Sato, M., Lacis, A., Ruedy, R., Tegen, I. and Matthews, E. (1998): Climate forcings in the Industrial era. Proc. Natl. Acad. Sci. USA, **95**, 12753–12758.

This document is provided by JAXA.

Haywood, J.M. and Ramaswamy, V. (1998): Investigations into the direct radiative forcing due to anthropogenic sulfate and black carbon aerosol. J. Geophys. Res., **103**, 6043–6058.

Haywood, J.M., Roberts, D.L., Slingo, A., Edwards, J.M. and Shine, K.P. (1997): General circulation model calculations of the direct radiative forcing by anthropogenic sulfate and fossil-fuel soot aerosol. J. Clim., **10**, 1562–1577.

Intergovernmental Panel on Climate Change (IPCC) (1996): Climate Change 1995: The Science of Climate Change, ed. by J.T. Houghton *et al.* Cambridge, Cambridge Univ. Press, 572 p.

Myhre, G. and Stordal, F. (1997): Role of spatial and temporal variations in the computation of radiative forcing and GWP. J. Geophys. Res., **102**, 11181–11200.

Myhre, G., Highwood, E.J., Shine, K.P. and Stordal, F. (1998a): New estimates of radiative forcing due to well mixed greenhouse gases. Geophys. Res. Lett., **25**, 2715–2718.

Myhre G., Stordal, F., Restad, K. and Isaksen, I.S.A. (1998b): Estimates of the direct radiative forcing due to sulfate and soot aerosols. Tellus, **50**, 463–477.

Myhre, G., Myhre, A. and Stordal, F. (2000): Historical evolution of total radiative forcing. submitted to Atmos. Environ.

Penner, J. E., Chuang, C.C. and Grant, K. (1998): Climate forcing by carbonaceous and sulfate aerosols. Clim. Dyn., **14**, 839–851.

Randel, W.J. and Wu, F. (1999): A stratospheric ozone trends data set for global modeling studies. Geophys. Res. Lett., **26**, 3089–3092.

Shaw, G.E., Stamnes, K. and Hu, Y.X. (1993): Arctic haze: Perturbation to the radiation field. Meteorol. Atmos. Phys., **51**, 227–235.

Shine, K.P. and Forster, P.M. de F. (1999): The effects of human activity on radiative forcing of climate change: a review of recent developments. to be published in Global and Planetary Change.

Stamnes, K., Tsay, S.-C., Wiscombe, W. and Jayaweera, K. (1988): A numerically stable algorithm for discrete-ordinate- method radiative transfer in multiple scattering and emitting layered media. Appl. Opt., **27**, 2502–2509.

WMO (1999): Scientific Assessment of Ozone Depletion. Global Ozone Research and Monitoring Project, World Meteorological Organization, Report No. 44.

(Received May 31, 2000; Revised manuscript accepted August 28, 2000)

This document is provided by JAXA.

This document is provided by JAXA.

Mem. Natl Inst. Polar Res., Spec. Issue, 54, 113–123, 2001

Scientific paper

Three years spectral resolved UV-measurements at Koldewey-Station (1997–1999)

Christian Groß, Helmut Tüg and Otto Schrems

Alfred Wegener Institute, Columbusstraße, 27568 Bremerhaven, Germany

Abstract: In May 1997 long-term measurements of spectral resolved UV-B irradiation (wavelength range of the instrument 280 to 322 nm) at the NDSC-Station in Ny-Ålesund (Spitsbergen) were started using a self-developed very fast multichannel spectroradiometer. In March 1998 a multichannel UV-A spectro-radiometer was installed at Ny-Ålesund to supplement the spectral range of the measurements from 318 to 400 nm. For the evaluation of the data with regard to changes in total ozone the ratio of the measured irradiation at two wavelengths (300 nm/320 nm) has been used to minimize the influence of other atmospheric parameters like clouds or aerosols. This ratio, called ozone index, is compared with ozone sonde data as well as daily TOMS data of total ozone. This comparison shows a good anticorrelation between the irradiation at short wavelengths and total ozone. Apart from ozone, influences of clouds and varying ground albedo have been investigated. The evaluation of the UV-B data has been supported by radiative transfer modeling.

1. Introduction

Since the discovery of the Antarctic ozone hole first noted by Chubachi (1984) and Farman *et al.* (1985), and more recently the seasonal ozone depletion in the northern high latitudes reported for example by Müller *et al.* (1997) and Rex *et al.* (1997), there is a strong interest in the changes of stratospheric ozone. A direct effect of ozone depletion is the increasing UV-B radiation reaching the Earth's surface. Comparison of UV data with total ozone were recently presented for mid latitude sites by Casale *et al.* (2000) or Krzyśin (2000). The scattering of UV-B radiation by aerosols and clouds plays also an important and complex role. A change in UV climate may possibly be detrimental to the biosphere (*e.g.* to marine life in the upper layers of the sea or to terrestrial vegetation) and to human (*e.g.* skin cancer).

One of the main objectives of UV measurements is the observation of long-term trends in UV irradiance. Among the most interesting geographical regions to study the changes in UV radiation are Antarctica and the Arctic due to the strong ozone depletion observed in the polar regions. Since 1997 the Alfred-Wegener-Institute records continuously UV-B in Antarctica (at the German Neumayer-Station and at the Argentinean Station Jubany on King George Island) as well as on Spitsbergen (NDSC-Station Ny-Ålesund).

This document is provided by JAXA.

2. The UV spectroradiometers

For the best long-term stability of the instrument in remote areas like Spitsbergen it is advantageous to avoid any movable parts like rotatable gratings as essential in scanning spectroradiometric systems. For this reason we have designed a non-scanning spectroradiometer which is based on a Bentham DM150 double monochromator with a multichannel detector system. The DM150 is operated with a comparatively broad center slit to allow the simultaneous detection of the whole UV-B range at 32 wavelengths. A low-resistance microchannel plate photomultiplier tube (MCP-PMT) with 32 channels working in single photon counting mode is used as detector. Due to the fixed gratings, our spectroradiometer is less sensitive towards transport by ship or aircraft, and it does not require recalibration during the Arctic campaigns from March until October.

The spectral global irradiance is measured with a teflon cosine diffuser. However, the data presented in this work are not cosine corrected. The spectral range of the UV-B instrument is from 280 nm up to 322 nm which leads to a distance of 1.35 nm between two channels due to the 32 detection channels of the MCP-PMT. The simultaneous detection of the total wavelength range enables a comparatively high time resolution. A spectrum can be recorded every second. However, in the routine operation mode 5 min averages are stored by the computer. The whole system is mounted in a weatherproof housing and the temperature is stabilized within 1°C. The entrance optics are covered by a quartz dome. Humidity inside the housing is kept below 20% by means of a drying agent (P_2O_5).

The spectroradiometer is calibrated in a laboratory in Bremerhaven prior installation at Spitsbergen and after its return. A 1000W FEL quartz-halogen lamp is used which was calibrated by the Physikalisch-Technische Bundesanstalt (PTB). The main quality assurance is given by comparison of the absolute energy calibration before the campaign and after the instruments return. All changes found up to now in 3 years have been below 5% for all wavelengths. Apart from this absolute energy calibration we use a 200 W quartz lamp from a slide projector with a very precise and stable power supply, to check energy calibration in field. Wavelength calibration is performed in the laboratory and checked again in field using a Penray mercury lamp.

A slightly modified instrument was built to measure the UV-A range. It is installed at Ny-Ålesund since March 1998, measuring from 318 nm up to 400 nm with the 32 detector channels corresponding to a distance of 2.65 nm between two channels. Beside this, the UV-A and UV-B instruments are quite similar, with identical recording and data storing modus.

Figure 1 shows the UV-A/B spectrum measured at Ny-Ålesund for March 20th 1998 at local noon. Results for our UV-B instrument, obtained during a German intercomparison of UV spectroradiometers in 1997 in Garmisch-Partenkirchen, are described in a report by Seckmeyer *et al.* (1997).

3. Daily UV-B irradiance

Figure 2 shows the daily UV-B irradiances integrated from 290–320 nm for the years 1997–1999. In 1997 the measurements began in May, whereas in the following years they

This document is provided by JAXA.

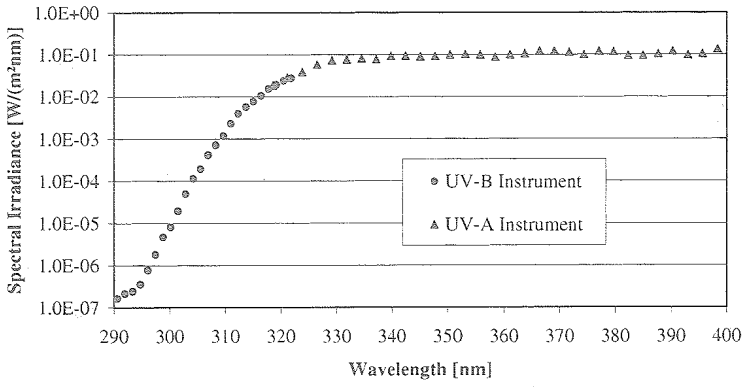


Fig. 1. UV-B/A spectrum measured at Koldewey-Station at March 20th 1998, 12.05 UTC.

restarted in March simultaneously with the polar sunrise. The figure shows the annual variation due to altering sun elevation with a maximum at midsummer with a large variability from day to day caused by fluctuating cloud conditions. A comparison of the three years also reflects the different weather situations. In 1998 there was a summer with a large amount of sunshine duration leading to 21 days with daily irradiance over 40 kJ/m^2. In 1997 only 10 days exceeded this value and in the summer of 1999, the value of 40 kJ/m^2 was exceeded only once.

Apart from these differences all datasets show a rather noisy distribution of daily irradiance due to the changes in attenuation by different cloud situations. This variation is low in spring before mid of May, high through the summer and starts to be low again in early (1998), mid (1997) or late (1999) September. This season dependent behavior of daily irradiance values is caused by changes in the ground albedo which shows a large annual variation around Spitsbergen. During winter and early spring the whole island and the frozen Kongsfjord, where the measuring site is located, is covered by snow leading to an albedo between 0.8 and 0.9. In late spring, when sea ice and snow are melting, the albedo decreases to about 0.1. Degünther *et al.* (1998) have recently shown that the ground albedo up to 50 km around the measuring site effects the UV radiation at ground. For this reason, melting of snow is a rather slow process in lowering the average albedo around the measuring site. In September a snow cover builds up again attended by a sudden increase of ground albedo.

Due to the high reflectance of the snow covered surface, the upward radiative flux on the ground is enhanced, compared to the snow free case. In the presence of clouds this upward flux is reflected downwards again. If clouds are absent the upward flux is scattered down again only by Raleigh scattering. The multiple reflection between snow and cloud cover enhances irradiance on the ground stronger than Rayleigh scattering only, this effect is recently evaluated for a measuring site in the Alps by Renaud *et al.* (2000). Thus the attenuating effect of clouds is partly compensated by this multiple reflection and daily irradiances in Fig. 2 are smoothed during the spring and autumn, when the measuring site is snow covered. The influences of ground albedo and cloud cover on the UV irradiance are evaluated by radiative transfer modeling in Section 6.

This document is provided by JAXA.

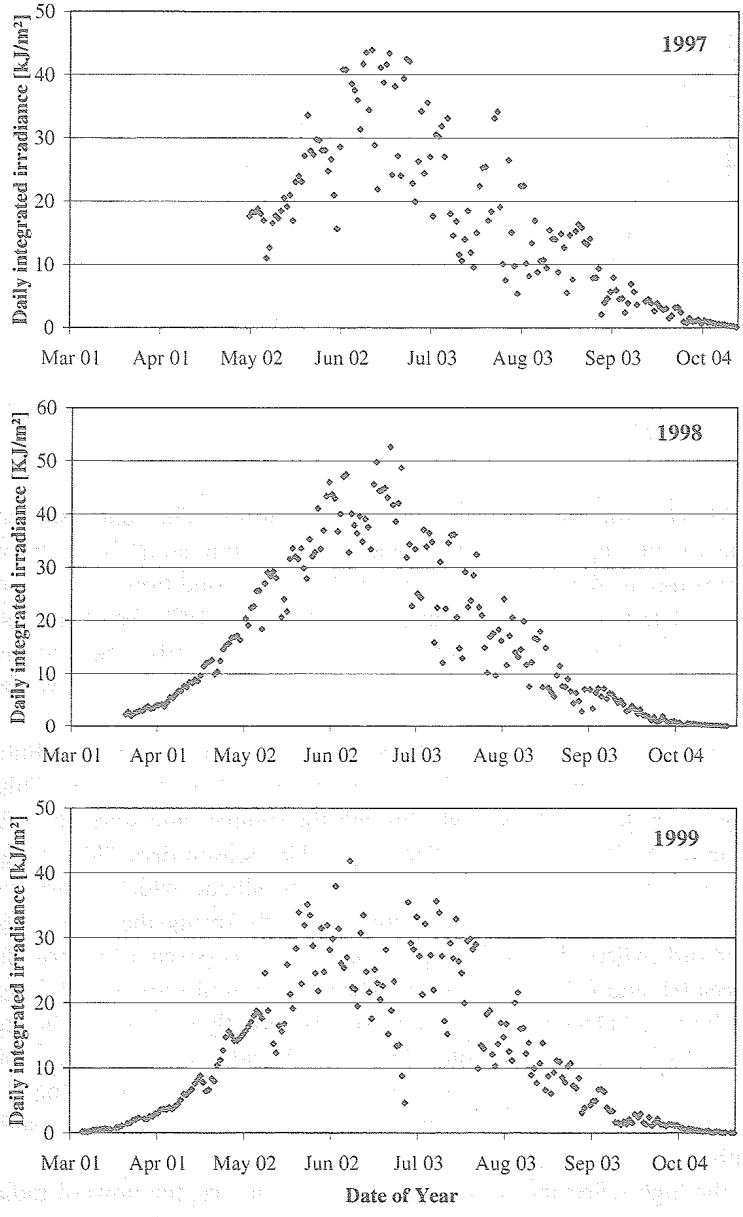


Fig. 2. Daily UV-B irradiances (280–320 nm) at Koldewey-Station.

4. Comparison of the UV-B data with total ozone columns

Apart from ozone, radiative transfer is influenced by several other atmospheric parameters like aerosols, clouds, etc.. To extract changes in the spectra which are due to

This document is provided by JAXA.

varying total ozone values from other effects, we use the ratio of the spectral irradiance measured at two wavelengths I (300 nm)/I (320 nm). This ratio is called ozone index in the following. This method is the principle of a Dobson photometer. In the wavelength range 300 to 320 nm the influences of aerosols and clouds have only a very weak dependence on wavelength. Seckmeyer *et al.* (1996) showed that cloud transmittance is not independent from wavelength, but they found only a weak decrease in the transmittance in the UV range of about 10% from 300 to 400 nm. This decrease is almost linear and therefore the effect from 300 to 320 nm is only about 2%. Kylling *et al.* (1997) explain this wavelength dependence as an upward scattering of photons from the cloud particles, which are then downscattered by the wavelength dependent Rayleigh scattering. Nevertheless, Mayer *et al.* (1998) showed that an extensive optical path enhancement of the photons in very thick clouds occurs by Mie scattering. This enhancement leads to an additional strong wavelength dependent absorption of the shortwave radiation by ozone in the cloud, which could cause large errors in the results of algorithms for total ozone determination. These errors increase with an increasing amount of tropospheric ozone, particularly ozone in the cloud, and increasing solar altitude, because then the path through the stratospheric ozone layer reaches the minimum and the absorption in the cloud becomes more important in relation to stratospheric absorption. Because on Spitsbergen solar elevation angle does not exceed 35° and air pollution is low there, tropospheric ozone is not a serious problem in data interpretation.

For a comparison of UV-B data with total ozone columns, we use ozone sonde data available for Ny-Ålesund, see for example König-Langlo (1997). But for a day by day comparison sonde data are to rare. thus we use satellite data from the TOMS instrument (Total Ozone Mapping Spectrometer). There are several ground based measurements of ozone performed at Ny-Ålesund by FTIR, DOAS, Differential Absorption LIDAR and millimeter-wave observations. An extensive comparison of all ozone data available in Ny-Ålesund is given by Langer (1999), pointing out several limitations for every system. The TOMS satellite data available showed a very stable behavior in this comparison (Langer, 1999, p. 197) and seemed to be suitable for relating with our 3 years of UV-B data.

Figure 3 shows the ozone index calculated from the 1998 daily UV spectra. These data are compared with total ozone data from TOMS and ozone sonde soundings. All UV spectra were measured at the same solar elevation angle of 30° (*i.e.* airmass 2.0), because ozone absorption depends on the optical path length through the ozone layer. This airmass is reached at 79° North between May 17th and July 29th only, therefore the comparison is restricted to this period. The figure shows a good anticorrelation between total ozone and the ozone index. However, one has to consider that there are some principle error sources in the comparison of ground based and satellite data. At first, there is only a finite coincidence in the time of the daily measurements and second the satellite records an average value over a footprint of 40×40 km^2. Keeping this in mind, the remaining discrepancy between ozone sonde and TOMS total ozone data within 10% is quite reasonable.

For 1997 and 1999 the comparison of UV-B and ozone data looks similar to Fig. 3. More interesting is the actual change in UV-B at the ground due to changes in the total ozone. We compare the ratios of the ozone index and the total ozone day by day for two years using average values around noon (± 1 h) to extend the period of comparison. This

This document is provided by JAXA.

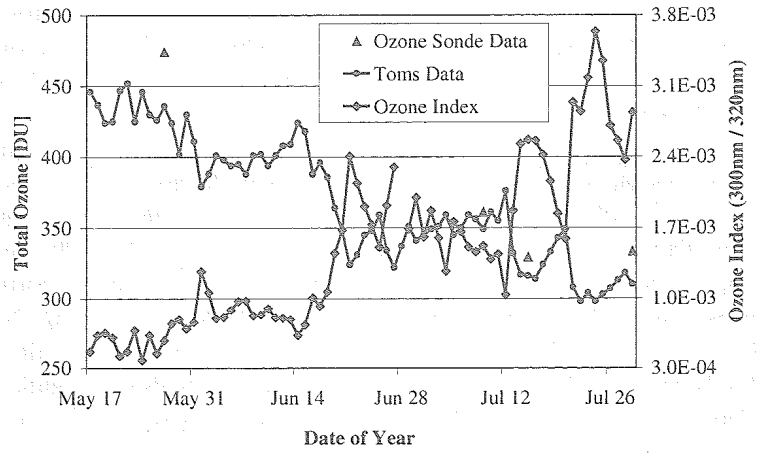


Fig. 3. Comparison of total ozone and ozone index at airmass 2.0 (Koldewey-Station 1998).

also weakens the possible error sources in the comparison with satellite measurements due to the footprint of the satellite. In Fig. 4 the ratios 1997/1998 are shown for the period from May to August, the solar elevation angle cancels down in the quotient. One can realize that small changes in the amount of total ozone cause large responses in the shortwave UV-B radiation at the Earth's surface. The picture is the same, when the 1999 data are included. In order to have a more quantitative comparison, we tried to find a functional correlation between the change in total ozone and in the ozone index. Assuming a simple Lambert-Beer law (1) to describe wavelength dependent attenuation of UV radiation by ozone we find equation (2) fitting the ratio of ozone indices as a function of TOMS data ratio. The parameter ΔB (0.0125 DU^{-1}) was fitted to the data of 97/98. This result quantifies the UV-B response to ozone variations: A 10 DU change in total ozone leads to a change of 12% in the ozone index.

$$I(\lambda) = I_0(\lambda) \exp(-B_\lambda[O_3]), \tag{1}$$

$$O_3 \text{ Index } (97/98) = \exp(-\Delta B \Delta O_3), \tag{2}$$

mit: $\Delta O_3 = [O_3]_{(97)} - [O_3]_{(98)}$ und $\Delta B = B_{300\,nm} - B_{320\,nm}$.

Figure 5 shows the result of the fit in comparison with the ratio of the measured ozone indices (1997/1998). Despite some outliers the fit matches within 20%, which is quite reasonable concerning discussed error sources. At some days the deviation is larger as for example at May 30th 1998. The reason is a large spatial gradient in the amount of total ozone for these days. At May 30th TOMS measured 430 DU at Koldewey-Station (78.93°N, 11.95°E) but 402 DU only 0.1° further north (79.03°N, 11.95°E) which corresponds to a distance of just 11 km. A reduction of the total ozone value from 430 DU to 402 DU leads to a reduction of function (2) from 2.97 to 2.09. This fits much better to the measured ratio of 1.63. This shows that the comparison of ground based UV measurements and TOMS data for some days are difficult, but considering the whole measuring period such extreme conditions are rather unusual.

This document is provided by JAXA.

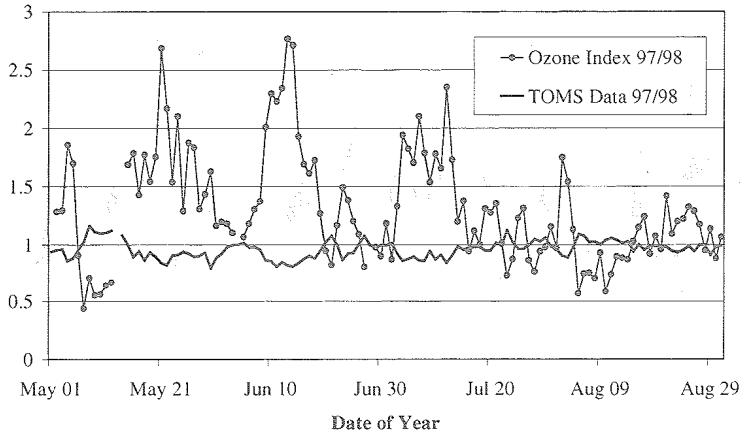


Fig. 4. Comparison of the ratios (1997/1998) of total ozone and ozone indices.

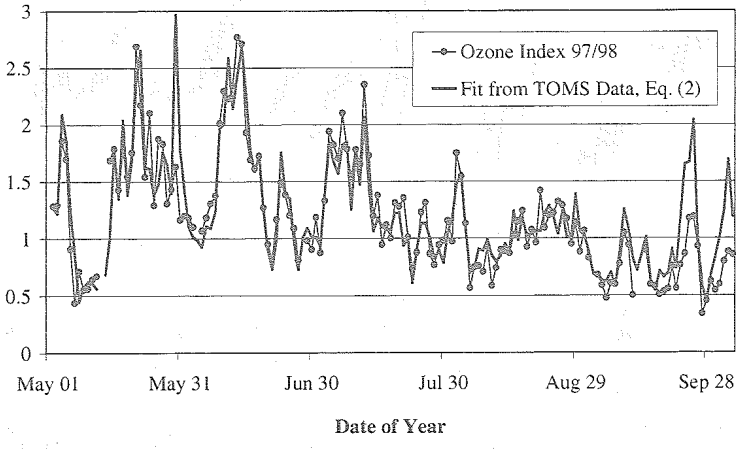


Fig. 5. The ratios of the ozone indices (1997/1998) as function of TOMS total ozone data.

We have been able to verify the relation between changes in total ozone and UV radiation on the basis of the 1999 data. Figure 6 shows the ratios 97/99 and 98/99 of the ozone indices in comparison with the fit. Although only the 97/98 data have been used for the fitting procedure it describes the ratios to 1999 as well.

5. Effects of clouds and ground albedo by UV radiative transfer modeling

The radiative transfer program *Libradtran* developed by Kylling and Mayer (1998) was applied to study the effects of clouds and ground albedo on the UV irradiance on the ground. *Libradtran* is based on a numerical solution of the 1 dimensional radiative transfer equation using the discrete-ordinate algorithmn introduced by Stamnes *et al.* (1988) or

This document is provided by JAXA.

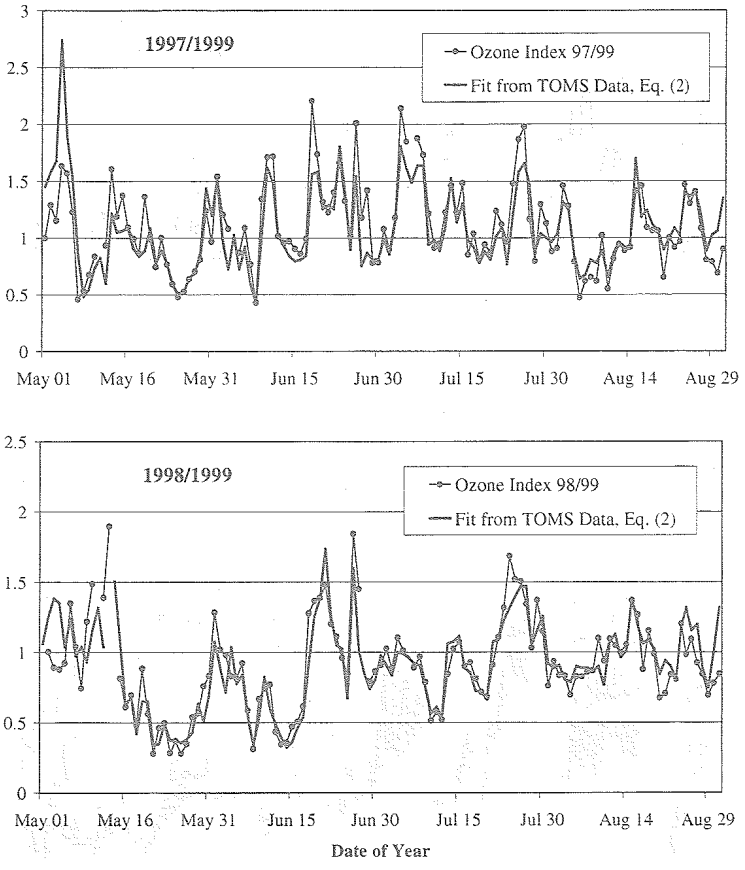


Fig. 6. The ratios of the ozone indices as function of TOMS data regarding to the 1999 data which were not included in the fitting procedure (eq. 2).

optional the two-stream radiative transfer solver. Due to the 1 dimensional description all cloud scenarios studied in the following are homogeneous cloud layers. Parameters to define these cloud covers are the altitude of the lower and upper cloud boundary, the liquid water content and the effective droplet radius. In this parameterization the optical properties of the cloud are calculated as described by Hu and Stamnes (1993). Aerosols are taken into account by employing the aerosol model of Shettle (1989).

For modeling of the interaction between cloud cover and ground albedo concerning UV radiative transfer we studied different cloud scenarios combined with the ground albedo of a snow covered (0.8) and a snow free (0.1) landscape. Figure 7 shows the modeling results for both albedo cases in a clear sky scenario and with a homogeneous cloud cover (with a lower/upper cloud boundary of 1 km/2 km, a liquid water content of 0.3 g/m^3, and an effective droplet radius of 10 micron). All calculations were done for 25° solar altitude, a total ozone value of 300 DU, and moderate maritime type aerosol conditions.

The figure shows that the cloud cover leads to a reduction of the spectral irradiance

This document is provided by JAXA.

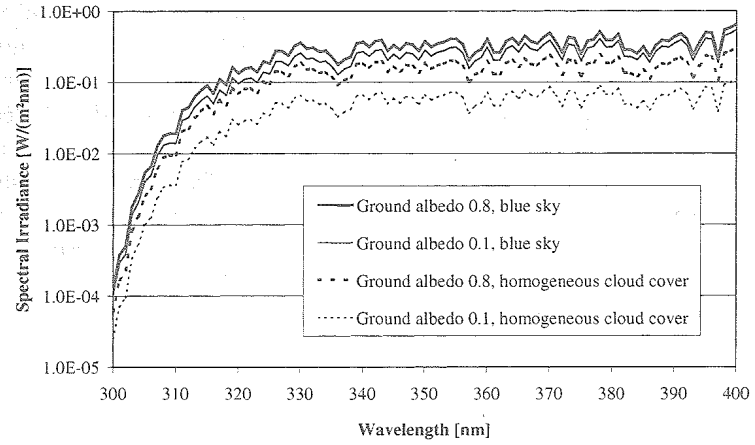


Fig. 7. Influence of ground albedo and clouds on UV irradiation at ground. The homogeneous cloud layer is determined through a lower boundary at 1 km, an upper boundary at 2 km, a liquid water content of 0.3 g/m³, and an effective droplet radius of 10 microns. All calculations were carried out at 25° solar altitude, 300 DU and moderate maritime type aerosol conditions.

Table 1. Integrated UV-A/UV-B irradiance at ground for 25° solar elevation in different ground albedo and cloud scenarios divided by clear sky values.

	Cloud 1	Cloud 2	Cloud 3
Ground Albedo 0.8	0.510/0.489	0.432/0.423	0.388/0.374
Ground Albedo 0.1	0.228/0.262	0.208/0.182	0.175/0.152

Cloud 1: liquid water content 0.3 g/m³, lower/upper boundary 1 km/2 km
Cloud 2: liquid water content 0.5 g/m³, lower/upper boundary 1 km/2 km
Cloud 3: liquid water content 0.2 g/m³, lower/upper boundary 1 km/3 km
Effective droplet radius for all clouds: 10 microns

at ground which is much larger in the snow free case. The reason for this behavior is the occurrence of multiple reflection between the snow surface and the cloud as discussed in Section 2. Table 1 gives quantitative results for the integrated irradiances (UV-A and UV-B) assuming different cloud scenarios. The reduction of the irradiance in snow free situations is more than twice as much as in the snow covered case. This gives the explanation for the obvious increase of noise in the daily UV irradiance during the melting of the snow in late spring and noise reduction with the first snowfalls in late summer shown in Fig. 2. The smoothing is not dependent on the weather condition of each single day. It is a more statistical statement in consequence of shifting up the-due to clouds-lower daily irradiance values of the ensemble in relation to the high values (sunny days).

6. Conclusions

During the first three years of our monitoring program the instrument proved to be

This document is provided by JAXA.

very stable and to work reliable under the extreme climatic conditions at Spitsbergen. Comparing the data from different years, the results show that the dominant influences are weather conditions and ground albedo. Due to the strong effects of clouds and the steep increase of intensity towards the long wavelengths, which are only little affected by ozone absorption, the influence of total ozone on radiative transfer is not visible in comparison to the measured integrated irradiance. The only visible effects are on the shape of the spectrum, represented by the ozone index. The data show an amplification of the 300 nm radiation at the surface by 12% for every 10 DU ozone loss with respect to 320 nm. Regarding a trend in UV radiation on the ground, as a result from all possible effects, it can be revealed that a longer period of observations is still needed before reliable statements can be made.

Acknowledgments

We gratefully acknowledge the help of the AWI staff involved in the accumulation of the data, in particular the personnel at Koldewey-Station (1997–1999): Thomas Seiler, Dirk Römermann, Thomas Schmitt, Tine Weinzierl, Nicole Spelten, and Christian Wille. We also acknowledge funding by the German ministry for Science, Education, Research and Technology (BMBF, grant #01 L09701/3). This paper is Alfred Wegener Institute contribution #1789.

References

Casale, G.R., Meloni, D., Miano, S., Palmieri, S., Siani, A.M. and Cappellani, F. (2000): Solar UV-B irradiance and total ozone in Italy: Fluctuations and trends. J. Geophys. Res., **105**, 4895–4901.

Chubachi, S. (1984): Preliminary results of ozone observations at Syowa Station from February 1982 to January 1983. Mem. Natl Inst. Polar Res., Spec. Issue, **34**, 13–19.

Degünther, M., Meerkötter, R., Abold, A. and Seckmeyer G. (1998): Case study on the influence of inhomogeneous surface albedo on UV irradiance. Geophys. Res. Lett., **25**, 3587–3590.

Farman, J.C., Gardiner, B.D. and Shanklin, J.D. (1985): Large losses of ozone in Antarctica reveal seasonal CLOX/NOX interaction. Nature, **315**, 207–210.

Hu, X.Y. and Stamnes, K. (1993): An accurate parameterization of the radiative properties of water clouds suitable for use in climate models. J. Clim., **6**, 728–742.

König-Langlo, G. and Marx, B. (1997): The Meteorological Information System at the Alfred Wegener Institute. Climate and Environmental Database Systems, by M. Lautenschläger and M. Reinke. Norwell, Kluwer Academic Publ.

Krzyśin, J.W. (2000): Total ozone influence on the surface UV-B radiation in the late spring-summer 1963–1997: An analysis of multiple timescales. J. Geophys. Res., **105**, 4993–5000.

Kylling, A. and Mayer, B (1998). Libradtran is a program for calculation of diffuse and direct UV and visible fluxes and intensities at any altitude. Available from http://www.uio.no/~arveky/libRadtran.html.

Kylling, A., Albold, A. and Seckmeyer, G. (1997): Transmittance of a cloud is wavelength-dependent in the UV range: Physical interpretation. Geophys. Res. Lett., **24**, 397–400.

Langer, J. (1999): Measurements of Arctic stratospheric ozone: Comparison of ozone-measurements at Ny-Ålesund, Spitsbergen, in 1997 and 1998. Ber. Polarforsch., **322**, 222 p.

Mayer, B., Kylling, A., Madronich, S. and Seckmeyer, G. (1998): Enhanced absorption of UV radiation due to multiple scattering in clouds: Experimental evidence and theoretical explanation. J. Geophys. Res., **D103**, 31241–31254.

Müller, R., Crutzen, P.J., Grooß, J.U., Brühl, C., Russell, J.M., Gernandt, H., McKenna, D.S. and Tuck, A.F. (1997): Severe chemical ozone loss in the Arctic during The winter of 1995–96. Nature,

This document is provided by JAXA.

389, 709–712.
Renaud, A., Staehlin, J., Fröhlich, C., Philipona, R. and Heimo, A. (2000): Influence of snow and clouds on erythemal UV radiation: Analysis of Swiss measurements and comparison with models. J. Geophys. Res., D105, 4961–4969.
Rex, M. and 23 colleagues (1997): Prologed stratospheric ozone loss in the 1995–96 Arctic winter. Nature, 389, 835–838.
Seckmeyer, G., Erb, R. and Albold, A. (1996): Transmittance of a cloud is wavelength-dependent in the UV range. Geophys. Res. Lett., 23, 2753–2555.
Seckmeyer, G., Mayer, B. and Bernhard, G. (1997): The 1997 Status of Solar UV Spectroradiometry in Germany: Results from the National Intercomparison of Spectroradiometers, Garmisch-Partenkirchen, August 1997. Shaker Verlag, Aachen, Germany.
Shettle, E.P. (1989): Models of aerosols, clouds and precipitation for atmospheric propagation studies. AGARD Conference Proceedings No. 454.
Stamnes, K., Tsay, S.-C., Wiscombe, W. and Jayaweera, K. (1988): Numerically stable algorithm for discrete-ordinate-method radiative transfer in multiple scattering and emitting layered media. Appl. Opt., 27, 2502–2509.

(Received April 4, 2000, Revised manuscript accepted September 22, 2000)

This document is provided by JAXA.

This document is provided by JAXA.

Mem. Natl Inst. Polar Res., Spec. Issue, 54, 125-131, 2001

Scientific note

Radiation and turbulence parameterizations at Ny-Ålesund, Svalbard Islands

Teodoro Georgiadis[1], Marianna Nardino[1], Francescopiero Calzolari[1], Vincenzo Levizzani[1], Jon Børre Ørbæk[2], Stefan Claes[2] and Roberta Pirazzini[3]

[1]*CNR-ISAO Institute of Atmospheric and Oceanic Sciences, Via Gobetti 101, 40129 Bologna, Italy*
[2]*Norwegian Polar Institute, Polar Environmental Centre, N-9296 Tromsø, Norway*
[3]*FIMR Finnish Institute of Marine Research, P.O. Box 33, FIN-00931 Helsinki, Finland*

Abstract: Two experimental campaigns were carried out at Ny-Ålesund during the spring of 1998 and the spring-summer of 1999 with the aim to study the daily evolution of surface turbulence and the influence of clouds on the surface radiation balance. Parameterizations of the surface roughness were derived from turbulence measurements performed with a sonic anemometer. The value of the roughness length was calculated. It was highly variable because of snow drift and changing surface conditions. The applicability of two long-wave incoming radiation parameterizations reported in literature was tested with data collected during the experiments.

1. Introduction

The impact of clouds on the Arctic climate is currently being widely investigated because of the complexity of the problem. In this frame the development of turbulence at the surface under different solar radiation availability, in terms of quantity and of partition in short- and long-wave, is of paramount importance.

The Ny-Ålesund international scientific base (78°55′N-11°56′E) represents an ideal outpost for interdisciplinary research on the land-ocean-atmosphere system.

The main aim of this study is to provide some basic information, even if limited in time and space, on physical quantities regarding radiation and turbulence useful in modeling schemes.

2. Methods

According to the general parameterization of Konzelmann *et al.* (1994), the incoming long-wave radiation (*Lwin*) can be expressed as follows:

$$\begin{aligned} Lwin &= \varepsilon_{cl}(1-N^p)\sigma T_a^4 + \varepsilon_{ov}N^q\sigma T_a^4 \\ &= [\varepsilon_{cl}(1-N^p)+\varepsilon_{ov}N^q]\sigma T_a^4, \end{aligned} \quad (1)$$

where ε_{cl} is the clear sky emittance, ε_{ov} the overcast sky emittance, σ the Stephan-Boltzmann

This document is provided by JAXA.

constant, T_a the air temperature, N the cloud amount, and p and q are coefficients determined by cloud characteristics. For clear sky emittance the value of Idso (1981) was used:

$$\varepsilon_{cl}=\left\{0.7+5.95\cdot 10^{-5}e_a\exp\left[\frac{1500}{T_a}\right]\right\}, \tag{2}$$

where e_a is the air water vapor pressure. From eqs. (1) and (2):

$$Lwin=\left[\left(0.7+5.95\cdot 10^{-5}e_a\exp\left(\frac{1500}{T_a}\right)\right)\cdot(1-N^p)+\varepsilon_{ov}\cdot N^q\right]\sigma T_a^4, \tag{3}$$

where the values of on p, q and ε_{ov} are obtained from experimental data and compared with those reported by Konzelmann *et al.* (1994).

If the contribution to the cloud amount of low and middle clouds is known, the parameterization proposed by De Rooy and Holtslag (1999) can be applied:

$$Lwin=a\left(\frac{e_a}{T_a}\right)^b\sigma T_a^4+cN-d(N-N_h), \tag{4}$$

where N_h is the low-middle cloud amount and the coefficients a, b, c and d are obtained experimentally from the best fit of eq. (4).

The turbulence measurements, performed with a sonic anemometer, allowed determination of the value of surface roughness length (z_0), a parameter commonly utilized in modeling schemes. The numerical determination followed the methodology of Sozzi *et al.* (1998).

An alternative way to obtain the value of the surface roughness length comes from considering the vertical profile of the wind speed in adiabatic conditions (Stull, 1988):

$$z_0=ze^{-uk/u_*}, \tag{5}$$

where u is the wind speed, u_* the friction velocity, z the measurement height, and k the von Karman constant (0.4).

3. Instrumentation set-up

The first campaign was conducted in the frame of the EC research project ARTIST (Arctic Radiation and Turbulence Interaction Study). The second was supported by the EU LSF (Large Scale Facility).

During the ARTIST experiment the anemometric and radiometric stations in the Kongsfjorden area were equipped with a sonic anemometer mod. USA-1 (Metek), a hygrometer KH20 (Campbell Sci.), and a radiometer mod. CNR1 (Kipp and Zonen) capable of measuring short and long-wave radiation components separately.

The radiometric measurements were recorded by a Campbell CR10 ET data logger every minute, then averaged every 10 min, and finally stored in a Campbell SM192 memory module.

The radiometer and the sonic anemometer were placed on the same mast at 1.5 m and 3.5 m height, respectively. The fast hygrometer KH-20 (Campbell Sci., USA) for moisture measurements was positioned on the same mast at 3.5 m height.

This document is provided by JAXA.

The data acquisition for the turbulence measurements was performed by a Meteoflux computer system (Servizi e Territorio).

The measurements started on 19 March and lasted until 14 April, 1998.

During the LSF experiment the instrumentation was substantially the same, except for the absence of the hygrometer and the different model of sonic anemometer (Metek mod. USAT1).

The anemometer data were stored on a PC hard disk after electronic processing performed by a programmable internal board, which computes two-axis rotations, the 15′ averages of the main physical quantities and standard deviations, and the momentum and sensible heat flux.

The radiometer and the anemometer were on the same pole at 3.5 and 1.5 m from the ground as in the previous experiment.

The measurements started on 7 May and lasted until 30 June 1999.

Data of cloud coverage, water vapor pressure and temperature, collected by the Koldeway, were utilized in the Lwin parameterizations.

4. Results and discussion

4.1. Radiation measurements

Table 1 reports the values of the coefficients of eqs. (3) and (4) that were obtained for both measurement campaigns.

Table 1. Values of the coefficients of the Konzelmann et al. (1994) and De Rooy and Holtslag (1999) parameterizations obtained as best fits, for ARTIST and LSF experiments.

Parameterization	Konzelmann			De Rooy and Holtslag			
	p	q	ε_{ov}	a	b	c	d
ARTIST experiment	6	4	0.979	1.15	1/11	64.47	49.10
LSF experiment	6	3	0.994	1.28	1/7	89.16	56.79
Konzelmann *et al.* curve	4	4	0.950				
De Rooy and Holtslag curve				1.2	1/7	70	50

Very good agreement between the coefficients of the parameterization of De Rooy and Holtslag (1999) and values derived from experimental data was found.

The trends of the Lwin measured by the radiometer were compared with the values parameterized by eq. (3). Good agreement was found as reported in the scatter plots of Fig. 1a-b. The higher scatter of the data for the LSF experiment is ascribable to the different surface features underlying the radiation station and the Koldewey station.

The same analysis was conducted by means of eq. (4); the results are reported in Fig. 2a-b. In this case the agreement between the measured and computed values is greater than in the previous case when the Konzelmann *et al.* (1994) parameterization was applied.

4.2. Turbulence measurements

The value of surface roughness length was computed from the turbulence measurements. The mean and median values of z_0 for each wind sector were computed to

This document is provided by JAXA.

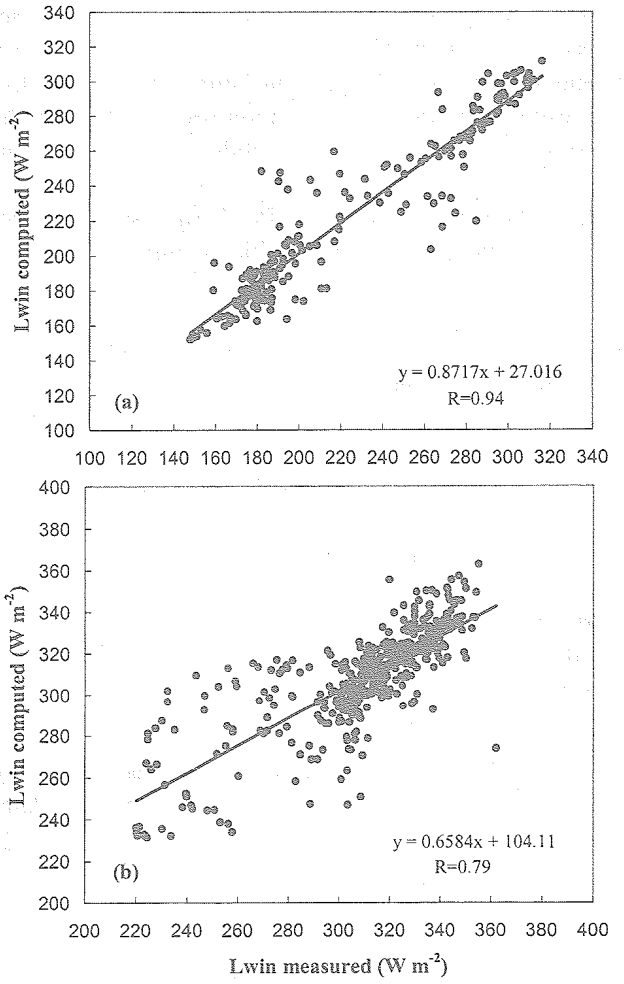


Fig. 1. Scatter plot between the longwave incoming radiation obtained through the Konzelmann et al. (1994) parameterization and that measured with the radiometer for (a) the ARTIST and (b) the LSF experiment.

characterize the surface around the measurement site which, considering the very flat territory of the fjord, are representative of a wide area south of the base. The mean values ranged from 3.4×10^{-3} to 8.2×10^{-1} m.

The highest value obtained can be attributed to the peculiar deployment of the instrumentation having a sodar system located very close to the sonic anemometer which perturbed the anemometer measurements for the determination of surface roughness within the corresponding wind sector. A second peak in the z_0 value was obtained for the wind direction from the mountain range, which highly perturbed the airflow.

In order to obtain a representative value for modeling purposes, the median, which allows exclusion of the contribution of the tail of the data distribution, was calculated for each series of observations.

This document is provided by JAXA.

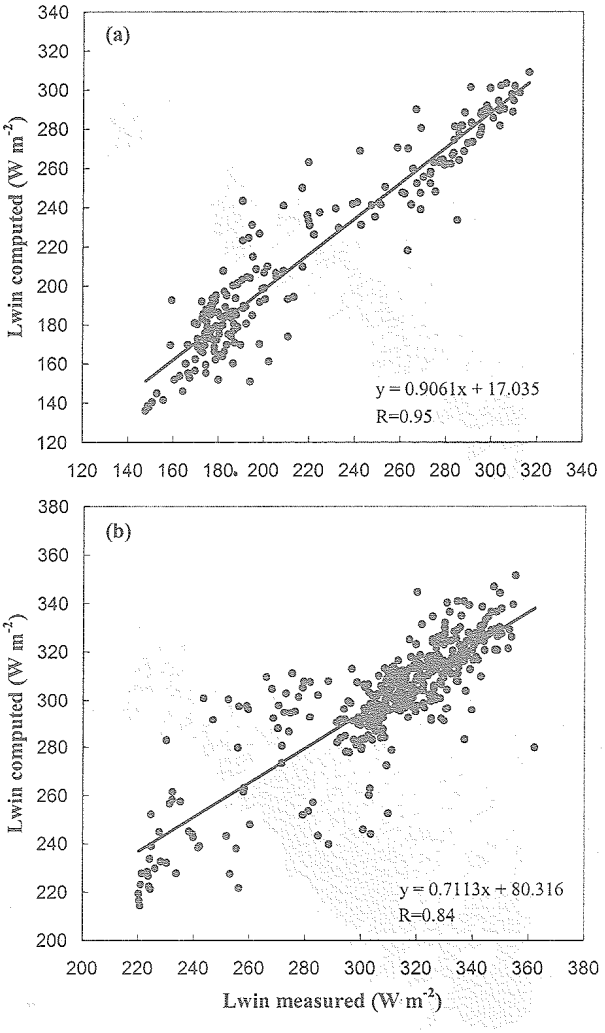


Fig. 2. Same as in Fig. 1 but with the longwave incoming radiation obtained through the De Rooy and Holtslag (1999) parameterization.

During the ARTIST experiment, z_0 resulted 8.9×10^{-4} m, while during the LSF experiment, z_0 resulted in 1.4×10^{-3} m which is closer to the characteristic values for snow and ice surfaces.

Utilizing eq. (5), the values of z_0 obtained from the slopes of the regression lines are equal to 1.3×10^{-4} m for the ARTIST experiment (Fig. 3a) and 2.5×10^{-3} m for the LSF experiment (Fig. 3b).

The discrepancy between the values obtained in the different experiments can be attributed to the total melting of the snow observed during the LSF campaign.

This document is provided by JAXA.

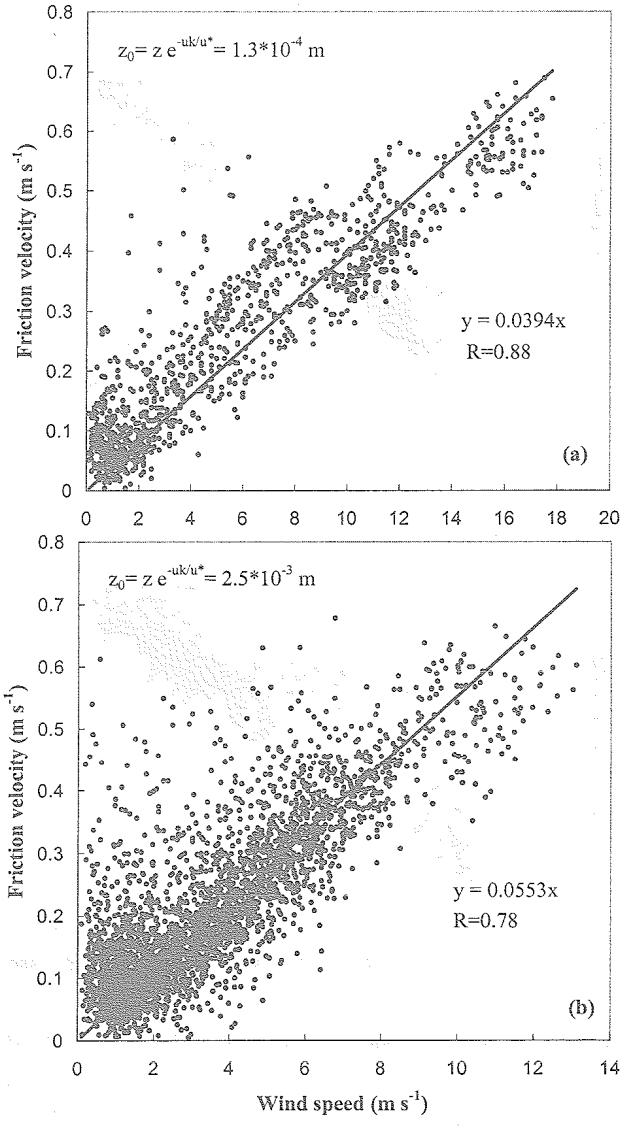


Fig. 3. Scatter plot between the friction velocity and the wind speed for (a) the ARTIST and (b) the LSF experiment.

5. Conclusions

The dependence of incoming longwave radiation on cloud amount has been parameterized using relationships reported in the literature.

Generally good agreement exists between the measured values and the parameterized Lwin computed by De Rooy and Holtslag (1999). The results show that the two parameter-

This document is provided by JAXA.

izations performed reasonably well in early spring conditions (ARTIST experiment), but produced larger errors in late spring, during an intense melting period (LSF experiment).

The surface roughness length obtained during the experiments can be utilized as an input parameter for modelling purposes provided that the prevailing wind direction is taken into account, and wind sectors directed from the mountain range are excluded.

Acknowledgments

The studies have been supported by the Training and Mobility of Research (TMR) Programme of the European Commission, within the framework of a Large Scale Facility grant NP 99/1-1, and by the ARTIST project funded by the European Commission DGXII within the 4th Framework Programme "Environmental and Climate" (Contract ENV4-CT97-0487). Special credit goes to the Alfred Wegener Institute for providing the Koldewey-Station data. The authors wish to thank Dr. Fabrizio Ravegnani, Mr. Ubaldo Bonafè and Mr. Giuliano Trivellone for their contributions to the ARTIST experimental project. Finally, Mr. Roberto Sparapani deserves recognition for his invaluable help in solving the many technical and logistic problems faced during the experiment.

References

De Rooy, W.D. and Holtslag, A.A.M. (1999): Estimation of surface radiation and energy flux densities from single-level weather data. J. Appl. Meteorol., **38**, 526–540.

Idso, S.B. (1981): A set of equations for full spectrum and 8- to 14-μm and 10.5 to 12.5μm thermal radiation from cloudless skies. Water Resour. Res., **17**, 295–304.

Konzelmann, T., Van de Wal, R.S.W., Greuell, W., Bintanja, R., Henneken, E.A.C. and Abe-Ouchi, A. (1994): Parameterization of global and longwave incoming radiation for the Greenland ice sheet. Global Planet. Change, **9**, 143–164.

Sozzi, R., Favaron, M. and Georgiadis, T. (1998): Method for estimation of surface roughness and similarity function of the wind speed vertical profile. J. Appl. Meteorol., **37**, 461–469.

Stull, R.B. (1988): An Introduction to Boundary Layer Meteorology. Dordrecht, Kluwer, 666 p.

(Received April 3, 2000; Revised manuscript accepted November 16, 2000)

This document is provided by JAXA.

This document is provided by JAXA.

Mem. Natl Inst. Polar Res., Spec. Issue, 54, 133–141, 2001

Scientific paper

Feasibility study on scientific balloon experiment at Ny-Ålesund

Hideyuki Honda, Naoki Izutsu and Nobuyuki Yajima

The Institute of Space and Astronautical Science (ISAS), 3-1-1, Yoshinodai, Sagamihara 229-8510

Abstract: This paper deals with the possibility of scientific ballooning in the Arctic (at Ny-Ålesund). This study is based on balloon experiments carried out at Syowa Station, Antarctica, from 1996 through 1999. Under typical flight conditions, such as five-hour flight duration at 30 km altitude, balloon trajectory simulation at Ny-Ålesund demonstrated the flight range within 150 km in June through August, and large possibility of payload recovery. A new type of super-pressure balloon developed by a Japanese balloon group, which promises a long duration flight at constant altitude, will be a useful platform. New onboard systems and ground facilities developed for the preceding balloon experiment in the Antarctic will be applicable to scientific observations over Arctic regions.

1. Introduction

Polar regions are interesting places to study atmospheric chemistry and physics in the stratosphere, and upper atmospheric physics. Scientific balloons are one of the most powerful and economical tools for those studies. Ballooning in those areas, however, encounters many difficulties, such as low temperature, insufficient facilities and logistics, and lack of skilled manpower.

One of the important subjects is meteorological conditions for a balloon experiment, especially surface wind speed, wind speed and direction in the troposphere and the stratosphere. These conditions directly affect observation time and the possibility of payload recovery. Other research subjects are onboard equipment and ground facilities. In the stratospheric air sampling project, National Institute of Polar Research (NIPR) has experienced ballooning at Syowa Station, Antarctica, in cooperation with the ballooning group of the Institute of Space and Astronautical Science (ISAS). The project included the simulation and analysis of flight trajectories, development of launching and tracking instrumentation, and recovery operation on sea ice and on the sea (Honda *et al.*, 1999a, b; Yajima *et al.*, 1999a; Aoki *et al.*, 1999). Technological achievements in the champaign are quite helpful when we consider the applicability of scientific experiments at the Arctic regions.

Scientific observation by a long duration balloon flight is one of the most effective research methods, comparing favorably with satellite observations. A super-pressure balloon, which has been developed by the ISAS balloon group (Yajima *et al.*, 1999b; Yajima, 2000), is one of the most promising candidates. More than one-month flight duration is possible for a super-pressure balloon, whereas a conventional zero-pressure balloon can fly

This document is provided by JAXA.

for only one week or less.

In this paper, the meteorological feasibility of a balloon experiment at Ny-Ålesund is discussed first. Then the new ballooning technology and the technological achievements in Antarctica, which are applicable to the Arctic balloon campaign, are explained.

2. Meteorological feasibility at Ny-Ålesund

From the viewpoint of ballooning, meteorological feasibility was studied. There are two important factors in ballooning operations: balloon launching and payload recovery. The former largely depends on the surface wind speed; the latter is affected by the wind speed and direction in the troposphere and stratosphere. Here, possibilities of payload recovery by trajectory simulation were first examined using the daily wind profiles over Ny-Ålesund in 1995. This was the same method that had been used in the Antarctic (Honda *et al.*, 1996a). The accuracy of the simulation was confirmed to be within 1 km through actual flights and recovery operations at Syowa Station, Antarctica (Honda *et al.*, 1996b). The capability of balloon launching was also estimated by considering daily surface wind speed data. For safety of balloon launching operations, wind speed of 3 m/s or less is suitable.

2.1. Trajectory simulation

A time-altitude profile during a five-hour observation duration at 30 km altitude was assumed, as shown in Fig. 1. The maximum altitude of the meteorological observation is often less than 28 km because the rubber balloon bursts, especially from January through March and November through December. Such profiles were not used in the trajectory calculation here. When the balloon burst altitude was between 28 km and 30 km, the wind speed and direction up to 30 km were considered to be the same as those at the balloon burst altitude.

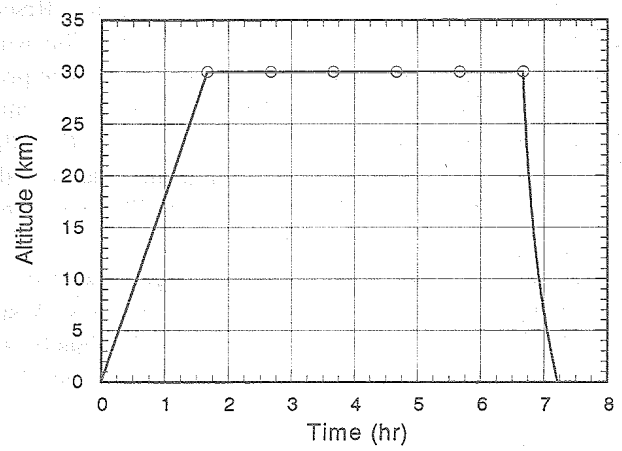


Fig. 1. Time-altitude profile used in trajectory calculation. Small circles indicate one-hour intervals after a ceiling altitude is reached.

This document is provided by JAXA.

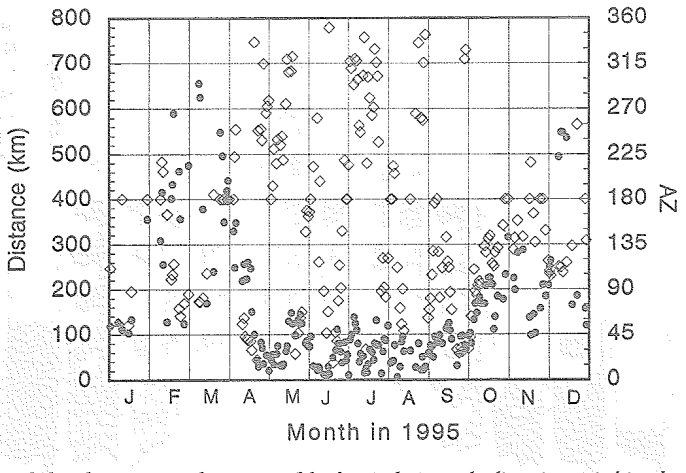


Fig. 2. Simulated landing point distances (black circles) and directions (white boxes) distribution from the launch pad in Ny-Ålesund, 1995. AZ indicates the direction, 0, 90 and 180 are north, east and south, respectively.

Balloon flight trajectories were calculated under the conditions described above. The distribution of the landing point distance and direction from Ny-Ålesund estimated for 1995 is shown in Fig. 2. The distance changes gradually throughout the year, being longer in winter and shorter in summer. The direction changes largely by two-month cycle in summer and is rather stable in winter. Westward (AZ around 270) is preferable for the payload recovery because of the open sea, which ensures that telemetered data can be received as low as sea level at the ground station without obstruction by mountains.

Figure 3 presents the results of the calculated distances between the estimated landing points and Ny-Ålesund. "No data" shown in the figure means that the calculation was not performed because no meteorological data were available or the balloon burst altitude was lower than 28 km. In the discussion below, the case of "no data" is excluded.

The landing points are categorized into five ranges, from one less than 50 km (expressed $<$ 50 km in the figure) to one not less than 200 km ($\geqq$200 km) in 50 km steps as shown in Fig. 3. All payloads are expected to land within 150 km of the launch pad from May through September. When the distance is limited to within 100 km for easier recovery operation, the occurrence ranges from 68% in May to 95% in August. In other months most landing points were farther than 150 km, and there will be little chance for recovery at short range.

Simulated trajectories for June, 1995, are plotted on the map as shown in Fig. 4. Most are within the 100-km circle as shown in Fig. 3. They are distributed on the sea and also on land. Landing on the island, however, has to be avoided for safety reasons and easier recovery operation. At Ny-Ålesund the recovery operation on the mountainside is more difficult than that on the sea because of the steep ice slopes. The balloon flight course can easily be controlled onto the sea by changing altitude by venting helium gas from the balloon or ballasting. According to analysis of the landing point distribution in the Antarctic work, the landing point distance and direction from the launching station varied only slightly day by day, and its tendency could be predicted easily (Honda *et al.*, 1999b).

This document is provided by JAXA.

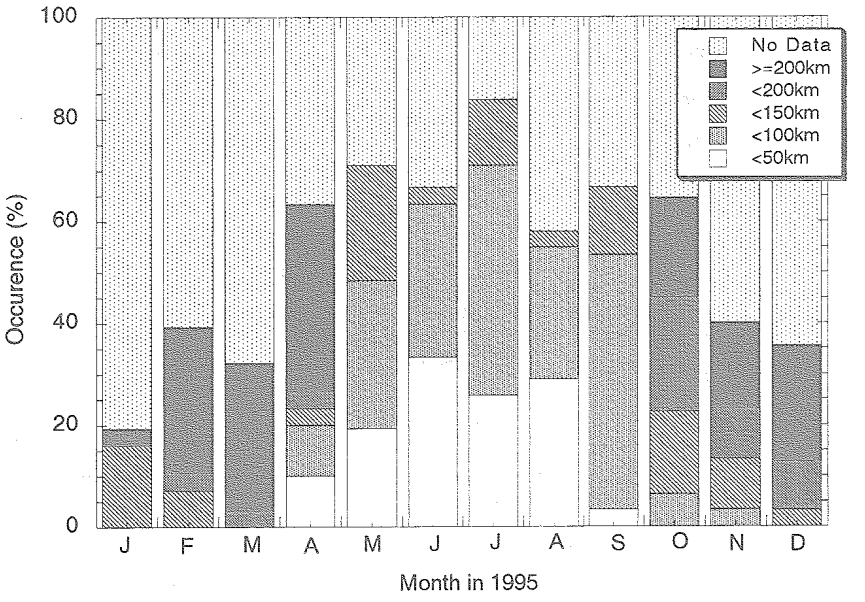


Fig. 3. Occurrence of simulated landing point distances, as shown in Fig. 2, classified into six categories. < 100 km includes landing point distances of at least 50 km but less than 100 km, for example. "No data" means that the calculation was not performed because no meteorological data were available or the balloon burst altitude was lower than 28 km.

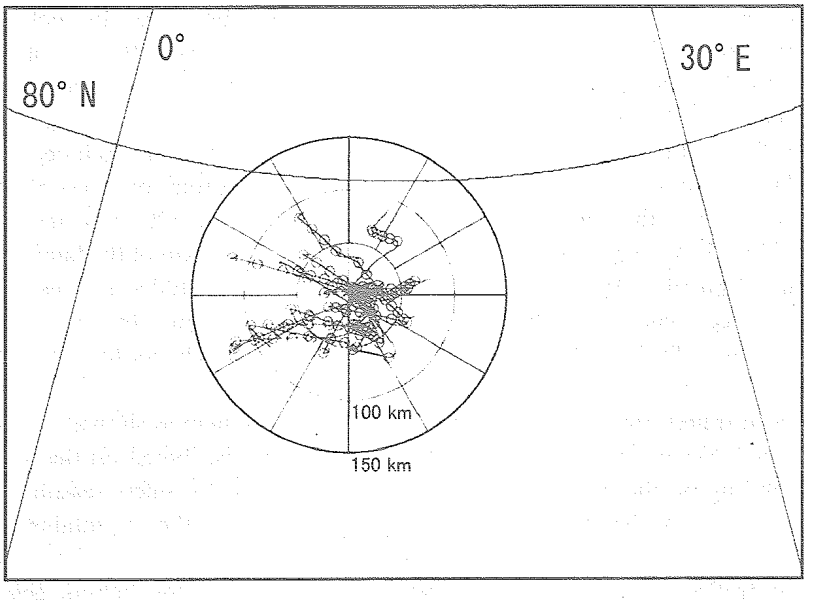


Fig. 4. Trajectories of June 1995 superimposed on a map of Ny-Ålesund. The three large circles indicate the distance from the launch pad, 50 km, 100 km and 150 km, respectively. Small circles on each trajectory present the same time and altitude as in Fig. 1.

This document is provided by JAXA.

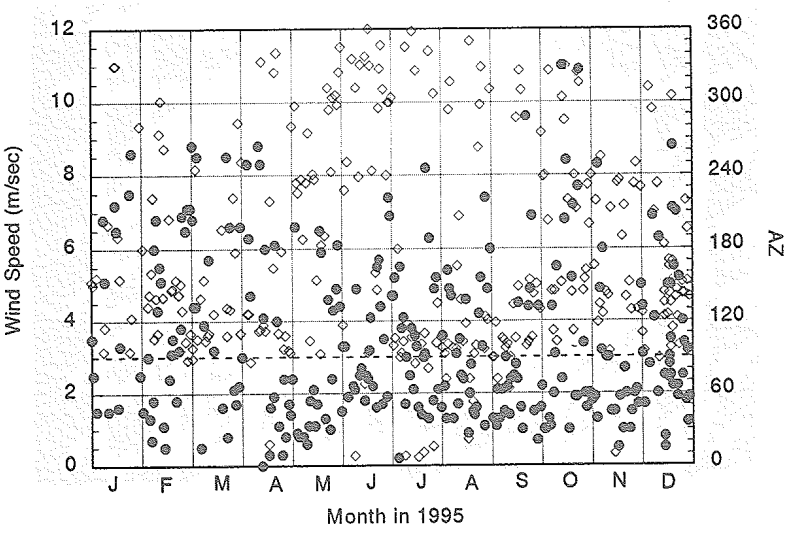


Fig. 5. Surface wind speed (black circles) and direction (white boxes) distribution at Ny-Ålesund in 1995. The broken line of 3 m/s indicates the maximum wind speed for safe launching of large balloons.

2.2. Surface wind

Another important factor for launching balloons, ground wind speed on the launching day, is plotted in Fig. 5, also for 1995. The broken line of 3 m/s indicates the maximum speed for safe launching operations of large balloons. The percentages of days having wind speed less than 3 m/s are 65%, 56%, 35%, 52% and 72% for May, June, July, August and September, respectively. The launching opportunities are not so limited compared to the situation in Japan. The wind direction at the surface is generally not a critical factor as long as the launch pad is open and no tall building or other obstacle nearby.

3. Ballooning facilities and instrumentation

Ballooning facilities and instrumentation, that are needed including balloon, a gas inflation system, a launch vehicle, an auto-track and telecommand system, and recovery equipment are given below. Some of these were designed for and used in the Antarctic from 1996 through 1999 (Honda *et al.*, 1999c, 2000; Izutsu *et al.*, 1999), and are equally useful for the Arctic balloon experiment.

3.1. Super-pressure balloon

The Japanese ballooning group has developed a new type of super-pressure balloon (Yajima *et al.*, 1999a; Yajima, 2000), for a long duration flight, longer than one month, at constant altitude. Figure 6 shows a 3000 m^3 super-pressure balloon in an indoor inflation test. The balloon made a successful flight on 15 May 1999 and became the first super-pressure balloon with a heavy payload in the world. Development of a larger balloon is now in progress.

The super-pressure balloon can fly on a circumpolar orbit when it is launched in a

This document is provided by JAXA.

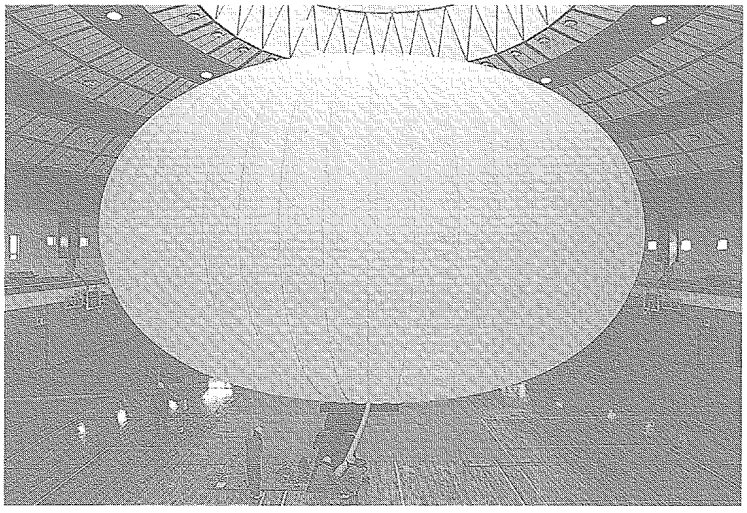


Fig. 6. A 3000 m^3 super-pressure balloon under an indoor inflation test.

polar vortex. It allows a scientific instrument to observe upper atmosphere by solar occultation method repeatedly and radiation from the earth surface continuously, for instance.

3.2. Power system

A large solar power generation system is under preparation for long duration flight using the super-pressure balloon. The system is made of several solar panels which can expand. When a balloon reaches its ceiling altitude, the stored panels are deployed downward. The system can follow the sun in order to achieve the maximum power generation efficiency.

3.3. Telecommunications system

There are two telecommunications systems; an ordinary one that was developed especially to be as simple as possible and a new one aimed at long duration flight. The former was used in the Antarctic campaign and functioned as expected (Honda *et al.*, 1999a; Yajima *et al.*, 1999a; Aoki *et al.*, 1999). The latter is under development.

A handy telemetry and telecommand system was designed for the Antarctic. The system consisted of a telemetry and a telecommand antenna, a biaxial rotator, an L band receiver, a telemetry demodulator, a transmitter and PCs. As the tracking range was limited within 150 km due to the recovery operation requirement in the Antarctic, a 15-element Yagi antenna was sufficient to receive the telemetry signal. The PC calculated the antenna attitude to direct it to the balloon using GPS data transmitted from the balloon. This method drastically simplified the auto-tracking system. The system required only a few staff members for one day to set up and test the antenna on a roof and the communications system in a room. For balloon experiments at Ny-Ålesund in the future, the receiving station may be set up on a mountain site for long range and wide coverage.

This document is provided by JAXA.

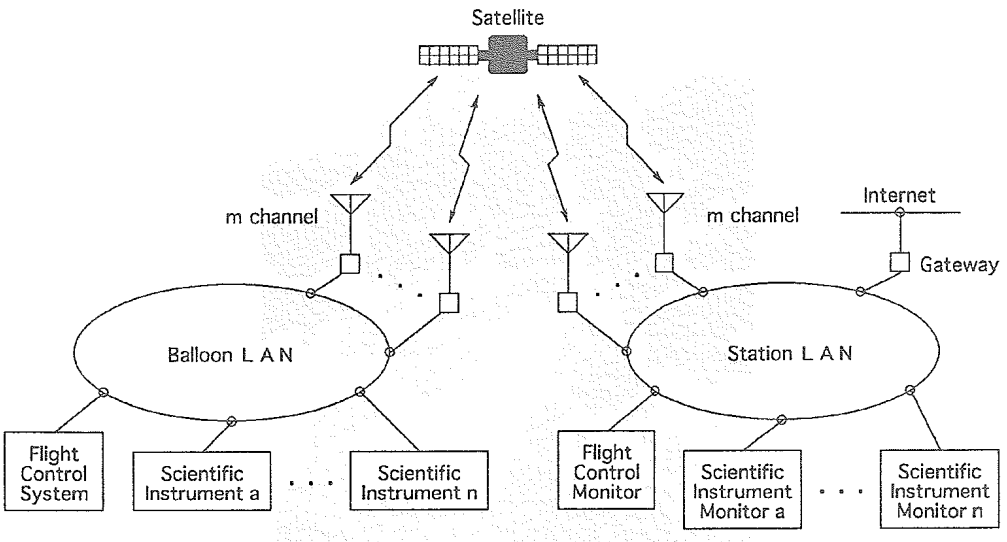


Fig. 7. Schematic diagram of a network configuration onboard the balloon, a telecommunications system, a ground station and Internet connections.

The new onboard system utilizes multiple satellite telephones as the communications system to be free from coverage of ground stations, to increase reliability and to improve total transmission capacity. This system can provide bidirectional communications, and onboard instruments can be manipulated interactively from the ground. A schematic of the concept of the new telecommunications system is shown in Fig. 7.

3.4. Network data transfer

Scientists in a remote office can access the onboard instruments and check the status in real time via the Internet, as has been demonstrated in the Antarctic (Honda *et al.*, 1999a, 2000). In Antarctica in 1998, all of the telemetry data were transferred to NIPR in Tokyo in real time through the computer network at Syowa Station via INMARSAT. This system was a powerful tool in both ballooning and the air sampling operation in the sense that engineers and scientists in Japan could monitor the status and data from the onboard systems in real time from the preparation stage of the payload instrument. They could also send instructions and advice to people at Syowa Station.

3.5. Launching facilities

A gas inflation system was designed, for the Antarctic work, to measure gas pressure and temperature precisely in order to determine the lift of the balloon, and to permit manual control of inflation speed. It could connect more than 100 helium gas bottles of 47 liters by volume, and has the capacity to inflate a balloon of 800 kg lift force within 30 min. A launcher for a small payload was also developed. It was capable of 80 kg lift force for a plastic balloon. Another launcher for a large balloon was installed in the previous balloon campaign called the Polar Patrol Balloon (PPB) (Ejiri *et al.*, 1993).

This document is provided by JAXA.

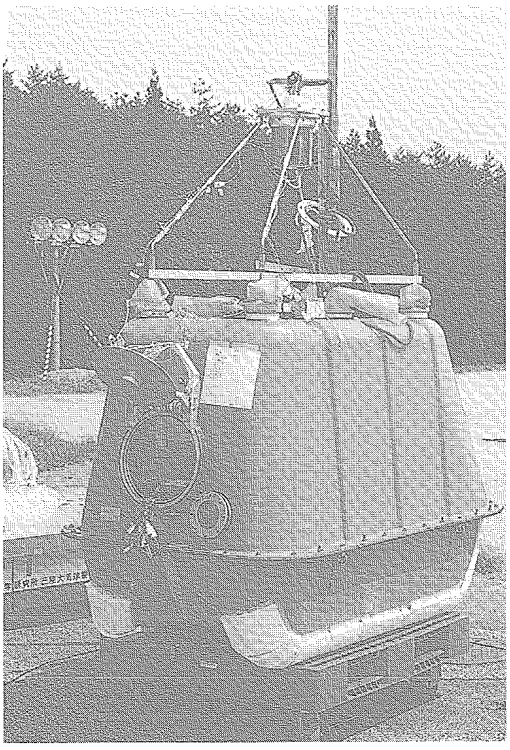


Fig. 8. A waterproof gondola in use.

3.6. Recovery system

In order to recover a payload, its exact positioning during flight and after landing is required. The former could be determined by transmitting onboard GPS data to the ground station, and the latter by continuous transmission of a beacon signal for direction finding. Since all payloads are landed on the sea in balloon experiments in Japan, they are recovered using a ship in cooperation with a helicopter. When a helicopter is used and the GPS data are transferred normally, no extra search time is required to find the payload compared to the conventional recovery operation only by a ship.

The Japanese ballooning group has already developed a multipurpose waterproof gondola made of FRP (Fiber Reinforced Plastic) (Akiyama *et al.*, 1992), which has a wide window allowing an optical instrument to observe the target without obscuration. It can house an instrument as large as 1.0 mW×0.6 mD×1.0 mH (see Fig. 8). It is already operational.

4. Conclusions

Scientific balloons are powerful platforms for scientific research in polar regions. Long duration flights are one of the candidates for future international collaborative scientific activities. The authors hope that the potential and merits of balloons will be realized in science in the Arctic using their new balloon technology as well as facilities developed for

This document is provided by JAXA.

ballooning in Antarctica.

References

Akiyama, H., Yajima, N., Okabe, Y., Honda, H., Noguchi, H., Ikeda, T., Andoh, Y., Nanjo, N., Ichijo, T. and Ikejiri, H. (1992): Flight test of an airtight and waterproof gondola made of FRP. Proc. of Scientific Balloon Symposium, 5–11 (in Japanese).

Aoki, S., Hashida, G., Machida, T., Okano, S., Yamanouchi, T., Morimoto, S., Honda, H., Namiki, N., Yajima, N. and Nakazawa, T. (1999): Collection of stratospheric air with balloon-borne cryogenic sampler over Syowa Station, Antarctica [II]—Balloon launching and payload recovery—. Uchû Kagaku Kenkyû-jo, Hôkoku, Tokushû (Inst. Space Astronaut. Sci., Spec. Issue), **39**, 87–106 (in Japanese with English abstract).

Ejiri, M., Kadokura, A., Hirasawa, T., Sato, N., Fujii, R., Miyaoka, H., Nishimura, J., Yajima, N., Yamagami, T., Kokubun, S., Fukunishi, H., Yamanaka, M. and Kodama, M. (1993): Polar patrol balloon experiment in Antarctica. Adv. Space Res., **13** (2), 127–130.

Honda, H., Aoki, S., Nakazawa, T., Morimoto, S. and Yajima, N. (1996a): Cryogenic air sampling system for measurements of the concentrations of stratospheric trace gases and their isotopic ratios over Antarctica. J. Geomagn. Geoelectr., **48**, 1145–1155.

Honda, H., Morimoto, S., Akiyama, H., Hashida, G., Aoki, S., Ui, H., Nakazawa, T., Yajima, N. and Yamanouchi, T. (1996b): A newly developed grab sampling system for collecting stratospheric air over Antarctica. Nankyoku Shiryô (Antarct. Rec.), **40**, 156–168.

Honda, H., Izutsu, N., Morimoto, S., Aoki, S., Hashida, G., Machida, T., Okano, S., Yajima, N., Yamagami, T., Namiki, N. and Balloon Group (1999a): Collection of stratospheric air with balloon-borne cryogenic sampler over Syowa Station, Antarctica [I]—Newly developed onboard instruments and ground systems—. Uchû Kagaku Kenkyû-jo, Hôkoku, Tokushû (Inst. Space Astronaut. Sci., Spec. Issue), **39**, 67–86 (in Japanese with English abstract).

Honda, H., Hashida, G., Morimoto, S., Aoki, S., Yamanouchi, T. and Nakazawa, T. (1999b): Feasibility study for recovering balloon payload at Syowa Station, Antarctica. Uchû Kagaku Kenkyû-jo, Hôkoku, Tokushû (Inst. Space Astronaut. Sci., Spec. Issue), **39**, 57–66 (in Japanese with English abstract).

Honda, H., Yajima, N., Yamagami, T., Aoki, S., Hashida, G., Machida, T., Morimoto, S., Okano, S., Yamanouchi, T. and Nakazawa, T. (1999c): Stratospheric air sampling experiment at Syowa Station, Antarctica. Proc. of 14th ESA Symp. on European Rocket and Balloon Programmes and Related Research, ESA SP-437.

Honda, H., Yajima, N., Yamagami, T., Aoki, S., Hashida, G., Machida, T. and Morimoto, S. (2000): Balloon operation for stratospheric air sampling at Antarctica. Adv. Space Res., **26** (9), 1369–1372.

Izutsu, N., Honda, H., Yajima, N., Morimoto, S., Aoki, S. (1999): Stratospheric air sampling balloon operation at Antarctica. Proc. of 1999 AIAA Symp., Norfork VA, 28 June–1 July, 257–265.

Yajima, N. (2000): A new design and fabrication approach for pressurized balloon. Adv. Space Res., **26** (9), 1357–1360.

Yajima, N., Honda, H., Aoki, S., Hashida, G., Morimoto, S., Machida, T. and Okano, S. (1999a): Improved scientific ballooning applied to the cryo-sampling experiment at Syowa Station. Adv. Polar Upper Atmos. Res., **13**, 167–175.

Yajima, N., Izutsu, N., Honda, H., Kurokawa, H. and Matsushima, K. (1999b): A new design concept of natural shape balloon for high pressure durability. Proc. of 1999 AIAA Symp., Norfork VA, 28 June–1 July, 221–230.

(Received May 23, 2000; Revised manuscript accepted October 17, 2000)

This document is provided by JAXA.

This document is provided by JAXA.

Mem. Natl Inst. Polar Res., Spec. Issue, 54, 143-151, 2001

Scientific paper

Climate change and its impacts on the arctic environment

Gunter Weller

Center for Global Change and Arctic System Research, University of Alaska Fairbanks, Fairbanks, Alaska 99775-7740, U.S.A.

Abstract: Regional assessments of climate change and its impacts are a high priority in the international programs on global change research. In the Arctic, climate models indicate an amplification of the global greenhouse warming, but the observed high-latitude climate trends over the last few decades are much more regional and patchy than predicted by the models. While considerable uncertainties remain in the long-term prediction of change there is some agreement between model results and observed trends by season on shorter time scales. The warming observed over the landmasses of the Arctic over the last few decades is matched by corresponding observed decreases in snow cover and glacier mass balances, by thawing of the permafrost, and by reductions in sea ice extent and thickness. The available evidence strongly suggests that the observed decrease in Northern Hemisphere sea ice extent is related to anthropogenic global warming. While uncertainties exist about the future, climate change in the Arctic during the past few decades can be shown to have had major impacts already on the arctic environment which will become much more pronounced if present trends continue.

1. Introduction

The Arctic plays a crucial role in global climate change. It is a sensitive indicator of change and its snow and ice features are good integrators of change. It also stores long-term climatic records in its glaciers and the Greenland ice sheet. The Arctic also affects the global climate directly through interactions between its atmosphere, ice cover, and oceans, and through a number of important feedback processes. Practically all climate models predict an amplification of the global greenhouse effect in the Arctic (IPCC, 1990, 1996; Everett *et al*., 1998).

Global greenhouse warming affects the arctic environment by melting ice and thawing permafrost. Practically all the snow and ice features of the Arctic will be affected in one way or another. The extent and thickness of the seasonal snow cover, sea ice, permafrost, glaciers and river and lake ice are all expected to decrease as the climate warms. These changes in turn will affect the polar ecosystems with their distinct fauna and flora. Socio-economic consequences to populations, industry, and lifestyles will be inevitable. Not all of these changes are necessarily negative; for example less sea ice may allow the opening of trans-Arctic shipping routes and offshore petroleum exploration (Weller, 1998).

The Arctic, in turn, can affect the global climate through polar feedback processes. The albedo-snow cover-temperature feedback (Kellogg, 1975) is one of the main causes of the

This document is provided by JAXA.

amplification of the greenhouse effect in the Arctic. Permafrost-trace gas-temperature feedbacks could also be important. If more CO_2 and CH_4 is released when permafrost thaws, this will increase the atmospheric temperature and will result in thawing more permafrost. Melting of glaciers and ice sheets raise the global sea level, and the collapse of large ice sheets has been postulated as a possible trigger of the major, rapid climate changes during the last ice age, as seen in the Greenland ice core results (Alley *et al.*, 1993).

2. Projected future climate impacts

The IPCC report *Climate Change 1995* (1996) includes a chapter (Chapter 7 of Working Group II on the cryosphere—the regions of snow and ice) on climate change and its likely impacts on the polar regions. This assessment states the degree of confidence that the IPCC had in its predictions, which include the following.

- Many components of the cryosphere are sensitive to changes in atmospheric temperature because of their thermal proximity to melting. The extent of glaciers has often been used as an indicator of past global temperatures (High Confidence).
- Projected warming of the climate will reduce the area and volume of the cryosphere. This reduction will have significant impacts on related ecosystems, associated people and their livelihoods (High Confidence).
- There will be striking changes in the landscapes of many high mountain ranges and of lands at northern high latitudes (High Confidence). These changes may be exacerbated where they are accompanied by growing numbers of people and increased economic activities (Medium Confidence).

For a scenario that doubles the atmospheric concentrations of CO_2, the following changes and associated impacts on the Arctic are likely, again listing the degree of confidence in these predictions.

- Pronounced reductions in seasonal snow cover, permafrost, glacier and periglacial features with a corresponding shift in landscape processes (High Confidence).
- Increases in the thickness of the active layer of permafrost and the disappearance of most of the ice-rich discontinuous permafrost over a century-long time span (High Confidence).
- Disappearance of up to a quarter of the presently existing mountain glacier mass (Medium Confidence).
- Less ice on rivers and lakes. Freeze-up dates will be delayed, and break-up will begin earlier. The river-ice season could be shortened by up to a month (Medium Confidence).
- A large change in the extent and thickness of sea ice, not only from warming but also from changes in circulation patterns of both atmosphere and oceans. There is likely to be substantially less sea ice in the polar oceans (Medium Confidence).

Many of these impacts are already being experienced in the Arctic, as shown in the next chapter.

3. Evidence of climate change

3.1. Twentieth century climate trends

Discussion of the detection of the greenhouse signal in the polar regions usually

This document is provided by JAXA.

revolves around two questions: (1) Are we now seeing the greenhouse signal in the high latitudes? (2) If not, how and when will the signal manifest itself? Chapman and Walsh (1993) examined the climate trends in the Arctic for the period 1961–1990, using the climate data set of the Climate Research Unit of the University of East Anglia (Jones *et al.*, 1986). Their analysis, as well as their updated results for 1966–1995, indicates considerable warming over the landmasses of Eurasia and North America, particularly in winter and spring. Over the last three decades, trends of up to 1.5℃ per decade have been towards higher temperatures. On the other hand there are also smaller areas of cooling of similar magnitude within the arctic regions, particularly in the South Greenland and Davis Strait area.

The available data also point to a more vigorous atmospheric circulation associated with a deepening of both the Icelandic and Aleutian Lows (Maxwell, 1995). The primary reason for a warmer climate in the Western Arctic, for example, is that more southerly flow occurs in winter coupled with less northerly flow of cold air from Siberia. Similarly the cooler climate in Southern Greenland is most likely related to a shift in the circumpolar wave pattern with increased northerly flow in that region. Whether this is triggered by the greenhouse effect is not clear at present.

3.2. Impacts on snow and ice

In many different parts of the world, pronounced reductions in seasonal snow, glaciers, permafrost and sea ice have been observed as a consequence of a warmer climate. In the Arctic, where the following observations have been made, these changes are particularly pronounced. Vinnikov *et al.* (1999) state that the probability of the observed trends

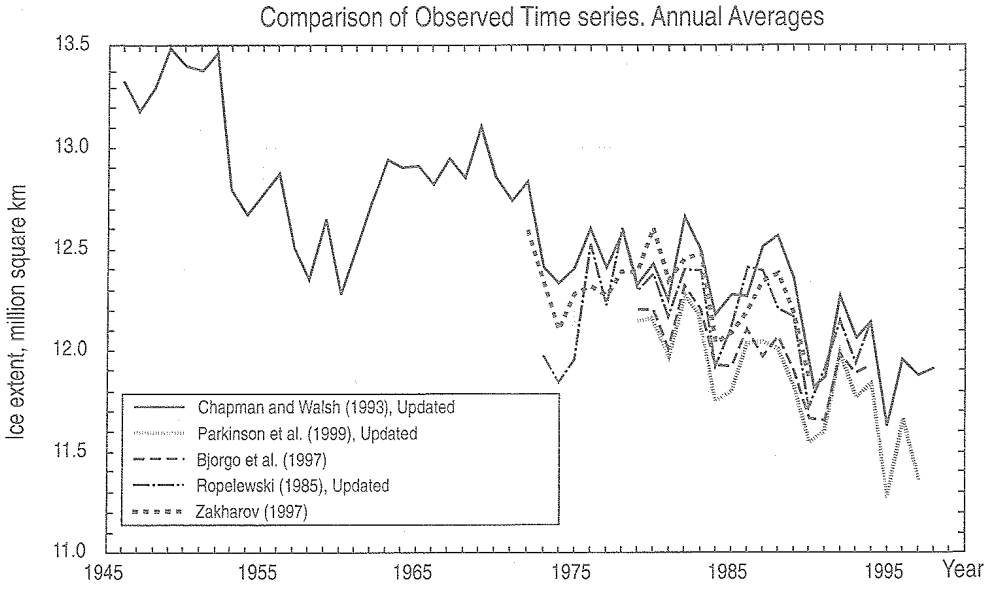


Fig. 1. Observed decrease of the Northern Hemisphere sea ice extent since 1945 (Vinnikov et al., 1999).

This document is provided by JAXA.

resulting from natural climate variability is less than 0.1 percent for the observed 1953–98 sea ice trends (Fig. 1). This strongly suggests that the observed decrease in Northern Hemisphere sea ice extent is related to anthropogenic global warming.

3.2.1. Sea ice

There have been substantial reductions in both ice extent and thickness in the Arctic in recent decades:

- The most recent study using passive microwave data from satellites through 1996 has shown Arctic sea ice extent decreasing by 2.9% (±0.2%) per decade (Cavalieri *et al.*, 1997).
- New extreme minimums of summer ice extent have been established repeatedly since 1980. The September ice extent in the Beaufort and Chukchi seas was 25% below the prior minimum value over the 45-year record (Maslanik *et al.*, 1999).
- Sea-ice extent in the Bering Sea has been reduced by about 5% over the last 40 years, with the steepest decrease occurring in the late 1970s (BESIS, 1997).
- Sea ice thickness, a sensitive indicator of climate change, has decreased by about 1.3 m, from 3.1 m to 1.8 m, in most of the deep water portion of the Arctic Ocean between

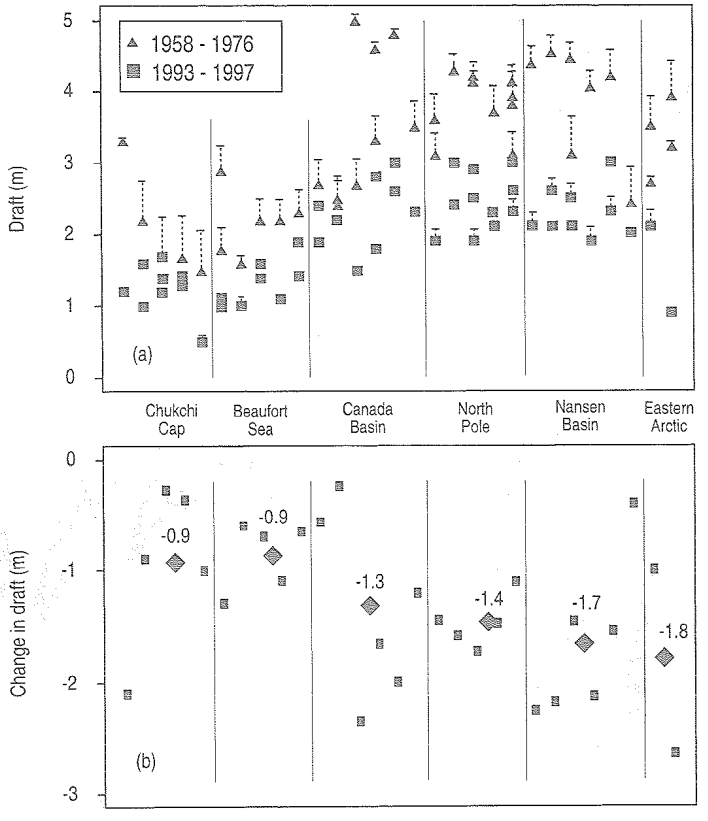


Fig. 2. Sea ice thickness reductions for various regions of the Arctic from submarine sonar data collected between 1958–1976 and 1993–1997 (Rothrock et al., 1999).

This document is provided by JAXA.

the 1960/1970s and the 1990s, based on submarine sonar records (Fig. 2 due to Rothrock *et al.*, 1999).

- The sea ice thickness decrease is greatest in the central and eastern Arctic and less in the Beaufort and Chukchi seas (Rothrock *et al.*, 1999).
- Observations at Barrow, Alaska, on the Beaufort Sea coast, showed sea ice to be only 1.4 m thick in 1998, compared with its normal thickness of 1.7–1.8 m; this is thinner than ever observed before (L. Shapiro, 1999, personal communication).

3.2.2. Glaciers and ice sheets

- Glaciers in the Arctic and subarctic regions have generally receded, with typical ice-thickness decreases of 10 m over the last 40 years (Fig. 3), but some glaciers have thickened in their upper regions (BESIS, 1997). A warming of 1°C, if sustained, appears to reduce glacier lengths by about 15%.
- The mass balance of Greenland is still uncertain, but there appears to have been a tendency towards increased melt area between 1979–1991 that ended abruptly in 1992, possibly due to the effects of the Mt. Pinatubo eruption (Abdalati and Steffen, 1997).
- Balances have been positive for European glaciers in Scandinavia and Iceland due to increased winter precipitation (Serreze *et al.*, 2000).
- Over the period 1961–1990, small melting glaciers worldwide have contributed about

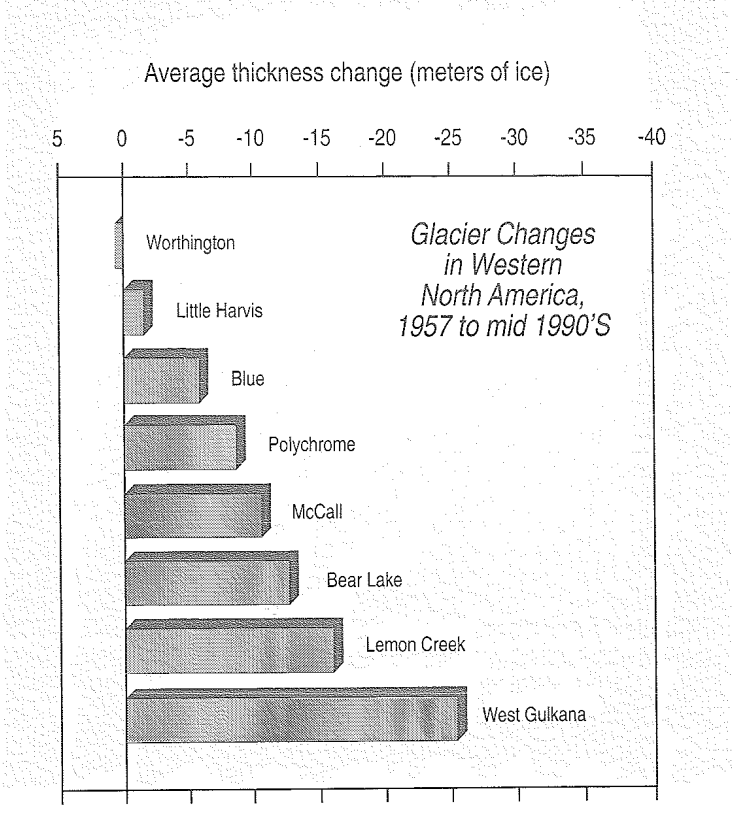


Fig. 3. Glacier mass balance changes in Western North America from 1957 to the mid-1990s (Sapiano et al., 1998).

This document is provided by JAXA.

7.36 mm to sea level rise, with the Arctic Islands contributing 1.36 mm, Alaska 0.54 mm, and Asia 3.34 mm (Serreze *et al.*, 2000).

3.2.3. Seasonal snow cover

- Cyclone and anticyclone frequency has increased over the Arctic between 1952–1989 (Everett *et al.*, 1998; Section 3.2).
- Annual snowfall has increased in the same period over northern Canada (North of 55°N) by about 20% and by about 11% over Alaska (Everett *et al.*, 1998; Section 3.2).
- While there is more snow in winter, satellite records indicate that since 1972 Northern Hemisphere annual snow cover on both continents has decreased by about 10%, largely due to spring and summer deficits since the 1980s (Serreze *et al.*, 2000).
- There has also been a decrease in snow depth in Canada since 1964, especially during spring, while winter depths have declined in some areas over European Russia since the turn of the century but have increased in others (Serreze *et al.*, 2000).

3.2.4. Permafrost

- Borehole measurements in continuous permafrost have shown warming of up to 2–4°C

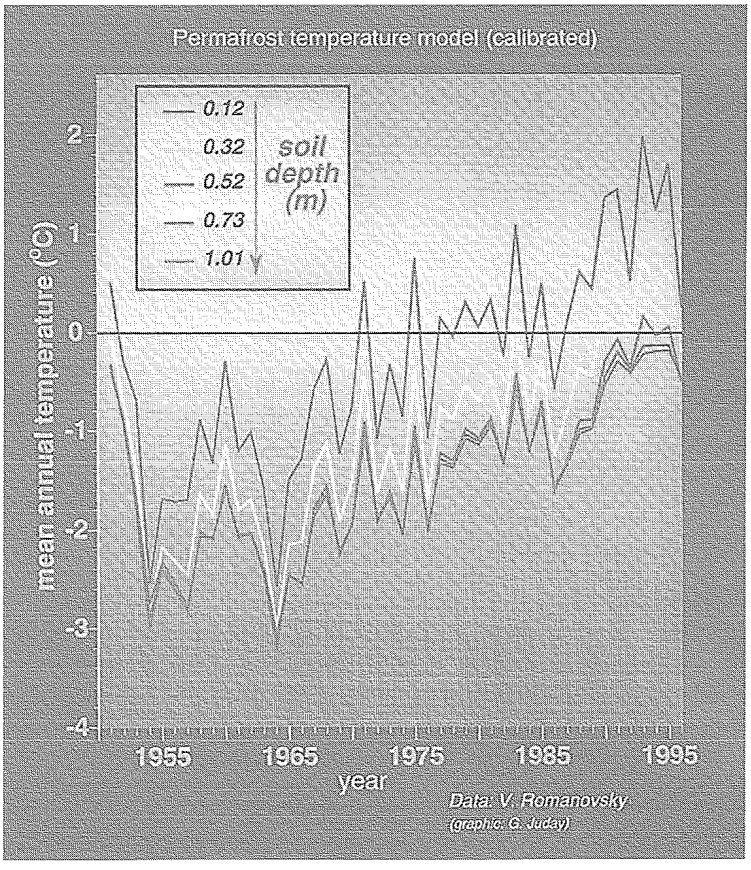


Fig. 4. Change in soil temperatures at various depths in permafrost terrain at Fairbanks, Alaska (V. Romanovsky, personal communication).

This document is provided by JAXA.

in northern Alaska over the last 80–100 years (Lachenbruch and Marshall, 1986).

- Discontinuous permafrost throughout Alaska has warmed (Fig. 4), and some of it is currently thawing from the top and bottom (Osterkamp, 1994).
- Near-surface permafrost has also become warmer by 0.6–0.7℃ in Siberia during the period 1970–1990; this warming may in part be due to a deeper snow cover in winter (Pavlov, 1994).

3.2.5. River and lake ice

- River and lake ice formation in Alaska occurs later in fall and breakup occurs earlier in spring, leading to shorter ice-covered periods. The annual breakup of the Tanana River ice in interior Alaska has been recorded since the 1920s and shows most breakup dates to occur in April in the 1990s compared with most of them occurring in May in the 1920s (Nenana Ice Classic, 1999).

3.3. Fingerprinting climate change

A view that has been proposed by climate researchers is that the "traditional" emphasis on sea ice extent and Arctic Ocean air temperatures as early indicators of change should be replaced with a broader "fingerprint" of many variables. This "fingerprint" should involve information from ice cores, sea ice concentration and thickness, sea surface temperatures, subsurface polar ocean temperatures, and high latitude precipitation. The set of variables in Table 1 summarizes the evidence of recent changes and provides such a "fingerprint." The observed changes are consistent with those anticipated from greenhouse influences. However, there are still problems since long records exist only for surface temperatures, and even these are not long enough to distinguish unambiguously the natural and man-made influences (Walsh *et al.*, 1996).

Table 1. Summary of changes observed in the Arctic over the last few decades of the 20th century (modified from Walsh et al., 1996).

Parameter	Trend	Comments
Surface temperature	Generally warmer	(on land, in winter/spring, but also some areas of cooling; unclear over Arctic Ocean)
Tropospheric temps.	Warmer	(lowest layers)
Stratospheric temps.	Colder	(summer only)
Precipitation	Increased	(over land, unknown over sea ice)
Extreme weather	Not yet assessed	
Ocean temps.	Warmer	(Central Arctic)
Snow cover extent	Reduced	(Eurasia, in spring; also in Canada and Alaska)
Snow cover depth	Reduced	
Sea ice extent	Reduced	(throughout the Arctic)
Sea ice thickness	Thinner	(throughout the Arctic)
Ice sheet elevation	Higher	(S. Greenland, no change in Canada)
Ice sheet surface melting	Increased	(S. Greenland)
Ice shelf extent	Reduced	(Canada)
Permafrost extent	Reduced	(Alaska, Canada, Siberia)

This document is provided by JAXA.

4. Societal and economic impacts of climate change

The societal and economic consequences of climate change in the Arctic are likely to be substantial but are not the subject of this paper. Reference to these impacts can be found in a number of publications (BESIS, 1997, 1998, 1999; Weller and Lange, 1999). Changes in the cryosphere, as a consequence of a warmer climate, that will lead to social and economic impacts have been summarized by the IPCC as follows:

- Widespread loss of discontinuous permafrost will trigger erosion or subsidence of ice-rich landscapes, change hydrologic processes, and release carbon dioxide (CO_2) and methane (CH_4) to the atmosphere (High Confidence).
- Cryospheric change will reduce slope stability and increase the incidence of natural hazards for people, structures and communication links. Buildings, other structures, pipelines and communication links will be threatened (High Confidence).
- Engineering and agricultural practices will need to adjust to changes in snow, ice and permafrost distributions (High Confidence).
- Thawing of permafrost could lead to disruption of petroleum production and distribution systems in the tundra, unless mitigation techniques are adopted. Reduced sea ice may aid new exploration and production of oil in the Arctic Basin (High Confidence).
- Improved opportunities for water transport, tourism and trade are expected from a reduction in sea, river and lake ice. These will have important implications for the people and economies of the Arctic (Medium Confidence).

References

Abdalati, W. and Steffen, K. (1997): Snowmelt on the Greenland ice sheet as derived from passive microwave data. J. Clim., **10**, 165–175.

Alley, R.B., Meese, D.A., Shuman, C.A., Gow, A.J., Taylor, K.C., Grootes, P.M., White, J.W.C., Ram, M., Waddington, E.D., Mayewski, P.A. and Zielinski, G.A. (1993): Abrupt increase in Greenland snow accumulation at the end of the Younger Dryas event. Nature, **362**, 527–529.

Bering Sea Impacts Study (BESIS) (1997): The Impacts of Global Climate Change in the Bering Sea Region. Oslo, International Arctic Science Committee, 41 p.

Bering Sea Impacts Study (BESIS) (1998): Implications of Global Change in Alaska and the Bering Sea Region. Proceedings of a Workshop at the University of Alaska, 3–6 June 1997. Center for Global Change and Arctic System Research, University of Alaska Fairbanks, 152 p. with appendix.

Bering Sea Impacts Study (BESIS) (1999): Assessing the Consequences of Climate Change for Alaska and the Bering Sea Region. Proceedings of a Workshop at the University of Alaska Fairbanks, 29–30 October 1998. Center for Global Change and Arctic System Research, University of Alaska Fairbanks, 94 p.

Cavalieri, D.J., Gloersen, P., Parkinson, C.L., Comiso, J.C. and Zwally, H.J. (1997): Observed hemispheric asymmetry in global sea ice changes. Science, **278**, 1104–1106.

Chapman, W.L. and Walsh, J.E. (1993): Recent variations of sea ice and air temperatures in high latitudes. Bull. Am. Meteorol. Soc., **74**, 33–47.

Everett, J.T., Fitzharris, B.B. and Maxwell, B. (1998): The Arctic and the Antarctic. The Regional Impacts of Climate Change: An Assessment of Vulnerability. A Special Report of IPCC Working Group II, ed. by R.T. Watson *et al.* Cambridge, Cambridge University Press, 85–103.

Intergovernmental Panel on Climate Change (IPCC) (1990): Climate Change. The Scientific Assessment, ed. by J.T. Houghton *et al.* WMO-UNEP, Geneva. Cambridge University Press, 364 p.

This document is provided by JAXA.

Intergovernmental Panel on Climate Change (IPCC) (1996): Climate Change 1995. Impacts, Adaptations and Mitigation of Climate Change: Scientific-Technical Analysis Contributions of Working Group II to the Second Assessment Report of the Intergovernmental Panel on Climate Change, ed. by R.T. Watson *et al.* WMO-UNEP, Geneva. Cambridge University Press, 876 p.

Jones, P.D., Raper, S.C.B., Bradley, R.S., Diaz, H.F., Kelly, P.M. and Wigley, T.M.L. (1986): Northern hemisphere surface air temperature variations, 1851-1984. J. Clim. App. Meteorol., **25**(2), 161-179.

Kellogg, W.W. (1975): Climatic feedback mechanisms involving the polar regions. Climate of the Arctic, ed. by G. Weller and S.A. Bowling. University of Alaska Fairbanks, Geophysical Institute, 111-116.

Lachenbruch, A.H. and Marshall, B.V. (1986): Changing climate: geothermal evidence from permafrost in the Alaskan Arctic. Science, **234**, 689-696.

Maslanik, J.A., Serreze, M.C. and Agnew, T. (1999): On the record reduction in 1998 Western Arctic sea ice cover. Geophys. Res. Lett., **26**, 1905-1908.

Maxwell, B. (1995): Recent climate patterns in the Arctic. Global Change and Arctic Terrestrial Ecosystems. Proceedings of Invited and Plenary Papers from the International Conference, 21-16 August 1993, Oppdal, Norway, ed. by W.C. Oechel *et al.* New York, Springer, 21-46.

Nenana Ice Classic: Alaska's coolest lottery (1999): Dates of the Nenana River ice breakup (from their webpage: http://www.ptialaska.net/-tripod/breakup.times.html).

Osterkamp, T. (1994): Evidence for warming and thawing of discontinuous permafrost in Alaska (abstract). EOS, **75**(44), Suppl., 85.

Pavlov, A.V. (1994): Current changes of climate and permafrost in the Arctic and sub-Arctic of Russia. Permafrost Periglacial Processes, **5**, 101-110.

Rothrock, D.A., Yu, Y. and Maykut, G.A. (1999): Thinning of the arctic sea-ice cover. Geophys. Res. Lett., **26**, 3469-3472.

Sapiano, J.J., Harrison, W.D. and Echelmeyer, K.A. (1998): Elevation, volume and terminus changes of nine glaciers in North America. J. Glaciol., **44**, 119-135.

Serreze, M.C., Walsh, J.E., Chapin, F.S. III, Osterkamp, T., Dyurgerov, M., Romanovsky, V., Oechel, W. C., Morison, J., Zhang, T. and Barry, R.G. (2000): Observational evidence of recent change in the northern high-latitude environment. Clim. Change, **46**(1-2), 159-207.

Vinnikov, K.Y., Robock, A., Stouffer, R., Walsh, J., Parkinson, C., Cavalieri, D., Mitchell, J., Garrett, D. and Zakharov, V. (1999): Global warming and northern hemisphere sea ice extent. Science, **286**, 1934-1937.

Walsh, J.E., Tanaka, H.L. and Weller, G. (1996): Wadati conference on global change and the polar climate, 7-10 November 1995, Tsukuba, Japan. Bull. Am. Meteorol. Soc., **77**, 1268-1273.

Weller, G. (1998): Regional impacts of climate change in the Arctic and Antarctic. Ann. Glaciol., **27**, 543-552.

Weller, G. and Lange, M., ed. (1999): Impacts of Global Climate Change in the Arctic Regions. Workshop on the Impacts of Global Change, 25-26 April 1999, Tromsø, Norway. Published for International Arctic Science Committee by Center for Global Change and Arctic System Research, University of Alaska Fairbanks, 59 p.

(Received March 31, 2000; Revised manuscript accepted July 31, 2000)

This document is provided by JAXA.

This document is provided by JAXA.

Mem. Natl Inst. Polar Res., Spec. Issue, 54, 153–159, 2001

Report

Summit Greenland environment observatory

Atsumu Ohmura

Institute for Climate Research, Swiss Federal Institute of Technology (ETH), CH-8057 Zurich, Switzerland (ohmura@geo.umnw.ethz.ch)

Abstract: A new movement to establish a permanent environment observatory at Summit in Greenland is under way between US and Europe. The initial motivation was to observe exchange processes between the atmosphere and the ice sheet surface to obtain the basic knowledge for the ice-core interpretation. It was, however, soon recognised that the objective necessitated the observations not only on the ice sheet surface, but also for the entire atmosphere including the middle atmosphere and the thermosphere. It became also obvious that the near-surface snow and firn layer should be investigated. To reach the goal the observations should be carried out year-round for a number of years. By the beginning of 1996 the idea was developed to establish an observatory for the integrated environment observation. As the first step a feasibility study for over-wintering at Summit was carried out during the 1997/1998 season with a four-man team. The project started its first year's operation in April 2000 and expects to carry out proposed observations for at least three years, until the final decision is made regarding the precise nature of the "permanent" observatory. The entire observation programme is multi-disciplinary. The author has been participating in the planning of the observatory from the start of the project. The present article was prepared to present an overview of the planned activities at the prospective observatory with emphasis on the field which the author has been primarily engaged in.

1. Introduction

Summit of Greenland is the region around the highest point on the Greenland ice sheet. During the summers from 1989 to 1993 Summit was a place of intensive ice-core boring activities. During those years two sites were drilled: GISP2 (72°35′N, 38°30′W, 3150 m a.s.l.) and GRIP (72°35′N, 37°39′W, 3230 m a.s.l.). The high-resolution history of the climate and atmospheric chemistry is being published (Dansgaard *et al.*, 1993; GRIP members, 1993). In the course of the core interpretation, however, a number of uncertainties were encountered. To decode the information archived in the ice cores, it has become necessary to understand the transfer processes of various matters between the atmosphere, the snow cover and firn layers. The initiative for the year-round observation at Summit came from the ice-core community. The other research disciplines joined the ice-core group to observe practically the entire environment in support of the core interpretation and also to pursue goals that can best be observed at this site. The old GISP2 drilling site was augmented to make the year-round observations possible.

This document is provided by JAXA.

2. Planned observations

The site of Summit is unique because of the high altitude in the high latitude regions of the Northern Hemisphere. The site is the third highest point within the Arctic Circle only after Gunnbjørns Fjeld (3700 m a.s.l.) and Mont Forel (3360 m a.s.l.). Because of the relatively low altitude of the tropopause in the Arctic the altitude of Summit represents the middle troposphere. The year-round dryness of the atmosphere, homogeneous nature of the snow surface and the large distances from anthropogenic emissions offer a unique opportunity to make various observations which are not possible at lower altitudes in the Arctic. The proposed observations are conceived to take advantage of the conditions prevailing at this site. The observations are grouped in the following themes:

1) Ice-core interpretation and tropospheric chemistry,
2) Energy balance and boundary layer processes,
3) Stratospheric physics and chemistry,
4) Atmospheric electricity,
5) Polar aeronomy and space sciences, and
6) Seismology and geodesy.

In view of the initial motivation of the project, the tropospheric chemistry has a considerable weight in the entire programme. The working process of the core-analyses is a kind of inversion to arrive at the boundary conditions (atmospheric time-series) starting from the solutions (cores). In this working procedure one traces back the natural processes in the opposite direction from how they happened. To proceed in this manner, it is necessary to understand each steps in the normal flow of natural processes, starting with the astronomical and atmospheric processes, covering the snow formation in the atmosphere, the surface deposition and the sintering process in the interior of the ice sheet. Tropospheric chemistry and boundary layer investigations must no doubt occupy the central position in this work. These investigations must be supported by the upper atmosphere studies on nuclear reactions, ionisation and photochemical reactions. Transfer processes from these layers to the ice sheet surface and subsequent transformations have also an important weight in the present programme. To obtain solid answers, the observations must be carried out year-round and over many years. Detailed observations will be carried out on the processes of the molecular-level integration of the atmospheric constituencies in the snow cover, including the snowfall, deposition and sublimation. Gas-phase measurements will include ozone, hydrocarbons, halocarbons and radon (Dibb, 1998). Further, aerosols and their ionic compounds will be considered (Bales, 1999). Besides obtaining a firm basis for chronological dating of ice-cores, it is believed that some of these components will help the core-analysts trace back the origins of air masses, providing hints on the paleo-atmospheric circulation and insights on human influence on the global atmosphere.

3. Energy balance and boundary layer processes

The author had the responsibility for formulating the European programme for investigating the ice sheet surface and atmospheric exchange processes. From the viewpoint of the primary objective of the ice-core interpretation, it is obvious that the goal can not

This document is provided by JAXA.

be achieved if the observation remains in the framework of conventional micrometeorology by observing only surface fluxes. The surface exchange must be understood in relation to large-scale atmospheric processes. This standpoint compels us to investigate the transport processes throughout the entire boundary layer by observations. Further, the results must be condensed in such a manner that they can be used to support the GCM-based numerical experiments. As a result the observation of the entire boundary layer combined with modern radiometry is proposed.

3.1. Boundary layer under stable conditions

The fluxes of various atmospheric characteristics are the result of the interaction of the atmosphere with the surface. Therefore, the processes in the entire boundary layer must be investigated in addition to the measurements of the consequences of the interaction. This is the basic frame of the experimental programme of the present study and aims at improving knowledge in the least understood regions in micrometeorology; namely the exchange processes in the stable atmosphere near the earth's surface. The investigation of the boundary layer under a stable stratification has been hindered by the fetch-effect that can survive over many kilometres. In the normally accessible areas it is not easy to gain ideal topographic conditions which satisfy the observational requirements for investigating the stable boundary layer. The area around Summit is one of the rare regions in the world that can be regarded as an ideal laboratory for experiments on the stable boundary layer. Firstly, the fetch is practically unlimited. Secondly, the surface is extremely homogenous, and thirdly high stability occurs frequently. From the wind-profile measurements of previous experiments on the Greenland ice sheet, the thickness of the planetary boundary layer is estimated to fluctuate between 200 m and 500 m above the surface (Ohmura, 1992; Ohmura *et al.*, 1994; Forrer and Rotach, 1997; Forrer, 1999). Within this layer and often within the lower half of the planetary boundary layer a thermocline appears which has a profound effect on the turbulent fluxes on the surface and the internal waves above the thermocline. Within the surface boundary layer turbulent fluxes and irradiances seem to be no longer constant. The divergences of sensible heat flux and radiative flux are, however, closely related. To grasp all these processes, the site will be equipped with a 50 m meteorological tower with 8 levels instrumented with sonic anemo-thermometers and Ly-α hygrometers, radiometers for radiative flux divergence measurement, a SODAR for continuous measurement of the height of the inversion, a wind-profiler which reaches up to 3000 m, a radio-sonde system and an aircraft equipped with the turbulence measuring system. Reliable turbulence measurements must be supported by high quality radiation data.

3.2. Radiation observation

Radiometry at Summit has three objectives that can be achieved on a medium time scale, that is, several years. The first objective is to provide accurate broad band irradiances to close the energy balance of the surface flux observations mentioned in the previous section. The second objective is to investigate the radiative characteristics of the atmosphere at a site with relatively small water vapour content and small amounts of low and middle clouds (Konzelmann and Ohmura, 1995). The third objective is the observation of the radiative divergence in the boundary layer to investigate its relationship with sensible heat flux. The atmospheric conditions at Summit are ideally suited for investigating the missing

This document is provided by JAXA.

absorption of solar radiation and also for observing radiative characteristics of the cirro-type cloud layers. The vast surface area with a homogenous snow cover helps accurate divergence measurements of radiative fluxes. To fulfil the accuracy requirements for these purposes, it was decided to adopt the scheme proposed for the Baseline Surface Radiation Network (BSRN) of the World Climate Research Programme (WCRP) (Ohmura *et al.*, 1998).

4. Long-term monitoring of atmospheric radiation

One of the most important goals in climate research is climate prediction. Presently, climate predictions are mostly based on models. In view of the possibility of grave economic and political influences of climate predictions, the prediction should not be based only on one method. The risk of all models committing the same error is too high. It is necessary to develop another climate prediction method that is independent of the model-based prediction method. This redundant prediction scheme is an added security, in case one of the above mentioned methods fails. The prediction of a natural phenomenon is possible in principle, if the precursor is detected early enough for organising response strategies. Such a prediction scheme must identify the very beginning of the processes which ultimately causes the phenomenon which we wish to predict. One example in other areas of earth science is the prediction of tsunamis by detecting the initiating earthquake. Another example in the climate system is the prediction of ENSO by knowing the start of the

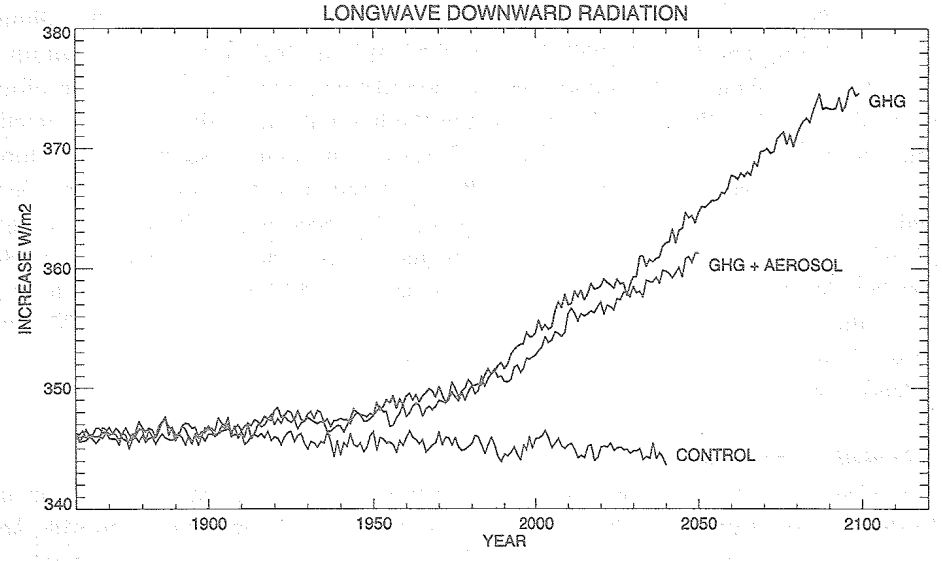


Fig. 1. Global mean longwave incoming radiation (W m^{-2}) for the last 140 years and future 100 years. The computation was made with ECHAM4/OPY3 T42 transient experiment based on the observed gas concentrations for 1860–1990. The future concentration is due to scenario IS92a. GHG denotes the scenario with only greenhouse gases. GHG + AEROSOL indicates the development with additional direct and indirect aerosol effect (SO_2) plus tropospheric ozone (Roeckner et al., 1999).

This document is provided by JAXA.

eastward movement of the warm water body in the tropical west Pacific.

In the case of climate change in the immediate future, it is envisaged that the enhanced greenhouse effect will become in due time powerful enough to dominate other climate factors. The enhanced greenhouse effect begins with an increase in longwave incoming radiation at the earth's surface. The author proposes to use the long-term monitoring of the longwave incoming radiation at the earth's surface as a means for predicting the onset of the greenhouse climate change. Figure 1 shows the simulated course of the global mean longwave incoming radiation for the next 100 years with ECHAM4 T42 coupled transient experiment, based on the scenario IS92a, carried out by Roeckner *et al.* (1999). The average rate of the IR increase is 2 W m^{-2} per decade. The increasing rate shows considerable regional variation. Figure 2 shows the global distribution of the increase in IR radiation, indicating the larger IR increase for the regions with smaller amounts of low and middle clouds. They are the desert and Polar regions of high altitudes. The site of Summit falls in such a fortunate spot on the Greenland ice sheet, indicating a 5 W m^{-2} change per decade. A zone of relatively large increase is seen over the sub-arctic oceans. This increase, however, is mainly caused by the temperature increase as the result of the recession of the sea-ice margins, and is outside the present consideration. Given the presently available accuracy of the longwave measurement of 3 W m^{-2} (Philipona *et al.*, 1995; Ohmura *et al.*, 1998), it must be possible to detect a systematic increase in longwave atmospheric radiation in about a decade or two at the location of Summit. This early detection of climate changes with the

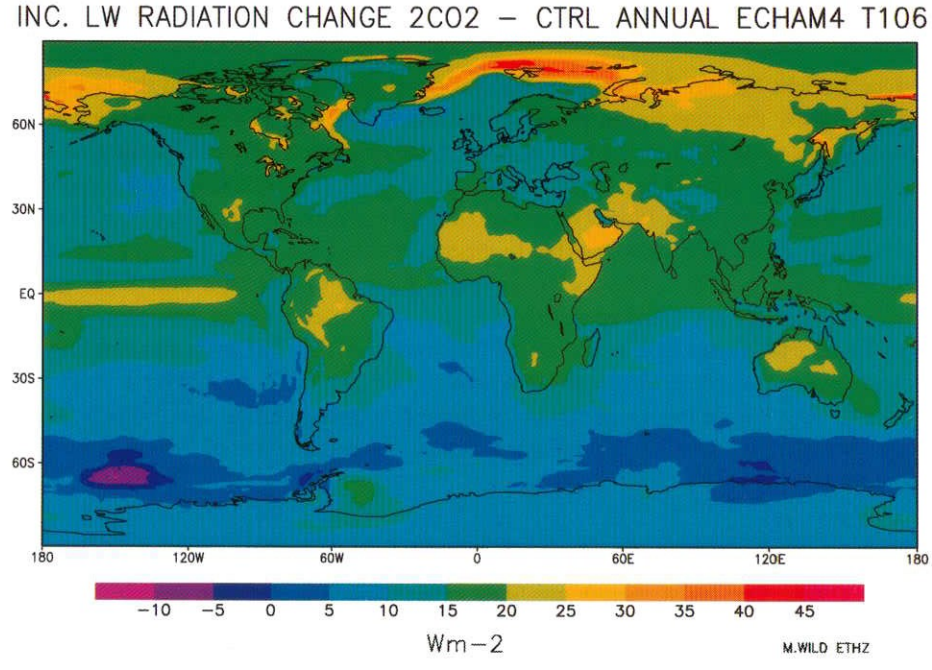


Fig. 2. Expected increase in annual mean longwave incoming radiation for the last decade in 21st century in W m^{-2} (based on the same experiment as in Fig. 1).

This document is provided by JAXA.

IR-monitoring is expected to happen at least one decade prior to the possible detection of the subsequent rise in air temperature. This fortunate delay in the temperature response is partly due to the storage of heat in the climate system, especially in oceans. The main reason for the early detection of a climate change from radiation rather than air temperature is, however, due to an extremely small year to year variation in longwave incoming radiation, which makes it easier to detect a long-term trend.

Besides longwave observations, the site will be equipped with instruments for all other shortwave and longwave components, including the Precision Filter Radiometer. This instrument will measure the change in aerosol optical depth for direct solar radiation. This measurement is meant to numerically evaluate the change in the direct aerosol effect, which could counter the enhanced greenhouse effect.

5. Closing remarks

The proposed Summit Greenland Environment Observatory offers a unique platform for environment observations, which are not possible in other regions of the Northern Hemisphere. It is especially suited for detecting long-term variation in radiation fields, which may cause climate changes. The activities at the observatory also provide an opportunity for cross-Atlantic co-operation which has proven to be a fruitful stimulation not only for scientific advancement but for training young scientists to understand different ways of thinking and behaviour between the similar but by now different cultures.

Acknowledgments

The thought behind the present work was developed in the course of the last ten years especially during the preparation phase of the BSRN/WCRP. The author wishes to thank Dr. John DeLuisi of NOAA, Boulder and Dr. Claus Fröhlich of World Radiation Centre, Davos for sharing valuable experiences over several years. The numerical experiments were performed within the Max-Planck-Institute (MPI) for Meteorology, Hamburg and ETH, Zurich co-operation. The author wishes to especially thank Dr. Erich Roeckner of MPI and Dr. Martin Wild of ETH. The Swiss National Science Foundation and ETH provided financial support for our participation in the Summit Observatory Programme. The major part of the IR instrument development was financed by ETH. The author is indebted to the past and present vice-presidents for research at ETH, Profs. Ralf Hütter and Albert Waldvogel. The GCM-based numerical experiments were carried out with a financial support provided by AVINA Foundation within the programme of Alliance for Global Sustainability ETH-MIT-Univ. Tokyo.

References

Bales, C.B. (1999): Year-round research gets boost at Summit of Greenland ice sheet. EOS, **80**, 51.

Dansgaard, W., Johnsen, S.J., Clausen, H.B., Dahl-Jensen, D., Gundestrup, N.S., Hammer, C.U., Hvidberg, C.S., Steffensen, J.P., Sveinbjörnsdottir, A.E., Jouzel, J. and Bond, G. (1993): Evidence for general instability of past climate from a 250-kyr ice-core record. Nature, **364**, 218–220.

Dibb, J. (1998): Team pioneers all-winter research at Greenland Summit. Arctic, **6**, 1–3.

This document is provided by JAXA.

Forrer, J. (1999): The structure and turbulence characteristics of the stable boundary layer over the Greenland ice sheet. Zürcher Klima-Schriften, **75**, 120 p.

Forrer, J. and Rotach, M. (1997): On the turbulence structure in the stable boundary layer over the Greenland ice sheet. Boundary-Layer Meteorol., **85**, 111–136.

GRIP members (1993): Climate instability during the last interglacial period recorded in the GRIP ice core. Nature, **364**, 203–207.

Konzelmann, T. and Ohmura, A. (1995): Radiative fluxes and their impact on the energy balance of the Greenland ice sheet. J. Glaciol., **41**, 490–502.

Ohmura, A. ed. (1992): Energy and mass balance during the melt season at the equilibrium line altitude, Paakitsoq, Greenland ice sheet. Department of Geography, ETH, Zurich, 94 p. (Progress Report, **2**).

Ohmura, A., Konzelmann, T., Rotach, M., Forrer, J., Wild, M., Abe-Ouchi, A. and Toritani, H. (1994): Energy balance for the Greenland ice sheet by observation and model computation. Snow and Ice Covers: Interactions with the Atmosphere and Ecosystems, ed. by H.G. Jones *et al.* Wallingford, IAHS Press, 85–94 (IAHS Publ. No. **223**).

Ohmura, A., Dutton, E., Forgan, B., Fröhlich, C., Gilgen, H., Hegner, H., Heimo, A., König-Langlo, G., McArthur, B., Müller, G., Philipona, R., Pinker, R., Whitlock, C.H., Dehne, K. and Wild, M. (1998): Baseline Surface Radiation Network (BSRN/WCRP): New precision radiometry for climate research. Bull. Am. Meteorol. Soc., **79**, 2115–2136.

Philipona, R., Fröhlich, C. and Betz, C. (1995): Characterization of pyrgeometers and the accuracy of atmospheric long-wave radiation measurements. Appl. Opt., **43**, 1598–1605.

Roeckner, E., Bengtsson, L., Feichter, J., Lelieveld, J. and Rodhe, H. (1999): Transient climate change simulations with a coupled atmosphere-ocean GCM including the tropospheric sulfur cycle. J. Clim., **12**, 3004–3032.

(Received May 31, 2000; Revised manuscript accepted July 24, 2000)

This document is provided by JAXA.

This document is provided by JAXA.

Mem. Natl Inst. Polar Res., Spec. Issue, 54, 161-168, 2001

Scientific paper

Atmospheric teleconnection between Japan and the Saint Elias Mountains, Yukon

Gerald Holdsworth

Arctic Institute of North America, University of Calgary, Calgary, Alberta, Canada T2N 1N4 (gholdswo@ucalgary.ca)

Abstract: Cross correlation between time series of (1) total precipitation for a combined four-station network in northern Japan and of (2) the net snow accumulation determined from an ice core obtained from Mount Logan (60.5°N, 5340 m) situated in the Saint Elias Mountains, Yukon, reveals high, statistically significant, cross correlation coefficients of +0.38 for annual data increasing up to +0.71 for seven point smoothing of the two 89 year series. The distance between sites is about 7000 km spanning the complete Pacific Ocean between latitudes of about 40°N and 60°N. A review of the extensive literature of oceanology and climatology for the North Pacific Ocean region indicates that a strong coupling exists between the ocean and the atmosphere especially up to and associated with the Polar Front Zone along which major cyclogenesis occurs during most months of the year. Cyclones track generally from west to east with a strong northerly component especially in the eastern (Gulf of Alaska) sector. Examination of these cyclones on GOES satellite images shows that weather systems can transport moisture from mid latitude ocean sources (<40°N) to high on Mount Logan over the top of the warm front zone and high above intervening coastal topography. Thus, the positive correlation between the two time series can be physically justified and qualifies the link as a genuine teleconnection.

1. Introduction

Teleconnections within the atmosphere are defined as linkages or correlations, over great distances, of weather or climate anomalies. They may be identified using routinely recorded meteorological variables (pressure, temperature, precipitation) as the diagnostic tool. The description, scientific bases and societal impacts of teleconnections are covered in a comprehensive volume edited by Glantz *et al.* (1991). It is now standard practice to identify teleconnections spanning distances of *order* 10^4 km. Teleconnections may be defined by either positive or negative cross correlation coefficients that are statistically significant at a nominal $\geq 5\%$ level. Negative correlations, associated with anomalies that switch sign on a regular basis, are commonly referred to as 'seesaws'. Here, I describe a positive (stable) precipitation teleconnection spanning a distance of over 7000 km right across the Pacific Ocean. An outline of how this teleconnection was originally discovered is given in Holdsworth (1992). I also describe a 'seesaw' teleconnection between two stations situated on the west coast of North America. Such teleconnections are not successfully produced in current Global General Circulation Models (GGCM's) because model

This document is provided by JAXA.

precipitation is not supported by realistic, regional-scale, cyclonic structures. Only very high spatial resolution (20 km×20 km) regional models (over a surface domain of $<10^4$ km× $<10^4$ km) are capable of doing this but then the domain is too restricted for looking at the physical basis for precipitation teleconnections over very large distances.

In this paper I avoid the numerical modeling approach to provide a detailed physical basis for the long distance correlation by using the wealth of published information, as well as satellite imagery, for studying the North Pacific oceanographic and atmospheric domains. These information resources show that there is a strong coupling between the ocean and the atmosphere for the breadth of the Pacific region at mid-latitudes and that cyclogenesis is frequently coherent, on a temporal basis, in the western and eastern Pacific regions. Intense cyclogenesis occurs along the polar front zone (Parker, 1980) extending across the North Pacific Ocean (Fig. 1).

In Section 2 the data will be presented, in Section 3 the cross correlation analyses results will be given and briefly discussed, and in Section 4, the physical basis for the long-distance cross correlation will be qualitatively explained. The overall results will be summarized and conclusions drawn in Section 5.

2. Data

Precipitation data for the stations in Japan were obtained from World Weather Records (1944, 1959, 1967) and from U.S.E.D.S. (1961-1987). Five stations with the longest records (Nemuro, Akita, Miyako, Tokyo and Nagasaki) were intially selected, but on the basis of known differences in regional climate, and on the basis of cross correlations made between station data, Nagasaki was eliminated and the records of the four northern region stations were combined into one mean record. This is referred to as the 'Northern Japan annual precipitation time series' (1889-1986). The corresponding net snow accumulation time series for Mount Logan is taken from data given in Holdsworth *et al.* (1992). The location of sites and stations referred to in this paper are given in Fig. 1 with coordinates given in Table 1. The four stations in northern Japan (J) are marked by black squares. On the eastern Pacific rim, Mt Logan (M) is marked by the black triangle. The stations S (Seward) and V (Victoria) are marked by black squares. The two time series from Japan and Mt Logan are plotted in Fig. 2. The remarkable correspondence in variance may be seen immediately and initially defines the west-east Pacific teleconnection, in empirical terms. Two other data sets that carry important information in the context of Pacific region atmospheric processes are the annual precipitation at Seward, Alaska and at Victoria, British Columbia. These series are shown in Fig. 3 and their significance will be discussed in the next two sections.

3. Data analyses and interpretation

The standard Pearson Product Moment Cross Correlation Coefficient (r) (see *e.g.* Thiébaux, 1994) has been calculated for pairs of (annual value) time series and for different amounts of smoothing applied to the raw series. The two series plotted in Fig. 2 have a cross correlation coefficient of $+0.38$ (significant at the 1% level). Progressive smoothing using 5-yr and 7-yr width filters increases the cross correlation coefficient successively to

This document is provided by JAXA.

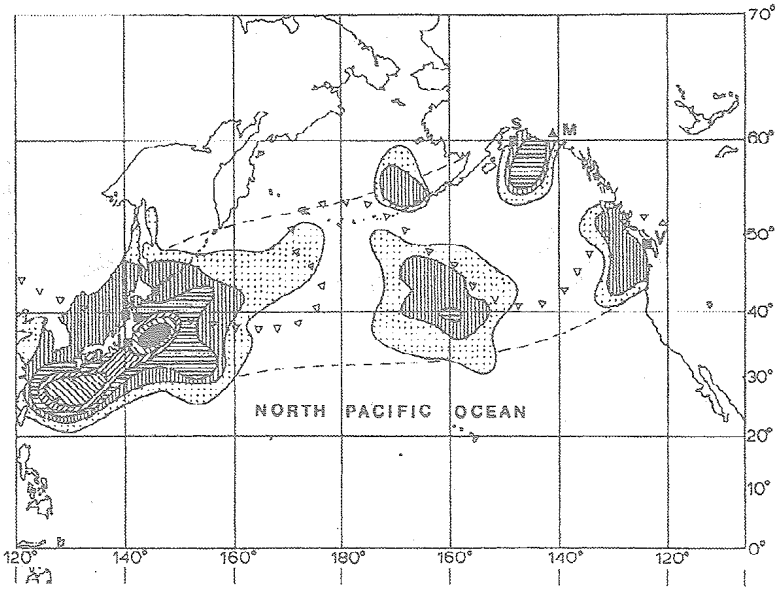


Fig. 1. Map of the North Pacific Ocean region (after Terada and Hanzawa, 1984). Stations in Japan (J) are shown by black squares (Table 1 lists the coordinates). Northeast Pacific rim stations or sites are Seward (S), Mt Logan (M) and Victoria (V). Contoured regions indicate intensity of cyclogenesis (for contour values see Figure 14 of Terada and Hanzawa, 1984). Black indicates highest intensity of cyclogenesis. These 'centers of action' are associated with the polar front. An instantaneous polar front position is given by the open inverted triangles (after Iribarne and Cho, 1980). The polar front generally occupies positions between the two dashed lines extending across the Pacific. In the text the accepted term 'polar front zone' is generally used to signify its broad and transient nature.

Table 1. Coordinates of sites or stations referred to in the text and beginning of record.

Mount Logan	60°37′N	140°31′W	5340 m	Records AD1693-
Seward, Alaska	60°07′N	149°27′W	76 m	Records AD1908-
Victoria, B.C.	48°25′N	123°19′W	70 m	Records AD1898-
Nemuro, Japan	43°02′N	145°35′E	27 m	Records AD1889-
Akita, Japan	39°43′N	140°06′E	10 m	Records AD1886-
Miyako, Japan	39°38′N	141°59′E	30 m	Records AD1884-
Tokyo, Japan	35°41′N	139°46′E	21 m	Records AD1876-
Nagasaki, Japan	32°44′N	129°52′E	13 m	Records AD1879-

+0.63 and +0.71 (Fig. 4). This latter coefficient is well above the 1% significance level and shows that both time series must contain considerable periodicity at decadal and higher wavelengths. Power spectra given in Holdsworth *et al.* (1992) for the Mount Logan series show peaks at 3.8 yrs (corresponding to ENSO frequency), at approximately 10–11 yrs, and at about two decades.

The application of a 7-yr filter to the data of Fig. 2 has accentuated these lower frequencies and the combined results show that the teleconnection, spanning over 7000 km,

This document is provided by JAXA.

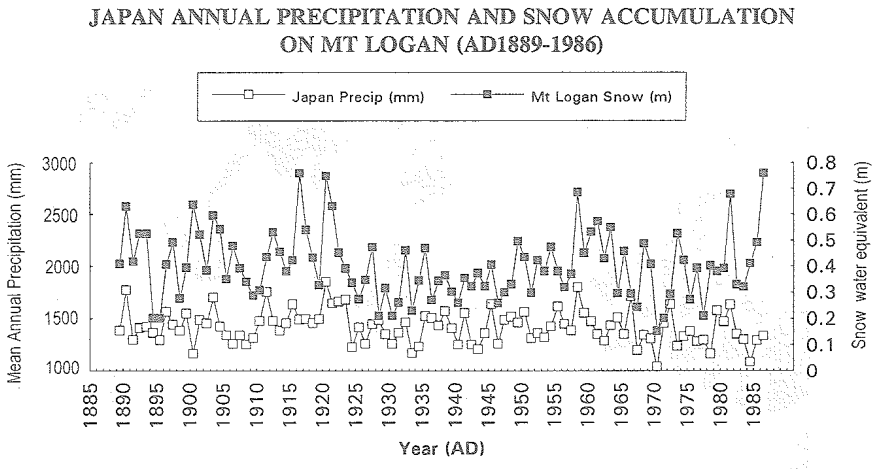


Fig. 2. Graph of Japan annual precipitation (unweighted mean of four stations in Northern Japan) and net snow accumulation (in water equivalent) for Mount Logan, Yukon.

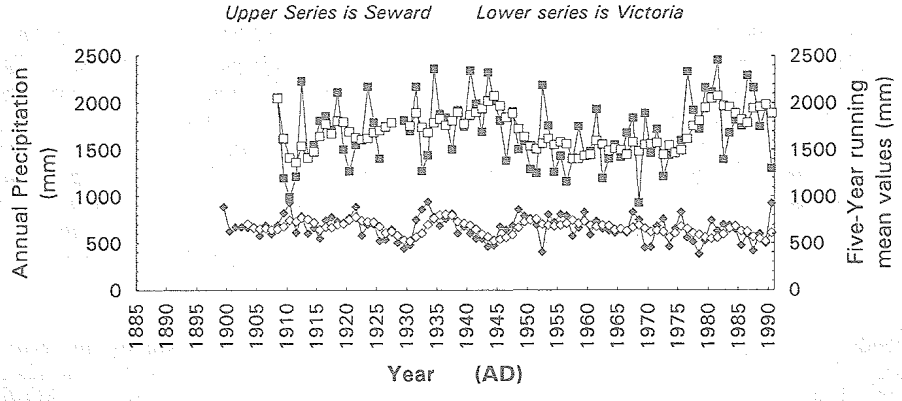


Fig. 3. Graph of total annual precipitation for Seward, Alaska (1908–1990) and for Victoria (Gonzales Heights), British Columbia (1899–1990). Data are smoothed by a 5-year filter for optimum correlation. The anti-correlation may be clearly seen for most of the series.

holds for a wide range of frequencies. This defines it as a stable, positive, teleconnection.

In Fig. 3 it is seen that the two North American time series (Victoria and Seward) are in anti-phase. The cross correlation coefficient is −0.41 for the 5-yr filtered series. This value is statistically significant at the 1% level. Such a result suggests the existence of a 'seesaw' teleconnection in a roughly north-south direction (spanning about 2200 km). This interpretation is broadly consistent with a study by Wallace and Gutzler (1981) who found 'seesaw' teleconnections in geopotential height fields in a north-south orientation for the north Pacific region in winter. They identified a *node* at about 50°N which lies between the two stations analysed here.

This document is provided by JAXA.

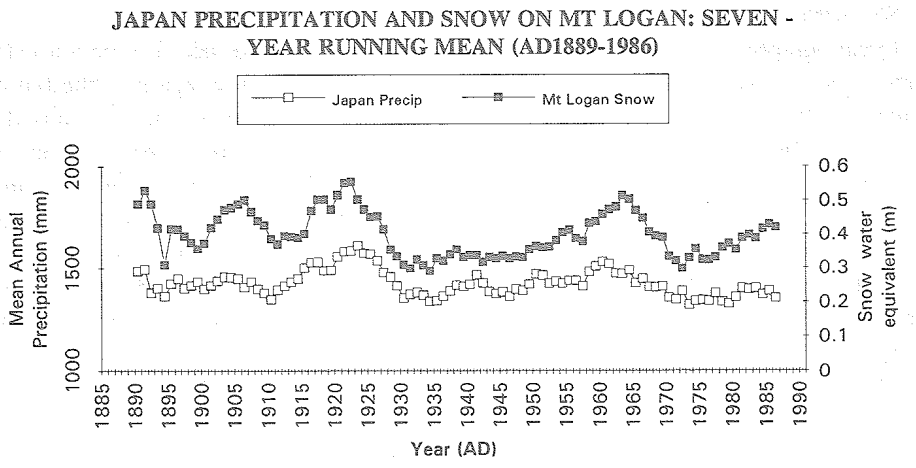


Fig. 4. Graph of Japan precipitation and Mount Logan net accumulation series from Fig. 2 smoothed with a 7-year filter to accentuate the decadal signal and produce the highest cross correlation coefficient (+0.71). See Table 2 for significance levels.

Table 2. Cross Correlation Coefficients (r) between stations/sites given in Table 1. Data have been smoothed by 5 and 7-yr filters. Statistical significance at the 5% and 1% levels apply to the annual data series. Levels for filtered series are slightly higher. A nil entry means r decreases from the value in the last box.

Station/site	Station/site	Annual data	5-yr r/mean	7-yr r/mean	Signif (5%)	Signif (1%)
Mt Logan	Japan (4 stn)	$r=0.38$	$r=0.63$	$r=0.71$	$r=0.200$	$r=0.256$
Nemuro	Akita	$r=0.33$	$r=0.41$	$r=0.40$	$r=0.199$	$r=0.254$
Miyako	Tokyo	$r=0.41$	$r=0.31$	$r=0.28$	$r=0.202$	$r=0.255$
Akita	Miyako	$r=0.317$	$r=0.322$		$r=0.194$	$r=0.253$
Tokyo	Nagasaki	$r=0.199$	$r=0.233$		$r=0.188$	$r=0.245$
Mt Logan	Victoria	$r=0.12$	$r=0.35$	$r=0.40$	$r=0.210$	$r=0.275$
Victoria	Seward	$r=-0.36$	$r=-0.41$		$r=0.224$	$r=0.293$

4. North Pacific oceanology and climatology

4.1. Scope

Only a brief review of the extensive literature on North Pacific region oceanology, meteorology, and climatology is possible here. The relevant information occurs in two general parts: ocean surface processes and atmospheric processes. Although consideration of atmospheric processes alone seems to be able to account for coherence in the North Pacific region atmosphere, a synthesis of the two types of information is attempted here as it appears to lead to a better understanding of how trans-Pacific, zonally linked, teleconnections in atmospheric anomalies can occur.

This document is provided by JAXA.

4.2. Sea surface data

Oceanographic data such as surface currents and Sea Surface Temperature (SST) (Terada and Hanzawa, 1984) clearly show strong coherence in the region of the Kuroshio Current Extension and its bifurcation near the North American coastline especially during the winter months. This east-northeasterly trending strip is the preferred location of the polar front along which intense cyclogenesis takes place especially during the fall and winter months. On satellite SST maps (www.fnoc.navy.mil/otis/archive/) the thermal structure of the Pacific Ocean may be clearly seen for all months of the year. Animations (www.cdc.noaa.gov/) of North Pacific SST's during an El Niño/La Niña cycle show the development of a warm water plume from the east coast of Japan to far out into the eastern Pacific. The position of the circumpolar vortex (a general term for the system bounded by the polar front and arctic front) is known to be modulated by this cycle (Angell and Korshover, 1985).

4.3. Atmospheric data

Figure 1 shows regions of preferred cyclogenesis for the North Pacific Ocean according to Terada and Hanzawa (1984). Preferred Centers of Action (COA) for cyclogenesis are located east of Japan, in the east central Pacific (near 40°N), north of the Aleutian chain, and in the Gulf of Alaska region (Terada and Hanzawa, 1984). Individual cyclones may travel from one COA to another. Also shown are the approximate preferred annual limits of the polar front (dashed lines). A specific winter-time polar front position at the 500 mbar level, is shown by the inverted open triangles (Iribarne and Cho, 1980). This case indicates strong meridional flow. Here, I refer to the polar front generally as the polar front zone (PFZ), because of its broad, as well as transient, nature. On the hemispheric scale, the PFZ is continuous, being the boundary between the polar air mass and subtropical air masses.

Satellite (GOES 10) images show that moisture for Gulf of Alaska cyclones often comes from as far south as below 40°N and from the mid-Pacific. Occasionally, major (winter) Gulf of Alaska cyclone tails are linked to western Pacific cyclones that have formed along the east coast of Japan. Synoptic weather maps for the entire North Pacific (http://weather.unisys.com/upper_air/ua_nhem_500p.html) show that low pressure systems are often occupying the western and eastern parts of the North Pacific simultaneously.

4.4. Synthesis of North Pacific Ocean data and modern analyses of atmospheric processes

By overlaying maps of oceanographic data with maps of atmospheric variables (pressure anomaly fields, the preferred zone of Rossby Waves, wind fields -including the Polar Front Jet Stream, precipitation intensity zones, synoptic charts and satellite images of moisture transport) it becomes apparent that there exists a strong zonal coherency in the atmosphere across the mid-latitude North Pacific. Recent modeling of the stationary wave propagating eastward off the high altitude Asian Plateaus (Plumb, 1985) shows its importance extending as far as the west coast of North America. Analyses of the geopotential height anomalies for the Pacific (Nigam *et al.*, 1999) also supports the existence of the stationary planetary wave field. This wave can be considered a type of 'carrier wave' supporting minor modulation by El Niños, internal decadal oscillations in the atmosphere (James and James, 1989) and including solar modulation (Christoforou and Hameed, 1997; Van Loon and Shea, 1999). Both ENSO and decadal scale signals are present in the power

This document is provided by JAXA.

spectrum of the Mount Logan time series (Holdsworth *et al.*, 1992). Further details of the ENSO signals and their related PNA-like teleconnection patterns are given in Moore *et al.* (2001).

5. Summary and conclusions

The results of this study show that there is strong coherence between the precipitation records from Japan, (representing the western margin of the mid-latitude North Pacific Ocean) and an ice core snow accumulation record from Mount Logan over a century scale time span. The cross correlation results imply that the high altitude precipitation received on Mount Logan is not derived locally but originates from mid-latitude, possibly mid-Pacific, waters where precipitation modulation processes are in synchroneity within a wide zonal swath across the Pacific. Isotopic data from Mount Logan (Holdsworth *et al.*, 1991) suggests that the ice core site is regularly receiving moisture from above the warm front zone of cyclones centered in the Gulf of Alaska, which implies that much of the water vapor for the snow has a long distance source south of the southern extremity of the Polar Front Zone (PFZ). A review of the extensive oceanographic, meteorologic and climatic data for the North Pacific, as well as a study of weather satellite images, reveals that this is the case. It also appears that a linkage of atmospheric anomalies spans the mid-latitude North Pacific. This linkage could be referred to as the Asia-Pacific-North-American linkage (APNA) evidently related to the PNA pattern of Wallace and Gutzler (1981) but more extensive than it. The APNA linkage seems to provide the physical basis for calling the remarkable cross correlation between precipitation records on either side of the Pacific, a teleconnection. An examination of precipitation records along the North American coastline reveals a persistent 'seesaw' in precipitation between Victoria, British Columbia and Seward, Alaska, which is at about the same latitude as Mount Logan but generally within the polar air mass. This type of teleconnection might be inferred from the results of Wallace and Gutzler (1981). Whereas there is a significant (positive) cross correlation between Mount Logan and Victoria, it is not as large as the one between Mount Logan and Japan. This result could only be due to the fact that complex topography is not *directly* interfering with precipitation processes on Mount Logan at high altitude.

The complete Mount Logan time series is nearly three centuries long. In principle it could be used as 'proxy' for generating an equivalent time series for Japan before the instrumental records. Unpublished, pre-instrumental, climate data for Japan, in the form of abstracted and 'indexed' diary records, are available (Professor M. Yoshimura of Yamanashi University), but these data have not yet been incorporated into the Japan data set. Future ice cores might extend the Mount Logan record back further. The data presented here could be useful for long term hydrologic and agricultural planning purposes.

Acknowledgments

I thank the National Institute of Polar Research (Tokyo) for enabling me to present this paper at the Second International Symposium on Environmental Research in the Arctic and for having it constructively reviewed. I also thank Professor M. Yoshimura for agreeing to provide his data for analysis.

This document is provided by JAXA.

References

Angell, J.K. and Korshover, J. (1985): Displacements of the North Circumpolar Vortex during El Niño 1963–83. Mon. Weather Rev., **113**, 1627–1630.

Christoforou, P. and Hameed, S. (1997): Solar cycle and Pacific 'centers of action'. Geophys. Res. Lett., **24**, 293–296.

Glantz, M.H., Katz, R.W. and Nicholls, N. (1991): Teleconnections linking worldwide climate anomalies. Cambridge, Cambridge University Press, 527 p.

Holdsworth, G. (1992): Ice cores as a source of long-term net precipitation data: a North American perspective. Using Hydrometric Data to Detect and Monitor Climatic Change, ed by G.W. Kite and R.D. Harvey. Saskatoon, Nat. Hydrol. Res. Inst., 107–120.

Holdsworth, G., Fogarasi, S. and Krouse, H.R. (1991): Variation of the stable isotopes of water with altitude in the Saint Elias Mountains of Canada. J. Geophys. Res., **96**, 7483–7494.

Holdsworth, G., Krouse, H.R. and Nosal, M. (1992): Ice core climate signals from Mount Logan, Yukon, AD1700–1987. Climate since AD1500, ed by R.S. Bradley and and P.D. Jones, London, Routledge, 483–504.

Iribarne, J.V. and Cho, H.-R. (1980): Atmospheric Physics. London, D. Reidel Publ.

James, I.N. and James, P.M. (1989): Ultra-low-frequency variability in a simple atmospheric circulation model. Nature, **342**, 53–55.

Moore, G.W.K., Holdsworth, G. and Alverson, K. (2001): Extra-tropical response to ENSO 1736–1985 as expressed in an ice core from the Saint Elias Mountain Range in Northwestern North America. submitted to Geophys. Res. Lett.

Nigam, S., Barlow, M. and Berbery, E.H. (1999): Analysis links Pacific decadal variabilty to drought and streamflow in United States. EOS, **80**, 621–625.

Parker, S.P. (1980): Ocean and Atmospheric Sciences. New York, McGraw-Hill Book Comp.

Plumb, R.A. (1985): On the three-dimensional propagation of stationary waves. J. Atmos. Sci., **42**, 217–229.

Terada, K. and Hanzawa, M. (1984): Climate of the North Pacific Ocean. Climate of the Oceans, ed by H. van Loon. Tokyo, Elsevier, 431–477 (World Survey of Climatology, **15**).

Thiébaux, H.J. (1994): Statistical Data Analysis for Ocean and Atmospheric Sciences. New York, Academic Press, 247 p.

U.S.E.D.S. (1961–1987): Monthly climatic data for the world. U.S. Environmental Data Service, **14** to **40**, NCDC, NOAA, Asheville, North Carolina.

Van Loon, H. and Shea, D.J. (1999): A probable signal of the 11-year solar cycle in the troposphere of the northern hemisphere. Geophys. Res. Lett., **26**, 2893–2896.

Wallace, J.M. and Gutzler, D.S. (1981) Teleconnections in the geopotential height field during the northern hemisphere winter. Mon. Weather Rev., **109**, 784–812.

World Weather Records (1944): Smithsonian Miscell. Coll. **79**, Smithsonian Institution, Washington, D.C.

World Weather Records (1959): Complete volume. U.S. Dept. Commerce, Washington, D.C.

World Weather Records (1967): Volume **4**, Asia. U.S. Dept. Commerce, Washington, D.C.

(Received March 22, 2000; Revised manuscript accepted August 30, 2000)

This document is provided by JAXA.

Mem. Natl Inst. Polar Res., Spec. Issue, 54, 169-182, 2001

Scientific note

Stable oxygen isotope ratio observed in the precipitation at Ny-Ålesund, Svalbard

Makoto Igarashi, Kokichi Kamiyama and Okitsugu Watanabe

National Institute of Polar Research, Kaga, 1-chome, Itabashi-ku, Tokyo 173-8515

Abstract: The stable oxygen isotope ratio ($\delta^{18}O$) in ice cores and surface snow pits samples obtained in Svalbard does not show a seasonal variation clearly. In preceding research, it has been reported that $\delta^{18}O$ is change by melting of the snow layer. However, to what degree $\delta^{18}O$ in snow changes after accumulation is not clear. We carried out the observation in Ny-Ålesund, northwestern part of Svalbard, in the 1993/94 winter season and 1994 summer season in order to investigate the initial values of $\delta^{18}O$ in precipitations.

Values of $\delta^{18}O$ both in winter and summer were almost same ($-4\sim-24$‰) as well as the average of each season was also almost same (-12.9‰, -12.3‰), which shows that $\delta^{18}O$ in precipitations does not have a clear seasonal variation.

It is known that the value of $\delta^{18}O$ in precipitation changes by the condensation temperature of water vapor. Temperature, at the height where the wettest air mass existed over northwestern Svalbard, changed almost same range in winter and summer, when the rain fell at Ny-Ålesund. And, there was a better correlation between $\delta^{18}O$ in precipitation and temperature of moist air masses than $\delta^{18}O$ in precipitation and air temperature at the observation site both in winter and in summer.

Therefore, fluctuation of $\delta^{18}O$ seemed to show the almost equal, even if the season was different. This fact can be regarded that one of the reasons why $\delta^{18}O$ of ice core drilled in Svalbard does not show the seasonal variation clearly.

1. Introduction

Dansgaard (1953) has indicated that past temperature is estimable by analysis of the stable oxygen isotope ratio ($\delta^{18}O$) in ice cores. The values of $\delta^{18}O$ in ice cores drilled on glaciers have been used for discussing paleoclimate. For example, climatic changes for several hundred thousand years have been clarified from ice cores obtained in Antractica and Greenland (*e.g.* Petit *et al.*, 1999; Dansgaard *et al.*, 1993). And seasonal variation of $\delta^{18}O$ was preserved for the last 8300 years in an ice core from Camp Century, northwestern Greenland (Johnsen *et al.*, 1972).

In Svalbard, research on the reconstruction of the climatic variation from $\delta^{18}O$ analysis has also been carried out. Goto-Azuma *et al.* (1995) drilled on Snøfjellafonna, northwestern Spitsbergen until 84 m depth, and found that the seasonal variation of $\delta^{18}O$ had partially been lost. This confirmed the finding that the seasonal variation of $\delta^{18}O$ was not recognizable in analysis of an ice core from Vestfonna on Nordaustlandet by Punning *et al.* (1986). The seasonal variation of $\delta^{18}O$ did not show clearly in analysis of surface snow

This document is provided by JAXA.

pit samples obtained in Austfonna on Nordaustlandet as well as ice cores (Iizuka *et al.*, 2000). The reason why the seasonal variation did not appear clearly in $\delta^{18}O$ was reported by Goto-Azuma *et al.* (1995) and Punning *et al.* (1986), as the snow melting after the accumulation on the glacier. However there is few data on the change of $\delta^{18}O$ in precipitation in these regions. We collected the precipitation in Svalbard in different season for the basic discussion.

2. Samples and methods

Precipitation sampling on the glacier over several months is not so easy. Therefore, precipitation samples were collected at Ny-Ålesund (78°56′N, 11°52′E, 35 m a.s.l.) in northwestern Svalbard (Fig. 1), where there is an observation base of the National Institute of Polar Research, and it is possible to stay for a long decade and to freeze the precipitation samples for the preservation on chemical analysis. Meteorological observations are carried out there regularly, and can be easily compared with results of analysis of the collected precipitation.

The investigation point at Ny-Ålesund is shown in Fig. 2. It is 1.6 km from the center of town and 0.2 km from the coast of Kongsfjord.

The precipitation sampling was carried out in winter 1993/94 and summer 1994. It is shown in Table 1. Precipitation could not be collected from December 16, 1993 to Janurary 31, 1994, because there was no investigator at Ny-Ålesund. During the obsevation period, there was precipitation for 36 days in winter and for 21 days in summer. Precipitation was observed as snowfall and rain both in winter and summer.

The sampling procedures between for snowfall and for rain were different. In case of snowfall, we collected fresh snow in a pre-cleaned plastic bag. Rain was concentrated in a

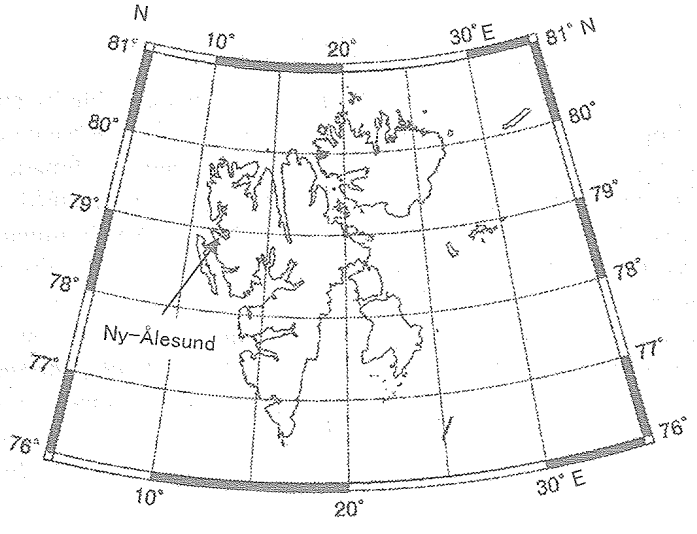


Fig. 1. Location of study area.

This document is provided by JAXA.

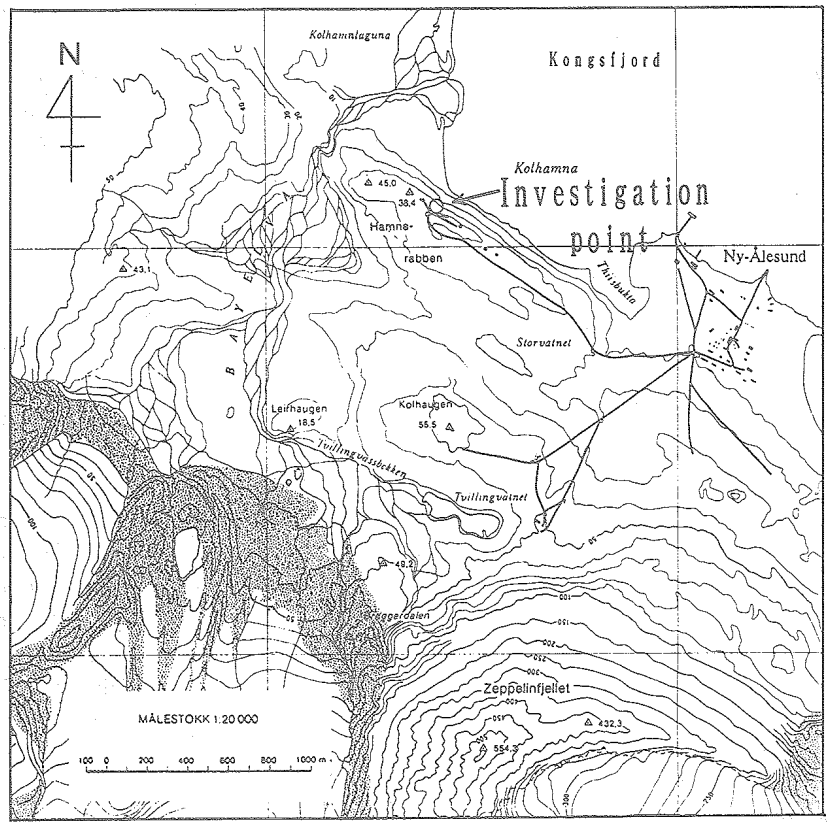


Fig. 2. Landforms and investigation point at Ny-Ålesund. The region where the mesh splashed is the end moraine.

Table 1. Outline of the observations.

	Date	The number of days of observation	The days with precipitation	The days of sample obtained
Winter 1993/94	1993.12.3~12.15 1994.2.1~3.15	56	36	31
Summer 1994	8.23~9.18	27	21	15

pre-cleaned plastic bottle with a funnel of diameter 0.3 m. We collected 100 m*l* samples to have enough for not only measurement of $\delta^{18}O$ but also determination of the chemical composition. And in the case of snowfall and rain, we collected samples every 6 hours at the time of meteorological observations. It is desirable to collect each sample in as short a time as possible because in Ny-Ålesund, the climate dramatically changes in a day during the polar night (Hanssen-Bauer *et al.*, 1990). During the summer, precipitation of 0.1 mm for 6 hours was necessary in order to collect a 100 m*l* sample. During the winter, it was not possible to collect a sufficient sample of 0.1 mm precipitation for 6 hours, as a sample was

This document is provided by JAXA.

collected when there was 0.1 mm precipitation for 12 hours. There was sufficient precipitation for sampling during 31 days in winter and 15 days in summer.

Each of the snowfall samples was melted in the laboratory at Ny-Ålesund and was kept in a pre-cleaned plastic bottle. After that, samples were kept frozen until measurement of $\delta^{18}O$. $\delta^{18}O$ was measured by mass spectrometer (Delta-E, finnigan-mat). The analytical error was $\pm 6\%$.

3. Characteristics of climate in this study period

Meteorological data were measured by the Norwegian Meteorological Institute 3 times per day (0700, 1300 and 1900; GMT+1) at Ny-Ålesund (Fig. 2). Sea-level pressure, surface air temperature, relative humidity and precipitation are shown in Table 2. Precipitation was observed 2 times per day (0700 and 1900; GMT+1). The deviation from the average of each quantity in each period from 1975 to 1989 is indicated in parentheses in Table 2, as well as the standard deviation of temperature within each period.

The deviation from surface mean temperature between 1975 and 1989 (−2.3) exceeded the standard deviation (0.6) only in August. The deviation of surface mean temperature in other months fell below the standard deviation (Table 2). Especially, the mean temperature during the winter of 1993/94 (December 3, 1993–March 15, 1994) agreed with the mean temperature between 1975 and 1989. And the deviation throughout the summer of 1994 (−0.9: August 23–September 19) was smaller than the standard deviation from August to September (1.1). This means that there was hardly a difference of mean temperature between the whole observation period in the summer and from 1975 to 1989. Large negative deviation appeared in August. It was about 4 times of the standard deviation (Std). This is because mean temperature (1.6℃) for the final 9 days of observation in August was 1.1℃ lower than the mean temperature (2.7℃) during August.

The deviation from mean value of sea-level pressure in March in the first half of the study period was the greatest difference from mean values.

Precipitation in January and February showed the large absolute value of deviations from the mean value. In January, the precipitation became only 4% of the mean value. As

Table 2. Meteorological data. Deviations from mean values between 1975 and 1989 are shown in parentheses.

	Sea-level pressure (hPa)		Temperature (℃) mean		Std.*	min.	max.	Relative humidity (%)		Precipitation (mm)	
Winter 1993/94											
12/3-3/15	1000.8	(−0.8)	−13.8	(0.0)	4.0	−32.8	4.4	69.9	(−6.1)	144.6	(26.6)
12/3-31	1005.5	(−0.6)	−11.9	(1.0)	4.6	−25.1	−0.7	62.6	(−10.4)	26.9	(1.6)
1/1-31	1007.6	(1.4)	−15.0	(−0.6)	4.0	−26.0	−1.6	58.5	(−15.5)	1.1	(−26.9)
2/1-28	1013.9	(5.6)	−14.7	(−0.1)	3.8	−32.2	4.4	82.1	(3.1)	97.5	(56.5)
3/1-15	994.3	(−15.4)	−13.6	(−0.1)	3.7	−32.8	0.6	85.4	(7.4)	19.1	(−4.6)
Summer 1994											
8/23-9/19	1007.2	(−2.4)	0.8	(−0.9)	1.1	−3.9	7.7	81.2	(−2.3)	46.5	(9.3)
8/23-8/31	1002.5	(−9.1)	1.6	(−2.3)	0.6	−3.9	7.7	74.7	(−10.3)	17.8	(5.9)
9/1-19	1009.5	(1.8)	0.4	(0.9)	1.6	−3.3	4.4	84.2	(2.2)	28.7	(3.4)

*The standard deviation of mean temperature in each period.

This document is provided by JAXA.

the result, the relative humidity was 15.5% lower than mean value. On the contrary, the amount of precipitation in February became more twice larger than mean value. However, the relative humidity was only 3% larger than mean value.

4. Results and discussion

4.1. Relationship between $\delta^{18}O$ and surface air temperature

$\delta^{18}O$ of the precipitation in winter 1993/94 is shown in Fig. 3a, and that in summer 1994 is shown in Fig. 4a. Surface air temperature measured at Ny-Ålesund is presented in the same figures in order to compare with the fluctuation of $\delta^{18}O$.

In winter, $\delta^{18}O$ varied between $-7.3‰$ and $-20.4‰$ (Fig. 3a), and between $-4.7‰$ and $-23.6‰$ in summer (Fig. 4a). The fluctuating range of $\delta^{18}O$ was about 6‰ larger in summer than in winter. The averages of $\delta^{18}O$ were $-12.9‰$ in winter and $-12.3‰$ in summer respectively.

Dansgaard *et al.* (1973) illustrated the relationship between $\delta^{18}O$ in precipitation collected in the Arctic, and surface mean temperature. They reported that the annual mean of surface temperature and that of $\delta^{18}O$ appeared to be proportional. The $\delta^{18}O$ mean value

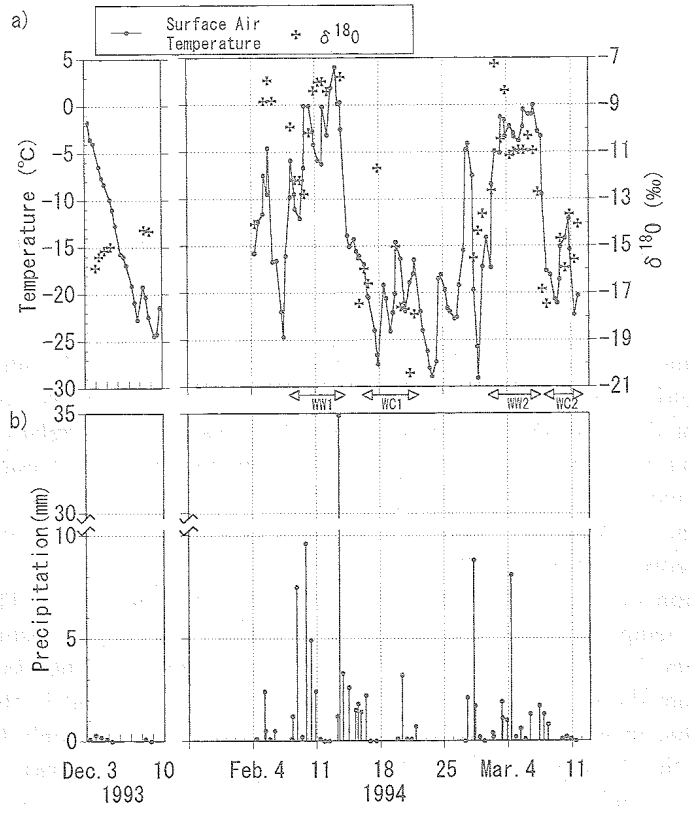


Fig. 3. $\delta^{18}O$ in precipitation, surface air temperature and precipitation at Ny-Ålesund in winter 1993/94. a) Surface air temperature and $\delta^{18}O$ in precipitation. b) Precipitation.

This document is provided by JAXA.

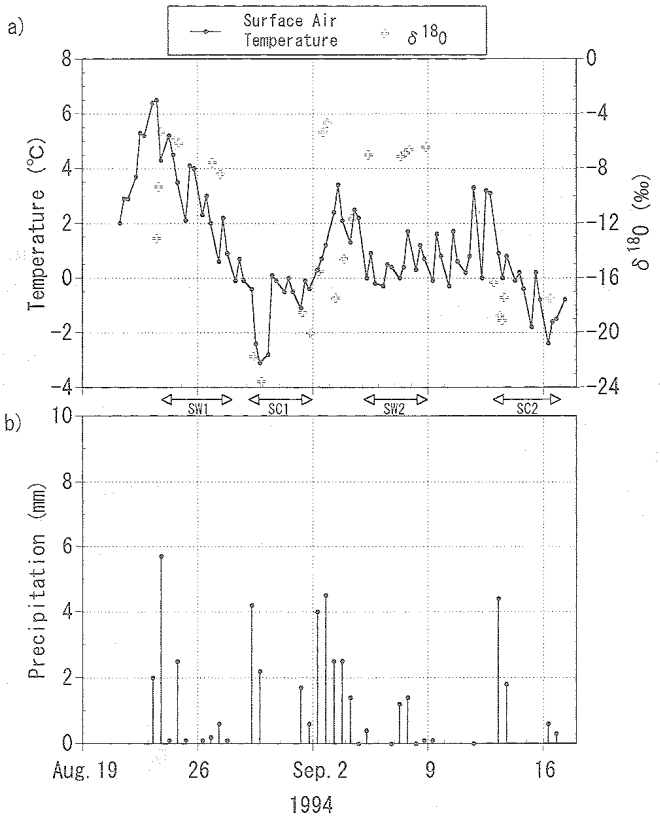


Fig. 4. $\delta^{18}O$ in precipitation, surface air temperature and precipitation at Ny-Ålesund in summer 1994. a) Surface air temperature and $\delta^{18}O$ in precipitation. b) Precipitation.

of all precipitation which we collected in Ny-Ålesund was −12.6‰, and surface mean temperature during the observation period was −8.9℃. This result agreed on proportional relationship of the other Arctic. Therefore, there appears to be correlation between the average of $\delta^{18}O$ in precipitation and surface mean temperature at Ny-Ålesund. We considered that the mean value of $\delta^{18}O$ in precipitation collected during this observation was almost usual at Ny-Ålesund because surface mean temperature was not so different from mean value between 1975 and 1989.

Fluctuation of $\delta^{18}O$ is related to temperature (Dansgaard, 1953). This means that features of the temperature during the observation period should reflect similar changes in $\delta^{18}O$. Frequency distributions of $\delta^{18}O$ in Ny-Ålesund and surface air temperature in winter and summer are shown in Fig. 5. The distribution of $\delta^{18}O$ (Fig. 5a) in the summer was longer than that in winter and the difference of both average were only 0.6‰, as it was mentioned earlier. However, the temperature distribution in summer was smaller than the one in winter. Temperature during each precipitation fluctuated between −28.9℃ and 0.1℃ in winter and between −3.9℃ to 7.7℃ in summer (Fig. 5b). The variation was about three times larger in winter than in summer. Average temperature were −13.8℃ in winter

This document is provided by JAXA.

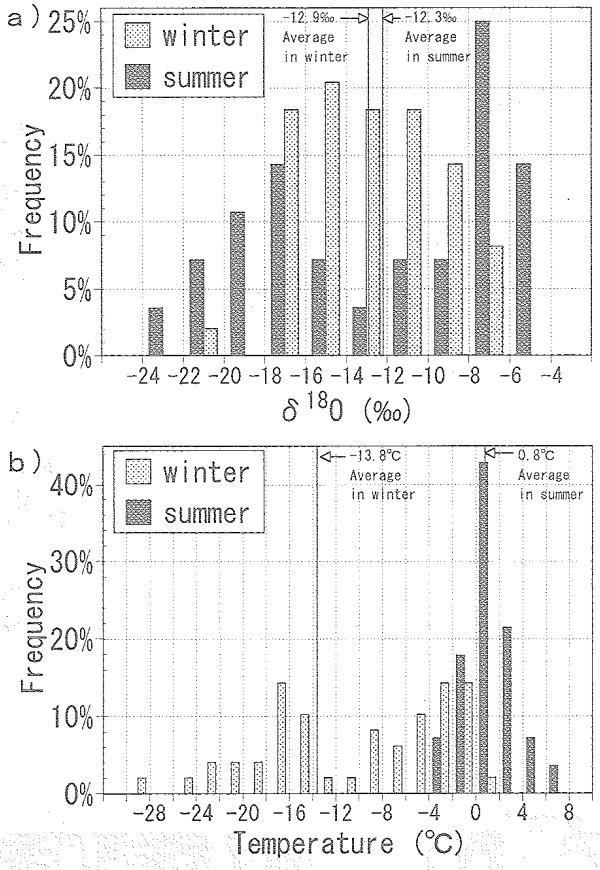


Fig. 5. Frequency distributions of $\delta^{18}O$ in Ny-Ålesund and surface air temperature in winter and summer. The total number of data are 49 in winter and 28 in summer. a) $\delta^{18}O$. b) Surface air temperature.

and 0.8℃ in summer, respectively. Large distribution of $\delta^{18}O$ occurs under the small distribution of temperature, and smaller distribution of $\delta^{18}O$ in winter under the large distribution of temperature, which indicated that the fluctuation of $\delta^{18}O$ does not depend upon only in the change of the surface air temperature.

4.2. Relationship between $\delta^{18}O$ and aerology data

In the previous section, we represented that it was difficult to explain the fluctuation of $\delta^{18}O$ only in the change of the local surface air temperature. Then, there is some possibility that the distribution of $\delta^{18}O$ depends under the atmospheric condition under the larger scale.

We used aerology data edited at NOAA-CIRES Climate Diagnostics Center. These data are compiled on a 2.5-degree latitude×2.5-degree longitude global grid and in 17 pressure levels (hPa: 1000, 925, 850, 700, 600, 500, 400, 300, 250, 200, 150, 100, 70, 50, 30, 20, 10). The grid point which is nearest to Ny-Ålesund is 80.0°N, 12.5°E. Temperature and

This document is provided by JAXA.

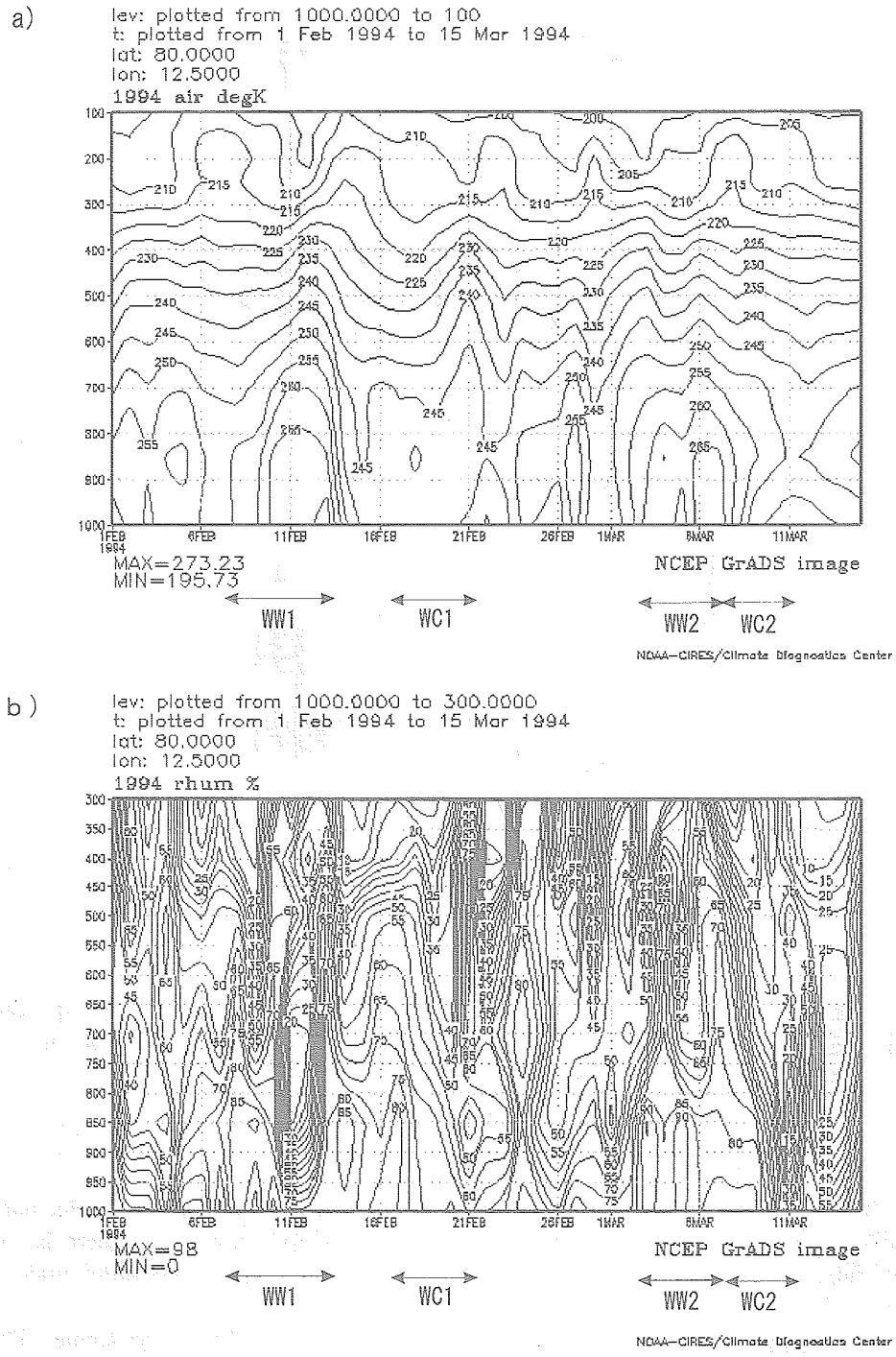


Fig. 6. Temperature and relative humidity at the grid point (80.0°N, 12.5°E) in winter 1994. a) Temperature. b) Relative humidity.

This document is provided by JAXA.

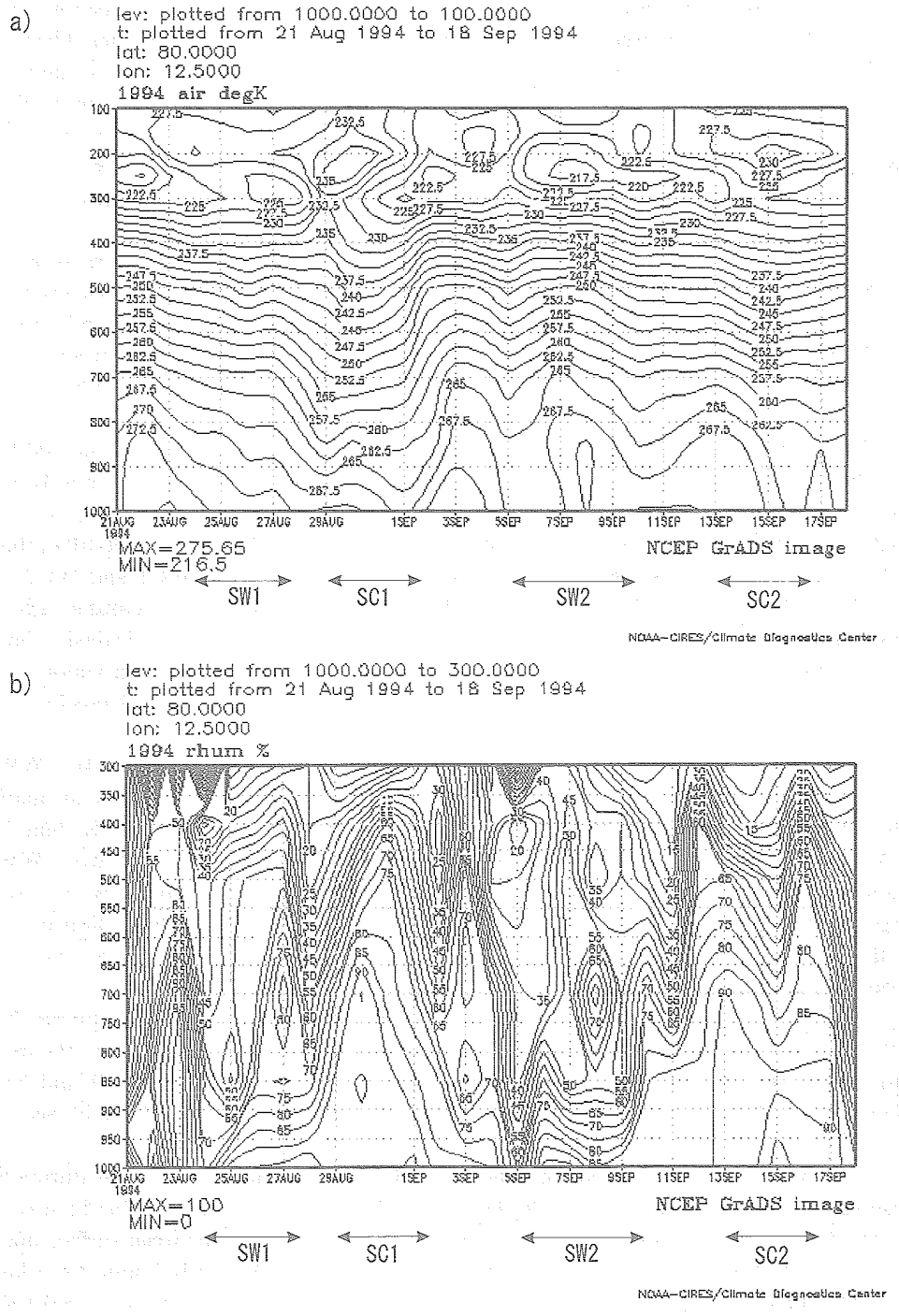


Fig. 7. Temperature and relative humidity of this grid point (80.0°N, 12.5°E) in summer 1994. a) Temperature. b) Relative humidity.

This document is provided by JAXA.

relative humidity at this grid point are shown in Fig. 6 (winter) and Fig. 7 (summer).

First, the relation between $\delta^{18}O$ and aerology data was examined in winter. Then, the following were divided: the period which the value of $\delta^{18}O$ was higher than the mean value (−12.9‰), and the period which it showed lower than that, as it was shown in Table 3. The periods in which two values were higher than the mean value continuously for several days were February 8–13 and March 2–7, and are called WW1 and WW2. The periods in which the value was lower than the mean value for several days were February 16–22 (except February 17; −11.7‰) and March 8–11, and are called WC1 and WC2.

In periods WW1 and WW2, there became the air masses which temperature were over 260 K from the surface to about 700 hPa (about 3000 m a.s.l.). In these two periods, there were the air masses which were the warmest throughout the observation period in February and March. Simultaneously, the values of the relative humidity of these warm air masses were over the 80%. These air masses apparently brought precipitation, because other wet air masses did not exist in WW1 and WW2.

In the meantime, temperatures of air masses between ground level and about 700 hPa were below 250 K in periods WC1 and WC2. The relative humidity in these periods were low value (below 70%), except for the layer over 850 hPa (below about 1400 m a.s.l.) became over 80% from February 16–17 and the layer between 700 hPa and 400 hPa (about 6500 m a.s.l.) became over 70% on February 21. Though in periods WC1 and WC2, the humidity was not very high, air masses in which temperature was almost constant existed between surface and a level of 700 hPa. It is likely that these air masses were inversion layer, and an ascending current was generated. In periods WC1 and WC2, the water vapor in the air was lifted from ground level into the sky by this ascending current, and precipitation occurred.

Properties of the air masses which brought about precipitation during WW1, WW2, WC1 and WC2 are collected in Table 3. From this table, the temperature of the air masses which brought about precipitation of WW1 and WW2 was higher at least 10 K than that of WC1 and WC2. The vertical extent of the moist air was also different between WW1, 2 and WC1, 2. In addition, amount of precipitation for WW1 and WW2 was over twice larger than that for WC1 and WC2. These results were suggested that fluctuation of $\delta^{18}O$ in the precipitation concerned with the characteristic of air masses which seemed to be supply source of the precipitation.

Then, the relation between $\delta^{18}O$ and aerology data was investigated in summer. The following were respectively extracted: Periods in which the $\delta^{18}O$ was higher than the mean value in summer (−12.3‰) for several days, are called SW1 (August 24–27) and SW2 (September 5–9), and periods in which low temperature persisted (SC1: August 29–September 1, SC2: September 13–16; *cf.* Table 3).

SW1 was one of the periods in which surface air temperature was highest during the observation period. In this period, the layer over 900 hPa (below 1000 m a.s.l.) was the highest for relative humidity (over 80%; Fig. 7b). The temperature between surface and a level of 900 hPa was over 267.5 K. In SW2, a layer which was similarly humid for a layer over 900 hPa existed. The temperature of this layer was over 265 K. Therefore, in SW1 and SW2 with high value of $\delta^{18}O$, the condensation of the water vapor which precipitated seemed to occur at low altitude and at high temperature.

In SC1 and SC2 where $\delta^{18}O$ was low, the layers between 600 hPa level (about 4000

This document is provided by JAXA.

Table 3. Properties of air masses which brought about precipitation and $\delta^{18}O$ during each period.

1993/94 Winter	WW1	WW2	WC1	WC2
Air masses				
Period	Feb. 8–13	Mar. 2–7	Feb. 16–22	Mar. 8–11
Vertical extent (hPa)	S*-700	S*-700	S*-850	S*-850
Temperature (K)	260–270	260–265	245–250	245–250
Precipitation (mm/half day)	0–34.9	0.1–8.1	0–3.2	0–0.8
$\delta^{18}O$				
Average (‰)	−9.8	−11.1	−16.6	−15.5
Maximum (‰)	−7.8	−7.3	−11.7	−13.7
Minimum (‰)	−12.8	−12.7	−20.4	−17.5

1994 Summer	SW1	SW2	SC1	SC2
Air masses				
Period	Aug. 24–27	Sep. 5–9	Aug. 29–Sep. 1	Sep. 13–16
Vertical extent (hPa)	S*-900	S*-900	S*-600	S*-600
Temperature (K)	267.5–275	265–270	245–270	250–267.5
Precipitation (mm/half day)	0.1–2.5	0–1.4	0.6–4.2	0.3–4.4
$\delta^{18}O$				
Average (‰)	−7.0	−6.8	−21.0	−17.8
Maximum (‰)	−5.8	−6.4	−18.5	−16.3
Minimum (‰)	−8.4	−7.1	−23.6	−19.1

*surface

m a.s.l.) and surface were high relative humidity, over 80%. Water vapor seemed to be condensing in these layer, since there was no other moist air. The temperature at the 600 hPa level was about 250 K in both periods.

The results in four summer periods are shown in Table 3. In SW1 and SW2, $\delta^{18}O$ clearly surpassed the mean value during the observation period, and the temperatures of the air masses which supplied the precipitation in these periods were over 265 K. $\delta^{18}O$ of SC1 and SC2 fell below the mean value, and the lowest temperature of the air masses which supplied the precipitation in these periods were below 250 K. The difference of the lowest temperatures between SW1, 2 and SC1, 2 was at least 15 K. Therefore, temperature of the air masses which supplied the precipitation seemed to be related to the change of the value of $\delta^{18}O$ in summer. Not only temperature but also amount of precipitation and extent of moist air were different between SW1, 2 and SC1, 2. Maximum Precipitations for half day in SW1 and SW2 were as almost half as that in SC1 and SC2. Moist airs in SW1 and SW2 existed only near surface, and in SC1 and SC2, spread from surface to 600 hPa level. It was found from these results that the characteristic of air masses brought precipitation influenced fluctuation of $\delta^{18}O$ in summer, same as winter.

4.3. Characteristic of variation of $\delta^{18}O$ in precipitations

Relationship between surface air temperatures and $\delta^{18}O$ in precipitations at Ny-Ålesund are appeared in Fig. 8. There is a week correlation between both in winter (R^2= 0.36; R^2 : Decision coefficient), and little in summer (R^2=0.22) as was suggested above.

In Table 3, we arranged the properties of air masses which brought about precipitation during 8 periods in both winter and summer. In winter, the temperature of the humid air

This document is provided by JAXA.

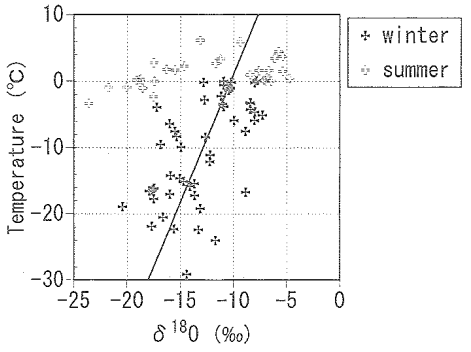


Fig. 8. The relationships between $\delta^{18}O$ and surface air temperature at Ny-Ålesund in winter and summer. The relationship in winter approximates the equation $T = 1.08\ \delta^{18}O + 3.63$ ($R^2 = 0.36$), and that summer the equation $T = 1.37\ \delta^{18}O - 3.52$ ($R^2 = 0.22$), T: surface air temperature, R^2: decision coefficient.

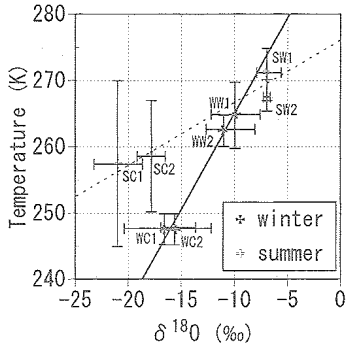


Fig. 9. The relationships between $\delta^{18}O$ and temperature of humid air masses which precipitations occurred in winter and summer. Vertical and horizontal bar means fluctuation range of temperature and $\delta^{18}O$ respectively. The relationship in winter approximates the equation $T = 2.82\ \delta^{18}O + 2.93 \times 10^2$ ($R^2 = 0.98$), and that summer the equation $T = 0.88\ \delta^{18}O + 2.75 \times 10^2$ ($R^2 = 0.93$), T: temperature of humid air mass, R^2: decision coefficient.

masses fluctuated between 245 K and 270 K. It fluctuated between 245 K and 275 K in summer. Though the maximum temperature was different by 5 K in winter and summer, the minima were equal. In Fig. 9, the relation between the temperature of the moist air masses and $\delta^{18}O$ in precipitations are shown, same as Fig. 8. Decision coefficient between both was 0.98 in winter and 0.93 in summer. Better correlations occurred between both in winter and summer. However there were the different equations which found the relationships between the temperature of the moist air masses and $\delta^{18}O$ in precipitations in winter and summer, as shown in Fig. 9, which possibly depended upon the atmospheric conditions in winter and summer. It means that $\delta^{18}O$ in precipitations at Ny-Ålesund in each season are approximated by these equations independently. From what has been discussed above, we can conclude that $\delta^{18}O$ in precipitations at Ny-Ålesund were decided by the temperature of the air mass in which the precipitation occurred.

A relation between $\delta^{18}O$ mean value of all precipitations during our observation and surface mean temperature at Ny-Ålesund agreed on proportional relationship of the other Arctic, as we mentioned in Section 4.1. It means that $\delta^{18}O$ during this observation was almost usual at Ny-Ålesund.

It has been reported that the seasonal variation of $\delta^{18}O$ was not recognizable in analysis of several ice cores from Svalbard, and the reason has been regarded that snow melted after it accumulated on the glacier in previous studies (Goto-Azuma *et al.*, 1995; Punning *et al.*, 1986. Besides, we could indicate other reason why the seasonal variation of $\delta^{18}O$ in precipitations did not recognize distinctly from this study.

This document is provided by JAXA.

5. Conclusions

Precipitation samples were collected at Ny-Ålesund in northwestern Svalbard in order to clarify the reason why the seasonal variation of $\delta^{18}O$ in ice cores from Svalbard was not so clear. We examined the relationship between $\delta^{18}O$ in precipitation and surface air temperature in winter and summer. Less correlation between $\delta^{18}O$ mean value in all precipitations during this observation and surface mean temperature was observed, not as it has previously been reported that there is generally a correlation between both in the polar regions. Therefore, it was indicated that present $\delta^{18}O$ observed value did not have the large difference from normal value. However, the extent of variation of $\delta^{18}O$ in winter and summer was similar in spite of a clearly difference of surface air temperature. It was concluded that in Ny-Ålesund, the fluctuation of $\delta^{18}O$ can not be explained only by the change of surface air temperature.

Then we examined the relationship between $\delta^{18}O$ change and aerology data. There was a correlation between temperature of the air masses which brought about the precipitation at Ny-Ålesund and $\delta^{18}O$ in both winter and summer. The relationships between both in winter and summer were found by the different equations, and $\delta^{18}O$ in each season are approximated by these equations independently.

In addition, we considered that it became a one of reason why the seasonal variation of $\delta^{18}O$ in analysis of several ice cores from Svalbard disappeared partly.

Acknowledgments

We would like to thank Drs. M. Wada and M. Kanawo for their help in collecting precipitation samples.

References

Dansgaard, W. (1953): The abundance of O^{18} in atmospheric water and water vapor. Tellus, **5**, 461–469.

Dansgaard, W., Johnsen, S.J., Clausen, H.B. and Gundestrup, N. (1973): Stable isotope glaciology. Medd. Grønl., **197**, 1–53.

Dansgaard, W., Johnsen, S.J., Clausen, H.B., Dahl-Jensen, D., Gundestrup, N., Hammer, C.U., Hvidberg, C.S., Steffensen, J.P., Sveinbjornsdöttir A.E., Jouzel, J. and Bond, G. (1993): Evidence for general instability of past climate from a 250-kyr ice-core record. Nature, **364**, 218–220.

Goto-Azuma, K., Kohshima, S., Kameda, T., Takahashi, S., Watanabe, O., Fujii, Y. and Hagen, J.O. (1995): An ice-core chemistry record from Snøfjellafonna, northwestern Spitsbergen. Ann. Glaciol., **21**, 213–218.

Hanssen-Bauer, I., Kristensen Solås, M. and Steffensen, E.L. (1990): The climate of Spitsbergen. Klima, **39/90**, 40 p. (DNMI-Rapport).

Iizuka, Y., Igarashi, M., Watanabe, K., Kamiyama, K. and Watanabe, O. (2000): Re-distribution of chemical compositions in the snowpack at the dome of Austfonna ice cap, Svalbard. Seppyo (J. Jpn. Soc. Snow Ice), **62**, 245–254 (in Japanese with English abstract).

Johnsen, S.J., Dansgaard, W., Clausen, H.B. and Langway, C.C., Jr. (1972): Oxygen isotopes profiles through the Antarctic and Greenland ice sheets. Nature, **235**, 429–434.

Petit, J.R. and 18 colleagues (1999): Climate and atmospheric history of the past 420,000 years from Vostok ice core, Antarctica. Nature, **399**, 429–436.

Punning, J.-M.K., Martma, T.A., Tyugu, K.E., Vaykmyae, R.A., Purshe, M. and Pinglo, F. (1986):

This document is provided by JAXA.

Stratification in an ice core from Vestfonna, Nordaustlandet. Geogr. Geol., **10**, 39–43.
Watanabe, O., Satow, K. and Fujii, Y. (1988): Depositional regime of the katabatic slope from Mizuho Plateau to the coast, East Antarctica. Ann. Glaciol., **10**, 188–192.

(Received May 9, 2000; Revised manuscript accepted October 23, 2000)

This document is provided by JAXA.

Mem. Natl Inst. Polar Res., Spec. Issue, 54, 183–191, 2001

Scientific note

Northern Eurasia glacier response to global climate change

Yuriy Kononov, Maria Ananicheva and Natalia Davidovich

Institute of Geography, Russian Academy of Sciences, Staromonetny per. 29 Moscow 109017, Russia

Abstract: One way to predict climate change in the future is reconstruction of former climates. This approach is called the method of paleoanalogues. In this paper the climatic reconstructions for Holocene optimum (scenario 1) and Eemian Interglacial (scenario 2) are used as paleoanalogues of possible future climate warming. Two techniques worked out by authors have been applied to calculate the change of the equilibrium line altitude (ELA): (1) based on calculations of ablation and accumulation on the Novaya Zemlya ice cap (the sufficient paleodata situation) and (2) on the other ice caps of the Eurasian Arctic (the insufficient paleodata situation). The latter involves the term "lower bottom of chionosphere" which under some assumptions is transformed into the ELA of each ice cap under climatic conditions of the Holocene and Eemian Interglacials.

According to these scenarios, the greatest changes of air temperature will be in the Arctic. For example, under global warming appropriate to scenario 1, the mean summer temperature in the Novaya Zemlya archipelago will rise by 4℃; according to scenario 2—by 8℃. By both scenarios the archipelagoes of Franz Joseph Land, Novaya Zemlya and Severnaya Zemlya will undergo the greatest warming in Northern Hemisphere. Annual precipitation will also reach maximum increase in this region (+100 mm under scenario 1 and +200 mm under scenario 2 in comparison with present values).

1. Introduction

Despite the last decades' trend toward retreat of glaciers, they are still a dominant factor in many high mountain landscapes and, in particular, on Arctic islands. More than 50% of the Arctic archipelagos are covered by ice caps and ice domes. The behavior of glacier systems in the lasting climatic trend toward warming in high latitudes is an important current research topic. Many papers on this topic have been published. Proposed scenarios of climate change involve different GCM schemes; however reconstructions of paleoclimates for interstadials (time between global glacier advances) and their use as possible analogous for future climate change represent an important direction in modern glacioclimatology.

In this paper paleoclimatic reconstructions of the Holocene optimum (5–6 thousand years ago) and Eemian Interglacial (120 thousand years ago) were used as scenarios for investigation of glacial response to possible climate change under two variants of global atmosphere warming. These reconstructions give spatial distributions of precipitation and air temperature (the climatic parameters which play the most important roles in glacier

This document is provided by JAXA.

development) for the whole Northern Hemisphere, with distinct regional differences.

2. Scenarios and methods

Calculations of the Arctic glaciers' response were carried out using the "principle of uniformity", that assumes contemporary relationships between glaciological and climatological parameters to be the same both in the past and future. Now glaciers exist in a wide corridor of the warmth and moisture alignment: from cold and dry conditions (where snow accumulation is lower than 50–100 mm per year, and mean summer temperature is −4, −6℃) to warm and humid ones (where snow accumulation is 3000–4000 mm annually and mean summer temperature is +5, +6℃). Actual data collected until the present time provide reliable links between glacier and climate characteristics for different types of glaciations.

The equilibrium line altitude (ELA), the basic glacier indicator, the level where annual accumulation equals annual ablation, directly depends on climate, first of all on the temperature and moisture regime. To obtain these parameters we used the following equations:

$$A = 1.33(t_{sum} + 9.66)^{2.85}, \quad (1)$$

$$C = X_{year} \cdot P \cdot K_{sn}, \quad (2)$$

$$X'_{year} = 9t_{sum}^{2} + 296t_{sum} + 645, \quad (3)$$

A—total melting (ablation), in mm, t_{sum}—mean summer temperature, ℃, C—annual accumulation in mm, X_{year}—annual precipitation at any altitude, mm, P—solid precipitation share in X_{year}, %, which depends mostly on mean monthly temperature, K_{sn}—coefficient of snow concentration on glaciers. X'_{year}—winter mass balance plus summer precipitation at the ELA, mm.

Formula 1 is a modification of a well known relation between snow melting and mean summer air temperature (Krenke and Khodakov, 1966), recalculated for the ELA zone (Krenke, 1982). Formula 2, summarizing empirical experience, has been widely used while compiling the World Snow and Ice Resources Atlas (Kotlyakov, 1998).

The third formula was derived from observations on 70 different glaciers at their ELA in various climatic belts presented in Ohmura *et al.* (1992).

Paleoclimatic scenarios are presented as maps which have been compiled from field data (Frenzl *et al.*, 1992) The points of sampling are not uniformly distributed throughout Northern Eurasia, so for some regions the spatial picture of climatic parameters was obtained by interpolation between rather scarce data. Therefore the degree of reliability for these areas is lower in comparison with those with dense sampling. This circumstance compelled the authors to use two different methods.

In case of sufficient data, we used the technique described in Davidovich and Ananicheva (1996). Specifically, we applied this technique to the Novaya Zemlya ice cap reconstruction in Holocene and Eemian Interglacial. This method involves calculation of the ablation vertical profiles for the glacier region by Formula 1 with the help of air temperature lapse rates and temperature discontinuities at glacier margins. When reconstructing climatic characteristics of the Novaya Zemlya islands, we assumed the annual

This document is provided by JAXA.

distribution of temperature and precipitation over the ice cap to be similar to the present-day one. The latter is distinctly maritime: the temperature extremes (minimum and maximum) take place in March and August, while the precipitation minimum occurs in February-March and maximum in August-September.

At present, the vertical gradient of air temperature over the existing ice cap, is noticeably greater (due to the cooling effect of the ice surface) than in free lower atmosphere and changes in reverse way through the year, with a winter minimum approaching the value of the dry adiabatic gradient. So for paleoreconstructions of warm periods we took the mean seasonal values 0.4℃/100 m in winter and 0.6℃/100 m in summer as the cooling effect of ice cap then was minimized. The mentioned method of treating the temperature discontinuities at the glacier surface is given in the same paper.

Since solid precipitation is not derived from paleogeographical data, this value was obtained by a nomogram, developed by E.G. Bogdanova of the State Geophysical Observatory (Bogdanova, 1976). The nomogram makes it possible to derive the solid precipitation component from the total amount by monthly air temperature and absolute altitude of the glacier (mean).

Paleo-temperatures and paleo-precipitation at different altitudes were calculated separately for 1) the modern ice sheet which occupies about 65% of Northern island's area in the middle and northern its parts, and 2) mountain glaciers which occupy about 7% of Southern island of the archipelago in its north. The two regions differ not only in the glaciation type, but also in subglacial landforms.

Vertical curves of glacier paleo-accumulation and paleo-ablation were built by Formulas 1 and 2. For the Novaya Zemlya ice cap the K_{sn} was assumed to be 1. The cross-section of the curves indicates the position of the ELA of the ice cap and mountain glaciation area in the two chosen time periods in the past.

The other approach was defined and used by Kononov and Ananicheva (1998) for the reconstruction of the former glaciation in Scandinavia *for the case of insufficient paleoclimate data.* A wealth of paleoclimate proxy data (lake level, pollen, diatoms, sediment stable isotopes, etc.) lies in the lowlands and intermountain basins outside the regions of interest. How can we exploit this resource of paleoclimate proxies in order to reconstruct mountain glaciation in the Arctic? This question was a primary motivating force for development of this approach.

For the reconstruction of glaciation in mountain areas (Arctic ice caps are located on elevated topography) we should identify the background value of some factor which combine both climatic and glaciologic components, can be obtained for region having past paleodata on climate, and can be extrapolated over wider (in particular mountain) territory. We consider that such factors can be obtained with the help of what we call the "chionosphere". The term was proposed by S.V. Kalesnik to describe the area (part of troposphere) where stable snow cover can persist all year round and glaciers can exist on the ground surface in favorable (elevated) relief forms (Kalesnik, 1963). This sphere of potential rather than actual glacierization should have a combination of warmth and moisture that permits annual solid precipitation on the horizontal surface to exceed their melting. The lower boundary of this sphere (H_h) corresponds to the climatic snow line, since in the free atmosphere climatic factors (temperature and precipitation) determine this level. While H_h touching the ground surface the relief factor enters into interaction, and then after glaciation

This document is provided by JAXA.

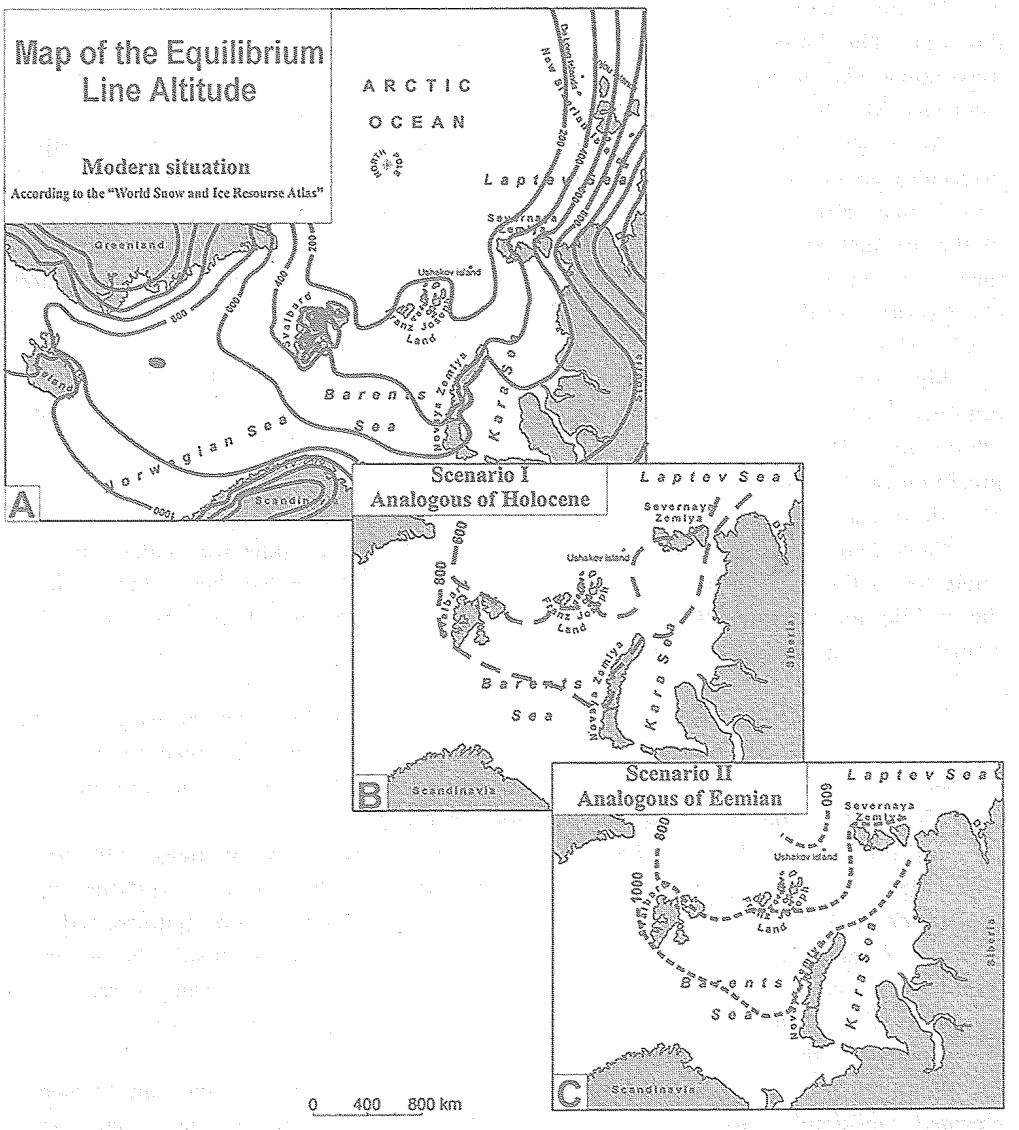


Fig. 1. Equilibrium line altitude of glaciation in the Eurasian Arctic at present time (A), reconstructed according to the paleoclimatic scenarios for Holocene Optimum (B) and Eemian interstadial (C).

has arisen, the glacier factor adds. In the latter case the lower boundary of the chionosphere "forms" ELA on glaciers. This method also supposes the use annual precipitation values as the analogue of accumulation.

The altitude of the chionosphere bottom over the major part of North polar area varies from 200–250 m to 1300–1500 m a.s.l. The chionosphere is at high altitude where it is cold and dry, in Greenland and the Canadian Arctic Archipelago, and is lowest over Arctic

This document is provided by JAXA.

islands near the sea ice edge. Its elevation under the central part of the Russian Arctic is 300–400 m. The altitude of the bottom boundary of the chionosphere is indicated by present-day equilibrium line altitudes (Fig. 1a, solid line).

If we can calculate the lower boundary of the chionosphere over plains and foothills we can extrapolate/interpolate to obtain average height for the wider territory including mountain regions. So in more detail the algorithm of calculations includes the following stages:

—Identification of the chionosphere lower boundary in the free atmosphere under the nearest place with sufficient paleoclimatic data and making the isoline "field" of the H_h;
—Interpolating or extrapolating the calculated H_h values over (mountain) regions, taking into account their local features;
—Transformation of the H_h values into ELA and constructing contours of the mountain ranges situated higher than the ELA;
—Determination of the whole glacier area which depends upon morphological and morphometric characteristics of both low and high mountain belts.

As has been said, H_h is not a direct equivalent of ELA, indeed in a previous paper (Kononov and Ananicheva, 1998) was shown that the relief forms have the greater effect on the ELA deviation from H_h. However, analysis of the difference between the presently observed ELA position on ice sheets of the Arctic archipelagoes and H_h, calculated by the described method has revealed that the influence of the relief cut in this region is insignificant and H_h can be considered to be the analogue of the ELA.

Paleoclimatic reconstructions as usual provide information about seasonal air temperature and annual total precipitation at the ground surface. In paleoglaciologic modeling it is acceptable to use mean summer temperature t_{sum} and annual precipitation X_{year} for while calculating mean annual ablation and accumulation.

The lower boundary of the chionosphere in free atmosphere was calculated by transformation of Formula 3: mean summer air temperature which corresponds to total precipitation, received by paleodata, is defined for the ELA. In this way we simulate the climatic situation as if the lower boundary of the chionosphere is located in a given place near the surface. Then, comparing values of the mean summer air temperature at the ELA and actual temperature (according to paleodata) at the ground surface, we obtain a temperature deviation, from which, together with the air temperature gradient, we can calculate an altitude where the deviation equals zero. This altitude coincides with the bottom boundary of the chionosphere. Taking the subsequent stages of the calculations (see above) we estimate the position of the glacier ELA and, as a result, the character and extent of glaciation in the past.

The method error (20%), caused by the series of assumptions, is acceptable in paleo-reconstructions but in case of forecasting seems too big. The main reason for the error lies in the assumption of correspondence between annual total precipitation and melting, calculated with Formula 1. In this paper this error is reduced by using Formula 3, since for this equation annual precipitation was measured at the equilibrium line altitude. Both described methods have been used for the Novaya Zemlya ice cap change under the paleoscenarios, the results were close.

This document is provided by JAXA.

3. Simulation of possible climate change in the Eurasian Arctic

Contemporary data on insular Arctic glaciation, collected for the newly published World Atlas of Snow and Ice Resources, were used for building the empirical relationship of the ELA and area of ice caps or reticular glaciers as the most widespread types in the Arctic. This relationship helps to estimate areas of former glaciation as well as possible glacier extent under climate change in the future. Depending on the lower chionosphere boundary position glaciers can occupy the whole island (for example, Ushakova Island) or some of its area (other glaciated islands of the Russian Arctic).

In accordance with the paleoscenarios, the major changes of air temperature took place in the high latitude belt. In the region of the Novaya Zemlya archipelago, for example, the mean summer air temperature will be 4℃ higher in the conditions of the global hemisphere

Table 1. Changes of some glaciological parameters for islands of the Eurasian Arctic under global warming by scenario 1.

Glacier region	Equilbrium line altitude (H) m a.s.l			Area under glaciers (S), km^2		
	Present-day	Forecasted	ΔH	Present-day	Forecasted	$\Delta S/\Delta$%*
West Spitsbergen, Svalbard	500	800	300	23719	7750	15969/67
Nordaustlandet, Svalbard	350	700	350	11135	2500	8635/78
Frans Josef Land	250	550	300	13735	0	13735/100
Novaya Zemlya	500	850	350	23645	5800	17845/75
Ushakova Island	150	450	300	325	0	325/100
Severnaya Zemlya	450	600	150	18325	7350	10975/60

*The percentage of glacier reduction (Δ, %) is given in the dominator as compared with the present glacier area.

Table 2. Changes of some glaciological parameters for islands of the Eurasian Arctic under global warming by scenario 2.

Glacier region	Equilbrium line altitude (H) m a.s.l			Area under glaciers (S), km^2		
	Present-day	Forecasted	ΔH	Present-day	Forecasted	$\Delta S/\Delta$%*
West Spitsbergen, Svalbard	500	900	400	23719	4250	19469/82
Nordaustlandet, Svalbard	350	800	450	11135	0	11135/100
Frans Josef Land	250	720	470	13735	0	13735/100
Novaya Zemlya	500	1100	600	23645	~500	23100/98
Ushakova Island	150	650	500	325	0	325/100
Severnaya Zemlya	450	850	400	18325	0	18325/100

*The percentage of glacier reduction (Δ, %) is given in the dominator as compared with the present time.

This document is provided by JAXA.

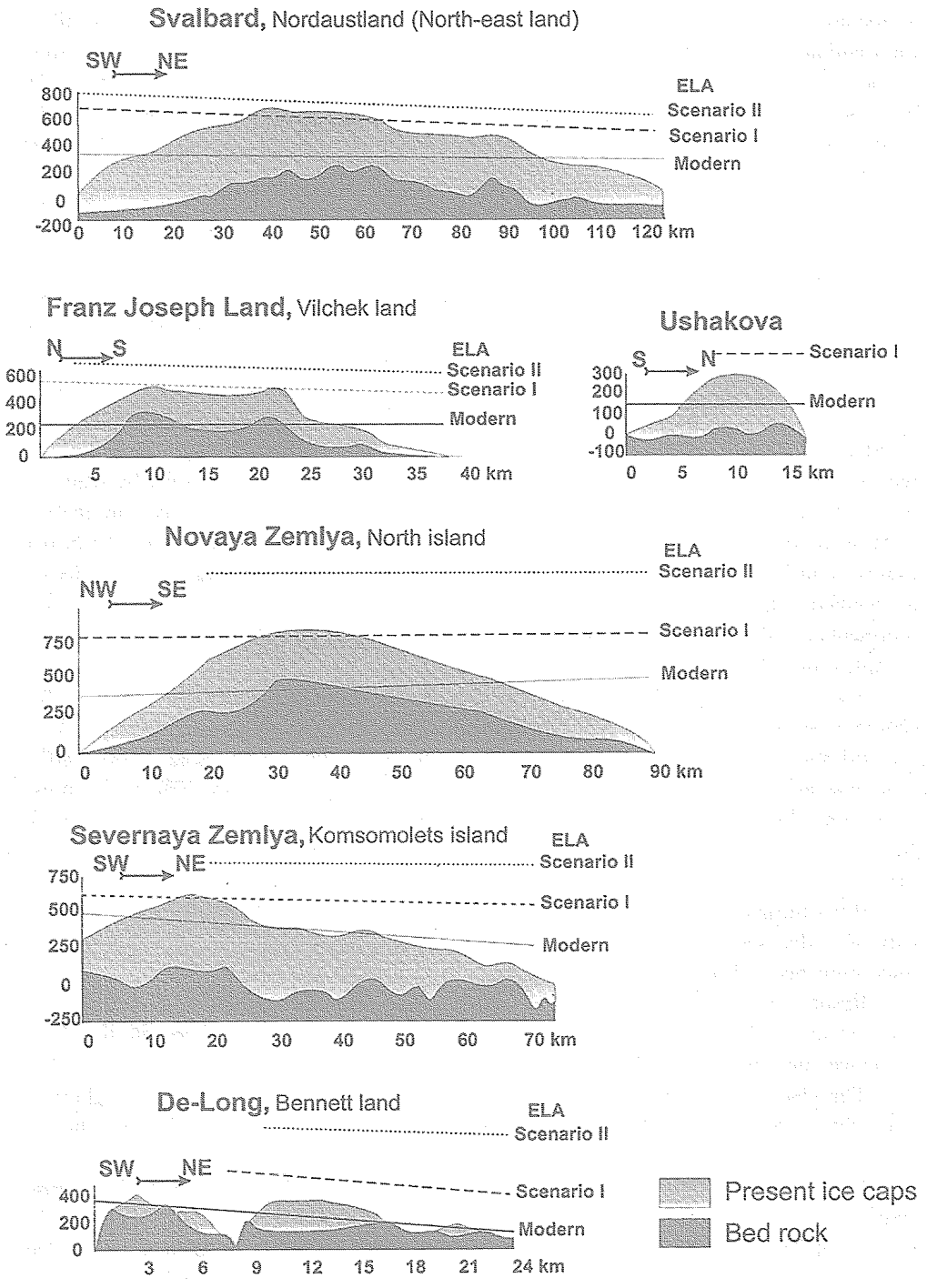


Fig. 2. The equilibrium line altitude change on glaciers of different Arctic islands according to the accepted paleoscenarios (the cross-sections are taken as presented in the World Atlas of Snow and Ice Resources, 1997)

This document is provided by JAXA.

temperature increase in the Holocene (scenario 1). Under global warming at 2℃, similar to the Eemian interstadial (scenario 2) it will be higher here at 8℃ than at present. However, in the belt between 20-40°N, regional climate will not change, and some mountain regions will face cooling. In general, within the Eurasian Arctic, the areas of most warming according to both scenarios will be the Frans Josef Land, Novaya Zemlya and Severnaya Zemlya archipelagos. Here annual precipitation will increase (+100 mm by scenario 1 and +200 mm by scenario 2) as compared with the present quantity. Calculation by the above stated methods gave forecasts for the main characteristics of insular Arctic glaciations for scenarios 1 and 2 (Tables 1 and 2).

From deviations of the calculated ELA values (ΔH) and glacier areas (ΔS), given in the tables, we can judge possible glacier situations in the Eurasian Arctic islands. We may say with certainly that under global warming according to scenario 1 (and also-scenario 2) the ice caps of Frans Josef Land and Ushakova Island will disappear completely; the remaining islands' glaciations will undergo significant reduction. The ELA of Frans Josef Land and Ushakova Island will exceed the tops of the archipelagos relief, resulting in removal of their ice caps. On other islands' ice caps the ELA shift upward by scenario 1 will be from 150 to 350 m (Fig. 1b, broken line); by scenario 2, from 400 to more than 600 m (Fig. 1c, dashed line). The maximum shift of the ELA is characteristic for the Novaya Zemlya and North-East Land (in the North-East of Svalbard Archipelago) as these ice caps are located in areas of great ocean influence and maritime climate type. Figure 2 graphically represents the shift of the ELA under both scenarios for those ice caps which will undergo complete degradation even under scenario 1.

The glaciation of Novaya Zemlya will undergo great reduction (75%) and will be replaced by mountain-valley glacier complexes (the same result is obtained by the first method, mentioned above). West Spitsbergen and Nordaustlandet will lose about 80% of their glaciated areas. The Severnaya Zemlya glaciers will cover only 40% of the present areas. On this archipelago small ice caps may survive only on the islands October Revolution and Bolshevik, maximum elevations of which exceed the forecasted ELA (600 m).

If warming corresponds to scenario 2 (Table 2, Fig. 1, dashed line, see also Fig. 2), ice caps will disappear from all of the Eurasian Arctic, because the ELA will exceed the maximum bedrock elevations everywhere.

Results of solid precipitation and melting calculation in this region also corroborate this statement (the reduced solid precipitation will not be able to compensate for sharply increased melting).

The glaciation of Svalbard will be survive only as a mountain-valley type glacier on West Spitsbergen Island. Possibly a mountain-valley glaciation will survive on the most elevated area-the southern part of the Northern Island.

In general we can conclude that glaciers will persist on those islands of the Eurasian Arctic which are favorable for their existence—elevated relief forms and topography. The glaciers of flat islands (Frans Josef Land, Nordaustlandet, Ushakova Island) will undergo intensive reduction under the "coolest" scenario 1 and disappear completely under the warm scenario 2.

This document is provided by JAXA.

References

Bogdanova, A.G. (1976): Method for calculation of solid and mixed precipitation proportion in their monthly standard. Mater. Glaciol. Issled. (Data Glaciol. Res.), **26**, Moscow, 202–207 (in Russian).

Davidovich, N.V. and Ananicheva, M.D. (1996): Prediction of possible changes in glacio-hydrological characteristics under global warming: south-eastern Alaska, U.S.A. J. Glaciol., **42**, 407–412.

Frenzl, B., Pecsi, M. and Velichko, A.A., ed. (1992): Atlas of paleoclimates and paleoenvironments of the northern hemisphere. Budapest.

Kalesnik, S.V. (1963): Glaciological Essays. Moscow, Uchpedgiz, 182 p. (in Russian).

Kononov, Y.M. and Ananicheva, M.D. (1998): Use of modern glacio-climatic relationships for the reconstruction of former glaciation (example of Scandinavia glaciation in Middle Valday). Mater. Glaciol. Issled., **84**, Moscow, 130–135 (in Russian).

Kotlyakov, V.M., ed. (1998): World Atlas of Snow and Ice Resources. Moscow, Institute of Geography, Russian Academy of Sciences, 392 p.

Krenke, A.N. (1982): Massexchange of glacial systems on the USSR territory. Leningrad, Gidrometizdat, 286 p. (in Russian).

Krenke, A.N. and Khodakov, V.G. (1966): The relationship between superficial ice melting with air temperature. Mater. Glaciol. Issled., **12**, Moscow, 153–164 (in Russian).

Ohmura, A., Kasser, P. and Funk, M. (1992): Climate at the equilibrium line of glaciers. J. Glaciol., **38**, 397–409.

(Received May 9, 2000; Revised manuscript accepted November 11, 2000)

This document is provided by JAXA.

This document is provided by JAXA.

Mem. Natl Inst. Polar Res., Spec. Issue, 54, 193–201, 2001

Scientific note

Effects on spectral reflectance from snow ageing

J-G. Winther[1], S. Gerland[1,3], J. B. Ørbæk[1], B. Ivanov[2], A. S. Zachek[2] and A. M. Bezgreshnov[2]

[1]*Norwegian Polar Institute, Polar Environmental Centre, N-9296 Tromsø, Norway (corresponding author's E-mail: winther@npolar.no)*
[2]*Arctic and Antarctic Research Institute, Bering 38, 199397 St. Petersburg, Russia*
[3]*Present address: Norwegian Radiation Protection Authority, Polar Environmental Centre, N-9296 Tromsø, Norway*

Abstract: This scientific note elaborates on the role that snow plays as an insulator for solar radiation on Arctic tundra and sea ice. We present spectral radiation data on i) surface reflectance, ii) attenuation in snow packs on land and on sea ice, and iii) under-ice irradiance. Our data is collected at Arctic tundra and fast-ice sites on Svalbard and in the Pechora Sea during spring melt-conditions. Although the spectrally-integrated surface reflectance, or albedo, decreases relative steadily in spring, we find that the infrared (IR) albedo decreases most strongly in the initial phase of snow melt while the visible albedo drops more quickly later on. The fact that the spectral signature of snow changes with time put restrictions on obtaining accurate satellite-derived narrow-band albedo measurements; however, new sensors will introduce significant improvements. Although thin, the presence of a snow cover fully dominates the exchange of solar radiation between the atmosphere and the sea ice-ocean system. Thus, a changing precipitation pattern (in time and space) in the Arctic Ocean can play a crucial role on sea-ice thickness distribution in a climate warming scenario. At last, this work suggests that the parameterisation of albedo in climate models could attempt to describe optical characteristics more realistically.

1. Introduction

The classical model work of Wiscombe and Warren (1980), Warren and Wiscombe (1980) and Warren (1982) thoroughly discusses the various factors affecting the albedo, such as snow depth, grain size, liquid water content, incident angle, and contamination. Later, a wide variety of field measurements and other theoretical studies of these relationships have been reported (*e.g.* Gerland *et al.*, 1999a,b; Grenfell *et al.*, 1981, 1994; Hall *et al.*, 1995; Knap and Reijmer, 1998; Liston, 1995; Perovich *et al.*, 1998; Steffen and Heinrichs, 1994; Winther *et al.*, 1999). Hence, during the last two decades we have gained a substantial knowledge on the reflective characteristics of snow.

Surface albedo is known to be one of the key parameters in the climate system in polar regions and very important in feedback processes (Curry *et al.*, 1995; IPCC TAR, in press). Obviously, a complicating factor for precise representation of snow cover and sea ice in large-scale models such as General Circulation Models (GCMs) is the extreme sub-grid

This document is provided by JAXA.

scale variability that occurs (Barry, 1996). Today, some GCMs make use of a time-dependent decay of snow albedo. Recent experiments with the ECHAM GCM have revealed that substantial improvement in the representation of snow albedo can be achieved when the shortwave albedo is treated separately in two bands, split at 700 nm (Ohmura, pers. commun., 2000). Therefore, it seems timely to utilise the detailed knowledge achieved in the previously-mentioned studies for improving the parameterisation of albedo in climate models. Furthermore, new generation satellite instruments, *e.g.* ESA's Envisat MERIS sensor, will enable us to measure spectral reflectance (in time and space) more accurately in future and they can provide improved input data for climate simulations. Also, in addition to being important for the surface energy-balance, attenuation of solar radiation determines how much radiation that is available for biological activity at the beginning of the growth season (*e.g.* for *collembola,* plants, moss, and lichen).

In this scientific note, we present data that illuminates various aspects of the reflection and attenuation behaviour of snow and sea ice. These examples are used in the following discussion where we indicate some future challenges concerning utilising information on spectral reflectance in climatic research.

2. Spectral reflectance measurements

2.1. Surface reflectance of melting snow at a tundra site

Figure 1 presents spectral reflectance from a tundra site near Ny-Ålesund at about 79°N on Svalbard for snow of various degrees of metamorphosis, surface blackening, and snow pack thickness measured in spring 1997. The data has been acquired by use of a FieldSpec spectroradiometer (Winther *et al.*, 1999). Curve 1 was acquired on 19 of May (clear skies) and represents dry, uncontaminated snow that had undergone minor metamorphosis. Curves 2 and 3 were taken on melting snow on June 8 and June 13, respectively (both cloudy days). By comparing Curves 2 and 3, it becomes clear that the decrease in reflectance is more pronounced in the near infrared (NIR) wavelength region than in the visible (VIS). This is partly caused by snow-grain growth. However, maybe more important is the increasing liquid-water content that replaces air with water between the ice grains. Then, because the spectral refractive index of liquid water is very close to that of ice for these wavelengths, the effective grain-size increases, and is followed by a decreasing reflectance. On contrary, the drop in reflectance in the VIS is more prominent than in the NIR between 13 and 19 of June (between Curve 3 and Curves 4 and 5) due to increasing surface blackening, mainly by local organic material transported from nearby snow-free areas as the snow cover depletes.

Curve 5 (cloudy) was acquired on a site in which a thin snow layer of 0.5 to 3 cm covered a 5–10 cm ice layer lying over the ground, with some free water present at the ice-soil interface. The low reflectance, in particular in the VIS region, is mainly caused by the thin layers of snow and ice covering the ground. In addition, the surface was strongly blackened by soil particles at this site. Curve 6 was measured over bare tundra.

Albedo is measured routinely at a nearby research station. Albedo is the spectral directional-hemispherical reflectance, *i.e.* it is the integral of reflectance over all (shortwave) wavelengths and reflection angles (Warren, 1982). For 19 of May, 8, 13, and 19 of June these values were 0.78, 0.76, 0.70, and 0.32, respectively. These values are marked as — on Fig. 1.

This document is provided by JAXA.

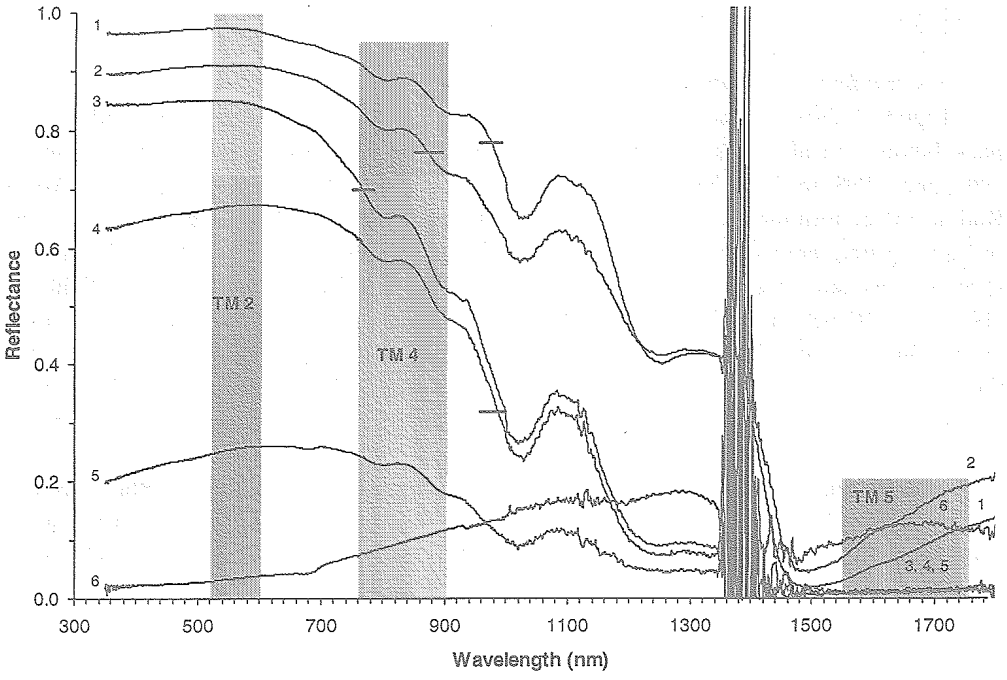


Fig. 1. Examples showing reflectance of snow with various degrees of metamorphosis, surface blackening, and snow pack thickness from Ny-Ålesund, Svalbard, in 1997. Curve 1 was acquired on May 19 (clear skies) and represents dry snow (snow thickness, s_h, = 45 cm) that had undergone minor metamorphosis and with an apparently unpolluted surface. Curves 2 and 3 were taken at melting snow surfaces on 8 and 13 of June, respectively (cloudy; s_h = 39 cm and 24 cm, respectively). Curves 4–6 were measured on 19 of June (cloudy). Curve 4 represents snow that had undergone about one month of snow metamorphosis and with some surface blackening (s_h = 5 cm). Curve 5 was acquired on a site where a thin snow layer of 0.5 to 3 cm covered a 5–10 cm thick ice layer sheltering the ground. In addition, the surface was strongly blackened by soil particles at this site. Curve 6 was measured over bare tundra. Spectrally-integrated albedo values from the nearby long-term albedo measuring site from 19 of May, 8, 13, and 19 of June, respectively, are marked on the figure as —. Finally, the wavelength ranges (or bands) covered by Landsat TM Bands 2, 4, and 5 are shown (from Winther et al., 1999). The small difference in reflectance between Curves 1 and 2 (dry snow < melting snow) is probably caused by different cloud conditions. The solar zenith angle was similar on these two days (~60 degrees).

The spectrally-integrated reflectance is, of course, often the most interesting figure for hydrological applications, *e.g.* for calculation of melt rates. Figure 1 shows that for the specific situation occurring in spring 1997, satellite-derived albedo in the NIR as measured, for example by Landsat TM Band 4, would in most cases yield slightly higher albedo estimates than the spectrally-integrated reflectance (285–2800 nm). However, important to notice here is that the variable spectral signature of melting snow makes it inappropriate to use one fixed satellite band throughout the melt season to acquire precise satellite-derived estimates of albedo. It should be noted that the large fluctuations around 1400 and 1800 nm are caused by the very small downward solar flux due to atmospheric absorption at these

This document is provided by JAXA.

wavelengths, *i.e.* a small signal to noise ratio.

2.2. Attenuation of radiation in a tundra snow pack

Figure 2 shows measured and modelled attenuation of radiation in a tundra snow pack before and after onset of melt. Measurements are obtained in the spring seasons of 1997 and 1998 in Ny-Ålesund using a Licor LI-189 PAR (Photosynthetically Active Radiation) quantum-meter along with snow parameters such as density, grain size, content of liquid water, temperature, thickness, and stratification (Gerland *et al.*, 2000). The model used is a two-stream 1-D model (Liston *et al.*, 1999) that is based on works by Schlatter (1972) and Brandt and Warren (1993). It can be used both with a constant or a variable extinction coefficient. Model input are snow grain-size, density, surface and soil albedo, and the spectrum of solar radiation as measured at the surface. Output from the model consists of downward and upward fluxes for 5000 layers, including the calculated extinction coefficient.

Overall, and in accordance with theory, solar radiation penetrates more efficiently into a snow pack after it has begun to melt since the effective grain-size increases when water becomes present, thus reducing the albedo (Fig. 2). Reasons for the relatively high degree of scatter in the measured data are mainly because i) they were collected throughout the

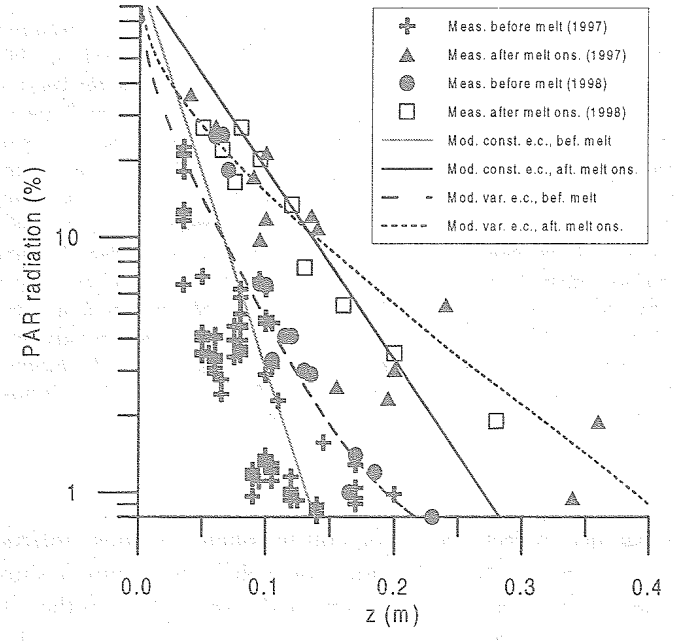


Fig. 2. In-situ attenuation-measurements of PAR and model simulations. Data is collected from various snow pits at Ny-Ålesund, Svalbard, before and after the onset of melt. The relative instrument reading Q(z)/Q(surface) is plotted at logarithmic scale versus snow thickness z above sensor. Model simulations are displayed for runs using constant and variable extinction-coefficients. Clearly, it can be seen that the snow pack becomes more transparent to solar radiation after the onset of melt (modified after Gerland et al., 2000).

This document is provided by JAXA.

melt period, *i.e.* over a time period when the snow pack gradually changed from dry to fully isothermal, and therefore the portion of the snow pack containing liquid water varied and ii) no distinguishing between measurements made under overcast or clear skies were made. It is known that the spectral composition of solar radiation received by a surface changes substantially during cloudy conditions since clouds absorb more of the infrared radiation than of the visible. Also, model simulations deviate somewhat from field measurements. We think this mainly is caused by a discrepancy between observed grain size (too large) and the real (optically) grain size where sub-grain size structures and non-spherical forms are important for scattering incidences to occur while these sub-structures are difficult to register by field methods (magnifying glass) (Grenfell and Warren, 1999).

2.3. Surface reflectance and under-ice irradiance of a fast-ice cover

Figure 3a shows surface albedo on a fast ice location in Kongsfjorden, Svalbard, for three stages in the development of snow melt during spring 1997 (Gerland *et al.*, 1999a). On 18 of May, the snow and sea-ice thickness were 20 cm and 70 cm, respectively. Average snow-density and grain-size were 318 kg/m^3 and 2 mm; the snow pack was dry. On 3 of June, the average density and snow grain size had increase to 356 kg/m^3 and 4 mm, respectively. However, the surface was covered by a thin layer of fresh snow with an observed grain size of 0.5 mm. The layer of freshly-fallen snow is the reason why the observed decrease in reflectance between 18 of May and 3 of June affects the visible albedo only (Fig. 3a). The explanation can be found in the fact that visible radiation penetrates deeper (*i.e.,* through the thin top-layer of snow) than infrared radiation does. The increased average grain-size decreases the visible albedo because the snow pack becomes more transparent and affected by the underlying sea ice whereas this does not happen in the infrared region where the thin, fresh snow-layer blocks out the IR radiation. Later, however, the fresh snow-layer thaws and then we experience a more pronounced decrease in the IR region. On 18 of June 1997, melting reached an advanced stage and only a little snow was left. Snow grains reached sizes of 5 to 10 mm, the surface was wet and melt ponds developed.

Figure 3b presents an experiment where irradiance was measured under the fast ice; first for an undisturbed situation and later for a sea-ice surface that had been cleared for snow. Thus, this enabled us to distinguish between the attenuation effect from sea ice only and from the original combined ice and snow-layer situation. The snow cover had a thickness of 21 cm, a temperature of −2.8℃, an average density of 260 kg/m^3, and with grain sizes varying from 0.1 to 5 mm (smallest grains at the top). Clearly seen on Fig. 3b, only about 1% of the irradiance at 550 nm reaches the water masses compared to the irradiance at the surface in the undisturbed case. After snow has been removed, about 27 times more solar radiation at 550 nm penetrates the sea ice and is thus received by the water masses beneath it. This relation factor is even higher for shorter and longer wavelengths.

2.4. Attenuation of radiation in snow that covers sea ice

An adequate understanding of shortwave radiative interactions in an atmosphere-sea ice-ocean system is critical for addressing issues such as sea-ice melt-rates, upper-ocean stratification processes, biological productivity-levels, as well as surface energy and mass-balance budget-calculations. Contrary to fast ice, pack ice is highly heterogeneous on

This document is provided by JAXA.

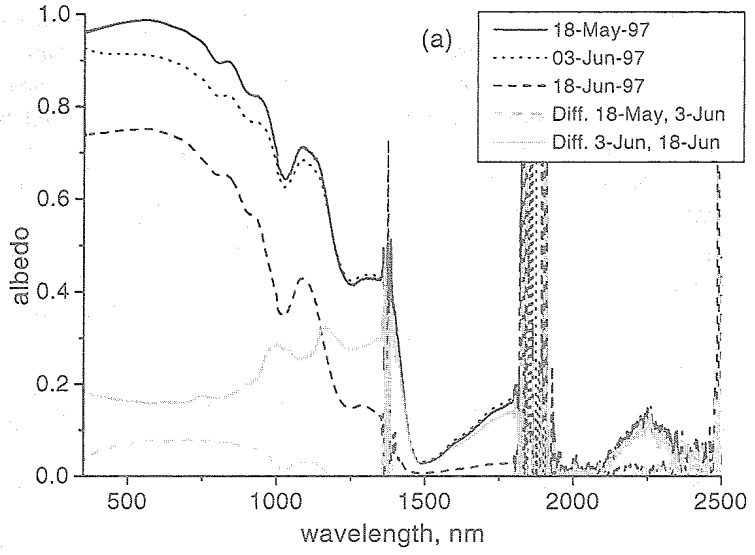


Fig. 3a. Surface reflectance from early-, mid-, and late spring season in 1997 over snow- covered sea ice in Kongsfjorden, Svalbard. Also plotted is the difference in albedo between 18 of May and 3 of June and between 3 of June and 18 of June. Note that the decrease in albedo appears in the visible region for the first period and to a larger extent in the infrared region for the latter.

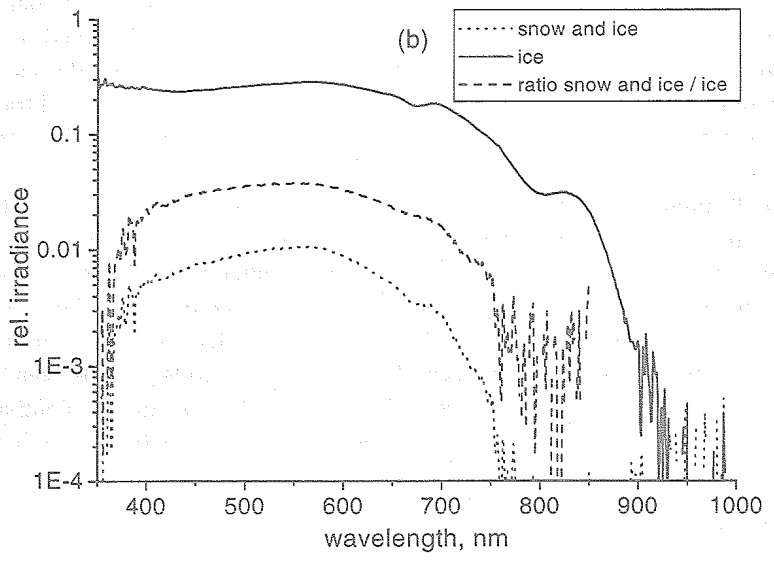


Fig. 3b. Under-ice irradiance measurements on fast ice in Kongsfjorden were acquired on 13 of May 1998. Spectral irradiance that reaches the water masses is plotted in percentage of the irradiance at the surface with and without snow on top of the sea ice (solid curve; snow was removed) (after Gerland et al., 1999a). It was stable, clear skies conditions on all observation days.

This document is provided by JAXA.

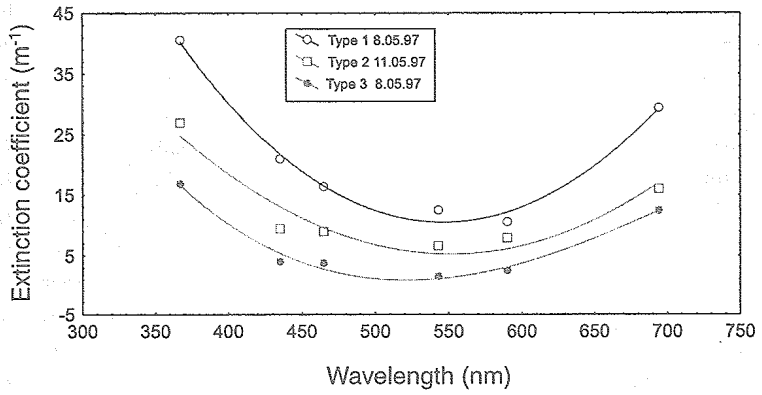


Fig. 4. Index for attenuation of irradiance in three different snow packs (all three were melting snow packs; other information n.a.) covering sea ice in the Pechora Sea, May 1997. Naturally, least attenuation is found in the central parts of the photosynthetic active region (around 550 nm) which also corresponds with under-ice measurements made on Svalbard (Fig. 3b).

horizontal scales of tens of meters due to the dynamic behaviour of drifting ice. Thus, the amount of solar radiation absorbed by the sea ice-ocean system is largely dependent on parameters such as brine volume, air-bubble distribution, ice thickness, presence of melt ponds, as well as snow-cover distribution and its characteristics.

Here, we only address one part of this extremely complex and highly varying system, namely the spectral extinction-coefficient of snow. Figure 4 shows how the PAR has attenuated at a fixed depth for three locations at 8 and 11 of May 1997 in the Pechora Sea. The largest penetration, or weakest attenuation, occurs in the central part of the PAR region at about 550 nm. This corresponds very well with under-ice irradiance measurements from Svalbard (Fig. 3b) showing that radiation at about 550 nm penetrates the snow-sea ice system most efficiently (*i.e.,* the curves in Figs. 3b and 4 have opposite curvatures). Another thing worthwhile mentioning is that relative large differences in attenuation occur over narrow wavelength-ranges, thus measurements by instruments averaging over broad bands will not detect these variations adequately. This has relevance for satellite-derived albedo measurements where the relative coarse spectral resolution of sensors often smooth out some of the spectral details present. Finally, a change of seasonal snow-characteristics as would happen in a warming scenario would have important impacts on the attenuation of solar radiation in snow packs, both in a terrestrial (Fig. 2) and marine environment (Fig. 4), with consequences on biological productivity.

3. Discussion and outlook

Our data shows that measurements of snow albedo, *i.e.* spectrally-integrated reflectance, using a narrow-band albedo as an indicator of shortwave albedo has severe weaknesses. This approach is commonly used in satellite remote-sensing studies but works inappropriately for melting snow because the spectral signature changes considerably

This document is provided by JAXA.

during the melt season. New sensors such as the NASA's Terra MODIS (launched in December 1999) and ESA's Envisat MERIS (launch planned in summer 2001) have a wide range of narrow bands and thus represent improved tools for accurate monitoring of broad-band albedo when combining various narrow satellite-bands.

In the beginning of the melt season the albedo drops fastest in the NIR region on tundra snow due to the increasing effective grain-size caused by the presence of liquid water and general metamorphosis of snow. Later, the VIS albedo reduction dominates due to contamination of the surface and a thinning snow pack. Interestingly, for one incident where fresh snow fell after the onset of melt, the reversed tendency happened over snow-covered fast ice on Kongsfjorden, Svalbard. Here, the initial snow cover was thin (about 20 cm). Thus, the underlying darker sea ice affected the visible surface albedo quickly after the onset of melt. Later on, the reduction in the NIR was most prominent. Held against the above findings from a tundra snow pack, this indicates that satellite-derived monitoring of broad-band albedo profits, at least for thin snow packs, from accounting for different spectral signatures for snow on land compared to snow on sea ice.

On the sea ice, even a thin snow layer (<20 cm) blocks out almost all solar radiation that otherwise would had been available for melting of sea ice and for absorption by the water masses beneath it. Undoubtedly, the snow-cover distribution plays a crucial role for solar energy-transfer between the atmosphere and the sea ice-ocean system; being important for marine biota production as well as in a climate context. For example, stratification due to sea-ice melt is known to trigger the bloom of phytoplankton production. Recently, an observed decrease in sea-ice extent and sea-ice thickness in the Arctic Ocean has received much attention (*e.g.* Rothrock *et al.*, 1999). These changes have to a large extent been attributed to an increase in air and/or ocean temperature. In addition, we think it is important to study precipitation patterns (*i.e.,* snow distribution) and changes in these in time and space and their effect on sea-ice thickness-distribution. In a climate regime where snow is absent only for about 3 months per year a change in snow thickness followed by a change in the timing of snow melt and disappearance will have a major effect on the amount of radiation available for sea-ice melt.

Finally, we would like to emphasise the need for improving the present relatively simple parameterisation of snow albedo in climate models. With the existing comprehensive observational data and models of the spectral-reflectance behaviour of snow combined with the improved monitoring capabilities provided by new satellite instruments, more realistic surface albedo should be used as input in future climate model-simulations.

Acknowledgments

We are grateful for fieldwork assistance by A. Blanco (University of Oulo, Finland), J. Boike (Alfred Wegener Institute, Potsdam, Germany), K. Sand (The University Courses on Svalbard, Longyearbyen), O.-G. Støen (Norwegian Polar Institute), personnel from the Norwegian Polar Institute's Research Station in Ny-Ålesund and personnel onboard the Russian icebreaker Akademik Federov. The Arctic and Antarctic Research Institute, the Norwegian Polar Institute, the Norwegian Research Council, and the NATO (CLG Grant No. EST.CLG.975781) are acknowledged for their funding support.

This document is provided by JAXA.

References

Barry, R.G. (1996): The parameterisation of surface albedo for sea ice and its snow cover. Progr. Phys. Geogr., **20**, 63–79.

Brandt, R.E. and Warren, S.G. (1993): Solar-heating rates and temperature profiles in Antarctic snow and ice. J. Glaciol., **39**, 99–110.

Curry, J.A., Schramm, J.L. and Ebert, E.E. (1995): Sea-ice albedo climate feedback mechanisms. J. Climate, **8**, 240–247.

Gerland, S., Winther, J-G., Ørbæk, J.B. and Ivanov, B. (1999a): Physical properties, spectral reflectance and thickness development of first year fast ice in Kongsfjorden, Svalbard. Pol. Res., **18**, 275–282.

Gerland, S., Winther, J-G., Ørbæk, J.B., Liston, G.E., Øritsland, N.A., Blanco, A. and Ivanov, B. (1999b): Physical and optical properties of snow covering Arctic tundra on Svalbard. Hydrol. Proc., **13**, 2331–2343.

Gerland, S., Liston, G.E., Winther, J-G., Ørbæk, J.B. and Ivanov, B. (2000): Attenuation of solar radiation in Arctic snow: field observations and modelling. Ann. Glaciol., **31** (in press).

Grenfell, T.C. and Warren, S.G. (1999): Representation of a nonspherical ice particle by a collection of independent spheres for scattering and absorption of radiation. J. Geophys. Res. **104**, 31697–31709.

Grenfell, T.C., Perovich, D.K. and Ogren, J.A. (1981): Spectral albedos of an alpine snowpack. Cold Reg. Sci. Tech., **4**, 121–127.

Grenfell, T.C., Warren, S.G. and Mullen, P.C. (1994): Reflection of solar radiation by the Antarctic snow surface at ultraviolet, visible and near-infrared wavelength. J. Geophys. Res., **99**, 18669–18684.

Hall, D.K., Riggs, G.A. and Salomonson, V.V. (1995): Development of methods for mapping global snow cover using moderate resolution imaging spectroradiometer data. Rem. Sens. Environ., **54**, 127–140.

IPCC TAR (2001): Intergovernmental Panel on Climate Change (IPCC) Third Assesment Report (in press).

Knap, W.H. and Reijmer, C.H. (1998): Anisotropy of the reflected radiation field over melting glacier ice: Measurements in Landsat TM Bands 2 and 4. Rem. Sens. Environ., **65**, 93–104.

Liston, G.E. (1995): Local advection of momentum, heat, and moisture during the melt of patchy snow covers. J. Appl. Meteorol., **34**, 1705–1715.

Liston, G.E., Winther, J-G., Bruland, O., Elvehøy, H. and Sand, K. (1999): Below-surface ice-melt on the coastal Antarctic ice sheet. J. Glaciol., **45**, 273–285.

Perovich, D.K., Roesler, C.S. and Pegau, W.S. (1998): Variability in Arctic sea ice optical properties. J. Geophys. Res. **103**, 1193–1208.

Rothrock, D.A., Yu, Y. and Maykut, G.A. (1999): Thinning of the Arctic sea-ice cover. Geophys. Res. Lett., **26**, 3469–3472.

Schlatter, T.W. (1972): The local surface energy balance and subsurface temperature regime in Antarctica. J. Appl. Meteorol., **11**, 1048–1062.

Steffen, K. and Heinrichs, J. (1994): Feasibility of sea ice typing with synthetic aperture radar (SAR): Merging of Landsat thematic mapper and ERS-1 satellite imagery. J. Geophys. Res., **99**, 22413–22424.

Warren, S.G. (1982): Optical properties of snow. Rev. Geophys. Space Phys., **20**, 67–89.

Warren, S.G. and Wiscombe, W.J. (1980): A model for the spectral albedo of snow. II: Snow containing atmospheric aerosols. J. Atmos. Sci., **37**, 2734–2745.

Winther, J-G., Gerland, S., Ørbæk, J.B., Ivanov, B., Blanco A. and Boike, J. (1999): Spectral reflectance of melting snow in a high Arctic watershed on Svalbard: Some implications for optical satellite remote sensing studies. Hydrol. Proc., **13**, 2033–2049.

Wiscombe, W.J. and Warren, S. (1980): A model for the spectral albedo of snow. I: Pure snow. J. Atmos. Sci., **37**, 2712–2733.

(Received April 3, 2000; Revised manuscript accepted July 3, 2000)

This document is provided by JAXA.

This document is provided by JAXA.

Mem. Natl Inst. Polar Res., Spec. Issue, 54, 203–207, 2001

Scientific note

Sudden climatic change

Roy M. Koerner

Geological Survey of Canada, Natural Resources Canada,
6012 Booth St, Ottawa, Ontario, K1A 0E8, Canada (rkoerner@nrcan.gc.ca)

Abstract: Studies of ice cores have shown that sudden climate changes (using $\delta^{18}O$ as a temperature proxy), were a common feature of past climate. Interplay between the Atlantic "conveyor belt" (or Thermohaline Circulation) and ice sheet melt-water is seen as the factor responsible for at least some of these sudden climatic changes. The Younger Dryas, 12.7–11.5 ky BP, is a well-studied example of such an event. Dansgaard-Oeschger events may be similarly explained. More recent research has attributed a sudden cooling, registered by a $\delta^{18}O$ step in 8.2 ky old ice in the Camp Century, Dye-3, GRIP and Agassiz ice cap cores, to sudden drainage, into the Atlantic, of glacial lakes on the southern margins of the decaying Laurentide ice sheet.

The question is whether a similar event could be triggered in the future by global warming and ice cap/Greenland ice sheet melt. In this paper, it is argued that all the classic sudden climatic change events occurred in the presence of the great Pleistocene Ice Sheets. It is unlikely that future melting of the northern circumpolar ice caps, glaciers and ice sheets would generate sufficient melt water to cause a similar event.

1. Introduction

Climatic change has come to the forefront of scientific research in response to the ongoing debate concerning the effect of industrial emissions of greenhouse gases on the radiative properties of the atmosphere. Models show that by increasing the concentrations of gases such as CO_2 and CH_4 in the atmosphere, climate will warm to levels high enough to seriously disrupt global society. Studies of past climates have, and are, playing a significant part in this debate. Only by putting ongoing climatic change in perspective can one determine how serious that disruption might become.

Paleo climate studies have been given a significant boost by recent successes in drilling deep ice cores from ice caps and ice sheets. For example, cores, covering 400000 years from Vostok, Antarctica (Jouzel *et al.*, 1993), have demonstrated the strong relationship between air temperatures and CO_2. In this case, CO_2 is seen as an amplifier rather than an initial cause of the temperature change. Cores from Greenland (Dansgaard *et al.*, 1971, 1985; Johnsen *et al.*, 1992) have also indicated that climatic change during the Pleistocene period was often rapid and dramatic. It is these kind of changes that are the concern of this note. This because if changes of several degrees C have occurred before they may occur with any future perturbations of climate. The consequences for society would be disastrous. This

This document is provided by JAXA.

paper argues that the abrupt changes recorded in the Greenland cores, all occurred in the presence of the great Pleistocene ice sheets. It has been suggested that the link between the ice sheets and climatic change was most probably meltwater releases from one of those ice sheets. The meltwater manifested itself climatically by either shutting or dramatically slowing down the northward, surface circulation of the Atlantic Ocean.

2. Sudden events

Abrupt changes in $\delta^{18}O$ (now termed *'Dansgaard/Oeschger events'*) were first found in Pleistocene ice from the Camp Century core (Dansgaard *et al.*, 1971). They were present also in the Dye-3 core from southern Greenland (Dansgaard *et al.*, 1985) and again in the summit-Greenland cores of both GISPII (Grootes and Stuiver, 1997) and GRIP (Johnsen *et al.*, 1992). GRIP also found similar abrupt events in Eemian Interglacial ice and considered them climatic (Johnsen *et al.*, 1998). However, study of the CH_4, $\delta^{18}O$ of O_2 records in the Eemian ice of the Vostok GRIP and GISPII cores (Chappellaz *et al.*, 1998), strongly suggests the interglacial events are dynamic (due to uneven ice flow over the bed) rather than climatic.

However, the sharp, unarguably climatic, (Dansgaard/Oeschger) events in the Pleistocene ice are thought to be the consequence of interplay between the big ice sheets, the Thermohaline circulation in the Atlantic, and consequent cooling of the air masses reaching Greenland and the north Atlantic coastline (*e.g.* Stocker and Marchal, 2000). Marshall and Clarke (1999) considered that high run-off variability from the north American continent may have kept the Thermohaline circulation in a similarly variable state; run-off variability itself was most likely ice-melt rather than rainfall dominated. In contrast, in the absence of the great Pleistocene Ice Sheets, the present (Holocene) interglacial period has had a relatively stable climate.

However, the Greenland and Canadian Arctic (Fig. 1) records have shown one dramatic climatic excursion 8.2 ka (thousands of calender years) ago. This event effected the sharpest $\delta^{18}O$ (temperature) excursion in the Holocene part of the ice core stable isotope records which represented a 4–8℃ drop in temperature in central Greenland (Alley *et al.*, 1997). Because the event occurred in a period that is, by definition, termed an interglacial it suggested that "warmth is not a guarantee of climate stability" (Alley, 2000). Thus, similar events could occur in the near future, especially when anthropogenic greenhouse forcing is perturbing climate. However, Barber *et al.* (1999) have related the 8.2 ka event to catastrophic drainage of massive lakes that were marginal to the Laurentide ice sheet. These lakes were released by the final collapse of the Laurentide ice sheet which had hitherto, dammed the natural drainage of these lakes to the sea. Barber *et al.*'s (1999) research shows that, although the event occurred in a warmer world, it was still triggered by a Pleistocene ice sheet albeit in its decaying stages. This scenario is *very* different to the present world where the large ice sheets have long disappeared.

The question is whether increased warming will cause sufficient melting of the Greenland Ice Sheet and the circum-polar ice caps to cause another upset of the Thermohaline circulation and a dramatic climatic change. Firstly, one should stress that the climate change picture over this period shows substantial variations in the patterns of circum-polar warming. While the western Canadian Arctic, Alaska, and Siberia are warming substantial-

This document is provided by JAXA.

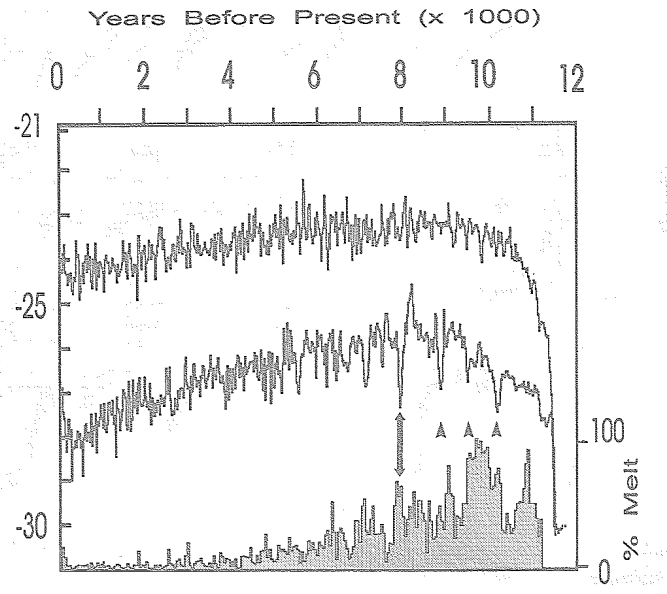


Fig. 1. Holocene records of stable isotopes ($\delta^{18}O$) for Penny Ice Cap, Southern Baffin Island (top), (Fisher et al., 1998), and Agassiz Ice Cap, Northern Ellesmere Island (middle) (Fisher et al., 1995), and melt% for Agassiz Ice Cap (bottom) (Koerner and Fisher, 1990). As a temperature proxy, the less negative the $\delta^{18}O$ values or the higher the melt percentage, the warmer the temperature. The melt percentage is assessed from the percentage of ice layers in an annual layer of ice in the core. The discrepancies, in terms of temperatures, represented between the ice melt% and the $\delta^{18}O$ values in the early Holocene, are believed due to the "contaminating" effect of melt water from the Laurentide ice sheet, on the latter (Koerner, 1988; Fisher, 1992). The double-headed arrow points to the 8.2 ka event. The 200 year discrepancy in the timing with the accurately-dated Greenland cores for this event, is due to slight dating errors in the Canadian cores. The three separate arrows point to possible similar events in the early Holocene. Extrapolation back from present-day $\delta^{18}O$ and Melt% values (where the mass balance of the ice caps is presently slightly negative) to the early Holocene shows warmer and hence more negative balances then.

ly, the same is not true for the Eastern Canadian Arctic and round to the east, to Svalbard (Dowdeswell *et al.*, 1997). Mass balance measurements on the ice caps in the Canadian Arctic (Fig. 2) and Svalbard do not show any trends of increased melting over the past 40 years although they do have slightly negative mass balances (Dowdeswell *et al.*, 1997; Koerner and Lundgaard, 1996). Secondly, the early Holocene was a period of very warm temperatures. Ice core records (*e.g.* Fig. 1) in conjunction with modern glacier mass balance measurements (Fig. 2) indicate that glacier mass balances were very negative at that time. The Greenland Ice Sheet, circumpolar ice caps, and the decaying Pleistocene ice sheets were all discharging far more melt water into the north Atlantic region than could be conceived of even in the warmer world of the anthropogenically warmed future. The Laurentide ice sheet alone was discharging melt water at an *average* rate, equivalent to about 1.0 cm sea level rise a year (Marshall and Clarke, 1999). This compares to sea level rise over the last 100 years of 1.0–2.0 mm/yr (Warrick and Oerlemans, 1990). Yet there is no evidence of a

This document is provided by JAXA.

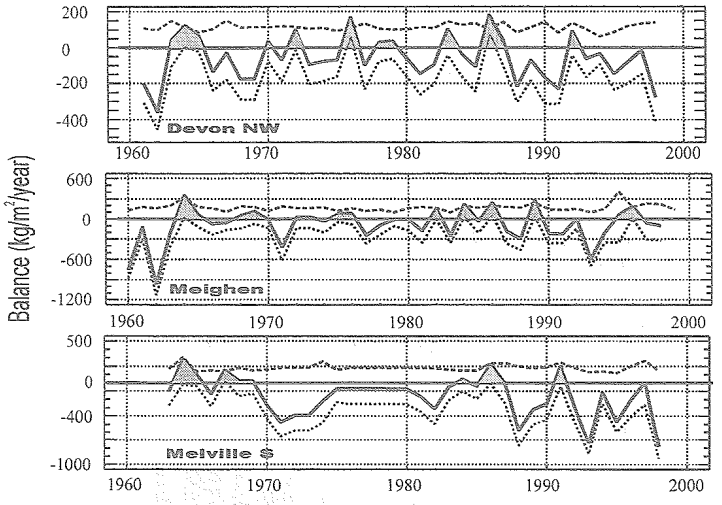


Fig. 2. Mass balance of 3 Canadian ice caps. The top line of the three in each profile, represents ***winter balance****, the middle line* ***net*** *(winter minus summer)* ***balance****, and the lowermost line* ***summer balance****. The records show no, overall, significant trend in any of the profiles, although the balance is slightly negative.*

major, *prolonged* shut-down of the Thermohaline circulation during the 10000 years of ice sheet retreat.

This is not to deny that the Thermohaline circulation is unlikely to be affected by future warming, rather that if it is affected, it will not be in the same way as the dramatic events of the past, registered in the ice core records.

References

Alley, R.B. (2000): Ice-core evidence of abrupt climate changes. Publ. Natl Acad. Sci. Online (PNAS Online), **97**(4), 1331–1334.

Alley, R.B., Mayewski, P.A., Sowers, T., Stuiver, M., Taylor, K.C. and Clark, P.U. (1997): Holocene climatic instability: A prominent, widespread event 8200 yr ago. Geology, **25**, 483–486.

Barber, D.C. and 10 others (1999): Forcing of the cold event of 8,200 years ago by catastrophic drainage of Laurentide lakes. Nature, **400**, 344–348.

Chappellaz, J, Brook, E., Blunier, T. and Malaize, B. (1998): CH_4 and $\delta^{18}O$ of O_2 records from Antarctic and Greenland ice: A clue for stratigraphic disturbance in the bottom part of the Greenland Ice Core Project and the Greenland Ice Sheet Project 2 ice cores. J. Geophys. Res., **102**, 26455–26470.

Dansgaard, W.S., Johnsen, S.J., Clausen, H.B. and Langway, C.C., Jr. (1971): Climatic record revealed by the Camp Century ice core. The Late Cenozoic Glacial Ages, ed by K.K. Turekian. Yale University Press, 37–56.

Dansgaard, W., Clausen, H.B., Gundestrup, N., Johnsen, S.J. and Rygner, C. (1985): Dating and climatic interpretation of two deep Greenland Ice Cores. Greenland Ice Core: Geophysics, Geochemistry, and the Environment, ed. by C.C. Langway, Jr. Washington, D.C., Am. Geophys. Union, 71–76 (Geophysical Monograph 33).

Dowdeswell, J.A. and 10 others (1997): The mass balance of Circum-Arctic glaciers and recent climate change. Quat. Res., **48**, 1–14.

This document is provided by JAXA.

Fisher, D.A. (1992): Possible ice core evidence for a fresh melt water cap over the Atlantic Ocean in the early Holocene. The Last Deglaciation: Absolute and Radiocarbon Chronologies, ed. by E. Bard and W.S. Broecker. 267–293 (NATO ASI Series, **12**).

Fisher, D.A., Koerner, R.M. and Reeh, N. (1995): Holocene climatic records from Agassiz Ice Cap, Ellesmere Island, NWT, Canada. The Holocene, **5**(1), 19–24.

Fisher, D.A. and 12 others (1998): Penny Ice Cap Cores, Baffin Island, Canada, and the Wisconsinan Foxe Dome Connection: Two States of Hudson Bay Ice Cover. Science, **279**, 692–695.

Grootes, P.M. and Stuiver, M. (1997): Oxygen 18/16 variability in Greenland snow and ice with 10^{-3} and 10^{5}-year time resolution. J. Geophys. Res., **102**, 26455–26470.

Johnsen, S.J. and 9 others (1992): Irregular glacial interstadials recorded in a new Greenland ice core. Nature, **359**, 311–313.

Johnsen, S.J. and 14 others (1998): The $\delta^{18}O$ record along the Greenland Ice Core Project deep ice core and the problem of possible Eemian climatic instability. J. Geophys. Res., **102**, 26397–26410.

Jouzel, J. and 16 others (1993): Extending the Vostok ice-core record of paleo climate to the penultimate glacial period. Nature, **364**, 407–412.

Koerner, R.M. (1988): Ice core records of paleo climate: the late glacial/early Holocene period: abstracts. 10th meeting of AMQUA, Amherst, Mass.

Koerner, R.M. and Fisher, D.A. (1990): A record of Holocene summer climate from a Canadian high-Arctic ice core. Nature, **343**, 630–631.

Koerner, R.M. and Lundgaard, L. (1996): Glaciers and global warming. Géogr. Phys. Quat., **49**, 429–434.

Marshall, S. and Clarke, G.K.C. (1999): Modeling North American freshwater runoff through the last glacial cycle. Quat. Res., **52**, 300–315.

Stocker, T.F. and Marchal, O. (2000): Abrupt climate change in the computer: Is it real ? Publ. Natl Acad. Sci. Online (PNAS Online), **97**(4), 1362–1365.

Warrick, R. and Oerlemans, J. (1990): Sea level rise. Climate Change, the IPCC Scientific Assessment. WMO Intergovernmental Panel on Climate Change. Cambridge University Press, 365 p.

(Received July 25, 2000; Revised manuscript accepted August 22, 2000)

This document is provided by JAXA.

This document is provided by JAXA.

Mem. Natl Inst. Polar Res., Spec. Issue, 54, 209–220, 2001

Scientific note

210-year ice core records of dust storms, volcanic eruptions and acidification at Site-J, Greenland

Yoshiyuki Fujii[1], Kokichi Kamiyama[1], Hitoshi Shoji[2], Hideki Narita[3], Fumihiko Nishio[4], Takao Kameda[2] and Okitsugu Watanabe[1]

[1]*National Institute of Polar Research, Kaga 1-chome, Itabashi-ku, Tokyo 173-8515*
[2]*Kitami Institute of Technology, Koencho 165, Kitami 090-0015*
[3]*Institute of Low Temperature Science, Hokkaido University, Kita-19, Nishi-8, Sapporo 060-0819*
[4]*Center for Environmental Remote Sensing, Chiba University, Yayoi-cho, Inage-ku, Chiba 262-8522*

Abstract: 210-year records of dust concentration, electrical conductivity, acidity (pH), non-sea salt sulfate (nss sulfate) and nitrate concentrations were obtained for an ice core from Site-J, Greenland. The ice core was well dated by counting annual cycles of the $\delta^{18}O$ profile and by tuning with time markers established for tritium peaks and the Laki 1783 eruption signal. Dust records in both ice cores from Site-J and Crête suggest that dust storms occurred in 1818, 1900, 1919, 1936 and 1943 over Greenland. Electrical conductivity shows remarkable peaks probably due to volcanic eruptions with VEI larger than 4. The anthropogenic effect on precipitation chemistry started in *ca.* 1860, 40 years earlier than the time previously reported. Nss sulfate increased remarkably, much more than nitrate, because of the rapid increase in solid fossil fuel combustion, but by the early 1970's, the nitrate concentration exceeded the nss sulfate concentration due to the intense increase in liquid fossil fuel combustion since the 1950's. The decrease in sulfate and nitrate concentrations started in the early 1970's. This is attributed to the spread of suppression facilities for anthropogenic pollutants emitted by the combustion of solid and liquid fossil fuels.

1. Introduction

As the Greenland Ice Sheet has much snow accumulation, the original stable oxygen isotope profile at the time of deposition is well preserved even though it has been smoothed by diffusive processes (*e.g.* Dansgaard *et al.*, 1973). Greenland ice cores, therefore, provide detailed climate and environment records over the past thousand years (*e.g.* Johnsen *et al.*, 1972; Mayewski *et al.*, 1990; Clausen *et al.*, 1998). There have been many works done on the climate and environment changes in the past with Greenland ice cores, but not many works on detailed environment changes in dust storms, volcanic eruptions and acidification during the past hundred years since the pre-Industrial Era. These signals in an ice core are well associated with atmospheric loading of aerosols, which play an important role in the climate system because of their direct or indirect interaction with solar and terrestrial radiation.

We present changes in dust concentration, electrical conductivity, acidity and major ions, and discuss dust storms, volcanic eruptions and anthropogenic acidification during the

This document is provided by JAXA.

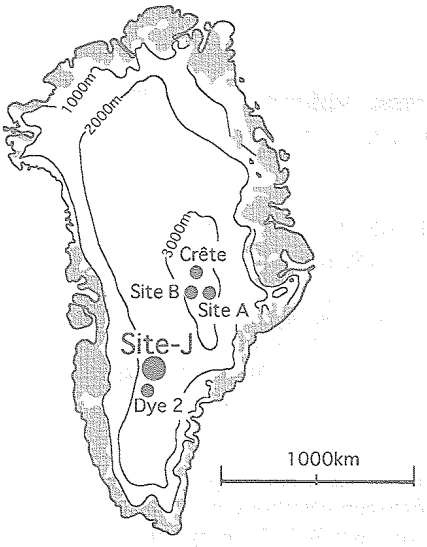


Fig. 1. Location of Site-J, Greenland. Ice core drilling sites referred to in this study are shown by small solid circles.

past 210 years on the basis of analyses of an ice core from Site-J (66°51.9′N, 46°15.9′W and 2030 m a.s.l.; Fig. 1) in southern Greenland. The place is far from any local anthropogenic sources and is thought to be ideal to evaluate the anthropogenic effect on the background level of atmospheric chemistry in the Arctic.

2. Ice core drilling and sample procedure

In 1989, we obtained a 205.15 m deep ice core at Site-J (Watanabe and Fujii, 1990), 50 km north from a previously drilling location, Dye 2 (66.2°N, 46.1°W; Langway *et al.*, 1985), with an electro-mechanical drill. After stratigraphic observation and electrical conductivity measurement (ECM), we cut the ice core at every 10 cm in depth to a depth of 168 m to obtain seasonal variation of $\delta^{18}O$ assuming the annual accumulation rate of 40 cm of ice at Site-J, referring to the rate of 37.4 cm at Dye-2 (Clausen and Hammer, 1988).

After removing the outer contaminated part, 5 mm thick, with a cleaned knife, we melted each ice sample in a Teflon container with a microwave oven in a science trench at the drilling site. We measured *in-situ* electrical conductivity of the melted samples and mixed samples prepared by mixing 10 successive samples, namely 1-meter long melted samples. These melted samples, and the frozen ice core deeper than 168 m, were brought back to Japan.

We carefully analyzed the melted samples in a class 1000 clean room to avoid contamination during processing and analyzing. The numbers of samples analyzed are 950 10-cm long samples continuously to 104 m in depth and 205 1-m long mixed samples to 205 m in depth.

3. Ice core dating

The ice core was precisely dated by counting annual cycles of the $\delta^{18}O$ profile to a

This document is provided by JAXA.

depth of 104 m as shown in Fig. 2. Tritium profile (Fujii, 1991) in the depth range from 15 to 23 m is also shown in Fig. 2, indicating reference horizons of 1959, 1963 and 1964 which are also obtained in other Greenland ice cores (*e.g.* Koide *et al.*, 1982). These tritium reference horizons are used to crosscheck the $\delta^{18}O$ dating for the upper 21-m layer where the $\delta^{18}O$ annual cycles are somewhat complicated.

The dating below this depth was achieved without many complications and high

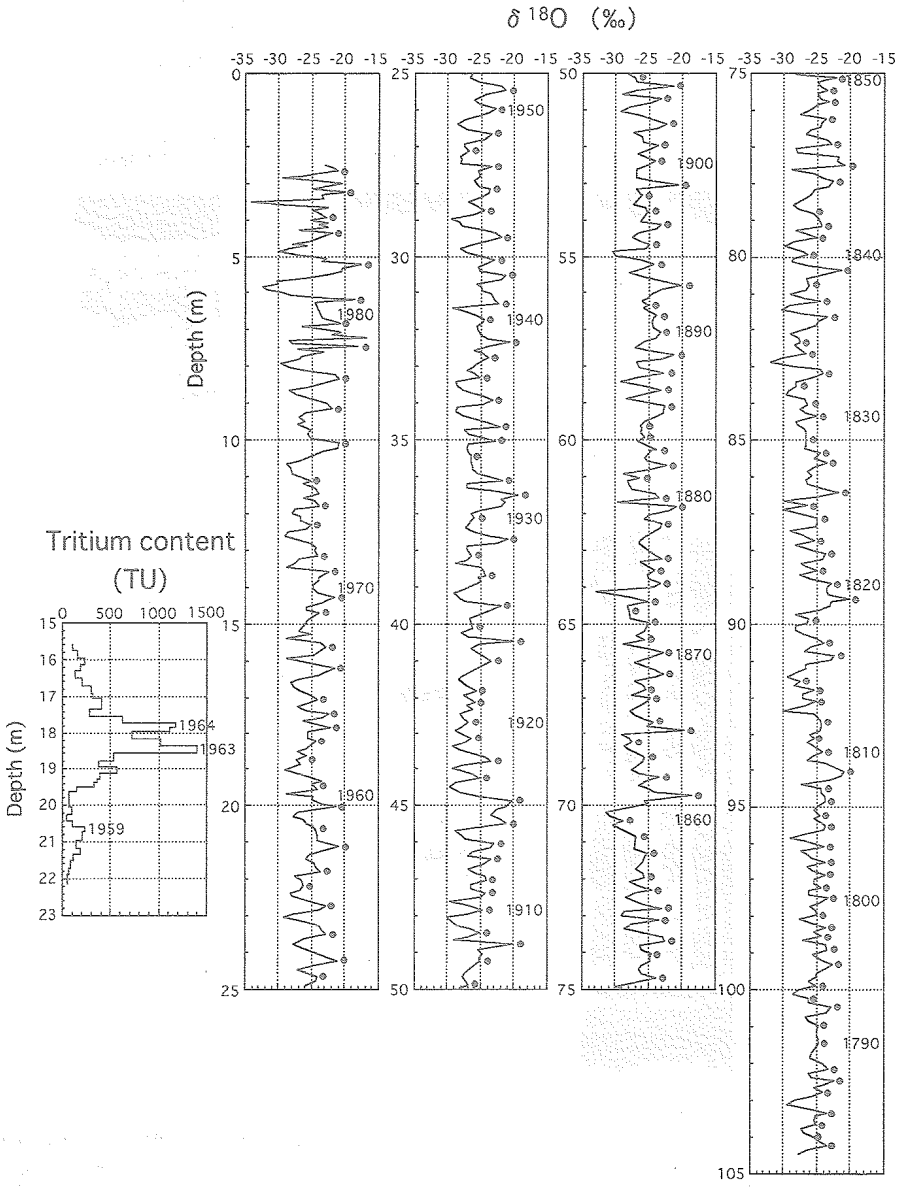


Fig. 2. Profiles of $\delta^{18}O$ and tritium content. Ice core dating was done by counting summer $\delta^{18}O$ peaks shown by black dots, and was crosschecked by tritium time markers.

This document is provided by JAXA.

precision was obtained to a depth of 104 m. The most distinct signal peak in ECM measurement observed at 103.63 m in depth is considered to be the Laki eruption in 1783 (Shoji *et al.*, 1991), which is the useful reference horizon in dating ice cores from Greenland (Clausen and Hammer, 1988). The dating by counting $\delta^{18}O$ annual cycles was tuned to be 1783 AD at this depth and estimation error is ± 2 years between these time markers.

4. Results and discussion

4.1. Acidity enhancement

To clarify formation of ice layers and change in acidity in the surface snow layer

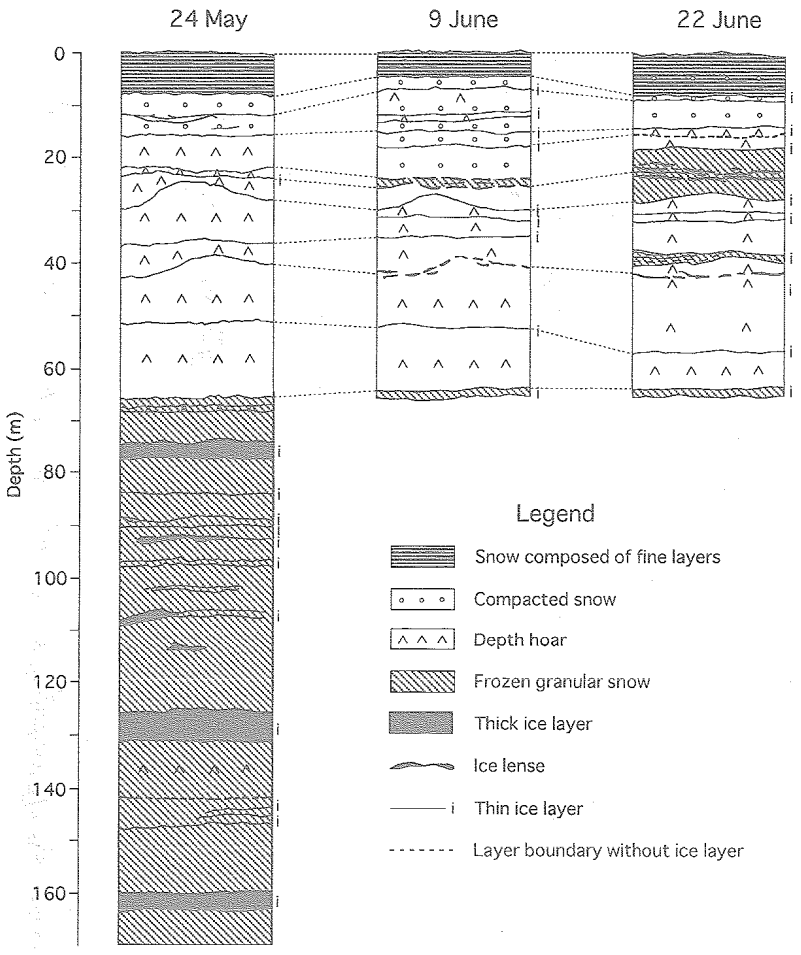


Fig. 3. Sequence of surface snow stratification at Site-J in early summer, 1989. The development process of thick ice layer is seen at around 25 cm in depth. Thick ice layers, seen at around 75, 130 and 160 cm in depth in the surface pit of 24 May, are the summer reference horizons. The surface of previous melting season appears at 65 cm in depth as the top of frozen granular snow.

This document is provided by JAXA.

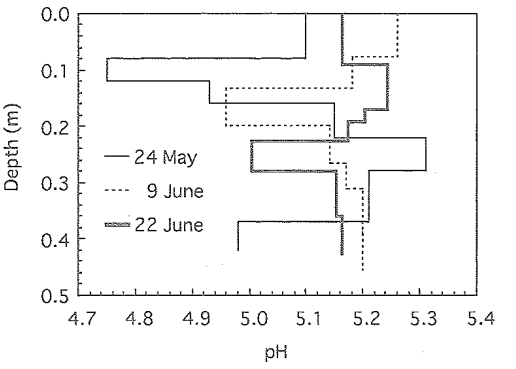


Fig. 4. Downward movement of high acidity layer observed in surface pit in early summer due to high acidic meltwater percolation.

during snow melt season, pit works were conducted on 24 May, and 9 and 22 June, near the drilling site. Figure 3 shows the sequential changes in stratification of the surface snow layer.

On the pit wall of 24 May, layers below 65 cm in depth were composed of frozen granular snow involving thick ice layers. The thick ice layers probably indicate summer horizons of each previous year. Development of frozen granular snow below 65 cm in depth suggests that some summer meltwater percolated into the snow layer deposited, at least in the previous year. The top of the frozen layer, therefore, indicates the end of the snow melt season of 1988.

Figure 4 shows the change in acidity in the surface 40 cm layer. As snow melted, the high acidity level at around 10 cm in depth moved downward and a thick high acidity ice layer developed at around 25 cm in depth by the middle of June. The high acidity in a thick ice layer is the result of concentration of acid in the surface snow layer by percolation of acidic meltwater.

4.2. Dust events

The bulk of the insoluble dust in the polar ice core is of continental origin (Hammer, 1977; Biscaye *et al.*, 1997). It has been transported over Greenland through the mid- and high troposphere and is considered to be a tropospheric background aerosol of continental origin (Hammer *et al.*, 1978; Svensson *et al.*, 2000).

Concentration and size distribution of dust in melted samples were analyzed for particles larger than 0.63 μm in diameter with a Coulter Counter TA-II in a clean room. This diameter is the minimum diameter measurable with the device. The result measured to a depth of 104 m is shown in Fig. 5. Peaks of dust concentration, which exceeds 3000 per 0.05 m*l*, are shown in this figure with the ages.

Steffensen (1988) analyzed dust concentration in two ice cores from central Greenland, that is, Site A and Site B, and discussed the detailed seasonal variations together with $\delta^{18}O$ and major anions. He showed these profiles in the period from 1890 to 1910, indicating a high dust concentration peak in 1899 in this period. Furthermore, Hammer (1989) showed the dust concentration profile in the Crête core, Greenland in the period 1815–1972. According to it, high dust peaks occurred in 1819, 1835, 1861, 1862, 1868, 1870, 1899, 1919, 1936 and 1942.

This document is provided by JAXA.

These studies suggest that dust storms appeared over Greenland at least in 1818 (or 1819), 1835, 1860 (or 1861), 1867 (or 1868), 1900 (or 1899), 1919 and 1936, during the past 210 years.

The source of the dust deposited on the Greenland ice sheet during the past several hundred years has not been studied yet. Steffensen (1988), however, suggested it to be continental origin from where vigorous atmospheric circulation, associated with the northward movement of the polar front, causes both horizontal and vertical transport of dust into the mid- and high troposphere of the Arctic in spring. Recent studies on mineralogy and Sr, Nd, and Pb isotope composition of dust in the Greenland deep ice core from GISP2 show that the most probable source area of the dust within marine isotope stage 2, between 23340 and 26180 calendar years BP, was in eastern Asia (Biscaye *et al.*, 1997). These studies suggest that the recent dust source is in eastern Asia as well. But there is a possibility of a local source, the western Greenland coast, where we saw a dust storm delay aircraft operation in spring.

4.3. Volcanic events

Many studies have revealed volcanic eruption signals in Greenland ice cores (*e.g.* Hammer *et al.*, 1980; Clausen and Hammer, 1988; Zielinski *et al.*, 1998; Clausen *et al.*, 1998).

Figure 6 shows the electrical conductivity profile to a depth of 104 m in the Site-J ice core. The electrical conductivity gradually increased with time due to anthropogenic acidification as discussed in the next section. There are many distinct peaks, which considerably exceed the background level as shown in Fig. 7. The layers that shows high electrical conductivity levels above the 2σ threshold value from the average are candidates of volcanic signals (Langway *et al.*, 1995). Taking into account the effect of anthropogenic acidification on the electrical conductivity, we take 2σ threshold values of 0.90 and 2.2 μS cm^{-1} and the averages of 1.4 and 2.3 μS cm^{-1} for the periods before and after 1950 AD from when pH used to drop to 5.1, respectively. With the help of precise dating of the core, probable volcanic eruptions with VEI (Volcanic Explosivity Index; Newhall and Self, 1982) larger than 4 are identified as shown in Fig. 6.

All of the explosive eruptions with VEI larger than 5 are identified here for volcanic eruptions located north of 8°S, except for eruption of Westdahl volcano in the Aleutian Islands in 1795. The largest signal is of Laki 1783, Iceland as revealed in other Greenland ice cores as mentioned above.

The second largest signal is seen in 1986 when two volcanic eruptions with VEI=4 took place at Augustine in Alaska and Chikurachki in the Kuril Islands (Simkin and Sibert, 1994). Such signals with high electrical conductivity are seen in the upper 20 m firn layer, formed from snow deposited with high anthropogenic acid content since early 1960's as described in the next section. Furthermore, these signals are the results of the enhancement of acidity by percolation of meltwater of high acid snow.

The Tambora eruption in Indonesia in 1815 was the most explosive with VEI=7, during the past 500 years (Simkin and Sibert, 1994). The signal is found in all Greenland and Antarctic ice cores (Clausen *et al.*, 1998). The Tambora 1815 signal is characterized by the double peaks of 1816 and 1817 as shown in Fig. 6, reaching the polar regions after one and two year delays following the eruption because of the southern hemisphere

This document is provided by JAXA.

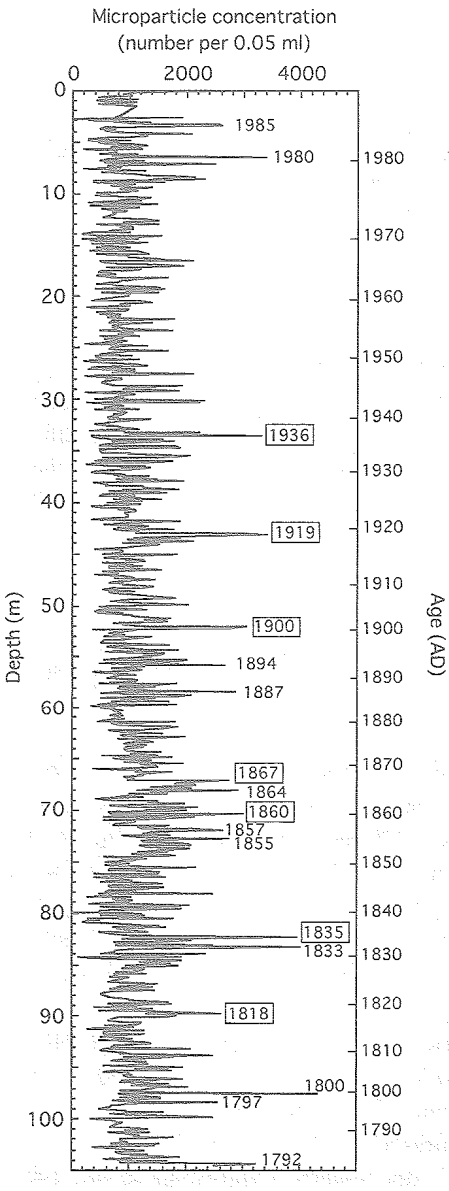


Fig. 5. Profile of total number of microparticles larger than 0.63 μm in diameter per 0.05 ml. High dust concentration peaks are shown with the age. Dust peaks indicated by dates in rectangles are found in other ice core, Greenland, suggesting that dust storms occurred over Greenland.

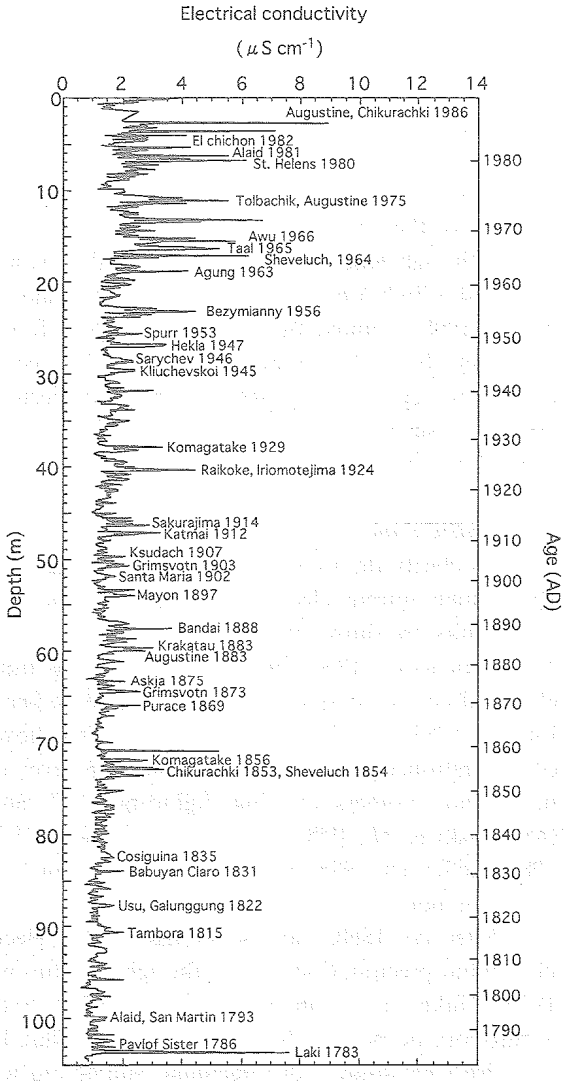


Fig. 6. Electrical conductivity profile. The distinct peaks are well associated with explosive volcanic eruptions with VEI larger than 4 in the equatorial region and the Northern Hemisphere.

This document is provided by JAXA.

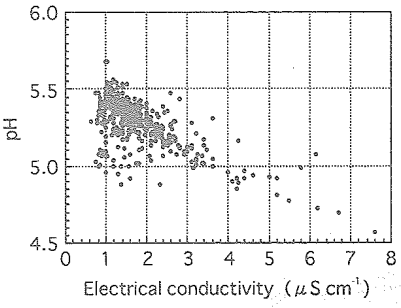


Fig. 7. Relation between pH and electrical conductivity. High electrical conductivity is well correlated with acidity, suggesting the effect of volcanic eruptions.

location of the volcano.

Although Katmai is located in Alaska, windward of Greenland, and the eruption in 1912 had a high VEI value of 6, the signal is not so distinct in the Site-J ice core. Clausen *et al.* (1998) pointed out that the signal is found in ice cores in central and northern Greenland but is barely detectable in ECM records of ice cores from the Dye 3, southern Greenland region. This suggests that the trajectory of volcanic clouds from the eruption may have shifted from central to northern Greenland. As Site-J is located in southern Greenland, the signal is not distinct in the ice core.

4.4. Acidification

To clarify the trend of anthropogenic acidification in Greenland since the Industrial Era, sulfate, nitrate, electrical conductivity and pH were analyzed for 1 m mixed samples. The results are shown in Fig. 8.

Prior to *ca.* 1860, the Site-J core records indicate no apparent trends for nss sulfate, electrical conductivity or pH, except for some perturbations due to volcanic events such as Laki in 1783 and Tambora in 1815. Nitrate shows a different trend from these trends. Its concentration remained at the 70–90 ppb level until *ca.* 1860. The principal sources of nitrate are biomass burning, lightning, NH_3 and N_2O oxidation, and NO exhalation (Mayewski *et al.*, 1990; Finkel and Langway, 1986; Clausen and Langway, 1989; Herron, 1982; Steffensen, 1988; Neftel *et al.*, 1985). But it is uncertain whether any of these sources varied or not.

After *ca.* 1860, increase in nss sulfate, electrical conductivity and acidity (pH) in Greenland precipitation started, though previous works reported *ca.* 1900 (Mayewski *et al.*, 1990; Finkel and Langway, 1986), suggesting that acidity increase is associated with anthropogenic pollutants transported from East Eurasia and North America.

Probable sources of Greenland sulfate are well documented (Mayewski *et al.*, 1990; Finkel and Langway, 1989; Clausen and Langway, 1989; Herron, 1982; Steffensen, 1988; Neftel *et al.*, 1985; Whung, 1994) with contributions from sea salt, biogenic emissions (dimethyl sulfide emissions on sea surface) and volcanic events as well as anthropogenic activity. The nss sulfate concentration after *ca.* 1860 shows good correlation with global solid fossil fuel (coal and lignite) production (Keeling, 1973; Boden *et al.*, 1990) until *ca.* 1960, suggesting that post-1860 acidification to *ca.* 1960 is mainly due to the increase in atmospheric Sox emitted by solid fossil fuel combustion (Fig. 9).

The depression in nss sulfate around 1930 (a similar trend was shown by Neftel *et al.*

This document is provided by JAXA.

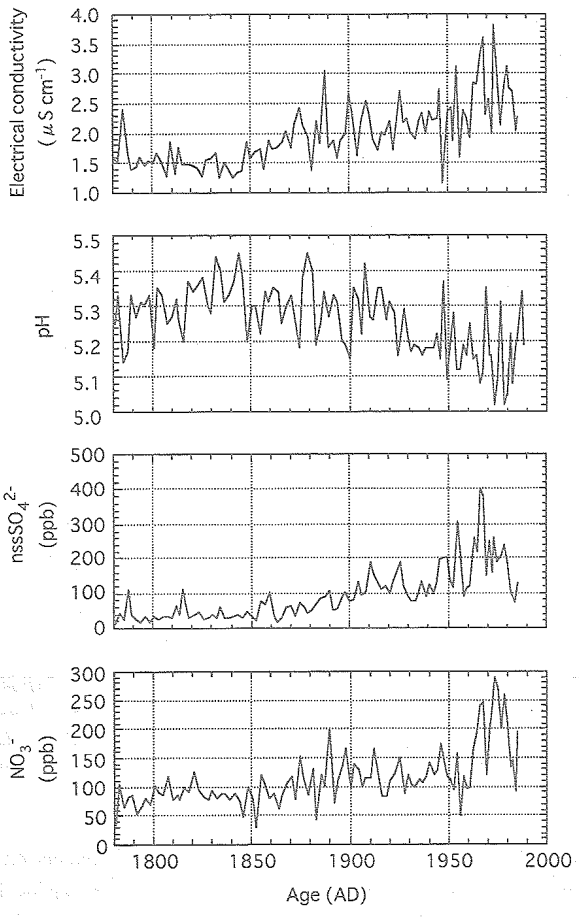


Fig. 8. Time series of the past 210 years of acidity (pH), electrical conductivity, nss sulfate and nitrate, showing acidification progress since ca. 1860, 40 years earlier than the time previously reported.

(1985) is probably associated with decrease in solid fossil fuel consumption during the economic depression. The background trend seems to have reached a maximum in the late 1960's as shown in the figure by Neftel *et al.* (1985). After the late 1960's, the nss sulfate concentration seems to have decreased or to have been stationary, even though fossil fuel consumption increased (Fig. 9). This is probably due to the increased use of sulfur removal equipment.

The background concentration of nitrate rose to 110–120 ppb from 80–90 ppb in *ca.* 1860 and remained at that level until *ca.* 1960. As there is no documented evidence of increases in lightning, NH_3 oxidation or NO-exhalation source strengths, we suggest that increase in anthropogenic biomass combustion is the most probable cause for the nitrate rise *ca.* 1860. After 1960, the concentration significantly increased from 100 ppb in 1960 to 290 ppb in the early 1970's due to the increase of fossil liquid fuel consumption (Fig. 9), followed by a clear decrease probably due to the spread of nitrogen removal equipment.

This document is provided by JAXA.

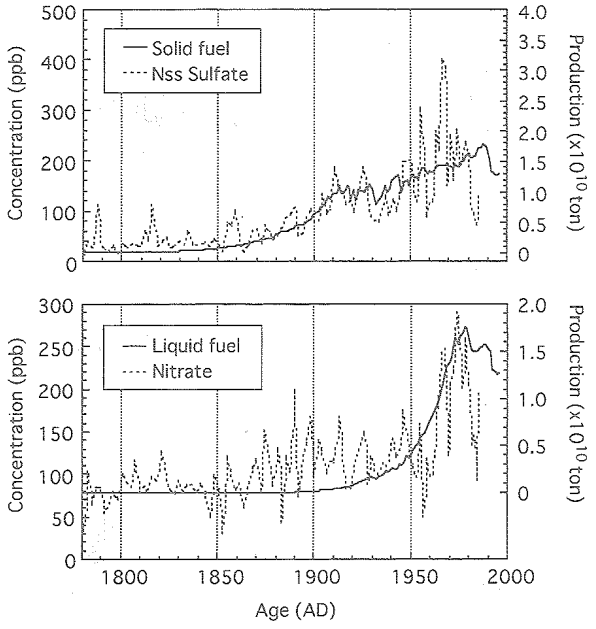


Fig. 9. Relation between major acid ions and fossil fuel production in America and Europe. Nss sulfate and solid fossil fuel production (above) and nitrate and liquid (thin dashed line) fossil fuels (below). These figures show acidification since ca. 1860, which is associated with anthropogenic pollutants emitted by the combustion of solid and liquid fossil fuels.

As reported by Mayewski *et al.* (1990), nss sulfate levels exceeded nitrate levels at the turn of the nineteenth century, reflecting the more intense increases in the emissions of anthropogenic SO_2 due to solid fossil fuel consumption, but nitrate levels again exceeded nss sulfate levels in the early 1970's in response to drastic increase in the emissions of NOx pollutants, probably due to liquid fossil fuel combustion (Fig. 9).

Nss sulfate (including volcanic origin) and nitrate concentrations increased by factors of 5.3 and 2.9 respectively from the period before *ca.* 1860 to recent decades.

5. Conclusions

On the basis of analyses done for pit samples and an ice core from Site-J, Greenland, we obtained the following results.

1) Acid in the surface snow layer percolates downward with meltwater and forms a high acid ice layer during the summer melting season.

2) Dust records in ice cores both from Site-J and Crête suggest that dust storms occurred in 1818 (or 1819), 1900 (or 1899), 1919, 1936 and 1942 over Greenland.

3) All the explosive eruptions with VEI larger than 5 from volcanos located north of 8°S are well identified in the electrical conductivity profiles.

4) Anthropogenic pollutants emitted by the combustion of solid and liquid fossil fuels have affected the sulfur and nitrogen cycles in the Arctic since *ca.* 1860. The mean

This document is provided by JAXA.

background levels of nss sulfate and nitrate concentrations were 45 ppb and 75 ppb, started to increase *ca.* 1860 and reached 400 ppb and 290 ppb in the late 1960's and early 1970's, respectively. Nss sulfate (including volcanic origin) and nitrate concentrations increased by factors of 5.3 and 2.9, respectively, from the period before *ca.* 1860 to recent decades.

Acknowledgments

We would like to express our sincere gratitude to Mr. Yoichi Tanaka and Mr. Morihiro Miyahara for their strong support of ice core drilling in Greenland. Our particular thanks are due to Dr. Henric Clausen and Dr. Niels Gundestrup of the University of Copenhagen for their various supports to our field work. Ice core samples were analyzed by Ms. Taeko Tominaga and Ms. Tomoko Kobayashi. We are grateful for their efforts. This research was carried out as a Monbusho (Ministry of Education, Culture, Sports and Science) International Scientific Research Program.

References

Biscaye, P.E., Grousset, F.E., Revel, M., Gaast, S., Ziilenski, G.A., Vaars, A. and Kukla, G. (1997): Asian provenance of glacial dust (stage 2) in the Greenland Ice Sheet Project 2 Ice Core, Summit, Greenland. J. Geophys. Res., **102**, 26765–26781.

Boden, T. A., Kanchiruk, P. and Farrell, M. P. (1990): Trends '90, A Compendium of Data on Global Change. Carbon Dioxide Information Analysis Center, Tennessee, U.S.A., 87–133.

Clausen, H.B. and Hammer, C.U. (1988): The Laki and Tambora eruptions as revealed in Greenland ice cores from 11 locations. Ann. Glaciol., **10**, 16–22.

Clausen, H. B. and Langway, C. C., Jr. (1989): The ionic deposits in polar ice cores. The Environmental Record in Glaciers and Ice Sheets, ed. by H. Oeschger and C.C. Langway, Jr. New York, J. Wiley, 225–247.

Clausen, H.B., Hammer, C.U., Hvidberg, C.S., Dahl-Jensen, D., Steffensen, J.P., Kipfstuhl, J. and Legrand, M. (1998): A comparison of the volcanic records over the past 4000 years from the Greenland Ice Core Project and Dye 3 Greenland ice cores. J. Geophys. Res., **102**, 26707–26724.

Dansgaard, W., Johnsen, S.J., Clausen, H.B. and Gundestrup, N. (1973): Stable isotope glaciology. Medd. Grønl., **197**, 2, 53 p.

Finkel, R.C. and Langway, C.C., Jr. (1986): Changes in precipitation chemistry at Dye 3, Greenland. J. Geophys. Res., **91**, 9849–9855.

Fujii, Y. (1991): Reply to Comments on '6000-year climate records in an ice core from the Hoghetta ice dome in northern Spitsbergen'. J. Glaciol., **37**, 186–188.

Hammer, C.U. (1977): Past volcanisms revealed by Greenland ice sheet impurities. Nature, **270**, 482–486.

Hammer, C.U. (1989): Dating by physical and chemical seasonal variations and reference horizons. The Environmental Record in Glaciers and Ice Sheets, ed. by H. Oeschger and C.C. Langway, Jr. New York, J. Wiley, 99–121.

Hammer, C.U., Clausen, H.B., Dansgaard, W., Gundestrup, N., Johnsen, S.J. and Reeh, N. (1978): Dating of Greenland ice cores by flow models, isotopes, volcanic debris, and continental dust. J. Glaciol., **20**, 3–26.

Hammer, C.U., Clausen, H.B. and Dansgaard, W. (1980): Greenland ice sheet evidence of post-glacial volcanism and its climatic impact. Nature, **288**, 230–235.

Herron, M.M. (1982): Impurity Sources of F^-, Cl^-, NO_3^- and SO_4^{2-} in Greenland and Antarctic precipitation. J. Geophys. Res., **87**, 3052–3060.

Johnsen, S.J., Dansgaard, W., Clausen, H.B. and Langway, C.C., Jr. (1972): Oxygen isotope profiles through the Antarctic and Greenland ice sheets. Nature, **235**, 429–434.

Keeling, C.D. (1973): Industrial production of carbon dioxide from fossil fuels and limestone. Tellus, **25**, 174–198.

This document is provided by JAXA.

Koide, M., Michel, R., Goldberg, E.D., Herron, M.M. and Langway, C.C., Jr. (1982): Characterization of radioactive fallout from pre- and post-moratorium tests to polar ice caps. Nature, **296**, 544–547.

Langway, C. C., Jr., Oeschger, H. and Dansgarrd, W., ed. (1985): Greenland Ice Cores: Geophysics, Geochemistry and the Environment, Washington D.C., Am. Geophys. Union, 118 p. (Geophys. Monog., **33**).

Langway, C. C., Jr., Osada. K., Clausen, H.B. and Hammer, C.U. (1995): A 10-century comparison of prominent bipolar volcanic events in ice cores. J. Geophys. Res., **100**, 16241–16247.

Mayewski, P.A., Lyons, W.B., Spencer, M.J., Twickler, M.S., Buck, C.F. and Whitlow, S. (1990): An ice-core record of atmospheric response to anthropogenic sulphate and nitrate. Nature, **346**, 554–556.

Neftel, A., Beer, J., Oeshger, H., Zurcher, F. and Finkel, R.C. (1985): Sulfate and nitrate concentrations in snow from South Greenland 1895–1978. Nature, **314**, 611–613.

Newhall, C.G. and Self, S. (1982): The volcanic explosivity index (VEI): An estimate of explosive magnitude for historical volcanism. J. Geophys. Res., **87**, 1231–1238.

Shoji, H., Clausen, H.B. and Kameda, T. (1991): Accumulation rate at Site-J and Dye-2, Greenland. Bull. Glacier Res., **9**, 85–88.

Simkin, T. and Sibert, L. (1994): Volcanoes of the World. 2nd ed. Arizona, Geosience Press Inc., 349 p.

Steffensen, J.P. (1988): Analysis of the seasonal variation in dust, Cl^-, NO_3^-, and SO_4^{2-} in two central Greenland firn cores. Ann. Glaciol., **10**, 171–177.

Svensson, A., Biscaye, P.E. and Grousset, F.E. (2000): Characterization of late glacial continental dust in the Greenland Ice Core Project ice core. J. Geophys. Res., **105**, 4637–4656.

Watanabe, O. and Fujii, Y. (1990): Outline of the Japanese Arctic Glaciological Expedition in 1989 (JAGE 1989). Bull. Glacier Res., **8**, 103–106.

Whung, P.Y., Saltzman, E.S., Spencer, M.J., Mayewski, P.A. and Gundestrup, N. (1994). Two-hundred-year record of biogenic sulfur in a south Greenland ice core (20D). J. Geophys. Res., **99**, 1147–1156.

Zielinski, G.A., Mayewski, P.A., Meeker, L.D., Gronvold, K., Germani, M.S., Whitlow, S., Twickler, M. S. and Taylor, K. (1998): Volcanic aerosol records and tephrochronology of the Summit, Greenland, ice cores. J. Geophys. Res., **102**, 26625–26640.

(Received May 31, 2000; Revised manuscript accepted September 18, 2000)

This document is provided by JAXA.

Mem. Natl Inst. Polar Res., Spec. Issue, 54, 221-225, 2001

Report

Japanese glaciological study efforts in the North Greenland Ice Core Project (NGRIP)

Hitoshi Shoji[1] and Okitsugu Watanabe[2]

[1]*Kitami Institute of Technology, 165 Koen-cho, Kitami 090-8507*
[2]*National Institute of Polar Research, Kaga 1-chome, Itabashi-ku, Tokyo 173-8515*

Abstract: Deep ice cores from polar ice sheets form a proxy data bank for global climate variations. Japanese researchers have been involved in international core drilling and analysis projects in Greenland since 1989. One of the major outcomes of the GRIP project is the possible existence of rapid climatic oscillation during the Eemian interglacial period. However, physical property observations suggest that this apparent oscillation could have resulted from complicated ice flow near the bed as revealed by disturbed cloudy band features. A new ice core project, NGRIP, is expected to resolve the above question.

1. Introduction

Japanese glaciological research operations have been performed in Greenland (Fig. 1) since 1989 in a systematic way as described by Watanabe and Fujii (1990). International collaboration efforts in field and laboratory works have been conducted with the University of Copenhagen (UCPH), Denmark during the GRIP (GReenland Ice-core Project) operation as summarized by Clausen *et al.* (1996). Study results on the GRIP ice core are reported with those of a sister project, GISP2, in GISP2 and GRIP (1998). One of the major outcomes from the GRIP operation is a finding of fast climatic oscillations during the Eemian interglacial period, which may suggest future instability in the Holocene climate. But another possibility is that this could be spurious if there is ice folding and/or boudinage near the bed as shown by disturbed layers of the cloudy band (GRIP Members, 1993; Dansgaard *et al.*, 1993). A new international project called NGRIP (North GRIP) was planned and organized for deep ice coring and analysis, especially for study of climatic instability before and during the Eemian period by UCPH in 1995. Japanese participated as members of NGRIP under the auspices of the National Institute of Polar Research (NIPR, PI: O. Watanabe).

2. Ice core analysis

Ice core analysis has been planned and conducted in Japan within the framework of NGRIP as shown in Fig. 2. Physical property measurements and mechanical tests are being conducted at the Institute of Low temperature Science (ILTS), Hokkaido University, Kitami Institute of Technology (KIT), Toyama University and NIPR in close collaboration

This document is provided by JAXA.

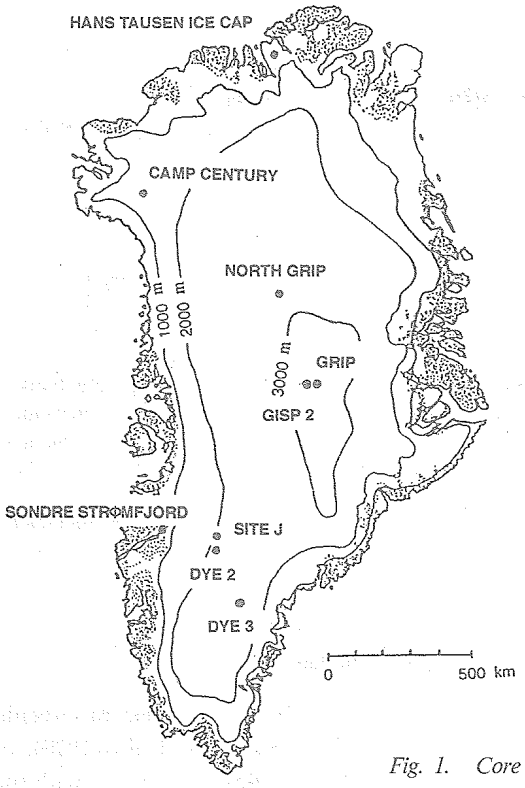


Fig. 1. Core drilling sites in Greenland.

with UCPH, Alfred Wegener Institute (AWI) in Germany, and others (Miyamoto *et al.*, 1997, 1999; Castelnau *et al.*, 1998; Pauer *et al.*, 1999). Chemical analysis and stable isotope study are conducted at NIPR as collaborative research with UCPH and others, although on a smaller scale. Gas analysis is planned and started at Tohoku University as a member of the NGRIP gas consortium.

Domestic NGRIP meetings have been held several times a year and their research plan is proposed in the NGRIP meeting in Copenhagen. Logistics expenses for Japanese participation are mainly covered by NIPR and the rest by other institutes to a lesser degree.

3. Field activities

NGRIP field activities are conducted from May to August each year. Approximately thirty persons join the NGRIP camp (75°06′N, 42°20′W). Transportation of both personnel and cargo is mainly by C-130 Herculus between Sondre Strømfjord (Kangerlussuaq) and the NGRIP camp.

Participants are assigned to certain tasks depending on their skills/background and interests. Some may work as drillers in a drilling trench (Fig. 3) and some as core processors in a science trench (Fig. 4). Nationality is not necessarily a factor for a task assignment. Two Japanese researchers participated as drillers in 1996. Six researchers joined the field work in 1997, three as core processors/loggers and three as drillers. One researcher participated as a

This document is provided by JAXA.

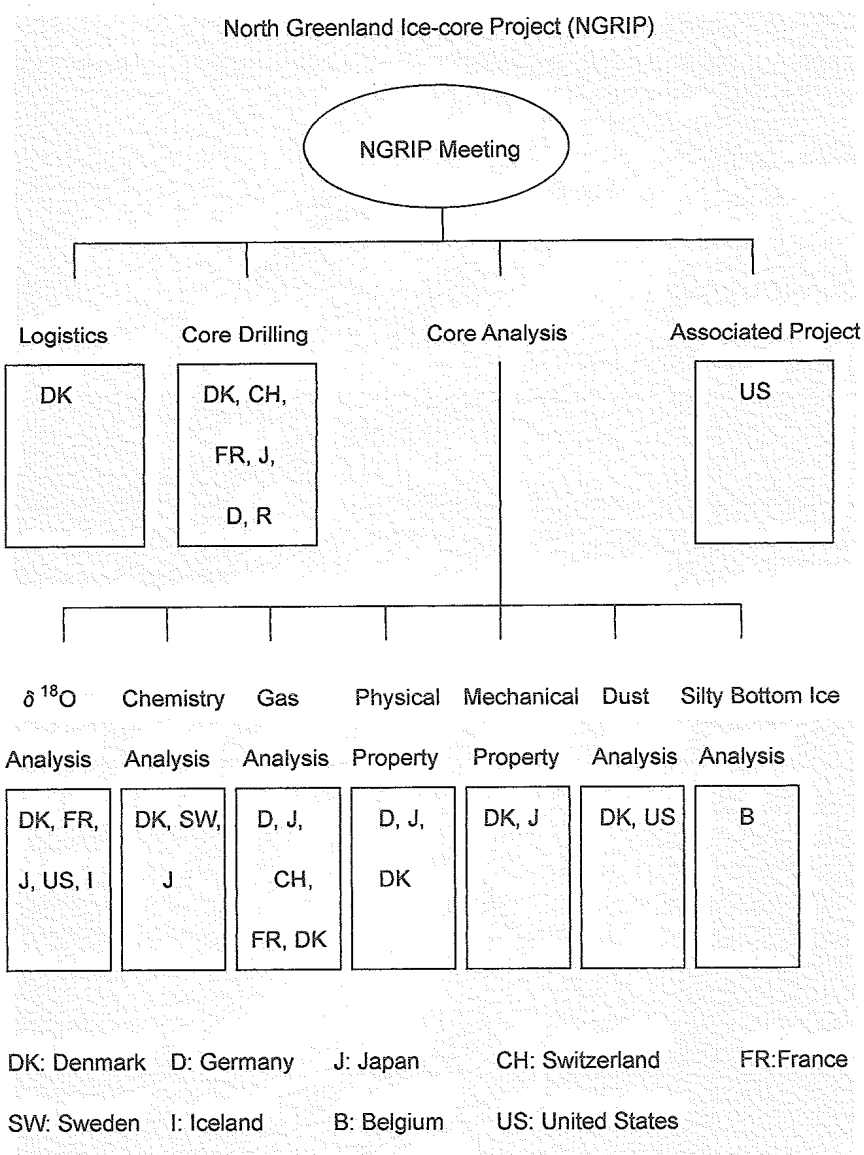


Fig. 2. Infrastructure of NGRIP and Japanese study efforts.

core processor/logger in 1998 and three researchers participated in 1999, two as core processors/loggers and one as a driller.

A pilot hole drilling was conducted in 1996 and a casing was made down to a depth of 93.1 m. A deep core drilling was started in a liquid filled hole from a depth of 111 m. The Core drilling was continued from a depth of 351 m in 1997 and completed down to a depth of 1373 m, where the drill was stuck and has never been recovered. Another new pilot hole drilling was started in 1998 at a position approximately 25 m from the first NGRIP hole. A new deep core (NGRIP2) was drilled down to a depth of 1751.47 m in

This document is provided by JAXA.



Fig. 3. Deep ice coring operation in NGRIP.



Fig. 4. Field core measurement on DC electric conductivity.

1999. A brittle zone has been encountered between about 800 and 1300 m in both deep holes.

Frozen ice core samples have been shipped to Japan by air with pit study samples collected near the surface, and laboratory analyses are under way.

This document is provided by JAXA.

4. Future collaboration

Eight Japanese researchers were scheduled to join the NGRIP field operation from KIT, ILTS, Hokkaido Univ., Tohoku Univ., Nagaoka Univ. Tech., NIPR and Geo. Tech. Co. Ltd. in 2000. They were to do field measurements, core drilling, processing and/or logging/packing as members of the NGRIP international project.

The Eemian age ice and also older ice were expected be extracted during the 2000 season, and to supply detailed information on fast climatic oscillation by core analysis. This should be a breakthrough in Greenland ice study and enables a bi-polar comparison with the Dome Fuji (Watanabe *et al.*, 1999; Hondoh *et al.*, 1999) and Vostok (Petit *et al.*, 1999), Antarctica core data for long term climate variations.

Acknowledgments

This study was supported by a Grant-in-Aid for Scientific Research from the Ministry of Education, Science, Sports and Culture, Japanese Government. We thank all members of the NGRIP project and Japanese participants in the field and laboratory research works.

References

Castelnau, O., Shoji, H., Mangeney, A., Milsch, H., Duval, P., Miyamoto, A., Kawada, K. and Watanabe, O. (1998): Anisotropic behavior of GRIP ices and flow in central Greenland. Earth Planet. Sci. Lett., **154**, 307–322.

Clausen, H.B., Gundestrup, N., Shoji, H. and Watanabe, O. (1996): Scientific research collaboration efforts for Greenland ice core studies. Mem. Natl Inst. Polar Res., Spec. Issue, **51**, 337–342.

Dansgaard, W. and 10 others (1993): Evidence for general instability of past climate from a 250-kyr ice-core record. Nature, **364**, 218–220.

GISP2 and GRIP (1998): Greenland Summit Ice Cores. J. Geophys. Res., **102**, 26315–26886.

GRIP Members (1993): Climate instability during the last interglacial period recorded in the GRIP ice core. Nature, **364**, 203–207.

Hondoh, T. and 15 others. (1999): Basic analyses of Dome Fuji deep ice core part 2: physical properties. Polar Meteorol. Glaciol., **13**, 90–98.

Miyamoto, A., Shoji, H., Narita, H., Watanabe, O., Clausen, H.B. and Hondoh, T. (1997): An attempt at deformation tests of deep ice core samples containing cloudy bands. Proc. NIPR Symp. Polar Meteorol. Glaciol., **11**, 87–93.

Miyamoto, A., Narita, H., Hondoh, T., Shoji, H., Kawada, K., Watanabe, O., Dahl-Jensen, D., Gundestrup, N.S., Clausen, H.B. and Duval, P. (1999): Ice-sheet flow conditions deduced from mechanical tests of ice core. Ann. Glaciol., **29**, 179–183.

Pauer, F., Kipfstuhl, J., Kuhs, W.F. and Shoji, H. (1999): Air clathrate crystals from the GRIP deep ice core: a number-, size- and shape-distribution study. J. Glaciol., **45**, 22–30.

Petit, J.R. and 18 others (1999): Climate and atmospheric history of the past 420,000 years from the Vostok ice core, Antarctica. Nature, **399**, 429–436.

Watanabe, O. and Fujii, Y. (1990): Outline of the Japanese Arctic Glaciological Expedition in 1989 (JAGE 1989). Bull. Glacier Res., **8**, 103–106.

Watanabe, O. and 16 others (1999): Basic analyses of Dome Fuji deep ice core, Part 1: Stable oxygen and hydrogen isotope ratios, major chemical compositions and dust concentration. Polar Meteorol. Glaciol., **13**, 83–89.

(Received June 1, 2000; Revised manuscript accepted July 27, 2000)

This document is provided by JAXA.

This document is provided by JAXA.

Mem. Natl Inst. Polar Res., Spec. Issue, 54, 227–242, 2001

Scientific paper

Studies on climatic and environmental changes during the last few hundred years using ice cores from various sites in Nordaustlandet, Svalbard

Okitsugu Watanabe[1], Hideaki Motoyama[1], Makoto Igarashi[1], Kokichi Kamiyama[1], Sumito Matoba[2], Kumiko Goto-Azuma[1], Hideki Narita[2] and Takao Kameda[3]

[1]*National Institute of Polar Research, Kaga 1-chome, Itabashi-ku, Tokyo, 173-8515*
[2]*Institute of Low Temperature Science, Hokkaido University, Kita-19 Nishi-8, Kita-ku, Sapporo 060-0919*
[3]*Kitami Institute of Technology, 165 Koen-cho, Kitami 090-8507*

Abstract: Ice coring and snow cover observations have been carried out at 3 sites in Nordaustlandet, Svalbard since 1995. The results of stratigraphic analyses, and chemical and $\delta^{18}O$ analyses from Vestfonna and Austfonna cores are presented here. The results from these sites show that most of the chemical constituents contained in the initial snow cover still remained in the ice cores, although re-distribution of them by melt water percolation had occurred. Anthropogenic increases in trace metals, sulfate and nitrate since about 1950 are detected. This suggests that ice-core chemistry records from Nordaustlandet, Svalbard, can be useful to reconstruct past atmospheric conditions. In addition to chemical records, $\delta^{18}O$ records, that correlate well with the temperature records in Svalbard, can be used to reconstruct past temperature changes.

1. Introduction

The Arctic region is a heat sink in the global climate system and acts as a convergent region of substances that are released into the atmosphere from various sources. It is believed that the types and amounts of substances vary with climatic and/or environmental fluctuations, so the state of these substances in the atmosphere in the Arctic can be considered as a kind of signal indicating what the climate and environment is like. Such substances, transported in the atmosphere over polar ice sheet or glacier, are eliminated by wash-out and dry fall-out processes from the atmosphere onto the snow surface. They become mixed into and then are fixed into the snow and ice structure.

The cryoshere covers over the Arctic. Its fluctuation affects or is affected by the global climate system. Svalbard is one of the most northern islands, where the fluctuation of the glacier system possibly affects and/or is affected by the Arctic climate. Svalbard is located in the European sector of the Arctic, where artificial activities have historically been active. Snow chemistry has been affected by human activities.

Ice coring and snow observations have been carried out at 3 sites in Nordaustlandet, Svalbard since 1995. The purposes of this research project are as follows: (1) to understand regional characteristics of post-depositional changes under present climatic conditions, and

This document is provided by JAXA.

(2) to reconstruct climatic and environmental changes in Svalbard during the last few hundred years (Watanabe, 1996). Topic (1) is necessary for the investigation on temperate glacier and (2) valid under the topics (1).

Since most of the glaciers in Svalbard suffer rather severe melting even in their highest parts (*e.g.* Hagen and Liestøl, 1990), ice-core investigations have not been paid enough attention. Interpretation of ice-core records from areas of high melt has often been misleading (Koerner, 1997), even if ice-core data exist. However, ice caps or glaciers with relatively heavy melt can still provide us with important climatic and environmental information, if the data are properly interpreted. Most of the sites studied in this research

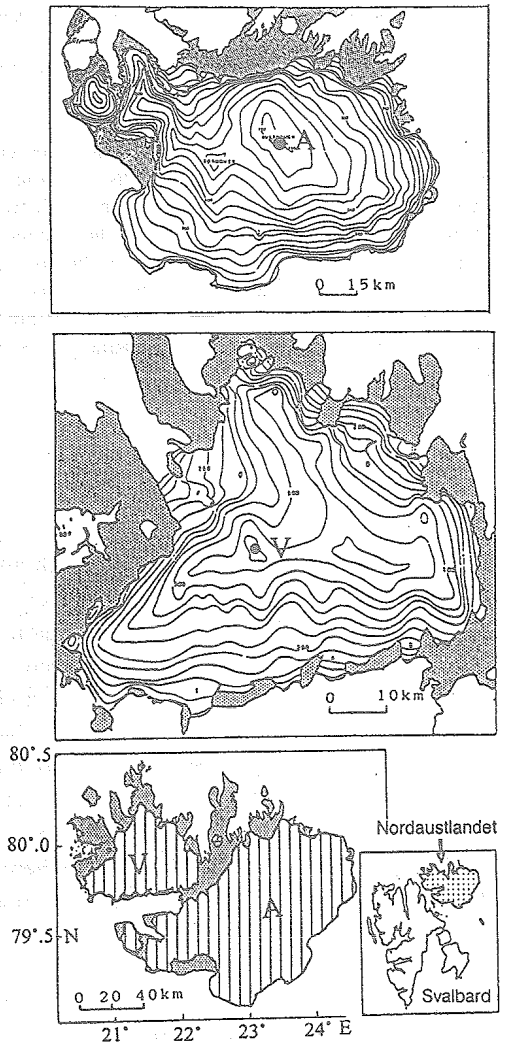


Fig. 1. Locations of drilling sites in Nordaustlandet, Svalbard. V: Vestfonna, A: Austfonna, ●: Drilling site.

This document is provided by JAXA.

project were located in the "percolation zone" and "dry snow zone", and melt water infiltration-refreezing conditions were different between the sites.

2. Ice coring in Nordaustlandet

2.1. Locations of ice coring site and glaciological condition

An ice core, reaching to the bottom of Austfonna glacier, was previously obtained by a Russian team (Arkhipov *et al.*, 1987); however, detailed analytical results of the core have not yet been published.

Glaciological conditions of the site above are as follows: ice thickness is 560–580 m

Table 1. Ice coring sites in Svalbard.

Drilling sites	Drilling date	Location	Altitude (m a.s.l.)	Drilling depth (m)	10 m ice temp. (℃)	Average density ($kg \cdot m^{-3}$) 0–10 (m)	Average density ($kg \cdot m^{-3}$) 10–20 (m)	Reference
Vestfonna	May-Jun. 1995	79°58′N, 21°01′E	600	210.0	−3.7	639	839	This study
Austfonna	Mar.-Apr. 1998	79°48′N, 24°00′E	750	118.6	−1.0	601	876	This study
Austfonna	Apr.-May 1999	79°50′N, 24°01′E	750	289.1	−2.8	649	840	This study
Høghetta Ice Cap	May-Jun. 1987	79°17′N, 16°50′E	1200	85.6	−11.0	(ice)	(ice)	Fujii (1990)
Snøfjellafonna	Jul.-Aug. 1992	79°08′N, 13°18′E	1190	83.9	−2.8	565	775	Kameda (1992)
Åsgårdfonna	Jun.-Jul. 1993	79°27′N, 16°43′E	1140	185.3	−6.8	808	881	Uchida (1996)

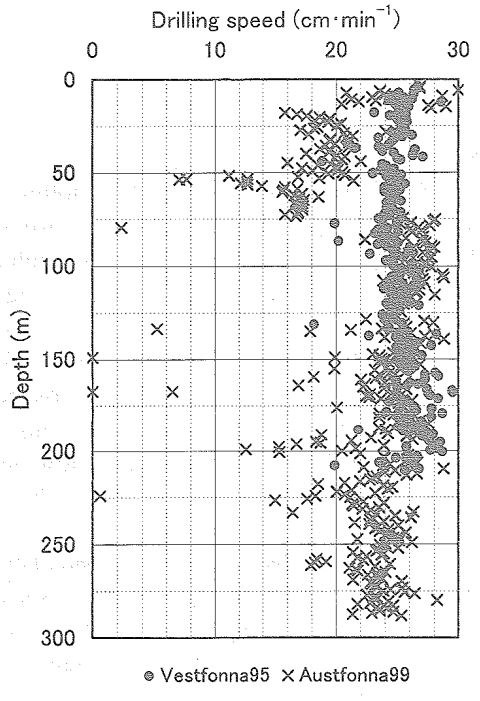


Fig. 2. Drill speeds at Vestfonna, and Austfonna drilling.

This document is provided by JAXA.

(Arkhipov *et al.*, 1987), annual accumulation rate is 0.5–0.6 $m \cdot yr^{-1}$ in water eq. (Sinkevich and Tarusov, 1989), and 10 m snow temperature is −4℃ (Zagorodonov and Arkhipov, 1990).

These are two glaciers in Nordaustlandet; Austfonna glacier and Vestfonna glacier. North Dome (Norddomen) of Austfonna glacier and the summit of Vestfonna glacier were selected as the representative ice coring sites (Fig. 1). Geographical and glaciological conditions are described in Table 1.

2.2. Coring operation

All the drilling operations were carried out in spring. All of the ice cores listed in Table 1 were excavated with electromechanical drills. The cores were drilled with the same electromechanical drill (Takahashi, 1996), whose length was 3.0 m. Diameters of the core and the bore hole were 94 mm and 129 mm, respectively.

Average drilling speeds at Vestfonna and Austfonna were 26.2 cm/min and 17.0 cm/min, respectively. Drilling speeds are plotted against depth in Fig. 2. Variations in drilling speed reflect variations in the physical properties of firn and ice. In general, ice (firn) becomes harder with decrease in ice (firn) temperature and also with increase in ice (firn) density, and thus drilling speed decreases. The greater drill speeds resulted from the much higher ice (firn) temperatures and thus the softer nature of ice (firn). At depths greater than 120–130 m, ice tends to break into pieces. At these depths, the ice core was fragile and easily broke, reflecting the change in physical properties of ice at 120–130 m depth. Although the drilling can take a 0.7–0.9 m long core in one drilling run, the ice layer may originally have fractures. The core obtained below 250 m in depth turned out to be in more stable condition.

3. Analytical results

3.1. Surface layer stratigraphy

Surface snow stratigraphical observations and snow sampling were carried out at snow pits near the three drilling sites. Due to irregularity of snow cover characteristics caused by selective melt water infiltration relating to the surface topography, pit observations were made at 3–5 locations around each drilling site. Snow cover stratigraphy provides information on the annual accumulation rate at the drilling sites, behavior of melt-water movement, formation mechanism of superimposed ice and other depositional phenomena.

The vertical distributions of stratigraphy, snow density, oxygen isotopic composition and chemical constituents are shown in Fig. 3. As is obvious from these profiles, the uppermost layer still retains its original condition during snow deposition. But homogenization by melt water infiltration occurred in the layer below 100–150 cm from the surface, taking the profiles into consideration.

From these data, these areas are judged to be in a "percolation zone". Annual layer boundaries can be recognized by the development of granular snow layers and dirt surface structures. In the surface snow cover in Vestfonna and Austfonna of 1995 and 1999 drilling sites, the uppermost annual layer was composed of 5–6 unit layers. Here a unit layers results from continuous deposition during a snowfall season. In these profiles of $\delta^{18}O$ and ion concentrations, two or three peaks in the annual layer exist. These phenomena may reflect

This document is provided by JAXA.

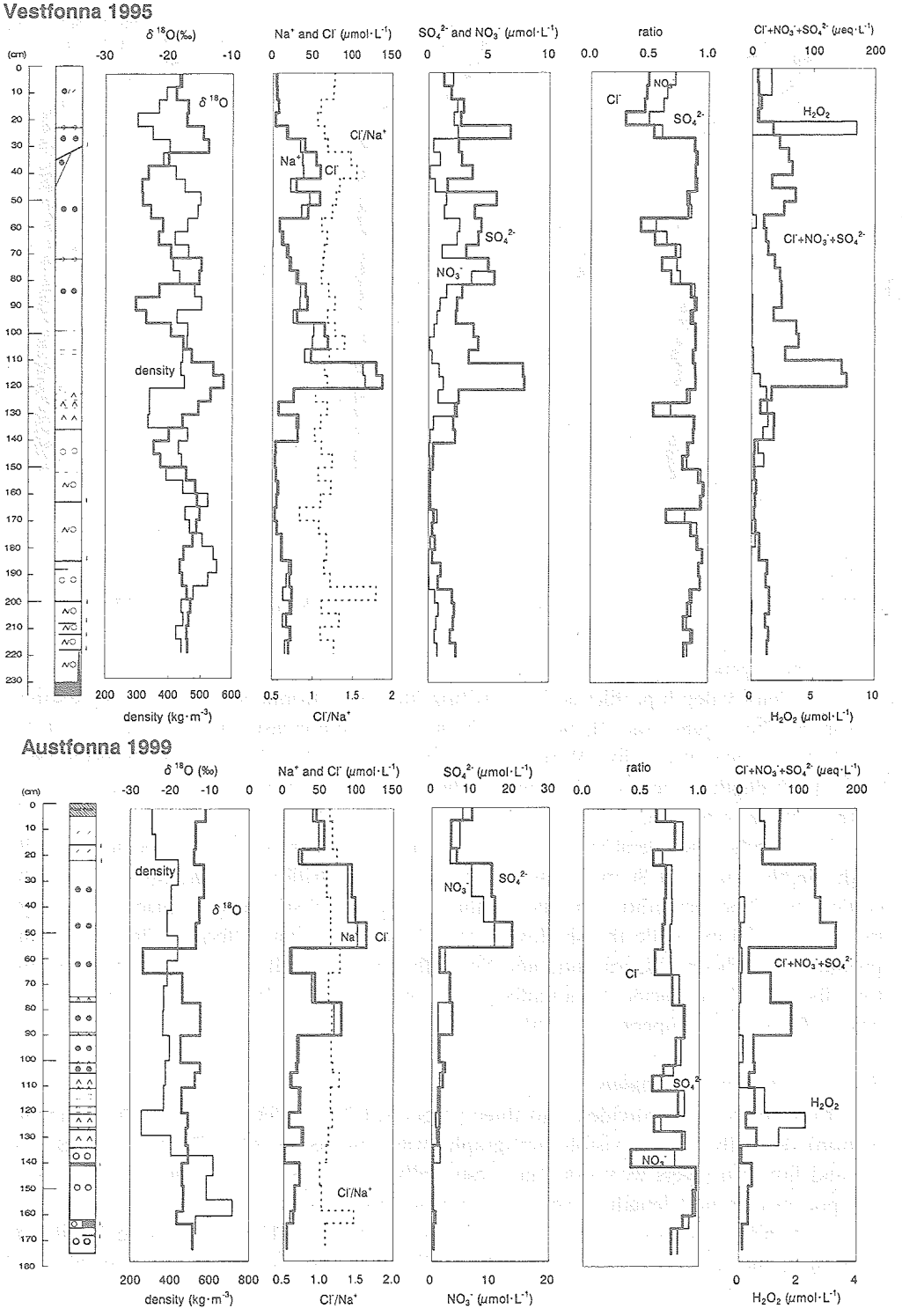


Fig. 3. Stratigraphic diagram of the surface snow cover at Vestfonna drilling site and Austfonna drilling site. Snow texture: solid circle (granular snow), Λ (depth hoar).

This document is provided by JAXA.

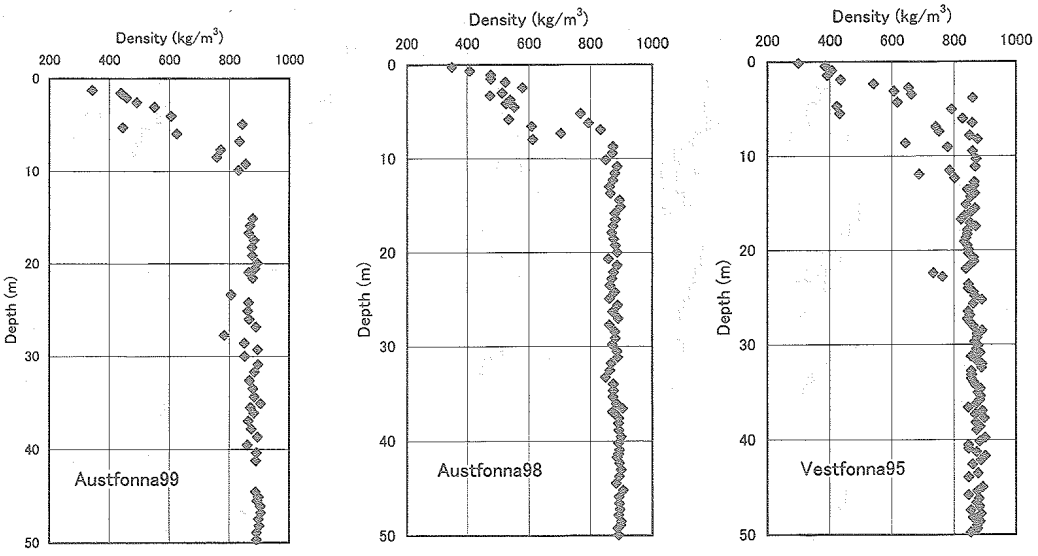


Fig. 4. Density-depth profiles at Vestfonna, and Austfonna coring.

meteorological conditions rather than seasonal variation (Motoyama *et al.*, 2001).

3.2. Physical properties

The density-depth profiles at three drilling sites in Vestfonna and Austfonna are shown in Fig. 4. The weights and diameters of the ice core were measured, *in situ*, at the site for the determination of density. As shown in this figure, change from firn to ice occurred in the 5–12 m depth range. Figure 4 suggests that melt water percolation played a major role in the firn/ice transition.

The borehole temperatures are shown in Fig. 5. Comparing these temperature profiles in the depth range of 0–80 m, it was considered that the drilling site on Austfonna was the coldest one. The temperature profiles in these 3 sites show similar tendencies in the depth range of 30–80 m, while the shallower parts look somewhat different. The temperature profiles of Høghetta, Åsgårdfonna and Snøfjellafonna, located on Spitsbergen, are shown for reference. These glaciers are all affected by melt water percolation. The behavior of melt water affected the temperature profiles near the surface.

3.3. Firn ratio measurements

Each ice core was divided into three parts (A: 60%, B: 25%, C: 15% in the horizontal section) vertically and the visible stratigraphy was observed *in situ*. The cores consisted of ice and firn; firn layers were dominant, especially in the upper part. The firn ratio means firn potion of a unit length of vertical section of a core.

Firn ratio profiles of 1995 and 1999 cores are shown in Fig. 6. The solid profiles are running means of 5 points at 2 m intervals (1995 core) and 7 points at 1 m intervals (1998 and 1999 cores).

There are two processes in ice formation. One is refreezing of surface melt water

This document is provided by JAXA.

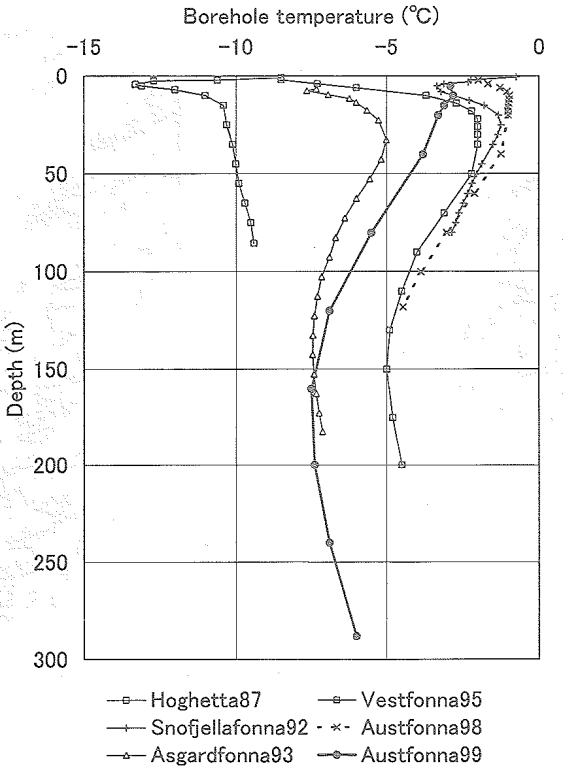


Fig. 5. Borehole temperature profiles at Vestfonna, Austfonna, Høghetta Ice Dome, Snøfjellafonna and Åsgårdfonna.

percolation to the lower firn layer; the other is compression of the firn layer by the weight of the upper layer. The latter process accelerates at higher snow temperature and/or with water soaking. This process has a close relationship with the ice temperature as shown in Fig. 5.

3.4. ECM measurements

For detection of acid layers and/or signals which originated from volcanic activities, ECM measurements are useful and were performed in situ. Some of the high ECM signals in the Arctic core correspond to those of large volcanic eruptions, such as Katmai 1912, Tambora 1815, Laki 1783 and so on (Table 2).

The ECM signal is the intensity of electric current between electrodes. After shaving about 1 cm off the cutting surface of the A part (60% in areal portion of core), ECM measurements were made vertically, with electrodes in direct contact with the ice surface. As seen in Fig. 7, several volcanic signals are extracted from the ECM measurements. Marked signals that originated from Icelandic Laki volcanic activity in 1783 were found at a depth of 106.23 m in the 1999 core.

In this figure, tritium concentration (TU) is added. The reference horizon of the 1963 radioactivity peak derived from a nuclear bomb test is found at a depth of 21.11–54 m in

This document is provided by JAXA.

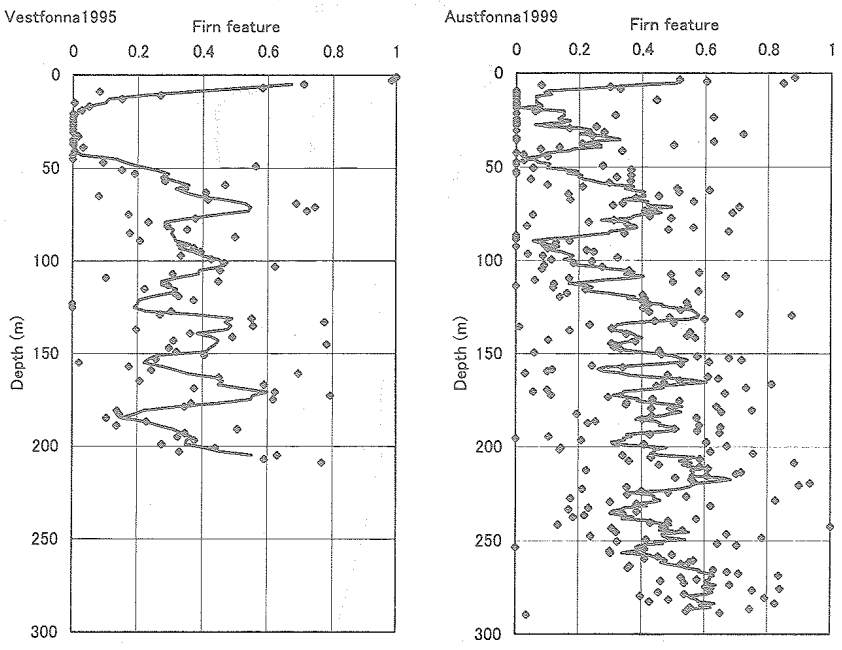


Fig. 6. Vertical profile of the firn ratio on Vestfonna core and Austfonna core.

Table 2. List of various events detected from Austfonna 1999 core.

Event	Year	Evidence	1999 Austfonna Core		Acc. rate (m-water•a^{-1})	Interval
			Depth (m)	Depth (m. w.eq)		
Hekla	1970	ECM peak	18.0	13.4		
Nuclear test (A)	1963	Tritium peak	21.3	16.3	0.45	Drilling-1963
δ^{18}O rise (B)	1920's	δ^{18}O profile	49.0	40.6	0.57	1963–1920
Katmai Santa Maria	1912(?) 1902(?)	ECM peak	52.2	43.5		
Tambora Unknown	1815(?) 1809(?)	ECM peak	96.4	83.3	0.48	1912 or 1902 –1815
Laki (C)	1783	ECM peak	106.6	92.9	0.32	1815–1783
Oræfajokull	1727	ECM peak	128.5	112.3	0.38	1783–1727
St. Helens (D) Berdarbunga (D)	1482(?) 1480(?)	ECM peak	220.3	195.1?	0.38	1783–1482 or 1480

the 1999 core. Laki signals, detected by ECM measurements, were also detected at 86 m (73.3 m-water equivalent) in the 1995 core and 15.3 m in the 1995 core, and tritium debris at 20.96 m in the 1998 core (Kameda *et al.*, 1993; Pinglot *et al.*, 1994).

3.5. Oxygen isotopic composition

Continuous oxygen isotopic composition measurements were made by MAT delta-E mass spectrometer along the whole depth of cores drilled in Nordaustlandet. The sample size corresponds to the estimated annual layer thickness. Results are shown in Fig. 8 together with those of Åsgårdfonna, and air temperature data observed at Isfjord Radio.

This document is provided by JAXA.

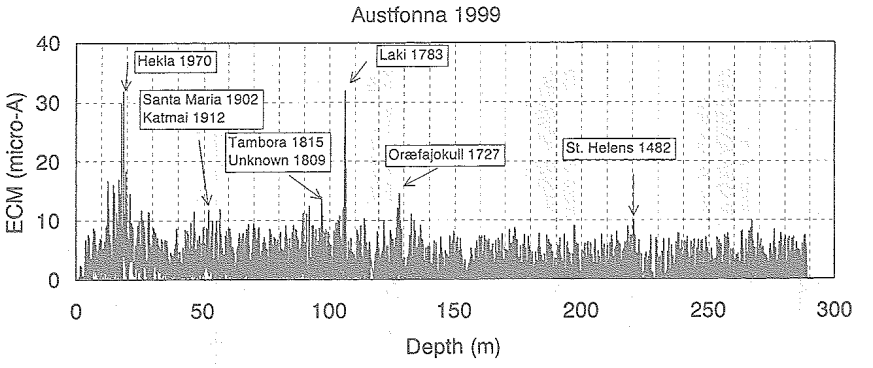


Fig. 7. ECM profile on Austfonna core. Thin arrow: Detected volcanic activity layer.

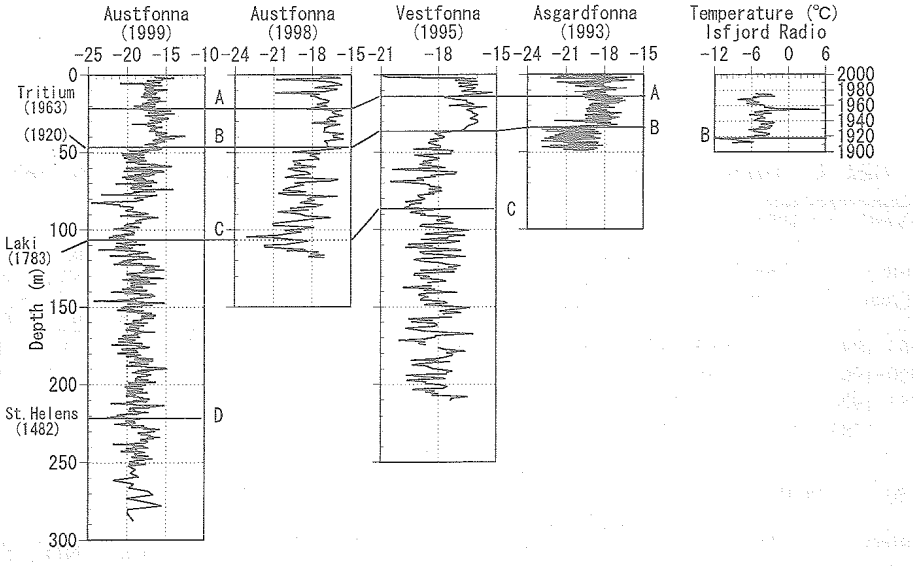


Fig. 8. Comparison of stable oxygen isotope profiles in Nordaustlandet core. Letters are reference horizons indicated by various events.

As seen in Fig. 8, oxygen profiles indicate the common tendency of climate change. Abrupt rise of temperature (or of $\delta^{18}O$) occurred at depths of 45 m in the Austfonna 1998 and 1999 cores and 35 m in the Vestfonna 1995 core. This abrupt rise of temperature may correspond to the temperature rise which occurred at the beginning of the 1920's, observed at Isfjord Radio meteorological station, which also corresponds to the general climatic tendency of the last century in the northern hemisphere (Hanssen-Bauer *et al.*, 1990).

3.6. Chemical constituents

The vertical concentration profiles for the cations Na^+ and Ca^{2+} and the anions SO_4^{2-} and NO_3^-, in the Austfonna 1999 core, are shown in Fig. 9. There is no obvious trend

This document is provided by JAXA.

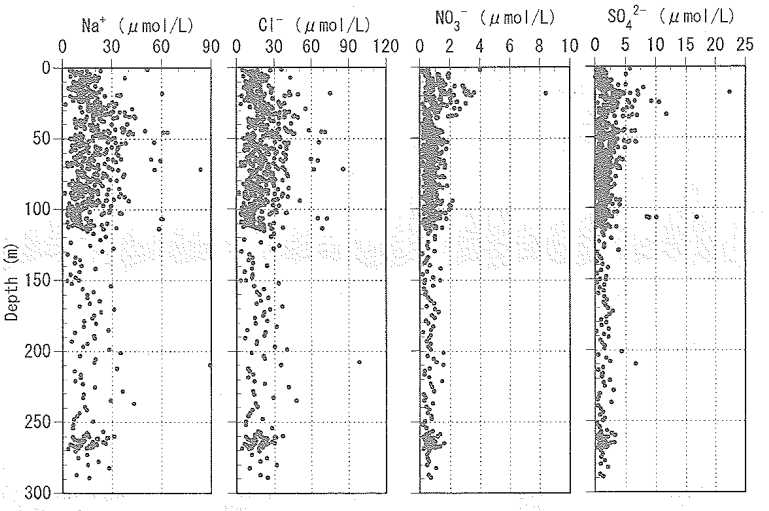


Fig. 9. Vertical profiles of chemical composition in Nordaustlandet cores.

Table 3. Average of annual chemical flux in the specific interval defined by the events.

1) Vestfonna 1995 Ice core

Interval (year)	Depth (m)	Concentration (μ mol·L^{-1})				Acc. rate (m-water·a^{-1})	Flux (m mol·m^{-2}·a^{-1})			
		Na^+	Ca^{2+}	NO_3^-	SO_4^{2-}		Na^+	Ca^{2+}	NO_3^-	SO_4^{2-}
1963–1995	0– 15.3	25.52	1.47	1.58	3.31	0.34	8.68	0.50	0.54	1.12
1920–1963	15.3– 36.9	24.92	0.91	0.70	2.32	0.43	10.71	0.39	0.30	1.00
1783–1920	36.9– 86.0	27.48	1.35	0.87	2.45	0.35	9.62	0.47	0.31	0.86
–1783	86.0–211	29.01	1.04	0.53	1.57					

2) Austfonna 1998 Ice core

Interval (year)	Depth (m)	Concentration (μ mol·L^{-1})				Acc. rate (m-water·a^{-1})	Flux (m mol·m^{-2}·a^{-1})			
		Na^+	Ca^{2+}	NO_3^-	SO_4^{2-}		Na^+	Ca^{2+}	NO_3^-	SO_4^{2-}
1963–1995	0– 20.9	15.88	0.73	1.54	1.88	0.45	7.15	0.33	0.69	0.85
1920–1963	20.9– 48.0	22.81	0.65	0.59	1.15	0.58	13.23	0.37	0.35	0.67
1783–1920	47.5–106.0	14.81	0.57	0.55	0.81	0.41	6.07	0.23	0.22	0.33
–1783	106.0–118.5	12.54	0.50	0.41	0.53					

3) Austfonna 1999 Ice core

Interval (year)	Depth (m)	Concentration (μ mol·L^{-1})				Acc. rate (m-water·a^{-1})	Flux (m mol·m^{-2}·a^{-1})			
		Na^+	Ca^{2+}	NO_3^-	SO_4^{2-}		Na^+	Ca^{2+}	NO_3^-	SO_4^{2-}
1963–1995	0– 21.3	14.57	0.53	1.32	2.06	0.45	6.55	0.24	0.60	0.93
1920–1963	21.3– 49.0	22.01	0.64	0.86	2.45	0.57	12.55	0.37	0.49	1.40
1783–1920	49.0–106.6	17.27	0.76	0.80	1.78	0.44	7.60	0.34	0.35	0.78
–1783	106.6–289	15.79	0.62	0.64	1.32					

This document is provided by JAXA.

reflecting climatic or environmental variability. SO_4^{2-} and NO_3^- concentrations increase in the recently deposited layer, at a depth of about 10 to 20 m, indicating recent acidification. The marked peak in SO_4^{2-} and acidity around 105 m in the 1999 core is believed to be due to the eruption of Laki in 1783.

Annual fluxes of ions at each site were estimated by multiplying mean ion concentrations by annual mean accumulation rates. Mean annual fluxes of several ions were calculated over the intervals between the reference horizons (marked with letters in Fig. 8). Horizon A is detected by the tritium peak, B by a sudden decrease of oxygen isotopic ratio, and C by the estimation for ECM measurement of Laki.

Table 3 lists the averaged concentrations of ions; annual mean fluxes of ions, and annual mean accumulation rates at these sites.

4. Ice-core dating

Ice-core dating with high resolution by annual layer counting was not possible, since snow melting and melt water percolation disturbed the seasonal variation of ions and $\delta^{18}O$. For the preliminary estimation, the 1999 core was dated by means of Nye's time scale assuming a constant accumulation rate. In applying Nye's time scale, if the glacier thickness (H^*) is taken to be 654 m (corresponding to 600 m in water), the age (t) of ice at depth Z as a function of the accumulation rate A at the glacier surface is given by the following formula:

$$t = (\text{drilling year}) - H^*(\ln (H/(H-Z))/A.$$

The average accumulation rates in the 1999 core between numbers of reference horizons are given in Table 2. First, to find a tentative "working" age, the average accumulation rate between 1999, the year of drilling, and 1963, the year of a nuclear test indicated by a local peak of tritium content, was found. In this way the average annual accumulation rate was found to be 507 mm of ice, equivalent to 465 mm of water.

The age given by the depth-year relationship was compared with the evidence of volcanic signals found by ECM as a check on accuracy; the difference between the two methods was within a few years in the upper layers. The older the age, the harder it becomes to identify the volcanic eruption responsible for a certain signal, but even so, the difference was less than about 10 years.

5. Reconstruction of the past environment and climate

It is well known that the oxygen and hydrogen isotopic composition ($\delta^{18}O$ and δD value) profiles are indicators of air temperature variability. The relationship between the stable isotope composition of water and air temperature on Nordaustlandet precipitation has not been clarified until now, because there occurred much local variation. However, relative fluctuation of air temperature can be determined.

In order to reconstruct climate change in Nordaustlandet, deviations from the average isotopic composition level, 50 years averages of isotopic composition were calculated. The relationship between the core age and $\delta^{18}O$ profile (indicating raw and running mean data) is shown in Fig. 10.

This document is provided by JAXA.

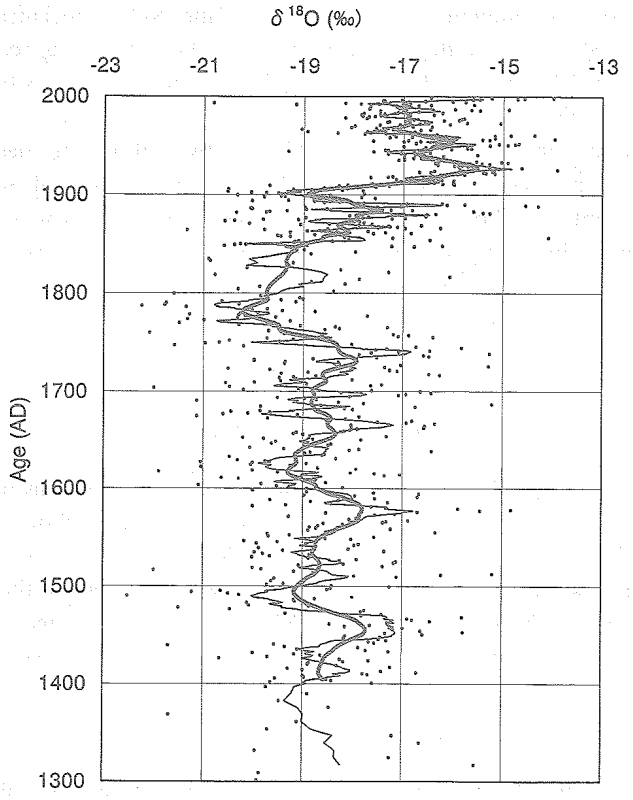


Fig. 10. Oxygen isotope profile on the estimated core age axis.

Inter-annual variability of oxygen isotope composition is shown as 50-year running means in Fig. 11. Open circles in the figure are 50-year means of isotope composition. The overall average from 1400 to 1900 is −18.7‰; since 1900, when air temperature has been rising rapidly, the average is −16.7‰.

The air temperature variability trend shown in the 1999 core shows that the most recent colder period, "Little Ice Age" (or Neoglaciation IV), ended around 1910, followed by a warming trend after about 1920. The difference of oxygen isotope composition between the Little Ice Age and the 20th century is about −2‰.

Before 1920, during the Little Ice Age, there were also prominent cool trends; from 1475 to 1550 (C1), from 1600 to 1650 (C2), from 1680 to 1720 (C3) and from 1750 to 1860 (C4). These decades do not exactly agree with the cooler periods in Europe during the Little Ice Ages found by Schove (1961); 1541–1680, 1741–1770 and 1801–1890, with overlap duration.

The 1750–1860 cold period (C4) is believed to correspond to the pronounced 1835–1870 cold period found at Site J on the Greenland Ice Sheet (Kameda *et al.*, 1995), but the cold period lasted longer in Nordaustlandet and the cooling, recorded by the difference in oxygen isotopic ratio, was stronger. The air temperature variability trend also shows general agreement with that in the Greenland Dye 3 core (Dansgaard *et al.*, 1975).

This document is provided by JAXA.

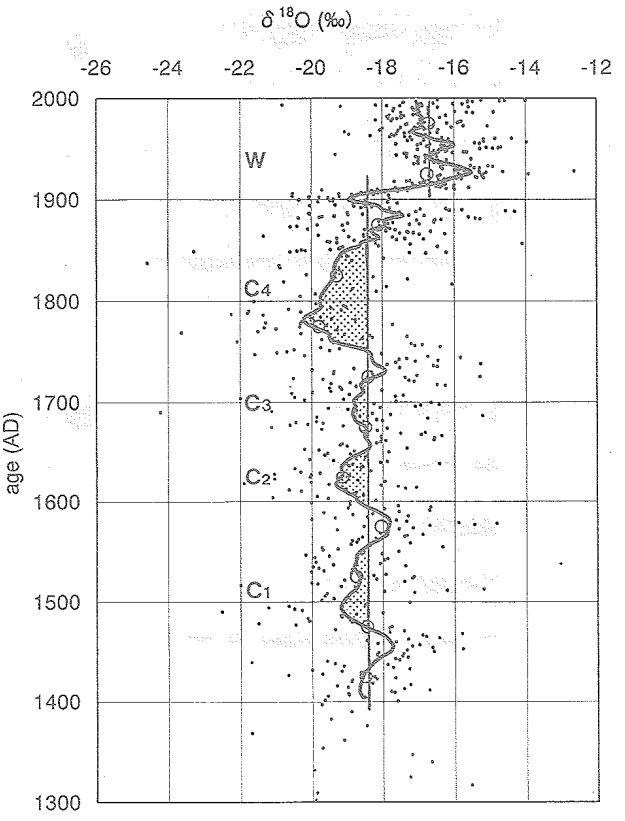


Fig. 11. Reconstruction of climatic and environmental change. Climatic phases during the little ice age. C (cold phase) 1: 1475-1554 AD, C2: 1596-1652, C3: 1676-1721, C4: 1752-1859, W (warm phase after little ice age): 1920-1999 AD.

The annual flux of several chemical compositions over the interval of C1-C4 cooler periods and the warmer period (W; after 1920) are shown in Fig. 12 and the numerical data in Table 4. Except for C3, the chemical fluxes of cooler periods (C1, C2 and C4) are of the same order and smaller value than those in the warmer period (W).

Since the Svalbard archipelago is located at the boundary between the multi-year sea ice pack and the seasonally ice-covered zone, the location of the multi-year sea ice limit changes from year to year. The remarkable decrease of the flux of major chemical constituents, Na^+, Cl^-, SO_4^{2-} and NO_3^- found in C3 may relate to cryospheric conditions such as sea ice distribution. The long cooler duration, as was estimated from Fig. 11 below the average line, was possibly responsible for the small fluxes.

As shown in Fig. 13, the correlation between the firn ratio and $\delta^{18}O$ was good from 1400 to 1750 and since 1900, but from 1750 to 1900, when there was strong cooling, there was a clear inverse correlation. This is in contradiction with the general trend for melting of accumulated snow to increase in a cold period. Perhaps it is possible to infer that during the Little Ice Ages the area covered by sea ice in the Barents Sea increased, the area of open

This document is provided by JAXA.

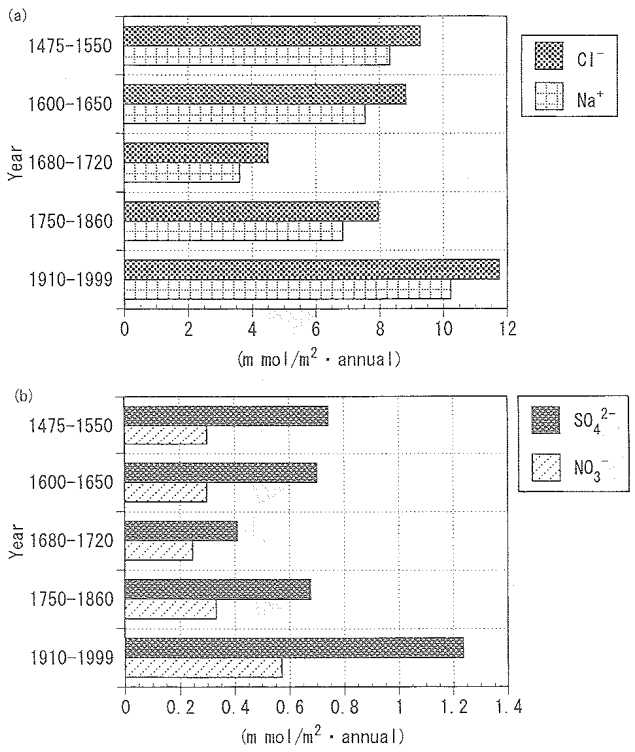


Fig. 12. Comparison of average annual chemical flux in the cold phase during the Little Ice Age.

Table 4. Average of annual chemical flux in the different climatic phase.

Depth (m)	Year	Climate phase	Acc. rate ($m \cdot a^{-1}$)	Na^+	Cl^-	NO_3^-	SO_4^{2-}
				($m\ mol \cdot m^{-2} \cdot a^{-1}$)			
0- 48.3	1999-1920	Warm	0.54	10.23	11.75	0.57	1.24
72.6-119.8	1860-1750	Cold 4	0.44	6.85	7.95	0.33	0.68
133.1-151.1	1720-1680	Cold 3	0.40	3.62	4.52	0.25	0.41
161.0-182.6	1650-1600	Cold 2	0.39	7.55	8.84	0.30	0.70
198.2-225.6	1550-1475	Cold 1	0.35	8.33	9.29	0.30	0.74

water in summer decreased and, particularly, that the amount of precipitation in summer decreased, so that there was the little cloud cover and little vapor transport. As seen in Table 3, compared to the period 1920-1963, the precipitation from 1783 to 1920 was lower (0.44 compared to 0.57 m-water$\cdot a^{-1}$) as was the Na^+ flux (7.60 compared to12.55 m mol$\cdot m^{-2} \cdot a^{-1}$); perhaps these figures support the above inference.

6. Concluding remarks

By comparing the multiple ice cores from different locations on Nordaustlandet, Svalbard archipelago, reconstruction of climatic and environmental change during the last

This document is provided by JAXA.

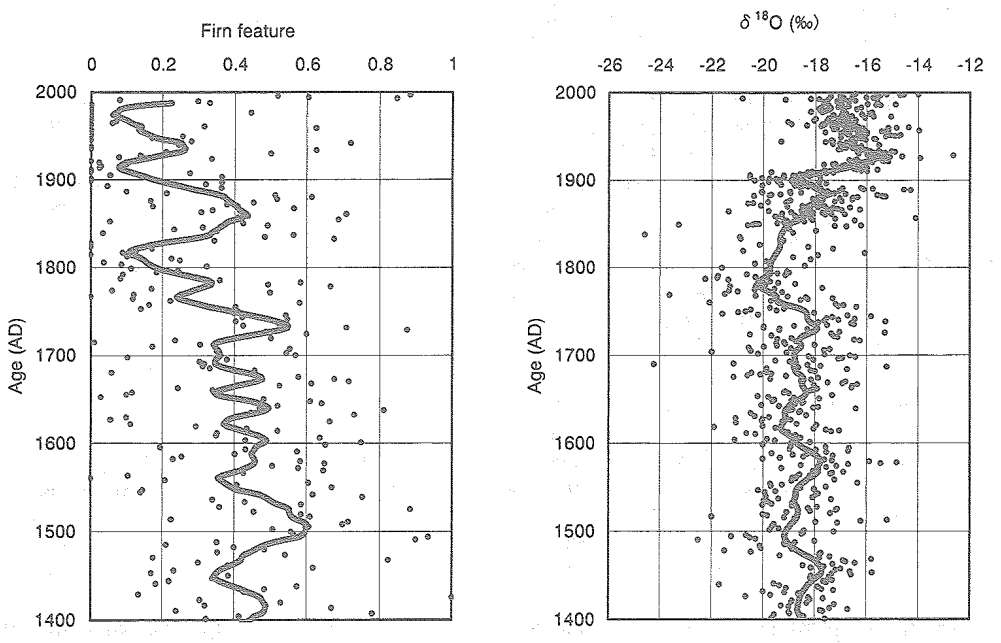


Fig. 13. Relation between firn ratio and climatic change at Austfonna.

few hundred years has been discussed.

The $\delta^{18}O$ records from Austfonna and Vestfonna ice cores correlated well with the temperature records since 1915 in Isfjord Radio. This suggests that $\delta^{18}O$ values recorded in ice cores would be important proxies for past temperatures in the Svalbard archipelago.

Ice core chemistry records can also be used to reconstruct past atmospheric conditions. Since our core analyses have not been completed yet, we need to perform preliminary analyses of the cores to obtain complete data sets. Also, we need to drill deep cores reaching the bedrock to reconstruct the Holocene climatic changes.

Acknowledgments

We would like to express our sincere gratitude to Dr. E. Isaksson and Prof. Jon Ove Hagen who are our cooperative researchers in Norway. The logistics section of the Norwegian Polar Institute in Longyearbyen supported our daily radio contacts. This research was supported by a Grant for an International Scientific Research Program of the Ministry of Education, Science, Sports and Culture (No. 08041114).

References

Arkhipov, S.A., Vaykmyae, R.A., Vasilenko, Ye.V., Zagorodnov, V.S., Zinger, Ye.M., Martma, T.A., Macheret, Yu.Ya., Punning, Ya.M.K., Samoylov, O.Yu., Sinkevich, S.A., Toots, M.D. and Troitskiy, L.S. (1987): Soviet glaciological investigations on Austfonna, Nordaustlandet, Svalbard in 1984–1985. Polar Geogr. Geol., **11**(1), 25–49.

This document is provided by JAXA.

Dansgaard, W., Johnsen, S.J., Reeh, N., Gundestrup, N., Clausen, H.B. and Hammer, C.U. (1975): Climatic changes, Norsemen and modern man. Nature, **255**, 24–28.

Hagen, J.O. and Liestøl, O. (1990): Long-term glacier mass-balance investigations in Svalbard, 1950–88. Ann. Glaciol., **14**, 102–106.

Hanssen-Bauer, I., Kristensen Solås, M. and Steffensen, E.L. (1990): The climate of Spitsbergen. DNMI-Rapport, Klima, **39/90**, 40 p.

Kameda, T., Narita, H., Shoji, H., Nishio, F., Fujii, Y. and Watanabe, O. (1995): Melt features in ice cores from Site J, southern Greenland: some implications for summer climatic since AD 1550. Ann. Glaciol., **21**, 51–58.

Kameda, T., Takahashi, S., Goto-Azuma, K., Kohshima, S., Watanabe, O. and Hagen, J.O. (1993): First report of ice core analyses and bore hole temperatures on the highest ice field on western Spitsbergen in 1992. Bull. Glacier. Res., **11**, 51–61.

Koerner, R.M. (1997): Some comments on climatic reconstruction from ice cores drilled in areas of high melt. J. Glaciol., **43**, 90–97.

Motoyama, H., Watanabe, O., Kamiyama, K., Igarashi, M., Goto-Azuma, K., Fujii, Y., Iizuka, Y., Matoba, S., Narita, H. and Kameda, T. (2001): Regional characteristics of chemical constituents in surface snow, Arctic cryosphere. submitted to Polar Meteorol. Glaciol.

Pinglot, J.F., Pourchet, M., Lefauconnier, B., Hagen, J.O., Vaikmae, R., Punning, J.M., Watanabe, O., Takahashi, S. and Kameda, T. (1994): Natural and artificial radioactivity in the Svalbard Glaciers. J. Environ. Radioact., **25**, 161–176.

Scove, D.J (1961): Solar cycles and the spectrum of time since 200 BC. Ann. N. Y. Acad. Sci., Art., **1**, 107–123.

Takahashi, A. (1996): Development of a new shallow ice-core drill. Seppyo (J. Jpn. Soc. Snow Ice), **58**, 29–37 (in Japanese with English abstract).

Watanabe, O. (1996): Japanese glaciological activities in the Arctic region. Mem. Natl Inst. Polar Res., Spec. Issue, **51**, 329–336.

Zagorodnov, V. and Arkhipov, S. (1990): Studies of structure, composition and temperature regime of sheet glaciers of Svalbard and Severnaya Zemlya: method and outcomes. Bull. Glacier Res., **8**, 19–28.

(Received May 31, 2000; Revised manuscript accepted October 23, 2000)

This document is provided by JAXA.

Mem. Natl Inst. Polar Res., Spec. Issue, 54, 243-251, 2001

Report

Field observations of the Japanese Arctic Glaciological Expeditions in Svalbard from 1993 to 1995

Kokichi Kamiyama, Hideaki Motoyama and Okitsugu Watanabe

National Institute of Polar Research, Kaga 1-chome, Itabashi-ku, Tokyo 173-8515

Abstract: The Japanese glaciological expedition continued its research in Svalbard from 1993 to 1995. The main interest is to clarify fluctuations of present and past Arctic environments. Ice coring provides past, and snow surveys present, climatic information. The corings were carried out on the central glacier in 1993, on small glacier near the seashore in 1994 and on a large glacier in the northernmost island in 1995. The snow survey was carried out mainly in 1994.

1. Introduction

The Arctic plays an important role in the global environment as a heat sink. Snow and ice cover the Arctic region, fluctuations in which affect the global climate. At the same time, environments far from the Arctic, such as biomass burning in the tropical regions and human activities in urban areas, affect the Arctic environment through transportation processes in the atmosphere (Legrand *et al.*, 1992).

Precipitation processes, fluctuating with season and year, importantly affect the glaciological environment. The annual fluxes of water and other substances onto the glacier through precipitation determine the composition of snow layers of the glacier. Snow layers record the glaciological environment produced by precipitation and metabolic processes after deposition.

A deep ice core obtained from a glacier is an archive of the snow layers. The record, observed in the deep ice core, has a close relationship with the atmospheric conditions at the times of deposition and sedimentation. The diagenetic process as well as the metabolic one will possibly alter the record. Through snow and ice surveys at various sites in Svalbard, we will try to obtain the information recorded in ice cores.

In the Arctic, Svalbard is the northernmost group of islands, in a unique environment. The Greenland Sea nearby brings warm water into the Arctic Ocean, where the climate is comparatively calmer than any other location in the similar latitude. In addition, the Greenland polynia occurring between Svalbard and Greenland, one of the biggest polynias in the ocean, is a major heat source to the atmosphere and brings water vapor into the Arctic region while driving a deep oceanic current toward the tropics. The climatic condition affects the glaciological environment in the Arctic. At the same time, the mass balance of the glaciers affects the climate through the area of snow cover and inflow rate of fresh water to the ocean. There are many glaciers located at various sites in Svalbard.

This document is provided by JAXA.

Each glacier has a unique glaciological environment (Hagen and Riestel, 1990). Some represent only local environments, and others appear to be correlated with the global climate (Ono, 1996).

The Japanese Arctic Glaciological Expedition in 1987 (JAGE-87), succeeded in obtaining an ice core at the top of Asgørdfonna (Høghetta) as the first experience in Svalbard for a Japanese glaciological group (Watanabe and Fujii, 1988). The ice drilling reached the bedrock at about 70 meters depth from the glacier surface. It was revealed that the core contained a 6000-year environmental record. Frozen petals and bacteria, preserved in the ice core near the bedrock, suggest the existence of 5000 to 6000 year old fossil ice formed in the warmest period after the last glacial period. The core record suggested that there was a big unconformity in deposition in the core, possibly because of the occurrence of a hiatus period. In the upper part of the core, we were able to trace almost continuous sedimentation back to a hundred years ago, and in the lower part, to detect the evidence for the occurrence of ice layers in a few thousand years during the warmer periods (Fujii *et al.*, 1990).

The coring site was located on the summit of the glacier. The depth of ice confirmed by drilling was not as deep as that estimated by radio echo sounding around the surrounding area. We might have been drilling in an old glacier, perhaps an isolated ice cap on top of the mountain.

The objective of research from 1993 to 1995 is to discuss the local fluctuation, revealed in the ice core on some locations in Svalbard.

2. Objectives of each expedition

2.1. General view

The project in 1993 was considered to be the second phase of JAGE-87. The prime objective was to obtain more precise and detailed information about the last 6000-year environmental records for comparison with those obtained by JAGE-87. Another coring over the top near by would help to clarify the paleo glacier environments through comparison of both ice core records.

The coring was carried out in Asgørdfonna, about 10 km north from the highest peak of Høghetta. The site was also a dome-like plateau, with flat glacier surface spread more widely than the site in 1987.

The research in 1994 was concentrated near Ny-Ålesund (NAL), one of the small settlements in Svalbard. Research on snow chemistry, as well as the atmospheric observations such as aerosol sampling, was carried out at NAL, including glaciological research on a glacier named Breggarbreen near by. Because the snow has a close relation to the atmospheric environment, the research was concentrated on the snow deposition and accumulation process as well as the metabolic process, with a shallow coring operation.

The operation in 1995 was treated as one of the Japanese Glaciological contributions for the Ice core Circum-Arctic Paleoclimate Program (ICAPP) of the International Arctic Scientific Committee (IASC). The target glaciers were located in the northern part of Svalbard. The northeast island, Nordaustlandet, is located in a unique position in Svalbard, low altitude and much snow cover near the Arctic Ocean. The glacier is also located near the Arctic Ocean, and any fluctuation of sea ice is reflected in the glacier environment

This document is provided by JAXA.

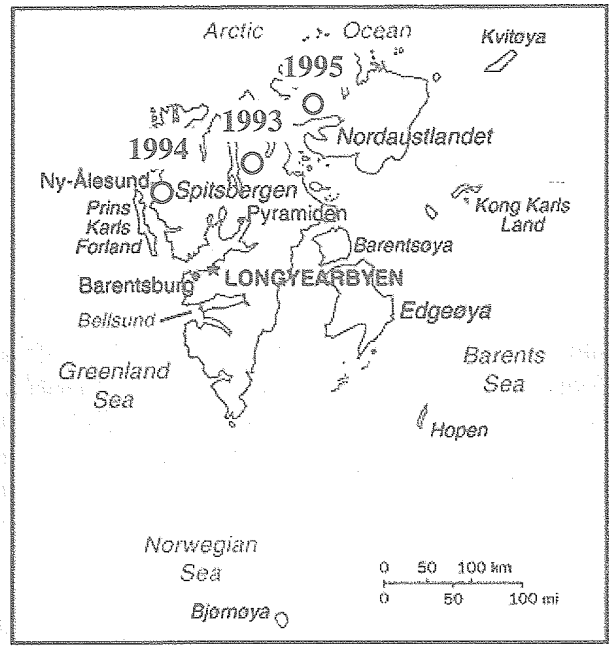


Fig. 1. Main observation sites in 1993, 1994 and 1995.

Table 1. Sampling sites with coring depth.

Sampling site	Location	Position	Year	Coring depth
Asgørdfonna	Spitsbergen	79°27′N, 16°43′E, 1140 m a.s.l.	1993	185.3 m
Ny-Ålesund	Spitsbergen	78°55′N, 11°56′E, 8 m a.s.l.	1993–94	49.0 m
Austre Brøggerbreen	Spitsbergen	78°52′N, 11°56′E, 450 m a.s.l.	1994	9.39 m
Vestfonna	Nordaustlandet	21° 1′N, 79°58′E, 600 m a.s.l.	1995	210.0 m
Høghetta Ice Cap	Spitsbergen	79°17′N, 16°50′E, 1200 m a.s.l.	1987	87.0 m
Snofjella basin	Spitsbergen	79° 8′N, 13°17′E, 1190 m a.s.l.	1992	24.4 m
Snofjella basin	Spitsbergen	79° 8′N, 13°19′E, 1160 m a.s.l.	1992	83.9 m

directly. The glaciological environment there will possibly reflects the Arctic environment with small local fluctuation. Japanese glaciological activities in the Arctic region, including the project, were introduced by Watanabe (1996).

Core records and snow surveys in Svalbard can help to clarify the Arctic glaciological environment and its local fluctuation. All the sampling sites are shown in Fig. 1 and Table 1 with coring depths. In Fig. 1, the main site in each year was marked in open circles on the map of Svalbard, obtained from the web site of the University of Texas central libraries (http://www.lib.utexas.edu/Libs/PCL/Map_collection/Map_collection.html).

2.2. Expedition in 1993

In the 1993 expedition, we tried to decrease the helicopter payload while carrying a

This document is provided by JAXA.

Table 2. Field members in 1993 coring.

Participant	Longyearbyen	Glacier	Ny-Ålesund
Kokichi Kamiyama	6/16–6/20, 7/19	6/20–7/14	7/14–7/19
Yoshitaka Suzuki	6/16–6/20, 7/19	6/20–7/14	7/14–7/19
Tsutomu Uchida	6/16–6/20, 7/19	6/20–7/14	7/14–7/19
Yoshitaka Yoshimura	6/16–6/20, 7/19	6/20–7/14	7/14–7/19
Akiyoshi Takahashi	6/16–6/20, 7/2–7/3	6/20–7/2	
Yoshiyuki Fujii	7/9–7/10, 7/19	7/10–7/14	7/14–7/19

drilling system capable of reaching more than 200 m depth. Under the situation, we tried to carry out the expedition with the smallest possible number of members, 4 members, for daily routine duties, plus specialists to developing the new drills (Takahashi, 1996) as shown in Table 2. The coring site was located at 79°27′N, 16°43′E at an altitude of 1140 m a. s. l. We obtained two cores of 185.3 and 49.0 m depth. The surface stratification of the snow and ice layers was observed on a snow pit wall nearby, and non-contaminated snow samples were obtained from the newly cut vertical snow walls.

2.2.1. Ice coring

Some of the scientific and logistic equipment, such as generators and tents, was stored at the Rabben station (R/S) of the Japanese Arctic Environmental Research Center (AERC) in NAL and other items at the home laboratory in Japan. All the luggage was gathered at Longyearbyen (LYB), a unique commercial airport in Svalbard, where we checked all of the coring instruments, assembling the winch with the mast to operate the drilling system. After obtaining food and oil, we prepared to leave for our coring site in Asgørdfonna by commercial helicopter with about 3000 kg of luggage. We reached the glacier on 16 June. One week of delay was forced by the weather because of difficulties in the first landing on the glacier. The drilling was done from 23 June to 12 July, 1993. The field members in the 1993 coring are listed in Table 2.

2.2.2. Sample procedure *in situ*

The drilling was done mainly by 3 members, and the logistic support by 1 member. During the coring operation, the sunshine became strong in the Arctic and the snow surface melted down gradually. The drill was stored in a bore hole at about 6-m depth from the surface to keep it in cold condition. Once ice packed the bore hole together with the drill, probably by freezing of melt water, and the drill was stuck until we recovered by digging a pit to the depth.

The core samples were cut less than 50 cm length and stored in a snow pit to keep them solid. It was difficult for us to maintain the pit under strong sunshine. At the coring site, vertical profiles of ice density, by measuring the core weight, and glacier temperature, using the bore hole, were observed. The visible stratification of the snow and ice layers, observed in the core samples, was recorded with the shapes and density of bubbles in the core sample. The observation and recording work was shared among 4 members. The vertical distribution of temperature and stratigraphy were discussed by Uchida *et al.* (1996).

2.2.3. Core storage and sample procedure in Ny-Ålesund

Some of the core samples were stored in the cold laboratory at R/S of AERC in NAL and others in the commercial cold room at LYB, depending upon the operation of

This document is provided by JAXA.

helicopters. Some of the surface snow samples were studied to determine biological activity after pre-treatments at NAL.

2.3. Expedition in 1994 together with core analyses at Ny-Ålesund

The expedition in 1994 was mainly aimed at sampling of precipitation and snow cover around NAL.

2.3.1. Background

For some elements of the core analyses, the samples must be preserved in the solid state. For example, measurement of electric conductivity (ECM) is only valid in the solid state. The ECM profile of the core is used to identify volcanic layers and to determine the period of sedimentation of ice core layers. To carry out some of the core analyses in situ or in a laboratory near the coring site is essential. Some chemical substances possibly change their concentration in the liquid phase, so they should be determined as soon as possible after melting. A cold room was opened at R/S of AERC in late 1994. We did some analyses of the ice core obtained in 1993 in the cold room. Some of the treated core samples were later subjected to the detailed study in the home laboratory in Japan.

Precipitation characteristics are basic information for determining the environmental record from the ice core analyses. Coring at Snofjella near NAL was carried out in 1992 (Takahashi *et al*., 1993). The site is considered to be representative of western Svalbard. In considering the core record, it is important to know the input from the atmosphere into the glacier. We tried to investigate the snow fallout and metamorphic process through the sedimentation process.

2.3.2. Field activity

Winter in 1993/1994:

The snow sampling and the core analyses were carried out at R/S of AERC in NAL, where two members stayed from 12/03 to 12/16 in 1993. Sampling was conducted of the snow fallout and snow pit. There was unusual heavy rain fall just before our arrival, causing the surface snow to melt down. After the rainfall, a little precipitation was observed during the stay.

1993 Core samples from the surface to 46 m were promised to be provided for obtaining vertical profiles of the artificial radionuclides, gross beta activities and Cs-137, to clarify the surface accumulation rate during the last several decades, under cooperative work with scientists of Norsk Polarinstitutt (Norwegian Polar Institute), Drs. J. O. Hagen and B. Lefauconnier. The core samples from the surface to 46-m depth in the upper part of the 185.3 m core were used for the investigation.

All of the core samples about 50 cm length, the 49.0 m core and rest of the 185.3 m core, were cut into half vertically. Each vertical half core was kept frozen in the cold laboratory in R/S. The other half was cut 10 cm horizontally into small pieces. Each piece was melted, after removing surface material which might have been artificially contaminated during the procedure. After analyzing the core samples in liquid phase, for example measuring electrical conductivity, pH and hydrogen peroxide (H_2O_2), the melted samples were carried to the home laboratory for future analyses. H_2O_2 should be determined just after melting, while it is difficult to process the whole core in a short stay.

Summer in 1994 and winter in 1994/1995:

In late summer 1994, precipitation and surface snow were sampled at NAL and also

This document is provided by JAXA.

Table 3. Field members for the research in Ny-Ålesund.

Participant	Duration in Ny-Ålesund	Seasons
Kokichi Kamiyama	12/03–12/15	Winter late in 1993
Makoto Igarashi	12/03–12/15	Winter late in 1993
Kokichi Kamiyama	02/01–03/15	Winter early in 1994
Makoto Igarashi	02/01–03/15	Winter early in 1994
Kokichi Kamiyama	8/22–9/20	Summer in 1994
Makoto Igarashi	8/22–9/20	Summer in 1994
Hideaki Motoyama	8/22–9/20	Summer in 1994
Fumihiko Nishio	9/01–9/15	Summer in 1994
Makoto Igarashi	1/19–3/23	Winter late in 1995
Kokichi Kamiyama	1/19–2/2, 3/1–3/14	Winter late in 1995
Yoshitaka Suzuki	2/23–3/23	Winter late in 1995

at Brøggerbrean near NAL. A 10 m core was also obtained from the glacier. Some parts of the core samples obtained in 1993, being stored in NAL, were melted for analysis. Snow sampling with core treatment was carried out at R/S. ECM measurement was carried out in the cold laboratory in NAL on stored solid cores in 1993 and on the 10 m core in 1994. Processing of the 1993 core was continued during the summer and winter. Finally, 652 pieces of melted samples were obtained from the surface to 50-m depth, and 1623 pieces from 50 m to 185 m.

For snow sampling as well as core analyses, field members stayed in NAL. The field members for the research in NAL are listed in Table 3.

2.4. Expedition in 1995

For coring in NordAustlandet, we cooperated with Russian and Norwegian scientists. In the past ten years, Russian scientists have been active in glaciological and geological research in northern Svalbard. They were familiar with NordAustlandet, especially on the view point of the logistics. They supported us in radio communication between our camp and the Russian settlement Barentsburg on Spitsbergen, and in helicopter operation and field observations. For forecasting the weather for helicopter landing, information from Barentsburg and Polish station received via Russian radio was useful. The large Russian helicopter, capable of carrying more than 3000 kg of luggage plus fuel for 400 miles of flight, made the operation much easier.

2.4.1. Duration and participants

Field members in the 1995 coring are listed in Table 4. In LYB, we prepared camping supplies with food, and checked the condition of all of the equipment, especially the drilling system. All of the members gathered in Barentsburg waiting for the helicopter, the operation of which depended on the weather over the target glacier. After drilling up to about 200 meters depth, we prepared to leave the glacier. After waiting for a week during heavy snowfall, we flew to NAL for core storage.

2.4.2. Coring procedure

In the field we tried to perform core analyses in situ. Three members were assigned to the drilling, and one to maintenance of ice core samples. The other 3 members were used only for the core analyses. These daily duties were rotated among these 7 members. The

This document is provided by JAXA.

Table 4. Field members in 1995 coring.

Participant	Longyearbyen	Barentsburg	Glacier	Ny-Ålesund
Kokichi Kamiyama	5/11-5/15, 6/16-6/17	5/15-5/19	5/19-6/11	6/11-6/16
Hideaki Motoyama	5/11-5/15, 6/16-6/17	5/15-5/19	5/19-6/11	6/11-6/16
Hideki Narita	5/11-5/15, 6/16-6/17	5/15-5/19	5/19-6/11	6/11-6/16
Sumito Matoba	5/11-5/15, 6/16-6/17	5/15-5/19	5/19-6/11	6/11-6/16
Moriatsu Miyahara	5/11-5/15, 6/16-6/17	5/15-5/19	5/19-6/11	6/11-6/16
Hideaki Yamazaki	5/11-5/15, 6/16-6/17	5/15-5/19	5/19-6/11	6/11-6/16
Arkihop	5/11-5/15, 6/16-6/20	5/15-5/19	5/19-6/11	6/11-6/16
Tevenkov	5/11-5/15, 6/16	5/15-5/19, 6/16-	5/19-6/11	6/11-6/16
Andry		5/15-5/19, 6/11-	5/19-6/11	6/11
Zinger	5/11-5/15	5/15-		

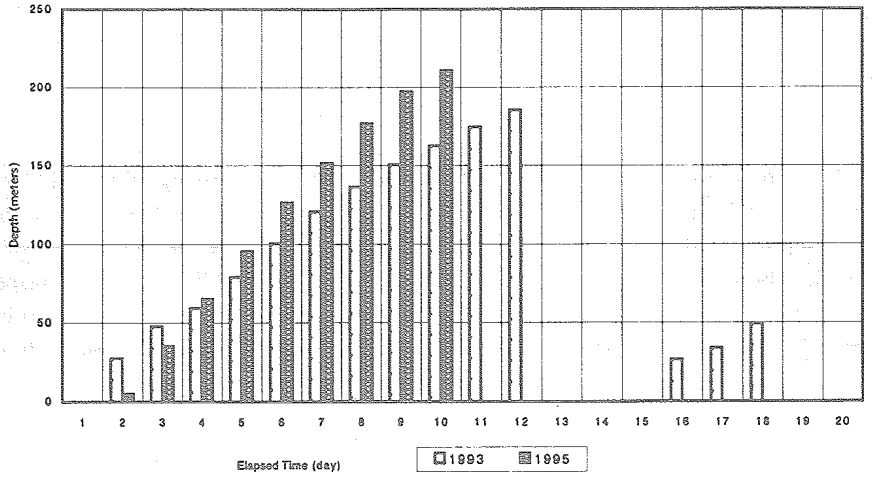


Fig. 2. Daily progress on the drilling depth in 1993 and 1995.

daily progress of drilling depth is shown in Fig. 2, with comparison to 1993. The delay in coring speed in 1993 was mainly due to the difficulty of removing core samples from the barrel.

All of the core samples were stored in the cold laboratory of AERC in NAL, where some ECM measurements were carried out by 2 members.

3. Activities

3.1. Observations and samples

Here we list our equipment in 1995 for the convenience of future research, in Table 5. Additional equipment was carried to obtain data immediately and reduce the risk and weight of samples carried back, at same cost in increased weight and number of members needed.

Some of the samples are still being analyzed. By determining the local and seasonal

This document is provided by JAXA.

Table 5. List for field equipment for core observation.

Equipments	Objection	Expedition
Core card	Record of core segments	93, 95
Core table, recording paper, camera,	Exact measurement for core lengths Observation for stratigraphy	93, 95
Band saw	Cutting cores vertically into half column Half column is cut into segments with cutting off the surface to keep from contaminant	95
Electric oven	Pretreated solid ice core sample into liquid phase	95
Portable electrical conductivity meter	Measurement of electrical conductivity for liquid core	95
Portable pH meter	Measurement of pH for liquid core	95
Flow line UV detector	Measurement of 210 nm absorbance for liquid core for estimating NO_3 concentration	95

fluctuations found in the core analysis and snow survey, we clarify the glaciological environment in the Svalbard region.

3.2. Observations in Svalbard

Expeditions were carried out also in 1998 and 1999, after missing 1996 and 1997. The expeditions in 1998 and 1999 were concentrated on Austfonna in NordAustlandet, the largest glacier in Svalbard, where the observation sites were the farthest from the main island of Spitsbergen among the glaciers in Svalbard. The expeditions were co-operative work with the Norsk Polarinstitutt. Reports on the expedition 1999 has been presented elsewhere (Watanabe *et al.*, 2000). Detailed reports, including these observations, have also been presented in the report for the scientific fund of the Ministry of Education, Science, Sports and Culture, No. 08041114 in Japanese (Watanabe, 1998).

References

Fujii, Y., Kamiyama, K., Kawamura, T., Kameda, T., Izumi, K., Satow, K., Enomoto, H., Nakamura, T., Hagen, J. O., Gjessing, Y. and Watanabe, O. (1990): 6000 year climate records in an ice core from the Hoghetta Ice Dome in northern Spitsbergen. Ann. Glaciol., **14**, 85–89.

Hagen, J. O. and Riestel, O. (1990) Long-term glacier mass balance investigations in Svalbard, 1950–88. Ann. Glaciol., **14**, 102–106.

Legrand, M., De Angelis, M., Staffelbach T., Neftel, A. and Stauffer, B. (1992) Large perturbations of ammonium and organic acids content in the Summit-Greenland ice core, fingerprint from forest fires? Geophys. Res. Letts., **19**, 473–475.

Ono, N. (1996) ENSO-like periodicities in the Arctic cryosphere. Mem. Natl Inst. Polar Res., Spec. Issue, **51**, 33–39.

Takahashi, A. (1996): Development of a new shallow ice core drill. Seppyo (Jpn. Soc. Snow Ice), **58**, 29–37 (in Japanese with English abstract).

Takahashi, S., Kobayashi, S. and Watanabe, O. (1993): Field activities of the Japanese Arctic Glaciological Expedition to the western Spitsbergen in 1991 and 1992 (JAGE 1991–1992). Bull. Glacier Res., **11**, 63–67.

Uchida, T., Kamiyama, K., Fujii, Y., Takahashi, A., Suzuki, T., Yoshimura, Y., Igarashi, M. and Watanabe, O. (1996): Ice core analyses and borehole temperature measurements at the drilling site on Asgardfonna, Svalbard, in 1993. Mem. Natl. Inst. Polar Res., Spec. Issue, **51**, 377–386.

Watanabe, O. (1996): Japanese glaciological activities in the Arctic region. Mem. Natl Inst. Polar Res.,

This document is provided by JAXA.

Spec. Issue, 51, 329–336.
Watanabe, O. (1998): Studies on Clio-environmental Variation in Arctic Cryosphere. Tokyo, Natl Inst. Polar Res., 131 p (in Japanese).
Watanabe, O. and Fujii, Y. (1988): Outline of the Japanese Arctic Glaciological Expedition in 1987. Bull. Glacier Res., 6, 47–50.
Watanabe, O., Kamiyama, K., Kameda, T., Takahashi, S. and Isaksson, E. (2000): Activities of the Japanese Arctic Glaciological Expedition in 1998 (JAGE 1998). Bull. Glaciol. Res., 17, 31–35.

(Received May 16, 2000; Revised manuscript accepted September 5, 2000)

This document is provided by JAXA.

This document is provided by JAXA.

Mem. Natl Inst. Polar Res., Spec. Issue, 54, 253–260, 2001

Report

Activities of the Japanese Arctic Glaciological Expedition in 1999 (JAGE 1999)

Hideaki Motoyama[1], Okitsugu Watanabe[1], Kumiko Goto-Azuma[1], Makoto Igarashi[1], Morihiro Miyahara[2], Tomoharu Nagasaki[3], Lars Karlöf[4] and Elisabeth Isaksson[4]

[1]*National Institute of Polar Research, Kaga 1-chome, Itabashi-ku, Tokyo 173-8515*
[2]*Nihon Link Co., Ltd, 2-7-32 Yodogawa, Miyazaki 880-0907*
[3]*Niigata University, Igarashi Ninomachi, Niigata 950-2102*
[4]*Norwegian Polar Institute, N-9296 Tromsø, Norway*

Abstract: To reconstruct climatic and environmental changes in Svalbard in the past several hundred years, an ice core was drilled on the summit of Austfonna ice cap, Svalbard (79°50′N, 24°00′E, 750 m a.s.l.) to a depth of 289 m in May 1999 by a Japan–Norway cooperative project. Ice core stratigraphy measurement, digital camera recording of the ice core, and measurements of bulk density and electrical conductivity of ice (ECM) were conducted *in situ*. Snow pit observations were carried out at three different sites. Fresh falling snow, drifting snow and surface hoar were sampled.

1. Introduction

The prime objective of the Japanese Arctic Glaciological Expedition (JAGE) is to study the climatic and environmental changes for the last few hundred years using ice cores from various areas of the Arctic cryosphere. Several shallow ice cores have been retrieved from Svalbard glaciers (Table 1). Previous research activities have already been outlined by Watanabe and Fujii (1998, 1990), Watanabe *et al.* (1993), Watanabe (1996), Watanabe *et al.* (2000) and Kamiyama *et al.* (2001). This research focuses on Japanese glaciological research activities on the top of Austfonna, Nordaustlandet, Svalbard in 1999.

2. Location of the ice coring site and its glaciological conditions

Austdomen, on the Austfonna ice cap (79°50′N, 24°00′E, 750 m a.s.l.), was selected for the ice coring site. It is 3 km north of the 1998 last ice coring site (Fig. 1: Watanabe *et al.*, 2000). The glaciological conditions were reported by Watanabe *et al.* (2000). The total area of the Austfonna ice cap is 8450 km^2 and the ice depth reaches 570 m. In order to determine the present regime and the hydrothermal state of the glacier, and to reconstruct past glacioclimatic conditions, radio echo sounding of the ice thickness, and thermal drilling of the glacier on the ice divide, were conducted in 1984, 1985 and 1987 on the Austfonna ice cap by Soviet scientists. Researchers observed that the ice on the divide of Austfonna was 550–570 m thick, and they obtained a 567 m ice core which covered the surface to the bed

This document is provided by JAXA.

Table 1. Ice coring in Svalbard by JAGE. Drilling period, position, 10 m ice temperature and surface ice density are summarized.

Date	Drilling sites	Latitude, longitude	Altitude (m a.s.l.)	Drilling depth (m)	10 m ice temp. (°C)	Ice density (kg/m^3)	
						0–10 m	10–20 m
May–June 1987	Høghetta Ice Dome	79°17′N, 16°50′E	1200	85.61 (bedrock)	−11.0	(ice)	(ice)
July–Aug. 1992	Snøfjellafonna	79°08′N, 13°18′E	1190	83.92	−2.8	565	775
		79°08′N, 13°19′E	1160	24.41			
June–July 1993	Åsgårdfonna	79°27′N, 16°43′E	1140	185.3, 49	−6.8	808	881
Sep. 1994	Brøggerbreen	78°52′N, 11°55′E	550	10	(0)	812	
May–June 1995	Vestfonna	79°58′N, 21°01′E	600	210	−3.7	639	839
Mar.–Apr. 1998	Austfonna	79°48′N, 24°00′E	750	118.62	−1.0	601	876
Apr.–May 1999	Austfonna	79°50′N, 24°00′E	750	289.075	−2.8	649	840

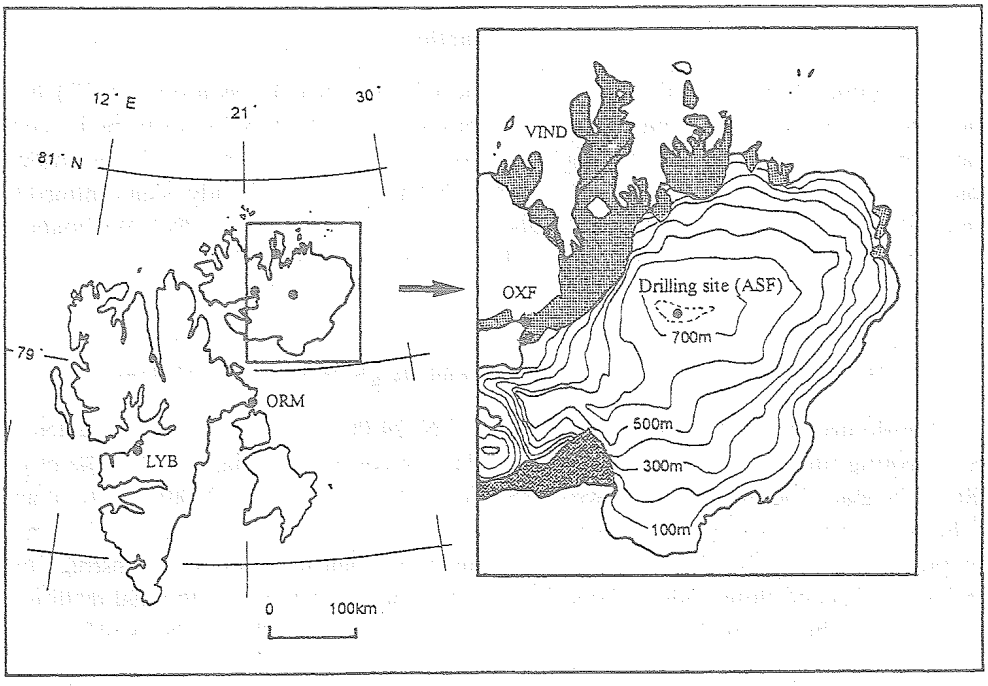


Fig. 1. Ice coring site on Austfonna, Svalbard. Dots indicate ice-free area (Watanabe et al., 2000).

This document is provided by JAXA.

rock. Some results have been published (Arkhipov *et al.*, 1987, Zagorodonov and Arkhipov, 1990).

3. Logistics

Our project (JAGE) and the ICEMASS project, whose purpose is to clarify the mass balance in the arctic cryosphere, were conducted at the same location and during the same season. In consideration of cost and weather risk, transportation of both sets of equipment was carried out in cooperation. The first incoming team (ICEMASS) and the last outgoing team (JAGE) used several flights of twin otter airplanes with skis (maximum pay load 1000 kg) for transportation of the main equipment. Two helicopter flights (maximum pay load 570 kg) were used for transportation of people in and out. The weight of the total incoming equipment (JAGE) including passengers was 4470 kg; the outgoing weight including the ice core was 4800 kg. Part of the outgoing equipment was temporarily deposited on the glacier because of bad weather, and was transported by a ship of Norwegian Polar Institute.

The ice coring site on the top of the ice cap was determined based on topographical observations by ICEMASS. We arrived there on April 25, 1999 and set up the camp

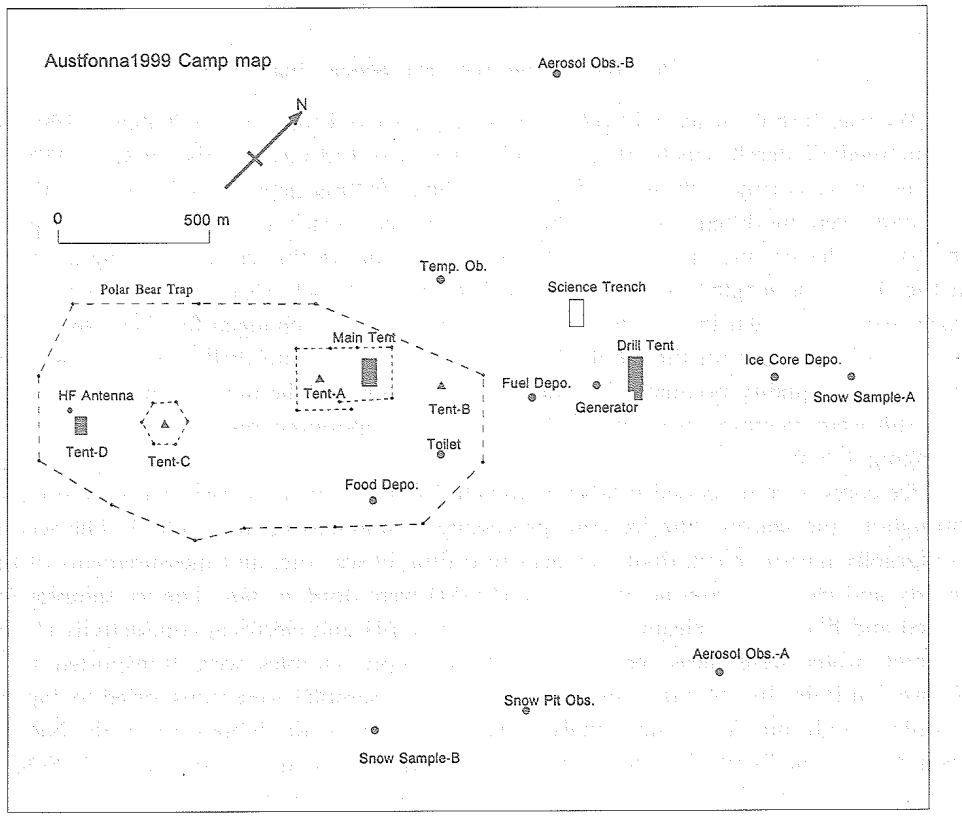
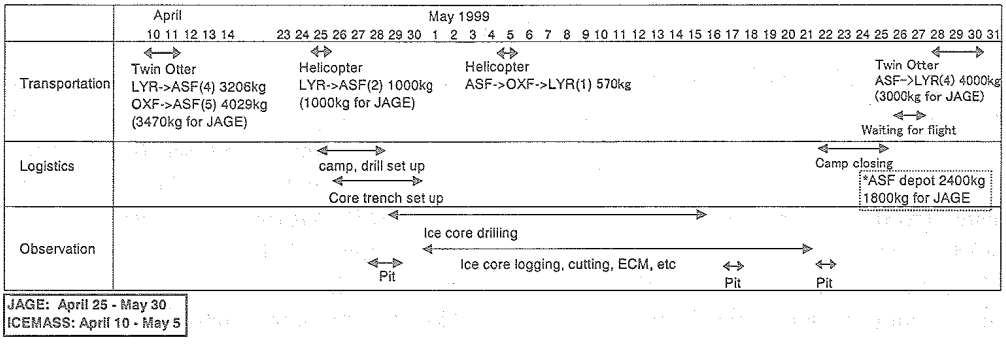


Fig. 2. Camp location map.

This document is provided by JAXA.

*Table 2. Schedule of flights and operations. LYR: Longyearbyen, ASF: Austfonna (drilling site), OXF: Oxfordhalvoya (drilling equipment and fuel deposit site), ( ): number of flights. *Depot equipment on ASF was transported to LYR in July 1999.*



equipment, drilling equipment and an ice core processing trench. The ice core drilling began on April 29. The outline of the camp is shown in Fig. 2. The drilling tent was damaged by a heavy snow storm in 1998, so we reinforced the tent and changed the practice period to a later date. The schedule of flights and operations is shown in Table. 2.

4. Ice coring, ice core processing

We used a shallow ice drill (D-2 type, Geo Tecs Co. Ltd, Japan, Takahashi, 1996) and an intermediate depth winch (W-4 type, Geo Tecs Co. Ltd.) as was also used in 1998. The progress of ice coring is shown in Fig. 3. The final drilling depth was 289.075 m. Various drill parts were modified, including the cutter, heel, core catcher, core barrel, winch power, anti-torque device and chip-ice separator. Characteristics of the ice core drilling are shown in Fig. 4. Coring length and drilling speed became stable below depths of 73 m and 59 m, respectively, as shown in Fig. 4a. The ice cutting pitch was changed for these depths. The average coring length for the whole depth was 76.1 cm/run, and drilling speed was 23 cm/min. Ice core quality became brittle deeper than 135 m, so the number of core pieces per each run were increased as shown in Fig. 4b. Consumption energy for drilling was stable, averaging 415 W.

Ice cores were processed in a snow trench. Room temperature was below zero Celsius throughout the season. The ice core processing is summarized in Table 3. The ice core stratigraphy measurement, digital camera recording of ice core, and measurements of bulk density and electrical conductivity of ice (ECM) were done *in situ*. The ice samples were melted and filled in pre-cleaned 50 m*l* bottles. The pH and electrical conductivity (EC) of the melt water were measured *in situ*. The ice core samples were transported to the Norwegian Polar Institute in Tromsø, Norway; water samples were transported to Japan in a cooled condition. A chemical analysis was performed at the laboratory of the National Institute of Polar Research. The analysis included the major soluble ions Cl, NO_3, SO_4, Na, K, Mg and Ca; stable oxygen isotope ratio and radioactivity (tritium).

This document is provided by JAXA.

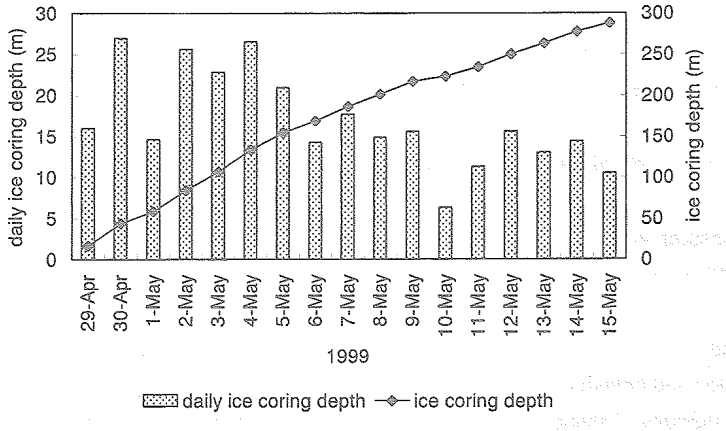


Fig. 3. Progress of ice coring.

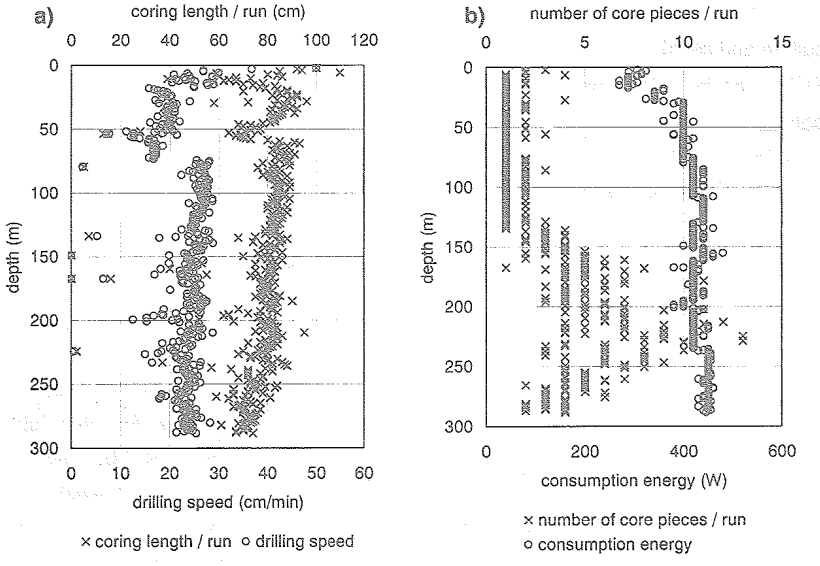


Fig. 4. Characteristics of ice core drilling. a) coring length per run or drilling speed versus ice coring depth. b) number of core pieces per run or consumption energy for drilling versus ice coring depth.

5. Glaciological and meteorological observations

Borehole temperatures were measured at depths of 5, 10, 15, 20, 40, 80, 120, 160, 200, 240, and 288 m. Snow pit observations were carried out; two near the drilling sites and one 2 km northward. The fresh falling snow and drifting snow were sampled in a timely manner. The frost accumulating around the surface of the tent ropes and the surface hoar

This document is provided by JAXA.

Table 3. Ice core processing.

temporary preservation ice core (90- 70 cm in length)

↓

transport to core processing trench

↓

density measurement

core length, core diameter, weight of the core

↓

core logging

fitting of top and bottom core

core stratigraphy: cutting position, boundary layer, quality of ice/snow (ice/bubble diameter and its density, degree of depth hoar, distinction of firn/superimposed ice)

marking of cutting position (within 50cm) and core direction

image recording by digital video camera

↓

core cutting and packing

A: ECM -> packing (keep freeze)

B: packing (keep freeze)

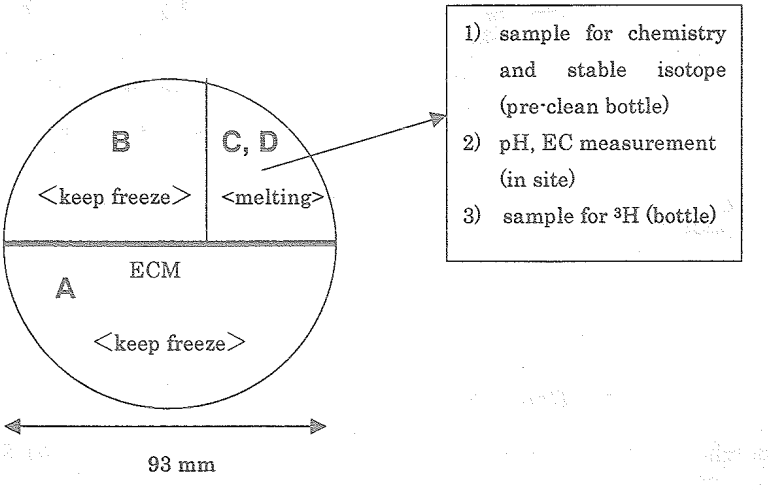
C: cleaning -> melting -> in bottle (keep freeze)

D: cleaning -> melting -> pH, electrical conductivity measurements

↓

transportation of samples to Tromsø Norway and Tokyo, Japan.

cutting plan



This document is provided by JAXA.

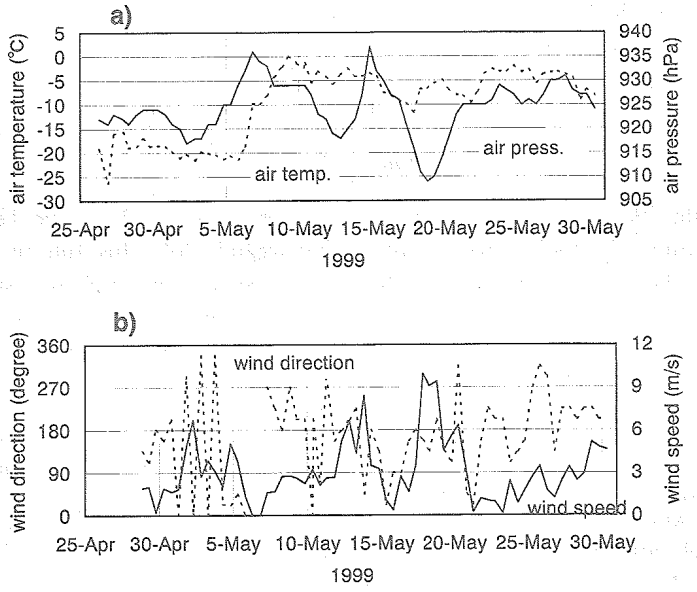


Fig. 5. Meteorological observations: a) air temperature and air pressure, b) wind speed and wind direction. Observations were conducted twice a day.

on the snow were sampled on occasion. The air up to 1 m above the snow surface was filtered using a cassette type collector with 4 filters. The aerosols were caught first by a 0.2 μm filter, and secondly the gas constituents in the air were caught by three alkaline filters. Air temperature (by portable thermometer), wind direction and wind speed (by portable anemometer), air pressure (by semiconductor type gauge), weather, cloud amount and type, and visibility were observed twice a day. Drifting and falling snow were sampled. Continuous air temperature and snow temperature near the snow surface were observed by automatic data recorders. The weather conditions are shown in Fig. 5. It is obvious that after May 7 the season quickly progressed into summer.

6. Participants

Principal Investigator in 1999 project:
Okitsugu Watanabe (National Institute of Polar Research)
Norwegian counterparts:
Elisabeth Isaksson (Norwegian Polar Institute)
Jon Ove Hagen (University of Oslo)
Field members
Field Leader: Hideaki Motoyama (National Institute of Polar Research)
Members: Makoto Igarashi (National Institute of Polar Research)
Tomoharu Nagasaki (Niigata University)
Morihiro Miyahara (Nihon Link Co. Ltd)
Tetsuhide Yamasaki (Independent polar explorer)

This document is provided by JAXA.

Lars Karlof (Norwegian Polar Institute)
Collaborator of the field operation:
Kumiko Goto-Azuma (National Institute of Polar Research)

Acknowledgments

We would like to express our sincere gratitude to Dr. Jon Ove Hagen and the ICEMASS group. The logistic section of the Norwegian Polar Institute in Longyearbyen supported our daily radio contact and flight schedule. This research was supported by a grant from the International Scientific Research Program of the Ministry of Education, Science, Sports and Culture (No. 10041130, PI O. Watanabe).

References

Arkhipov, S.A. and 11 colleagues (1987): Soviet glaciological investigations on Austfonna, Nordaustlandet, Svalbard in 1984–1985. Polar Geogr. Geol., **11**(1), 25–49.

Kamiyama, K., Motoyama, H. and Watanabe, O. (2001): Field observations of the Japanese Arctic Glaciological Expeditions in Svalbard from 1993 to 1995. Mem. Natl Inst. Polar Res., Spec. Issue, **54**, 243–251.

Takahashi, A. (1996): Development of a new shallow ice core drill. Seppyo (J. Jpn. Soc. Snow Ice), **58**, 29–37 (in Japanese).

Watanabe, O. (1996): Japanese glaciological activities in the Arctic region. Mem. Natl Inst. Polar Res., Spec. Issue, **51**, 329–336.

Watanabe, O. and Fujii, Y. (1988): Outline of the Japanese Arctic Glaciological Expedition in 1987. Bull. Glacier Res., **6**, 47–50.

Watanabe, O. and Fujii, Y. (1990): Outline of the Japanese Arctic Glaciological Expedition in 1989 (JAGE 1989). Bull. Glacier Res., **8**, 103–106.

Watanabe, O., Takahashi, S. and Kobayashi, S. (1993): Outline of the Japanese Arctic Glaciological Expedition (JAGE) in 1991–1992. Bull. Glacier Res., **11**, 63–67.

Watanabe, O., Kamiyama, K., Kameda, T., Takahashi, S. and Isaksson, E. (2000): Activities of the Japanese Arctic Glaciological Expedition in 1998 (JAGE 1998). Bull. Glacier Res., **17**, 31–35.

Zagorodnov, V. and Arkhipov, S. (1990): Studies of structure, composition and temperature regime of sheet glaciers of Svalbard and Severnaya Zemlya: method and outcomes. Bull. Glacier Res., **8**, 19–28.

(Received May 17, 2000; Revised manuscript accepted July 6, 2000)

This document is provided by JAXA.

Mem. Natl Inst. Polar Res., Spec. Issue, 54, 261-269, 2001

Scientific note

In-situ snow temperature monitoring at an Arctic tundra site: A comparison of manual and automatic measurements

Sebastian Gerland[1,2], Jan-Gunnar Winther[1] and Knut Sand[3]

[1]*Norwegian Polar Institute, Polar Environmental Centre, 9296 Tromsø, Norway*
[2]*present address: Norwegian Radiation Protection Authority, Polar Environmental Centre, 9296 Tromsø, Norway*
[3]*SINTEF Civil and Environmental Engineering, 7465 Trondheim, Norway*

Abstract: The physical properties of snow in the Arctic play an important role for the surface energy balance and Arctic biota. By measuring snow temperatures, the physical condition of the snowpack can be monitored. Conventionally, snow scientists measure snow temperature vs. depth in snow pits. An alternative to those destructive and time-consuming measurements is automated temperature logging using permanently installed sensors. At an Arctic research site on Svalbard we did both, manual and automatic snow temperature measurements. The measurements were performed before and after the onset of melt in May and June 1998, when various snow properties change quickly. Our results show that in the lower part of the snowpack, both datasets deviate usually not more than ±0.2℃. In the upper part of the snow pack, measurements are often distorted by solar radiation, especially after the onset of melt, once the snow is more transparent due to metamorphosis. When measuring in snow pits, shadowing the surface can reduce this effect. A substantial advantage of the automatic measurements is the better temporal resolution and the non-destructiveness. On the other hand, from manual snow-pit measurements, multi-parameter datasets in combination with sampling on regional scales can be collected.

1. Introduction

1.1. Motivation

The physical properties of snow in the Arctic environment play an important role for the surface energy balance. There are several reasons why scientists are interested in high-resolution snow-temperature data: Both the spatial and temporal distributions are directly connected with the energy balance at the atmosphere-soil interface. Regional changes in the thermodynamic properties of the snow may reflect climate-change processes and in parallel enable for prediction of them. Condition and changes of the snowpack can also affect the survival conditions for animals and plants, both those that depend on snow-free tundra and those depending on snow being present. Further, temperature data measured manually and automatically in snow are often required and used in snow models (*e.g.*, SNTHERM.89, Jordan, 1991). Whereas temperature measurements in deeper snow turned out to be less complex, near-surface measurements are especially affected by radiation influence/sensor heating and melt-water percolation.

This document is provided by JAXA.

1.2. History

Despite snow (pit) temperature measurements are a kind of a standard measurement within glaciology and snow hydrology, very little research focused so far on the technical problems when measuring temperature of snow near the surface. Automatic measurements using fixed sensors and data loggers are also exposed to possible errors. The aspect of stabilization of measurements after bringing temperature sensors into the snow environment was discussed by Seppälä (1992). The fact that solar radiation may lead to higher temperatures in the snow near the surface while air temperatures are further below 0℃ ("greenhouse effect") is known and investigated (*e.g.*, Brandt and Warren, 1993; Liston *et al.*, 1999).

1.3. Aims

In this study, we aim at evaluating and quantifying measurement errors connected to both automatic and manual snow-temperature measurements as well as pointing out advantages and disadvantages of both methods, using data from a field campaign near Ny-Ålesund on Svalbard (Gerland *et al.*, 1999, 2000; Winther *et al.*, 1999, 2001). Data from manual temperature measurements during spring 1998 are compared with automatic measurements obtained with a thermistor string, installed in the field before the beginning of snow fall in summer 1997. In spring, temperature can be expected to vary much both on a spatial and a time scale.

2. Location

The measurements were taken 2 km west of the settlement Ny-Ålesund in a flat tundra area near the river Bayelva and the hill Leirhaugen. Ny-Ålesund is located at about 79°N ashore Kongsfjorden on the northwestern side of the Svalbard archipelago (Fig. 1). Despite its high Arctic location, due to a branch of the Gulf Stream, the climate on the western coast of Svalbard is relative mild. Because this location is favourable in many respects (local infrastructure, logistics) also studies from related fields like hydrology and soil science are going on in the same area (Harding and Lloyd, 1997; Sand and Bruland, 1999; Roth *et al.*, 1998). The site starts to be covered with snow in fall (earliest September, latest December); the snow is melting in June. The snow thickness at the end of the accumulation season (end of May 1998) was about 0.65 m (including a *ca.* 10 cm thick basal ice layer).

3. Instruments and measurements

Manual snow-temperature measurements were made every 2 or 3 days in snow pits immediately after digging. For that we used a portable electronic thermometer (Digitron 3204, Digitron Instrumentation Ltd., Hertford, England) with a metal Pt100 sensor/needle probe (length 13 cm, diameter 3 mm). The product maker calibrated the sensor and refers to an absolute accuracy of ±0.2℃. The measurements were done by inserting the needle probe into the snow wall of the pit that is closer to the sun, avoiding that the solar radiation affects the wall directly. Readings were taken after approximately 10–20 s, when temperature recording had stabilised. The vertical spacing between individual measurements was usually 5 cm, near the surface less. The measurements were always started near the surface at the uppermost measurement location. During the near-surface measurements a 20 cm × 30 cm

This document is provided by JAXA.

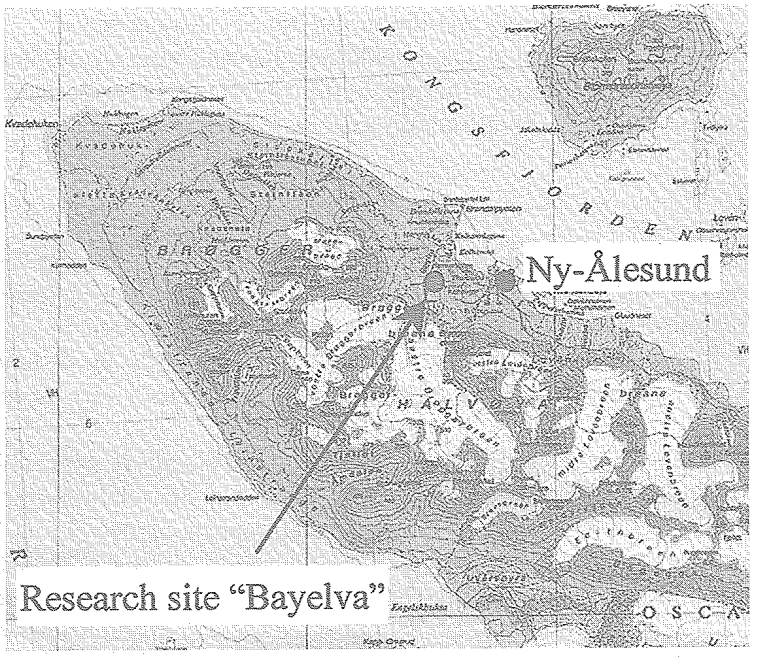


Fig. 1. Location map of research area. The research site located about 2 km west of Ny-Ålesund, Svalbard, it is marked by an arrow (map base: A7-Kongsfjorden, 1:100000, Norwegian Polar Institute, 1990).

plastic sheet was used to cover the surface above the measurement point in order to avoid direct heating of the sensor. As we intended to measure every time in pristine snow, we had to move the snow pit location slightly from day to day. Further, in order to keep the thermistor-string site operating and undisturbed, we had to dig the snowpits for the manual measurements in a distance of 10–20 m off that site. Due to locally varying snow covers, snow thicknesses for individual snow pits before beginning of melt varied by up to 10 cm.

Snow temperatures were measured automatically hourly with the help of a thermistor string (type TS-13ASV, Lakewood Systems Ltd., Edmonton, AB, Canada) and a data logger (type Lakewood R-X-16 data storing unit). The string was installed on a wooden stake during the snow-free season in 1997 with sensors placed at 0, 10, 25, 45 and 65 cm above the soil surface. Additionally, an air-temperature thermistor (type Lakewood R-XTP-5) was installed within a radiation shield at 2 m above the surface. The thermistors are placed within a plastic mantle (both outer length and diameter 2 cm, respectively), mounted on a cable (diameter 7 mm). The cable was fixed with cable ties directly to the stake, so that the sensors could not move relatively to the stake. In order to reduce heating by solar radiation, the cable and sensors were covered with white paint. The absolute accuracy of the thermistors after information of the producer is ± 0.4℃. Next to the thermistor string, an automatic ultrasonic snow-level sensor (type SR50, Campbell Scientific Ltd., Shepshed, United Kingdom) registered the level of the snow surface relative to the sensor mounting hourly. The data were stored on a Campbell CR500 data logger. With the help of these measurements, we were able to determine the snow thickness and the distance

This document is provided by JAXA.

between the individual thermistors and the surface for all measurements.

The two systems for manual and automatic measurements were not absolutely calibrated versus each other after purchase. However, in the context of this paper, the emphasis lays on the comparison of relative temperature variations with time and space.

4. Results

Manual temperature measurements in snow pits (Fig. 2) every other day show how the warm air heats the snow over time and how the snow temperature increases with time deeper into the snow pack. On 6 June 1998, temperature decreases more or less linear with depth, as it is typical for this location just before the onset of melt. By 14 June, the entire snow pack is in an isothermal condition. Surface-snow temperatures vary for different days only within 0.2°C.

The temperature time-series dataset measured with the thermistor string (Fig. 3a) gives only values at four different levels in the snow pack, but the relatively high temporal resolution shows the gradients with time at these levels more accurately. From 7 June 1998 onwards, the air temperature stayed more or less permanently above 0°C, therefore we took this date as the time of "onset of melt". This is about one week before snow temperatures reach the state of equi-temperature (Fig. 2). In the time series from automatic measurements (Fig. 3a), we further see the diurnal temperature variations in near-surface snow layers, which cannot be identified in our snow pit data (but are overlaid them). The sensor at 45 cm above soil surface shows these variations already before the onset of melt, whereas the sensors deeper in the snow are only affected for a short time between onset of melt and

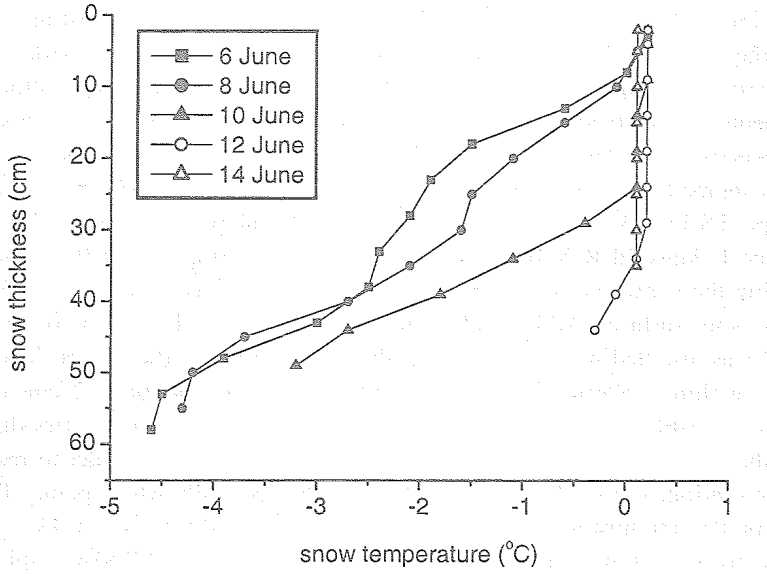


Fig. 2. Snow-pit temperatures from spring 1998, from 6 to 14 June 1998 every other day. The location of the snow pit was changed from one observation day to the next by a few metres in order to measure in pristine snow.

This document is provided by JAXA.

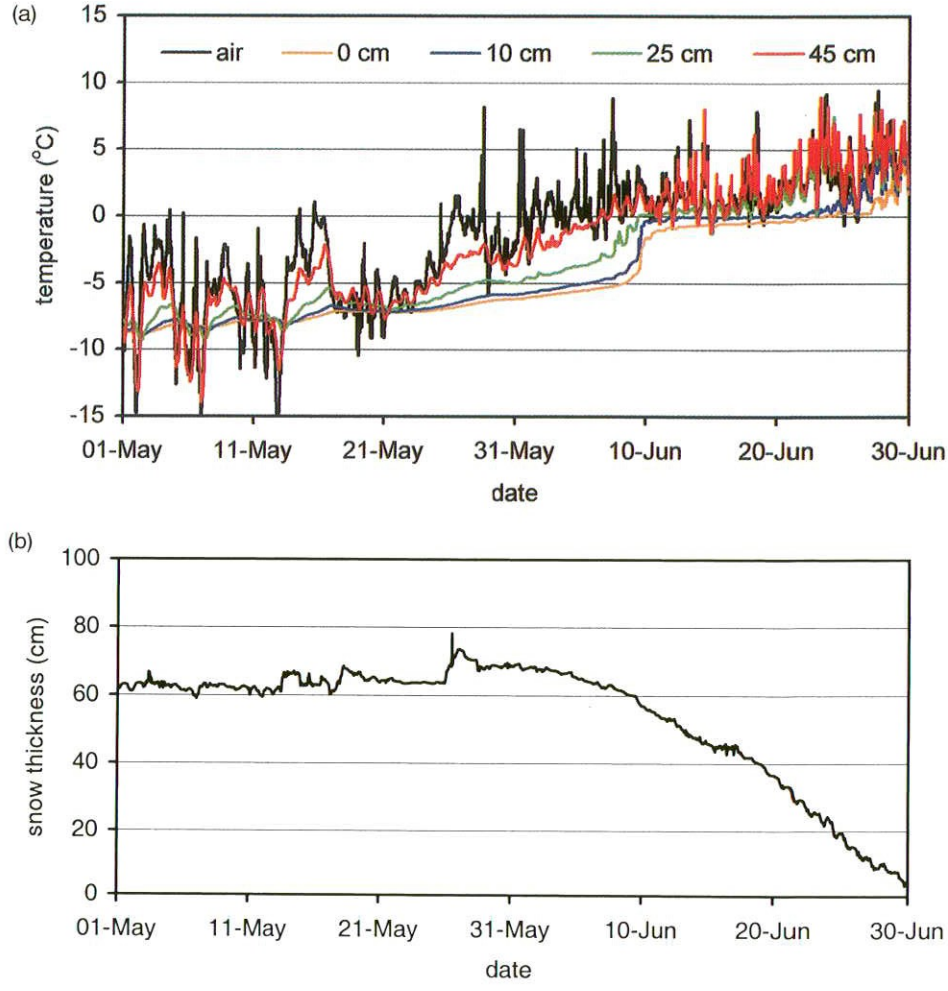


Fig. 3. Time series from spring 1998 with air temperature and thermistor-string data (a), and snow thickness (b). The snow thickness is calculated from automatic snow-level measurements next to the thermistor string.

temperature equilibrium. The development of snow thickness (Fig. 3b) shows a characteristic slope with decreasing snow thickness, after the melting has started. Further, gradual decreasing of snow-thicknesses after fresh snowfalls (settling, wind transport) is recognisable.

In Fig. 4 we show further manual measurements, here also from May, this time in order to compare them with automatic temperature logging.

5. Discussion

In-situ snow-temperature measurements can be disturbed by solar radiation and heat

This document is provided by JAXA.

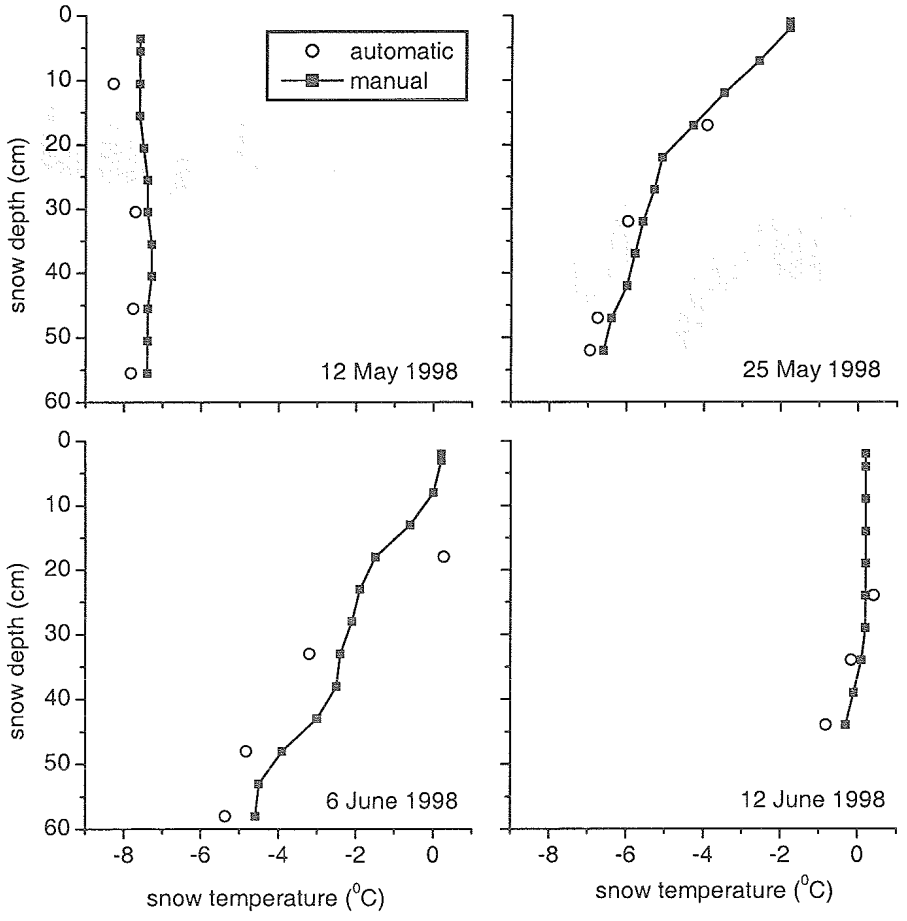


Fig. 4. Comparison of manual and automatic measurements (from 12 and 25 May, 6 and 12 June 1998). Where the snow thickness for pits and the thermistor-string spot varied slightly, depths were corrected linearly in order to be able to compare both datasets. Near-surface thermistors show higher temperatures than snow-pit data already before the onset of melt.

transport by migration of air or liquid water. In this research note, we want to focus most on the disturbances caused by solar radiation. Because of the plastic sheet used in connection with manual near-surface measurements, these readings are less affected by solar radiation. However, even with shadowing the snow above the sensor, manual measurements show systematically too high values (+0.2℃) near the surface; this could be due to scattered solar radiation, which reaches the needle probe from the sides, despite of the plastic sheet above. The sensors of the thermistor string are at all times exposed to potential heating by scattered solar radiation penetrating the snow. Accordingly, when comparing manual and automatic measurements (Fig. 4), the near-surface thermistors show higher temperatures than snowpit data for 25 May, 6 and 12 June 1998. The fact that this is not the case for our measurements on 12 May is probably connected to a lower sun angle and less transparent

This document is provided by JAXA.

snow earlier in the season (Gerland *et al.*, 2000). The increase of snow transparency during spring, connected to snow metamorphosis, is a known effect. Modelling and measurements showed that after the onset of melt, solar radiation in the Photosynthetically Active Radiation range (PAR, 400–700 nm wavelength) can exhibit still 5% of the surface intensity at 20 cm depth (Gerland *et al.*, 2000). The comparison of measurement from 12 June 1998 shows that the depth down to where automatic measurements were affected by scattered solar radiation was at least 25 cm. Before the onset of melt, solar radiation is attenuated to the 5%-level already at 10-cm depth. The offset of about 0.2℃ in absolute temperature at deeper levels (Fig. 4) might be either showing the limit of instrument calibrations and accuracy, or it is connected to scattering light from the snow-pit walls, penetrating the snow and heating the sensor.

Looking more in general on the heat balance at a temperature sensor within the snowpack, the situation can be described by the differential equation

$$C\frac{dT}{dt} = -k(T_m - T_s) + R,$$

with C as the heat capacity, T_m as the measured temperature at a certain time t, T_s as the snow temperature, k as the conductivity coefficient that is influenced by the coupling between the sensor and the surrounding snow, and R representing net radiation. The net radiation depends on incoming and reflected solar radiation, snow transparency, sensor depth, and sensor albedo. In theory, if the temperature measurements could be performed without radiation influence, the measured temperature would equal the snow temperature after a certain time (depending on k and difference between the initial sensor temperature and snow temperature). However, in reality the net radiation disturbs the measurements more or less. Sensor designs providing good thermal coupling to the surrounding snow and high sensor albedo in combination with a measurement setup with only little or reduced radiation influence will improve the measurement results.

From our comparison and the nature of the instrument setups of manual and automatic snow temperature measurements, we can summarise advantages and disadvantages (see also Table 1): An advantage of manual measurements is that the spatial resolution can be chosen as high as desired, disturbing effects from solar radiation can be partly excluded, and the snow layering is undisturbed from the setup. Further, parallel snow pit measurements of other physical and structural snow properties may ease the interpretation of the data measured. On the other hand, a plus of automatic measurements is that they are

Table 1. Advantages (+) and disadvantages (−) of manual and automatic snow temperature measurements.

Aspect	Manual measurement	Automatic measurement
Time resolution	−	++
Depth resolution	++	+
Areal resolution	+	−
Destructiveness	−−	+
Solar rad. disturbance	−	−−
Time and manpower	−	+

This document is provided by JAXA.

non-destructive, and therefore measurements are possible at exactly the same location over longer times. Automatic measurements enable further to measure snow temperatures at high resolution in time, such that diurnal changes and fast temperature changes can be recorded and investigated. Substantial disadvantages of automatic measurements are the possible effects of solar radiation, especially near the surface, and possible heat and water transport along the string cable. The thermistor string setup itself might also disturb and alter the snow layering and melting. Areal measurements comparable to regional snow-pit studies are usually limited because of logistic and financial reasons, which do not allow to install as many thermistor strings in one area as desired. Manual measurements on the other hand require more time and manpower and their destructiveness set limits for certain monitoring studies. The experiments further showed that also snow-pit measurements are affected by solar radiation. A major disadvantage of manual snow temperature measurements in pits is the low temporal resolution. The "snapshot" character of the data hides diurnal and weather-dependent temperature variations (*e.g.*, cooling at night, warming during day). Possible misinterpretation can only be avoided by having time series with high temporal resolution.

6. Conclusions

In the lower part of the snowpack, automatic measurements with hourly time resolution reproduce snow temperatures above Arctic tundra in general well, as it could be confirmed by snow pit reference measurements. However, especially near the surface, manual and automatic measurements of snow temperature may contain inaccuracies caused by different error sources (*e.g.*, sensor heating by solar radiation, distortions by the measurement setup). It is not possible to conclude that one method consistently is more accurate than the other. The biggest advantage of automatic measurements is the high temporal resolution, which makes this method suitable for long-term monitoring studies, and which resolves fast, diurnal temperature changes. On the other hand, within surveys over larger areas in order to cover spatial variations of snow parameters, manual measurements are usually the only affordable option. Further, snow-pit studies enable snow scientists to do *in-situ* multi-parameter studies including sampling and subsequent sample analysis.

If one wants to minimise the disadvantages of each method, a combined use of automatic and manual measurements is optimal. For example, a few automatic sites could help within a regional study to correct snow-pit data for daily temperature variations, or snow-pit surveys could be used to correct near-surface thermistor-string temperature data for solar-radiation influence. While using thermistor strings for snow temperature monitoring in remote areas, simultaneous automatic snow-thickness measurements help to define the distance between individual sensors and the snow surface. This information is necessary to evaluate logged temperature data for possible errors connected with solar radiation.

Acknowledgments

We thank the personnel of the research station of the Norwegian Polar Institute (NP) in Ny-Ålesund (Sverdrup Station), namely Lars-Edin Svaasand and Stefan Claes for

This document is provided by JAXA.

maintaining the automatic logger equipment throughout the year. We are grateful to Julia Boike (Alfred Wegener Institute for Polar and Marine Research, Germany) and Boris Ivanov (Arctic and Antarctic Research Institute, Russia) for helping in performing the manual temperature measurements. Constructive criticism by an anonymous reviewer is gratefully acknowledged. The preparation of this manuscript was supported through the NATO Collaborative Linkage Grant No. EST.CLG.975781. This study was funded through the Norwegian Research Council (NFR) and NP and was performed within a project in the NFR-ALV (Arctic Light and Heat) programme.

References

Brandt, R.E. and Warren, S.G. (1993): Solar-heating rates and temperature profiles in Antarctic snow and ice. J. Glaciol., **39**, 99–110.

Gerland, S., Winther, J-G., Ørbæk, J.B., Liston, G.E., Øritsland, N.A., Blanco, A. and Ivanov, B. (1999): Physical and optical properties of snow covering Arctic tundra on Svalbard. Hydrol. Processes, **13**, 2331–2343.

Gerland, S., Liston, G.E., Winther, J-G., Ørbæk, J.B. and Ivanov, B.V. (2000): Attenuation of solar radiation in Arctic snow: field observations and modelling. Ann. Glaciol., **31**, 364–368.

Harding, R.J. and Lloyd, C.R. (1997): Measurements of water and energy fluxes from a high latitude tundra site in Svalbard. Proc. 11th Int. Northern Research Basins Symposium and Workshop, Alaska, The Water and Environmental Research Centre, University of Alaska, Fairbanks, 73–93.

Jordan, R. (1991): A one-dimensional temperature model for a snow cover—technical documentation for SNTHERM.89. CRREL Spec. Rep., **91-16**, 50 p.

Liston, G.E., Winther, J-G., Bruland, O., Elvehøy, H. and Sand, K. (1999): Below-surface ice-melt on the coastal Antarctic ice sheet. J. Glaciol., **45**, 273–285.

Roth, K., Boike, J., Gerland, S. and Kopsch, C. (1998): Spatial and seasonal variations of liquid water content in snow and permafrost soils using time domain reflectometry. Abstract, Supplement to Eos Transactions, **79**, 269.

Sand, K. and Bruland, O. (1999): Water balance of three high Arctic river basins in Svalbard. Proc. 12th Int. Northern Research Basins Symposium and Workshop, Iceland, Engineering Research Inst., University of Iceland, 270–283.

Seppälä, M. (1992): Stabilization of snow temperature in Dronning Maud Land, Antarctica, January 1989. Geogr. Ann., **74A**, 227–230.

Winther, J-G., Gerland, S., Ørbæk, J.B., Ivanov, B., Blanco, A. and Boike, J. (1999): Spectral reflectance of melting snow in a high Arctic watershed on Svalbard: some implications for optical satellite remote sensing studies. Hydrol. Processes, **13**, 2033–2049.

Winther, J-G., Gerland, S., Ørbæk, J.B., Ivanov, B., Zachek, A.S. and Bezgreshnov, A.M., (2001): Effects on spectral reflectance from snow ageing. Mem. Natl Inst. Polar Res., Spec. Issue, **54**, 193–201.

(Received April 3, 2000; Revised manuscript accepted September 18, 2000)

This document is provided by JAXA.

This document is provided by JAXA.

Mem. Natl Inst. Polar Res., Spec. Issue, 54, 271–278, 2001

Scientific note

The geochemical phenomenon—Local geochemical fields in a glacier

V. N. Makarov

Permafrost Institute, Siberian Branch, Russian Academy of Sciences, Yakutsk, Russia

Abstract: Geochemical fields in alpine cold and warm glaciers were studied. Local geochemical fields of typomorphic elements were found to form in the ice and on the surface of glaciers overlying ore bodies and endogenic geochemical haloes. The formation of local cryogenic geochemical fields in the glaciers results from sharp geochemical heterogeneity and geochemical processes in underlying rocks which cause cryogenic migration of chemical elements and compounds in the glacier. The thickness of geochemical fields, (134 m) is limited by ice thickness in the studied glaciers.

1. Introduction

It is believed that the chemical composition of glaciers is controlled by regional factors and reflects changes in the environment and atmosphere throughout the existence of glacier ice, and the material accumulated in a glacier changes very little after its deposition due to low temperature. Studies conducted by the author in alpine glaciers of the Tien-Shan indicate the existence of local geochemical fields, whose formation is caused by geochemical maxima in underlying rocks, in alpine glaciers.

2. Methodology

The chemical composition of rocks, glacier ice, snow cover and natural water was studied. Ice samples were obtained from the surfaces of glaciers and boreholes drilled through the glaciers. A wide range of chemical elements was analyzed in the samples using quantitative spectrometry and atom-adsorption methods. For gold determination, a flameless atomizer mounted on a Perkin-Elmer-603 spectrophotometer was used.

3. Results

Mountain glaciers accumulate and hold atmospheric moisture as firn ice for a considerable time; they represent a unique source of information on changes in the chemical content of the atmosphere. It is believed that precipitated material accumulated in the glaciers does not change significantly from the moment of its fall due to low temperatures (Langway, 1970; Kotlyakov and Gordienko, 1982). Our investigations conducted in the glaciers of the Tien-Shan enable us to establish the existence of local geochemical fields, the

This document is provided by JAXA.

formation of which is not related to global climatic factors.

The formation of local geochemical fields in the glaciers results from the sharp geochemical heterogeneity and the geochemical processes occurring in underlying rocks. These geochemical processes cause migration of chemical elements and compounds within ice and snow layers. In the glaciers, migration of chemical elements occurs as ion diffusion along liquid pellicles covering ice and snow crystals at temperatures below or close to 0℃ (Fletcher, 1962; Kvlividse *et al.*, 1978; Makarov *et al.*, 1990). Cryogeochemical fields have been detected in glaciers of different types: in valley and hanging glaciers, in warm and cold glaciers.

Local geochemical fields have qualitative (chemical elements and their compounds) and quantitative (concentration of elements, parameters of geochemical fields) characteristics, which depend on the geochemical peculiarities of underlying rocks. These characteristics exhibit regular patterns within the glacier.

Geochemical fields were studied in alpine cold and warm glaciers situated at 4000–5000 m elevation. Cold glaciers are underlain by rocks with negative temperature. The frozen stratum consists of two layers, the upper layer being the glacier, and the lower one being the bedrock. Warm glaciers rest on positive-temperature rocks. The temperature profile of the glaciers consists of an upper 10–15 m zone with temperatures of 4–5℃ below zero, a middle zone down to a depth of 25–30 m with sharply increasing temperatures up to 1–0.6℃ below zero, and a lower zone extending to the glacier bed with a zero-gradient 0℃ isothermal curve.

Geochemical fields are discussed below for the example of Lysyi Glacier. It is a hanging glacier located at 4050–4200 elevation. The maximum ice thickness at the study site is 60 m. Thermometric measurements in holes drilled through the glacier show that the ice temperature varies from −6℃ at the surface to −2.5℃ in the bottom layer.

The glacier overlies an ore body of a gold-tungsten deposit over a length of about 300 m. An adit was made in the glacier (4070 m level). The ice was studied at the contact with and at several distances from underlying rocks. The rocks are ore metasomatites. The glacier bottom is at 4050 m elevation in its deepest part. The content of microelements in the ice at the ice-rock contact is a few tens times higher than the background chemical concentrations in the glacier (Table 1).

The maximum concentration of elements in the geochemical halo occurs at the immediate contact with metasomatites and decreases in the series (in parentheses are degrees of contrast of the anomalies, i.e. the ratio of anomalous concentrations to background values): Cu(80)–Zn(30)–W(20)–Au, Cr(10)–Ag, Sn(7)–V(5)–Mo, Pb(3). There is a clear relationship between the concentration of chemical elements in the ice contacting the rocks and the concentration of ore elements in the ores.

Concentrations of the elements typomorphic for the ore body and endogenic halos gradually decrease in the glacier with increasing distance from the ore zone (Table 2). Within 50–60 m (the glacier thickness) concentrations of heavy metals decrease nonuniformly in the series: Zn(60)–Cu(40)–W(10)–Au, Ag, Sn, Pb, Be(5)–Mn, Mo(4)–Cu, Ni(2). The most abrupt decreases occur in the concentrations of zinc, copper and tungsten. The least contrasting changes are characteristic of cobalt and nickel, whose concentrations decrease two-fold.

Concentrations of Be, Pb and Sn in the glacier decrease steadily, already reaching

This document is provided by JAXA.

Table 1. Content of components in the glacier at the contact with rocks.

Components	Ore*	Ice				Ore*	Lysyi Glacier ice, Background values, N=28**
Distance between samples, m		0.3	35	25	15		
pH	7.9	7.4	7	6.9	7.1	7.75	7.3
Eh, mV	467	470	490	510	505	405	502
Mineralization, mg/*l*	0.027	40.6	35.6	35.1	38.2	0.020	49
Ca^{++}, mg/*l*	0.236	9.5	5.3	5.3	4.2	0.194	5.3
Mg^{++}, mg/*l*	0.095	0.6	1.9	0.3	1.3	0.112	1.6
$Na+K^{+}$, mg/*l*	0.161	4.8	4.0	7.9	7.8	0.100	6.2
NCO^{-}_{3}, mg/*l*	0.305	30.8	21.6	21.6	18.5	0.249	24.0
Cl^{-}, mg/*l*	0.020	3.3	3.7	3.3	3.3	0.018	4.1
$SO^{=}_{4}$, mg/*l*	0.167	6.6	6.6	7.8	12.3	0.139	9.6
Au, $10^{-3}\mu g/l$	1000	14	2	2	1	60	1.4
W, $\mu g/l$	200	20	15	10	15	20	1
Ag, $\mu g/l$	1.5	0.2	0.03	0.03	0.07	0.5	0.03
Mo, $\mu g/l$	7	7	2	2	5	10	2
Pb, $\mu g/l$	20	5	2	2	3	15	1.4
Sn, $\mu g/l$	5	3	2	2	3	2	0.4
Zn, $\mu g/l$	50	300	200	10	200	15	10
Cu, $\mu g/l$	500	150	150	100	50	20	1.8
Cr, $\mu g/l$	50	30	30	15	7	50	3
V, $\mu g/l$	200	20	5	5	10	30	4

Notes: *concentration of microelements in ore-g/t, Au-mg/t. **N=28-number of samples.

background values at a distance of 35 m from the ore body, while Mn concentration, even at the glacier surface, remains five times higher than the background value. Concentrations of Zn, Cu and W decrease slightly within the first twenty meters from the glacier bottom, then decrease sharply near the surface. The reverse distribution is characteristic of gold and molybdenum, although their concentrations at the glacier surface are still higher than the background concentrations. The redox potential decreases with depth from 505 to 470 mV (specific Eh value is 0.3–1.1 mV/m).

Anomalies of indicator-elements of gold ore mineralization in the glacier form above both the ore body and the primary haloes, reflecting the composition of endogenic mineralization (Fig. 1).

The distribution of chemical elements along the glacier surface is also nonuniform. Anomalies of gold, zinc, copper, tungsten and chromium at the glacier surface occur above the ore body with practically no shift (Fig. 2). Negative anomalies above the ore zone are formed by sulfates and Eh values. Some indicator-elements (Ag, Sn, Pb, Zn, Sc, Be) form more contrasting anomalies at the glacier surface above the north-eastern part of the ore body. These anomalies coincide with the enriched sections of the ore body where concentrations of heavy metals increase 2–5-fold.

Thus, superimposed haloes of indicator-elements form in the glacier overlying the ore body. The composition of the superimposed haloes corresponds to those of the ore body

This document is provided by JAXA.

Table 2. Variation in chemical composition of ice with depth, Lysyi Glacier.

Component	Measurement unit	Depth		
		Surface	30 m	50 m
Elevation a.s.l.	m	4100	4070	4050
PH		7.2	6.95	7.45
Eh	mV	510	500	470
Mineralization	mg/*l*	32.4	33.9	40.6
Ca	mg/*l*	4.7	5.3	9.5
Mg	mg/*l*	1.6	0.95	0.6
Na+K	mg/*l*	5.0	5.9	4.8
Fe^{3+}	mg/*l*	0.3	0.25	0.3
NH_4	mg/*l*	0.2	1.0	0.1
HCO_3	mg/*l*	21.5	21.6	30.8
SO_4	mg/*l*	6.6	7.2	6.6
Cl	mg/*l*	3.3	3.5	3.3
NO_2	mg/*l*	0.01	1.0	0.01
Au	10^{-3} μg/*l*	1.75	2.0	14.0
W	μg/*l*	2	12.5	20
Mo	μg/*l*	2	2	7
Ag	μg/*l*	0.05	0.05	0.2
Cu	μg/*l*	4	125	150
Pb	μg/*l*	1	2	5
Zn	μg/*l*	15	100	250
Sn	μg/*l*	0.5	2	3
Cr	μg/*l*	1	22	18
Be	μg/*l*	0.06	0.18	0.30
Mn	μg/*l*	150	450	600
Co	μg/*l*	1.5	1.5	3
Ni	μg/*l*	3	6	7.5

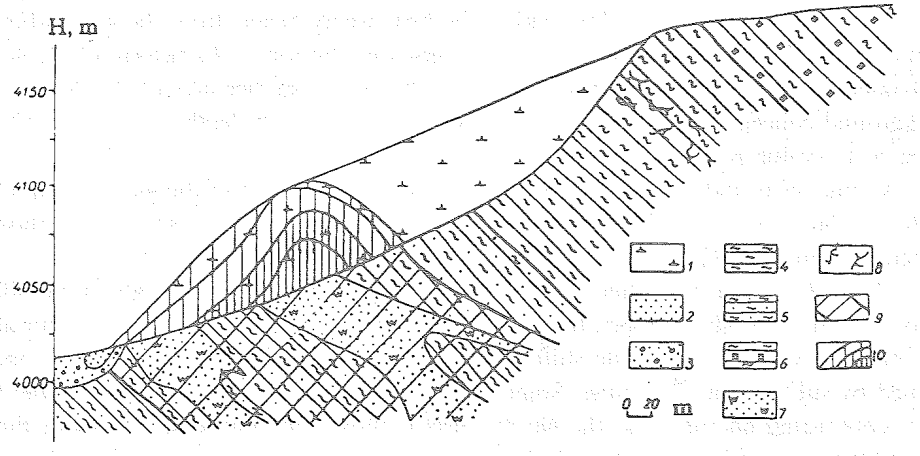


Fig. 1. The geochemical field above the ore zone and the endogenic halo.
1-ice; 2-sand; 3-gravel; 4-shale; 5-sandstone; 6-limestone; 7-ore body; 8-shatter zone; 9-endogenic halo; 10-geochemical field in the ice (spacing in cross-hatch shows the degree of contrast of the geochemical field).

This document is provided by JAXA.

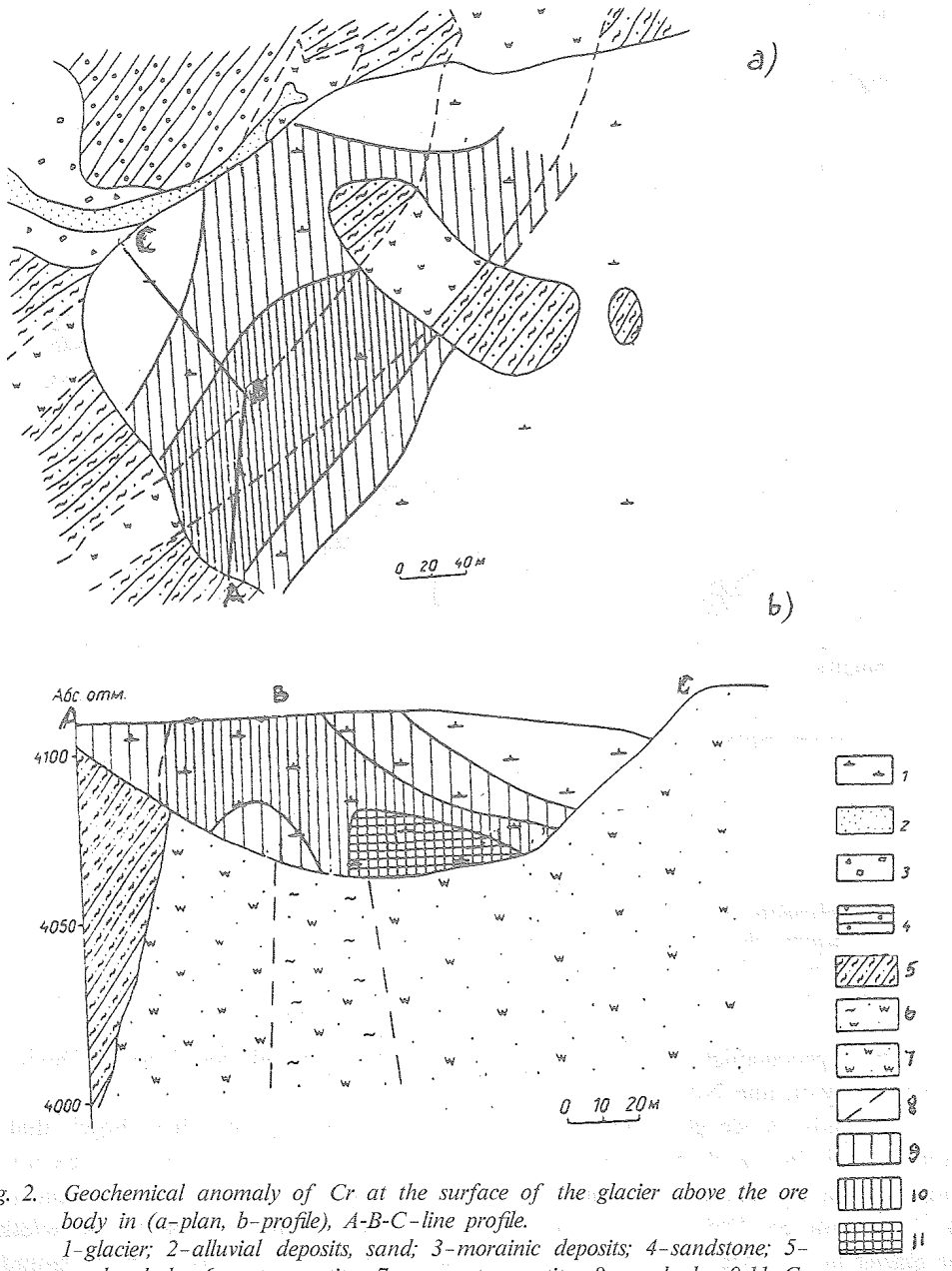


Fig. 2. Geochemical anomaly of Cr at the surface of the glacier above the ore body in (a-plan, b-profile), A-B-C-line profile.
1-glacier; 2-alluvial deposits, sand; 3-morainic deposits; 4-sandstone; 5-sandy shale; 6-metasomatite; 7-ore metasomatite; 8-ore body; 9-11-Cr concentration on the glacier surface, μg/l: 9-3-10, 10-10-20, 11-20-30.

and the endogenic halo. More contrasting geochemical anomalies form in the glacier above the greater enriched sections of the ore body (see Figs. 1 and 2). The vertical range of migration of indicator-elements (Au, W, Pb, Cr, Cu) and, correspondingly, the thickness of the superimposed halo in Lysyi Glacier is 50–60 m.

This document is provided by JAXA.

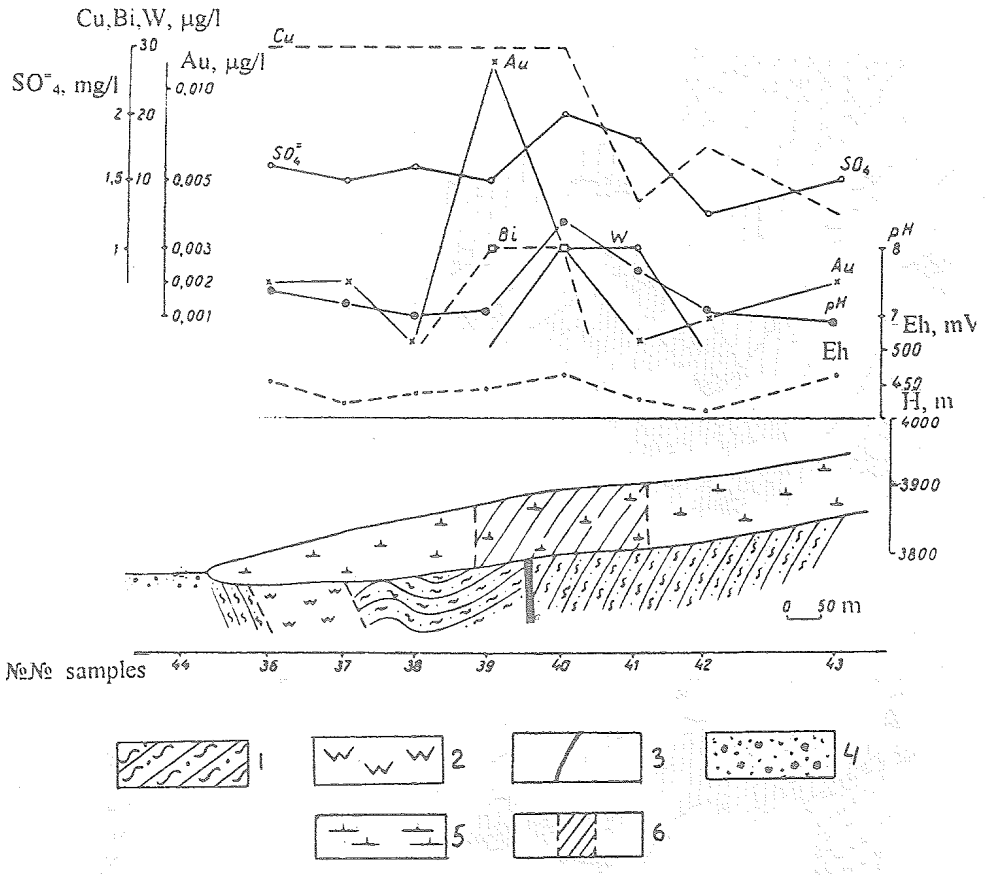


Fig. 3. Geochemical profile along the surface of Boordu Glacier above the ore zone. 1-metamorphic shale; 2-metasomatic rock; 3-ore metasomatite; 4-sandy shale; 5-glacier; 6-cryogenic halo.

Similar geochemical studies were also carried out in other glaciers: Boordu, Davidova, Petrova, Sarytor, and No. 121.

The study of ice geochemistry at the Boordu Glacier surface has shown that an anomaly of indicator-elements exists in the lower part of the glacier tongue. The complex anomaly (Au, Bi, W, $SO^{=}_4$) is located above the conjectured extension of the ore zone (Fig. 3). Contrasting geochemical anomalies were also found in Davidov Glacier. The width of the glacier in its lower part is 0.8–0.9 km; the ice thickness determined by radio sounding is up to 134 m with an average of 75 m. According to thermometric measurements, the ice has a temperature of −6℃ at a depth of 5 m and is near the melting point below 30 m depth. The depth range of 40 to 109 m is filled with pressure melt water; the ice temperature here is not lower than −0.5℃. A near-bottom layer of warm, water-containing (1–2% by volume) ice probably exists in the middle and upper parts of the glacier tongue.

The glacier tongue in its middle and upper parts has fissures and is divided longitudinally by a medial moraine into two branches. These branches differ in activity. The

This document is provided by JAXA.

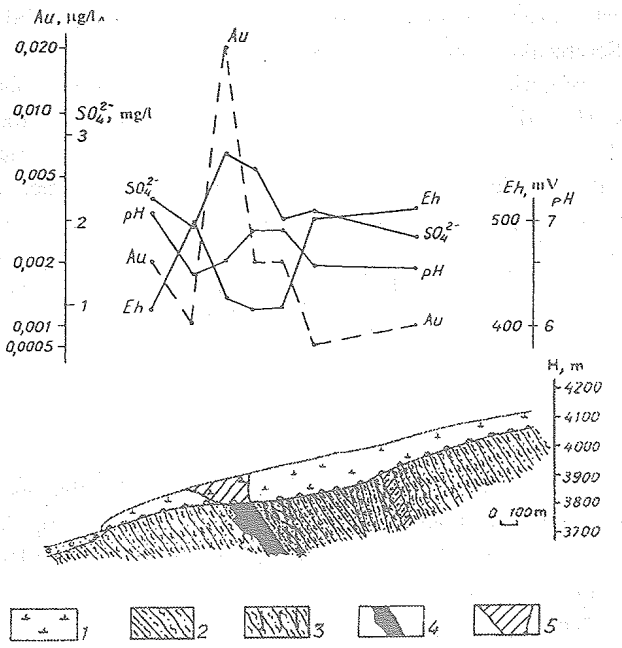


Fig. 4. Geochemical profile along the surface of Davidov Glacier above the ore zone. 1-glacier; 2-sandy shale; 3-metamorphic shale; 4-ore metasomatite; 5-cryogenic halo.

movement rate of the surface of the right branch in summer is 1-2 cm/day; the left branch is more active, moving at 1-4 cm/day. The angle of slope of the tongue is 5-6°. Down the glacier there is a large outwash plain between the tongue and the terminal ridge of the 80-90-m-high moraine.

The glacier is asymmetrical in cross section, with its ice thickening towards the left margin. The bottom layer of the glacier consists of ice containing a relatively large amount of morainic debris a few meters to 11 m in thickness. The upper layer consists of relatively clean ice.

Distinct geochemical anomalies of the elements typomorphic for the ore body and endogenic halo (Au, W, Pb, Cr, Cu, Sn) exist at the glacier surface. The contrast of anomalies decreases in the series: Au(20)-Pb(5)-Cr, Cu, Mo(3)-W, Sn(2). The geochemical haloes are located within the projection of the ore zone onto the glacier surface. The anomalies extend over a length of 150-200 m in the direction of glacier movement (Fig. 4).

It is known that the chemical composition of glaciers is controlled by regional factors and reflects changes in the environment and atmosphere throughout the existence of glacier ice, and the material accumulated in a glacier changes very little after its deposition, due to low temperature. Our studies indicate the existence of local geochemical fields in alpine glaciers whose formation is caused by geochemical maxima in underlying rocks, and is not dependent on regional climatic factors.

The rate of formation of geochemical fields in glaciers is of great interest. It is known that the movement rate of large glaciers in the Tien-Shan is 40 to 130 m/yr. Glaciologists estimate that the full mass cycle in glaciers of the inner Central Tien-Shan occurs within 450-900 years. Glaciers on flat mountain tops with the slowest mass circulation bear

This document is provided by JAXA.

evidence of far earlier events. They may contain ice layers which formed as much as 1500–2000 years ago (Serebriakov and Orlov, 1988).

Therefore the migration rate of chemical elements forming geochemical fields at the surfaces of glaciers should be no less than 10 cm/yr for a cold glacier located on a flat top and more than 40 cm/yr for a warm valley glacier. Only at these rates of sub-vertical migration would geochemical fields form on the surface of a glacier, at least within its tongue. However, actual geochemical fields on the surfaces of glaciers are only slightly shifted in the direction of glacier movement. The high formation rates and the morphology of geochemical fields, as well as the distribution of positive and negative ions in the ice on the glacier surface, are adequately explained by the electrochemical model of geochemical field formation (Sato and Mooney, 1960; Semenov, 1955).

4. Conclusions

The formation of local cryogenic geochemical fields in the glaciers results from sharp geochemical heterogeneity and geochemical processes in underlying rocks which cause cryogenic migration of chemical elements and compounds in the glacier. Migration of chemical elements occurs as ion diffusion along liquid-like films enveloping ice crystals. Cryogenic geochemical fields have been detected in glaciers of different types (valley and hanging; warm and relatively cold).

Cryogenic geochemical fields have qualitative (chemical elements and compounds) and quantitative (concentration of elements, extension of haloes) characteristics distributed regularly within the glacier and on its surface. Theoretically, their vertical range may reach hundreds of meters; the measured thickness is limited by ice thickness in the studied glaciers, *i.e.* 134 m. The composition of geochemical fields depends on the geochemistry of underlying rocks.

When studying glaciers for paleoclimatic reconstruction and quantitative assessment of substance input, account must be taken of their geochemical heterogeneity related to the existence of local geochemical fields.

References

Fletcher, N.H. (1962): Surface structure of water and ice. Philos. Mag., **7**, 255 p.

Kotlyakov, V.M. and Gordienko, F.G. (1982): Izotopnaya i Geochimicheskya Glaciologia. Gidrometeoizdat, Leningrad, 288 p.

Kvlividse, V.I., Kiselev, V.F., Krasnushkin, A.V. *et al.* (1978): An NMR study of the phase transition of water in models and in frozen clays. Proc. Third Inter. Cond. on Permafrost. Edmonton, Alberta, Canada, Vol. **1**, 113 p.

Langway, C.C. (1970): Stratigraphic Analysis of a Deep Ice Core from Greenland. Boulder, Geol. Soc. Am., 186 p. (Spec. Paper, Geol. Soc. Am. **125–170**).

Makarov, V.N., Fedoseev, N.F. and Fedoseeva, V.I. (1990): Geokhimia Snezhnogo Pokrova Iakutii. Yakutsk, IMZ SO AN SSSR, 152 p.

Sato, M. and Mooney, H.M. (1960): The electrochemical mechanism of sulfide selfpotentions. Geophysics, **25**, 226–249.

Semenov, A.S. (1955): Electrorasvedka Metodom Estestvennogo Elektricheskogo Pola. Leningrad, 446 p.

Serebriakov, L.R. and Orlov, A.V. (1988): Tian-Shan Glasamy Glaciologa. Moskva, Nauka, 144 p.

(Received May 19, 2000; Revised manuscript accepted November 24, 2000)

This document is provided by JAXA.

Mem. Natl Inst. Polar Res., Spec. Issue, 54, 279-290, 2001

Scientific paper

Determination of ice flow velocity in Svalbard from ERS-1 interferometric observations

Bernard Lefauconnier[1,2], Didier Massonnet[3] and Geir Anker[1]

[1]*Norsk Polarinstitutt, Tromsø, Norway*
[2]*University of Silesia, Poland*
[3]*CNES, Toulouse, France*

Abstract: Based on ERS-1 data recorded in autumn 1991, differential interferogrammes have allowed the determination of the ice flow of north-west Spitsbergen glaciers.

The highest velocity of the d'Arodesbreen and the Fjortendejulibreen, observed in their equilibrium zone, was 3 cm and 6.6 cm per day, respectively. The large Kronebreen (700 km^2) is fed by two plateaux, Isachsenfonna and Holtedahlfonna. Along the longitudinal axis of Isachsenfonna, the velocity was near constant, around 20 cm per day over a distance of 20 km, while the velocity on Holtedahlfonna increased from near zero in the higher basin to 52 cm per day at 15 km to the calving front. The obtained velocities were in excess of 48% of the annual average velocity measured by GPS at three locations. Interferometric pairs were obtained at the end of the ablation period when the presence of subglacial meltwater can still lead a high velocity.

These relatively high rates of velocity indicate that the basal sliding of Isachsenfonna and Holtedahlfonna is important and that the glacier sole must be at the melting point down to the front. The present temperature distribution in the glacier is still possibly influenced by a surge, which occurred 130 years ago.

1. Introduction

After Goldstein *et al.* (1993) applications of INSAR techniques for glacier monitoring have been described and demonstrated in a number of papers. As examples, Rignot *et al.* (1996) who presented an overview of the literature have retrieved the surface topography and ice velocity over a large ice field from SIR-C data and, by using ERS-1 and ERS-2 tandem missions, determination of the ice velocity over an Alpine glacier has been obtained by Karim *et al.* (1998).

Sixty per cent of the Svalbard archipelago is covered by glaciers, which represent in total an area of about 40000 sq. km (Hagen *et al.*, 1993). For a high number of cirque glaciers, the ice flow fall in a range between zero and 30 m per year. Such velocities are also encountered in the accumulation area of ice caps, while their outlets can flow at several tens of centimetres per day in summer time. It could be estimated that 60 to 70% of the glacier surface in Svalbard is possibly subjected to such a velocity range, which is also the range of expected detection from INSAR techniques applied on ERS-1 data.

Based on data from ERS-1, clear fringes were firstly obtained over a high number of

This document is provided by JAXA.

glaciers in Svalbard and an analysis of the images of coherence has made it possible to delimitate ice stream boundaries, to discriminate between slow and fast ice motion and to detect surging glaciers (Lefauconnier *et al.*, 1994a). By geodetic methods, a mean velocity of between 2 and 2.15 m per day with peak of 4.50 m per day at the beginning of July was measured at the calving front of Kronebreen by Voigt (1965) and Lefauconnier *et al.* (1994b). A similar result has recently been obtained by using the tandem ERS1–ERS2 (Eldhuset *et al.*, 2000). Also from tandem data, maximum velocities over three glaciers have been estimated by Wangensteen and Weydahl (1999).

From interferogrammes based on ERS-1 data obtained along a single track combined with the use of an accurate DEM and of an ice flow model, ice velocity fields have been obtained over three glaciers (Lefauconnier *et al.*, 1996a, b). The aim of the present paper is to present briefly this work, to validate the results by ground control and discuss the findings in a glaciological context.

2. Surveyed site

This area is one with a mostly alpine type relief comprised of terrain between 0 and 1400 m a.s.l. and numerous glaciers and ice fields from a few km^2 up to 1000 km^2 in extent, some of which have a calving front.

2.1. D'Arodesbreen and Fjortendejulibreen

The d'Arodesbreen (79°09′N and 12°04′E, Fig. 1) is a valley glacier, mainly facing the satellite look. The area of the glacier basin is of 16 km^2 and the length 10 km. This glacier is well individualised without any tributary. The glacier top reaches 750 m a.s.l, surrounding mountains culminate at 980 m a.s.l. The Fjortendejulibreen (79°07′N and 12°13′E, Fig. 1), is a calving glacier, which also mainly faces the satellite look. Its area is 81 km^2 and its length 18 km. Its head is partly fed by the Isachsenfonna around 900 m a.s.l. and surrounding mountains culminate at 1300 m a.s.l.

2.2. Kronebreen (Isachsenfonna and Holtedahlfonna)

The Kronebreen, (78°58′N, 13°11′E, Fig. 1) is the most active glacier in Svalbard. Its calving front is about 4 km wide and the central part, with many crevasses is moving close to 800 m per year (Lefauconnier *et al.*, 1994b). The main outlet is fed by two "fonna" (accumulation plateau): Isachsenfonna with a top above 900 m a.s.l. and Holtedahlfonna at 650 m but which is partly supplied by another fonna culminating at 1200 m. The total area is about 700 km^2, with a maximum length of 43 km. The net accumulation over the fonna together with the narrowing of the outlet and the buoyancy at the front causes an increase in velocity and high flow speed at the front, which will be discussed below. The flow of Holtedahlfonna is facing the satellite look while the flow of Isachsenfonna, which is also facing the satellite look in its higher basin, turn then to an angle of 30° toward the satellite sight. Over the two basins, the surveyed zone presents a slope average of less than 2°.

This document is provided by JAXA.

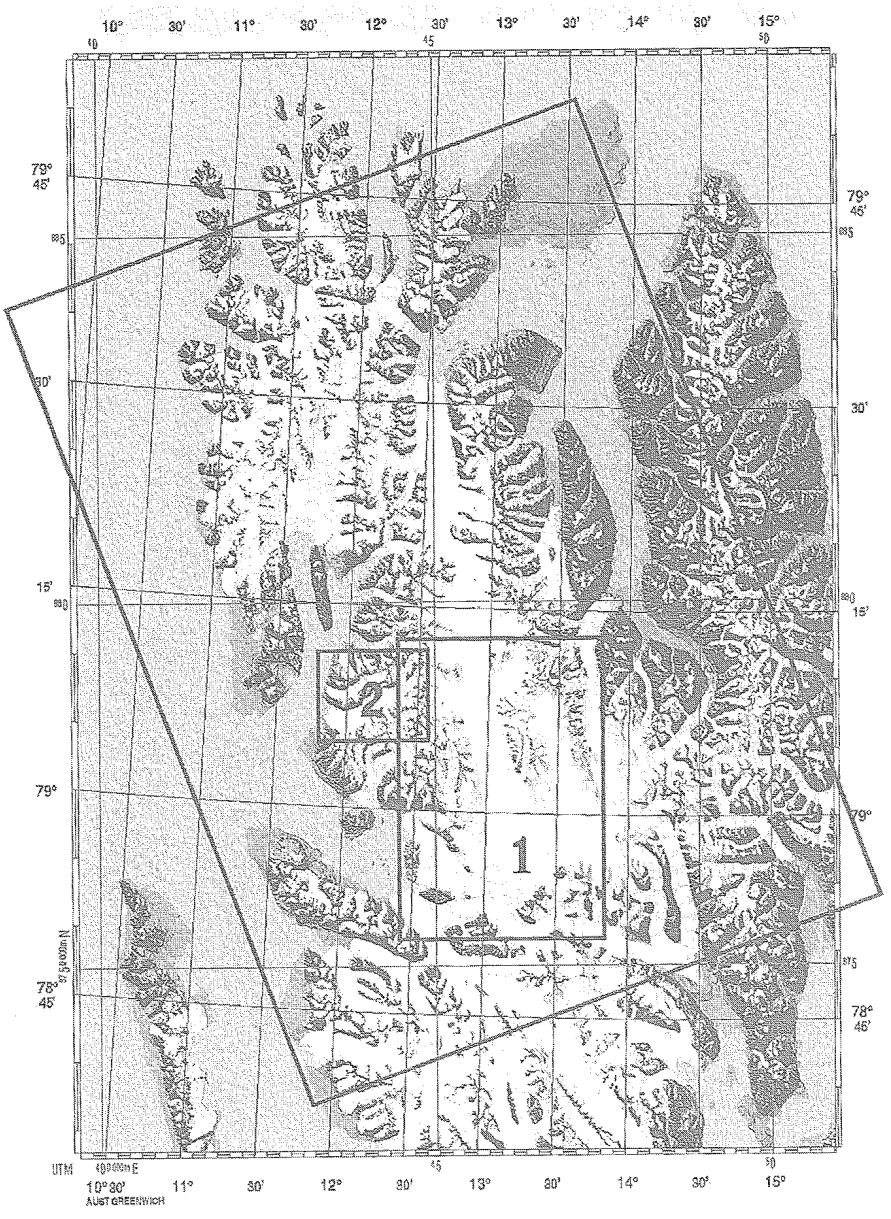


Fig. 1. Map of the northwest Spitsbergen and location of the test sites; 1: Kronebreen; 2: D'Arodesbreen and Fjortendejulibreen.

3. Method

3.1. ERS-1 data and DEM

Eleven ERS-1 scenes recorded at the summer-autumn transition were analysed. The

This document is provided by JAXA.



Fig. 2. Differential interferogramme over northwestern Spitsbergen from ERS-1 data recorded on ascending orbits the 17 and the 23 September 1991 (six days interval). The image is oriented to the North and covers the area of one complete ERS-1 scene (100 × 120 km). Despite of the scale, clear fringes are visible on several glaciers on the eastern part of the image while due to the meteorological condition the western part is characterised by a low coherence and lack of fringes. Inverse conditions as well as radar features were observed between the 23 September and the 3 October and on the nine days interval interferogramme not presented here.

images of phase and of coherence and obtained interferogrammes were analysed and the validity of the data to determine the ice movement from glaciers located in the area was assessed (Rossi, 1994). Three scenes recorded at the end of the ablation period were associated to the best coherence. The interferometric pairs used in this paper were based on the following combinations: scenes of the 17 September with the 23 September (six days interval, Fig. 2) and 23 September with 2 October (nine days interval). Due to the meteorological conditions during the period of the data takes (see Lefauconnier *et al.*,

This document is provided by JAXA.

1994a), clear fringes are present in the central and eastern part of the interferogramme with the six days interval, while the fringes are clear in the western part of the interferogramme with the nine days interval. The two interferogrammes were then used according to the location of the studied site.

Due to the tormented relief of the area (see Fig. 1), a DEM obtained from SAR interferogrammes was not accurate enough to be used. A DEM was then obtained from maps at the 1/100000 based on aerial stereo photogrametry. In Svalbard there are number of trigonometric reference points with an accuracy better than one meter in the three coordinates. The contour lines on rock sides are estimated to be associated to a possible error less than 5 m in height. On the other coordinates, the error depends of the slope and could be more than 10 m. The DEM that was used for the project is available on Arc-Info data, digitised from a scanning. Thus, due to the chain of treatment, errors in position are usually in the 20 m range.

The fringe pattern caused by the orbital trajectories and the elevation of the terrain (with one topographic fringe corresponding to 30 m in elevation) were simulated and removed to produce differential interferogrammes where the fringes are due to the ice movement.

3.2. Flow line model

The general behaviour of glaciers is known and over ideal, small glaciers with well-defined basins, the flow lines correspond to a description made by Reid (1896). It is therefore possible to roughly estimate the flow direction at the glacier surface. If the surface is taken as reference, the ice is submitted to a submergence velocity in accumulation area and an emergence velocity in ablation area (Paterson, 1994), which are not determined in the present work. We nevertheless propose a model of the flow direction and the results, as well as the possible influence of the vertical component of the movement, will be discussed for the studied glaciers.

Both Isachsenfonna and Holtedahlfonna have a very weak slope (less than 2°). The laminar flow parallel to the surface and basal sliding dominate, and we are able to assume that, with the exception of a few areas, the real flow vectors follow the surface. Determination of the flow direction is made by taking into account information from air photos and satellite imagery. An important source of help in this determination is provided by the INSAR data themselves (see Lefauconnier *et al.*, 1994a). This is because the images of coherence show lack of coherence at the border of ice streams as well as at the confluence between two ice-streams. Hence, using Kronebreen as an example, especially on the Holtedahlfonna (Fig. 4), which is flowing toward the satellite look, the fringe morphology is used as the representation of real isotachytes. We therefore believe that the main central flow line is at least accurately detected.

3.3. Determination of the ice flow velocity

A grid of points is plotted every 500 m on the DEM and for each point, data on slope and aspect of the slope are extracted from the Arc-Info file. As the hypothesis is made on the flow direction we used then the relation (1):

This document is provided by JAXA.

$$\frac{2Vt}{\lambda}k \cdot s = n \qquad \text{as} \qquad V = \frac{n\lambda}{2tk \cdot s}, \tag{1}$$

where V is the velocity; t is the period between the data takes on which the interferogramme is based, λ is the wave length of the radar (56 mm); $k \cdot s$ is the scalar product of the coordinates in a cartographic system of the velocity vectors at each point of the grid (k) and the line-of-sight vector of the satellite (s); n is the number of fringes. The components of the line-of-sight vector are: 0.93; −0.21 and −0.32 for the vertical, North and East respectively and the coordinates of the vectors at each points of the grid (k) are obtained by using the following relation (2):

$$\begin{array}{ll} \text{Vertical:} & (\cos\theta), \\ \text{North} & (\cos\varphi.\ \sin\theta), \\ \text{East} & (\sin\varphi.\ \sin\theta), \end{array} \tag{2}$$

where θ, is the angle between the zenith and the flow direction and φ is the angle between the flow direction and North. The ellipsoidal shape of the Earth introduces negligible offset to θ, especially in Polar Regions.

On the interferogrammes, mountains and nunataks are all presented in black and the first fringe, which is clearly independent from these black zones, is counted as $n=1$. Due to the alpine relief the field of fringes is complex and the counting is then made manually. The counting is difficult or impossible on the western part of the Isachsenfonna and over the higher basin of Holtedahlfonna. In the lower part of the glacier where the velocity is too high and where there are many crevasses, no fringes were visible. Clear fringes are nevertheless seen over more than 50% of the glacier surface of Kronebreen, over about 80% of the Fjortendejulibreen and all over the d'Arodesbreen. The results are plotted on maps and due to the fact that the model cannot take into account small local topography, errors in the flow direction are detected and a few abnormal values, usually in the higher tributary basins, are eliminated.

4. Results

4.1. D'Arodesbreen and Fjortendejulibreen

For these glaciers, the interferogramme is shown in Fig. 3 and the obtained flow vectors in Fig. 5. The DEM is based on data (air photos and maps) from 1970. From this year to 1991 the slope over the main part of the basin may not have changed consistently except at the front where, due to high ablation, the elevation and dip of the slope may have changed drastically.

Over d'Arodesbreen, linear flow dominates and thus the results are accurate in the central basin, while they may be underestimated in the accumulation basin since a slight increase in the angle of the slope may have occurred. At the front, an important change of the surface topography through time due to the melting invalidates any possible result and the visible long vectors in the figure close to the front do not represent real values. The most accurate finding is then close to the equilibrium line where the velocity is 3 cm per day (a1 in Fig. 5).

Linear flow and basal sliding also dominate over the main basin of the Fjortendejuli-

This document is provided by JAXA.

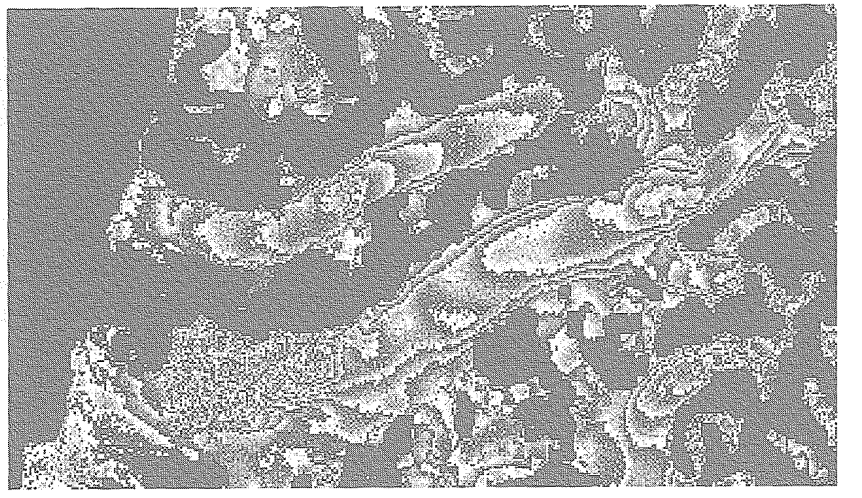


Fig. 3. Part of the differential interferogramme (16 × 13 km, 9 days interval) over the d'Arodesbreen and the Fjortendejulibreen (see location noted 2 on Fig. 1).



Fig. 4. Part of the differential interferogramme (34 × 42 km, 6 days interval) over Kronebreen. There are no visible fringes in the lower basin of the glacier (to the west) due to high velocity of the termini and the high number of crevasses (see location noted 1 on Fig. 1).

This document is provided by JAXA.

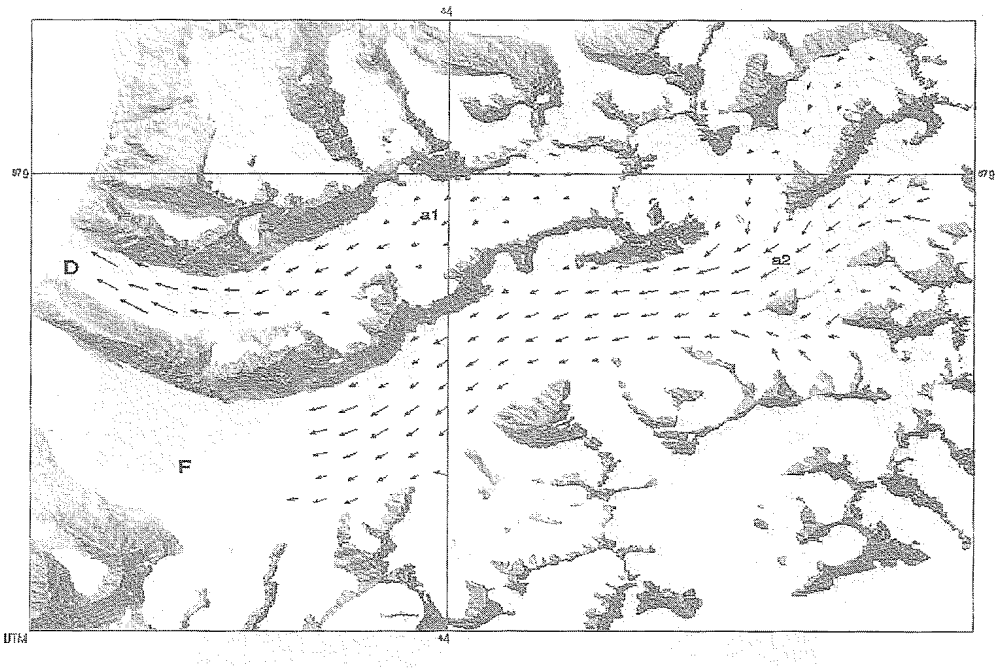


Fig. 5. Ice velocity over d'Arodesbreen (D) and Fjortendejulibreen (F). The figure is oriented to the north and the glaciers are also noted on 2 in Fig. 1. There are no results at the front of Fjortendejulibreen due to a high number of crevasses. Over d'Arodesbreen, the velocities are slightly underestimated at the glacier head. Highly overestimated velocities at the front lead to unrealistic results. Daily velocities, around the equilibrium lines; a1: 3.0 cm; a2: 6.6 cm.

breen. The results have the same source of error in the higher basin as for the d'Arodesbreen. At the front, higher velocities and the presence of crevasses cause a lack of coherence and no fringes are visible. A maximum velocity of 6.6 cm (a2 in Fig. 5) is found close to the equilibrium line, which is of the same order of magnitude that velocity measured geodetically in the same zone by Ahlmann (1948) between mid-June to mid-August 1934.

4.2. Kronebreen

The interferogramme is shown in Fig. 4 and the flow vectors in Fig. 6. The velocity is remarkably regular, around 20 cm per day over 20 km along the longitudinal axis of Isachsenfonna. The velocity over Holtedahlfonna increases from near zero to 52 cm per day along a transect terminating at 15 km to the calving front (c1 in Fig. 6). At the front, a mean annual value of between 200 to 215 cm per day was reported for 1964 (Voigt, 1965) as well as for 1986 (Lefauconnier *et al.*, 1994b) with in both cases, peaks of 450 cm per day at the beginning of July. Even if the data on which the DEM is based are from 1966, the slope of these wide basins did not appear to change significantly (the mean dip of the slope is less than 2°). The fringe morphology in this basin indicates a regular surface and possible variation in velocities due to local change in the slope are limited.

One source of error may come from the counting of the fringes. The determination of the first fringe which is sometimes largely spread and not clearly defined, is not easy in all

This document is provided by JAXA.

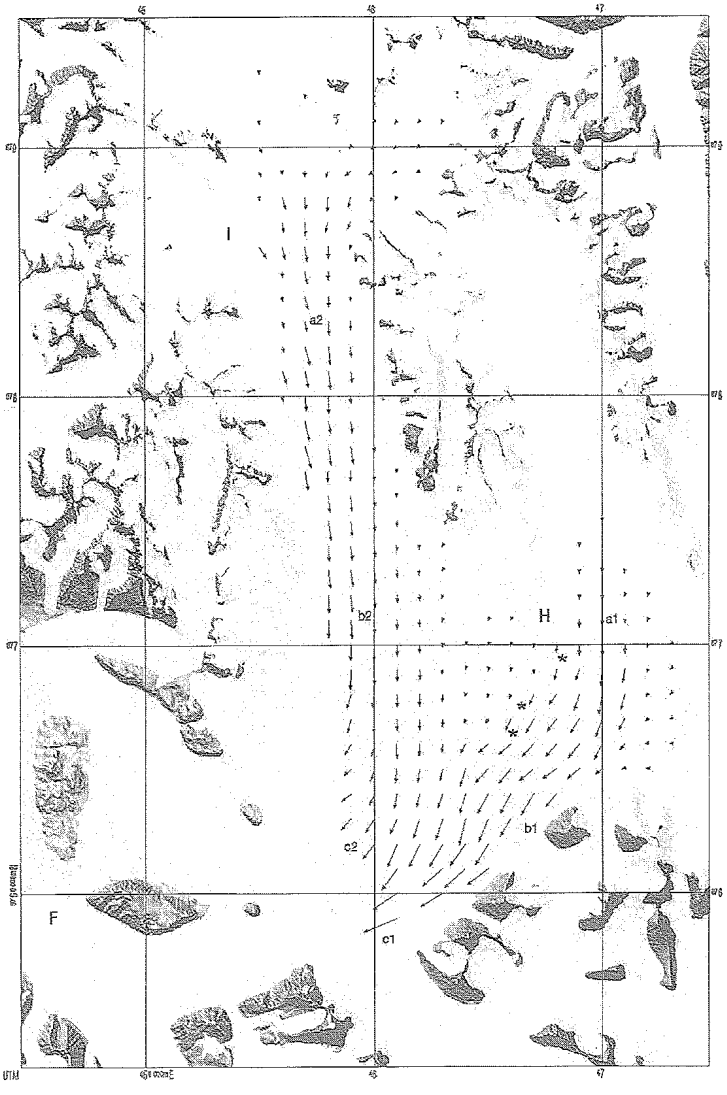


Fig. 6. Ice velocity over Kronebren: I: Isachsenfonna; H: Holtedahlfonna; F: calving front. The figure is oriented to the north and the glacier is also noted on 1 in Fig. 1. Interpretation of fringes is not possible in the western part of the Isachsenfonna and the relief influences the fringe morphology on its eastern part. The lack of vectors over the terminal tongue of the glacier is due to a lack of fringes (corresponding to a high velocity and presence of many crevasses). The dots indicate the location of the stakes used as ground control and noted S10, S05, S11 from the East to the West (see also Table 1).
Velocities per day; a1: 7.5 cm; b1: 32.0 cm; c1: 52.0 cm; a2: 20.0 cm; b2: 22.0 cm; c2: 21.0 cm.

parts of the scenes. Repeated independent counting from diverse locations always gave the same number of fringes over Isachsenfonna and an uncertainty of one fringe on Holtedahl-

This document is provided by JAXA.

fonna. In the later case, this uncertainty leads a possible error relatively important in the higher basin but of only 2% at point c1 (*e.g.* that the velocity is 51 or 52 cm per day). The atmospheric component of the interferometric measurement, the most common artefact to the technique, is not likely to significantly bias measurements with such high amplitudes.

4.3. Ground control

Three aluminium stakes (S11; S05 and S10 in Fig. 6) were settled in May 1996 on Holtedahlfonna for geodetic control by GPS. Their position was recorded again in May 1997, after 366 days. Table 1 presents the results of both interferometric and ground control measurements. The recorded movement of the stakes allows the validity of the flow model to be assessed at the three points. There was an error of 5° in the flow direction at stake S10 (see Table 1). This stake was settled on a gentle bump and the local aspect of the slope is not taken into account by the flow model. The accuracy of the model is confirmed at the two other points (with an error of only 1° in the flow direction and an error of 1% in the velocity (see Table 1). The velocities obtained from the fringes exceed the result from ground measurements by 48%. This discrepancy may be due to the fact that the velocity determination was made over 6 days just at the end of the ablation period, when the subglacial water pressure can still lead to high velocity rates. During the ablation period, velocities twice the mean annual value have been recorded at the front of this glacier in 1964 (Voigt, 1965) and 1986 (Lefauconnier *et al.*, 1994b).

Table 1. Comparison of velocities obtained at three stake locations, by the INSAR method and by GPS. S10, S05 and S11 are three stakes settled over Holtedahlfonna (see Fig. 6).

N of days	Method	Ice flow ($cm\,d^{-1}$)		
		S11	S05	S10
	INSAR			
6 days	A) Based on ice flow model	22.50	20.30	14.30
6 days	B) Based on the real flow line (from GPS)	22.80	20.10	14.60
366 days	GPS	15.20	13.00	10.40
	Difference in the flow line direction (A/B)	*1°7*	*0°7*	*4°57*
	Ratio INSAR/GPS values	*150%*	*155%*	*140%*

5. Discussion and conclusion

In this paper results have been based on data recorded along ascending orbits only. In order to estimates glacier velocities it was then necessary to propose an ice flow model for each surveyed glacier. Such models cannot be precise in all parts of the different glaciers. Moreover, The DEM is based on data recorded about twenty years before the records from the radar. If, in twenty years, the topography does not change consistently over the main areas of the glaciers, a small change occurs in the higher part of the accumulation area and an important change occurs at the front. Then, the findings must be considered as valid over

This document is provided by JAXA.

the central basin only, and in particular close to the equilibrium line. In accumulation areas, where the vectors from the models cannot take into account the submergence velocity, the result provides only a fairly broad indication of the ice movement. At the fronts, changes in the glacier geometry and undetermined emergence velocities prohibit any realistic result. In order to improve the results over these two areas, the DEM would have to be based on data recorded as close as possible to the dates of the satellite passage and the results based on interferogrammes obtained from both ascending and descending orbits as demonstrated for example by Joughin *et al.* (1998) and Karim *et al.* (1998).

Historical data from one glacier (Fjortendejulibreen) and a ground control at three locations on the main glacier (Kronebreen) allow a rough validation of the results. The results have important glaciological implications. On Kronebreen, if a higher velocity at the end of the ablation period compared to the annual value is typical, our estimate of 48% in September–October is highly significant in a glaciological context. It would therefore be interesting to carry out more surveys of the glaciers behaviour during the rapid summer to the slow winter flow regime transition and to eventually detect shifts from extensive flow to less extensive flow and even possible local compressive flow. Further, since a large part of Isachsenfonna has been found to move almost as a single block over 20 km, it would also be of interest to examine up-glacier of the main zone with extensive flow.

Kronebreen like most Svalbard glaciers is a sub-polar or polythermal glacier with both cold and temperate ice volumes. The fairly high rate of movement, even if favoured by the buoyancy at the front, indicates that basal sliding is important and that the temperate ice layer which originates in the firn area of the accumulation zone must be continuous to the front and at least all over the glacier sole of Holtedahlfonna. Observation of sediments on an overturned iceberg by Glasser and Hambrey (2000) seems to support this suggestion and additionally indicates that the glacier slides over soft sediments. Such a basal sediment layer is also an index of a high rate of erosion and fresh water release into the fjord.

Since the Kronebreen has experienced a surge shortly before 1869 (Liestøl, 1988), the transfer of ice from the high basin to the ablation area may have facilitated the extension of the temperate layer toward the sea. A sustained high velocity together with a significant glacier thickness may have prevented a marked change in the distribution of cold and temperate ice layers until today.

An extension of the analysis of the interferometric ERS-1 data presented in this paper will, in a future work allow to obtain information on the flow regime of about 15 to 20 glaciers in the area and, for the Kronebreen, the main glacier presented here, to check for a possible detection of the change in ice velocity at the end of the ablation period.

Acknowledgments

The work, which was first conducted within a direct co-operation between the CNES and the Norwegian Polar institute, has later on received a support from the ESA through a consortium led by Matra CapSystem. We also thank Michel Fily from the LGGE in Grenoble, Andy Hodson from the University of Sheffield, Elisabeth Isaksson, and Trond Eiken from the Norwegian Polar Institute.

This document is provided by JAXA.

References

Ahlmann, W.S. (1948): Glaciological research on the North Atlantic coasts. R. Geogr. Soc. Res. Ser.

Eldhuset, K., Andersen, P.H., Hauge, S., Isaksson, E. and Weydahl, D.J. (2000): ERS tandem INSAR processing for DEM generation, glacier motion estimation and coherence analysis on Svalbard. to be published in Int. J. Remote Sensing.

Glasser, N.F. and Hambrey, M.J. (2000): Sedimentary characteristics of iceberg debris, Kongsfjorden, Svalbard. submitted to J. Glaciol.

Goldstein, R.M., Engelhardt, H., Kamb, B. and Froloch, R.M. (1993): Satellite radar interferometry for monitoring ice sheet motion: Application to an Antarctic ice stream. Science, **262**, 1525–1530.

Hagen, J.O., Listøl, O., Roland, E. and Jørgensen, T. (1993): Glacier atlas of Svalbard and Jan Mayen. Norsk Polarinstitutt Meddelelser, **129**, 141 p.

Joughin, R.J., Kwok, R. and Fahnestok, M.A. (1998): Interferometric estimation of three-dimensional ice-clow using ascending and descending passes. IEEE Trans. Geosci. Remote Sensing, **38**(1), 25–37.

Karim, E.M., Vachon, P.W., Geudtner, A., Gray, L., Cumming, I.G. and Brugman, M. (1998): Validation of Alpine glacier velocity measurements using ERS tandem-mission SAR data. IEEE Trans. Geosci. Remote Sensing, **36**(3), 25–37.

Lefauconnier, B., Chorowicz, J., Deffontaine, B., Parrot, J.F., Rudant, J.P., Massonnet, D. and Rabaute, T. (1994a): Validation of SAR (Synthetic aperture radar) data from ERS-1 on Spitsbergen, Svalbard. Preliminary glaciological and geomorphological interpretation. Proceedings Second ERS-1 symposium Space at the Service of our Environment, Hamburg, Germany, 11–14 October 1993, ESA SP-**361**, 171–176.

Lefauconnier, B., Hagen, J.O. and Rudant, J.P. (1994b): Flow speed and calving rate of Kongsbreen glacier, Svalbard, using SPOT images. Polar Res., **13**, 59–65.

Lefauconnier, B., Massonnet, D., Anker, G., Querrien, E. and Bouissou, O. (1996a): Ice monitoring in Spitsbergen. INSAR Science Application Report. Report to Matra Capsystem and the ESA. October 1996.

Lefauconnier, B., Massonnet ,D., Rossi, M., Pinglot, J.F., Bouissou, O., Kerrien, E. et Anker, G. (1996b): Validation de données INSAR (interférométrie radar), application à l'estimation de la vitesse d'écoulement des glaciers du Spitsberg. Rapport à l'Institut Français pour la Recherché et la Technologie Polaire , IFRTP. Octobre 1996.

Liestøl, O. (1988): The glaciers in the Kongsfjorden area, Spitsbergen. Norsk Geogr. Tidsskr., **42**, 221–238.

Paterson, W.S.B. (1994): The Physics of Glaciers. 3rd ed. Oxford, Pergamon Elsevier Sciences, 480 p.

Reid, F.H. (1896). The mechanisms of glaciers. J. Geol., **4**, 912–928.

Rignot, E., Forster, R. and Isacks, B. (1996): Interferometric radar observations of Glaciar San Rafael, Chile. J. Glaciol., **42**, 279–291.

Rossi, M. (1994): Assessment of ice flows in glaciers of western Spitsbergen using differential interferometry. Proc. of 6th International ISPRS Symposium on Physical Measurements and Signatures in Remote Sensing. Val d'Isère, France 17–21 January 1994, 437–442.

Voigt, U. (1965): Die Bewegung der Gletscherzunge der Kongsvegen, Kingsbay, Vestspitsbergen. Petermanns Geogr. Mitteil., **1**, 8 p.

Wangensteen, B. and Weydahl, D. J. (1999): Mapping glacier velocities at Spitsbergen using ERS Tandem SAR data. Proceedings of IGARSS, Vol. IV, Hamburg, Germany, 28 June–2 July 1999, 1954–1956.

(Received April 18, 2000; Revised manuscript accepted December 13, 2000)

This document is provided by JAXA.

Mem. Natl Inst. Polar Res., Spec. Issue, 54, 291–299, 2001

Scientific note

Ocean tides and loading in the Nordic Seas

M. S. Bos and T. F. Baker

Proudman Oceanographic Laboratory, Bidston Observatory, Bidston Hill, Prenton, CH43 7RA, United Kingdom (msb@pol.ac.uk)

Abstract: A set of recent published global ocean tide models and two local ocean tide models are compared in the Nordic Seas with a set of tide gauge observations and with each other. For the M2 harmonic, a mean standard deviation of 23% was found compared with the observed tidal amplitudes. For the other constituents this number is even larger, between 34% and 51%. These differences will, to some extent, average out when the ocean loading is calculated but for the displacement ocean loading at Ny-Ålesund significantly different phase-lag values were obtained compared to those published by the International Earth Rotation Service (IERS).

1. Introduction

Several studies have compared global ocean tide models with tide gauge data and with each other within a latitude range of −66° to 66° North (Andersen *et al.*, 1995; Shum *et al.*, 1997). This region corresponds with the coverage of the TOPEX/POSEIDON satellite from which altimetry data is assimilated in most modern ocean tide models. The ERS1/2 satellites have a higher northern latitude limit of 82° but so far inaccurate orbit determination has limited its use for measuring the tides. Outside this region only tide gauge observations are available and a hydrodynamic ocean tide model must be used to map the tides. Lyard (1997) extended these comparisons with his own and 2 other models over the Arctic but since then new hydrodynamic ocean tide models have been published and therefore a new comparison has been made in this paper.

Next, it is interesting to investigate if these new models produce significantly different vertical displacement ocean loading values in this area. At Ny-Ålesund and Tromsø, Very Long Baseline Interferometer (VLBI) measurements are made while at Høfn VLBI measurements have been made in the past. In addition, all three stations are equipped with Global Positioning System (GPS) receivers. Both types of instruments are capable of sub-*cm* accuracy and since ocean loading effects are of this order of magnitude the loading at these three sites will be given.

2. Description of available ocean tide models

The tides in the Nordic Seas, assumed to encompass the Norwegian Sea, Greenland Sea and the Barents Sea, are difficult to model due to lack of accurate knowledge of the

This document is provided by JAXA.

bathymetry. Furthermore, the seasonally changing ice coverage in the Arctic influences the dynamics of the tides. For the diurnal tides, there are also trapped shelf waves present which need again precise bathymetry for correct representation.

In this study eight models are used. The oldest global ocean tide model used is the Schwiderski model which is denoted as SCHW (Schwiderski, 1980). It is given on a $1^\circ \times 1^\circ$ grid and is included for reference purposes. Next are the two global ocean tide models ORI. 96 and NAO.99, an update of ORI.96, both given on a $0.5^\circ \times 0.5^\circ$ grid (Matsumoto *et al.*, 1995, 1999).

Another set of global ocean tide models which cover the Nordic Seas are FES94.1, FES95.2 and FES98. All three are based on a finite element grid transformed to a regular latitude/longitude grid. FES94.1 and FES95.1 are given on a $0.5^\circ \times 0.5^\circ$ grid (Le Provost *et al.*, 1994; Lyard, 1997), FES98 on $0.25^\circ \times 0.25^\circ$ (Lefèvre *et al.*, 2000). FES94.1 is a pure hydrodynamic model while FES95.2 has assimilated TOPEX/POSEIDON data globally. Lyard then also improved the model in the Arctic. He studied the influence of ice on the tides by doubling the bottom friction coefficient over ice covered regions and found only a small influence over the deep water. More effect was observed in shallow water. FES98 assimilated tide gauge data, but not altimetry.

A local ocean tide model by Gjevik, Nøst and Straume, here after referred to as the GNS model, is given on a $0.5^\circ \times 0.25^\circ$ grid (Gjevik and Straume, 1989; Gjevik *et al.*, 1994). Kowalik and Proshutinsky (1993, 1994) also developed a local ocean tide models of the Arctic and is denoted as the KP model. They model the influence of ice coverage and mention that the effect is small for the deep water.

All models capture the main features of the tides. Only the SCHW model misses the amphidrome south of Spitsbergen for the M2 harmonic. This is probably caused by the coarse grid resolution. For the semi-diurnals, the tides in the Nordic Seas are mainly driven by the tides coming from the North Atlantic Ocean which are propagating partly into the Barents Sea where they are dissipated. The rest continues through the Fram Strait into the Arctic Sea. In Fig. 2 the tidal pattern is given for the FES98 model.

The diurnal tides are driven in the same way but the influence of the gravitational potential forcing is larger. The presence of trapped waves is noticeable. See for example the Yermak plateau or the entrance to the shelf between Norway and Svalbard. The tidal pattern for the O1 harmonic can be seen in Fig. 3.

3. Comparison between tide gauges and ocean tide models

Most tide gauge data are obtained from the International Hydrographic Office and only those with a length of observation longer than 30 days were selected. Gjevik also provided tide gauge observations made in the Barents Sea. Another constraint was that all models should cover the gauges, which reduced the list to 52 gauges. Their positions are shown in Fig. 1. The White Sea has been excluded from the comparison, since the errors in this region are up to 1 m and will dominate all the other gauges. The same problem was encountered by Lyard (1997). It must be noted that the tidal amplitude is small for the diurnals making errors in the observations more significant.

The standard deviation σ between the model and the gauges was, for each harmonic, calculated with the following equation:

This document is provided by JAXA.

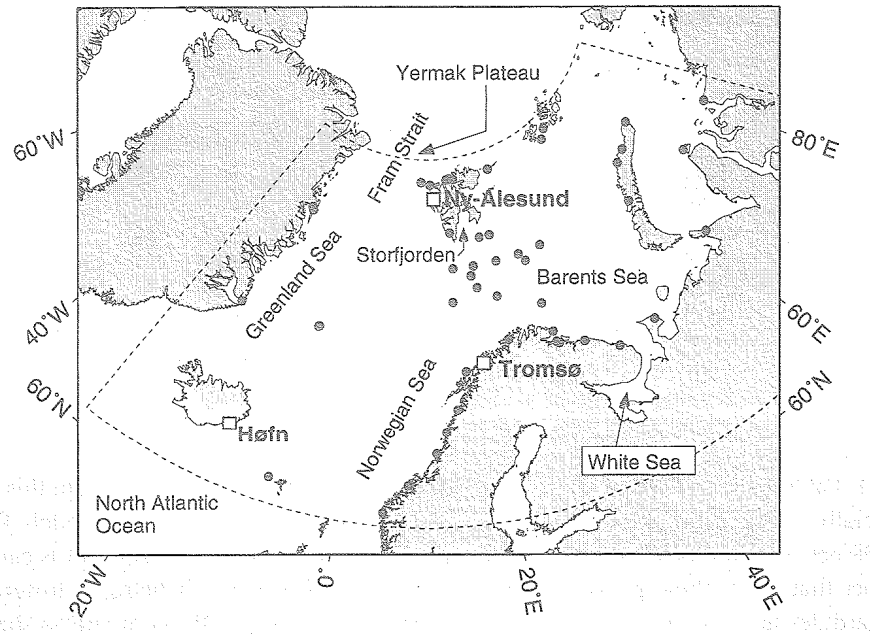


Fig. 1. The black dots give the location of the 52 tide gauges and the white squares of the 3 VLBI/GPS stations. The dashed line indicates the region used for comparing ocean tide models.

Table 1. Standard deviation σ between tide gauges and ocean tide models in cm. Also the percentage of σ compared to the average amplitude of the tide at the gauges is given.

	M2		S2		N2		K1		O1	
Model	cm	%	cm	%	cm	%	cm	%	cm	%
FES94.1	12.71	27	7.55	44	5.54	51	4.11	58	2.39	66
FES95.2	9.32	20	5.06	30	6.10	56	2.45	34	1.76	48
FES98	9.51	20	5.43	32	3.09	29	2.30	32	1.57	43
ORI.96	10.09	22	5.02	29	3.80	35	2.97	42	2.36	65
NAO.99	8.86	19	5.60	33	4.13	38	3.00	42	1.82	50
GNS	13.19	28	5.93	35	3.11	29	2.32	33	-	-
KP	8.24	18	5.89	35	4.69	43	3.25	46	1.65	45
SCHW	12.26	26	4.91	29	4.39	40	3.14	44	1.37	38
Average	10.52	23	5.67	33	4.36	40	2.94	41	1.85	51

$$\sigma^2 = \frac{1}{N}\sum_{i=1}^{N}\frac{1}{2}\left| Z_i^{\text{gauge}} - Z_i^{\text{model}} \right|^2. \qquad (1)$$

In this equation Z^{gauge} and Z^{model} are the tides written in complex form. This standard deviation can be interpreted as the root-mean-square of the averaged variance at each gauge. Because the variance is taken over one tidal period the factor 1/2 appears. The results are listed in Table 1.

The results for FES95.2, KP and SCHW are in good agreement with Table 4 of Lyard

This document is provided by JAXA.

Table 2. Standard deviation σ between tide gauges and ocean tide models in cm for harmonic M2. Also the percentage of σ compared to the average amplitude of the tide at the gauges is given.

	Storfjorden		White Sea		South Barents	
Model	cm	%	cm	%	cm	%
FES94.1	8.18	25	56.62	71	44.12	43
FES95.2	8.25	26	35.51	44	30.02	30
FES98	7.29	23	51.63	64	30.98	31
ORI.96	25.49	90	-	-	48.26	43
NAO.99	21.34	66	39.06	48	35.47	35
GNS	21.57	67	51.61	65	35.99	35
KP	10.20	31	31.50	41	23.39	23
SCHW	35.47	111	-	-	32.92	32

(1997). Table 1 shows that the FES94.1 model is not the most accurate model in this region. Especially for the diurnal harmonics it has a much larger σ than the other models. Overall, FES98 performs the best although not by a large margin. Part of this good fit is caused by the fact that 18 of these gauges are assimilated into FES98 which helps in lowering the standard deviation. However, with 34 non-assimilated gauges left the comparison should be fairly independent. In specific areas the errors are much larger such as in the Storfjorden (south of Spitsbergen), in the White Sea and in the south of the Barents Sea. The results of the comparisons in these areas are presented in Table 2.

4. Differences between the FES98 and other ocean tide models

The previous section compared tide models with gauges which were mostly at the coast. Now the standard deviation will be taken between each model and FES98. If the same values are obtained then this is a good indication that the accuracy of the models within the domain is the same as at the boundary. Tide gauge comparisons can then be used as an index for the overall accuracy. The results are given in Table 3.

Table 3 shows a relatively small standard deviation of FES98-FES95.2 which is

Table 3. The averaged standard deviation σ between the gridpoints of an ocean tide model and FES98 in cm. The area of averaging is drawn in Fig. 1. Next, the percentage of σ compared to the average amplitude of FES98 over the region is given.

	M2		S2		N2		K1		O1	
Model	cm	%	cm	%	cm	%	cm	%	cm	%
FES94.1	6.31	15	4.15	27	3.67	40	2.52	37	1.17	29
FES95.2	5.08	12	2.26	15	3.76	41	1.47	21	0.57	14
ORI.96	10.58	24	4.47	29	3.59	39	2.75	40	1.63	40
NAO.99	10.27	24	4.79	31	4.05	44	2.60	38	1.40	35
GNS	12.12	28	3.62	24	2.71	30	2.18	32	-	-
KP	8.29	19	3.81	25	3.71	41	2.60	38	0.88	22
SCHW	12.09	27	4.01	26	2.63	29	2.46	36	0.92	22
Average	9.25	21	3.87	25	3.45	38	2.37	35	1.04	27

This document is provided by JAXA.

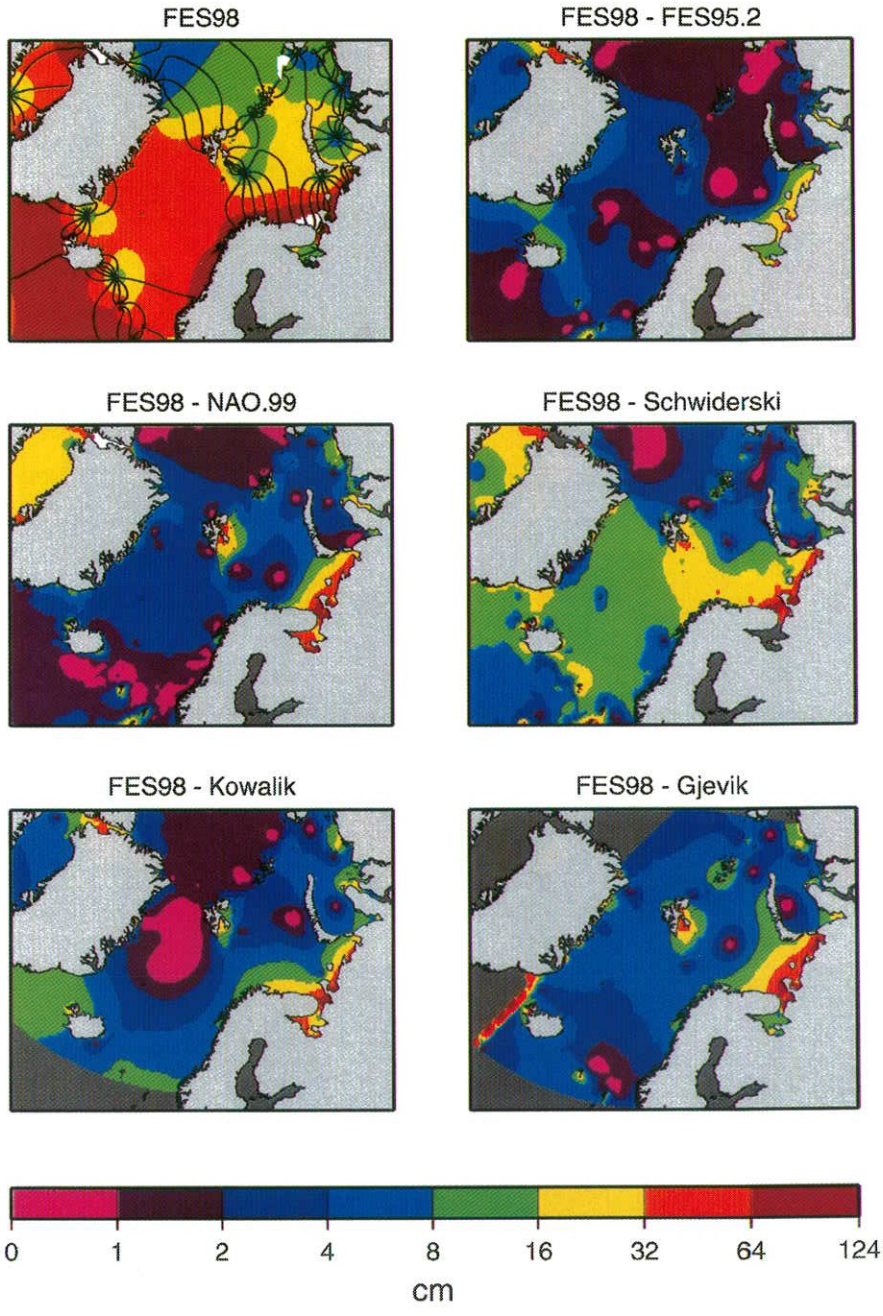


Fig. 2. The M2 tides in the Nordic Seas as given by the FES98 model and the vector difference between FES98 and 5 ocean tide models, for M2.

This document is provided by JAXA.

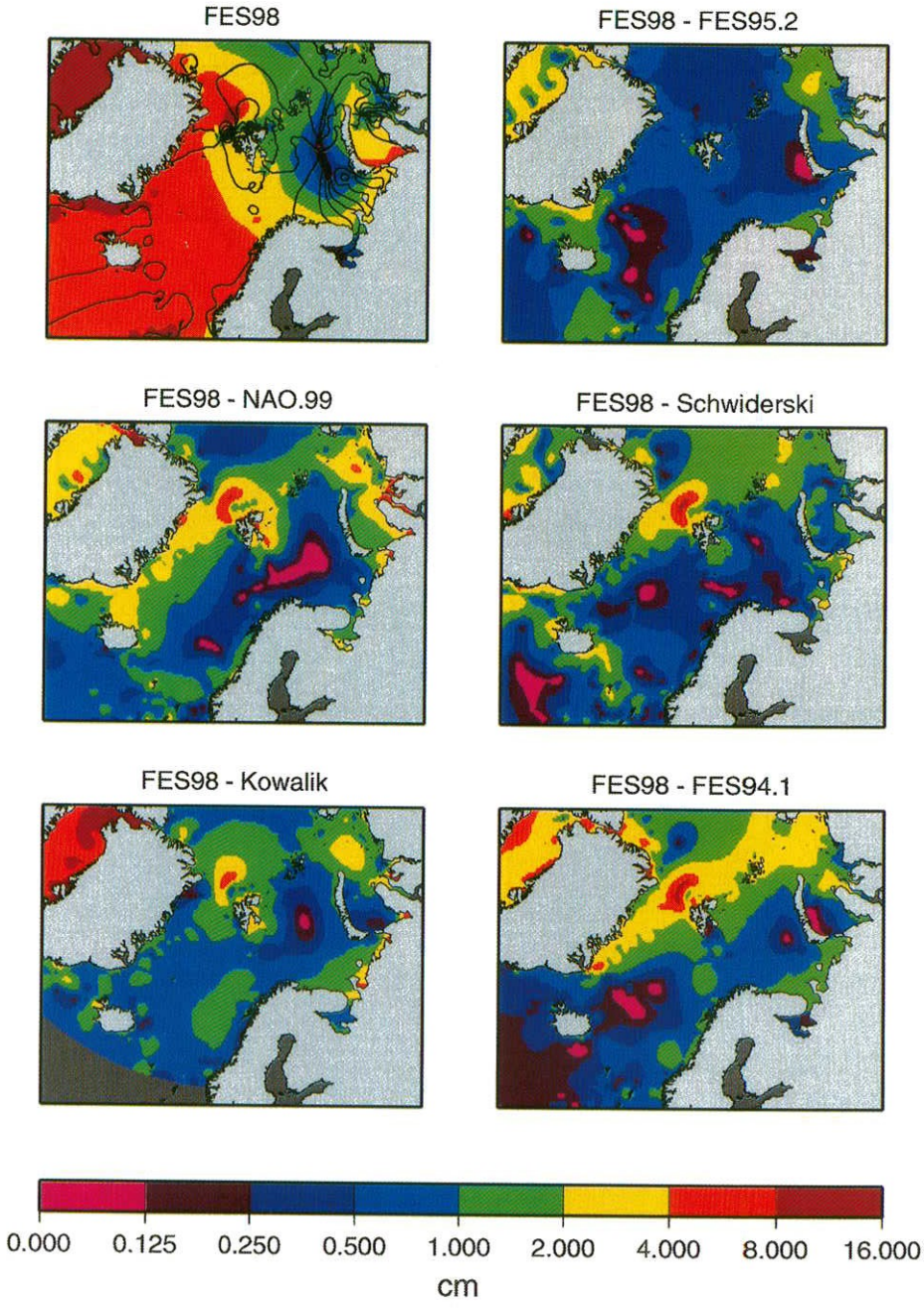


Fig. 3. The O1 tides in the Nordic Seas as given by the FES98 model and the vector difference between FES98 and 5 ocean tide models, for O1.

This document is provided by JAXA.

understandable since these models are produced on the same finite element grid. For the diurnals the obtained values are significantly smaller than compared with the gauges. Especially the low O1 values between FES98-KP and FES98-SCHW are striking. The spatial distribution of the vector differences, $|Z^{model1} - Z^{model2}|$, is shown in Figs. 2 and 3. For harmonic M2 the large differences in the South of the Barents Sea, the White Sea and in the Storfjorden are clearly visible. The large difference of SCHW and GNS, to a lesser extent, with FES98 in the Norwegian Sea will have a large influence on the loading values at Ny-Ålesund as discussed in the next section. For harmonic O1, the most striking feature is the difference between FES98 and all models over the Yermak Plateau North of Spitsbergen.

5. Vertical ocean loading displacements

Due to the fact that the weight of the tidal water mass varies spatially with time and the elasticity of the Earth, deformations of the ocean bottom occur which are propagated to the land. For each harmonic the amount of deformation can be calculated as follows:

$$h(r) = \int_A \rho Z(r') G(|r - r'|) dA. \tag{2}$$

In this equation $h(r)$ is the vertical displacement at a specific location r, again given in its complex form. The integral is taken globally over all water masses and ρ is the mean density of sea water. Z is the complex tidal amplitude and G is a Green's function which determines how much deformation a pointload of 1 *kg* at a distance $|r - r'|$ causes at the station at r. For the ocean loading values presented in Table 4 the Green's function of the Preliminary Reference Earth Model is used and the tidal water mass is conserved by subtracting a uniform layer with a certain phase-lag globally from the ocean tide model. Finally, the ocean tide models are linear interpolated near the stations to a gradual refined grid to assure that the assumption of a pointload representing the continuous waterload remains valid and to improve the fit with the coastline. The finest grid size is about 50 *m* which is small enough since the contribution of the ocean tides within a 1 *km* radius around the station to the loading cannot be more than 0.14 *mm* for a 0.5 *m* tide.

The International Earth Rotation Service (IERS) also gives the vertical ocean loading displacement values for Ny-Ålesund, Tromsø and Høfn, calculated by Scherneck (McCarthy, 1996). He uses the FES94.1 model and from Table 4 one can see that the same results are obtained. It must be mentioned that the GNS and KP models were extended outside their domain with values from FES98. For Ny-Ålesund the semi-diurnal tides from the Norwegian Sea have the largest contribution to the ocean loading. From Fig. 2 one can see that for harmonic M2 the GNS and SCHW models will deviate the most from the other models. This is confirmed in Table 4. For Tromsø, the Norwegian Sea is also of importance but this station is also more influenced by tides in the North Atlantic which are more uniform between all models. At Høfn the influence of the North Atlantic is even stronger. The FES94.1 has overall a poor comparison with tide gauge observations and this shows up in Table 4 in high amplitudes for harmonics S2 and N2 and a very low amplitude for K1. The phase-lags for these three harmonics are also significantly different from the other models.

This document is provided by JAXA.

Table 4. Vertical displacement ocean loading values for the VLBI/GPS stations. Amplitude is given in mm and the Greenwich phase lags positive.

Ny-Ålesund, Spitsbergen

	M2		S2		N2		K1		O1	
Model	mm	°	mm	°	mm	°	mm	°	mm	°
Scherneck	8.37	175	3.74	−120	2.66	170	0.47	27	1.47	−109
FES94.1	8.25	175	3.71	−120	2.63	170	0.44	27	1.48	−109
FES98	8.55	180	2.94	−132	1.83	155	0.83	−40	1.94	−116
ORI.96	8.20	177	2.92	−134	1.42	154	1.02	−61	2.00	−124
NAO.99	7.44	178	2.45	−145	1.19	151	1.02	−43	1.85	−125
GNS	9.24	168	3.25	−144	2.03	159	1.32	−33	-	-
KP	8.60	182	3.37	−139	2.15	160	0.68	−74	1.93	−125
SCHW	8.62	204	3.24	−116	1.77	180	1.43	−20	1.66	−121

Tromsø, Norway

	M2		S2		N2		K1		O1	
Model	mm	°	mm	°	mm	°	mm	°	mm	°
Scherneck	9.50	169	4.43	−141	3.31	148	2.38	−18	2.06	−107
FES94.1	9.76	169	4.55	−141	3.41	147	2.43	−17	2.09	−107
FES98	10.01	174	3.43	−143	2.20	148	2.37	−32	2.23	−115
NAO.99	10.15	174	3.18	−150	1.73	152	2.27	−29	2.26	−115
SCHW	11.67	192	4.10	−134	2.33	160	2.48	−17	1.88	−115

Høfn, Iceland

	M2		S2		N2		K1		O1	
Model	mm	°	mm	°	mm	°	mm	°	mm	°
Scherneck	11.64	−16	4.78	16	2.15	−39	5.56	−50	3.30	−110
FES94.1	11.48	−16	4.75	16	2.10	−39	5.60	−50	3.36	−110
FES98	11.97	−19	4.96	18	2.30	−42	5.58	−50	3.23	−113
NAO.99	11.98	−17	4.82	22	2.43	−39	5.56	−51	3.41	−109
SCHW	12.26	−23	4.82	29	2.53	−29	5.22	−43	2.92	−117

6. Conclusions

It has been shown that the mean standard deviation in ocean tide models of the Nordic seas for the M2 harmonic is 23% compared with the average amplitude at the tide gauges. For the other harmonics this error is even larger. Problem areas are the Storfjorden, the White Sea and the South of the Barents Sea. Comparisons with the tide gauges have also shown that FES94.1 and SCHW models perform worse than the other models. Especially for the K1 harmonic, FES94.1 has a large standard deviation which shows up as a very different phase-lag of the vertical ocean loading displacement value at Ny-Ålesund. Overall, the ocean loading amplitude values obtained are quite similar for all ocean tide models and their difference will mainly be measurable by their different phase-lags. For loading the most important errors are caused by relatively small errors in the amplitude and phase-lag in the Norwegian Sea because this region is coherent in phase for the semi-diurnal tides causing a large loading effect.

This document is provided by JAXA.

Acknowledgments

The first author would like to thank the Norwegian Polar Institute for their travel grant to the Second International Symposium on Environmental Research in the Arctic and the Fifth Ny-Ålesund Scientific Seminar in Tokyo.

References

Andersen, O.B., Woodworth, P.L. and Flather, R.A. (1995): Intercomparison of recent ocean tide models. J. Geophys. Res., **100**, 25261–25282.

Gjevik, B. and Straume, T. (1989): Model simulations of the M2 and the K1 tide in the Nordic Seas and Arctic Ocean. Tellus, **41A**, 73–96.

Gjevik, B., Nost, E. and Straume, T. (1994): Model simulations of the tides in the Barents Sea. J. Geophys. Res., **99**, 3337–3350.

Kowalik, Z. and Proshutinsky, A.Y. (1993): Diurnal Tides in the Arctic Ocean. J. Geophys. Res., **98**, 16449–16468.

Kowalik, Z. and Proshutinsky, A.Y. (1994): The Arctic Ocean tides. The Polar Oceans and Their Role in Shaping the Global Environment, ed. by O. Johannessen *et al*. Washington, D.C., Am. Geophys. Union, 137–158 (Geophysical Monograph Vol. 85).

Le Provost, C., Genco, M.L., Lyard, F., Vincent, P. and Canceil, P. (1994): Spectroscopy of the world ocean tides from a finite-element hydrodynamic model. J. Geophys. Res., **99**, 24777–24797.

Lefèvre, F., Lyard, F.H. and Le Provost, C. (2000): FES98: A new global tide finite element solution independent of altimetry. Geophys. Res. Lett., **27**, 2717–2720.

Lyard, F.H. (1997): The Tides in the Arctic Ocean from a finite element model. J. Geophys. Res., **102**, 11611–15638.

Matsumoto, K., Ooe, M., Sato, T. and Segawa, J. (1995): Ocean tide model obtained from TOPEX/POSEIDON altimetry data. J. Geophys. Res., **100**, 25319–25330.

Matsumoto, K., Takanezawa T., Sato, T. and Ooe, M. (1999): NAO.99 Tidal Prediction System. TOPEX/POSEIDON and Jason-1 Science Working Team Meeting, Saint-Rapaël (abstract), 8.

McCarthy, D.D., ed. (1996): IERS Technical Note 21. Observatoire de Paris.

Schwiderski, E.W. (1980): On charting global ocean tides. Rev. Geophys. Space Phys., **18**, 243–268.

Shum, C.K., Woodworth, P.L., Andersen, O.B., Egbert, G.D., Francis, O., King, C., Klosko, S.M., Le Provost, C., Li, X., Molines, J.M., Parke, M.E., Ray, R.D., Schlax, M.L., Stammer, D., Tierney, C.C., Vincent, P. and Wunch, C.I. (1997): Accuracy assesment of recent ocean tide models. J. Geophys. Res., **102**, 25173–25194.

(Received March 27, 2000; Revised manuscript accepted July 17, 2000)

This document is provided by JAXA.

This document is provided by JAXA.

Mem. Natl Inst. Polar Res., Spec. Issue, 54, 301–317, 2001

Scientific paper

Inversion of global tide gauge data for present-day ice load changes

Hans-Peter Plag[1] and Hans-Ulrich Jüttner[2]

[1]*Norwegian Mapping Authority, Kartverksveien 21, N-3511 Hønefoss, Norway*
[2]*Institute for Geophysics, University Kiel, Kiel, Germany*

Abstract: Trends in relative sea level as recorded by the large number of coastal tide gauges are used to derive new constraints on trends in the Antarctic and Greenland ice sheets on century time scales. Based on the sea-level equation, which describes the spatial pattern of sea-level changes due to changes in the ice masses, for each ice sheet the finger-print function for a constant trend is derived. These finger-print functions are used to determined the best-fit trends from the tide gauge trends.

A fit to all tide gauge trends excluding only those with unreasonably large values indicates negative rates of approximately −50 mm/yr for the Antarctic ice sheet and −50 to −100 mm/yr for the Greenland ice sheet, with the latter strongly depending on the model used to predict the post-glacial signal. However, excluding tide gauge trends from lower latitudes, the fit results in positive trends for both the Antarctic and Greenland ice sheets. This high sensitivity of the inversion to a zonal selection of tide gauges indicates that the tide gauge trends may be contaminated by a latitude-dependent steric effect due to zonal warming of the ocean water.

1. Introduction

The 1995 IPCC assessment (Houghton *et al.*, 1996) focuses on the uncertainties in our knowledge of global change, and with respect to changes in the cryosphere, Warrick *et al.* (1996) emphasize the large uncertainties in the contribution of the ice sheets to sea level changes (see Table 1). These uncertainties are due to several circumstances. Firstly, the accuracy of satellite altimetry over ice is still not sufficient to determine the change in the surface height of the large ice sheets, particularly over areas with steep topography, on a level required to reduce the uncertainties. Secondly, the response of glaciers and ice sheets to climate change happens on long time scales of possibly up to several centuries. Therefore, the input forcing function (*i.e.* climate variability) is not well enough determined both in space and time to drive ice mass balance models satisfactorly. Moreover, ground observations to constrain the ice models are scarce compared to the extent of the ice sheets and cover only in a few cases time periods of decades and centuries. Thirdly, observations of global ocean mass (GOM) changes would help to constrain the overall mass balance of the cryosphere. However, the determination of GOM changes from relative sea level (RSL) observations at tide gauges are hampered by the temporal and spatial structure of the global data set as well as the complex physical relation between GOM and RSL. Moreover, global ocean volume (GOV) changes can be due to both mass changes and temperature changes

This document is provided by JAXA.

Table 1. Uncertainties in factors contributing to global sea-level change. The numbers are according to Warrick et al. (1996).

Source	Estimated rate of sea level change (mm/yr)
Steric effects	0.2 to 0.7
Antarctica	−1.4 to 1.4
Greenland	−0.4 to 0.4
Glaciers	0.2 to 0.5
Continental ground waters	−0.5 to 0.7

(steric volume changes), and the separation is not easily achieved. In addition, RSL is affected by other factors than GOV changes constituting a high "noise" level in RSL. Fourthly, the determination of GOM changes from satellite altimetry is still not possible with sufficient accuracy due to the short interval of observation and problems in the separation of steric (volume) and mass effects.

In this unsatisfactory situation, additional observational evidence or methodological approaches that can help to constrain changes in the cryosphere should be sought. Here we attempt a new exploitation of the global tide gauge data set for constraints on changes in the cryosphere. Based on the physical relation between ice load and GOM changes and RSL, an inversion of the local trends at the tide gauges for trends in the large ice sheets is carried out.

GOM and GOV constitute two quantities characterising the ocean as a reservoir in the global hydrological cycle. Changes in GOM and GOV are directly related to changes in the hydrological cycle and therefore to climate change. On climatological time scales, the cryosphere has the greatest potential to contribute to changes in GOM, a fact which has been documented very clearly during the ice ages. GOV changes (for constant mass) are due to density changes resulting primarily from heat exchange with the atmosphere. It is important to note that GOM and GOV are absolute numbers.

Sea level, on the other hand, always is a relative quantity given with respect to a coordinate system (*e.g.* a geocentric coordinate system) or a reference plane (*e.g.* a geoid model or the reference ellipsoid). Sea level describes how the GOM is distributed in a given topography of the Earth surface. This distribution depends on many different factors, such as the Earth's topography, the (time-variable) geoid, changes of the Earth's rotation, atmospheric circulation, heat and salinity distribution in the ocean, ocean circulation, present and past mass movements in the Earth system, the viscoelastic properties of the Earth's interior, sedimentation, and even anthropogenic subsidence due to groundwater, gas, or oil extraction.

Whenever mass is exchanged between the ocean and any other reservoirs, sea level is changed in a complex way. A mass movement from or to the ocean changes all geocentric and relative positions of the planes relevant to sea level, *i.e.*, ocean bottom, the reference ellipsoid, the geoid and the sea surface.

Nevertheless, in most studies of the past twenty years, observations of coastal RSL obtained with tide gauges have been used to estimate a global sea level rise (GSLR) and to convert this into a GOV changes without taking into account the complex relation between local RSL and GOV (for a review, see Warrick *et al.*, 1996). Based on a unique data set of monthly mean sea levels derived from tide-gauge observations, the global trend

This document is provided by JAXA.

has been estimated to be of the order of 1–2.5 mm/yr. This relatively wide range mainly is due to the selection criteria used by the different researchers to select subsets of tide gauges. In earlier studies, simple arithmetic averages of selected subsets of tide gauges were considered to be representative for the GSLR (*e.g.* Barnett, 1984). Gornitz and Lebedeff (1987) used geological data to separate the present-day trend from past geological contributions, while Peltier and Tushingham (1989) corrected for the present-day RSL changes due to the last glaciation on the basis of geophysical models. One major conclusion from these studies concerns the length of the records required to determine a reliable local trend at any given tide gauge: due to large decadal to inter-decadal variability of coastal sea level, a record length of the order of 50 years appears to be necessary to determine local trends with a precision of 0.5 mm/yr. Recently, Douglas (1991, 1992, 1995) selected a small number of tide gauges with long records in areas considered as tectonically stable and corrected the local trends for the post-glacial contribution. He then used the consistency of the local trends at these tide gauges as indication that they represent the GSLR.

A few authors have criticised the approach used to determine a GSLR from tide gauges (Pirazzoli, 1989, 1993; Gröger and Plag, 1993; Plag, 1993). Plag (1993) even claimed that it is not possible to determine a global sea level change from tide gauges due to their poor spatial sampling. Previous studies used the complex relation between GOM changes and RSL changes only for the correction of the postglacial rebound effect due to the last deglaciation. Utilising the full physical relationship between sea level and GOM changes, the tide gauges could well be sufficient to constrain the mass movement having contributed to the observed trends in local RSL. This is attempted here for the first time.

It is well known that the disintegration of the last great ice sheets produced a distinct spatial pattern, a finger-print, in RSL, with rather different temporal characteristics of the RSL in the near-intermediate and far field of the load changes (see, *e.g.*, Quinlan and Beaumont, 1982; Lambeck, 1993). The elastic response of the Earth to present-day changes in the cryosphere can be expected to produce a similar finger-print, which should be present in the tide gauge data. Based on these finger-prints, tide gauge trends, in principle, can be inverted for ice load changes.

In the next section, we will first present the well-known equation for RSL changes due to surface mass changes on a visco-elastic and self-gravitating Earth, and specialise this sea-level equation for century scale processes on a simplified Earth model. Based on this equation, in Section 3, we will introduce the concept of finger-prints, which describe sea-level changes due to changes in the thickness of large ice sheets. The finger-print functions are then used to define a model function, which describes local RSL trends as a super-position of the finger-print functions of several ice sheets. In Section 4, we will discuss the RSL databases and the quality of the RSL trends, that can be derived from this database. Results for ice thickness changes of the Antarctic and Greenland ice sheets determined in a fit of the model function to the RSL trends are presented in Section 5 and the sensitivity of the ice thickness trends on different selection criteria for tide gauges are considered. Finally, an interpretation of the results is attempted in Section 6.

2. Sea level changes due to surface mass movements

A linar description of the relation between changes in the Earth's ice cover and RSL

This document is provided by JAXA.

was first given by Farrell and Clark (1976) as the hydrostatic relative sea level equation on a viscoelastic Earth, which we write here as

$$\xi(\vartheta,\lambda,t)=c(t)+\int_{-\infty}^{t}\int_{0}^{t}\int_{0}^{2\pi}G(\vartheta,\lambda,\vartheta',\lambda',t-t')$$
$$\frac{\mathrm{d}}{\mathrm{d}t'}\{\rho_w O(\vartheta',\lambda',t')\xi(\vartheta',\lambda,t')+\rho_l[1-O(\vartheta',\lambda',t')]\eta(\vartheta',\lambda',t')\}\sin\vartheta'\,\mathrm{d}\lambda'\,\mathrm{d}\vartheta'\,\mathrm{d}t'. \quad (1)$$

Here, ξ is the sea level change relative to the (deformable) solid Earth surface. G is the Green's function for sea level defined below, O is the ocean function, defined as

$$O(\vartheta,\lambda,t):=\begin{cases}1 \text{ on oceans}\\ 0 \text{ on continents}\end{cases}, \quad (2)$$

and η the cumulated ice load change due to mass added or removed from land. $c(t)$ is determined such that mass is conserved, *i.e.*

$$\langle\xi(t)\rangle_O=-\frac{\rho_l\langle\eta(t)\rangle_E}{\rho_w\langle O(t)\rangle_E} \quad (=\text{eustatic change}), \quad (3)$$

where $\langle\cdot\rangle_E$ denotes an average over the Earth's surface, *e.g.*

$$\langle\eta\rangle_E=\frac{1}{4\pi}\int_0^{\pi}\int_0^{2\pi}\eta(\vartheta,\lambda)\sin\vartheta\,\mathrm{d}\lambda\,\mathrm{d}\vartheta, \quad (4)$$

and $\langle\cdot\rangle_O$ indicates an average over the oceans, *e.g.*

$$\langle\xi\rangle_O=\frac{\langle O\xi\rangle_E}{\langle O\rangle_E}=\frac{\int_0^{\pi}\int_0^{2\pi}O(\vartheta,\lambda)\xi(\vartheta,\lambda)\sin\vartheta\,\mathrm{d}\lambda\,\mathrm{d}\vartheta}{\int_0^{\pi}\int_0^{2\pi}O(\vartheta,\lambda)\sin\vartheta\,\mathrm{d}\lambda\,\mathrm{d}\vartheta}. \quad (5)$$

Strictly speaking, ξ as defined by eq. (1) is a continuation of RSL on the continents as well and the true RSL has to be defined as

$$\hat{\xi}:=O\xi. \quad (6)$$

However, the function ξ has the decisive advantage over $\hat{\xi}$ of being continuous at the coastlines. Since most of the sea-level stations are located at coastlines of continents where $\hat{\xi}$ has discontinuities, approximations to $\hat{\xi}$ must fail to give correct values of RSL in these stations. Approximations to ξ, on the other hand, have no problem with these locations.

Equation (1) does not consider any dynamic effects in the ocean due to the mass movements, *i.e.*, it is assumed that all processes are slow enough for the ocean to respond hydrostatically to the changes. Dickman (1997) estimated dynamic effects due to seasonal melting and growth of the Antarctic ice sheet and found these effects at annual time scales to be of the order of a few mm. Thus, for considerations of century trends in the ice sheets, dynamic effects safely can be neglected.

Based on a Maxwell rheology and a simple Earth model, Farrell and Clack (1976) showed that the viscous contribution 1000 years after a significant mass change is still of the order of 10% of the initial combined instantaneous effect of elastic deformation and gravitation. Moreover, the spatial pattern of the sea-level changes is not significantly changed by the viscous contribution. Gasperini *et al.* (1986) considered present-day cryogenic forcing of perturbations in the Earth's rotation and found that a transient

This document is provided by JAXA.

rheology may be important in the modelling of the response due to such a forcing on time scales of centuries. However, for an initial first order study, we assume that the most important contribution to the sea-level change pattern is due to the instantaneous elastic response. We will discuss the validity of this assumption below together with the results of the inversion.

As discussed in Farrell (1972) and Peltier (1974) for the elastic and viscoelastic case, respectively, the Green's function G can be computed for a given spherically symmetric elastic (viscoelastic) isotropic Earth model (SNRE(V)I) model. Thus, for a known load history, the sea-level variations can be computed for such a simplified Earth model.

In specialising eq. (1) for century-scale sea-level changes on an elastic Earth, we assume that changes in the load history are linear trends everywhere, therefore, at any given tide gauge, we expect a linear trend.

For a SNREI Earth, the Green's function for sea level is deduced by Farrell and Clack (1976) to be

$$G(\vartheta,\lambda,\vartheta',\lambda')=\frac{3}{4\pi\rho_\circ}\sum_{n=0}^{\infty}(1+k_n-h_n)P_n(\cos\theta)$$
$$=\frac{3}{4\pi\rho_\circ}\sum_{n=0}^{\infty}(1+k_n-h_n)P_n(\sin\vartheta\sin\vartheta'\cos(\lambda-\lambda')+\cos\vartheta\cos\vartheta'), \qquad (7)$$

where ϑ is the angle between the observer and the load, and k_n and h_n are the elastic load Love numbers for the incremental gravitational potential due to the elastic deformation of the Earth and the vertical crustal displacement, respectively, and $\rho_\circ$ ist the mean density of the Earth. Thus, the sea-level change with respect to a benchmark fixed on the crust is given as the sum of the vertical movement described by h_n, and the geoid change given by $1+k_n$. Here, the one accounts for the Newtonian potential of the mass being moved on the Earth's surface and k_n accounts for the deformations of the Earth's interior.

With this Green's function, we may simplify eq. (1) and write it as

$$\xi(\vartheta,\lambda)=\frac{1}{g_\circ}\Big(\phi(\vartheta,\lambda)-\langle\phi\rangle_O\Big)-\Big(H(\vartheta,\lambda)-\langle H\rangle_O\Big)-\frac{\rho_1\langle\eta\rangle_E}{\rho_w\langle O\rangle_E}. \qquad (8)$$

Here, H is the radial displacement of the Earth's surface and ϕ the incremental gravitational potential generated by the total ice and water load on the Earth and by the accompanying deformation of the Earth. Both, H and ϕ depend on the global distribution of ξ. It is worthwhile to note that ξ is the quantity observed at a given tide gauge but is not equivalent to the geocentric sea-level as measured by satellite altimetry.

Passing over to harmonic developments, *e.g.*

$$\xi(\vartheta,\lambda)=\sum_{n=0}^{\infty}\sum_{m=-n}^{n}\xi_{nm}Y_{nm}(\vartheta,\lambda), \qquad (9)$$

results into

$$H_{nm}=\frac{3}{\rho_\circ}\frac{h_n}{2n+1}\Big(\rho_w\hat{\xi}_{nm}+\rho_1\eta_{nm}\Big), \qquad (10)$$

$$\phi_{nm}=\frac{3g_\circ}{\rho_\circ}\frac{1+k_n}{2n+1}\Big(\rho_w\hat{\xi}_{nm}+\rho_1\eta_{nm}\Big), \qquad (11)$$

and

This document is provided by JAXA.

$$\hat{\xi}_{nm}=(-1)^m\sum_{p=0}^{\infty}\sum_{q=0}^{\infty}\sum_{j=-p}^{p}\sqrt{\frac{(2n+1)(2p+1)(2q+1)}{4\pi}}\begin{pmatrix}n & p & q\\ 0 & 0 & 0\end{pmatrix}\begin{pmatrix}n & p & q\\ -m & j & m-j\end{pmatrix}O_{qm-j}\xi_{pj}, \tag{12}$$

$$\langle H\rangle_O=\frac{1}{4\pi\langle O\rangle_E}\sum_{n=0}^{\infty}\sum_{m=-n}^{n}(-1)^m H_{nm}O_{n-m}, \tag{13}$$

$$\langle \phi\rangle_O=\frac{1}{4\pi\langle O\rangle_E}\sum_{n=0}^{\infty}\sum_{m=-n}^{n}(-1)^m \phi_{nm}O_{n-m}, \tag{14}$$

where g_o is the gravitational acceleration at the surface of the Earth and the symbols $\begin{pmatrix}n_1 & n_2 & n_3\\ m_1 & m_2 & m_3\end{pmatrix}$ denote Wigner 3-j symbols known from the theory of coupling of angular momentums in quantum mechanics (see *e.g.* Edmonds, 1957). Thereby, the sea level eq. (8) may be rewritten in terms of spherical harmonic coefficients as

$$\begin{aligned}\xi_{nm}=3\frac{1+k_n-h_n}{2n+1}\Bigg\{&\frac{\rho_1}{\rho_o}\eta_{nm}\\ &+(-1)^m\frac{\rho_w}{\rho_o}\sum_{p=0}^{\infty}\sum_{q=0}^{\infty}\sum_{j=-p}^{p}\sqrt{\frac{(2n+1)(2p+1)(2q+1)}{4\pi}}\begin{pmatrix}n & p & q\\ 0 & 0 & 0\end{pmatrix}\begin{pmatrix}n & p & q\\ -m & j & m-j\end{pmatrix}O_{qm-j}\xi_{pj}\Bigg\}\\ -\Bigg\{&\frac{3}{O_{00}}\frac{\rho_w}{\rho_o}\sum_{p=0}^{\infty}\sum_{q=0}^{\infty}\sum_{r=0}^{\infty}\sum_{j=-p}^{p}\sum_{i=-q}^{q}\frac{1+k_p-h_p}{2p+1}\sqrt{\frac{(2p+1)(2q+1)(2r+1)}{4\pi}}\begin{pmatrix}p & q & r\\ 0 & 0 & 0\end{pmatrix}\begin{pmatrix}p & q & r\\ -j & i & j-i\end{pmatrix}O_{p-j}O_{rj-i}\xi_{qi}\\ &+\frac{3}{O_{00}}\frac{\rho_1}{\rho_o}\sum_{p=0}^{\infty}\sum_{j=-p}^{p}(-1)^j\frac{1+k_p-h_p}{2p+1}O_{p-j}\eta_{pj}+\sqrt{4\pi}\frac{\rho_1}{\rho_w}\frac{\eta_{00}}{O_{00}}\Bigg\}\delta_{n0}\delta_{m0}.\end{aligned} \tag{15}$$

Equations (9) and (15) are linear. Therefore, taking time derivatives, it is seen that formally the same equations are satisfied by sea-level and ice-load trends. Thus, eq. (15) in principle can be used to invert local RSL trends determined at a sufficient number of tide gauges for trends in the ice sheets.

3. The concept of finger-print function

We will, for the time being, assume that we are able to determine reliable RSL trends at a sufficient number of tide gauges and correct these trends for all other effects not due to present-day changes in the ice loads. Below, we use $\alpha=\dot{\xi}$ and $\beta=\dot{\eta}$ to denote the linear trends in sea-level and the ice sheets, respectively. α_i denotes the trend in RSL at the i-th tide gauge.

There are two main approaches for the inversion of the available sea-level observations for ice-load trends. The first one is to fit spherical harmonic coefficients α_{nm} up to a maximal degree n_o by a least squares method to station data $\alpha_i=\alpha(\vartheta_i,\lambda_i)$ using eq. (9). Then, eq. (15) is inverted for the harmonic coefficients β_{pj} up to the same maximal degree n_o. This yields the spatial distribution of the linear trend in the ice-load. However, the solution is subject to major uncertainties due to the spatially incomplete distribution of tide gauges with most sites located along the coasts of the northern hemisphere. Moreover, the number of unknowns β_{pj} is large and may exceed the number of tide gauges with reliable trends for any reasonable value of n_o.

Therefore, the second approach is to reduce the number of unknowns through parametrising the ice-load trends. Then eqs. (9) and (15) can be used together to determine

This document is provided by JAXA.

the parameters of the ice load by a least squares method. If there are only a few free parameters to adjust, this avoids much of the uncertainties of the former solution. However, the quality of this solution depends strongly on the selected ice-load model. If the ice-load model is incorrect, the solution based on it might be misleading.

Below we will explore the second approach. For that, we assume a constant trend in ice cover over each of the major ice sheets. This assumption is not justified by the known processes on ice sheets and glaciers, where large spatial variations in ablation or accretion are observed. However, the spatial resolution of the tide gauge data set is not good enough to resolve small-scale variability. Nevertheless, we should be able to determine whether the Greenland and Antarctic ice sheets are on average increasing or decreasing. Therefore, the assumption can be justified as a first step.

For linear changes on each of the major ice sheets we can computed the finger-print in the RSL trends for a unit trend. Let $g^{(k)}$ be the characteristic function of the k-th glacier, defined as

$$g^{(k)}(\vartheta,\lambda)=\begin{cases} 1 & \text{on the glacier number } k \\ 0 & \text{otherwise} \end{cases} \tag{16}$$

with harmonic development

$$g^{(k)}(\vartheta,\lambda)=\sum_{n=0}^{\infty}\sum_{m=-n}^{n} g_{nm}^{(k)} Y_{nm}(\vartheta,\lambda). \tag{17}$$

Assuming that the sea-level eq. (8) has a unique solution for η replaced with any of the characteristic functions (16), these solutions shall be called the *finger-print functions* of the k-th glacier and be denoted $f^{(k)}(\vartheta,\lambda)$. Then, the corresponding solutions of eq. (15) yield the harmonic coefficients $f_{nm}^{(k)}$ of these finger-print functions, *i.e.*

$$\begin{aligned} f_{nm}^{(k)}=3\frac{1+k_n-h_n}{2n+1}\Bigg\{&\frac{\rho_1}{\rho_o}g_{nm}^{(k)} \\ &+(-1)^m\frac{\rho_w}{\rho_o}\sum_{p=0}^{\infty}\sum_{q=0}^{\infty}\sum_{j=-p}^{p}\sqrt{\frac{(2n+1)(2p+1)(2q+1)}{4\pi}}\begin{pmatrix} n & p & q \\ 0 & 0 & 0 \end{pmatrix}\begin{pmatrix} n & p & q \\ -m & j & m-j \end{pmatrix}O_{qm-j}f_{pj}^{(k)}\Bigg\} \\ -\Bigg\{\frac{3}{O_{00}}\frac{\rho_w}{\rho_o}&\sum_{p=0}^{\infty}\sum_{q=0}^{\infty}\sum_{r=0}^{\infty}\sum_{j=-p}^{p}\sum_{i=-q}^{q}\frac{1+k_p-h_p}{2p+1}\sqrt{\frac{(2p+1)(2q+1)(2r+1)}{4\pi}}\begin{pmatrix} p & q & r \\ 0 & 0 & 0 \end{pmatrix}\begin{pmatrix} p & q & r \\ -j & i & j-i \end{pmatrix}O_{p-j}O_{rj-i}f_{qi}^{(k)} \\ &+\frac{3}{O_{00}}\frac{\rho_1}{\rho_o}\sum_{p=0}^{\infty}\sum_{j=-p}^{p}(-1)^j\frac{1+k_p-h_p}{2p+1}O_{p-j}g_{pj}^{(k)}+\sqrt{4\pi}\frac{\rho_1}{\rho_w}\frac{g_{00}^{(k)}}{O_{00}}\Bigg\}\delta_{n0}\delta_{m0}. \end{aligned} \tag{18}$$

With these finger-prints, the trend at tide gauge i may be approximated as

$$\alpha_i=\sum_{k=1}^{K}\beta_k f^{(k)}(\vartheta_i,\lambda_i)+c, \tag{19}$$

where β_k is the (unknown) constant trend for the k-th ice mass, $f^{(k)}$ the unit finger-print function for this ice mass, K the number of ice masses considered, ϑ_i and λ_i are the geographical coordinates of the tide gauge, and c is a constant included to account for a global sea level change not being due to ice load changes. Finally, the β_k can be estimated in a least squares fit of eq. (19) to the trends determined from the tide gauges.

For practical calculations the eqs. (15) and (18) have to be truncated at a maximal degree n_o. This results in the matrix equation

$$\sum_{p=0}^{n_o}\sum_{j=-p}^{p}A_{nm,pj}^{(n_o)}\xi_{pj}=\sum_{p=0}^{n_o}\sum_{j=-p}^{p}B_{nm,pj}^{(n_o)}\eta_{pj}, \tag{20}$$

This document is provided by JAXA.

with matrix elements

$$A^{(n_o)}_{nm,pj} := \delta_{np}\delta_{mj} + \frac{3}{O_{00}}\frac{\rho_w}{\rho_o}\sum_{q=0}^{n_o}\sum_{r=0}^{n_o}\sum_{i=-q}^{q}\frac{1+k_q-h_q}{2q+1}\sqrt{\frac{(2p+1)(2q+1)(2r+1)}{4\pi}}\begin{pmatrix} p & q & r \\ 0 & 0 & 0\end{pmatrix}\begin{pmatrix} p & q & r \\ j & -i & i-j\end{pmatrix}O_{q-i}O_{r\,i-j}\delta_{n0}\delta_{m0} - 3(-1)^m\frac{\rho_w}{\rho_o}\frac{1+k_n-h_n}{2n+1}\sum_{q=0}^{n_o}\sqrt{\frac{(2n+1)(2p+1)(2q+1)}{4\pi}}\begin{pmatrix} n & p & q \\ 0 & 0 & 0\end{pmatrix}\begin{pmatrix} n & p & q \\ -m & j & m-j\end{pmatrix}O_{qm-j}, \quad (21)$$

and

$$B^{(n_o)}_{nm,pj} := 3\frac{1+k_n-h_n}{2n+1}\frac{\rho_l}{\rho_o}\delta_{np}\delta_{mj} - \left\{(-1)^j\frac{3}{O_{00}}\frac{\rho_l}{\rho_o}\frac{1+k_p-h_p}{2p+1}O_{p-j} + \frac{\sqrt{4\pi}}{O_{00}}\frac{\rho_l}{\rho_w}\delta_{p0}\delta_{j0}\right\}\delta_{n0}\delta_{m0}. \quad (22)$$

With matrix

$$S^{(n_o)} := \mathrm{A}^{(n_o)^{-1}}B^{(n_o)}, \quad (23)$$

the solution of the matrix eq. (20) reads $\xi_{nm} = \sum_{p=0}^{n_o}\sum_{j=-p}^{p} S^{(n_o)}_{nm,pj}\eta_{pj}$.

By this, approximations $f^{(k,n_o)}$ to the footprint functions $f^{(k)}$ are defined as

$$f^{(k,n_o)}_{nm} := \sum_{p=0}^{n_o}\sum_{j=-p}^{p} S^{(n_o)}_{nm,pj}g^{(k)}_{pj}, \quad (24)$$

$$f^{(k,n_o)}(\vartheta,\lambda) := \sum_{n=0}^{n_o}\sum_{m=-n}^{n} f^{(k,n_o)}_{nm}Y_{nm}(\vartheta,\lambda). \quad (25)$$

It has to be shown that these approximations actually converge in a certain sense to the true footprint functions $f^{(k)}$. Furthermore, an n_o has to be found, for which the approximations are sufficiently close to the footprint functions $f^{(k)}$ for all glaciers.

No mathematically rigorous proof of convergence of the approximation to the footprint functions is attempted here. Instead, in Fig. 1, the trends predicted at individual tide gauges are given as function of the cut-off degree n_o. At all tide gauges, the trend predictions are stable for $n_o > 40$ and no significant variations occur at higher values of n_o. It is interesting to note here that the trends at tide gauges in the far field do not show large variations from gauge to gauge, while at gauges closer to the ice loads large variations in the predicted trends are found.

In Fig. 2 the boundaries of the ice sheets are given for the cut-off degree of $n_o = 69$. This approximation represents the boundaries of the ice sheets already to a great detail.

The finger-prints of the Antarctic and Greenland ice sheets are given in Fig. 3. For a unit increase of the Antarctic ice sheet, sea level will basically tilt from South to North with very little dependency on longitude, while a similar increase of the Greenland ice sheet will result in an opposite tilt from North to South but additionally a dependency on longitude for high northern latitudes.

The finger-prints of Antarctic and Greenland to a large extent are anti-correlated. This may cause problems in separating the effect of the two ice sheets if the overall trends have opposite sign. Furthermore, the success of a fit of the model function to the tide gauge trends depends also on the geographical distribution of the tide gauges. This will be discussed in the next section.

This document is provided by JAXA.

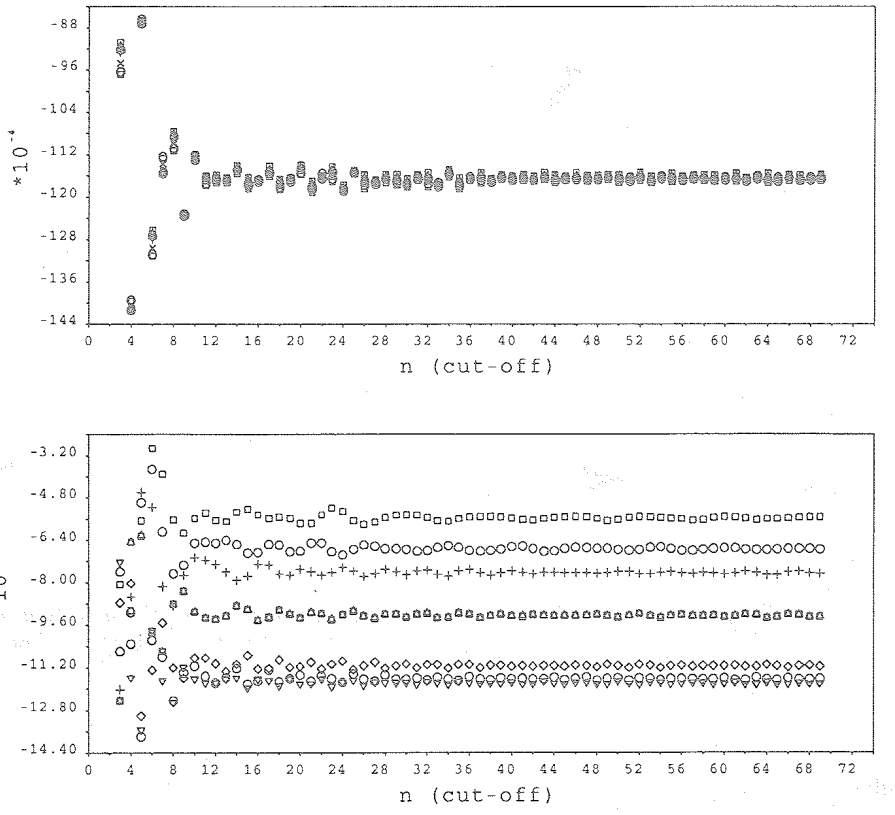


Fig. 1. Trends predicted by equally weighted finger-prints of the Antarctic, Greenland, and Iceland ice sheets as function of the cuf-off degree n_o. Upper diagram: Stations from the coast around Great Britain, lower: from New Zealand. Each symbol represents an individual tide gauge.

4. Determination of RSL trends at tide gauges

The global tide gauge data set provided by the PSMSL (Spencer and Woodworth, 1993) contains more than 1700 records of monthly mean sea levels. These time series are of variable quality and length. The PSMSL separates the total data set into a so-called Metric data set and a Reviced-Local-Reference data set, with the latter one comprising all the records with a well-documented history of the tide-gauge benchmark. For trend determinations, only records in the RLR subset can be used. In this data set, there are 988 records with at least five years of data, with the longest of them covering a span of nearly 200 years.

In Fig. 4 we show the trends as determined from the RLR tide gauges. All trends up to ± 10 mm/yr are displayed. The figure reveals a large scatter of the local trends, which partly can be explained by known tectonic movements and partly by postglacial rebound. To improve the quality of the attempted fit of eq. (19), we have to use as many trend values as possible. Therefore, it is necessary to account for as many disturbing influences as

This document is provided by JAXA.

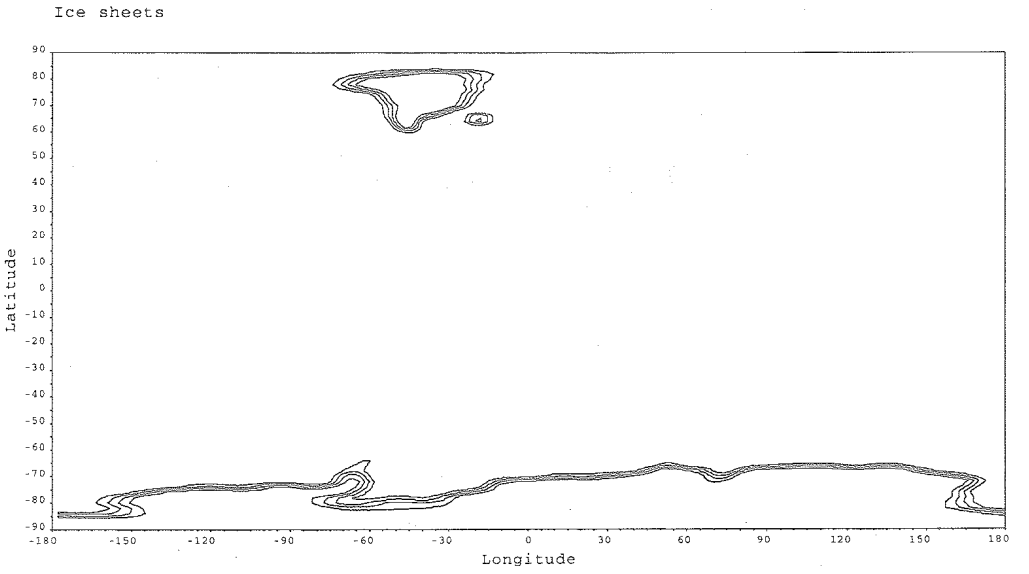


Fig. 2. Approximation of the ice sheet functions to degree 69. The nominal value inside and outside the ice sheets is 1 and 0, respectively. The approximation does not deviate from these values more than 0.02 except at the boundaries, which have a steep slope. Isolines are from 0 to 1 with step 0.2.

possible.

Basically, the local trends determined from tide gauges are significantly affected by (1) tectonic movements, (2) postglacial rebound, and (3) decadal to interdecadal variability. We will discuss these effects one by one.

(1) Large parts of the ocean's coasts are in deformation areas associated with plate tectonics (see, *e.g.* Fig. 6 in Stein, 1993). In most of these regions, the tectonically caused vertical crustal movements are dominated by short spatial scales of the order of 30 to 100 km (see *e.g.* Emery and Aubrey, 1991). Thus, the ice mass finger-print is distinctively different from the tectonical signal in sea level and a contamination of the β_k due to tectonic motion should be small. With respect to the long-wavelength ice signal, the tectonical signal can be considered as noise. Moreover, in many geographical regions the vertical crustal motion is of the order of ± 1 mm/yr and thus smaller than the expected local signal due to ice mass changes. Therefore, we have not taken any measure to decontaminate the tide gauge trends for tectonical vertical crustal motion.

(2) The present-day postglacial signal (PGS) in sea level may be highly correlated with the finger-print of present-day changes in ice sheets. Fortunately, elaborated models exist for the PGS and these models can be used to decontaminate the tide gauge trends for the PGS. However, inter-model differences are still considerable. Therefore, we have used a suite of models in the determination of the ice sheet trends. Moreover, a scale factor was introduced for the PGS in order to allow for uncertainties in the global amplitude of the PGS. Thus, eq. (19) is modified to

This document is provided by JAXA.

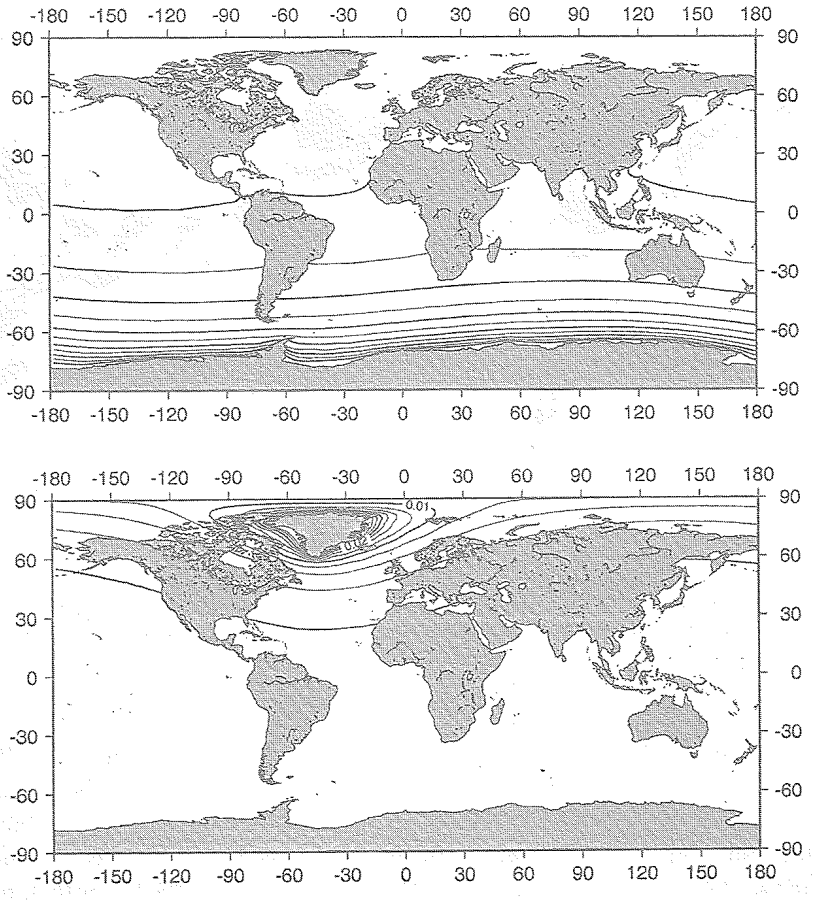


Fig. 3. RSL finger print of a uniform ice load change across the complete Antarctic (upper diagram) and Greenland (lower diagram) ice sheets. For Antarctica, isolines are from −0.01 to 0.045 with step −0.005. Spacing of thick lines is 0.01 and zero line is the third line from top. For Greenland, isoline are from 0. to 0.0275 with step 0.0025. Spacing of thick lines is 0.01 and zero line is the first line from bottom.

$$\alpha_i = \sum_{k=1}^{K} \beta_k f^{(k)}(\vartheta_i, \lambda_i) + \gamma p_i + c, \tag{26}$$

where p_i is the PGS at the tide gauge i and γ the (unknown) scale factor for a given PGS model. It should be mentioned here, however, that since the PGS is closely correlated with the present-day changes, any errors in the PGS will bias the estimates of the present-day changes.

(3) Interannual to multidecadal variations in RSL are mainly due to similar variations in atmospheric and oceanic circulation. In sea-level at costal locations, these variations are of the order of several cm, and thus significantly bias trends determined from records of less than several decades. To determine a local trend from an individual tide gauge with an accuracy of 0.5 mm/yr, records of 60 years are required in most coastal regions (*e.g.* Zerbini

This document is provided by JAXA.

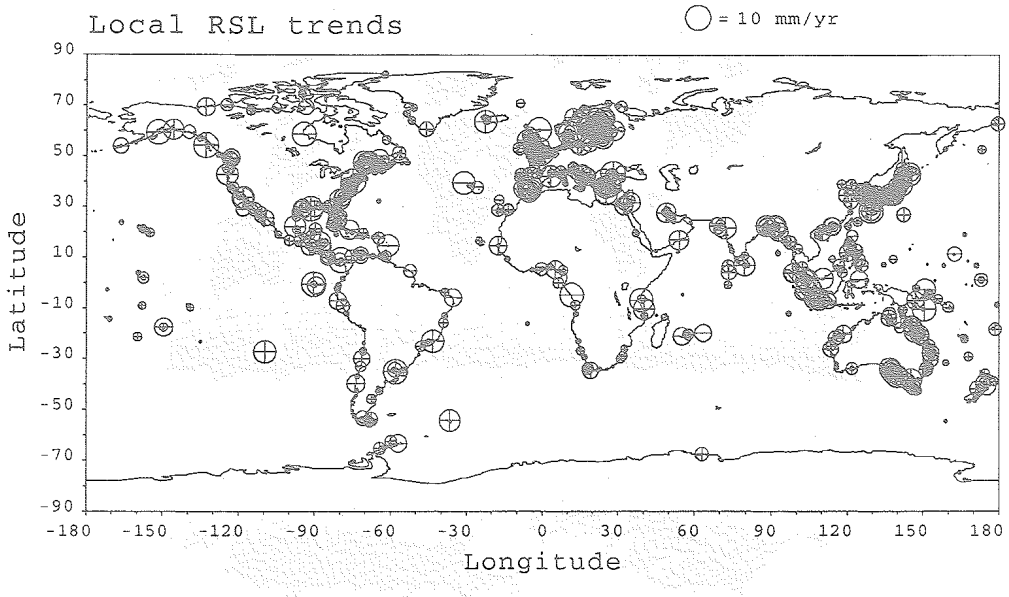


Fig. 4. Local RSL trends determined from tide gauges. The diameter of the circles at each tide gauge are proportinal to the trend with positive and negative trends indicated by a plus or minus sign, respectively.

et al., 1996). Both, tide gauge studies (*e.g.* Sturges, 1987; Gröger and Plag, 1993) and satellite altimetry observations (*e.g.* Nerem *et al.*, 1997) have shown that the interannual to multi-decadal sea level variations are spatially coherent over large regions. Therefore, based on a high-quality long record in a given region, shorter records can be decontaminated for the interannual to multidecadal variability (Sjöberg, 1987; Plag, 1988). For that, time series of the monthly differences between the a given shorter record and the base record are computed. These differences are nearly free of the interannual to multidecadal variability. The trend of these differences plus the long-term trend at the base station thus is a decontaminated long-term trend at the station with the shorter record.

In the present study, only the local RSL trends are used without any corrections for interannual to multidecadal variability.

5. Antarctic and Greenland ice thickness changes

The anti-correlation of the Greenland and Antarctic finger-prints in large geographical regions may cause problems if the changes of these two ice sheets have opposite signs. However, taking into account the position of the available tide gauges, the predicted trends at a considerable number of tide gauges depend on the spatial pattern of either the Antarctic or Greenland ice sheets alone while the other ice sheet only contributes a small constant (Fig. 5). Iceland, on the other hand is too close to Greenland for its finger-print to be separable from the Greenland finger-print.

It can be concluded that particularly the tide gauges in the near to medium field of a given ice sheet will be able to detect the finger-print. Thus, Southern hemisphere gauges will

This document is provided by JAXA.

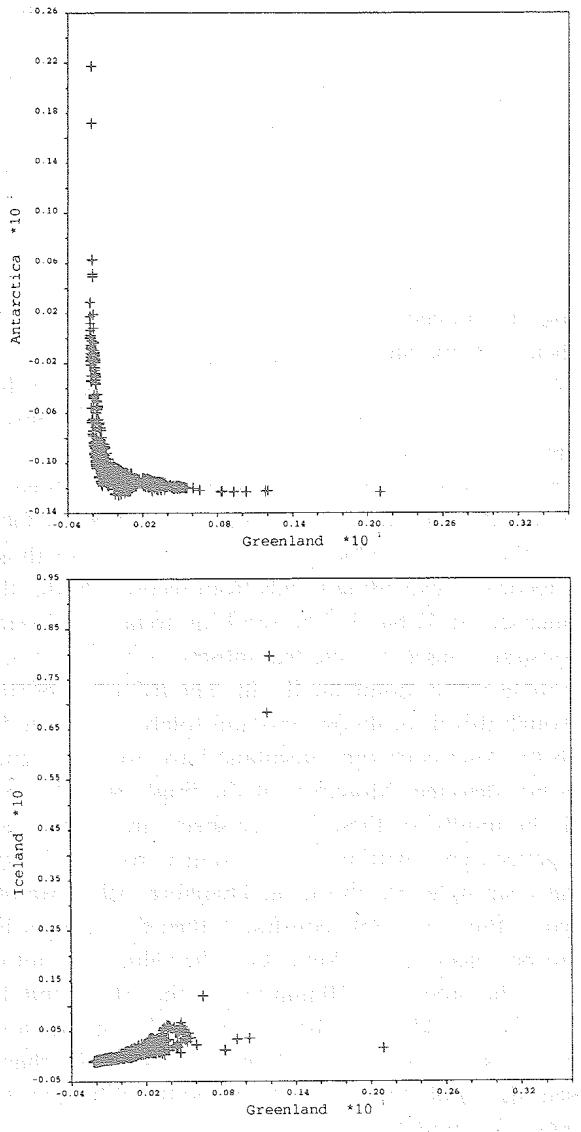


Fig. 5. Comparison of RSL finger prints at tide gauges. Upper diagram: Antarctica versus Greenland; lower diagram Iceland versus Greenland.

constrain the Antarctic ice sheet while Northern hemisphere gauges will do the same for the Greenland ice sheet. Tide gauges at higher latitudes will have a greater effect on the inversion than those at lower latitudes.

Changes in the two large ice sheets having the same sign should result in a finger-print detectable in sea level. Thus, the sum of a unit increase in both ice sheets displays an increase of sea level close to the ice sheets and a decrease at lower latitudes. However, in large geographical regions, a negative change in the Antarctic ice sheet would be correlated

This document is provided by JAXA.

Table 2. Parametres of the postglacial rebound models from Mitrovica (1996, personal communication).

	Model 1	Model 2
Lithosphere	120 km	120 km
Upper mantle viscosity	1×10^{21} Pas	1×10^{21} Pas
Lower mantle viscosity	2×10^{21} Pas	4.75×10^{21} Pas
Ice model	ICE-3G	ICE-3G

with a positive change for Greenland. Changes with opposite sign for these ice sheets therefore will be difficult to separate.

Based on eq. (26) the finger-print functions have been fitted to the trend data set. In this fit, two different models for the PGS have been used, which only differ in the lower mantle viscosity (Table 2).

In the fit, different constraints have been applied to select subsets of the trend values. These constraints are (1) the latitude ϑ excluding trends from a latitude band centred around the equator; (2) the absolute value of the trend T, excluding those trends larger than a limit; (3) length of record L, excluding trends from records shorter than a lower bound. The results are summarised in Table 3. The resulting trends in the ice sheets are strong dependent on the constraints used to selected subsets of the trend values. Without any constraints, the large trend values dominate the fit. The reduction of standard deviation of the trend data set through this fit is almost zero and solely due to the PGS and the global rise c while the trends for Antarctica and Greenland have opposite sign. Thus, a fingerprint of these ice sheets is not detected. Moreover, if the finger-print for both Greenland and Iceland are included, the results for these two ice sheets are unreasonably large.

Using only tide gauge trends within $|T|<12$ mm/yr reduces the number of gauges by only 7.7% but this has a strong effect on the fit. Therefore, below we only discuss fits with this constraint applied. If this is the only constraint, then the rates for both Antarctica and Greenland turn out to be negative. For Antarctica, the value does not depend on the PGS model selected and is of the order of -50 mm/yr. On the other hand, for Greenland, PGS model 1 gives decreases of the order of -100 mm/yr while the rates for model 2 are of the order of -50 mm/yr. The scale factor for PGS model 2 is smaller than for model 1, while the constant c representing a global rise in sea level and the reduction of standard deviation of the total fit are larger for model 2.

If the length of the tide gauge record is used as additional constraint with $L>240$ months, then the negative rate for Greenland is rather large (-189 mm/yr) while the rate for Antarctica is much smaller (-22 mm/yr). However, constraining the length of the time series removes a large fraction of the tide gauges at higher latitudes, *i.e.* in the near-field. Therefore, this may not be a reasonable constraint.

Eliminating all trends from tide gauges within $|\vartheta|<30°$ reduces the number of tide gauges by almost 30%. However, applying this together with the constraint $|T|<12$ mm/yr, results in rates of -29 mm/yr and -124 mm/yr for the Antarctic and Greenland ice sheets, respectively. That is, both ice sheets appear to be decreasing.

The combined constraints $|\vartheta|>50°$ and $|T|<12$ mm/yr is the only set resulting in large positive rates for both ice sheets. These constraints eliminate all tide gauges in the far

This document is provided by JAXA.

Table 3. Results of the fits of eq. (26) to the tide gauge trends. The model function is denoted by nI, pm, with n number of ice sheets included, and m number of PGS model. Constraints are applied for latitude ϑ, trend T and record length L. N is the number of stations meeting the constraints. All rates are in mm/yr. Rates are for Antarctica (Ant.), Greenland (Green.) and Iceland (Ice.) and the remaining global average c. The scale factor γ for the PGS model is relative. σ_0 and σ_{res} are the standard deviation of the trend values and the residuals with respect to the model fit, respectively. Red. is the reduction in the standard deviation in %.

Model	$\lvert\vartheta\rvert$ °	$\lvert T\rvert$ mm/yr	L months	N	Ant.	Green. mm/yr	Ice.	γ	c	σ_0 mm/yr	σ_{res}	Red. %
3I, p1				988	−124	580	1600	0.88		11.14	10.93	1.9
3I, p1, c				988	71	−405	1318	0.96	2.11	11.14	10.93	1.9
2I, p1, c				988	88	−258		0.97	2.32	11.14	10.94	1.8
2I, p2, c				988	88	−181		0.91	2.44	11.14	10.92	2.0
2I, p1, c	>30			708	114	−130		1.00	2.24	10.79	10.56	2.1
2I, p1, c	>30	<12		661	−29	−124		0.83	0.75	3.80	3.34	12.1
2I, p1, c	>30		>240	410	35	−127		0.84	1.33	3.80	3.25	14.4
2I, p1, c	>30	<12	>240	404	12	−154		0.81	1.16	3.02	2.31	23.5
2I, p1, c	>50	<12		216	86	340		0.88	0.36	4.02	3.00	25.4
2I, p1, c			>240	529	1	−214		0.83	1.26	4.09	3.60	12.0
2I, p1, c		<20	>240	526	−4	−191		0.83	1.13	3.40	2.83	16.8
2I, p1, c		<15	>240	524	−12	−195		0.81	1.03	3.23	2.65	18.0
2I, p1, c		<12	>240	521	−22	−189		0.81	0.95	3.09	2.48	19.7
2I, p1, c		<20		959	−13	−114		0.84	1.04	4.95	4.65	6.1
2I, p1, c		<15		937	−58	−93		0.83	0.48	4.22	3.90	7.6
2I, p1, c		<12		921	−56	−117		0.83	0.51	3.88	3.51	9.5
2I, p2, c		<20		959	−16	−57		0.77	1.10	4.95	4.63	6.5
2I, p2, c		<15		937	−59	−31		0.77	0.57	4.22	3.86	8.5
2I, p2, c		<12		921	−57	−52		0.78	0.61	3.88	3.47	10.6

field. Thus, the near-field gauges appear to be best fitted by a growth of both ice sheets. The global signal represented by c appears to be very small (<0.4 mm/yr). The large dependency of the results on the far-field gauges included or excluded may be due to another latitude-dependent signal in the RSL trends, super-imposed on the ice sheet finger-prints. For example, a latitude-dependent warming of the ocean with relatively large warming at lower latitudes would bias the estimated rates for the ice sheets towards lower values and might even cause negative rates for actually growing ice sheets.

6. Discussion

Reasonably selected subsets of the RSL trends determined from the global tide gauges database indicate negative rates of approximately −50 mm/yr for the Antarctic ice sheet and −50 to −100 mm/yr for the Greenland ice sheet. However, the results depend on the selection criteria. Excluding the tide gauges in the far field of the ice sheets results into positive trends for both ice sheets. This high sensitivity of the estimated rates for the ice sheets to the latitudinal constraint for the selection of tide gauges indicates that the rates of relative sea-level changes determined from tide gauges may be contaminated by another

This document is provided by JAXA.

latitude-dependent factor.

This factor may be a combined effect of steric volume changes and changes in the ocean circulation, which both may have a significant latitude-dependent part. Interdecadal variability in ocean circulation and water temperature induces similar sea level variations, which effect trends in relative sea level determined from time series of up to several decades. Taking into account that many tide gauge records cover the last 30–50 years, a bias of the trends can be expected. However, observational data on ocean circulation and density are sparce (Warrick *et al.*, 1996) and the spacial pattern of steric sea-level changes cannot be determined confidently from these observations.

The geographical distribution of steric sea-level variations can also be determined from ocean circulation or coupled atmosphere-ocean circulation models (*e.g.* Gregory, 1993; Bryan, 1996). However, results still show little similarity between different models and, therefore, have low confidence.

Nevertheless, to improve the inversion of the tide gauge data, models for the steric effect need to be taken into account. For example, output from different advanced global circulation model simulations for the last hundred years could be used to study the sensitivity of the inversion to this factor.

Another potential bias of the estimated rates is due to uncertainties in the models used to compute the pgs. (Huybrechts and Le Meur (1999) modelled the present-day pgs of Antarctica and found that this signal may be significantly larger that the one predicted by the models used here. Therefore, the use of more advanced models for the pgs would be an additional improvement of the fits presented here.

Acknowledgments

The postglacial rebound signal was computed from data sets provided by J.X. Mitrovica. The tide gauge data was taken from the database maintained by the *Permanent Service for Mean Sea Level*.

References

Barnett, T.P. (1984): The estimation of "global" sea level change: a problem of uniqueness. J. Geophys. Res., **89**, 7980–7988.

Bryan, K. (1996): The steric component of sea level rise associated with enhanced greenhouse warming: a model study. Clim. Dyn., **12**, 545–555.

Dickman, S.R (1997): Detection of hypothetical global warming effects. Ann. Geophys., **15** (Supl. I), C32.

Douglas, B.C. (1991): Global sea level rise. J. Geophys. Res., **96**, 6981–6992.

Douglas, B.C. (1992): Global sea level acceleration. J. Geophys. Res., **97**, 12699–12706.

Douglas, B.C. (1995): Global sea level change: Determination and interpretation. Rev. Geophys., IUGG suppl., 1425–1432.

Edmonds, A.R. (1957): Angular momentum in quantum mechanics. Princeton, Princeton University Press.

Emery, K.O. and Aubrey, D.G. (1991): Sea Levels, Land Levels, and Tide Gauges. Berlin, Springer.

Farrell, W.E. (1972): Deformation of the Earth by surface loads. Rev. Geophys. Space Phys., **10**, 761–797.

Farrell, W.E. and Clark, J.A. (1976): On postglacial sea level. Geophys. J. R. Astron. Soc., **46**, 647–667.

Gasperini, P., Sabadini, R. and Yuen, D.A. (1986): Excitation of the earth's rotational axis by recent

This document is provided by JAXA.

glacial discharges. Geophys. Res. Lett., **13**, 533–536.
Gornitz, V. and Lebedeff, S. (1987): Global sea level changes during the past century. Sea Level Fluctuations and Coastal Evolution, ed. by D. Nummedal *et al.* Soc. Econ. Palaeontol. Miner., 3–16 (Spec. Publ., Vol. 41).
Gregory, J.M. (1993): Sea level changes under increasing atmospheric CO_2 in a transient coupled ocean-atmosphere gcm experiment. J. Clim., **6**, 2247–2262.
Gröger, M. and Plag, H.-P. (1993): Estimations of a global sea level trend: Limitations from the structure of the PSMSL global sea level data set. Global Planet. Change, **8**, 161–179.
Houghton, J.T., MeiraFilho, L.G., Callander, B.A., Harris, N., Kattenberg, A. and Maskell, K., ed. (1996): Climate Change 1995—The Science of Climate Change. Cambridge, Cambridge University Press.
Huybrechts, P. and LeMeur, E. (1999): Predicted present-day evolution patterns for ice thickness and bedrock elevation over Greenland and Antarctica. Polar Res., **18**, 299–306.
Lambeck, K. (1993): Glacial rebound of the British Isles -I. Preliminary model results, II. A high-resolution, high precision model. Geophys. J. Int., **115**, 941–990.
Nerem, S.M., Rachlin, K.E. and Beckley, B.D. (1997): Characterization of global mean sea level variations observed by TOPEX/POSEIDON using empirical orthogonal functions. Surv. Geophys., **18**, 293–302.
Peltier, W.R. (1974): The impulse response of a Maxwell Earth. Rev. Geophys. Space Phys., **12**, 649–669.
Peltier, W.R. and Tushingham, A.M. (1989): Global sea level rise and the Greenhouse effect: Might they be connected? Science, **244**, 806–810.
Pirazzoli, P.A. (1989): Present and near-future global sea-level changes. Palaeogeogr., Palaeoclimatol., Palaeoecol., **75**, 241–258.
Pirazzoli, P.A. (1993): Global sea-level changes and their measurement. Global Planet. Change, **8**, 135–148.
Plag, H.-P. (1988): A regional study of Norwegian coastal long-period sea-level variations and their causes with special emphasis on the Pole Tide. Berl. Geowiss. Abhandl. Reihe A, **14**, 1–175.
Plag, H.-P. (1993): The "sea level rise" problem: An assessment of methods and data. Proceedings of the International Coastal Congress, Kiel 1992, Frankfurt, P. Lang Verlag, 714–732.
Quinlan, G. and Beaumont, C. (1982): The deglaciation of Atlantic Canada as reconstructed from the post glacial relative sea-level record. Can. J. Earth Sci., **19**, 2232–2246.
Sjöberg, L.E. (1987): Comparison of some methods of determining land uplift rates from tide gauge data. ZfV, **2**, 69–73.
Spencer, N.E. and Woodworth, P.L. (1993): Data holdings of the Permanent Service for Mean Sea Level, Tech. rep., Permanent Service for Mean Sea Level, Bidston, UK, 81 p.
Stein, S. (1993): Space geodesy and plate motion. Contributions of Space Geodesy in Geodynamics: Crustal Dynamics, ed. by D.E. Smith and D.L. Turcotte. Washington, D.C., Am. Geophys. Union, 5–20 (AGU Geodyn. Ser., Vol. 23).
Sturges, W. (1987): Large-scale coherence of sea level at very low frequencies. J. Phys. Oceanogr., **17**, 2084–2094.
Warrick, R.A., Provost, C.I., Meier, M.F., Oerlemans, J. and Woodworth, P.L. (1996): Changes in sea level. Climate Change 1995—The Science of Climate Change, ed. by J.T. Houghton *et al.* Cambridge, Cambridge University Press, 359–405,
Zerbini, S. and 15 colleagues (1996): Sea level in the Mediterranean: a first step towards separation of crustal movements and absolute sea-level variations. Global Planet. Change, **14**, 1–48.

(Received April 3, 2000; Revised manuscript accepted July 27, 2000)

This document is provided by JAXA.

This document is provided by JAXA.

Mem. Natl Inst. Polar Res., Spec. Issue, 54, 319-330, 2001

Scientific note

The determination of the reference point of the VLBI antenna in Ny-Ålesund

Paolo Tomasi[1,2], Pierguido Sarti[1,3] and Maria Rioja[1,4]

[1]*Istituto di Radioastronomia, CNR, Via Gobetti 101, 40129 Bologna, Italy*
[2]*Istituto di tecnologia informatica spaziale CNR, Centro di Geodesia Spaziale, 75100 Matera, Italy*
[3]*DISTART Universita' di Bologna, Bologna, Italy*
[4]*Observatorio Astronomico Nacional, Alcala, Spain*

Abstract: We present here, the results of a campaign of measures carried on between August 25th and September 8th, 1999, in Ny-Ålesund, to tie the reference point of the VLBI antenna on the ground marks.

A number of Leica retro-targets has been attached (glued) all over the structure of the antenna, and their positions determined (horizontal and vertical angles, along with distance whenever it was possible) with respect to a local reference network. The positions of two points at opposite edges of the elevation axis have also been pinpointed and measured (only horizontal and vertical angles, in this case), to determine the vertical component of the reference point and to measure the offset between the elevation and azimuth axes. The local reference network has been measured using direct and inverse intersection depending on different position and mutual visibility of pillars. Occasionally some pillars have been measured using both methodologies. Furthermore, trigonometric levelling has been performed for connecting the levelling bolts of the six closest pillars to the 3-D network adjustment results and therefore obtain an univocal determination of the height of the VLBI reference point tight to the altimetric control network.

The positions of several markers on the antenna have been measured for 8 antenna azimuth angles, uniformly spread along 360 degrees, in steps of 45 degrees, with the VLBI antenna at the same elevation angle, nearly at the zenith direction. In order to test the position of the elevation axis, we did similar measures on a selected number of markers at different antenna elevation angles, in the range from 90 to 45 degrees, in steps of 15 degrees, for a fixed azimuth angle.

The analysis of these measures provide both coordinates for the position of the reference point of the VLBI antenna, and an estimate of the offset between the elevation and azimuth axes in the antenna of Ny-Ålesund. The offset vector from the reference pillar selected (marker 91) is $X=21.830\pm0.001$ m and $Y=18.787\pm0.001$ m, while the height referred to the levelling bolt of the same pillar (marker 91b) is $Z=10.269\pm0.001$ m.

In the last section we list some suggestions for modifications of the local reference network around the VLBI antenna in order to simplify similar future campaigns of measurements.

This document is provided by JAXA.

1. Introduction

Very Long Baseline Interferometry (VLBI) technique applied to geodesy provides estimates of baseline lengths and their temporal variations on scales of thousands of kilometres, with sub-centimetre accuracy. However, the measurements with this technique correspond to a precise point on the antennas, the reference point of the VLBI antenna. Sometimes this point is called "invariant point", since its position is not variable in space at different pointing angles of the VLBI antenna and it remains in a fixed position during VLBI observations. For antennas with azimuth-elevation mounting, as generally is the case for single dish radio telescope, this point is located along the azimuth axis of the antenna. It coincides with the intersection of the elevation and azimuth axis if the two axes intersect. If the two axes do not intersect it is the projection of the elevation axis onto the azimuth

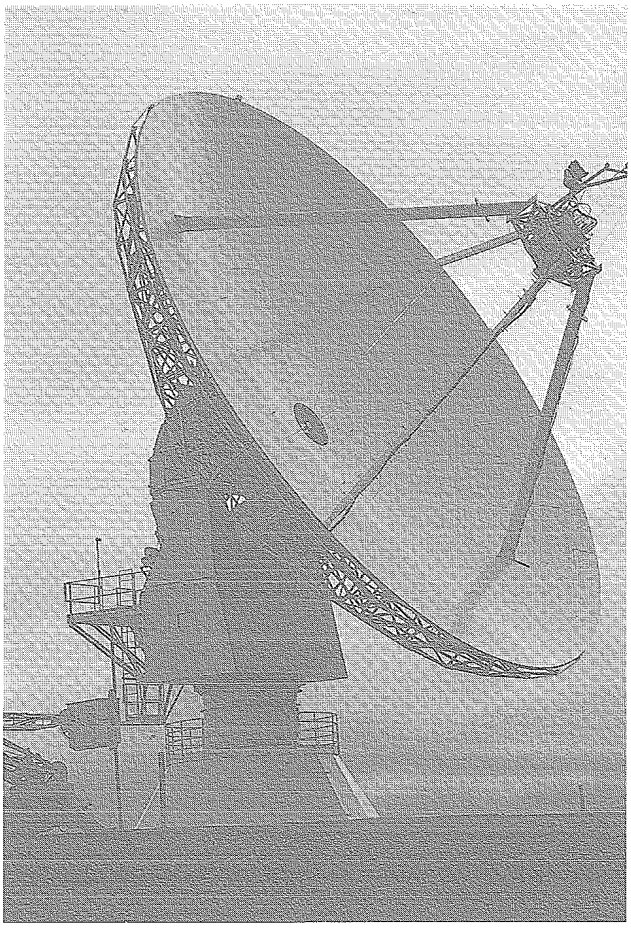


Fig. 1. The Ny-Ålesund VLBI antenna. A 20 m diameter dish with the S/X receiver in the primary focus.

This document is provided by JAXA.

axis. The second is the case for the VLBI antenna in Ny-Ålesund, with a diameter of 20 m and an axis offset around half a meter (Fig. 1).

The importance of linking the invariant point of a VLBI antenna to a local reference network is well known as a way to disentangle the possible (even unlikely) local movements of the antenna in respect to the ground, and the crust movements. In absence of that measurement we cannot be sure that local movements of the antenna and/or its basement do not affect the VLBI geodetic measurements.

In particular, for Ny-Ålesund, there is an unexpected and incomprehensible result that makes this measurement even more necessary: the significant discrepancy between the vertical velocities measured with GPS and VLBI techniques at this site. This suggests that some problems are present locally with one of the techniques (or even with both). For example, there are recent suspects of local motion at the GPS pillar. But also the VLBI antenna, even with its basement deeply dug into bedrock and permafrost could experience some local motion that should be detected, if present. Otherwise any interpretation of vertical motion detected up there in terms of crust motion would make no sense.

There are different ways of determining the position of the reference point of a VLBI antenna, depending on the antenna characteristics, *i.e.* whether the reference point is visible and physically identified, or whether this point is not visible or not physically identified. In the first case, this point can be used as a target for a total station (a theodolite equipped with a diastimeter), and any local motion will be easily detected and directly measured with a proper monitoring. If this is not the case, as it is for Ny-Ålesund, the reference point must be determined using the positions of some targets on the structure of the antenna, using a theodolite or a total station, at different pointing angles of the antenna. The strategy we have used to measure the positions of the markers was based on fundamental principle of direct intersection.

The motion of a generic point on the antenna structure during the motion of the antenna itself is contained in a surface with toric shape (Fig. 2). If the two axes intercept this surface becomes a sphere. A single point on the antenna, with a rotation only around

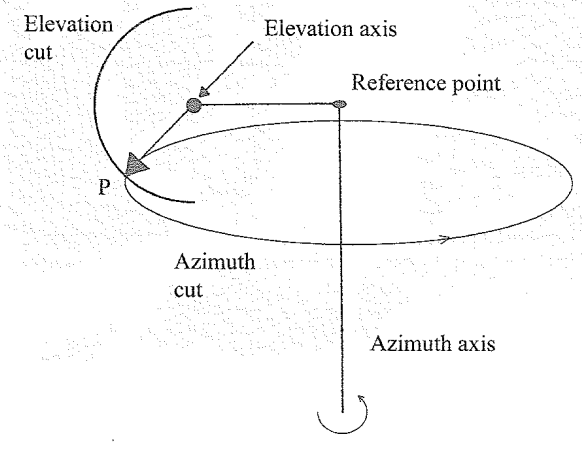


Fig. 2. A scheme of the motion of a generic point on the antenna during a rotation in azimuth and in elevation.

This document is provided by JAXA.

the azimuth axis, will move along a circumference, lying in a plane parallel to the horizontal plane. This is true under the assumption that structural deformations of the antenna, due to different effects (in general gravity and thermal deformation) are negligible. Hence, a sufficiently large set of measurements of the positions of a generic point on the antenna allows determination of the invariant point and the axis offset. That means motions around the vertical and the elevation axes. This second kind of motions (and measures) can be avoided, if it is possible to identify the elevation axis itself placing two targets at the opposite edges. In this case the position of the elevation axis can be determined and its distance from the vertical axis can be measured with indirect methods.

2. The measurements

We used standard Leica prisms for linking different pillars around the VLBI antenna and measure the local reference network while Leica tape targets were used for the antenna itself. The elevation axis of the antenna has been visualized, using two pins at the opposite ends of that axis (Fig. 3). A way to test that the two pins really represent the elevation axis would be to verify they are not moving during a run in elevation of the antenna. For the

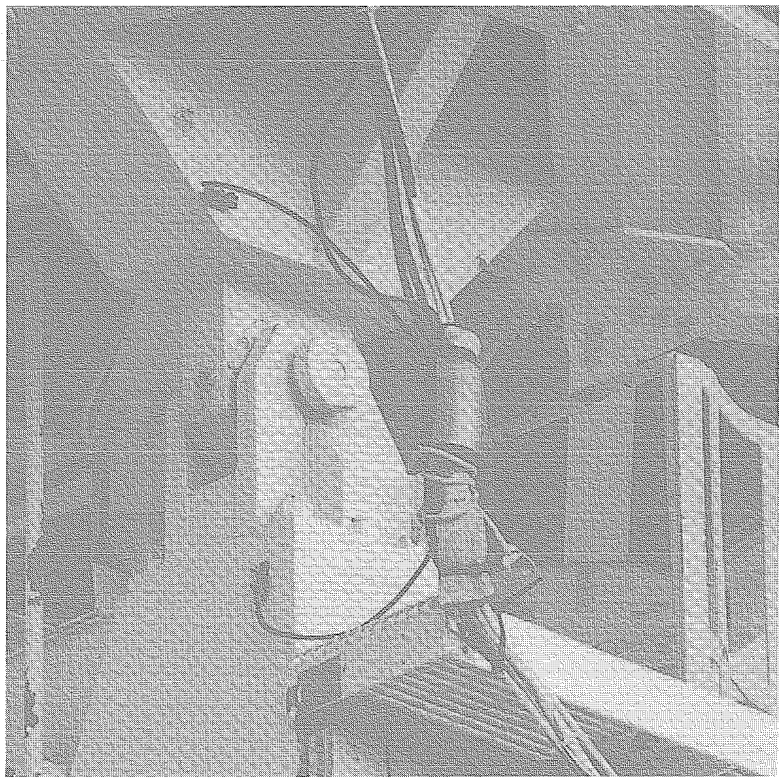


Fig. 3. Particular of the elevation axis of the VLBI antenna in Ny-Ålesund where the pin (marker 50) has been set up. One of the Leica tape target used for testing the marker 50, is also visible. At the symmetric opposite side the marker 51 has been set up in the same way.

This document is provided by JAXA.

Ny-Ålesund antenna this easy test cannot be used, due to the fact that the pins are not turning with the antenna, while it is moving in elevation. Instead, we verified with a wooden meter, that two fixed points on the other sides of the rotating part of the antenna, at distances of about 50 cm from the pins, kept their distance to the pins constant during an elevation run within half a millimetre. Afterwards, another more precise test was done measuring the positions of one pin, and four targets on the structure of the antenna, at different elevation angles. This has been done, from two pillars at one fixed azimuth angle.

As described above we used several Leica tape targets on the antenna structure and two pins for identification of the elevation axis. In particular we used 26 Leica tape targets regularly distributed on the back of structure holding the VLBI dish. With the antenna pointing nearly to the zenith, ten targets were placed on the upper part; eight on the lower part; four near the elevation axis; four on the structure that support the gear of the elevation movements (see Fig. 4 for a detail of one marker on the lower part of the antenna). One of the reasons for using a large number of targets on the antenna is that this kind of measurement has never been tried before, hence it was difficult to define a priori how many points are needed to identify the rotation centre of the antenna, with the required precision. However, the main reason to use a large number of targets was the shape of the control network around the antenna. See Fig. 5 for the positions of the pillars and the VLBI antenna, as results of the measures presented here. Most of the pillars are so nearby that it is nearly impossible from these to target any point on the upper part of the antenna, while the ones on the lower part are reachable only with small zenith angles. The targets on the

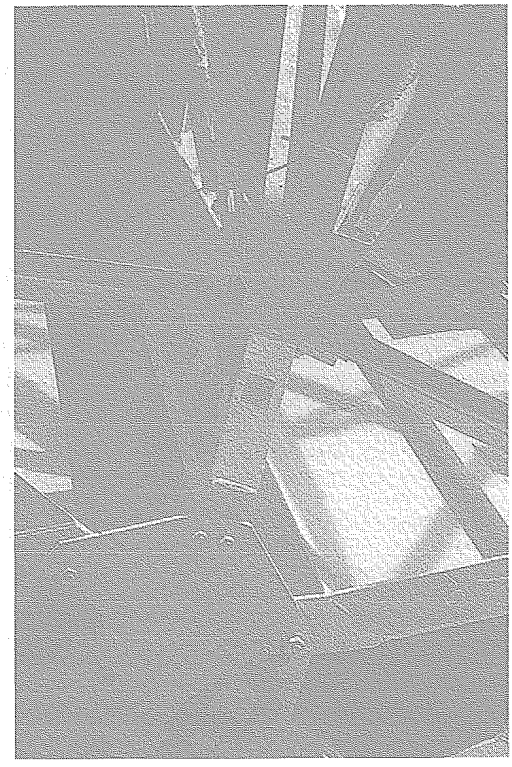


Fig. 4. One of the Leica tape target placed on the lower part of the structure supporting the VLBI dish.

This document is provided by JAXA.

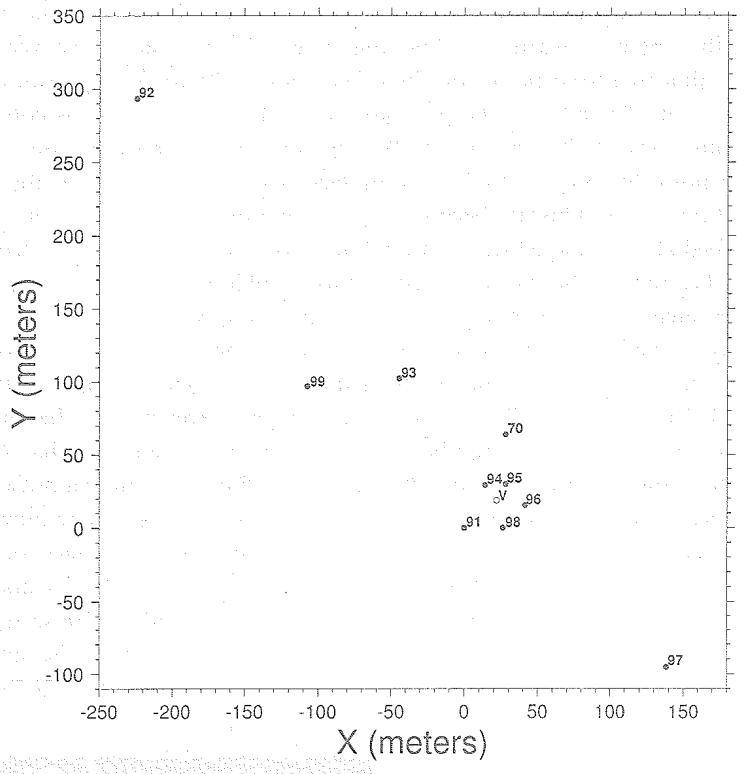


Fig. 5. The local control network around the Ny-Ålesund VLBI antenna. The VLBI antenna position (its azimuth axis) is marked by an open circle and a letter V. The pillars are marked with filled circle and the reference number used also in Table 1. The origin of the axis is pillar 91. The pillars 99 and 70 are not permanent and have been added using a tripod.

upper part are very useful when observing from distant pillars because in most cases the ones on the lower part were not visible.

The existing local control network and the targets on the VLBI antenna have been measured using two Wild total stations: TC2000 and TC2002. The eight pillars that constitute the original control network are made of concrete, deeply dug into bed rock, with a central Wild top screw for horizontal reference and an ex-centric levelling bolt for height reference (Fig. 6) and they constitute the planimetric and altimetric control network respectively. Thermal insulation layers protect all the pillars in order to reduce the effect of the sun. More details on the control network can be found in a paper by Hernes and Rekkedal (1997).

Due to the presence of buildings not all the pillars are mutually visible. In order to measure the network and the VLBI antenna, using forward intersection and inverse resection methods, two control points have been added using tripods: point 99 and point 70 on Fig. 5. This was particularly important to connect pillar 92 to the network, making the measurements made from there usable, and at the same time, enlarge the dimension of

This document is provided by JAXA.



Fig. 6. One of the pillars of the control network around the VLBI antenna of Ny-Ålesund. It is visible the metal plate on the top of the pillar with the Wild central screw for horizontal reference and the ex-centric levelling bolt for height reference. All the pillars are equipped in the same way.

the network towards north-west and south-east direction. In fact, mostly for local topography reasons the pillars of the network are aligned in the opposite direction, as clearly visible on Fig. 5. For technical reasons the point 91 has been moved and substituted by point 61, with a possible difference in the vertical component of the position of the two points. It should be noted that, as clearly shown in Table 1, after the data analysis, this vertical difference turned out to be zero. Along with usual triangulation, some trigonometric levelling has been performed, in order to tight the measurements to the levelling bolts and therefore allow a unique height reference.

It should be noted that, as mentioned in the previous section, moving the antenna only around the vertical axis, all the targets on the antenna draw an arc of circumference. These arcs have different radii for every target and different heights, but all centres are aligned along the vertical rotation axis. Measuring the position of a target at least in three different azimuth positions, allows us to determine the radius and the centre of the corresponding circumference. We have then completed the coverage of antenna positions in the range of azimuth angles between 0 and 360 degrees, with a span of 45 degrees, with eight different azimuth positions. We added yet another position (ninth) (with different interval in azimuth) in order to make measurable one of the points that identify the elevation axis (point 51). At the end we proceeded with a new set of measurements, now fixing the azimuth position of the antenna, and varying the elevation angle. The fixed azimuth

This document is provided by JAXA.

position (about 74 degrees) was selected to guarantee a good visibility of four targets on the antenna from pillars 61 and 98, at different elevation angles. In this case we measured the positions of the point 50 (one of the pins at the edge of the elevation axis) and other four targets around it. This has been done at different antenna elevation angles in a range of 45 degrees, in steps of 15 degrees. This procedure has been used to verify the precision of point 50 as indication of the position of the elevation axis.

3. Data analysis

The data acquired during the observation campaign have been combined in different files that have been edited and reviewed several times in order to correct the errors resulted from an incorrect measurement coding or other coarse mistakes. Merging these files, two worksheets have been created, one for each total station, totally containing more then 4500 rows. Each row of the worksheets corresponds to a collimation to a point of the general network (pillars and targets on the VLBI antenna). Therefore, each row contains at least two angles (one azimuth and one zenith) and, if measured, one distance. The data of each stratum have been combined applying Bessel's rule, thus obtaining one determination of the angle for each couple of direct and inverse observation (theodolite with vertical circle on the left and on the right respectively). The determinations originating from different strata and different total stations have been averaged obtaining one value for each angle. The distances measured at targets on VLBI antenna have been corrected applying an additive constant of 34.4 mm since no correction was imposed on the theodolite and the Leica retro-reflecting prisms that were used on pillars need no correction. In order to calculate the effect of the refractive index of the atmosphere the meteorological data collected at Ny-Ålesund weather station were used. It was the closest operating meteorological station while the measurements where taken and it is located at approximately 800 m from the VLBI antenna. The data recorded by the sensors located at 10 m above the sea level were used. Temperature and pressure have been inserted into Barrel and Sears' formula and a ppm correction of the distance has been calculated. As expected, the maximum correction value obtained by considering all the days of measurements was negligible, when applied to the distances involved in the survey. In hotter days the temperature rose up to 7–8℃ (usually being only a few degrees above zero) and it was sufficiently low to remain the ruling parameter for calculating the correction that resulted in a maximum value of 9 ppm. Only a small number of pillars have reciprocal distances that exceed a couple of hundreds metres resulting in a few tens of measurements. Applying the atmospheric effect to those measurements the corrections resulted well within the precision of the diastimeter. Therefore no corrections for refractivity were introduced. The same reasons apply to the measured vertical angles. All the data have been analysed using STAR*NET V.4, a 2-D or 3-D least squares adjustment program for networks measured using angles and/or distances, produced by STARPLUS SOFTWARE INC. A total number of 1163 observations were used to estimate 475 parameters (3-D co-ordinates of points belonging to the general network); 368 measures of distances, 413 azimuth angles, 381 zenith angles and one fixed bearing. The a priori standard errors we have introduced for the adjustment are quite strict and are as follow:

— 0.0003 gon for Leica prisms on pillars and 0.0004 gon for Leica retro tapes located on

This document is provided by JAXA.

VLBI antenna for azimuth angles measured by both total stations

— 1 mm for distances to Leica prisms and 4 mm to Leica retro tapes when measured with TC2002; 2 mm to prisms and 4 mm to retro tapes when measured with TC2000. With both instruments, when observing at Leica retro-tapes, a different a priori standard error should be introduced depending on the diastimeter's signal incidence angle (Russo and Stumpo, 1993). In this particular case (retro-tape targets on the structure of the antenna having an unpredictable orientation) there hasn't been any possibility to account for this effect. However it should be mentioned that no response was obtained if the incident angle was larger than 40–50 gon from the vertical of the Leica tape target.

— 0.0006 gon and 0.0008 gon for both instruments for zenith angles for prisms and retro tapes respectively.

In order to determine the differences in elevation of the altimetric control network we have performed trigonometric levelling, using a 44 cm INVAR rod, on the levelling bolts of pillars 91, 93, 94, 95, 96 and 98. These altimetric points are named adding a "b" to the pillar number. Distances between the theodolite and the levelling bolts have been determined using the variable parallactic method. According to the formulae that characterise the methods, a proper propagation of the errors affecting the distances and the elevations has been performed and, for the latter, these errors have been used as a priori standard errors in the adjustment procedure. To perform the adjustment we have used STAR*LEV V.1.1, a least squares level network adjustment package from STARPLUS SOFTWARE INC.

4. Results

Both adjustments passed the chi-square test at 5% level giving the results showed in Tables 1 and 2. As mentioned before the pillar 91 has the same horizontal position as pillar 61, but a vertical displacement was allowed during adjustment process. No difference has been found in the vertical direction, as shown in Table 1. The coordinates in Table 1 are expressed in a local orthogonal reference frame arbitrarily centred at pillar 91 (or 61) with X-axis directed to pillar 98. The three components of the targets on the VLBI antenna, at different azimuth angles, have been also determined, with errors on the three components similar or sometimes larger then those obtained for the pillars.

In order to determine the position of the projection of the VLBI antenna's azimuth axis on the $Z=0$ plane, all the x and y coordinates of the 25 points where used to determine an equal number of circle's centres. We have used a program that performs this calculation using a least squares approach. All these estimated centres should coincide and identify the azimuth axis on $Z=0$. Nevertheless some small differences are evident and therefore the mean x-y position, its r.m.s. and the r.m.s. of the population were calculated. The results are $X=21.830\pm0.001$ m and $Y=18.787\pm0.001$ m, in the previous defined local reference system, and these components represent the planimetric position of the reference point of the VLBI antenna, *i.e.* the location of the azimuth axis of the antenna.

Analysing the values of the z coordinates of each rotating point, in some cases a difference was found. The circle described by each rotating point should have a unique height, being exactly the z values of the rotating point. Thermal deformations and/or inclination of the azimuth axis in respect to the local vertical can cause such effect. In order to analyse the characteristic of these differences, further investigation has been done. Using

This document is provided by JAXA.

Table 1. Results obtained from forward intersection measurements 3-D adjustment.

Pillar name	X(m)	Y(m)	Z(m)
61	0.000±0.000	0.000±0.000	0.000±0.000
91	0.000±0.000	0.000±0.000	0.000±0.000
92	−224.117±0.001	293.503±0.000	−2.668±0.001
93	−44.397±0.000	102.319±0.000	1.232±0.000
94	14.233±0.000	29.269±0.000	0.561±0.000
95	28.182±0.000	29.934±0.000	−0.337±0.000
96	41.190±0.000	15.247±0.000	−0.640±0.000
97	138.434±0.000	−95.235±0.000	−2.623±0.000
98	26.116±0.000	0.000±0.000	0.077±0.000
99	−107.309±0.001	96.849±0.001	−0.030±0.001
70	28.197±0.000	63.727±0.000	−5.249±0.000

Table 2. Rsults obtained from trigonometric levelling adjustment.

Point name	Elevation (m)	Std. dev (m)
91b	0.000	0.000
93b	1.233	0.003
94b	0.564	0.002
95b	−0.334	0.001
96b	−0.641	0.001
98b	0.074	0.001
91	0.217	0.001
93	1.449	0.001
94	0.778	0.001
95	−0.119	0.001
96	−0.422	0.001
98	0.294	0.001

a least square approach, the equations of the different planes univocally determined by the rotating points have been computed. Then the normal vectors to these planes have been determined, and the direction of the mean vector has been computed. This latter vector should represent the best 3-D determination of the VLBI azimuth rotation axis. Its deviation from the local vertical is 0.02±0.04 deg, well within the errors and the pointing precision of the VLBI antenna.

Using the total stations (TC2000 and TC2002) the measure of the distance of the two markers (50 and 51) that define the elevation axis of the VLBI antenna was not possible. In this case only horizontal and vertical angles have been measured and therefore a full 3-dimensional best fit using STAR*NET was impossible for the lack of the needed redundancy. On the contrary the same program has been used in two dimensions for computing the positions of the two markers at the different azimuth angles. Then all the azimuth angles measured from the different pillars have been used to compute the vertical component (Z) of these points. The mean of these vertical components has been computed with its standard deviation.

The result is $Z=10.052\pm0.001$ m and this is the vertical component of the reference point of the VLBI antenna, obtained using the loosely defined height reference system

This document is provided by JAXA.

having origin in the intersection point of the axes of the theodolite on pillar 91. A univocal determination has been obtained using the data acquired with the trigonometric levelling. The differences in elevation between the levelling bolts and the heights of the axes intersection point of the theodolite on each pillar are shown in Table 2 and are a comprehensive solution that allows the tight of the planimetric local network (obtained using a 3-D adjustment) to the altimetric local network.

Considering the results shown in Table 2 the height of the VLBI antenna reference point referred to the 91b bolt is $Z = 10.269 \pm 0.001$ m. The same point's height is connected to the other five bolts of the altimetric control network presented in Table 2, using results shown in this table.

The distance between the elevation axis, as defined by the position of marker 50 and 51, at six different azimuth angles (other 3 azimuth angles cannot be used for this purpose) and the invariant point has been also computed and the resultant axis offset is 0.524 ± 0.003 m.

A final computation was needed for verifying the stability of the marker number 50, that identifies the elevation axis. In order to do that the distances from four different markers to the marker 50 have been computed, using the results of the markers positions during the elevation run, at fixed azimuth angle. The distances of the markers to the pin (marker 50), varied from 3.8 m to 0.34 m and their errors have been estimated to be 0.001 m. Then we can conclude that the elevation axis is defined by marker 50 within a circle with radium equal to 0.5 mm. Similar measures can not be performed for marker 51. However the results of the preliminary test, with the same results as the ones for marker 50, suggest that the marker 51 has the same behaviour as marker 50.

5. Final remarks

We have planned to measure the reference point of the VLBI antenna at Ny-Ålesund in the Spitzbergen Island. The task was completed successfully, with the determination of the three coordinates of the reference point with an error of 0.001 m in each coordinate. Also the antenna offset (the distance between elevation and azimuth axes) has been determined with an error of 0.003 m.

The use of Leica tape targets, instead of other kind of retro reflectors has been quite useful even if the work, due to the control network shape and weather conditions, was quite hard and time consuming.

It is well known that a single measure of the reference point, never measured before for this antenna, is only the starting point for a subsequent series of regular measures. In this respect we are suggesting here also some technical development that could make the following measures a bit easier and shorter.

First of all for this particular antenna is not difficult to materialize the reference point. On the VLBI antenna, not far from the elevation axis, there is a platform that can be modified and used to place a target at the reference point position. As soon as the point is materialized, even if it is not visible from all the present pillars, it can be measured quite easily in a short time (less then one day).

As a second item we point to the shape of the control network. Many limitations are related to the topography of the area. These are the presence of the airport on one side and

This document is provided by JAXA.

steep slope on the other, and a number of buildings that put a severe limitation on mutual visibility of the reference pillars. However some of the pillars are too nearby the antenna itself, and that makes measures to the antenna difficult and sometime impossible. In some cases it is possible to move the pillar (or build a new one) a bit farther from the VLBI antenna. In particular this should be possible for pillar 98 and 96. Moreover pillars 94 and 95 are almost unusable and there is not much space left on this side of the VLBI antenna. It might be possible to build a new pillar at the position of our point 70 (made available using a tripod).

Acknowledgments

The authors would like to thank the people at the Ny-Ålesund VLBI station for the help during and after the observations, and in particular Helge Digre and David Holland for their invaluable support. We would also to thank H.P. Plag for important suggestions for the application preparation and for the useful discussion on the way to carry on the measures.

We want to thank Prof. M. Unguendoli of the Bologna University for the use of one of the Total station (TC2000). We would also thank the referee K. Shibuya for his important suggestions and comments that allow us to present the paper in this present form.

The work at Ny-Ålesund has been supported by LSF grant n. NMA 99/1-12.

References

Hernes, G.M. and Rekkedal, S. (1997): Ny-Ålesund geodetic observatory station report 1996–1997. Proceedings of the 12th working meeting on European VLBI for geodesy and astrometry. Honefoss, Norway, 54–57.

Russo, P. and Stumpo, D. (1993): Una tecnica per il rilievo dei punti di appoggio in fotogrammetria terrestre. Bollettino della SIFET, 2, 145–156 (in Italian).

(Received April 26, 2000; Revised manuscript accepted August 31, 2000)

This document is provided by JAXA.

Mem. Natl Inst. Polar Res., Spec. Issue, 54, 331–336, 2001

Report

Scientific achievements in the First Chinese Expedition to the Arctic Ocean

Zhaoqian Dong[1] and Weijia Qin[2]

[1]*Polar Research Institute of China, Shanghai 200129, China*
[2]*Chinese Arctic and Antarctic Administration, Beijing 100860, China*

Abstract: The First Chinese Arctic Expedition to the Arctic Ocean was carried out from July 1 to September 8, 1999, aboard the icebreaker R/V Xuelong supported by two helicopters and a boat, organized by the Chinese Arctic and Antarctic Administration, State Oceanic Administration. Twenty five scientists in the scientific disciplines of physical oceanography, marine chemistry, marine biology, biogeochemistry, marine geology, glaciology, atmospheric science and fisheries from ten research institutions and universities in China, as well as scientists from the National Institute of Polar Research, Japan and the Korean Ocean Research and Development Institute, took part in the field investigations and cooperative research. The working areas covered the Canadian Basin, Chukchi Sea in the Pacific sector of the Arctic Ocean, and the Bering Sea.

The following data and samples were obtained during that expedition. For oceanography, operations of more than 100 CTD deep stations and 70 XBT and XCTD probes (to the depth of 1000 m) were completed, and 1423.6 Mb model VM ADCP (Acoustic Doppler Current Profiler) data were obtained. For geology, sediment samples by box sampler and multi-tube sampler in 41 locations and 47.92 m of column sediment samples in 17 locations were collected. Vertical and horizontal trawls in 110 locations were made for biology and ecology, and EK-500 and 792DSG fish-finder in over 5800 nautical miles and 19 trawls were operated. A variety of samples of sea water, air and snow and sea ice cores etc. for research on chemistry, isotopes, primary productivity, microbiology, phytoplankton, nanoplankton, aerosols and samples from sediment traps were obtained at two stations on ice floes. Boundary and upper-air observations including ozone and ice-radar measurements of ice thickness were also made. The northernmost station was at 77°N in the Canadaian Basin.

All samples and data are now being analyzed and results of scientific research have been published. Cooperative research on our data and samples obtained by the expedition with foreign scientists is most welcome.

1. Introduction

Chinese Arctic research goes back to the 1950s. Before the present expedition, Chinese scientists in a variety of scientific disciplines had been involved in Arctic scientific and social research, by cooperation and participation with many Arctic research programs of several Arctic countries, including the former Soviet Union, Norway, Germany, Canada, Japan and the U.S.A. And valuable scientific results in geology and geophysics, atmo-

This document is provided by JAXA.

sphere and space physics, oceanography, glaciology, social and cultural science were published. To prepare for our National Arctic Scientific Expeditions, scientists and management staff were sent to several Arctic countries for training before a non-governmental Arctic expedition in 1995, with logistic support being provided by foreign countries.

In 1996, China became a member of the International Arctic Science Committee (IASC), The Chinese Arctic & Antarctic Administration (CAA), the State Oceanic Administration started to prepare a national long-term Arctic research plan and make more contributions to the IASC and international Arctic research programs.

Implementation of the plan started with the First Chinese Arctic Expedition to the Arctic Ocean from July 1 to September 8, 1999, aboard icebreaker R/V Xuelong, supported by two helicopters and a boat to make observations at drifting ice stations. The expedition was organized by the Chinese Arctic and Antarctic Administration, State Oceanic Administration (1999, 2000). It included a comprehensive Arctic research program mainly on Arctic Ocean-Atmosphere-Ice interactions and the environment. Twenty-five scientists in the scientific disciplines of physical oceanography, marine chemistry, marine biology, biogeochemistry, marine geology, glaciology, atmospheric science and fisheries from ten research institutions and universities in China as well as scientists from NIPR, Japan and KORDI, Korea took part in the field investigations. The working areas included the Canadian Basin and Chukchi Sea in the Pacific sector of the Arctic Ocean, and the Bering Sea.

2. General scientific objectives and research priorities

There are three major scientific objectives in the science program of the First Chinese Expedition to the Arctic Ocean. The research priorities are listed under each objective item.

2.1. The role of the Arctic in relation to global change and its influence on climate in China

(1) Structure at the boundary layer between the ocean, sea-ice and the atmosphere, and physical mechanism of energy and material exchanges in the Arctic region.
(2) Thermodynamic interactions among ocean, ice and the atmosphere in the Arctic sea ice zone.
(3) Atmosphere and radiation balance at different surfaces in response to weather systems.
(4) Vertical exchange of energy and material between stratospheric and troposphere layers and its influence on the climate in China.
(5) Vertical ozone profile in the stratosphere, troposphere and boundary layers and its relation to UV-B radiation.
(6) Study of atmospheric components, pollen, sedimentary minerals and aerosols.
(7) CO_2 flux at the sea surface and carbon balance in the ocean-sea ice-atmosphere system.
(8) Physical structure of sea ice, chemical properties of ice and snow and the relation to climate and human activities.
(9) Present sedimentary processes in the Chukchi Sea and analysis of environmental change records.
(10) Detection of volatile fatty acids, hydrocarbons and other organic pollutants at the surface water of the Arctic Ocean and their role in organic geochemistry.

This document is provided by JAXA.

(11) UV-B radiation effects on physiology and ecology of phyto-plankton, biochemical processes and primary productivity in the Arctic Ocean.

2.2. Water mass exchange between the Arctic Ocean and the northern Pacific Ocean and its influence on the circulation in the northwest Pacific

(1) Water masses, their structure and formation mechanism in the Bering Sea and in the Chukchi Sea and Canadian Basin of the Arctic Ocean.
(2) Vertical convection and horizontal circulation, and their role in transporting material and energy in the Bering Sea, and in the Chukchi Sea and Canadian Basin of the Arctic Ocean.
(3) Water exchange processes in the Arctic Ocean and their relation to northwest Pacific and conditions of China seas.

2.3. Ecosystems in the Arctic Ocean and Bering Sea and their relation to Chinese fisheries

(1) Ecological structure in the Arctic Ocean and Bering Sea, structure of biological communities and bio-diversity in Arctic sea ice.
(2) Primary productivity and new productivity in the Arctic Ocean and Bering Sea.
(3) Plankton structure and its relation to fisheries.
(4) Fishery resources in the Arctic Ocean and the Bering Sea.

3. Investigation area, time and vessel

3.1. Area

- Bering Sea: 54–61°N, 174°E–174°W.
- Chukchi Sea and Canadian Basin: 66–76°N, 165–175°W.
- Ice Station: 76–77°N, 170°W.

3.2. Time

From July 1st to September 8th, 1999.

3.3. Observation platforms

The major observation platform is our icebreaker R/V Xuelong, managed by Polar Research Institute of China in Shanghai, State Oceanic Administration, with two helicopters and a boat for scientific observation. The total investigation distance was 14113.6 nautical miles and took 1238 hours.

A 0.3×1.0 km ice floe with thickness of 4.5 m in the Canadian Basin was used as a natural platform for our Ice Station. Comprehensive observations of the atmosphere, sea ice ecology, carbon cycling, physical oceanography, snow and ice sampling, coring and radar sounding were successfully carried out for six days. Another ice floe in the same basin was also used for an observation platform for two days. And then it was broken.

This document is provided by JAXA.

4. Data and samples obtained

4.1. Physical oceanography

One hundred and ten hydrographic deep stations were completed and the following data were obtained.

- Deep Mark IIIc CTD: 50 Mb (reached the bottom).
- FSICTD(MCTD): 30 Mb (0–200 m).
- VM-ADCP: 1423.6 MB (75 kHz, sampling interval: 30 or 60 s).
- XBT & XCTD: 70 probes in 55 locations above 1000 m.
- Automatic SST records on the track of the Xuelong.

4.2. Chemical oceanography

Water sampling was successfully carried out and the following samples were obtained for chemical analysis such as dissolved oxygen and nutrients.

- At 175 depths in the Chukchi Sea, water was sampled in 33 locations and 239 oxygen and nutrients data were obtained.
- At 336 depths in the Bering Sea, water was sampled in 29 locations and 2016 oxygen and nutrients data were obtained.
- At 27 depths in four locations trace element measurements of sea water were carried out.

4.3. Marine geology

A QNC-2-2 Sediment Box Sampler, A DDC4-2 Sediment Gravity Sampler (Sediment Core length: 350 cm), Gravity Corers and DSC-2 Multi-corers were used to obtain bottom sediment samples for a variety of analyses including ^{14}C, $\delta^{13}C$, $\delta^{18}O$, ^{210}Pb, Sr, organic matter, $CaCO_3$, SiO_2, trace matter, micro-paleorganism and segment minerals.

- Sediment samples by Box Sampler and Multi-Tube Sampler were obtained in 41 locations.
- Total 47.92 m column sediment samples were obtained in 17 locations.

4.4. Snow and sea ice

- 47 surface snow samples.
- 13 sea ice cores (Total length: 46.3 m) for analysis of sea ice structure, ice algal assemblages and inorganic ions.
- Ice thickness and structure measurements at 29 sections in 7 locations by PulseEKKO 100A radar (made in Canada).
- Snow and sea ice temperature measurements at many locations.

4.5. Atmospheric sciences

- 150 air samples for study of atmospheric chemistry and pollutants.
- 180 samples of aerosol and gases HNO_3, SO_2, NH_3 in the atmosphere in 1860 hours by four-stage open face sampler (made in U.S.A.).
- 8804 data of underway routine air observations and ozone sounding at 16 locations (altitudes up to 20000 m) by DigiCora II MW15 GPS wind finder sounding system, Väisalä RS80-25GE Radiosonde and 6A ECC Ozonesonde, made by Science Pump

This document is provided by JAXA.

Corporation, U.S.A.

- 136 hour observations at boundary layer between air/sea/snow & sea ice.

4.6. Marine biology and fisheries

- 71 nanoplankton samples.
- Phytoplankton samples at 14 stations.
- 45 microbes samples.
- Chl-a samples at different depths in 49 hydrological stations and 20 surface samples on the track of the Xuelong.
- 792DSG color fish finder (ATLAS, Germany) was operated for 423 hours (distance about 5800 nautical miles), and 19 trawls were made.
- 72-hour observation of short-term fluxes of diatom and particulate organic carbon in pack ice area.

4.7. Carbon cycling

- 4 sets of sediment traps each for 70 hours sampling.
- 2 bottom column samples of sediment at water depth of 2090 m for analyzing particulate organic matter.
- 26 Samples for analyzing C, N, P, Si and contents of suspended particle organic carbon.
- Samples at different levels in 46 locations and 29 bottom surface sediment for study of marine bacteria.

4.8. The role of sea-ice- atmosphere interaction

- Several Mb of solar radiation, albedo, etc. at different surfaces.
- More than ten Mb of routine data by auto-weather station.
- 8000 Mb of satellite sea ice distribution and thickness data.

4.9. Mapping

- 4200 sets of data in Epoch 15 for GPS positioning at two locations on Arctic sea ice.
- Absolute and relative gravity measurements at two locations.
- Collected information for Arctic digital mapping.

5. Some preliminary results

- All data obtained during the expedition are being processed.
- Net radiation seems to vary daily and absorption of radiation energy may reach to 100W/m^2 on the air/snow interface; turbulent heat flux shows obviously daily change and momentum flux has no notable daily change, which is different from observations at an interface between air and land.
- A great temperature inversion around an altitude of 400 m at 73.4°N, 165°W was observed during the expedition.

This document is provided by JAXA.

Acknowledgments

The authors thank the organizers, scientists and the crew of the R/V Xuelong in the expedition for information making this report possible.

References

Chinese Arctic and Antarctic Administration, State Oceanic Administration (1999): Field Implementation Program of the First China Arctic Scientific Expedition, May 1999. 48 p (in Chinese).

Chinese Arctic and Antarctic Administration (2000): Report on The First China Arctic Scientific Expedition. China Ocean Press, January 2000, 201 p. (in Chinese).

(Received May 15, 2000; Revised manuscript accepted August 22, 2000)

This document is provided by JAXA.

Mem. Natl Inst. Polar Res., Spec. Issue, 54, 337-341, 2001

Report

Greenland Sea in winter

Hajime Ito

National Institute of Polar Research, Kaga 1-chome, Itabashi-ku, Tokyo 173-8515

Abstract: The necessity to carry out observations in the Greenland Sea in winter is emphasized, and the background which makes such observations so important is described. Recent efforts are reported.

1. Introduction

Winter conditions in the Greenland Sea are poorly known. This short article points out that observation of the sea in the dark months is important.

Oceanic phenomena are inherently seasonal, so it is generally true that complete understanding requires observations in all seasons. In the Greenland Sea, however, a quite interesting additional motive for winter observation exists.

2. Role of the Greenland Sea

2.1. Arctic Ocean

The Arctic Ocean is one of the largest semi-closed marine basins in the world Ocean, together with the Mediterranean Sea. The basin is connected to the world ocean system through one channel/strait. The channel functions as a river mouth, while the basin itself is equivalent to the main river with a great width and small gradient, which gathers water from the tributaries, which in this case are ordinary rivers on land. The Greenland Sea is the river mouth. This simplified schemes "leaks" through Bering Strait, the Canadian Arctic Archipelago and the Barents Sea.

Figure 1 shows the Arctic Ocean drainage basin. It is a large drainage basin. The land area of the basin alone extends over 1548500 km^2, which exceeds one tenth of the entire land area of the earth. Ten percent of all precipitation falling on land would be collected in this basin, if precipitation were uniform worldwide. Furthermore, the precipitation in the basin has more or less uniform properties, as it falls under a unique physical environment, i.e. in the Arctic.

The Arctic Ocean supplies a large quantity of fresh water with particular characteristics to the global water circulation. Therefore hydrological investigation of the Arctic Ocean is necessary to clarify the structure and mechanism of the global water cycle.

2.2. Runoff

Discharge measurement at river mouths is one of the most important observation

This document is provided by JAXA.

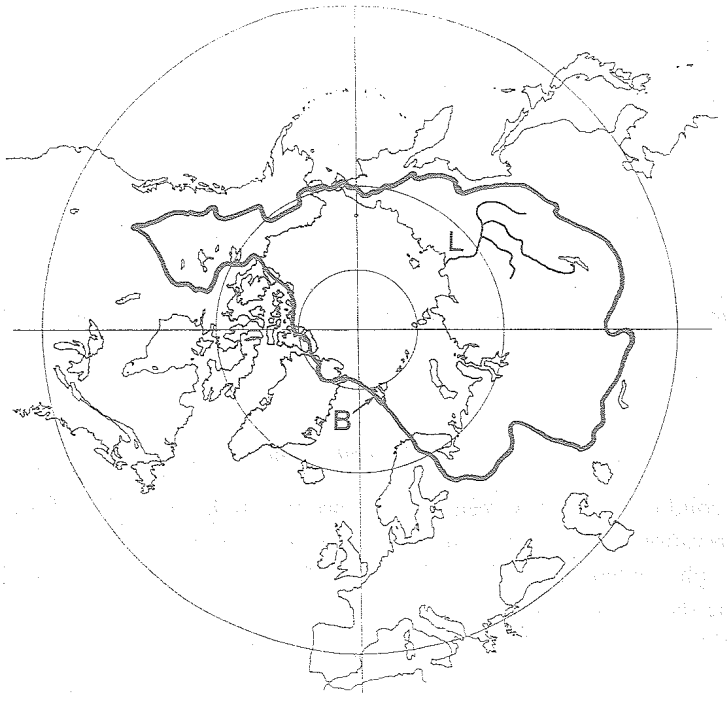


Fig. 1. Drainage basin of the Arctic Ocean.

components in hydrological research. Water behavior in the area of the Arctic "river mouth" (the Greenland Sea) is rather complicated, with currents flowing in two opposite directions simultaneously, from the Arctic Ocean to the Atlantic and vice versa. In the present study, the scheme is simplified. Streams at different depths and locations have different directions, into the basin and out of it. There must be a net runoff, which pumps out the net basin precipitation and keeps the water level of the basin unchanged. Part of the net runoff flows out of the basin at the surface, the rest finds its escape route at depth, analogous to ground water.

Assessment of the runoff is not easy. In contrast to its great width, the depth of the surface runoff is rather small, a couple of meters at most. Underneath the surface flow lies a thick layer of seawater. The "riverbed" in this case consists of water, not rock, and the river water penetrates into the "ground", *i.e.* into the seawater, without much difficulty and at any point. This makes measurement complicated in many ways. The worst complication is the difficulty in assessing the travel route of each water particle. The travel time since the particle left the land until it arrives at the "gauging station" in the Greenland Sea cannot be estimated with the desired accuracy.

Some discharge records are shown in Fig. 2. Two tributaries of the Arctic Ocean "River", the Lena in Russia and the Bay in Spitsbergen, are chosen. Among hundreds of rivers nourishing the Arctic Ocean, these two are not necessarily typical or representative in any sense. The selection of rivers is thus arbitrary. The observation years were also chosen arbitrarily. They present similar discharge patterns. Strong seasonal variation is noticed in

This document is provided by JAXA.

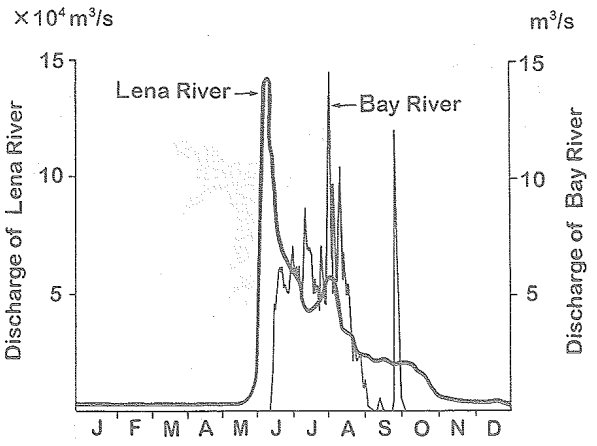


Fig. 2. Discharges of two Arctic rivers.
Positions of the gauging stations are indicated in Fig. 1 by L and B respectively. Thick curve: Lena River in 1958 (redrawn from Mostahov, 1972). Thin curve: Bay River in 1993 (drawn with the data collected by NVE, Norwegian Water Resources and Energy Administration). Letters on the abscissa stand for months, e.g. J for January, June or July.

both diagrams. The water properties are also expected to vary drastically with the season.

Each tributary has its own discharges; some of them may very similar by to that in Fig. 2. The sum of the tributary discharges, together with the net precipitation falling directly on the Arctic Ocean, will give the total discharge at the river mouth.

Tributaries are located at various distances from the river mouth, and the discharges from them arrive at the river mouth after different travel times. Some particles may stay quite long in the "river", perhaps even years or tens of years.

The summing of the discharge is, hence, far from simple. Let us consider the peak discharge of June, measured in the Greenland Sea. Only part of the water observed at the gauging station, would correspond to the annual peak discharges of tributaries. Thus, observations have to be made all year round, not only at the particular time of a year of immediate interest. Without winter observations, for instance, the full summer variation is not obtained either. Year-round observation in the Greenland Sea is the only way to investigate the full annual water cycle of the Arctic Ocean.

3. Field observations

3.1. Past studies

The northern Greenland Sea has been observed intensively in recent decades, mainly by European oceanographers. Most of the observations were, however, carried out in summer. Among a rather large volume of publications two are mentioned here: one of the oldest modern investigation (Muench *et al.*, 1987) and one involving the author directly (Ito *et al.*, 1994).

Norwegian fishing boats go up as far north as 81 degrees in winter every year. They must have made some measurements for their own purposes but the data are not in the

This document is provided by JAXA.

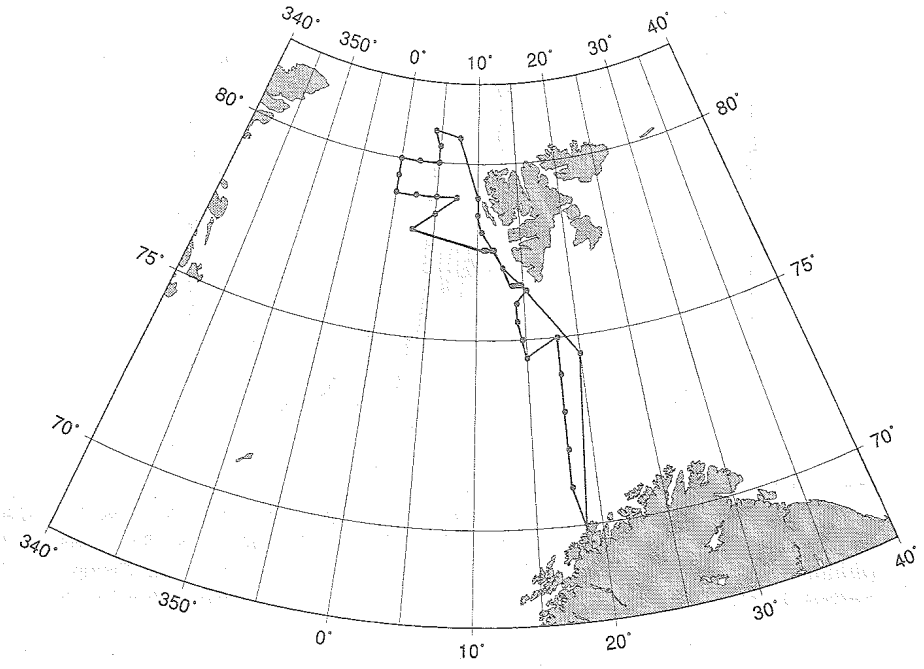


Fig. 3. Cruise route of the Ivan Petrov, January 1999. Black circles show locations of oceanographic stations.

public domain. The present author has requested to use one of the boats as an observation platform, but was refused.

Russian boats may also have sailed in the Greenland Sea in winter, either for fishing or for other (perhaps naval) purposes, and may have possibly collected some data. Access to their data is also difficult.

The research vessel Jan Mayen sailed to Isfjorden/Kongsfjorden in December 1994. Although the cruise was limited to the fjords and along the coast of Spitsbergen, this was the only modern winter expedition focused on oceanographic observations up to the last two years. The data obtained are kept in UNIS, University System of Svalbard (Vigdis Tverberg, personal communication).

3.2. Recent years

A Japanese-Russian joint cruise was conducted using a Russian vessel Ivan Petrov in January 1999 in the Greenland Sea. The cruise report has been published (Ito, 1999) and only the cruise route with stations is given here (Fig. 3). Research results are not presented in either the report or in the present article. Some of the cruise participants present their results in this Symposium Proceedings, and others are preparing for later opportunities.

Two research cruises were carried out in February in the Greenland Sea, in 1999 and in 2000 by the Norwegian Polar Research Institute, Tromsø and Scott Polar Research Institute, Cambridge, respectively. The results will be reported by the respective institutions. Hopefully, these recent cruise are a sign that winter research in the Greenland Sea is finally

This document is provided by JAXA.

starting to attract attention.

References

Ito, H. (1999): Cruise Observations in the Greenland Sea and Barents Sea, January 1999. Nankyoku Shiryô (Antarct. Rec.), **43**, 361–365.

Ito, H., Osterhus, S. and Ushio, S. (1994): Temperature Profiles of the Greenland Sea in the Summer of 1993: Oceanographic Observation on the R/V Lance Cruise. Nankyoku Shiryô (Antarct. Rec.), **38**, 68–71.

Mostahov, S.E. (1972): Reka Lena (Lena River). Yakutsk, Yakutskoe Kniznoe Izdatelctvo, 144 p. (in Russian).

Muench, R.D., Martin, S. and Overland, J.E., ed. (1987): MIZEX special issue. J. Geophys. Res., **92** (C7), 6715–7225.

(Received May 30, 2000; Revised manuscript accepted July 21, 2000)

This document is provided by JAXA.

This document is provided by JAXA.

Mem. Natl Inst. Polar Res., Spec. Issue, 54, 343–348, 2001

Scientific note

The International North Water Polynya Study (NOW): A progress report

L. Fortier[1], M. Fortier[1], M. Fukuchi[2], D. Barber[3], Y. Gratton[4], L. Legendre[1], T. Odate[2] and B. Hargrave[5]

[1]*GIROQ, Département de Biologie, Université Laval, Ste-Foy, QUE, G1K 7P4, Canada*
[2]*National Institute of Polar Research, Kaga 1-chome, Itabashi-ku, Tokyo 173-8515*
[3]*CEOS, Department of Geography, University of Manitoba, Winnipeg, MAN, R3T 2N2, Canada*
[4]*INRS-Eau, 2800 rue Einstein, Ste-Foy, QUE, G1V 4C7, Canada*
[5]*Department of Fisheries & Oceans, Bedford Institute of Oceanography, Dartmouth, NS, B2Y 4A2, Canada*

Abstract: After three highly successful, multidisciplinary expeditions totaling 180 days at sea, what have we learned about the functioning, ecological importance, and future of the North Water ecosystem? The scientific program of NOW comprises 13 projects tightly integrated around a central hypothesis that links spatial and temporal gradients in biological productivity and carbon export to the hydrographic/meteorological forcing of the North Water.

Preliminary interpretations from observations and modeling efforts are summarized concerning (among several other topics), the relative importance of sensible and latent heat processes in maintaining the polynya; the duration, intensity and nature of biological production in the North Water; and the export of carbon to the pelagic food web and at depth.

1. Introduction

Arctic polynyas are large areas of open water or thin ice in the midst of the thick ice pack that covers the Arctic Ocean and adjacent seas (Stirling and Cleator, 1981). Because they remain free of ice in winter, some polynyas serve as feeding, mating, spawning and over-wintering grounds for key species of birds and mammals in the Arctic marine ecosystem (Stirling, 1980; Stirling and Cleator, 1981). Accordingly, polynyas have been compared to oases in terrestrial deserts. Perhaps more importantly, they are suspected to be focal points for the intense production of the plankton herbivores that ensure the transfer of the solar energy fixed by plankton microalgae to Arctic cod, seals, polar bear and native man. A significant fraction of the biogenic carbon produced in polynyas could be sequestered at depth. Polynyas are predicted to increase in area and frequency in response to global climate warming (Gradinger, 1996) and, to some extent, could be models of the response of the Arctic ocean to global warming.

The North Water in northern Baffin Bay is perhaps the most productive ecosystem north of the Arctic circle. It is located at latitudes that will be impacted early and most strongly by the present trend in climate warming. In January, the North Water area is

This document is provided by JAXA.

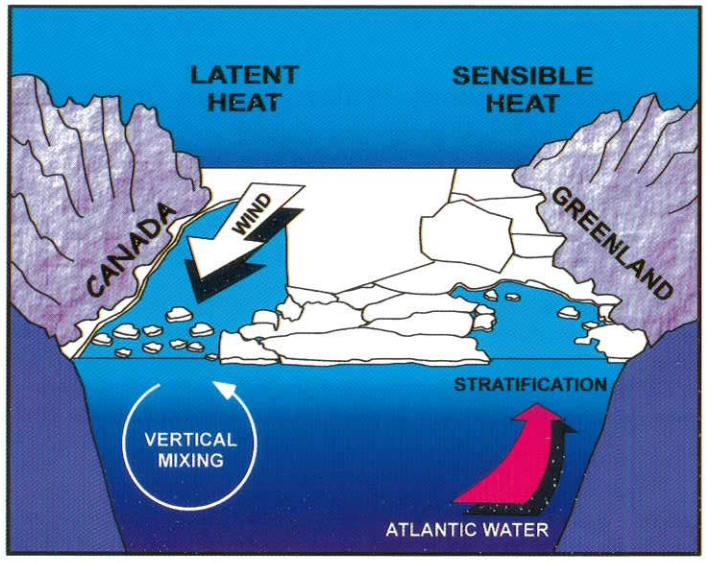


Fig. 1. Schematic representation of opening mechanisms of the North Water.

almost completely covered with thin drifting ice < 30 cm thick (Steffen, 1986; Steffen and Lewis, 1988). In late March or early April, the polynya starts to expand along the Greenland coast and begins to spread South and West between the islands of Ellesmere, Devon and Baffin to the West and Greenland to the East. The North Water reaches its maximum extent in July (*ca.* 90000 km^2) before merging with the open waters of Baffin Bay in August (Dunbar, 1969; Dunbar *et al.*, 1967). The mechanical removal of ice by currents and strong winds (latent heat) coming from Smith Sound in winter has long been considered the most important factor keeping the polynya open (Dunbar *et al.*, 1967). The recent discovery of warm water cells along the Greenland coast (Steffen and Ohmura, 1985) suggest that upwelling of warmer water (sensible heat) could also favour the opening of the polynya in spring (Fig. 1).

The functioning of the North Water ecosystem, its role in the overall Arctic biota and its potential response to global warming are the subjects of the *International North Water Polynya Study (NOW)* conducted within the International Arctic Polynya Programme (IAPP) of the Arctic Ocean Science Board (AOSB). In March 1997, the NOW Research Network was funded by the Natural Sciences and Engineering Research Council of Canada (NSERC) with the objective of assembling the international expertise necessary to conduct NOW. Thirty scientists from 7 Canadian universities, the Department of Fisheries and Oceans, the Canadian Wildlife Service, the Atmospheric Environment Service and the Department of National Defense form the Canadian component of the Research Network. Thirty additional investigators from Japan (12), the United States of America (9), Denmark (5), Poland (2), the United Kingdom (1) and Belgium (1) complete the Network.

The science program of NOW rests on the central hypothesis that both sensible and latent heat mechanisms contribute to the opening of the polynya, maintaining a west-east

This document is provided by JAXA.

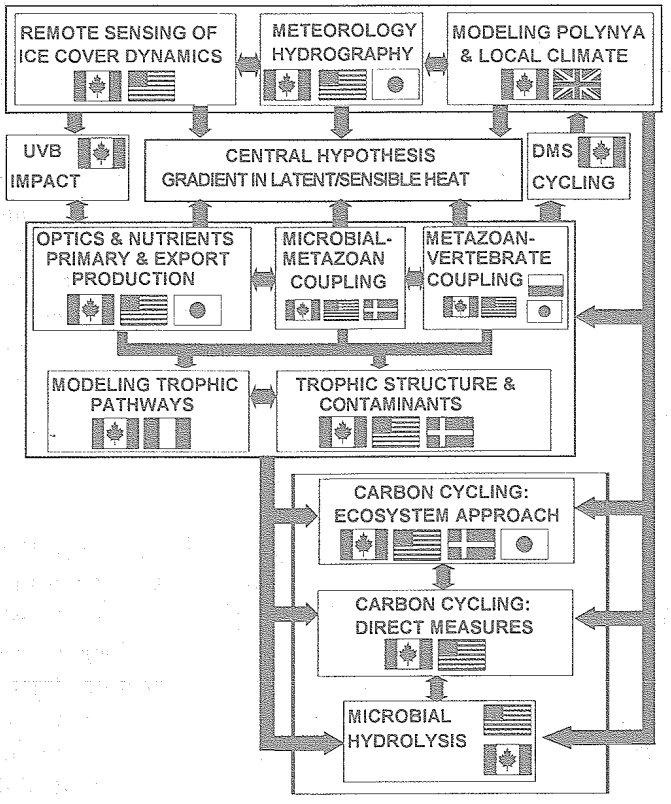


Fig. 2. NOW research net work and information flow.

gradient in biological productivity. In areas and at times when sensible heat prevails (upwelling), the stratification of the surface layer resulting from the melting of the ice cover triggers a diatom bloom immediately after the opening of the waters. When latent heat prevails (winds and currents), the algal bloom is delayed until solar heating stratifies the surface layer. Built around this central hypothesis, the science program is made of three modules that each integrate several sub-projects (Fig. 2): (1) physical generation of the North Water; (2) the North Water pelagic ecosystem; (3) biogeochemical cycling in the North Water. After three successful expeditions to the North Water in 1997 (August–September), 1998 (April–July) and 1999 (August–October), the international network is now in a position to assess inter-annual variability in the biological productivity of the ecosystem in relation to ice cover dynamics and climate.

2. Expeditions

2.1. 1997

Work at sea started in August 1997 with a 19 days expedition on board the Canadian Coast Guard icebreaker Louis S. St-Laurent. The successful deployment of 9 instrument

This document is provided by JAXA.

lines supporting 14 current meters, 6 ADCPs, 3 CTDs, one tide gauge and 10 sediment traps allowed scientists to record the winter conditions that led to the opening of the polynya in the spring of 1998, as well as the annual cycle of exportation of organic matter to depth. Hydrographic and biological measurements were taken at 19 stations covering the region of the North Water. Measurements on station included profiles of temperature, salinity, light transmittance, fluorescence and chlorophyll *a* concentration. Helium and tritium, microbial densities and processes as well as picoplankton densities were sampled/measured at selected depths. Plankton nets were hauled for the determination of zooplankton and juvenile fish areal densities. In between stations, salinity, temperature and chlorophyll *a* were continuously monitored. XBT profiles were obtained along some of the sampling transects. Mammal and bird abundance was monitored during the displacements of the ship in the North Water and in Lancaster Sound during the return trip to Resolute. In addition to ship-based operations, two teams studied bird ecology on the Canadian (Coburg Island) and Greenlandic (Hakluyt Island) coasts of the North Water.

2.2. 1998

The 1998 expedition to the North Water was an historical success. From 26 March to 29 July, over 100 experts took rotations on board the icebreaker CCGS Pierre Radisson to study the oceanography, ecology and biogeochemistry of the North Water. From the multitude of measurements taken, we can stress the continuous logging of satellite images, of meteorological and hydrographical conditions, measurements of light, CO_2, contaminants, DMS, thorium, fluorescence and chloropigments, sampling of microbes, of picoplankton, of zooplankton and fish larvae, and the surveying of marine birds and mammals. Apart form ship-based operations, the helicopter and zodiacs were used to describe the structure of the forming ice, the development of ice algae, to install weather stations, sediment traps and gill nets, and to record marine mammals vocalizations. Canadian and Danish teams studied bird ecology on both shores of the polynya and a joint Canada-Poland team based at Cape Hershel monitored ice formation and the influx of salt, heat and plankton from the Arctic into the North Water. In total, over 12000 researcher-days of intense work at sea and on land enabled the scientists to describe, dissect and quantify the functioning of the ecosystem, from its forcing by winds and currents to the fate of the carbon assimilated in its waters, including the entire food web from viruses to whales.

2.3. 1999

This third and last expedition of the NOW was jointly funded by Canada, Japan and the USA. The main scientific objectives of the expedition were (1) to recover the instruments moored in July 1998, which recorded circulation and the deep flux of particles in the polynya from August 1998 to August 1999, (2) to quantify pre-winter primary and secondary productions in the area, and (3) to identify the biological sources of the significant deep particle flux measured in the fall of 1997 by the moored instruments. All three objectives were fulfilled and the overall operation was a great success. 34 of the 43 instruments moored in 1998 and 1 trap moored in 1997 were recovered and over 75 sampling stations were carried out. In addition in 1999, careful preparation made possible a call of the ship to the Grise Fjord (Canada) and Qaanaaq (Greenland) communities. During the visits, the Community was invited onboard to see for themselves the work of

This document is provided by JAXA.

the scientists and to discuss with them. The information provided during the visits resolved some concerns that the local populations may have had about the impact of the scientific operations on the region. These activities also increased the awareness of local people about the importance of the research in a context of climate change and the potential benefits to their Community.

The spectacular success of the NOW field program reflects months of careful preparation by scientists and professionals all over the world. Our success is also, in large part, attributable to the extraordinary competence and enthusiastic support of the Polar Continental Shelf Project in Resolute and to the officers and crew of the CCGS Louis S. St-Laurent and Pierre Radisson. From August 1997 to October 1999, the different teams have logged 169 days of shiptime in the North Water (190 days at sea when including voyages to and from the area). Overall, this represents 6543 scientist-day at sea, not including the field work of our teams at Cape Hershel, Coburg Island and Hakluyt Island.

3. Preliminary results

Obviously, the gigantic volume of samples and data collected during the three expeditions will take many years to digest. However, the main dynamics of the North Water ecosystem are already emerging. Among several preliminary results of significance:

1) Once the ice bridge forms in Nares Strait, the strong northerly winds (30–70 knots) prevailing in April and May drive the ice cover southward and away from the Canadian coast while the upwelling of warm water and warmer air temperature help melt the ice cover on the Greenland side. The two mechanisms could be linked, the upwelling on the eastern side being fuelled by the wind induced North-South flux on the western side. A surprising and spectacular observation: the North Water can open in less than 24 hours.

2) Above-freezing near-surface temperatures were recorded as early as April in the eastern part of the polynya, consistent with the hypothesis that sensible heat processes (both oceanic and radiative) contributed to the melting of the ice cover along the Greenland Coast.

3) The intense primary production starts as early as April in the North Water, immediately fuelling the reproduction of large herbivorous copepods such as *Calanus glacialis*. By comparison, the onset of the phytoplankton bloom and reproduction of *Calanus glacialis* does not occurs until July in nearby Barrow Strait. The algal biomass measured in the polynya are as high as the highest ever measured in the ocean. In agreement with the predictions of the central hypothesis, the algal bloom starts along the Greenland coast and propagates West to the Canadian side.

4) Data from sediment traps moored in August 1997 and recovered in July 1998 indicate that a strong vertical flux of organic matter persists from June to November, reflecting at least 5 months of plankton production. Elsewhere in the Arctic, the season of plankton production typically last less than 2 months.

4. The future

The exceptional data set obtained on the physic, biology and biogeochemistry of the North Water represents one of the most comprehensive studies ever of an Arctic marine

This document is provided by JAXA.

ecosystem. The presentation and synthesis of this data is being achieved through international workshops and special sessions at international conferences (ASLO-AGU, January 2000, San Antonio; Sea-Ice Symposium, February 2000, Mombetsu; this symposium, February 2000, Tokyo; ASLO, Copenhagen, June 2000) and upcoming special issues of Atmosphere & Ocean and Deep-Sea Research.

All the while, participants in the Network are planning a new initiative to pursue the international collaboration and apply the Network's complementary expertise to the study of the changing Arctic Ocean. The emerging CASES (Canadian Arctic Shelf Exchange Study) is an international program to understand and model the response of the Canadian Arctic shelf ecosystem to atmospheric, oceanic and continental forcing, in the present context of warming of the Arctic. CASES is providing a unique opportunity to study the large Cape Bathurst polynya that is part of the circum-arctic system of flaw lead polynyas that characterise Arctic shelves and play a central role in the dynamics of the Arctic ice sheet and the formation of Arctic deep water. Accordingly, at its last meeting in January 2000 in San Antonio, the Steering Committee of the IAPP has decided that CASES would constitute phase III of the IAPP.

References

Dunbar, M. (1969): The geophysical position of North Water. Arctic, **22**, 438–441.

Dunbar, M.J., Dunbar, M. and Nutt, D.C. (1967): The Baffin Bay-North Water Project. Report Number 1. AINA Research Paper, **45**, 71 p.

Gradinger, R. (1996): Climate change and biological oceanography of the Arctic Ocean. The Arctic and Environmental Change, ed. by P. Wadhams *et al.* The Netherlands, Gordon and Breach Publishers, 77–86.

Steffen, K. (1986): Ice conditions of an Arctic polynya: Northwater in winter. J. Glaciol., **32**, 383–390.

Steffen, K. and Lewis, L.E. (1988): Surface temperatures and sea ice typing of northern Baffin Bay. Int. J. Remote Sensing, **9**, 409–422.

Steffen, K. and Ohmura, A. (1985): Heat exchange and surface conditions in North Water, northern Baffin Bay. Ann. Glaciol., **6**, 178–181.

Stirling, I. (1980): The biological importance of polynyas in the Canadian Arctic. Arctic, **33**, 303–315.

Stirling, I. and H. Cleator. (1981): Polynyas in the Canadian Arctic. Can. Wildl. Serv. Occas. Pap., **45**, 77 p.

(Received June 22, 2000; Revised manuscript accepted August 24, 2000)

This document is provided by JAXA.

Mem. Natl Inst. Polar Res., Spec. Issue, 54, 349–364, 2001

Review

Persistent organic pollutants in Arctic animals in the Barents Sea area and at Svalbard: Levels and effects

Geir Wing Gabrielsen and Espen O. Henriksen*

Department of Biology, The Norwegian Polar Institute, The Polar Environmental Centre, N-9296 Tromsø, Norway (geir@npolar.no)

Abstract: At Svalbard and in the Barents Sea area, high levels of persistent organic pollutants (POPs) have been found in glaucous gull (*Larus hyperboreus*), arctic fox (*Alopex lagopus*) and polar bear (*Ursus maritimus*). Studies of the possible toxic effects on the hormone-, vitamin-, enzyme-, immune- and reproduction system have been conducted during the last 5–10 years. Data obtained both from laboratory and field studies indicate that the present POP levels have an influence on biochemical-, physiological- and immunological parameters in glaucous gull and polar bear. In these two species, studies are currently being conducted in order to relate POP levels to biological/toxic effects both on individuals and populations.

1. Introduction

A thorough review of the levels and effect of the persistent organic pollutants (POPs) in Arctic animals is beyond the scope of a single symposium lecture. In this paper we will try to outline what is known about the levels and effects of POPs in marine mammals and seabirds, which are living in the Barents Sea area and at Svalbard. For a more complete review of these issues we refer the reader to the Arctic Monitoring and Assessment Programme report (AMAP, 1998) and to the reviews by Muir *et al.* (1992, 1999), Thomas *et al.* (1992), MacDonald and Bewers (1996), Bard (1999), and Skaare *et al.* (2000).

The AMAP report (1998) lists and documents several threats to the Arctic ecosystem from long-range transported contaminants, in particularly from POPs. Most POPs that are found in the Arctic comes from distant industrial and agricultural sources. They accumulate in biotic lipids and biomagnify in food chains (Ottar, 1981; Muir *et al.*, 1992). Consequently the highest POP levels in Arctic marine food chains have been found in top predators such as glaucous gull (*Larus hyperboreus*)(Bogan and Bourne, 1972; Gabrielsen *et al.*, 1995), arctic fox (*Alopex lagopus*) (Wang-Andersen *et al.*, 1993) and polar bear (*Ursus maritimus*) (Bernhoft *et al.*, 1997). The finding of high POP levels in tissues and blood of these species raises questions if these levels are high enough to be associated with possible biological effects on individuals and populations.

*Present address: Faculty of Fisheries and Natural Science, Høgskolen i Bodø, N-8049 Bodø, Norway (Espen.Henriksen@hibo.no).

This document is provided by JAXA.

In the first part of this paper we will briefly present our knowledge of POPs in Arctic mammals and seabirds. At the last part, we will present data obtained on the biological effects in polar bear and glaucous gull, and data on temporal trends of POPs in Arctic seabirds and marine mammals.

2. Persistent organic pollutants

Environmental contaminants include both industrial chemicals, such as polychlorinated biphenyl (PCBs), hexachlorobenzene (HCB), chlorinated pesticides, such as DDT, chlordanes, hexachloro-cyclohexane (HCH), aldrin/dieldrin, polychlorinated boranes (Toxaphenes) and industrial byproducts such as polychlorinated dibenzo-p-dioxins (PCDDs), polychlorinated dibenzofurans (PCDFs), polybrominated biphenyls (PBBs) and polybrominated diphenyl ethers (PBDEs) (Muir *et al*., 1992). Most of these contaminants were developed and put into production more than 50 years ago. The highest production of most of these contaminants was at the end of the 1960's and the start of 1970's (Blus, 1995; Voldner and Li, 1995). Substances like PBBs and PBDEs are still being produced globally at an estimated 150000 tons a year (Sellstrøm and Jansson, 1995). The brominated compounds are being heavily used in electronic equipment such as computers and TV sets, which means that the production and release into the environment is expected to increase in the years to come.

The presence of anthropogenic chlorinated contaminants in the Arctic, especially in the marine environment, have been documented in the literature since the 1970's (AMAP, 1998). In Arctic marine organisms, the first case of POPs (DDT, PCB and toxaphene residues) was reported in the 1970's in Arctic seals (Holden, 1972). In the Arctic area, high levels of POPs were documented in glaucous gulls from Bjørnøya (Bear Island) in the early 1970's (Bourne and Bogan, 1972; Bogan and Bourne, 1972). In polar bears, POPs were also documented in Canada at the beginning of the 1970's (Bowes and Jonkel, 1975). The concern about levels of pollutants in the Arctic increased with the comprehensive surveys performed in the 1980's and 90's (AMAP, 1998).

The production and use of most chlorinated compounds listed above were stopped in Europe and North America in the 1980's and 1990's. Some pesticides (such as DDT and toxaphenes) are still being produced and used in Asia, Africa, South America and in some eastern European countries (AMAP, 1998).

In this article we focus on PCB, DDT, toxaphenes and PBB/PBDE, since these contaminants dominate at higher trophic levels in the marine environment. For these contaminants we also have the best knowledge of distribution, levels and fate in the Arctic environment. So far, studies on effects of contaminants in arctic animals have mainly been focused on the possible effects of PCBs. In the cases where PCBs are suspected to cause adverse effects, it is difficult to exclude a contributing adverse influence from other contaminants.

2.1. PCB

PCBs are mixtures of chlorinated hydrocarbons that have been heavily used since 1930 for many industrial purposes such as dielectrics in transformers and large capacitors, heat exchange fluids, paint additives, in carbonless copy paper and plastics (Fisher, 1999). There

This document is provided by JAXA.

are 209 possible PCBs (congeners), of which *ca.* 100 have been found in biological samples (McFarland and Clarke, 1989). The properties of PCBs depend on the number of Cl-atoms and their position and include low water solubility, high stability, and semi-volatility, which favor long range transport. With regard to the effect on wildlife, PCBs have been linked to reproductive and immunotoxic effects. In the Baltic sea PCB was linked to reproductive failure in ringed seal (*Phoca hispida*) and grey seal (*Halichoerus gryphus*) (Blomkvist *et al.*, 1992).

2.2. DDT

DDT and its metabolities (DDD and DDE) have been found in biota since 1940's. After the war, DDT was used extensively as a pesticide on a variety of agricultural crops (*i.e.* cotton and peanuts) and to prevent the spreading of diseases to humans by insects (*i.e.* malaria and typhus). DDT and related compounds are very persistent in the environment and their half-life in soil range from 10–15 years. DDT received a lot of publicity in the 1970's for its adverse effects on bird reproduction, causing eggshell thinning (Ratcliffe, 1967). DDT has also been linked with feminization and altered sex ratios of a western gull (*Larus occidentalis*) population of the coast of southern California and in herring gulls (*Larus argentatus*) in the Great Lakes (Fox, 1992).

2.3. Toxaphenes

Toxaphene is an insecticide, which was introduced in 1949. In the US it became the most widely used insecticide by 1975. It has been used on cotton, cereal grains, fruits, nuts, and vegetables, as well as to control ticks and mites in livestock (Fisher, 1999). Toxaphene is a complex mixture of many hundred of different compounds, chiefly chlorinated bornanes. Toxaphene is highly insoluble in water, comparably resistant to ultraviolet sunlight, and its half-life in soil is 10–15 years. Toxaphene is highly toxic to animals and humans. The list of effects of toxaphene in laboratory animals includes neurotoxicity, carcinogenicity and induction of hepatic biotransformation enzymes (De Geus *et al.*, 1999).

2.4. PBBs and PBDEs

Brominated flame retardants are used in high concentrations in electric equipment such as computers, television sets, in textiles, cars and other applications (De Boer *et al.*, 1998). Humans may absorb PBBs and PBDEs emitted from electronic circuit boards and plastic computers and cabinets (Zelinski *et al.*, 1993). PBBs and PBDEs show high lipophilicity, high resistance to degradation, and are expected to bioaccumulate easily in food chains. Both PBBs and PBDEs are listed as compounds that effect the regulation of thyroid and steroid hormones. High levels of PBDEs have been found in seals and dolphins from the North Sea and the Atlantic (De Boer *et al.*, 1998).

2.5. Accumulation of POPs in marine animals

POPs originating in industrial and agriculture areas are mainly transported to the Arctic via winds, ocean currents and rivers (Barrie *et al.*, 1992). Once transported to the Arctic, low temperatures promote their condensation and deposition (Ottar, 1981; Wania and Mackay, 1993). Since POPs are lipophilic they are easily incorporated into food chains, especially in the marine environment. The substances are mainly incorporated into the

This document is provided by JAXA.

organisms fat (*bioaccumulation*) (Barrie *et al.*, 1992; MacDonald and Bewers, 1996). At lower trophic levels the uptake occurs both through the diet and direct partitioning from seawater to the body lipids (*bioconcentration*) (Walker *et al.*, 1996). At higher trophic levels the uptake occurs mainly through the diet, which results in increased concentrations of substances in the food chain (*biomagnification*) (Walker *et al.*, 1996; Barron *et al.*, 1995). Accordingly, we find the lowest POP levels in phytoplankton and zooplankton, while we find the highest levels in the top of the food chain.

2.6. POP levels in Arctic animals

There are large differences in POP levels in Arctic animals. These differences may be attributed to many factors such as exposure time, ability to metabolize contaminants, ability to excrete compounds, seasonal variation in body mass, age and sex (Bignert *et al.*, 1993; Henriksen *et al.*, 1996). For example, the sex difference in POP levels often seen in birds partly reflects the fact that female birds are able to deposit the lipophilic compounds into the egg. In polar bears, considerable amounts of POPs are also transferred via milk from the mother to the cub. This is one of the main reasons for lower levels of some POPs in sexually mature female polar bears than in males (Bernhoft *et al.*, 1997).

Mapping the levels of anthropogenic pollutants in the Arctic has shown that the problem is mainly related to the marine ecosystem. POP levels in terrestrial species (all herbivorous) such as the Svalbard reindeer (*Rangifer tarandus platyrhynchus*), Svalbard ptarmigan (*Lagopus mutus hyperboreus*), geese (barnacle geese (*Branta leucopsis*), and pink footed geese (*Anser brachyrhynchus*)) are close to background levels (AMAP, 1998).

In general the POP levels in most marine species from the Barents Sea area are low when compared to the Baltic and the North Sea. High POP levels and possibilities of biological effects are mainly associated with species at the top of the food chains: the glaucous gull, the arctic fox and the polar bear. In glaucous gulls, the PCB levels are within the levels that cause reduced hatching success in wild and captive birds (AMAP, 1998). For polar bear and arctic fox, the PCB levels are within the levels that cause effects on reproduction in laboratory mammals (AMAP, 1998).

2.7. POP levels in marine food chains

In most marine species investigated at lower trophic levels in the Barents Sea area, the POP levels are low compared to species at lower trophic levels from the sub-arctic and temperate areas (0.01–0.2 ppm, lipid weigth concentrations) (Borgå *et al.*, 2001). For example, in copepods (*Calanus* spp.), euphausiids (*Thysanoessa* spp.) and amphipods (*Parathemisto libellula*) the POP levels are similar to the levels found in the Canadian Arctic (Muir *et al.*, 1999). In fish species, such as polar cod (*Boreogadus saida*) and cod (*Gadus morhua*), the POP levels are low when compared to the levels found in cod from the North- and Norwegian Seas (AMAP, 1998). The POP content in seawater, phyto- and zooplankton is dominated by HCH and HCB. In zooplankton, polar cod and cod from the Barents Sea, pattern of Chlordanes, DDTs and HCHs was dominated by compounds from the technical mixtures. This is similar to the POP pattern found in the Bering Sea and north Pacific (Tanabe *et al.*, 1984; Kawai *et al.*, 1988; Hargrave *et al.*, 1992; Ray *et al.*, 1999). The patterns found in zooplankton and fish may indicate that these species have a low ability to metabolize POPs (Borgå *et al.*, 2001). The low POP levels found in species at

This document is provided by JAXA.

lower trophic level are mainly explained by their position in the food web, their lipid content, their relatively short life span, as well as their migration routes.

2.8. Seabirds

Seabird species living in the Arctic are contaminated by the same POPs as seabirds living in the south (AMAP, 1998). The POP levels in seabirds are mainly determined by their feeding habits. Common eider (*Somateria mollissima*), which feed on benthic organisms, and little auk (*Alle alle*), which mainly feed on copepods, have low POP levels (0.5–1.0 ppm)(Savinova *et al*., 1995). However, in fish-eating species such as kittiwakes (*Rissa tridactyla*), common and Brunnich's guillemots (*Uria aalge* and *Uria lomvia*) and puffins (*Fratercula arctica*) the POP levels are somewhat higher (1.0–5.0 ppm) than in common eider and in little auk. The highest POP levels (1.0 to 40 ppm) are found in herring gull, glaucous gull, great black-backed gull (*Larus marinus*) and the great skua (*Stercorarius skua*)(Savinova, Skaare and Gabrielsen, unpublished). The POP levels in these gull species are 5–10 times higher than the other seabird species in the same area. In seabirds, the PCB is the major POP in all species, followed by DDT, Chlordane, HCB and HCH (Savinova *et al*., 1995; Borgå *et al*., 2001). The high POP levels in gulls reflects their position on the top of the Arctic food web. The levels of POP in different seabird species may also be explained by their migration pattern during the winter. Guillemots from low Arctic colonies in Canada have shown higher PCB and HCB levels than guillemots from high Arctic colonies (Braune and Donaldson, 2000). Most seabird species from Svalbard, which migrate south to the North- or Norwegian Seas during the winter, have higher POP levels than seabirds that live in the Arctic throughout the winter (Savinova, Skaare and Gabrielsen, unpublished).

2.9. Seals

The POP levels in different seal species from the Barents Sea area are low (10–50 times lower) when compared to seal species from the North- and the Baltic Sea. The PCB levels in ringed seal, harp seal (*Phoca groenlandica*), bearded seal (*Erignathus barbatus*) and Atlantic walrus (*Odobenus rosmarus*) are an average of 1.0–5.0 ppm (AMAP, 1998). The PCB levels in blubber of harp seal from the East Ice (Russian area) was three times higher (3.0 ppm) than the levels in West ice (Greenland area)(Espeland *et al*., 1997; Kleivane *et al*., 1997). However, this comparison is confounded by a significant difference in blubber thickness between the two areas (less blubber in the East Ice seals). A recent geographical trend study of PCB and DDT in ringed seal blubber have shown higher levels - in samples from the Yenisey Gulf in the Russian Arctic, Svalbard and east Greenland when compared to west Greenland and the Canadian Arctic (Muir *et al*., 2000). The highest levels of toxaphene have been found in harp seal collected east of Svalbard (Wolkers *et al*., 2000). The levels of the toxaphene congeners Tox 26 and Tox 50 in harp seals collected east of Svalbard were 20 times higher than in ringed seal samples west of Svalbard (Wolkers *et al*., 1998) and four times higher than in seals from the Canadian Arctic (Zhu and Nordstrom, 1993). The POP levels in seals are mainly determined by their feeding habits. The PCB levels in bearded seal and walrus, which are feeding on benthic organisms, is lower than in ringed - and harp seals, which mainly feed on fish and amphipods.

Most seal species show large variations in POP levels in the blubber, which can be

This document is provided by JAXA.

related to food intake and seasonal variation in body mass. Usually, the lowest body mass (lowest blubber thickness and highest POP level) occurs after giving birth, during lactation or in the molting period. The usage of blubber throughout this period will release POPs, which can have toxic effects on the immune- and reproductive system of the seal pups. However, mapping of the contaminant levels in most seal species from the Barents Sea area show that the levels are well below the levels which cause biological effects on seals (AMAP, 1998).

2.10. Whales

The levels of POPs in different whale species are also reflected by their feeding habits. Beluga (*Delphinapterus leucas*), narwhale (*Mondon monoceros*) and harbour porpoise (*Phocoena phocoena*), which feed mainly on fish, have higher POP levels (5–6 ppm) in their blubber than the minke whale (*Balaenoptera acutorostrata*) (2–4 ppm), which feeds on krill and amphipod. The levels of POPs increase with age and there are large differences between males (highest level) and females. There are also geographical differences in the POP levels in whales. This is mainly explained by their migration pattern. In minke whales the levels of POPs are higher on the coast of Lofoten Island in northern Norway when compared to the Svalbard area and the Kola area (Kleivane and Skaare, 1998).

In blubber samples of harbour porpoise from northern Norway, very high PCB levels (20–30 ppm) have been found. The levels of PCB and DDT are the highest measured in any whale species from the Arctic (AMAP, 1998). The reason for the high PCB levels in harbour porpoise from northern Norway is not fully understood. When compared to laboratory animals, the PCB levels in the blubber of the porpoise are high enough to have an effect on the immune system. High POP levels have also been found in beluga whales from the Gulf of St. Lawrence in Canada. Autopsy of stranded whales from this area did reveal cancer in the stomach and intestines (Martineau *et al.*, 1994). This was not found in animals from other areas. Such a finding is not described in dead whales found in Norwegian areas.

2.11. Arctic fox

The arctic fox is an opportunistic feeder, which eats cached food, scavenged carcasses of seabirds, terrestrial birds, seals, Svalbard reindeer and Svalbard ptarmigans (Fuglei, 2000). Some arctic foxes follow polar bears on the sea ice, feeding on remnants of seals killed by polar bears (Hiruki and Stirling, 1989). The levels of PCBs in arctic fox show a great variation (1.0–45 ppm), which probably reflects what they feed on (Wang-Andersen *et al.*, 1993; Severinsen and Skaare, 1997). Foxes sampled on the coast, which are feeding on marine species, have higher POP levels than foxes living inland, feed on carcasses of reindeer and terrestrial birds. When compared to POP levels in foxes from northern Europe and the Canadian Arctic, the levels in foxes from Svalbard are high (AMAP, 1998). The reason for this may be that foxes on Svalbard eat more marine species than foxes in Europe and in Canada.

The arctic fox shows seasonal variation in body weight and food intake throughout the year. In the late autumn (November), the fat content in arctic foxes is 20% of the body mass, while in late spring (June) the fat content is less than 6% of their body mass (Prestrud and Nilssen, 1992). Since PCBs are released during fat mobilization, there is reason to

This document is provided by JAXA.

believe that most of the PCBs in females are transported to the pups either when giving birth or transferred via milk. The POP levels in arctic fox at Svalbard are as high as in polar bear from Svalbard. It is reason to believe that the present POP levels, which are found in some individuals at Svalbard, are having an effect on the immune and reproduction system. At the present there are no studies going on to determine the effects of POPs on individuals or populations of arctic foxes from the Svalbard area.

2.12. Polar bears

Mapping of the contaminant levels in polar bear have shown high POP levels (5–80 ppm, average 25 ppm) in polar bears from east Greenland, Svalbard and Frans Josef Land (Russia), when compared to Alaska and Canada (Bernhoft *et al.*, 1997; Norstrom *et al.*, 1998; Andersen *et al.*, 2001). When compared to Alaska and Canada, the PCB levels are 2–6 times higher at Svalbard (Norstrom *et al.*, 1998; Bernoft *et al.*, 1997; AMAP, 1998). At Svalbard the PCB levels are 8–10 times higher than the levels found in ringed seal from the same area (Severinsen *et al.*, 2000). Polar bears feed mainly on the energy rich blubber layer of the seal (Stirling and McEwan, 1975), in which the POPs are accumulated, with the consequence that they are exposed to very high POP levels. During periods of reduced food intake in polar bears, stored lipids are released to meet the energy demands. During lipid mobilisation, however, the lipid-associated POPs are released to the blood resulting in POP exposure. At Svalbard the highest PCB levels are found in males, in which the levels increase with age (Bernhoft *et al.*, 1997).

Several explanations have been presented for the high PCB levels in polar bears from Svalbard and Franz Josef Land. One explanation may be that the polar bear at Svalbard and Frans Josef Land is exposed to local contamination due to transport of ice (in which POPs are incorporated in the Kara Sea), which are melted in the eastern part of Svalbard (Alexander, 1995; Pfirman, 1995, 1997). Another explanation is that polar bears feed on harp seals which migrate from the White Sea to the northern Barents Sea during the winter/spring (Kleivane *et al.*, 2000). Higher PCB levels in harp seals from the east ice when compared to the west ice as well as higher POP levels in harp seal compared to ring seal and bearded seal from the Svalbard and Frans Josef Land area may explain the high levels found in polar bears.

In polar bear there are large differences in PCB/DDT levels. These differences in POP levels are mainly explained by their feeding habits, sex differences and seasonal changes in body mass. During lactation the females deliver a lipid rich milk (40% fat) with a high content of PCB/DDT to the cub. Due to the transfer of contaminants via milk, there is reason to believe that the polar bear cub is exposed to POPs in a sensitive period of rapid growth and development.

3. Effects of POPs on birds and marine mammals

POP exposure has been associated with a variety of disorders in birds and mammals. Effects on the immune system (De Swart *et al.*, 1996; Grasman *et al.*, 1996), the endocrine system (Brouwer *et al.*, 1986) and internal organs (Bergman *et al.*, 1992; Reijnders, 1994) have been described in both laboratory animals as well as in marine birds and mammals from contaminated areas.

This document is provided by JAXA.

In field studies of Arctic free-living wildlife, it is difficult to prove a causal relationship between a suspected effect and specific contaminants. Thus, assessments of possible effects are based on associations between biological parameters and tissue residues of contaminants. Some biological responses (or *biomarkers of exposure*) are quite specifically related to contaminant exposure (*e.g.* cytochrome P450 enzyme activities or accumulation of highly carboxylated porphyrins), but are difficult to interpret in terms of consequences for the health of the individual, not to say the population (Peakall, 1992). Other responses may be more directly coupled to the survival or reproduction of the individual, but influenced by a large variety of confounding factors. In the following, we will review associations that have been reported between biological parameters and contaminant levels in vertebrates from the Svalbard area.

3.1. Polar bears

The POP levels in polar bears from Svalbard are comparable to the levels found in Baltic ringed seals, which have a negative effect on the reproduction and survival rate of young seals (Olsson *et al.*, 1992). A low cub production at Svalbard compared to Alaska and Canada might indicate that the POPs are already affecting the cub production in this area (Wiig *et al.*, 1998). Furthermore, it has recently been hypothesized that PCB and other POPs may be involved in the relatively high incidence of female pseudohermaphroditism in polar bear from Svalbard (Wiig *et al.*, 1998).

Many planar halogenated hydrocarbons (that is, dioxin-like compounds, which include some of the PCBs) have a common pattern of toxic effects that is associated with affinity to the aryl hydrocarbon (Ah) receptor and induction of isoforms from the cytochrome P4501A (CYP1A) subfamily (Poland and Knutson, 1982). Preliminary results from 13 polar bears from Svalbard show a positive correlation ($P=0.026$) between CYP1A and total PCB concentration in white blood cells (Skaare *et al.*, 2000a).

Vitamin A homeostasis can be severely altered by exposure to POPs, and several vitamin A deficiency-like symptoms are associated with intoxication by polyhalogenated aromatic hydrocarbons (Zile, 1992). Some PCB metabolites can disturb the formation of the protein complex responsible for retinol (vitamin A) and thyroxin transport (Brouwer *et al.*, 1986). In harbour seals fed fish from polluted waters, retinol and thyroid hormones in plasma was depressed, compared to seals fed fish from less polluted waters (Brouwer *et al.*, 1989). In polar bears from Svalbard, Skaare *et al.* (2000b) found a negative correlation between plasma retinol and PCB concentration ($r^2=0.11$, $P=0.003$). The ratio of total thyroxin to free thyroxin in plasma was also significantly negatively correlated to total PCB in plasma ($r^2=0.08$, $P=0.013$) (Skaare *et al.*, 2000b).

Many studies have demonstrated adverse effects of PCB and dioxin-like compounds on the immune system of experimental animals (see *e.g.* review by Tryphonas, 1994). In captive harbor seals fed fish highly contaminated with POPs, several measures of cell-mediated and humoral immune function were depressed compared to seals fed less contaminated fish (De Swart *et al.*, 1996). Immunoglobulin G (IgG) is the most abundant class of antibodies in mammals, and consequently an essential part of the humoral immune system. IgG levels indicate the ability of the bears to mount an immune response when re-exposed to a pathogen. In a sample of 52 polar bears from Svalbard, age- and sex-corrected level of IgG was negatively correlated with total PCB ($r^2=0.08$, $P=0.029$) and HCB ($r^2=0.13$, $P=$

This document is provided by JAXA.

0.005) (Bernhoft *et al.*, 2000). The PCB levels in the bears were within the range found to give immunotoxic effects in experimental animals (Bernhoft *et al.*, 2000). The association between POPs and IgG could indicate a contaminant-induced immunosuppression in Svalbard polar bears, with possible consequences for the susceptibility to infectious diseases.

3.2. Glaucous gulls

Possible biochemical effects of organochlorine contaminants in glaucous gulls were studied in a sample of forty adult individuals collected from colonies on Bjørnøya in the Barents Sea (Henriksen *et al.*, 2000a). Selected POPs, microsomal cytochrome P450 associated enzyme activities, highly carboxylated porphyrins (HCPs), retinol and retinyl palmitate, were quantified in liver samples.

As mentioned above, many POPs, in particular 2,3,7,8-tetrachlorodibenzo-p-dioxin (TCDD) and dioxin-like PCBs, can interfere with vitamin A homeostasis in experimental animals (Zile, 1992). Vitamin A is mainly stored as retinyl palmitate in lipid droplets of liver stellate cells (Blomhoff, 1994). In herring gulls from colonies in eastern Canada, liver retinoid concentrations were inversely related to the extent of TCDD-contamination in eggs from the same colonies (Spear *et al.*, 1986; Anonymous, 1991). In the sample of forty glaucous gulls from Bjørnøya, no significant relationships were found between liver retinoid concentrations and PCB levels (Henriksen *et al.*, 2000a). The hepatic vitamin A stores in glaucous gulls from Bjørnøya were larger than in herring gulls from contaminated locations in North America (Anonymous, 1991).

Briefly, cytochrome P450 activities have two aspects. In the first place, induction of P450 enzymes can be recognised as a biochemical effect per se, with consequences for the metabolism of endogenous compounds. Secondly, the P450 activities give an indication of the organisms metabolic capacity, and the potential for formation of metabolites, which in some cases are toxic. 7-ethoxyresorufin *O*-deethylase (EROD) activity is catalysed by isoenzymes from the cytochrome P4501A (CYP1A) subfamily, which are induced by planar POPs with affinity for the aryl hydrocarbon (Ah) receptor (Poland and Knutson, 1982; Peakall, 1992). When hepatic microsomes are incubated with testosterone, the pattern of hydroxylated testosterone metabolites reflects the activities of a range of cytochrome P450 proteins (Paolini *et al.*, 1997). Alterations in testosterone hydroxylase activities may have consequences for the steroid hormone status, and thereby affect reproductive capacity. TCDD exposure at environmentally realistic levels increased 2β-, 6β-, and 15α-testosterone hydroxylation activities in captive female great blue herons (*Ardea herodias*) (Sanderson *et al.*, 1997). In the glaucous gull sample (Henriksen *et al.*, 2000a), a weak positive association was found between hepatic EROD activity and PCB-levels. This may indicate induction by PCBs, but the EROD activities were low compared to other studies on fish-eating birds. Microsomal testosterone hydroxylase activity was only observed at the 6β-position and could not be related to levels of POPs. The low P450 associated enzyme activities in the glaucous gull suggests that they have a low capacity for metabolising POPs, which may contribute to the high accumulation of POPs in this species.

Disturbances in the heme biosynthetic pathway can lead to elevated levels of highly carboxylated porphyrins (HCP) in the liver (Marks, 1985). In free-living birds, the only known cause of HCP elevation is exposure to POPs (Fox *et al.*, 1988; Kennedy *et al.*, 1998). In herring gulls from the Great Lakes, hepatic HCP levels were elevated, compared

This document is provided by JAXA.

to herring gulls from less polluted colonies (Fox *et al.*, 1988). Among forty glaucous gulls sampled on Bjørnøya (Henriksen *et al.*, 2000a), HCPs were only elevated (138 pmol g^{-1}) in a single sample. The remaining samples contained low levels of HCPs (<30 pmol g^{-1}). It may not be a coincidence that the sample with elevated HCPs also had the highest levels of several POPs, including PCB-118, which is very porphyrinogenic in chicken embryo hepatocytes cultures (Lorenzen *et al.*, 1997). The findings of Kennedy *et al.* (1998) suggested that PCB-118 was an important contributor to porphyria in Great Lakes herring gulls. In these gulls, HCPs were consistently elevated whenever the liver level of PCB-118 exceeded 1.5 $\mu g\ g^{-1}$ wet weight (Kennedy *et al.*, 1998). In comparison, the PCB-118 level was 1.9 $\mu g\ g^{-1}$ wet weight in the single glaucous gull with elevated HCPs.

The weak association between EROD activity and PCB levels, and the low level of HCPs, suggest that these biochemical parameters were unaffected by OCs in most of the sampled gulls in the study by Henriksen *et al.* (2000a). Thus, the glaucous gulls seem not to be particularly sensitive towards Ah-receptor mediated effects.

Suppressed immune function has been associated with exposure to POPs in herring gulls from the contaminated Great Lakes area (Grasman *et al.*, 1996). If establishment and/or survival of intestinal macroparasites is limited by host immunity, we would expect increased parasite intensities in animals with high organochlorine burdens, such as the glaucous gull. In a sample of 40 glaucous gulls from Bjørnøya in the western Barents Sea, numbers of intestinal macroparasites were compared with hepatic levels of selected POPs (Sagerup *et al.*, 2000). After controlling for nutritional condition, no single parasite species was significantly associated with concentrations of PCBs or chlorinated pesticides. However, the intensity of all nematodes grouped together was positively correlated with 10 of the 14 POP concentrations measured. The strongest correlations were with p,p′-DDT, Mirex, total PCB, and PCB congeners 28, 118, 153, 138, 170, and 180. Although correlative and collected in the absence of immunological data, these data suggests that POPs might affect immune function in the glaucous gull.

Contamination by some POPs may result in behavioural impairments in birds (Peakall, 1996; McCarty and Secord, 1999). In a recent study by Bustnes *et al.* (2000) patterns of incubation and nest site attentiveness were examined in relation to PCB (polychlorinated biphenyls) loads, measured in blood, of 27 glaucous gulls from two different breeding areas at Bjørnøya. The levels of PCB in the blood samples ranged from 52 ppb to 1079 ppb (wet weight). PCBs were positively related to the proportion of time absent from the nest site, both overall and when not incubating, and to the number of absences, when controlling for a set of covariates (sex, breeding area ect.) known to influence behaviour. Bustnes *et al.* (2000) concluded that the increased absence from the nest site of glaucous gulls with high loads of PCB suggests that their reproductive motivation, possibly through endocrine disruption, or their ability to conduct some complex behaviour, were affected. PCB contamination could thus lead to increase energetic costs during incubation, and reduced reproductive output.

3.3. Harp seals

Testosterone hydroxylase activity was measured in harp seals by Wolkers *et al.* (2000). No correlation with PCBs were found, however, the CYP3A-like activity correlated significantly and strongly ($r^2=0.50$, $P<0.05$) with toxaphene residues. If the insecticide

This document is provided by JAXA.

toxaphene actually does affect this enzyme-activity in the harp seal liver, it means that the regulation of sex hormones could be disturbed.

4. Temporal trends in POPs in Arctic seabirds and marine mammals

Despite that several contaminants have been taken out of production and use in the 1970s and 1980s, we can see that it takes a long time before the POP levels decrease in seabirds and marine mammals in the northern Barents Sea area (AMAP, 1998). Trend studies of DDT and PCB levels in seabird eggs and marine mammals (seal and whales) from the Arctic and sub-Arctic show a clear reduction during the last 15–20 years (Barrett *et al*., 1996; AMAP, 1998). For example, in eggs from northern Norway there is a reduction in DDT and PCBs of 80–90% between 1973 and 1993 (Barrett *et al*., 1996). In the Canadian Arctic a similar reduction has been shown in eggs from guillemots, Fulmars and Kittiwakes (Braune and Donaldson, 2000). Such a decrease in PCB/DDT levels may indicate a reduction in production and use of organic pollutants. In marine mammals (seal and whales) the reduction in DDT and PCBs are not as strong as observed in seabirds. There is a lack of trend data from the Barents Sea area (except for polar bear). However, trend data from north west Canada show a strong decrease (5 times) in PCBs and a lower (3 times) decrease in DDT from 1972 to 1991 (AMAP, 1998). This is in contrast to data from seals and walruses from North-east Canada and Greenland which show no decrease in PCBs and DDT in a period of 15 years (AMAP, 1998). A reduction of PCBs and DDT was also found in Arctic foxes from Svalbard from 1970 up to present (E. Fuglei, pers. com). When it comes to the toxaphene and brominated compounds we do not have long trend data. However, it is reasonable to believe that there has been an increase in these contaminants in seabirds and marine mammals since the beginning of 1980s.

The most abundant PCB congener, PCB 153, decreased significantly in polar bear plasma from Svalbard during the 1990s (Henriksen *et al*., 2000b). Temporal data with high resolution from high Arctic biota are sparse (Muir *et al*., 1999). To our knowledge, the data from polar bears is the first detailed description of a temporal trend of PCB in high Arctic biota during the 1990s. The shape of the decline could suggest a levelling off in the latter part of the sampling period. Data from other marine mammals in the Canadian Arctic suggest a decline since the 1970s, but a levelling of during the 1980s and early 1990s (Muir *et al*., 1999). Stabilisation of PCB concentrations has also been observed in Great Lakes herring gull eggs (Stow, 1995). Continued monitoring will be necessary to verify if the observed decline in the Norwegian Arctic is levelling off or not.

Acknowledgments

The authors want to thank Myra Finkelstein, University of California Santa Cruz, Katrine Borgå and Kjetil Sagerup, The Norwegian Polar Institute, for constructive comments on the manuscript.

References

Alexander, V. (1995): The influence of the structure and function of the marine food-web on the

This document is provided by JAXA.

dynamics of contaminants in Arctic Ocean ecosystems. Sci. Total Environ., **161**, 593–603.
AMAP (1998): AMAP Assessment Report: Arctic Pollution Issues. Arctic Monitoring and Assessment Programme (AMAP) Oslo, Norway. p.xii+859.
Andersen, M., Lie, E., Belikov, S.E., Boltunov, A.N., Derocher, A.E., Garner, G.W., Skaare, J.U. and Wiig, Ø. (2001): Geographic variation of PCB congeners in polar bear (*Ursus maritinus*) from Svalbard east to the Chukchi Sea. Polar Biol., **24**, 231–238.
Anonymous (1991): Toxic chemicals in the Great Lakes and associated effects. Minister of Supply and Services Canada.
Bard, S.M. (1999): Global transport of anthropogenic contaminants and consequences for the Arctic marine ecosystem. Mar. Pollut. Bull., **38**, 356–379.
Barrett, R.T., Skaare, J.U. and Gabrielsen, G.W. (1996): Recent changes in levels of persistent organochlorines and mercury in eggs of seabirds from the Barents Sea. Enviorn. Pollut., **92**, 13–18.
Barrie, L.A., Gregor, D., Lake, R., Muir, D., Shearer, R., Tracey, B. and Bidleman, T. (1992): Arctic contaminants- sources, occurrence and pathways. Sci. Total Environ., **122**, 1–74.
Barron, M.G., Galbraith, H. and Beltman, D. (1995): Comparative reproductive and developmental toxicology of PCBs in birds. Comp. Biochem. Physiol., **112C**, 1–14.
Bergman, A., Olsson, M. and Reiland, S. (1992): Skull-bone lesions in the Baltic grey seal (*Halichoerus gryphus*). Ambio, **21**, 517–519.
Bernhoft, A., Wiig, Ø. and Skaare, J.U. (1997): Organochlorines in polar bears (*Ursus maritimus*) at Svalbard. Environ. Pollut., **96**, 1–16.
Bernhoft, A., Skaare, J.U., Wiig, Ø., Derocher A.E. and Larsen H.J. (2000): Possible immunotoxic effect of organochlorines in polar bear (*Ursus maritimus*) at Svalbard. J. Toxicol. Environ. Health, **59**, 561–574.
Bignert, A., Göthberg, A., Jensen, S., Litzen, K., Odsjö, T., Olsson, M. and Reutergårdh, L. (1993): The need for adequate biological sampling in ecotoxicological investigations—a retrospective study of 20 years pollution monitoring. Sci. Total Environ., **128**, 121–139.
Blomhoff, R. (1994): Transport and metabolism of vitamin A. Nutr. Rev., **52**, S13–S23.
Blomkvist, G., Roos, A., Jensen, S., Bignert, A. and Olsson, M. (1992): Concentrations of sDDT and PCB in seals from Swedish and Scottish waters. Ambio, **21**, 539–545.
Blus, L.J. (1995): Organochlorine pesticides. Handbook of Ecotoxicology, ed. by D. J. Hoffman *et al.* Boca Raton, Lewis Publ., 275–300.
Bogan, J.A. and Bourne, W.R.P. (1972): Organochlorine levels in Atlantic seabirds. Nature, **240**, 358.
Borgå, K., Gabrielsen, G.W. and Skaare, J.U. (2001): Biomagnification of organochlorines along a Barents Sea food chain. Environ. Pollut., **113**, 187–198.
Bourne, W.R.P. and Bogan, J.A. (1972): Polychlorinated biphenyls in North Atlantic seabirds. Mar. Pollut. Bull., **3**, 171–175.
Bowes, G.W. and Jonkel, C.J. (1975): Presence and distribution of polychlorinated biphenyls (PCB) in arctic and subarctic marine food chains. J. Fish. Res. Board Can., **32**, 2111–2113.
Braune, B.M. and Donaldson, G.M. (2000): Trend in organochlorine concentrations in seabird eggs from the Canadian Arctic: 1975–1998. Workshop on Persistent Organic Pollutants (POPs) in the Arctic: Human Health and Environmental Concerns. Rovaniemi, Finland, Jan. 2000, AMAP Report 2000:1, Abstract 27.
Brouwer, A., Van den Berg, K.J., Blaner, W.S. and Goodman, D.S. (1986): Transthyretin (prealbumin) binding of PCBs, a model for the mechanism of interference with vitamin A and thyroid hormone metabolism. Chemosphere, **15**, 1699–1706.
Brouwer, A., Reijnders, P.J.H. and Koeman, J.H. (1989): Polychlorinated biphenyl (PCB)-contaminated fish induces vitamin A and thyroid hormone deficiency in the common seal (*Phoca vitulina*). Aquat. Toxicol., **15**, 99–106.
Bustnes, J.O., Bakken, V., Erikstad, K.E., Mehlum, F. and Skaare, J.U. (2000): Patterns of incubation and nest site attentiveness in relation to polychlorinated biphenyl (PCB) contamination in Glaucous Gulls. J. Appl. Ecol. (in press).
De Boer, J., Wester, P.G., Klamer, H.J.C., Lewis, W.E. and Boon, J.P. (1998): Do flame retardants threaten ocean life? Nature, **394**, 28–29.
De Geus, H.J., Besselink, H., Brouwer, A., Klungsøyr, J., McHugh, B., Nixon, E., Rimkus, G.G., Wester,

This document is provided by JAXA.

P.G. and De Boer, J. (1999): Environmental occurrence, analysis, and toxicology of toxaphene compounds. Environ. Health Perspect., **107**, 115–144.

De Swart, R.L., Ross, P.S., Vos, J.G. and Osterhaus, A.D.M.E. (1996): Impaired immunity in harbour seals (*Phoca vitulina*) exposed to bioaccumulated environmental contaminants: Review of a long-term feeding study. Environ. Health Perspect. Suppl., **104**, 823–828.

Espeland, O., Kleivane, L., Haugen, S. and Skaare, J.U. (1997): Organochlorines in mother and pup pairs in two arctic seal species; Harp seal (*Phoca groenlandica*) and hooded seal (*Cystophora cristata*). Mar. Environ. Res., **44**, 315–330.

Fisher, B.E. (1999): Most unwanted persistent organic pollutants. Environ. Health Perspect., **107**, A18–A23.

Fox, G. A. (1992): Epidemiological and pathobiological evidence of contaminant-induced alterations in sexual development in free-living wildlife. Chemically-induced Alterations in Sexual and Functional Development: The Wildlife/Human Connection, ed. by T. Colborn and C. Clement Princeton Sci. Publ., 147–158.

Fox, G.A., Kennedy, S.W., Norstrom, R.J. and Wigfield, D.C. (1988): Porphyria in herring gulls: A biochemical response to chemical contamination of Great Lakes food chains. Environ. Toxicol. Chem., **7**, 831–839.

Fuglei, E. (2000): Physiological adaptations of the arctic fox to high Arctic conditions. Dissertation for the degree of Doctor Scientiarum. University of Oslo, Norway.

Gabrielsen, G.W., Skaare, J.U., Polder, A. and Bakken, V. (1995): Chlorinated hydrocarbon in glaucous gulls (*Larus hyperboreus*) in the southern part of Svalbard. Sci. Total Environ., **160/161**, 337–346.

Grasman, K.A., Fox, G.A., Scanlon, P.F. and Ludwig, J.P. (1996): Organochlorine-associated immunosuppression in prefledgling Caspian terns and herring gulls from the Great lakes: An Ecoepidemiological study. Environ. Health Perspect. Suppl., **104**, 829–842.

Hargrave, B.T., Harding, G.C., Vass, W.P., Erickson, P.E., Fowler, B.R. and Scott, V. (1992): Organochlorine pesticides and polychlorinated-biphenyls in the Arctic-Ocean food web. Arch. Environ. Contam. Toxicol., **22**, 41–54.

Henriksen, E.O., Gabrielsen, G.W. and Skaare, J.U. (1996): Levels and congener pattern of polychlorinated biphenyls in kittiwakes (*Rissa tridactyla*), in relation to mobilization of body-lipids associated with reproduction. Environ. Pollut., **92**, 27–37.

Henriksen, E.O., Gabrielsen, G.W., Trudeau, S., Wolkers, J., Sagerup, K. and Skaare, J.U. (2000a): Organochlorines and possible biochemical effects in glaucous gulls (*Larus hyperboreus*) from Bjørnøya, the Barents Sea. Arch. Environ. Contam. Toxicol., **38**, 234–243.

Henriksen, E.O., Derocher, A.E., Bustnes, J.O., Gabrielsen, G.W., Wiig, Ø. and Skaare, J.U. (2000b): Monitoring PCBs in polar bears: lessons learned from Svalbard. submitted to J. Environ. Monitoring.

Hiruki, L.M. and Stirling, I. (1989): Population-dynamics of the arctic fox, *Alopex lagopus*, on Banks Island, Northwest Territories. Can. Field-Nat., **103**, 380–387.

Holden, A.V. (1972): Monitoring organochlorine contaminants in marine environment by the analysis of residues in seals. Marine Pollution and Sealife, ed. by M. Ruivo. Surrey, FAO, 266–272 (Fishing News Book).

Kawai, S., Fukushima, M., Miyazaki, N. and Tatsukawa, R. (1988): Relationship between lipid composition and organochlorine levels in the tissues of Striped dolphin. Mar. Pollut. Bull., **19**, 129–133.

Kennedy, S.W., Fox, G.A., Trudeau, S., Bastien, L.J. and Jones, S.P. (1998): Highly carboxylated porphyrin concentration: a biochemical marker of PCB exposure in herring gulls. Mar. Environ. Res., **46**, 65–69.

Kleivane, L. and Skaare, J.U. (1998): Organochlorine contaminants in northeast Atlantic minke whales (*Balaenoptera acutorostrata*). Environ. Pollut., **101**, 231–239.

Kleivane, L., Espeland, O., Fagerheim, K.A., Hylland, K., Polder, A. and Skaare, J.U. (1997): Organochlorine pesticides and PCBs in the East ice harp seal (*Phoca groenlandica*) population. Mar. Environ. Res., **43**, 117–130.

Kleivane, L., Severinsen, T. and Skaare, J.U. (2000): Biological transport and mammal to mammal

This document is provided by JAXA.

transfer of organochlorines in arctic fauna. Environ. Sci. Technol., **15**, 626–639.
Lorenzen, A., Kennedy, S.W., Bastien, L.J. and Hahn, M.E. (1997): Halogenated aromatic hydrocarbon-mediated porphyrin accumulation and induction of cytochrome P4501A in chicken embryo hepatocytes. Biochem. and Pharmacol., **53**, 373–384.
MacDonald, R.W. and Bewers, J.M. (1996): Contaminants in the arctic marine environment: priorities for protection. ICES J. Mar. Sci., **53**, 537–563.
Marks, G.S. (1985): Exposure to toxic agents: The heme biosynthetic pathway and hemoproteins as indicator. CRC Crit. Rev. Toxicol., **15**, 151–179.
Martineau, D., De Guise, S., Fournier, M., Shugart, L., Girard, C., Lagacé, A. and Béland, P. (1994): Pathology and toxicology of beluga whales from the St. Lawrence estuary, Quebec, Canada. Past, present and future. Sci. Total Environ., **154**, 201–215.
McCarty, J.P. and Secord, A.L. (1999): Nest-building behavior in PCB-contaminated tree swallows. The Auk, **116**, 55–63.
McFarland, V.A. and Clarke, J.U. (1989): Environmental occurrence, abundance, and potential toxicity of polychlorinated biphenyl congeners—considerations for a congener-specific analysis. Environ. Health Perspect., **81**, 225–239.
Muir, D.C.G., Wagemann, R., Hargrave, B.T., Thomas, D.J., Peakall, D.B. and Norstrom, R.J. (1992): Arctic marine ecosystem contamination. Sci. Total Environ., **122**, 75–134.
Muir, D., Braune, B., DeMarch, B., Norstrom, R., Wagemann, R., Lockhart, L., Hargrave, B., Bright, D., Addison, R., Payne, J. and Reimer K. (1999): Spatial and temporal trends and effects of contaminants in the Canadian Arctic marine ecosystem: a review. Sci. Total Environ., **230**, 83–144.
Muir, D., Innes, S., Cleement, M., Riget, F., Dietz, R., Kleivane, L., Skaare, J., Severinsen, T., Nakata, H. and Tanabe, S. (2000): Circumpolar trends of PCBs and organochlorine pesticides in the Arctic marine environment inferred from levels in ringed seals. Workshop on Persistent Organic Pollutants (POPs) in the Arctic: Human Health and Environmental Concerns. Rovaniemi, Finland, Jan. 2000, AMAP Report 2000:1, Abstract 49.
Norstrom, R.J., Belikov, S.E., Born, E.W., Garner, G.W., Malone, B., Olpinski, S., Ramsay, M.A., Schliebe, S., Stirling, I., Stishov, M.S., Taylor, M.K. and Wiig, Ø. (1998): Chlorinated hydrocarbon contaminants in polar bears from eastern Russia, North America, Greenland, and Svalbard: Biomonitoring of Arctic pollution. Arch. Environ. Contam. Toxicol., **35**, 354–367.
Olsson, M., Andersson, O.E., Bergman, A.E., Blomkvist, G., Frank, A. and Rappe, C. (1992): Contaminants and diseases in seals from Swedish waters. Ambio, **21**, 561–562.
Ottar, B. (1981): The transfer of airborne pollutants to the Arctic region. Atmos. Environ., **15**, 1439–1445.
Paolini, M., Pozzetti, L., Sapone, A., Biagi, G.L. and Cantelli-Forti, G. (1997): Development of basal and induced testosterone hydroxylase activity in the chicken embryo in ovo. Br. J. Pharm., **122**, 344–350.
Peakall, D.B. (1992): Animal Biomarkers as Pollution Indicators. London, Chapman & Hall. (Chapman & Hall Ecotoxicology Ser. 1).
Peakall, D.B. (1996): Disrupted patterns of behavior in natural populations as an index of ecotoxicity. Environ. Health Perspect. Suppl., **104**, 331–335.
Pfirman, S.L., Eicken, H., Bauch, D. and Weeks, W.F. (1995): The potential transport of pollutants by Arctic sea-ice. Sci. Total Environ., **159**, 129–146.
Pfirman, S.L., Colony, R., Nurnberg, D., Eicken, H. and Rigor, I. (1997): Reconstructing the origin and trajectory of drifting Arctic sea ice. J. Geophys. Res., **102**, 12575–12586.
Poland, A. and Knutson, J.C. (1982): 2,3,7,8-tetrachlorodibenzo-p-dioxin and related halogenated aromatic hydrocarbons: Examination of the mechanism of toxicity. Ann. Rev. Pharm. Toxicol., **22**, 517–554.
Prestrud, P. and Nilssen, K. (1992): Fat deposition and seasonal variation in body composition of arctic foxes in Svalbard. J. Wildl. Manage., **56**, 221–233.
Ratcliff, D.A. (1967): Decrease in eggshell weight in certain birds of prey. Nature, **215**, 208–210.
Ray, S., Paranjape, M.A., Koenig, B., Paterson, G., Metcalfe, T. and Metcalfe, C. (1999): Polychlorinated biphenyls and other organochlorine compounds in marine zooplankton off the east coast of

This document is provided by JAXA.

Newfoundland, Canada. Mar. Enviorn. Res., **47**, 103–116.
Reijnders, P.J.H. (1994): Toxicokinetics of chlorobiphenyls and associated physiological responses in marine mammals, with particular reference to their potential for ecotoxicological risk assessment. Sci. Total Environ., **154**, 229–236.
Sagerup, K., Henriksen, E.O., Skorping, A., Skaare, J.U. and Gabrielsen, G.W. (2000): Intensity of parasitic nematodes increases with organochlorine levels in the glaucous gull. J. Appl. Ecol., **37**, 1–9.
Sanderson, J.T., Janz, D.M., Bellward, G.D. and Giesy, J.P. (1997): Effects of embryonic and adult exposure to 2,3,7,8-tetrachlorodibenzo-p-dioxin on hepatic microsomal testosterone hydroxylase activities in great blue herons (*Ardea herodias*). Environ. Toxicol. Chem., **16**, 1304–1310.
Savinova, T.N., Polder, A., Gabrielsen, G.W. and Skaare, J.U. (1995): Chlorinated hydrocarbons in seabirds from the Barents Sea area. Sci. Total Environ., **160/161**, 497–504.
Sellstrøm, U. and Jansson, B. (1995): Analysis of tetrabromobisphenol A in a product and environmental-samples. Chemosphere, **31**, 3085–3092.
Severinsen, T. and Skaare, J.U. (1997): Levels of heavy metals and persistent organic components in some terrestrial animals from Svalbard. The AMAP International Symposium on Enviorn. Pollution of the Arctic, Tromsø, Norway, June 1–5, 1997. Extended Abstracts, Vol. **1**, 407–409.
Severinsen, T., Skaare, J.U. and Lydersen, C. (2000): Spatial distribution of persistent organochlorines in ringed seal (*Phoca hispida*) blubber. Mar. Environ. Res., **49**, 291–302.
Skaare, J.U., Bernhoft, A., Derocher, A.E., Gabrielsen, G.W., Goksoeyr, A., Henriksen, E., Larsen, H. J.S., Lie, E. and Wiig, Ø. (2000a): Organochlorines in top predators at Svalbard-occurence, levels and effects. Toxicol. Lett., **112**, 103–109.
Skaare, J.U., Bernhoft, A., Wiig, Ø., Norum, K.R., Haug, E., Eide, D.M. and Derocher, A.E. (2000b): Relationships between plasma levels of organochlorines, retinol and thyroid hormones from polar bears (*Ursus maritimus*) at Svalbard. submitted to J. Toxicol. Environ. Health.
Spear, P.A., Moon, T.W. and Peakall, D.B. (1986): Liver retinoid concentrations in natural populations of herring gulls (*Larus argentatus*) contaminated by 2,3,7,8-tetrachlorodibenzo-p-dioxin and in ring doves (*Streptopelia risoria*) injected with a dioxin analogue. Can. J. Zool., **64**, 204–208.
Stirling, I. and McEwan, E.H. (1975): The calorific value of whole ringed seals (*Phoca hispida*) in relation to polar bear (*Ursus maritimus*) ecology and hunting behaviour. Can. J. Zool., **53**, 1021–1027.
Stow, C.A. (1995): Great Lakes herring gull egg PCB concentrations indicate approximate steady-state conditions. Environ. Sci. Technol., **29**, 2893–2897.
Tanabe, S., Tanaka, H. and Tatsukawa, R. (1984): Polychlorobiphenyls, SDDT, and hexachlorocyclohexane isomers in the western North Pacific ecosystem. Arch. Environ. Contam. Toxicol., **13**, 731–738.
Thomas, D.J., Tracey, B., Marshall, H. and Norstrom, R.J. (1992): Arctic terrestrial ecosystem contamination research. Sci. Total Environ., **122** (1–2), 135–164.
Tryphonas, H. (1994): Immunotoxicity of polychlorinated biphenyls: Present status and future considerations. Exp. Clin. Immunogenet., **11**, 149–162.
Voldner, E.C. and Li, Y.F. (1995): Global usage of selected persistent organochlorines. Sci. Total Environ., **161**, 201–210.
Walker, C.H., Hopkin, S.P., Sibly, R.M. and Peakall, D.B. (1996): Principles of Ecotoxicology. London, Taylor & Francis.
Wania, F. and Mackay, D. (1993): Global fractionation and cold concensation of low volatility organochlorine compounds in polar regions. Ambio, **22**, 10–18.
Wang-Andersen, G., Skaare, J.U., Prestrud, P. and Steinnes, E. (1993): Levels and congener pattern of PCBs in Arctic fox, Alopex lagopus, in Svalbard. Enviorn. Pollut., **82**, 269–275.
Wiig, Ø., Derocher, A.E., Cronin, M.M. and Skaare, J.U. (1998): Female pseudo-hermaphrodite polar bears at Svalbard. J. Wildl. Dis., **34**, 792–796.
Wolkers, J., Burkow, I.C., Lydersen, C., Dahle, S., Monshouwer, M. and Witkamp, R.F. (1998): Congener specific PCB and polychlorinated camphene (toxaphene) levels in Svalbard ringed seals (*Phoca hispida*) in relation to sex, age, condition and cytochrome P450 enzyme activity. Sci. Total Environ., **216**, 1–11.

This document is provided by JAXA.

Wolkers, H., Burkow, I.C., Lydersen, C. and Witkamp, R.F. (2000): Chlorinated pesticide concentrations, with an emphasis on polychlorinated camphenes (toxaphenes), in relation to cytochrome P450 enzyme activities in harp seals (*Phoca groenlandica*) from the Barents Sea. Environ. Toxicol. Chem., **19**, 1632–1637.

Zelinski, V., Lorenz, W. and Bahadir, M. (1993): Brominated flame retardants and resulting PBDD/F in accidental fire residues from private residences. Chemosphere, **27**, 1519–1528.

Zhu, J. and Norstrom, R.J. (1993): Identification of polychlorocamphenes (PCCs) in the polar bear (*Ursus maritmus*) food chain. Chemosphere, **27**, 1923–1936.

Zile, M.H. (1992): Vitamin A homeostasis endangered by environmental pollutants. Proc. Soc. Exp. Biol. Med., **201**, 141–153.

(Received April 14, 2000; Revised manuscript accepted September 20, 2000)

This document is provided by JAXA.

Mem. Natl Inst. Polar Res., Spec. Issue, 54, 365–375, 2001

Scientific note

Arctic Ocean change and consequences to biodiversity: A perspective on linkage and scale

Eddy Carmack and Fiona McLaughlin

Institute of Ocean Sciences, 9860 West Saanich Road, Sidney, B.C. V8L 4B2, Canada

Abstract: In the Arctic Ocean at least two climate-linked, contiguous domains are linked to ecosystems through both bottom-up (e.g. changes in light and nutrient regimes) and top-down (*e.g.* changes in fish and large predator populations) regulation. The first is the $\sim 7 \times 10^6$ km^2 seasonal ice zone (SIZ) which affects light and nutrient regimes, and also provides a solid surface upon which large mammals travel, rest, reproduce and hunt. The second is the $\sim 10 \times 10^3$ km long riverine coastal domain (RCD), driven by runoff, which affects light, nutrient and carbon regimes and provides a pathway for the dispersal and migration of marine biota. Sustained observation of marine mammal and bird behaviour may unlock 'top-down' information to an important ecological question raised by Malcolm Ramsay (pers. comm.), namely: What environmental conditions prompt certain animals to be in a certain place at a certain time, and how will they respond to changing climate conditions? Finally, it is noted that the Arctic is not an isolated sea, but rather is interconnected to the water masses and ecosystems of the Pacific and Atlantic.

1. Introduction

Conservation of biodiversity, particularly those components upon which humans depend for survival, is arguably the most pressing challenge facing environmental scientists in the new century (*cf.* Levin, 1999). This challenge must be addressed against a backdrop of rapidly changing environmental conditions and constraints, and nowhere is this backdrop changing more rapidly than in the Arctic.

Prior to the 1990s, the water mass structure of the Arctic Ocean was generally held to be in steady state. However growing evidence of change has been documented in both the Arctic Ocean water column (*cf.* Carmack *et al.*, 1995, 1997; McLaughlin *et al.*, 1996; Morison *et al.*, 1998; Steel and Boyd, 1998) and in its ice cover (Kwok and Rothrock, 1999). Such studies appear to parallel climate model predictions that climate warming will occur first and most intensely in high-latitude regions (Walsh and Crane, 1992). How, then, will biota respond?

The disproportionate influence of climate warming on Arctic physical and biological systems may also be linked to critical temperatures involving the melting of sea ice and snow. Physically this involves two main positive feedback mechanisms: the first is the so-called albedo feedback mechanism associated with the melting of snow and ice; the second is associated with the release of natural greenhouse gases (*e.g.* methane, CO_2) stored

This document is provided by JAXA.

in the permafrost and hydrate layers at high latitudes. Biologically, the disproportionate influence of warming may alter the floating ice cover, and change the timing and strength of river freshet. It is the purpose of the following research note to review the basic structure of the Arctic Ocean; highlight recent observations of change; speculate on potential biological consequences; and, finally, discuss how changes in the physical environment may produce bottom-up and top-down consequences.

2. Ocean structure

The Arctic is a salt-stratified ocean. This allows the Arctic Ocean the stratification it requires to support an ice cover. The Arctic mixed-layer consists of the upper 50 or so meters wherein changes involving the annual melt-freeze cycle and river water disposition occur. Below this seasonally variable mixed-layer lies a complex of cold, salt-stratified layers known collectively as the Arctic halocline. This layer insulates the Arctic Ocean and keeps the upper cold waters cold and the underlying warm waters warm. Regionally, the various components of the Arctic halocline can be ascribed to (1) ice melt mixed with Atlantic-origin water, (2) Pacific-origin inflow waters (summer and winter), and (3) brine-enriched shelf drainage. Water mass boundaries separating waters of different source are found both in the vertical and the horizontal, and such boundaries are now known to shift from submarine ridge to ridge on inter-decadal time-scales. Such shifts are likely to alter downstream conditions in the North Atlantic as a result of the displacement of freshwater (McLaughlin, 2000). It is also important to view the Arctic mixed-layer and halocline as components of a much larger oceanographic feature, the northern hemisphere halocline, a domain bounded by sharp subarctic fronts in both the Pacific and Atlantic oceans. It is this latter feature that ultimately defines the presence or absence of both ice cover and deep convection at high latitudes.

Below the cold halocline lie components of the Atlantic layer, situated below the Arctic thermocline and above the effective sill depth of the Lomonosov Ridge (about 1600 m). Water within this layer enters from the North Atlantic via Fram Strait and the Barents Sea and moves counter-clockwise as narrow (about 100 km) cores following shelf-break and ridge topography. The deep waters of the Arctic Ocean lie below the effective sill depths of the Lomonosov and Alpha/Mendeleyev ridges and are among the most isolated in the world.

Arctic Ocean outflow occurs via both Fram Strait and the West Greenland Current (Woodgate *et al.*, 1999) and through the Canadian Arctic Archipelago (Melling, 2000), and both outflows are complex. For example, transformations within the East Greenland Current are thought to play a role in the formation of Denmark Strait Overflow Water (Strass *et al.*, 1993). Outflow through the Canadian Arctic Archipelago occurs across an extremely large and complex arctic shelf, studded with islands, and characterized by interconnected sub-basin, tidal and buoyancy-driven boundary currents.

3. Arctic environmental change

It is currently thought that there are two main ways that the Arctic Ocean might impact on global climate, and both relate to the high-latitude hydrological cycle (*cf.* Aagaard and

This document is provided by JAXA.

Carmack, 1989, 1994). The first is through its effect on the surface heat balance, *i.e.* the role of the ocean, sea ice and clouds in the local radiation balance and albedo. The second is through its effect on the global thermohaline circulation, *i.e.* the regulation of deep-water formation rates. But, climate change is a two-way street, and we must also ask the question: How will global climate variability impact back, regionally, upon the Arctic and its biodiversity?

3.1. What are the signs of Arctic change?

This past decade has witnessed remarkable variability in the physical environment of the Arctic region, variability that may have consequences to all forms of life. Figure 1 depicts a number of key changes in a cartoon 'climate clock' where each passing hour records different physical changes.

- One o'clock: Perturbations in the amount of low salinity water exiting the Arctic have affected the upper waters of the entire North Atlantic Ocean (and perhaps the thermohaline circulation) on decadal time scales (Dickson *et al.*, 1988; Belkin *et al.*, 1998).
- Two o'clock: Temperature of Atlantic origin water entering through Fram Strait and the Barents Sea has increased (Quadfasel *et al.*, 1991; Carmack *et al.*, 1995, 1997; Morison *et al.*, 1998; Grotefendt *et al.*, 1998).
- Three o'clock: Transport of surface waters toward exit points at Nares and Fram straits has increased (Newton and Sotirin, 1997).

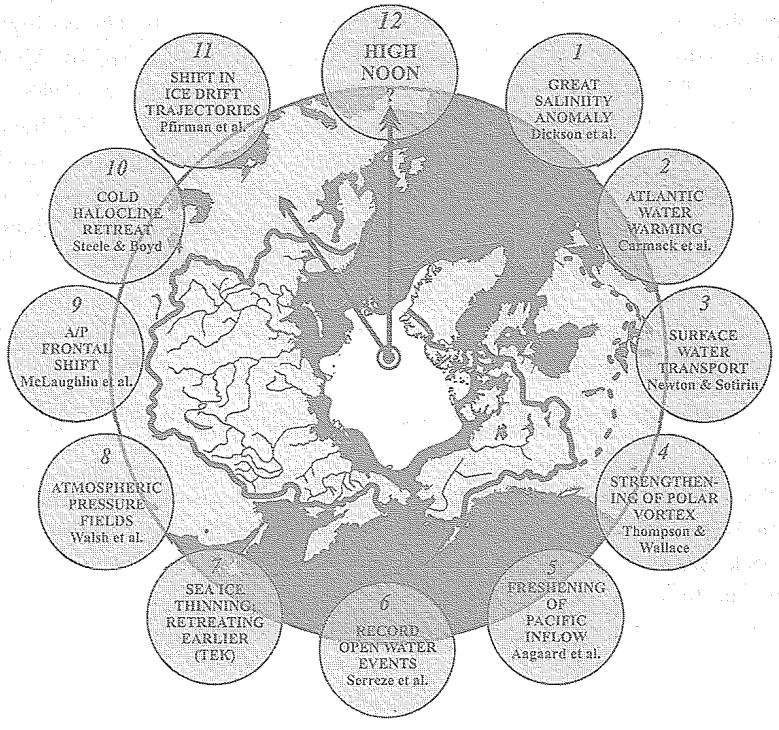


Fig. 1. 'Climate clock' summarizes the physical changes observed in the 1990s.

This document is provided by JAXA.

- Four o'clock: Polar vortex has strengthened and the Arctic Oscillation is now recognized as a fundamental mode of the global atmosphere (Thompson and Wallace, 1998).
- Five o'clock: Salinity of Pacific origin water entering through Bering Strait has decreased (Aagaard, pers. comm.)
- Six o'clock: Record areas of open water during summer (Serreze *et al.*, 1995).
- Seven o'clock: Sea ice has been noted to be decreasing in areal extent, thinning, more mobile, melting earlier and re-freezing later (Traditional Ecological Knowledge).
- Eight o'clock: Mean atmospheric pressure over the Arctic has decreased, reflective of an increased number of atmospheric cyclones entering the arctic system (Walsh *et al.*, 1996).
- Nine o'clock: A basin-wide water mass front separating Atlantic and Pacific water masses has abruptly shifted from one ridge system (the Lomonosov) to another (the Alpha-Mendeleyev) (McLaughlin *et al.*, 1996).
- Ten o'clock: Areal extent of the so-called cold halocline (which provides static stability to the water column) has retreated (Steele and Boyd, 1998).
- Eleven o'clock: Large-scale trajectories of sea-ice have changed (Pfirman *et al.*, 1997).
- Twelve o'clock: As in the western film "High Noon" this is a time when the protagonist (mankind) must take moral and decisive action—in this case with the environment—or forever live with the consequences.

3.2. What are the potential consequences to biota?

Variability in the physical environment is likely to be reflected in the realm of living nature, including changes in species abundance, community structure, seasonal distributions, geographic range, migration patterns and reproductive success. The ecological importance of biota living below, within and above sea ice has been discussed by Alexander and Chapman (1981), Burns *et al.* (1981), Bradstreet (1982), Grebmeier *et al.* (1988) and Welch *et al.* (1992). Stirling and Derocher (1993) and Tynan and DeMaster (1997) have discussed consequences of climate change to marine mammals. Drawing from these works, among others, we present Fig. 2 as a 'biological clock' that summarizes a number of conceptual scenarios, both bottom-up and top-down, that might follow from climate change.

- One o'clock: Warming will result in longer ice-free periods, particularly in the seasonal ice zone.
- Two o'clock: Increased open water will increase wind-mixing, upwelling, and wintertime brine rejection (convection), and thus increase the availability of nutrients to phytoplankton.
- Three o'clock: Increased open water will increase the availability of underwater light to phytoplankton, especially in the seasonal ice zone.
- Four o'clock: Increased rainfall predicted under global warming will increase the export of organic terrestrial material (POC, DOC) to coastal domains.
- Five o'clock: Decreased ice cover will decrease ice algae production with consequences to the marine food web.
- Six o'clock: Rising sea level, combined with increased temperatures and open water areas, will accelerate coastal erosion.
- Seven o'clock: Shifting water mass fronts and currents will affect fish migration and behaviour.
- Eight o'clock: Altered habitat conditions in both rivers and coastal seas may affect the

This document is provided by JAXA.

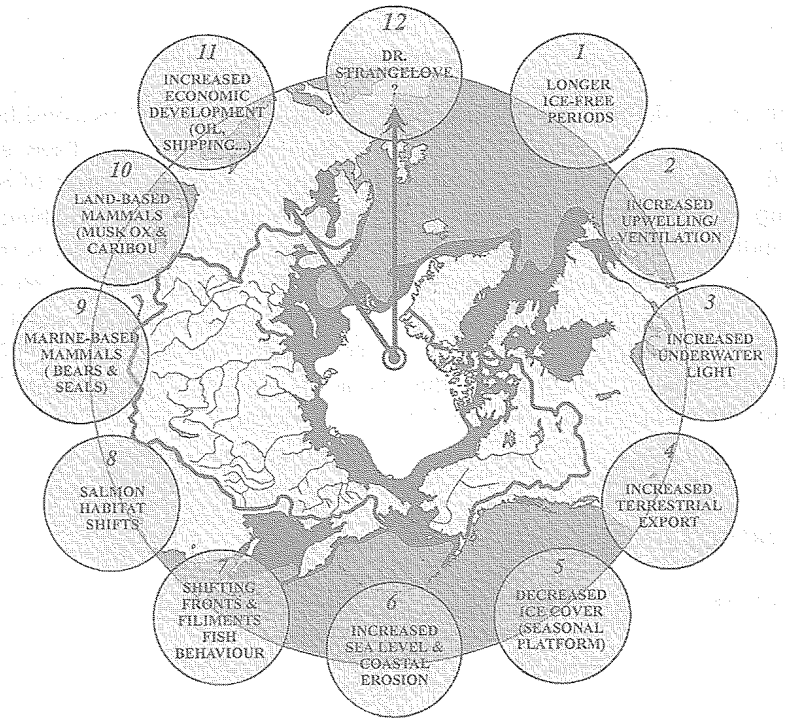


Fig. 2. 'Biological clock' summarizes a number of biological scenarios that might follow from climate change.

distribution of anadromous fish.

- Nine o'clock: Marine-based animals (*e.g.* seals, bears) that depend on an ice platform will be seriously impacted by loss of habitat.
- Ten o'clock: Land-based mammals (*e.g.* caribou) that depend on a reliable seasonal platform of ice for migration will be impacted.
- Eleven o'clock: A warmer climate will attract extractive, resource-based industries (*e.g.* oil, mining) with the result that human conditions and impacts will change.
- Twelve o'clock: As in the film "Dr. Strangelove" which refers to a doomsday device buried in the Arctic capable of extinguishing all life, the cumulative effects of climate change may trigger natural doomsday devices (*i.e.* runaway feedback mechanisms) that the Arctic may possess. For example, the release of billions of tonnes of methane (a greenhouse gas) held beneath the frozen Arctic surface could be triggered by global warming with catastrophic effects.

The above 'clock' maintains a separation in the responses of plankton, fish and mammals to environmental change, whereas in fact, they are coupled, a point discussed below.

This document is provided by JAXA.

4. Discussion

Wilson (1999) defined biodiversity as: "The variety of organisms considered at all levels, from genetic variants belonging to the same species through arrays of species to arrays of genera, families and still higher taxonomic levels; (it) includes the variety of ecosystems, which comprise both the communities of organisms within particular habitats and the physical conditions under which they live." Biodiversity thus refers to what is there. More recently the term biocomplexity has been applied and refers to how what is there senses and interacts with its environment. Biocomplexity views nature as a complex adaptive system, wherein the problem of pattern and scale is the central challenge (*cf.* Levin, 1992). To link biodiversity to climate simply requires that we accommodate all scales from that of the molecular to that of the climate (Fig. 3). This 'working through scales' is typically done in either ascending or descending order. The bottom-up approach views trophic interactions

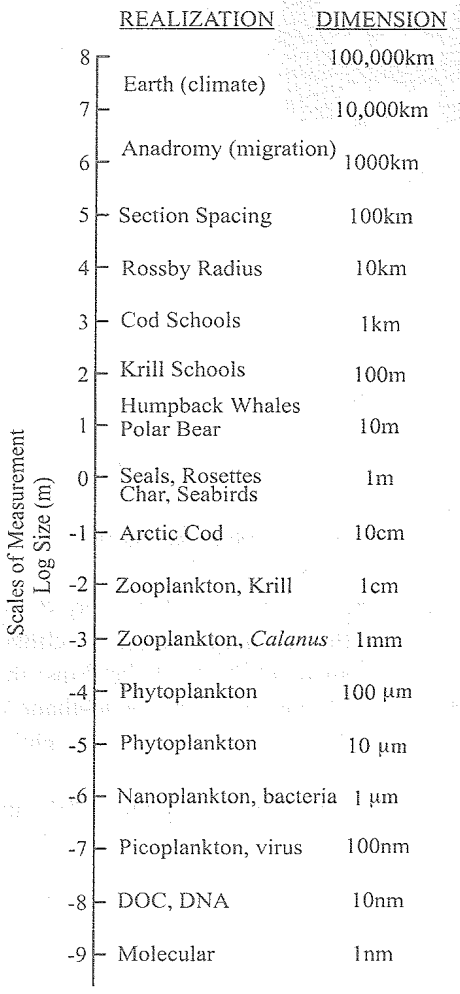


Fig. 3. Scales linking climate to biota.

This document is provided by JAXA.

as a chain beginning with small scales and working upward (*e.g.* turbulence delivers nutrients which fuel primary production, and so on). The top-down approach begins at some larger scale and works downward to understand, for example, the role of predators in shaping trophic structure. It is commonly assumed that climate change effects bottom-up changes (*e.g.* nutrients, underwater light conditions), and that anthropogenic impacts (*e.g.* fishing, whaling) work in a top-down mode. Seldom is the full set of scales linking climate to biodiversity within a contiguous ecological domain accommodated. In the Arctic, two climate-linked, contiguous domains can be identified where global warming may impact ecosystems from the bottom-up and the top-down.

4.1. Seasonal ice zone (SIZ)

Each year over 7 million square kilometres of sea-ice freezes and melts in the Arctic, an area about the size of the Australian continent. The top of this solid cover serves as floating platform for many large mammals, such as polar bears and seals and the underside provides a rich habitat for plankton and fish. Global warming, by shrinking and thinning the seasonal sea-ice, affects the geographical range and survival of many Arctic species. Shorter duration of ice cover by earlier break-up and later freeze-up may also impact on the timing of annual cycles critical to the Arctic environment.

Viewing recent changes from the bottom-up, a number of consequences may be anticipated. Longer ice-free periods will significantly increase underwater light availability. (At present, ice lingers through May and June, months of high insolation.) A delayed freeze-up will also expose more open water to forcing by autumn storms. Retreat of the SIZ into the central Arctic basins will impact nutrient availability on shelves during summer and autumn through increased mixing and upwelling. There may be an increase in productivity should the SIZ routinely retreat past the shelf break and allow coastal upwelling of nutrient-rich water from the basin interior.

Taking a top-down view we can ask: Could climate change in the Arctic Ocean also pose a threat of extinction to seals that require snow and ice to birth their young? Or polar bears that hunt only from sea ice? Or non-marine animals such as some populations of caribou that depend on a solid and reliable ice cover for their seasonal migrations to calving grounds? Removal and/or replacement of such predators from the adaptive ecosystem will clearly have top-down consequences.

4.2. Riverine coastal domain (RCD)

A key process in the transport of fresh water through the Arctic is via the formation of gravity-driven, buoyancy-boundary currents (Muchow and Carmack, 1997). Such flows form when fresh, low-density water is discharged into the higher-density ocean, and are deflected to the right by the Coriolis force. In the Northern Hemisphere, buoyancy-boundary currents travel in a clockwise sense, with landmasses always to the right in the direction of flow. The dimension of buoyancy-boundary currents scales with the Rossby radius $R_R=(g^* h)^{1/2}/f$, where g^* is the reduced gravity, h is depth, and f the Coriolis term; in the Arctic R_R ~10 km. This parameter scales the width of currents driven by coastal runoff.

The multiple sources of freshwater discharge from northern North America, combined with ice and snow melt, may enable the formation of a quasi-contiguous domain, here

This document is provided by JAXA.

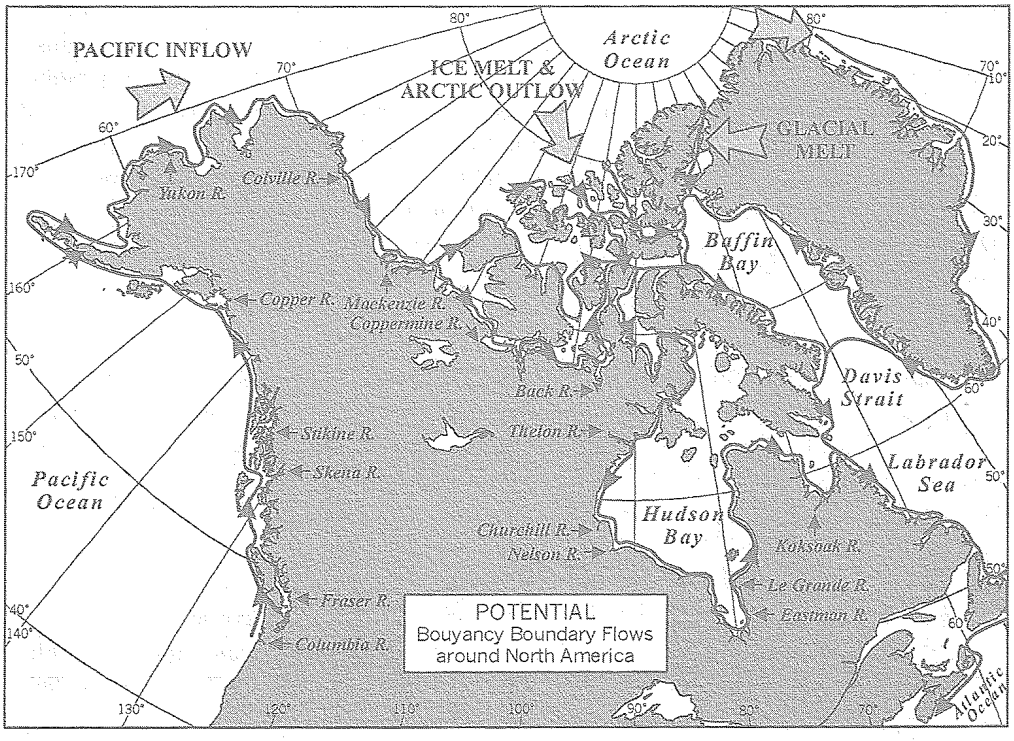


Fig. 4. Schematic representation of potential buoyancy-driven boundary flow around northern North America.

called the Riverine Coastal Domain (RCD), which extends around the northern part of the continent. This concept is shown schematically in Fig. 4. The RCD is not stationary or continuous; it is highly idealized in that it ignores wind and tidal forcing. However, it is (a) contiguous—more or less continuous around the entire continent; and (b) terrigenous—having a strong influence of land/ocean interaction. This contiguous and terrigenous ribbon around North America, if demonstrated, could provide an important migration and dispersal corridor for biota, and is of sufficient size and extent to be strongly linked to the climate system.

Taking a bottom-up view, some consequences of climate variability on the RCD are evident. Climate models predict increased precipitation in high-latitudes under greenhouse gas warming. This may result in altered runoff and export of terrestrial carbon (POC, DOC) to coastal ecosystems. Increased runoff may also alter erosion, suspended load transport, and thus the turbidity and light climate of coastal waters.

Top-down impacts may be even more important, as it is clear that such a pathway would play a major role in dispersal. Many anadromous fish species (salmon, cisco, char) use the RCD as a migration (and perhaps navigation) pathway. Do recent observations of increased numbers of Pacific salmon in Arctic rivers signal new colonizations associated with global warming? Finally, the ecological consequences of macro-plankton grazers, carried by density currents over great distances to new pastures, because of a changing

This document is provided by JAXA.

physical environment, are beyond speculation.

5. Concluding remarks

Although this note has focused on the impacts to arctic biota of changing climate, the effects of human activity upon this fragile ecosystem must also be weighed. In the Canadian Arctic we should inquire, for example, has the abundance and diversity of life in Arctic waters changed since the time Henry Larsen sailed aboard the *St. Roch*? Since the time John Franklin's party sailed aboard the *Erebus* and *Terror*? Since Parry, Hudson and Frobisher entered the Arctic in search of a trade route? Has removal of top predators by whaling, hunting and fishing irreversibly altered the trophic dynamics of Arctic waters, thereby changing productivity and increasing vulnerability to climate change? Likely, the answer to each question is yes. But, can the magnitude of such change be measured or understood? Likely, it cannot. Nevertheless, an important beginning can be made by studying oral history, examining archaeological records and reviewing scientific data that already exists.

Around the world, Aboriginal Peoples have long held that all nature is interconnected. Certainly, this is true of the oceans surrounding North America. Low salinity waters from the Pacific Ocean flow northward through Bering Strait carrying nutrient-rich waters into the Arctic Ocean. This water floods the upper layers of the Beaufort Sea, and much of it eventually exits eastward from the Arctic Ocean through the Canadian Arctic Archipelago and into the North Atlantic via the Labrador Sea. In this way, Pacific waters transiting the Arctic, may eventually condition the marine habitat of Atlantic fishes. This simple example shows that we cannot truly understand changes that occur in one ocean without viewing the entire system.

Acknowledgments

This brief contribution is dedicated to the vision, inspiration and scientific leadership of Malcolm Ramsay, who woke us both to the beauty and importance of the Arctic's living nature.

References

Aagaard, K. and Carmack, E.C. (1989): The role of sea ice and other fresh water in the Arctic circulation. J. Geophys. Res., **94**, 14485–14498.

Aagaard, K. and Carmack, E.C. (1994): The Arctic Ocean and climate: A perspective. The Polar Oceans and Their Role in Shaping the Global Environment: The Nansen Centennial Volume, ed. by O.M. Johannessen *et al*. Washington, D.C., Am. Geophys. Union, 5–20 (Geophys. Monogr. Ser., **85**).

Alexander, V. and Chapman, T. (1981): The role of epontic algal communities in Bering Sea ice. The Eastern Bering Sea Shelf: Oceanography and Resources, Vol. 2, ed. by D.W. Hood and J.A. Calder. Seattle, Univ. Washington Press, 773–780.

Belkin, I. M., Levitus, S., Antonov, J. and Malmberg, S. (1998): "Great Salinity Anomalies" in the North Atlantic. Progr. Oceanogr., **41**, 1–68.

Bradstreet, M.S.W. (1982): Occurrence, habitat use and behaviour of seabirds, mammals and arctic cod at the Pond Inlet ice edge. Arctic, **35**, 28–40.

This document is provided by JAXA.

Burns, J.J., Shapiro, L.H. and Fay, F.H. (1981): Ice as a marine mammal habitat in the Bering Sea. The Eastern Bering Sea Shelf: Oceanography and Resources, Vol. 2, ed. by D.W. Hood and J.A Calder. Seattle, Univ. Washington Press, 781–797.

Carmack, E.C., Macdonald, R.W., Perkin, R.G., McLaughlin, F.A. and Pearson, R.J. (1995): Evidence for warming of Atlantic water in the southern Canadian Basin of the Arctic Ocean: Results from the Larsen-93 expedition. Geophys. Res. Lett., **22**, 1061–1064.

Carmack, E.C., Aagaard, K., Swift, J.H., Macdonald, R.W., McLaughlin, F.A., Jones, E. P., Perkin, R. G., Smith, J.N., Ellis, K.M. and Kilius, L. (1997): Changes in temperature and tracer distributions within the Arctic Ocean: Results from the 1994 Arctic Ocean Section. Deep-Sea Res., **44**, 1487–1502.

Dickson, R.R., Meincke, J., Malmberg, S. and Lee, A.J. (1988): The "Great Salinity Anomaly" in the northern North Atlantic. Prog. Oceanogr., **20**, 103–151.

Grebmeier, J.M., McRoy, C.P. and Feder, H.M. (1988): Pelagic-benthic coupling on the shelf of the northern Bering and Chukchi Seas. I. Food supply, sources and benthic biomass. Mar. Ecol. Progr. Ser., **48**, 57–67.

Grotefendt, K., Logemann, K., Quadfasel, D. and Ronski, S. (1998): Is the Arctic Ocean warming. J. Geophys. Res., **103**, 27679–27687.

Kwok, R. and Rothrock, D.A. (1999): Variability of Fram Strait ice flux and the North Atlantic Oscillation. J. Geophys. Res., 104, 5177–5189.

Levin, S.A. (1992): The problem of pattern and scale in ecology. Ecology, **73**, 1943–1967.

Levin, S.A. (1999): Fragile Dominion: Complexity and the Commons. Reading, Perseus Books, 250 p. (Helix books).

McLaughlin, F.A., Carmack, E.C., Macdonald, R.W. and Bishop, J.K. (1996): Physical and geochemical properties across the Atlantic/Pacific water mass front in the southern Canadian Basin. J. Geophys. Res., **101**, 1183–1197.

McLaughlin, F.A. (2000): The Canada Basin 1989–1995: Upstream Events and Far-Field Effects of the Barents Sea Branch 2000. Ph.D. Dissertation, University of Victoria, Victoria, British Columbia, 85 p.

Melling, H. (2000): Exchanges of freshwater through the shallow straits of the North American Arctic. The Freshwater Budget of the Arctic Ocean, ed. by E.L. Lewis. Amsterdam, Kluwer Academic Publ., 479–502.

Morison, J., Steele, M. and Anderson, R. (1998): Hydrography of the Upper Arctic Ocean measured from the nuclear submarine USS Pargo. Deep-Sea Res., Part 1, **45**, 15–38.

Munchow, A. and Carmack, E.C. (1997): Synoptic flow and density observations near an Arctic Shelf Break. J. Phys. Oceanogr., **27**, 1401–1419.

Newton, J.L. and Sotirin, B.J. (1997): Boundary undercurrent and water mass changes in the Lincoln Sea. J. Geophys. Res., **102**, 3393–3403.

Pfirman, S.L., Colony, R., Nürnberg, D., Eicken, H. and Rigor, I. (1997): Reconstructing the trajectory and origin of Arctic sea ice. J. Geophys. Res., **102**, 12575–12586.

Quadfasel, D., Sy, A., Wells, D. and Tunik, A. (1991): Warming in the Arctic. Nature, **350**, 385.

Serreze, M.C., Maslanik, J.A., Key, J.R. and Kokaly, R.F. (1995): Diagnosis of the record minimum in Arctic sea ice area during 1990 and associated snow extremes. Geophys. Res. Lett., **22**, 2183–2186.

Steele, M. and Boyd, T. (1998): Retreat of the cold halocline layer in the Arctic Ocean. J. Geophys. Res., **103**, 10419–10435.

Stirling, I. and Derocher, A.E. (1993): Possible impacts of climate warming on polar bears. Arctic, **46**, 240–246.

Strass, V.H. and Farbach, E. (1993): U. Schauer, and L. Sellmann, Formation of Denmark Strait Overflow Water by mixing in the East Greenland Current. J. Geophys. Res., **98**, 6907–6919.

Thompson, D.W.J. and Wallace, J.M. (1998): The Arctic Oscillation signature in the wintertime geopotential height and temperature fields. Geophys. Res. Lett., **25**, 1297–1300.

Tynan, C.T. and DeMaster, D.P. (1997): Observations and predictions of Arctic climate change: Potential effects on marine mammals. Arctic, **50**, 308–322.

Walsh, J.E. and Crane, R.G. (1992): A comparison of GCM simulations of Arctic climate. Geophys. Res.

This document is provided by JAXA.

Lett., **19**, 29–32.
Walsh, J.E., Chapman, W.L. and Shy, T.L. (1996): Recent decrease of sea level pressure in the Central Arctic. J. Clim., **9**, 480–486.
Welch, H.E., Bergmann, M.A., Siferd, T.D., Martin, K.A., Curtis, M.F., Crawford, R.E., Conover, R.J. and Hop, H. (1992): Energy flow through the marine ecosystem of the Lancaster Sound Region, Arctic Canada. Arctic, **45**, 343–357.
Wilson, E.O. (1999): The Diversity of Life. New York, W.W. Norton, 424 p.
Woodgate, R.A., Farbach, E. and Rohardt, G. (1999): Structure and transports of the East Greenland Current at 75°N from moored current meters. J. Geophys. Res., **104**, 18059–18072.

(Received June 6, 2000; Revised manuscript accepted August 2, 2000)

This document is provided by JAXA.

This document is provided by JAXA.

Mem. Natl Inst. Polar Res., Spec. Issue, 54, 377-392, 2001

Review

Vernal export and retention of biogenic matter in the north-eastern North Atlantic and adjacent Arctic Ocean: The role of the Norwegian Atlantic Current and topography

Paul Wassmann

Norwegian College of Fishery Science, University of Tromsø, N-9037 Tromsø, Norway

Abstract: The abundance of suspended chlorophyll *a* (Chl *a*) and particulate organic carbon (POC) and its vertical export was investigated on the shelf off northern Norway, off Spitsbergen and in the Barents Sea during biological spring. Accumulation of suspended Chl $a > 100$ mg m^{-2} was only observed in the Barents Sea marginal ice zone and at a distance from the shelf break. Suspended POC concentrations were less variable. Similar results were found for the vertical export of Chl *a* and POC from the upper layers. It is suggested that the high retention rates of suspended biogenic matter along the shelf break of the Norwegian Sea and the Arctic Ocean north of Spitsbergen, sites influenced by branches of the North Atlantic Current, are caused by top-down regulation of phytoplankton biomass by overwintered and advected zooplankton. Thus a tight coupling appears to exist between primary and secondary production on the shelf areas off northern Norway and Spitsbergen during spring. Classical vernal blooms are not the rule in the area and can only be observed when the distance to the shelf break is significant, advection of zooplankton occasionally is restricted and stratification supports rapid accumulation of phytoplankton.

1. Introduction

The dynamics of vertical flux of biogenic matter, and to a lesser extent also the composition of exported matter has been recurrently investigated in a variety of ecosystems. Major seasonal, as well as regional and inter-annual variations, have been encountered with regard to the quantity and composition of the material exported from the upper water column. Loss of organic matter from the upper water column mainly takes place through settling of phytoplankton cells, plankton-derived detritus and zooplankton faecal pellets. Regional, seasonal and interannual variations have thus been attributed to differences in primary production (Platt *et al.*, 1988) as well as retention and export food chains (*e.g.* Peinert *et al.*, 1989; Wassmann, 1998). The current understanding of the dynamics involved in daily and seasonal changes in vertical flux is though rudimentary. This is particularly true for sub-arctic and arctic areas, which experience large seasonal variations. In these areas the vertical flux is strongly dominated by episodic events on daily, weekly, seasonal and annual time scales (Wassmann *et al.*, 1996).

There are several oceanic areas where, in spite of high nutrient concentrations, phytoplankton is not abundant, *i.e.* high nutrient/low chlorophyll regions (HNLC).

This document is provided by JAXA.

Among those areas we find several pacific areas such as the Gulf of Alaska (Frost, 1987; Parsons and Lalli, 1988; Taniguchi, 1999) and the north-western Pacific Ocean (Odate, 1994; Taniguchi, 1999) or the Southern Ocean (Smith and Nelson, 1985; Martin *et al.*, 1990). Other factors than light and macro nutrient availability must be responsible for the lack of phytoplankton biomass accumulation. For example: water column stability (Nelson *et al.*, 1987; Townsend *et al.*, 1993; Huisman *et al.*, 1999), absence of essential micro nutrients (Martin and Fitzwater, 1988) or extensive grazing by zooplankton (Frost, 1991; Miller, 1993; Odate, 1994). Recent information reveals that similar scenarios are also encountered on the north Norwegian shelf (*e.g.* Wassmann *et al.*, 1999a). Here the new production was >120 g C m^{-2} y^{-1} (Slagstad *et al.*, 1999), macro nutrients became hardly limiting at the shelf break (Wassmann *et al.*, 1999a) and phytoplankton biomass was low and entirely dominated by pico- and nanoplankton (Ratkova *et al.*, 1999; Verity *et al.*, 1999). The mesozooplankton biomass was high (Halvorsen and Tande, 1999) and vertical export of carbon was moderate to high and not dominated by phytoplankton, but faecal pellets and detritus (Andreassen *et al.*, 1999). The pelagic trophic structure obviously regulates the total suspended biomass, its species composition as well as the export of biogenic matter.

A major corollary of the traditional large organism food chain model is that each trophic level is primarily resource-limited. Enhanced nutrients supply at the bottom of the food chain will yield higher biomass of phytoplankton, zooplankton and fish (*e.g.* Legendre, 1990). This perspective has been challenged for its universal applicability (Verity and Smetacek, 1996). The food web structure on the north Norwegian shelf suggests that top-down control is as important as resource limitation: (a) a dearth of large phytoplankton, despite significant NO_3 and $Si(OH)_4$ consumption (Wassmann *et al.*, 1999a), (b) low abundance of large protozoans, despite tremendous abundances of their prey (Ratkova *et al.*, 1999); (c) high concentrations of mesozooplankton (Halvorsen and Tande, 1999) which cannot feed efficiently on small flagellates. The scenario implies that predation by the large copepods and euphausiids keep pace with the growth of large phyto- and protozooplankton, minimising their respective competition with and predation on small cells. The food web is thus characterised by joint regulation by resource availability and predation (Verity and Smetacek, 1996). This dual dependency indicates that the structure of the food web can indeed complicate relationships between primary production, grazing, and sedimentation (Andreassen *et al.*, 1996; Wassmann, 1998; Verity *et al.*, 1999).

The north Norwegian shelf shares similarities with HNLC regions. However, here the cause for the low phytoplankton stock is to be found in the substantial grazing pressure by overwintering mesozooplankton which is advected to the north by the Norwegian Atlantic Current. The question arises if the Nordic Seas, its encircling shelves and the adjacent Arctic Ocean are characterised by tendencies towards high nutrient/low chlorophyll conditions, which are caused by grazing? What consequences have the advection of Atlantic water and zooplankton for the production and fate of biogenic matter in the Arctic Ocean? In order to answer these questions, the present investigation reviews, compiles and recalculates published information by Andreassen *et al.* (1996), Andreassen and Wassmann (1998), Andreassen *et al.* (1999), Ratkova *et al.* (1999) and Wassmann *et al.* (1999a) on the suspended biogenic matter and its vertical export during biological spring along the pathway of the North Atlantic Current, *i.e.* the Norwegian shelf, the shelf of west and north of Spitsbergen and the adjacent Barents Sea.

This document is provided by JAXA.

2. Geographic and hydrographic description of the investigation area

The shelf off northern Norway is characterised by shallow banks and a steep shelf break. Fjords continue by trenches penetrating to the shelf break, separating the shelf into shallow coastal banks (Fig. 1). The shelf off northern Norway borders to the Norwegian

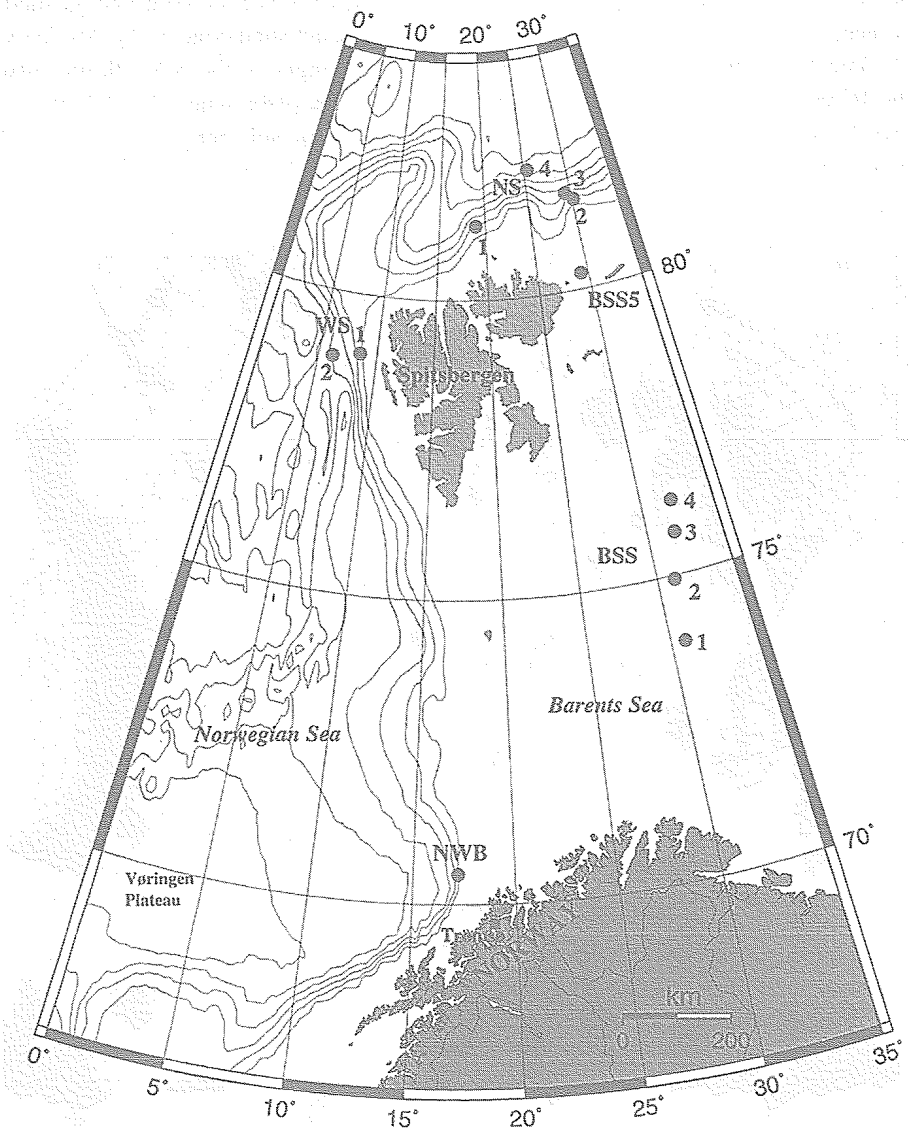


Fig. 1. The investigated and adjacent areas, the north Norwegian coast, the Barents Sea, the west-Spitsbergen shelf and the shelf of the Arctic Ocean north of Spitsbergen. The positions of the investigated sites are indicated. NWB = Nordvestbanken, WS = west Spitsbergen, NS = north Spitsbergen, BSS = Barents Sea shelf.

This document is provided by JAXA.

Sea. The Barents Sea, which is situated to the east of the Norwegian Sea between northern Norway and Spitsbergen, is part of the large shelf-seas bordering the Eurasian Arctic. This continental shelf is wide, with water depths ranging from 100 to 400 m. The shelf west and north off Spitsbergen is narrow, with penetrating trenches and a steep shelf break descending to more than 2000 m. This area shows great resemblance to that off northern Norway. To the north of Spitsbergen the shelf fringes the Arctic Ocean.

The investigation area is dominated by the Norwegian Atlantic Current (NAC), which transports warm Atlantic water northwards along the Norwegian continental shelf, to Spitsbergen, the Barents Sea and eastward along the Eurasian shelf edge of the Arctic Ocean (Fig. 2). The NAC splits into several branches. A broad tongue of the NAC flows eastward into the Barents Sea. Subduction under Arctic water takes place when the Atlantic water turns north. Another branch continues along the west side of Spitsbergen creating the West Spitsbergen Current (WSC). Also here subduction of Atlantic water occurs north of

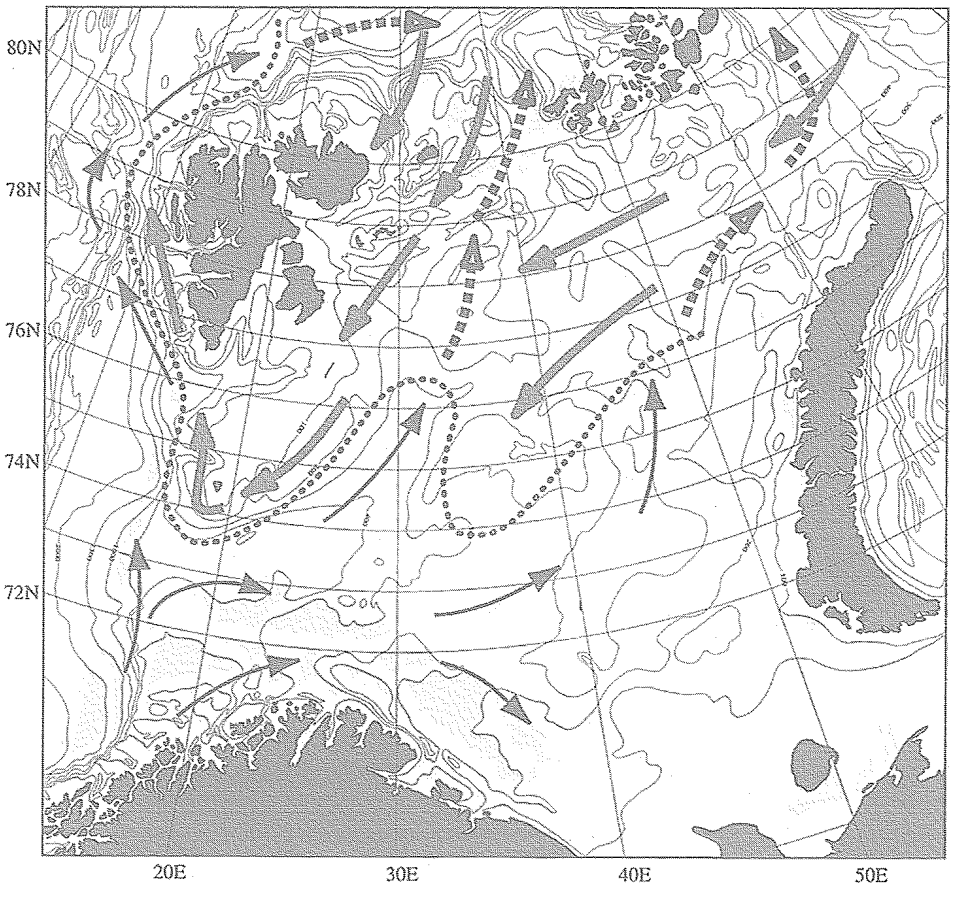


Fig. 2. Main features of the surface current system in the investigated area. Dark, full lines: North Atlantic Current (NAC) and West Spitsbergen Current (WSC). Dark, dashed lines: Subducted NAC/WSC water. Grey lines: Arctic water. Also shown is the mean position of the Polar Front (dotted line).

This document is provided by JAXA.

Spitsbergen. At the Yearmark Plateau (north of Spitsbergen) the subducted WSC splits and the eastern branch continues along the shelf break, enters the Arctic Ocean and is joined by branches of Atlantic water from the Barents Sea through the Victoria and St. Anna troughs (west and east of Franz Joseph Land, respectively). The NAC hence creates a marine environmental continuum which extends from the south-eastern Norwegian Sea into the Barents Sea, along the western coast of Spitsbergen and to the Eurasian shelf break of the Arctic Ocean (Blindheim and Loeng, 1981; AMAP, 1998).

In the northern part of the Barents Sea cold Arctic waters from the north-east meets the warm Atlantic water flowing from the south-west, giving rise to a distinct front, the Polar Front, where the subduction of Atlantic water occurs. On the western side of Spitsbergen between the coast and the WSC, cold Arctic water flows north, creating the cold West Spitsbergen Coastal Current (WSCC). The water of the WSCC origins from the Arctic Ocean and flows between Nordaustland and Franz Josef Land as the East Spitsbergen Current (ESC) onto the Barents Sea shelf, and continues around the southern end of Spitsbergen as the WSCC.

Along the NAC/WSC continuum data from Nordvestbanken (NWB) (Andreassen *et al.*, 1999; Ratkova *et al.*, 1999; Wassmann *et al.*, 1999a), the West Spitsbergen shelf (WS) (Andreassen *et al.*, 1996) and the North Spitsbergen shelf (NS) (Andreassen *et al.*, 1996) have been selected (Fig. 1). These data are contrasted by those derived from a north-south gradient crossing the Barents Sea (BBS) who is under the influence of the ESC and the MIZ (Andreassen *et al.*, 1996; Andreassen and Wassmann, 1998).

3. Suspended biomass and vertical export

The suspended Chl *a* concentrations varied considerably between 10 to 400 mg m^{-2} during spring in the investigated area (Table 1). The highest concentrations were encountered in the MIZ of the Barents Sea while all shelf stations under the influence of the NAC had $<$ 50 mg m^{-2}. Even on the north Norwegian shelf characterised by high new production, the Chl *a* concentrations were low. Thus the entire northern shelf region appears to be characterised by "blue water" scenarios despite of high nutrient depletion and productivity. The suspended POC concentrations varied less over the entire area: 3–18 g m^{-2}. They reflect both the accumulation of phytoplankton (for example at BSS4 in the MIZ) as well as nitrate depletion (which reflects new production) in various systems (far higher at NWS than at WS and NS). The vertical export of Chl *a* followed a similar pattern: low rates along the shelf, but high rates in the MIZ of the Barents Sea (Table 1). However, the range was an order of magnitude greater, from 0.03 to almost 5 mg Chl *a* m^{-2} d^{-1}. Similar to the suspended fraction, the range of vertical export rates of POC was less than that of Chl *a*: about 20 to 350 POC m^{-2} d^{-1}. The highest rates were encountered on the north Norwegian shelf and in the Barents Sea MIZ while the lowest rates were found west and north of Spitsbergen. This coincides with the high and nitrate depletion rates in these waters, respectively.

The daily loss rates of Chl *a* and POC reflect similar scenarios than those of presented above (Table 2): low loss rates along the NAC continuum (average 0.36 and 0.78% d^{-1} for Chl *a* and POC, respectively) while high rates prevail in the MIZ of the Barents Sea (average 1.95 and 3.0% d^{-1} for Chl *a* and POC, respectively). Maximum loss rates up to

This document is provided by JAXA.

Table 1. Integrated suspended chlorophyll a (Chl a; mg m^{-2}) and particulate organic carbon (POC; g m^{-2}) (0–100 m, except BSS 1 (0–60 m). Vertical flux of chlorophyll a (Chl a) and particulate organic carbon (POC) at 100 m (60 m at BSS 5) (mg m^{-2} d^{-1}). Data from two stations during April and May at NWB (1994), four stations during May at BSS 1–4 (1993) and July at BSS 5 (1991) and six station during June/July at WS and NS (1991) are shown.

Station	NWB1	NWB2	WS1	WS2	NS1	NS2	NS3	NS4	BSS1	BSS2	BSS3	BSS4	BSS5
Suspended biomass													
Chl *a*	20	49	40	50	20	15	20	25	145	80	150	400	70
POC	11.1	17.2	11.6	12.2	7.0	3.3	5.2	8.5	8.7	4.8	9.0	24.0	6.1
Vertical export													
Chl *a*	0.1	0.2	0.05	0.05	0.03	0.2	0.03	0.03	0.35	4.8	2.8	1.2	0.9
POC	130	315	24	32	17	22	76	26	195	350	320	260	47

Table 2. Daily vertical loss rates of chlorophyll a (Chl a) and particulate organic carbon (POC) at 100 m (% d^{-1}). Also shown is the residence time (d) of Chl a and POC in the upper 100 m (=100/daily loss rate). Remark: 60 m at BSS 4 and 5.

Station	NWB1	NWB2	WS1	WS2	NS1	NS2	NS3	NS4	BSS1	BSS2	BSS3	BSS4	BSS5
Daily vertical loss rates													
Chl *a*	0.5	0.4	0.1	0.1	0.2	1.3	0.2	0.1	0.2	6	1.9	0.3	1.3
POC	1.2	1.8	0.2	0.3	0.2	0.7	1.5	0.3	2.2	7.3	3.6	1.1	0.8
Residence time													
Chl *a*	200	250	1000	1000	500	77	500	1000	500	17	53	200	46
POC	83	56	500	333	500	143	67	333	45	14	28	55	75

7% d^{-1} were encountered, clearly indicating the large-scale vertical export of biogenic matter in the MIZ. The residence times vary analogue to the daily loss rates. For Chl *a* they are several hundred days along the NAC continuum. They were as low as 14 and 17 days for Chl *a* and POC, respectively, in the MIZ of the Barents Sea.

Significant accumulation and vertical export of phytoplankton biomass were only encountered in areas at a distance to the main NAC current (*e.g.* the central Barents Sea) and the shelf edge. Stratification during spring will promote the vernal bloom development and vertical export (*e.g.* in the MIZ). In all other areas along the shelf of the NAC continuum, vernal blooms were not encountered. Vertical export of biogenic matter is thus not a simple function of nitrate depletion or standing stock. Below I will try to analyse why this is so and what general conclusions could be deduced from the data presented in Tables 1 and 2.

4. Physical environment, phytoplankton growth and vertical flux: The significance of bottom-up regulation

In arctic and sub-arctic seas, the environment is highly dynamic both on a seasonal and interannual times scale. Thus physical processes strongly influence the pelagic community and the vertical flux of biogenic particles (Wassmann *et al.*, 1996). It is widely accepted that the seasonal development of water column stabilisation, in combination with increasing solar radiation in spring, is a prerequisite of vernal spring blooms (Smetacek and Passow,

This document is provided by JAXA.

1990). In ice-covered environments, water column stability by ice melt, the depth of the stratified surface water as well as photosynthetic active radiation, control the magnitude and time development of the bloom (Sakshaug and Holm-Hansen, 1984; Sakshaug and Skjoldal, 1989). Melting sea ice is the only important source of fresh water in the entire region during spring. In contrast, the spring bloom on the north Norwegian shelves and in the southern part of the Barents Sea dominated by Atlantic water, takes place in almost non-stratified waters (Skjoldal and Rey, 1989; Wassmann *et al.*, 2000). Limited vertical mixing appears to support cell growth, giving rise to a bloom (Eilertsen, 1993: Townsend *et al.*, 1993). Wind strength and direction, along with radiation and ice cover, play a crucial role for the onset, development and fate of the spring bloom in arctic and sub-arctic waters (Sakshaug, 1997; Slagstad and Wassmann, 1997).

Vertical stability, mixing and upwelling determine the amount of nutrients available and thus the new production. The level of turbulence also influences the composition of primary producers (Margalef, 1978; Kiørboe, 1993). Turbulence and shear increase the collision rates of particles in the water column and may thus increase the aggregation of sticky particles (*e.g.* Kiørboe, 1993). Advection of water may influence the prevalence of zooplankton along with the NAC (*e.g.* Halvorsen and Tande, 1999; Slagstad *et al.*, 1999) and the Barents Sea (*e.g.* Ådlandsvik and Loeng, 1991; Pedersen, 1995). The physical oceanography determines primarily the new production and hence the upper limit of export production from the euphotic zone (Platt *et al.*, 1988). Physical oceanography determines further the dynamics of vertical flux indirectly through mixing, shear, timing of spring bloom, aggregation, phytoplankton species composition and through over-wintering, advection and retention of zooplankton (Wassmann *et al.*, 1996).

The daily and seasonal changes of the vertical flux of biogenic matter are thus the result of complex interactions of biological and physical factors, which could be circumscribed as *bottom-up regulation*. The quantity and quality of sinking biogenic material reflects also the prevailing structure of the pelagic system, in particular zooplankton (Wassmann, 1998). The latter impact could be describes as *top-down regulation*, which will be discussed further in the next sections. Thus, both the complexities of the physical environment and the pelagic community are important in structuring planktonic ecosystems and influence vertical flux (Silver and Gowing, 1991; Verity and Smetacek, 1996).

5. Meso- and macrozooplankton and top-down regulation

The deep Norwegian Sea is an important area for over-wintering of meso- and macrozooplankton, and its early ascend in the Norwegian Sea has been shown to potentially control the early spring bloom (Bathmann *et al.*, 1990). These zooplankton populations on the north Norwegian shelf are primarily advected into the area with the Norwegian Coastal Current (NCC) and the NAC (Slagstad and Tande, 1996; Halvorsen and Tande, 1999). As early as March, over-wintering mesozooplankton may be imported onto the shelf off northern Norway and further north (Slagstad and Tande, 1996). At NWB in March 1994 a mesozooplankton biomass of 0.3 g C m^{-2} was recorded, and already in April mesozooplankton biomass at the shelf break (~4 g C m^{-2}; K. Tande, unpubl. res.) equalled levels which are usually reached in late summer in north Norwegian fjords (Tande, 1991; Falkenhaug *et al.*, 1995; Pasternak *et al.*, 2000). Mesozooplankton biomass attained

This document is provided by JAXA.

maxima up to 20 g C m^{-2} at Nordvestbanken in May and a high average biomass (2.3–3.4 g C m^{-2}) prevailed throughout summer and autumn (K. Tande, unpubl. res.).

The average seasonal grazing rate of mesozooplankton at NWB may have been 31–94 g C m^{-2} (Verity *et al.*, 1999), indicating that mesozooplankton grazing was sufficient to consume the entire new production in spring. The low Chl *a* concentration (Table 1), a high new production rate of about 120 g C m^{-2} y^{-1} (Slagstad *et al.*, 1999) and high grazing estimates (Verity *et al.*, 1999) all suggest significant top-down regulation of phytoplankton biomass at NWB in 1994. Due to the lack of more detailed information from West Spitsbergen, indications of grazing controlled phytoplankton biomass are not well supported by data, but low suspended Chl *a* stocks (Table 1) and the character of the sedimented material indicate that zooplankton grazing was important (Andreassen *et al.*, 1996). Thus the NAC/WSC continuum along the Norwegian Sea shelf supports top-down regulation of phytoplankton biomass.

Sedimentation of phytoplankton and ice algae was low in areas covered by multi-year ice north of Spitsbergen, as could be expected due to the low nutrient consumption and phytoplankton biomass (Andreassen *et al.*, 1996). Microscopic examination indicated that sedimentation of faecal pellets was more important for vertical flux of biogenic matter than sinking algae at all NS stations. This is supported by reports of relatively high mesozooplankton biomass in the area (González and Smetacek, 1994). Faecal pellets produced by sub-ice fauna may also be a source for sinking faecal pellets (Werner, 1997). Due to light-limited growth of phytoplankton even low grazing rates might have been sufficient to control the phytoplankton biomass. Zooplankton and sub-ice fauna were important factors in regulating the vertical flux in areas covered with multi-year ice by producing faecal pellets, also by controlling suspended and sinking phytoplankton biomass. It is suggested that a substantial fraction of the zooplankton present along and on the shelves fringing the Eurasian section of the Arctic Ocean is advected into the region by the NAC/WSC (Fig. 2). For an evaluation of this transport for the pelagic-benthic coupling in the Arctic Ocean, see below.

Although the concentration of suspended Chl *a* was higher in the Barents Sea compared to the Norwegian Sea shelf, the vertical flux data indicated retention of phytoplankton biomass due to grazing also here (Andreassen and Wassmann, 1998). Thus even during "typical" vernal bloom conditions with "green" waters (Wassmann *et al.*, 1999b), retention of phytoplankton is significant. Calanoid copepods are regarded as the main herbivorous species during spring in the central Barents Sea (Båmstedt *et al.*, 1991; Tande, 1991). Experiments carried out by Hansen *et al.* (1996) indicated low copepod biomass and grazing rates in the euphotic zone at BSS 1–4 in spring 1993. Consequently the suspended Chl *a* concentrations were high. However, variability in overwintering and the concomitant grazing impact on phytoplankton development has a dominating impact on phytoplankton biomass and pelagic-benthic coupling (Peinert *et al.*, 1989; Wassmann and Slagstad, 1993). As a consequence, grazing pressure can be expected to vary with the magnitude of zooplankton present during early spring, giving rise to variable top-down control.

To the extent that the grazing potential of mesozooplankton has been estimated in the area at all, results are only available for the most dominant copepod species (Båmstedt *et al.*, 1991; Hansen *et al.*, 1996). The role of macrozooplankton species such as euphausiids, pteropods, amphipods and gelatinous taxa and under-ice fauna were so far rarely evaluated.

This document is provided by JAXA.

Euphausiids for example, are important contributors to zooplankton biomass in the south-western and western Barents Sea (Dalpadado and Skjoldal, 1991). Euphausiids have been shown to give rise to rapid sedimentation of organic matter through fast sinking pellets in the area (Bathmann *et al.*, 1991; Riebesell *et al.*, 1995).

Microzooplankton can, by high grazing rates, the production of small and slow sinking faecal pellets and coprophagy retain biomass and nutrients in the upper layers (Antia, 1991; Buck and Newton, 1995; Taniguchi, 1999). Their pellets were less prominent at NWB, reflecting pelagic retention (Wassmann *et al.*, 1999c). At BSS stations during spring 1993 microzooplankton grazing was shown to be higher than copepod grazing in the Barents Sea (Hansen *et al.*, 1996). Microzooplankton grazing was largest at BS4 and BS1 (Hansen *et al.*, 1996), both stations with low daily Chl *a* loss rates (Table 2). BS2 and BS3 experienced lower microzooplankton grazing pressure coinciding with larger vertical flux of Chl *a*. At NWB protozooplankton became a most significant prey of food-limited mesozooplankton (Verity *et al.*, 1999; Slagstad *et al.*, 1999).

The classical bottom-up view (*e.g.* Margalef, 1978) regards the hydrodynamic conditions as the most important factor in regulating phytoplankton biomass, species composition and consequently vertical export of biogenic matter. A top-down oriented perspective, however, explains the composition and biomass of phytoplankton species as a function of grazing pressure, escape from grazing and competition, in addition to dependence of light, nutrients and turbulence conditions (*e.g.* Kiørboe, 1993; Wassmann, 1998). Pico- and nanoplankton biomass is usually controlled by protozooplankton due to similar growth rates of predator and prey. Low over-wintering populations and slow reproductive response of mesozooplankton in relatively shallow coastal environments typically prevents a high grazing pressure on large phytoplankton cells, allowing an accumulation of phytoplankton biomass (*e.g.* the spring bloom). Spring blooms in shallow environments are therefore usually dominated by large phytoplankton forms and characterised by large-scale vertical export of ungrazed cells (Kiørboe, 1993). However, such scenarios are not encountered on the NAC/WSC-dominated shelves fringing the eastern Norwegian Sea and Arctic Ocean where zooplankton appears to play a pivotal role throughout the productive season.

6. Zooplankton advection and vertical export: Importance of interannual variation

Mesozooplankton exerting a substantial grazing pressure on phyto- and protozooplankton during spring, seems to be a prevalent feature of both the north Norwegian shelf and off-shelf areas (Peinert *et al.*, 1987; Slagstad *et al.*, 1999). A slow start of the spring bloom due to low water column stability on the shelf and large mesozooplankton biomass during early spring couple primary production and consumers tightly along the shelves flushed by the NAC (*e.g.* Andreassen *et al.*, 1996; Halvorsen and Tande, 1999; Wassmann *et al.*, 1999a). In contrast, zooplankton is obviously not able to prevent accumulations of phytoplankton during spring in fjords (Reigstad *et al.*, 2000) and in the Barents Sea (Skjoldal and Rey, 1989; Wassmann *et al.*, 1999b).

Interannual variation of vertical flux in the Barents Sea has been suggested due to variation in hydrography, ice-cover and advection of zooplankton from the Norwegian Sea (Wassmann *et al.*, 1996; Slagstad and Wassmann, 1997). Sensitivity testing of a simulation model for the Barents Sea indicated that the number of over-wintering and advected

This document is provided by JAXA.

copepods represents one of the most important variables in the Barents Sea ecosystem (Wassmann and Slagstad, 1993). The results presented here indicate that advection of zooplankton might have even greater implications at the shelf off Northern Norway, West-Spitsbergen, in the southern Barents Sea and probably also north of Spitsbergen, giving rise to control of both phytoplankton biomass, species composition as well as influencing the vertical flux. Earlier reports describing classical spring blooms on the shelf off Northern Norway (Rey, 1981; Hegseth *et al.*, 1995), suggest that interannual variation exists. The NWB results from Nordvestbanken may thus indicate that top-down control may vary between years.

Both the timing of the onset of phytoplankton production and the size of the local over-wintering population or advected zooplankton biomass are thus important factors influencing the regulation of the vernal bloom and its vertical export. The late onset of reproduction and a long generation time of each mesozooplankton cohort typically gives rise to a mismatch between primary and secondary production in the central Barents Sea and in fjords in northern Norway (Eilertsen *et al.*, 1989; Tande, 1991; Reigstad *et al.*, 2000). An important key for the regulation of the vertical flux of phytoplankton in these areas is therefore the timing between advection of mesozooplankton and the development of phytoplankton growth during spring.

Variation in hydrodynamic conditions may influence the interannual magnitude of new production and zooplankton abundance (Slagstad and Wassmann, 1997; Vernet *et al.*, 1998; Wassmann *et al.*, 1999b). Thus both the potential vertical flux and retention of biogenic matter must vary interannually. The onset of the phytoplankton growth season is mainly confined to a time interval of a couple of weeks between April to June, varying slightly between different areas. The phytoplankton accumulation starts earlier and develops more rapid in the MIZ. This is due to earlier and stronger stratification compared to the southern Barents Sea and the shelf area off northern Norway, where phytoplankton blooms are caused by periodically reduced vertical mixing (Heimdal, 1974; Rey and Loeng, 1985). The MIZ region is also most remote to the major over-wintering areas for mesozooplankton in the Norwegian Sea. Consequently, advection of zooplankton to these areas may be more sporadic, dependent on transport time and usually occurs later in the season (*e.g.* Reigstad *et al.*, 2000).

Long-term observations from weather ship M in the Norwegian Sea show that the ascent of copepods is characterised by considerable interannual variation. Maximum abundance may occur as early as April or as late as August (Lie, 1968). This suggests that the timing between primary production and advection of grazers may be subjected to strong interannual variations. Low over-wintering success of mesozooplankton in the Norwegian Sea, or changes in current pattern can also result in less advection of mesozooplankton onto and along the shelf, as has been suggested for the southern and central Barents Sea (Pedersen, 1995). Consequently, in years with low zooplankton abundance during spring, a classic phytoplankton bloom with a predominance of export food chains may develop on the shelf off northern Norway and result in stronger spring sedimentation of phytoplankton-derived matter. Accordingly, during years of strong and early zooplankton advection a similar situation as found at NWB may be expected in the southern Barents Sea and around Spitsbergen.

This document is provided by JAXA.

7. Advection of zooplankton into and top-down regulation in the Arctic Ocean?

Recent investigations of the physical oceanography of the Eurasian Basin imply that significant amounts of Atlantic water are annually advected into the basin, mainly along the shelf break north of Spitsbergen and through the St. Anna Trough between Franz Josef Land and Novaya Zemlya (AMAP, 1998). The flow through the Barents Sea varies between 2-3 Sv (Ådlandsvik and Loeng, 1991) while the boundary current close to the Lomonossov ridge is about 5 Sv (F. McLaughlin and E. Carmack, pers. com.). In addition, intermittent draining of several Sv of cool and salty water masses which accumulate in the Barents Sea basins during sea ice formation, adds to the discharge of Atlantic water into the Arctic Ocean (Midttun and Loeng, 1987). Water of NAC-origin flows as a boundary current subducted under the Arctic water and the halocline in a circular pattern along the Eurasian shelf break towards the east (Fig. 2). It crosses the Arctic Ocean along the Lomonosov or Alpha Ridge to the Canadian side and leaves, mixed with Arctic water, through the Fram Strait. At times modified Barents Sea water may penetrate along the entire Siberian coast into the Beaufort Sea area (F. McLaughlin and E. Carmack, pers. com.).

Many of the zooplankton species living in the subarctic region, have life cycles of one year or longer and overwintering at depth based on lipid reserves. It is suggested that the high abundance of zooplankton, which characterises the NAC (Noji *et al.*, 1999), is advected through the Barents Sea and along the West- and North-Spitsbergen shelf into the Arctic Ocean, probably also in winter (Pedersen *et al.*, 1995). Atlantic species have frequently been detected in the northern Barents Sea (*e.g.* Falk-Petersen *et al.*, 1999) and north of Spitsbergen and Novaya Zemlya (Mumm, 1993). Some of the expatriates in these Arctic waters, for example the typical Atlantic species *Calanus finmarchicus*, is out of the temperature range favourable for spawning (Falk-Petersen *et al.*, 1999). The consequent supply of allochthonous biomass from the south-west and north onto the Barents Sea shelf and from west to east along the Eurasian shelf into the Arctic Ocean is thus based on "down-stream" NAC/WSC production. It derives partly from the previous year. Similar scenarios with advection of *Neocalanus plumchrus* through Bering Straight into the western Beaufort Sea have been detected (S. Smith, pers. com.). Annual carbon budgets inside the Arctic Ocean can thus not be in balance with regard to meso- and macrozooplankton as only their contemporary grazing and growth, but not all of their biomass is based on the autochthonous production.

Massive differences in zooplankton standing stock have been detected along gradients between the NAC/WSC and East-Greenland Current (Noji *et al.*, 1999), suggesting that far more zooplankton is advected into than out of the Arctic Ocean. This suggests a net loss of zooplankton biomass in the Eurasian basin, which could be caused by decreased spawning success by the expatriates, carnivory, or death. Similar to the net advection of zooplankton into the headwaters of fjords and estuaries (Lewis and Thomas, 1986), the ecological setting of zooplankton in the Arctic Ocean could be rephrased by the proverb "one foot in the grave" (Soetaert and Herman, 1994), which was applied for large-scale death of advected zooplankton in an estuary. The advective net flux of zooplankton into the Arctic Ocean is regulated by both the climatologically varying strength of NAC inflow, modifications in the Barents Sea and inter-annual differences in zooplankton abundance

This document is provided by JAXA.

outside the Arctic Ocean. The import of zooplankton also implies that at least the boundary current region of the Arctic Ocean may be top-down controlled as suggested by data from Andreassen *et al.* (1996). The Arctic Ocean is thus not an almost closed system with modest abiotic and biotic variability, but it is an open, variable, advective and circular system subject to considerable climatic and biogeochemical variability.

8. Conclusion

The hydrodynamic conditions on subarctic and arctic shelves off northern Norway, off Spitsbergen and in the Barents Sea play a major role in favouring export production out of the euphotic zone. The advection of variable magnitudes of NAC/WSC water, including nutrients and plankton, is of utmost significance for the function of the region. Advection is not only regulated by NAC/WSC mass flow, but also by the configuration of the shelf. Troughs, coastal banks and the shape of the slope and shelf break region modify the impact of the NAC/WSC on the pelagic ecosystem dynamics. Suspended biomass and vertical export are strongly modified by zooplankton grazing and *in situ* recycling. The present data suggest that biological and physical processes *in concert* regulate vertical flux of phytoplankton and biogenic matter along the NAC/WSC continuum. Significant accumulation of phytoplankton biomass during spring can be encountered at a distance to the shelf break (*e.g.* the central Barents Sea) or areas restrained from regular, large-scale water exchange (*e.g.* fjords). Stratification during spring will promote the vernal bloom development (*e.g.* the MIZ). In all other areas under the influence of the NAC, vernal blooms can only be encountered during events of insignificant zooplankton advection. The advection of zooplankton and its concomitant top-down regulation of suspended biomass and vertical export, calls for a new manner to study the plankton ecology of the north-eastern North Atlantic and adjacent Arctic Ocean. It calls for what Matthews and Heimdal (1980) call an "ecology of advection". It further points at the pivotal, but still not sufficiently reckoned role of zooplankton for global marine productivity (*e.g.* Banse, 1992, 1995).

Joint regulation by resource availability (bottom-up) and predation (top-down) offers a new conceptual framework in which the apparent regulation of the pelagic trophic structure and the pelagic-benthic coupling in subarctic and arctic areas in northern Norway, Spitsbergen, the Barents Sea and the Arctic Ocean may be resolved. Future studies need to expand the basic knowledge regarding the importance of pelagic key species, which shape the carbon flow. The entire size spectra of phytoplankton consumers, their role in structuring the pelagic carbon flow, their life cycles and where they were spawned, is essential to acquire a comprehensive understanding of the retention and export potential in the region.

Acknowledgments

I grateful acknowledge the invitation and financial support by the organisers of the symposium "Second International Symposium on Environmental Research in the Arctic and Fifth Ny-Ålesund Scientific Seminar" and Mitsuo Fukuchi. Thanks to the members of the sedimentation group at the Norwegian College of Fishery Science, University of Tromsø, who by active co-operation in the laboratory and the field, interpretations of the results and vivid discussions contributed significantly to this manuscript. Discussions with

This document is provided by JAXA.

Fiona McLaughlin and Eddy Carmack were important for the scope of the manuscript. The research programme ALV, supported by the Norwegian Research Council, and the European Union in the framework of the MAST programme, contract no. MAS2-CT93-0069, MAS3-CT96-0056 (Ocean Margin EXchange—OMEX) and ENV4-CT97-0637 (Barents Sea system investigation—BASIS) supported this work.

References

Ådlandsvik, B. and Loeng, H. (1991): A study of the climatic system in the Barents Sea. Polar Res., **10**, 45–49.

AMAP (1998): The influence of physical and chemical processes on contaminant transport into and within the Arctic. AMAP Assessment Report: Arctic Pollution Issues, Chap., 25–116.

Andreassen, I.J. and Wassmann, P. (1998): Vertical flux of phytoplankton and particulate biogenic matter in the marginal ice zone of the Barents Sea in May 1993. Mar. Ecol. Prog. Ser., **140**, 1–14.

Andreassen, I., Nothing, E.-M. and Wassmann, P. (1996): Sedimentation of particulate matter on the shelf of northern Spitsbergen. Mar. Ecol. Prog. Ser., **137**, 215–228.

Andreassen, I., Wassmann, P. and Ratkova, T. (1999): Seasonal variation of vertical flux of phytoplankton and biomass on the north Norwegian shelf break. Sarsia, **84**, 227–238.

Antia, A.N. (1991): Microzooplankton in the pelagic food web of the East Greenland Sea and its role in sedimentation processes. Ber. Sonderforschungsbereich 313, Univ. Kiel, **33**, 1–110.

Båmstedt, U., Eilertsen, H.C., Tande, K.S., Slagstad, D. and Skjoldal, H.R. (1991): Copepod grazing and its potential impact on the phytoplankton development in the Barents Sea. Polar Res., **10**, 339–354.

Banse, K. (1992): Grazing, temporal changes of phytoplankton concentrations, and the microbial loop in the open sea. Primary Productivity and Biochemical Cycles in the Sea, ed. by P.G. Falkowski and A.D. Woodhead. New York, Plenum Press, 409–440.

Banse, K. (1995): Zooplankton: Pivotal role in the control of ocean production. ICES J. Mar. Sci., **52**, 265–277.

Bathmann, U.V., Noji. T.T. and Bodungen B. v. (1990): Copepod grazing potential in late winter in the Norwegian Sea—A factor in the control of spring phytoplankton growth? Mar. Ecol. Prog. Ser., **60**, 225–233.

Bathmann, U., Fischer, G., Müller, P.J. and Gerdes, D. (1991): Short-term variations in particulate matter sedimentation of Kapp Norvegia, Weddell sea, Antarctica: relation to water mass advection, ice cover, plankton biomass and feeding activity. Polar Biol., **11**, 185–195.

Blindheim, J. and Loeng, H. (1981): On the variability of Atlantic influence in the Norwegian and Barents seas. Fiskeridir. Skr. Havunders., **17**, 161–189.

Buck, K.R. and Newton, J. (1995): Fecal pellets flux in Dabob Bay during a diatom bloom: Contribution of microzooplankton. Limnol. Oceanogr., **40**, 306–315.

Dalpadado, P. and Skjoldal, H.R. (1991): Distribution and life history of krill from the Barents Sea. Polar Res., **10**, 443–460.

Eilertsen, H.C. (1993): Spring blooms and stratification. Nature **363**, 24.

Eilertsen, H.C., Tande, K.S. and Hegseth, E.N. (1989): Potential of herbivorous copepods for regulating the spring phytoplankton bloom in the Barents Sea. Rapp. P.-V. Cons. Int. Explor. Mer, **188**, 154–163.

Falk-Petersen. S., Pedersen, G., Kwasniewski, S. and Nøst, E. (1999): Spatial distribution and life-cycle timing of zooplankton in the marginal ice zone of the Barents Sea during the summer melt season in 1995. J. Plankton Res., **21**, 1249–1264.

Falkenhaug, T., Nordby, E., Svendsen, H. and Tande, K. (1995): Impact of advective processes on displacement of zooplankton biomass in a North Norwegian fjord system: a comparison

This document is provided by JAXA.

between spring and autumn. Ecology of Fjords and Coastal Waters, ed. by H.R. Skjoldal *et al*. Amsterdam, Elsevier Sci., 45–72.

Frost, B.W. (1987): Grazing control of phytoplankton stock in the open subarctic ocean: a model assessing the role of meso-zooplankton, particularly the large calanoid copepods Neocalanus spp. Mar. Ecol. Prog. Ser., **39**, 49–68.

Frost, B.W. (1991): The role of grazing in nutrient-rich areas of the open sea. Limnol. Oceanogr., **36**, 1616–1630.

González, H.E. and Smetacek, V. (1994): The possible role of the cyclopoid copepod *Oithona* in retarding vertical flux of the zooplankton faecal material. Mar. Ecol. Prog. Ser., **113**, 233–246.

Halvorsen, E. and Tande, K.S. (1999): Physical and biological factors influencing the seasonal variation in distribution of zooplankton across the shelf at Nordvestbanken, Northern Norway, in 1994. Sarsia, **84**, 279–292.

Hansen, B., Christiansen, S. and Pedersen, G. (1996): Plankton dynamics in the Marginal Ice Zone of the central Barents Sea during spring: carbon flow and structure of the grazer food chain. Polar Biol., **16**, 115–128.

Hegseth, E.N., Svendsen, H. and Quillfeldt, C.H.v. (1995): Phytoplankton in fjords and coastal waters of Northern Norway: environmental conditions and dynamics of the spring bloom. Ecology of Fjords and Coastal Waters, ed. by H.R. Skjoldal *et al*. Amsterdam, Elsevier Sci., 45–72.

Heimdal, B.R. (1974): Composition and abundance of phytoplankton in the Ullsfjord area, North Norway. Astarte, **7**, 17–42.

Huisman, J., Oostveen, P.v. and Weissing, F.J. (1999): Critical depth and critical turbulence: Two different mechanisms for the development of phytoplankton blooms. Limnol. Oceanogr., **44**, 1781-1787.,

Kiørboe, T. (1993): Turbulence, phytoplankton cell size, and the structure of pelagic food webs. Adv. Mar. Biol., **29**, 2–72.

Legendre, L. (1990): The significance of microalgal blooms for fisheries and for the export of particulate organic carbon in oceans. J. Plankton Res., **12**, 681-699.

Lewis, A.G. and Thomas, A.C. (1986): Tidal transport of planktonic copepods across the sill of a British Columbia fjord. J. Plankton Res., **8**, 1079–1089.

Lie, U. (1968): Variation in the quantity of zooplankton and propagation of *C. finmarchicus* at station M in the Norwegian Sea 1959–66. Fiskeridir. Skr. Havunders., **14**, 121–128.

Loeng, H. (1991): Features of the physical oceanographic conditions of the Barents Sea. Polar Res., **10**, 5–18.

Margalef, R. (1978): Life-forms of phytoplankton as survival alternatives in an unstable environment. Oceanol. Acta, **1**, 493-509.

Martin, J.H. and Fitzwater, S. (1988): Iron deficiency limits phytoplankton growth in the north east Pacific subarctic. Nature, **331**, 341–343.

Martin, J.H., Fitzwater, S. and Gordon, R.M. (1990): Iron deficiency limits phytoplankton growth in Antarctic water. Global Geochem. Cycles, **4**, 5–12.

Matthews, J.B.L. and Heimdal, B. (1980): Pelagic productivity and food chains in fjord systems. Fjord Oceanography, ed. by H.J. Freeland *et al*. New York, Plenum Press, 377–398.

Midttun, L. and Loeng, H. (1987): Climatic variations in the Barents Sea. The Effect of Oceanographic Conditions on Distribution and Population Dynamics of Commercial Fish Stocks in the Barents Sea; Proc. 3rd Soviet-Norwegian Symposium, ed. by H. Loeng. Bergen, Inst. Mar. Res., 13–27.

Miller, C. (1993): Pelagic production processes in the Subarctic Pacific. Prog. Oceanogr., **31**, 1–15.

Mumm, N. (1993): Composition and distribution of mesozooplankton in the Nansen Basin, Arctic Ocean, during summer. Polar Biol., **13**, 451–461.

Nelson, D.M., Smith, W.O., Gordon, L.I. and Huber, B.A. (1987): Spring distributions of density, nutrients and phytoplankton biomass in the ice edge zone of the Weddell-Scotia Sea. J.

This document is provided by JAXA.

Geophys. Res., **92**, 7181–7190.
Noji, T.T., Rey, F., Miller, L.A., Børsheim, K.Y. and Urban-Rich, J. (1999): Fate of biogenic carbon in the upper 200 m of the central Greenland Sea. Deep-Sea Res. Part II: Topical Studies in Oceanography, **46**, 1497–1509.
Odate, T. (1994): Plankton abundance and size structure in the northern North Pacific Ocean in early summer. Fish. Oceanogr., **3**, 267–278.
Parson, T.R. and Lalli, C.M. (1988): Comparative oceanic ecology of the plankton communities of the subarctic Atlantic and Pacific oceans. Oceanogr. Mar. Biol. Ann. Rev., **23**, 317–359.
Pasternak, A., Arashkevich, E., Wexels Riser, C., Ratkova, T. and Wassmann, P. (2000): Seasonal variation in zooplankton and suspended faecal pellets in the subarctic fjord Balsfjorden, northern Norway, in 1996. Sarsia, **85**, 439–452.
Pedersen, G. (1995): Factors influencing the size and distribution of the copepod community in the Barents Sea with special emphasis on *Calanus finmarchicus* (Gunnerus). Dr. Scient. thesis, Norwegian College of Fishery Science, University of Tromsø.
Pedersen, G., Tande, K. and Ottesen, G. O. (1995): Why does a component of *Calanus finmarchicus* stay in the surface waters during the overwintering? ICES J. Mar. Sci., **52**, 523–531.
Peinert, R., Bathmann, U., Bodungen, B.v. and Noji, T. (1987): The impact of grazing on spring phytoplankton growth and sedimentation in the Norwegian current. Mitt. Geol.-Paläontol. Inst. Univ. Hamburg, **62**, 149–164.
Peinert, R., Bodungen, B.v. and Smetacek, V. (1989): Food web structure and loss rate. Productivity of the Ocean: Present and Past, ed. by W. Berger *et al*. Chichester, J. Wiley, 35–48.
Platt, T., Harrison, W.G., Lewis. M., Li, W., Sathyendranath, S., Smith, R. and Vezina, A. (1988): Biological production of the oceans: the case for a consensus. Mar. Ecol. Prog. Ser., **52**, 77–88.
Ratkova, T.N., Wassmann, P., Verity, P.G. and Andreassen, I. (1999): Abundance and biomass of pico-, nano- and microplankton along a transect on Nordvestbanken, north Norwegian shelf, in 1994. Sarsia, **84**, 213–226.
Reigstad, M., Wassmann, P., Ratkova, T., Arashkevich, E., Pasternak, A. and Øygarden, S. (2000): Comparative spring vertical export of biogenic matter in north Norwegian fjords. Mar. Ecol. Prog. Ser., **201**, 73–89.
Rey, F. (1981): The development of the spring phytoplankton outburst at selected sites off the Norwegian coast. The Norwegian Coastal Current, ed. by R. Sætre and M. Mork. University of Bergen, 649–680.
Rey, F. and Loeng, H. (1985): The influence of ice and hydrographic conditions on the development of stress on marine organisms. Marine Biology of Polar Regions and Effect of Stress on Marine Organisms, ed. by J.S. Gray and M.E. Christiansen. Chichester, J. Wiley, 49–63.
Riebesell, U., Reigstad, M., Wassmann, P., Noji, T. and Passow, U. (1995): On the trophic fate of *Phaeocystis pouchetii* (Hariot): VI. Significance of *Phaeocystis*-derived mucus for vertical flux. Neth. J. Sea Res., **33**, 193–203.
Sakshaug, E. (1997): Biomass and productivity distributions and their variability in the Barents Sea. ICES J. Mar. Sci., **54**, 341–350.
Sakshaug, E. and Holm-Hansen, O. (1984): Factors governing the pelagic production in Polar oceans. Marine Phytoplankton and Productivity, ed. by O. Holm-Hansen *et al*. New York, Springer, 1–18 (Lecture Notes on Coastal and Estuarine Studies No. 8).
Sakshaug, E. and Skjoldal, H.R. (1989): Life at the ice edge. Ambio, **18**, 60–67.
Silver, M.W. and Gowing, M.M. (1991): The "Particle" Flux: Origins and biological components. Prog. Oceanogr., **26**, 75–113.
Skjoldal, H. and Rey, F. (1989): Pelagic production and variability of the Barents Sea ecosystem. Biomass and Geography of Large Marine Ecosystems, ed. by K. Sherman and L. Alexander. Boulder, Westview Press, 243–283.
Slagstad, D. and Wassmann, P. (1997): Climate change and carbon flux in the Barents Sea: 3-D

This document is provided by JAXA.

simulations of ice-distribution, primary production and vertical export of particulate organic matter. Mem. Natl Inst. Polar Res., Spec. Issue, **51**, 119–141.

Slagstad, D. and Tande, K.S. (1996): The importance of seasonal vertical migration in the across shelf transport of *Calanus finmarchicus*. Ophelia, **44**, 189–205.

Slagstad, D., Tande, K. and Wassmann, P. (1999): Modelled carbon fluxes as validated by field data on the north Norwegian shelf during the productive period in 1994. Sarsia, **84**, 303–317.

Smetacek, V. and Passow, U. (1990): Spring bloom initiation and Sverdrup's critical-depth model. Limnol. Oceanogr., **35**, 228–234.

Smith, W.O. and Nelson, D.M. (1985): Phytoplankton blooms produced by a receding ice edge in the Ross Sea: spatial coherence with the density field. Science, **227**, 163–166.

Soetaert, K. and Herman, P.M.J. (1994): One foot in the grave: zooplankton drift into the Westerschelde estuary (The Netherlands). Mar. Ecol. Prog. Ser., **105**, 19–29.

Tande, K. (1991): *Calanus* in North Norwegian fjords and in the Barents Sea. Polar Res., **10**, 389-408.

Taniguchi, A. (1999): Differences in the structure of the lower trophic levels of pelagic ecosystems in the eastern and western subarctic Pacific. Prog. Oceanogr., **43**, 289–315.

Townsend, D.W., Keller, M.D., Sieracki, M.E. and Ackleson, S. (1993): Spring phytoplankton blooms in the absence of vertical water column stratification. Nature, **360**, 59–62.

Verity, P.G. and Smetacek, V. (1996): Organism life cycles, predation, and the structure of marine pelagic ecosystems. Mar. Ecol. Prog. Ser., **136**, 277–293.

Verity, P., Wassmann, P., Ratkova, T.N. and Andreassen, I.J. (1999): Seasonal patterns in composition and biomass of autotrophic and heterotrophic microplankton communities on the north Norwegian shelf. Sarsia, **84**, 265–278.

Vernet, M., Matrai, P.A. and Andreassen, I.J. (1998): Synthesis of particulate and extracellular carbon by phytoplankton at the marginal ice zone in the Barents Sea. J. Geophys. Res., **103**, 1023–1037.

Wassmann, P. (1998): Retention versus export food chains: processes controlling sinking loss from marine pelagic systems. Hydrobiologia, **363**, 29–57.

Wassmann, P. and Slagstad, D. (1993): Seasonal and annual dynamics of carbon flux in the Barents Sea: A model approach. Polar Biol., **13**, 363–372.

Wassmann, P., Andreassen, I., Reigstad, M. and Slagstad, D. (1996): Pelagic-benthic coupling in the Nordic Seas: The role of episodic events. P.S.Z.N. I: Mar. Ecol., **17**, 447–471.

Wassmann, P., Andreassen, I. and Rey, F. (1999a): Seasonal variation of nutrients and suspended biomass along a transect on Nordvestbanken, north Norwegian shelf, in 1994. Sarsia, **84**, 199–212.

Wassmann, P., Ratkova, T.N., Andreassen, I., Vernet, M., Pedersen, G. and Rey, F. (1999b): Spring bloom development in the marginal ice zone and the central Barents Sea. P.S.Z.N. I: Mar. Ecol., **20**, 321–346.

Wassmann, P., Hansen, L., Andreassen, I. and Urban-Rich, J. (1999c): Suspended and sinking faecal pellets along a transect on north Norwegian shelf break. Sarsia, **84**, 239–252.

Wassmann, P., Reigstad, M., Øygarden, S. and Rey, F. (2000): Seasonal variation in hydrography, nutrients, primary production and suspended biomass in the subarctic fjord Balsfjord, northern Norway, in 1996. Sarsia, **85**, 237–249.

Werner, I. (1997): Ecological studies on the Arctic under-ice habitat—Colonisation and processes at the ice-water interface. Ber. Sonderforschungsbereich 313, Univ. Kiel, **70**, 1–167.

(Received April 4, 2000; Revised manuscript accepted July 24, 2000)

This document is provided by JAXA.

Mem. Natl Inst. Polar Res., Spec. Issue, 54, 393-407, 2001

Scientific paper

The upper layer circulation in Kongsfjorden and Krossfjorden — A complex fjord system on the west coast of Spitsbergen

Randi Ingvaldsen[1], Marit Bø Reitan[2], Harald Svendsen[3] and Lars Asplin[1]

[1]*Institute of Marine Research, Bergen, Norway*
[2]*STATOIL, Research and Technology, Stavanger, Norway*
[3]*Geophysical Institute, University of Bergen, Bergen, Norway*

Abstract: The upper layer circulation in the fjord system of Kongsfjorden and Krossfjorden is investigated based on field observations and a numerical hydrodynamical model. Rotational dynamics have a considerable influence on the circulation pattern in the fjords, but due to the complex topography of the fjord system, horizontal pressure-gradients caused by the sea-surface elevation are established rather fast. This counteracts the rotational dynamics, and the expected circulation pattern with a brackish current confirmed to the right hand side (as seen from the head of the fjord) are not always the case. The upper layer circulation seems to be dominated by the wind field, especially since the effect of the wind is quite persistent after the cessation of the wind.

Strong interaction is shown to take place between the fjord arms, and in the common fjord mouth there might develop an anticyclonic eddy. The exchange between the shelf areas and Kongsfjorden seems to be strong, and processes in the common mouth might propagate far into the fjord as internal Kelvin waves. As a combination of the rotational dynamics and the fjords location and width, the upper layers in Krossfjorden are somewhat more isolated from the shelf compared to Kongsfjorden.

1. Introduction

During the last decade, investigations related to marine biological aspects, sedimentation and hydrology has been performed in the fjords of Svalbard including Kongsfjorden (*e.g.* Weslawski *et al.*, 1994; Dowdeswell and Tranter, 1993; Hagen and Lefauconnier, 1993). However, with the exception of the hydrographic mapping of some fjords at West-Spitsbergen carried out by Weslawski *et al.* (1991, 1994), little is known about the physical oceanography in the fjords of Spitsbergen. Investigations considering the formation and transport of deep water has been carried out in Storfjorden (*e.g.* Quadfasel *et al.*, 1988; Schauer and Fahrbach, 1999). Considering other Arctic fjords, a few investigations has been performed in Greenland fjords (*e.g.* Lewis and Perkin, 1982). Since biological processes to a great extent are governed by physical processes, a thorough knowledge of the physics is decisive in order to understand the variations of the biological conditions. A better knowledge of the circulation in the Kongsfjorden-Krossfjorden system will be beneficial for the interpretation of the biological and chemical data sampled in the fjords. Polar areas are ecologically very vulnerable. The fjords in Svalbard are supplied with freshwater with a

This document is provided by JAXA.

high sediment content, and an alteration of the freshwater supply related to *e.g.* climatic changes, may therefore affect the biological production. The productivity is low and an increased runoff due to an increased air temperature may therefore affect the ecology of the fjords considerably through the alteration of the salinity, stratification and transparency of the upper layer (Eilertsen *et al.*, 1989; Weslawski *et al.*, 1994; Hasle and Heimdal, 1998). It is therefore crucial to have knowledge about the upper layer circulation in the fjord system.

Rotational dynamics (Coriolis force) have been shown to have an significant impact on fjord dynamics in wide, stratified fjords (Proehl and Rattray, 1984; Cushman-Roisin *et al.*, 1994; Asplin *et al.*, 1999). Kongsfjorden-Krossfjorden is a complex and wide fjord system being stratified due to runoff from the glaciers. The fjord dynamics are therefore expected to be strongly affected by the Coriolis force, both within each fjord arm and also in relation to exchange processes between the fjord arms.

The present paper aims to give a description of the upper layer circulation in the complex fjord system of Kongsfjorden and Krossfjorden. No attempt is made here to investigate the deeper layers of the fjords. The investigation is based on numerical simulations and data sampled on two cruises in 1994 and 1995. Some of the results has been presented in two thesis (reports) by Ingvaldsen (1996) and Reitan (1996).

2. Material and methods

2.1. Field observations

The field program was carried out on two cruises in September 1994 and August 1995. Repeated hydrographic mapping of the fjord system were performed with a CTD covering a dense station net (Fig. 1). On both cruises, 2 moorings with Aanderaa current meters RCM 4 and RCM 7 (Aanderaa Instrument, 1987) were deployed, one in each fjord (Fig. 1). The moorings were deployed for a period of 5–6 days, and the measuring depths were

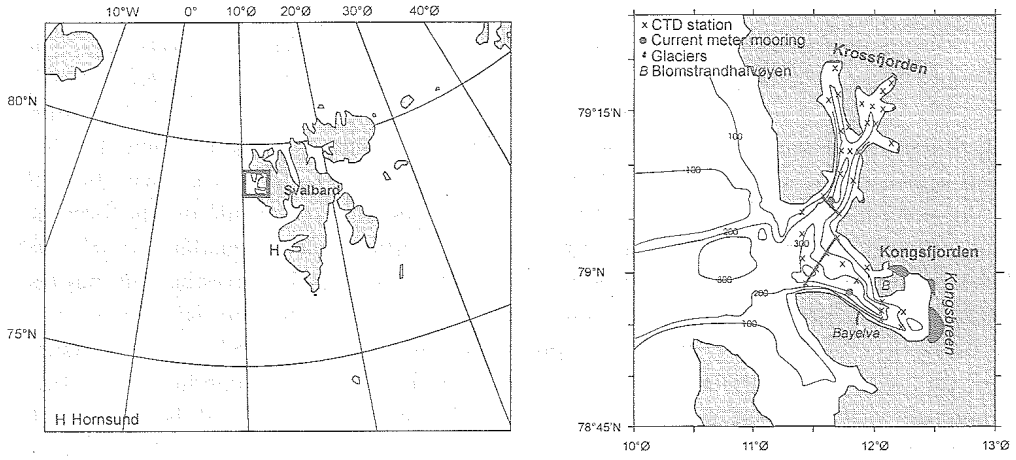


Fig. 1. Map of the investigated area (left). Sketch of the fjord system (right) showing bottom topography, the position of the CTD-stations, the current meter moorings and the sections (black lines) used in the text.

This document is provided by JAXA.

2, 10, and 30 m. The principal shortcoming of the RCM 4 is its inability to record currents accurately in regions affected by surface wave motions, therefore the RCM 7 was used as the upper two instruments. The residual current was obtained by removing the tidal component using an order 4 Butterworth filter with a cut-off period of 40 hours (Roberts and Roberts, 1978). To examine the brackish current Lagrangian drifters were used. The drifter is a simple construction consisting of a floating body (15×10×5 cm), attached by a 40 cm string to a 3-dimensional cross consisting of 2 quadratic, perpendicular plates. The drifters were dropped along a cross section of the fjord and recovered after 10–30 min of drifting period. To ensure minimal influence of the tides, all experiments were performed during nip or spring tide, when the tidal currents are at a minimum. Wind direction and speed was recorded by a permanent automatic meteorological station on board the ship.

2.2. The numerical model

The numerical model used for the simulations was the Ecom3D. Ecom3D is a three-dimensional, primitive equation, time-dependent, σ-coordinate, free surface estuarine and coastal ocean circulation model (Blumberg and Mellor, 1987; Mellor, 1996). This model, being the twin of the Princeton Ocean model, has been applied in a number of studies, including fjord and coastal dynamics relevant for fjord and coastal areas of Northern Norway (Cushman-Roisin *et al.*, 1994; Asplin, 1995; Leth, 1995; Svendsen, 1995).

2.2.1. Model design

The modelled area comprises the fjord system and the adjacent coastal area west to 25 km off the fjord mouth. The model domain terminates with sponge-like boundaries towards the north, west and south that operate under the condition called FRS (Flow Relaxation Scheme, see Martinsen and Engedal, 1987). A rectangular uniform grid with resolution 500 m in both the x-(north) and y-axis (east) were used. The vertical resolution (expressed in z-coordinates) varies from 0.2 m near the surface to 30 m near the bottom with 15 of a total of 21 σ-levels in the upper 15 m. The simulations were carried out with a flat bottom of 100 m depth, *i.e.* far deeper than the upper layer which is the subject of investigation. The initial conditions were of no water velocities, no sea-surface elevations and a constant temperature field of 2.5℃ including the supplied freshwater. The salinity field was horizontally homogeneous, but with a stratification in the vertical, increasing from a salinity of 32 at the surface to 34.5 at 100 m depth. The forcing of the model included local wind stress and freshwater supply. The wind was channelled along the fjord arms (*i.e.* into or out off), and the wind speed was kept constant over the entire area. The wind speed was increased linearly from 0 to 6.5 cms^{-1} in 6 hours, then held constant for 2 days, before it was reduced linearly to 0 during 6 hours. A thorough comparison between model and data are performed in Ingvaldsen (1996) and Reitan (1996), and their results showed that the model gives qualitatively good results, although there is some quantitative discrepancies between the model results and the data.

2.2.2. Freshwater sources

The most important freshwater sources to arctic fjords are calving and ablation from glaciers, but also melting of fast ice, direct precipitation on the fjord surface, and land/riverine outflow contribute to the freshwater supply (Weslawski *et al.*, 1994). According to Lefauconnier *et al.* (1994) the freshwater supply due to calving from Kongsbreen (Fig. 1) are 0.25 km^3year^{-1}. The discharge from Bayelva, the largest river in the fjord system, is

This document is provided by JAXA.

estimated to only 0.095 km^3year^{-1} (Hagen and Lefauconnier, 1993). Weslawski *et al.* (1991) estimated the total freshwater content in Kongsfjorden to be about 0.3 km^3. Compared to this the calving from Kongsbreen as estimated by Lefauconnier *et al.* (1994) contribute to more than 80% of the total freshwater supply. A total freshwater content of 0.3 km^3 gives for a melting season of three months (June–August) an average freshwater volume flux of 40 m^3s^{-1}. No estimates of the freshwater runoff in Krossfjorden are available, but calving from the glacier boarding in the left fjord arm are relatively large (Den Norske Los, 1992). It is probably the largest source in Krossfjorden, although freshwater is also supplied from all the other glaciers in the fjord. As the glaciers in Kongsfjorden are by far the largest, and are also calving most frequently on Svalbard (Lefauconnier *et al.*, 1994), it is assumed that the freshwater supply to Kongsfjorden is larger than to Krossfjorden. Anyhow, numerical simulations with different freshwater supplies have shown that the circulation in the fjord system is not sensitive for the amount of freshwater supplied, as well as the fraction supplied in the two fjords (Ingvaldsen, 1996). Melt water from the glaciers are supplied as sub-surface discharge (Liestøl, 1988). In the numerical model the freshwater is supplied at the surface, but as discussed in Ingvaldsen (1996) there are indications that the sub-surface discharges are not important for the upper layer circulation in central and outer parts of the fjords. This might be due to most of the freshwater being supplied at the surface by calving from the glaciers.

2.2.3. The cases

Three cases were simulated. Characteristics for the cases are shown below.

The freshwater driven case: Runoff from three sources: 55 m^3s^{-1} from the head of Kongsfjorden and 15 m^3s^{-1} from the head of each of the two main fjord arms in Krossfjorden. No wind.

The freshwater and down-fjord wind driven case: Runoff as the first simulation. After the freshwater driven circulation is established, a down-fjord wind field of 6.5 ms^{-1} is superposed. The wind forcing is present for 2 days before tuned of.

The freshwater and up-fjord wind driven case: Same as above, but with up-fjord wind.

3. Results and discussion

In the following discussion, periods dominated by either freshwater driven circulation or combined wind-freshwater driven circulation are identified in the field observations. However, when analysing the field observations, one must keep in mind the "memory" of the fjord system, i.e. the inertia of the system. Based on an analysis of observed surface layer response to a varying wind field, Svendsen (1981) found that more than 10% of the current in 2 m depth was related to the wind action with a lag of 6 hours. Furthermore, remote forcing of the coastal waters outside the fjord system might in periods dominate the local fjord dynamics as shown by *e.g.* Svendsen (1977) and Asplin *et al.* (1999).

Rotational effects are important if the width of a fjord is larger than the internal radius of deformation (*i.e.* the ratio of the internal wave speed to the Coriolis parameter, *e.g.* Gill, 1982). A rough two-layer approach based on the observed vertical density distribution gives a Rossby radius of 3.1 km (H_{surf}=15 m, H_{low}=245 m, ρ_{surf}=1026.3 kgm^{-3}, ρ_{low}=1027.8 kgm^{-3}, $f=1.43.10^{-4}s^{-1}$). Kongsfjorden are about 8 km wide in central parts and Krossfjorden about 6 km. Thus the rotation of the earth is important for the flow. This is confirmed

This document is provided by JAXA.

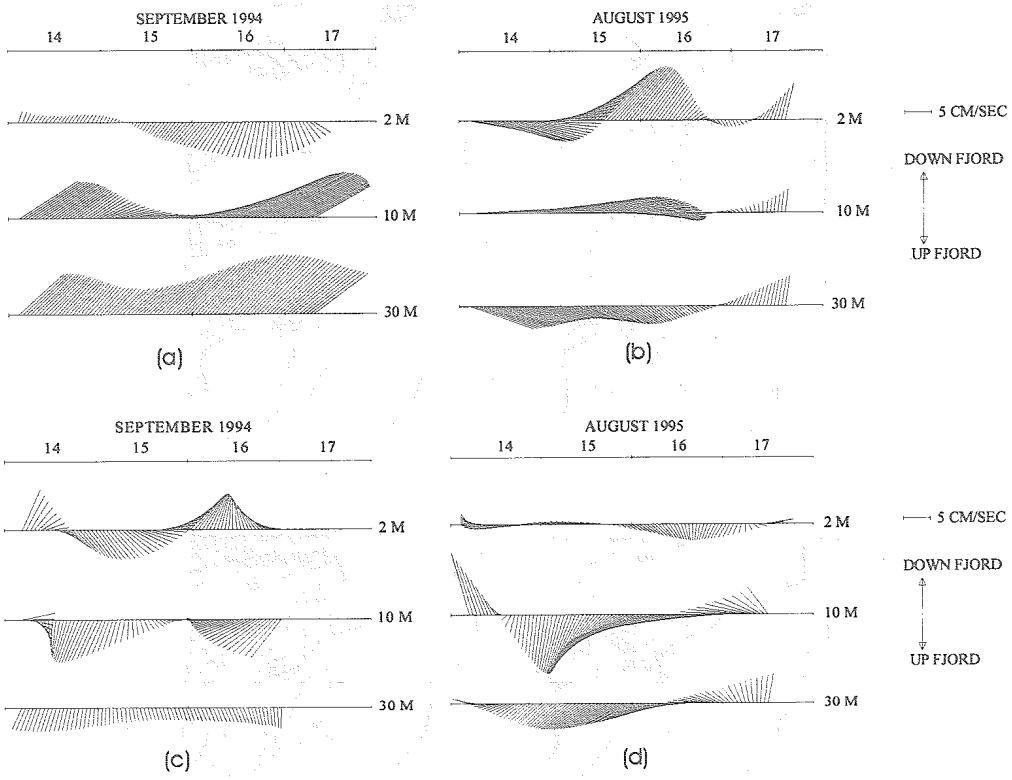


Fig. 2. Current velocities from the moorings in Kongsfjorden in (a) September 1994, (b) August 1995, and in Krossfjorden in (c) September 1994 and (d) August 1995.

by the time series from the current meter moorings which show the current to be deflected towards the right hand side (Fig. 2).

A fjord broader than the internal radius of deformation may, under the influence of a wind field, experience a wind-driven cross-fjord volume transport (Ekman transport). The piling up against the side will lead to cross-fjord horizontal density gradients. The transient behaviour due to the distortion of the interface will travel as an internal Kelvin wave with the shore on the right side (looking in the direction of propagation) having a width comparable to the internal radius of deformation. In a similar way a distortion of the density field at the coast, *e.g.* by coastal downwelling/upwelling broken by a fjord mouth, may generate internal Kelvin waves which can propagate into and inside a fjord.

3.1. The freshwater driven circulation

The mapped surface salinity and temperature distribution shown in Fig. 3 are sampled during calm conditions and are expected to mainly reflect the freshwater driven flow. The general feature of the hydrography is the appearance of fresher and colder water on the northern side of Kongsfjorden and the western side of Krossfjorden, indicating the importance of the rotational dynamics in deflecting the brackish water current to the right. The deflection is reproduced by the numerical model (Fig. 4a), which shows the effect to be

This document is provided by JAXA.

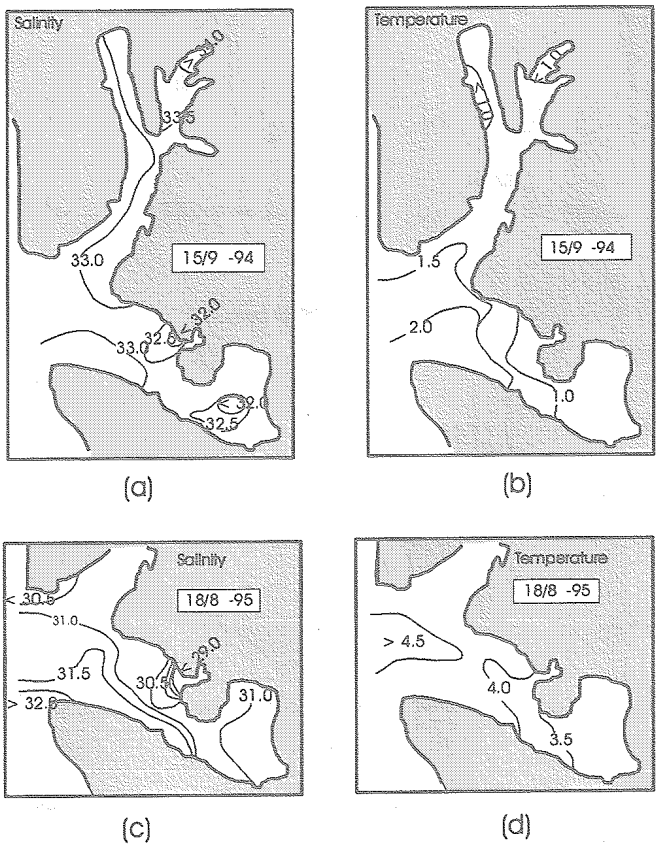


Fig. 3. Horizontal distribution of salinity and temperature in the surface layer during calm conditions.

particularly conspicuous when the flow passes around Blomstrandhalvøyen and the junction between the fjords. The flow describes a semi-circle movement, where the Coriolis acceleration acts in the direction of a centripetal acceleration. It is also a possibility that the lateral friction in the boundary layer along the fjord side may have an amplifying effect. Frictional torques act to reduce the relative vorticity within the frictional boundary layer on the landward side of a boundary flow, and a negative relative vorticity will cause a deflection towards the side of the fjord. After a while the stacking up of water in the bight boarding Blomstrandhalvøyen builds up a cross-fjord pressure gradient which displaces the flow towards the left hand side of the fjord in that area (Fig. 4b). The gradient is enhanced by discharge from the glacier in the lagoon as seen by the low saline water in the area (Fig. 3a and c). The displacement of the flow in Kongsfjorden is confirmed by the drifter experiments performed in this area during calm winds (Fig. 5), showing the highest velocities in the middle of the fjord, and low velocities with a cross-fjord component in the bay of Blomstrandhalvøyen. The inflow along the southern side of the fjord is not expected to be connected to the freshwater driven flow, and will be discussed later. The brackish water current seems to be limited to the upper 5–6 m in central and outer parts of both

This document is provided by JAXA.

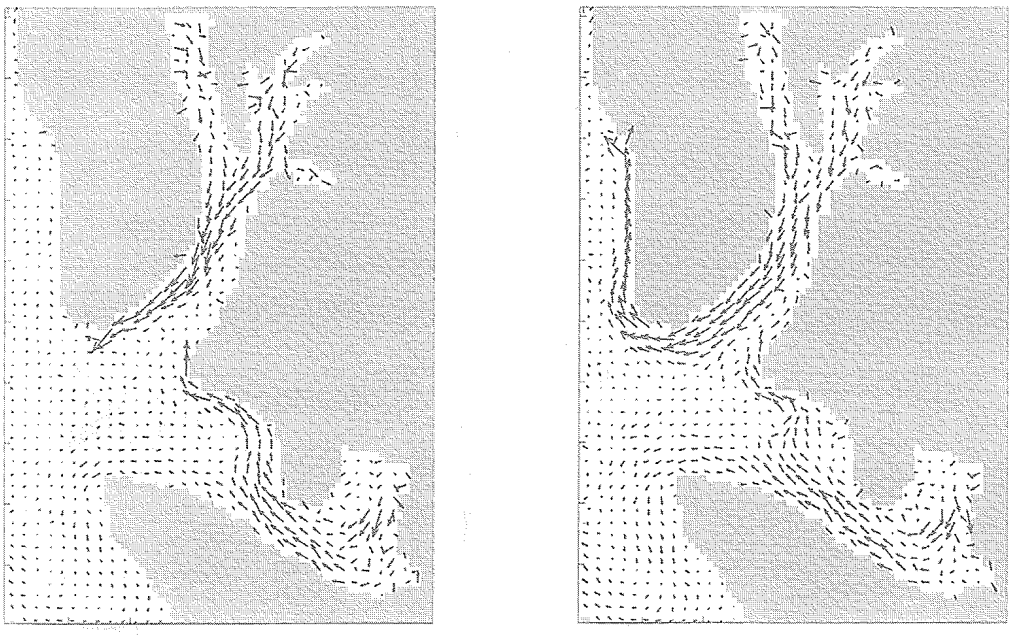


Fig. 4. Current velocities at surface after (a) 5 days, and (b) 8 days simulation time of the freshwater driven case.

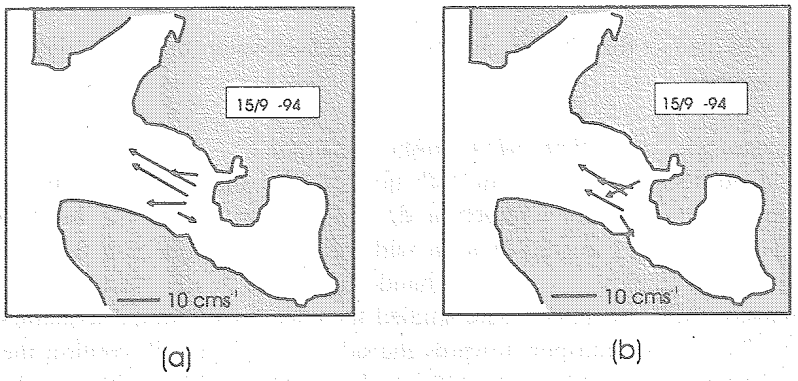


Fig. 5. Drifter experiments performed during calm conditions.

fjords (Fig. 6a and c). The velocities in the core are 5–20 cms^{-1}. The saline water in the inner parts of the fjord, as observed in the surface layer maps (Fig. 3), may have two reasons; entrainment of saline water to ascent freshwater from below the glacier, and the fjords "memory" of wind-driven upwelling happened the previous day. Generally, the temperature are higher and the salinity lower in August 1995 compared to September 1994,

This document is provided by JAXA.

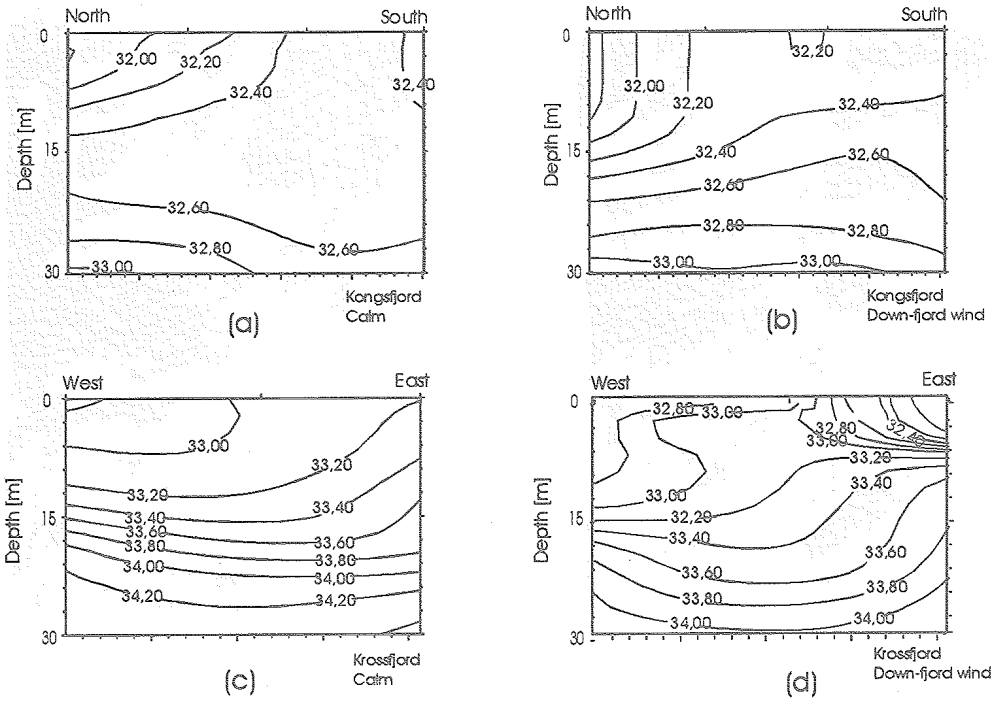


Fig. 6. Observed distribution of salinity in cross sections (looking up-fjord) in Kongsfjorden during (a) calm conditions and (b) down-fjord wind, and in Krossfjorden during (c) calm conditions and (d) down-fjord wind.

which is due to the fact that the air temperature and freshwater supply are higher in August than in September.

3.2. Freshwater and down-fjord wind driven circulation

These conditions were present in both fjords during the samplings shown in Fig. 7. The surface layer hydrography reflects a down-fjord flow along the northern side of Kongsfjorden. Compared to the situation with no wind, the brackish flow seems to be narrower and more confirmed to the right hand side. This is in accordance with the findings by Cushman-Roisin *et al.* (1994) who studied the effect of rotational dynamics on fjord circulation. The Ekman transport towards the side of the fjord will confirm the extent of brackish water and give an increase of the water level. Downwelling, with a resulting deeper brackish layer on the right hand side, and upwelling (and possibly an out-cropping of the interface at the surface), are expected on the left hand side (Cushman-Roisin *et al.*, 1994). This shows up nicely in the vertical section from Kongsfjorden (Fig. 6b), where the depth of the brackish layer is about 15 m, although out-cropping of the interface is not present. The numerical simulations show that the wind has a pronounced intensificating effect on the flow in both fjords (Fig. 8a). In the narrowest part of Kongsfjorden the current has a strong component towards the left hand side, while in the outer parts it is towards the right hand side. This is in very good accordance with the drifter experiments performed during

This document is provided by JAXA.

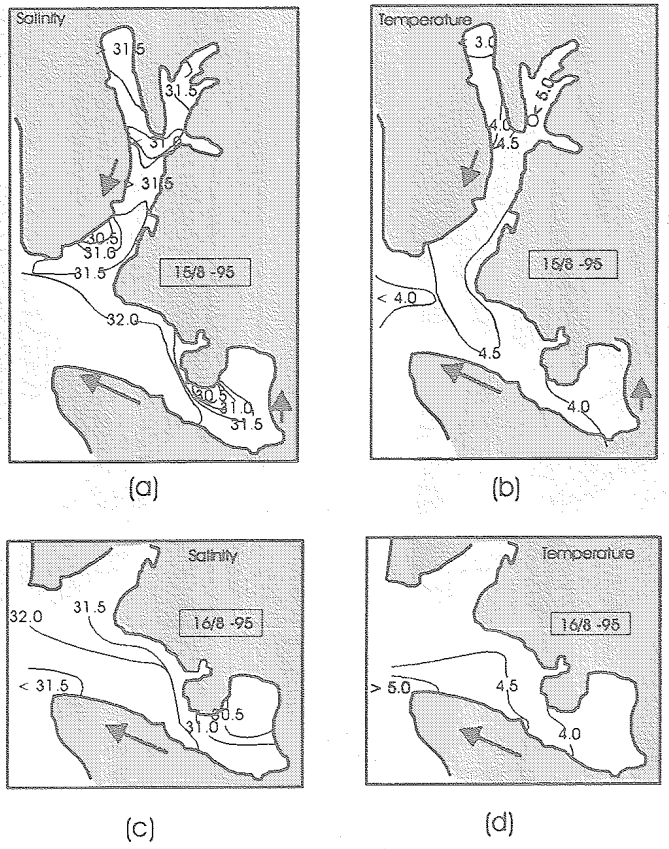


Fig. 7. Horizontal distributions of salinity and temperature in the surface layer during down-fjord wind. The heavy arrow represents the wind conditions during the mapping (1 cm = 5 ms^{-1}).

down-fjord wind (Fig. 9a–c). Due to its lesser width and more complicated topography, there is a more complicated structure in Krossfjorden (Fig. 8a), a result also evident from the surface layer maps (Fig. 7a). Because of the accumulation of surface waters from Kongsfjorden and the common fjord mouth, the waters of Krossfjorden must cross the fjord towards the left hand side in outer parts to escape the fjord (Fig. 8a). This is consistent with the drifter experiments (Fig. 9d–e).

An interesting feature of the fjord system arises after the cessation of the wind (Fig. 8b). In Krossfjorden the freshwater driven circulation is re-established after a few days (due to higher velocities when the fjord is under the influence of wind, a different scaling are used in this figure compared to Fig. 4). In Kongsfjorden the effect of the wind is more persistent, and even 5 days after the wind cessation, the freshwater driven circulation is not re-established (Fig. 8b). As the wind seldom is calm for that long, this means that the pure freshwater driven flow is a rare event in Kongsfjorden. Another interesting phenomena is the anticyclonic circulation developing in the mouth of the fjord system. The longevity of the eddy suggest a geostrophic balance, as the level of energy then are at a minima while all other motion requires more energy to be sustained. Such an anticyclonic eddy might also

This document is provided by JAXA.

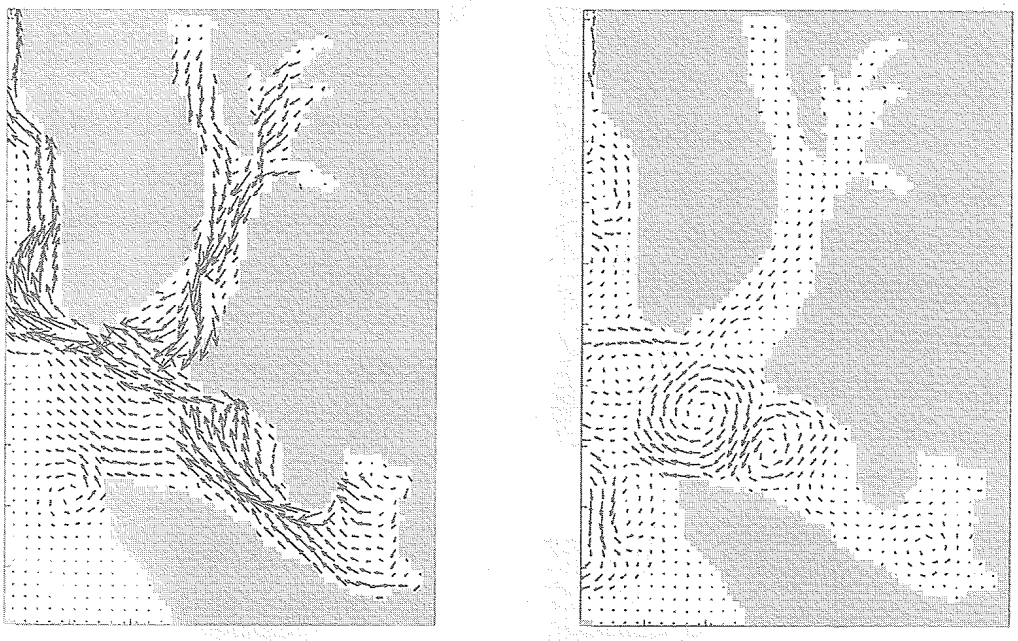


Fig. 8. Current velocities at surface after (a) 1 day with wind forcing and (b) 5 days after the wind has ceased in the freshwater and down-fjord wind driven case.

develop during calm conditions (Ingvaldsen, 1996).

3.3. Freshwater and up-fjord wind driven circulation

These conditions did not appear during any of the surface layer mappings, and seems to be a more seldom occurring event than down-fjord wind (Reitan, 1996). However, on August 17, 1995, the conditions in Kongsfjorden are close, with the exception for the down-fjord wind in the inner part of the fjord (Fig. 10). The effect of the wind is mainly to stack up water at the head, being reflected in the salinity distribution which indicates a cross-fjord front at the Blomstrandhalvøyen. The drifter experiment performed in the Kongsfjorden shows, as expected, an up-fjord current (Fig. 12), being strongest along the left hand side of the fjord, in accordance with the simulations (Fig. 11a). The reduction in the velocity field at the narrowest part of Kongsfjorden is due to an internal Kelvin wave generated by the wind (Reitan, 1996). These waves propagate into and around the fjord with the fjord side on the right looking in the direction of the wave propagation as described by Svendsen (1995). During the period with up-fjord wind the water level at the head of the fjords increase significantly, and when the wind cease this water flush out as a strong brackish water current. Consequently, a circulation similar to the freshwater driven flow, although much stronger, is re-established 2 days after the cessation of the wind (Fig. 11b). As in the simulation with down-fjord wind, an anticyclonic eddy is developed after the cessation of the wind.

This document is provided by JAXA.

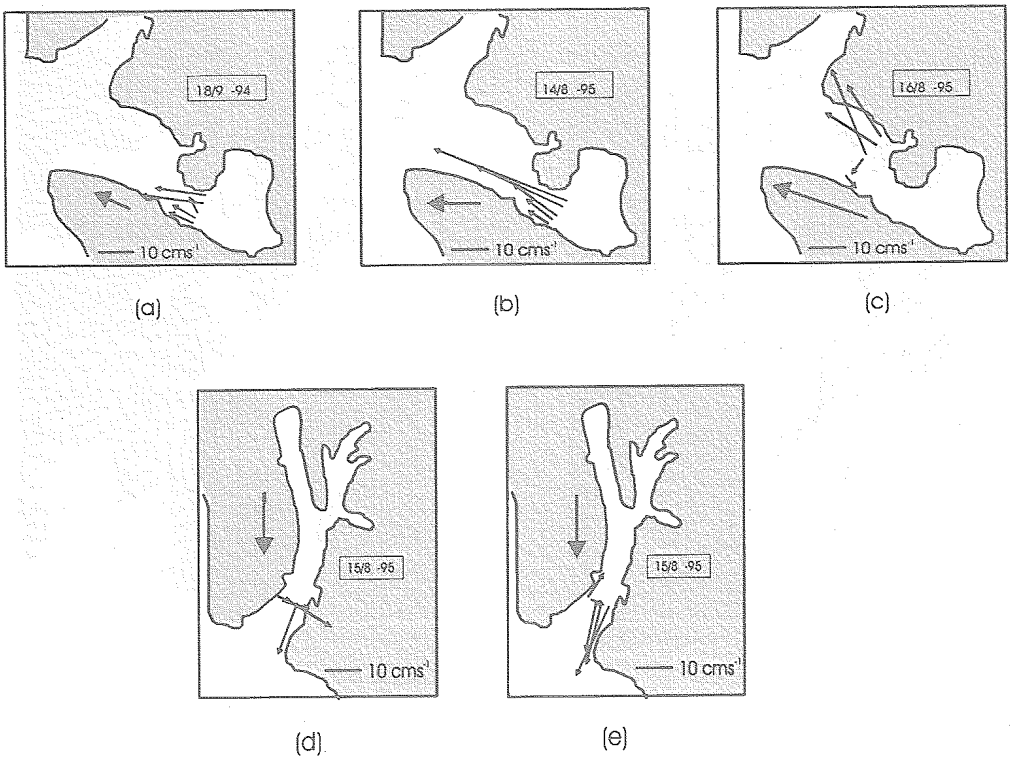


Fig. 9. Drifter experiments performed during down-fjord wind. The heavy arrow represents the wind conditions during the mapping (1 cm=5 ms^{-1}).

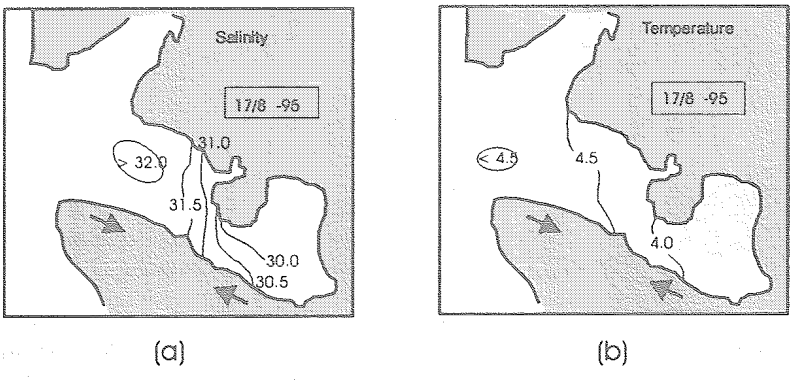


Fig. 10. Horizontal distributions of salinity and temperature in the surface layer during up-fjord wind. The heavy arrow represents the wind conditions during the mapping (1 cm=5 ms^{-1}).

3.4. Exchange of water

The numerical simulations show that with calm conditions the freshwater driven flow from Kongsfjorden continue into Krossfjorden as a wedge on the eastern side (Fig. 4). The

This document is provided by JAXA.

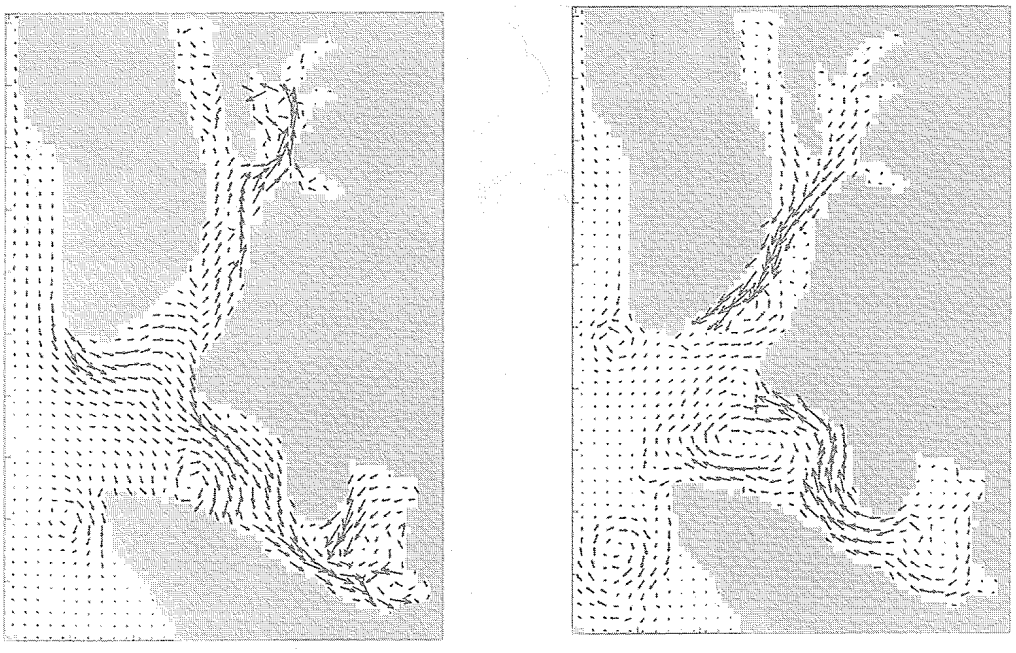


Fig. 11. Current velocities at surface after (a) 1 day with wind forcing and (b) 2 days after the wind has ceased in the freshwater and up-fjord wind driven case.

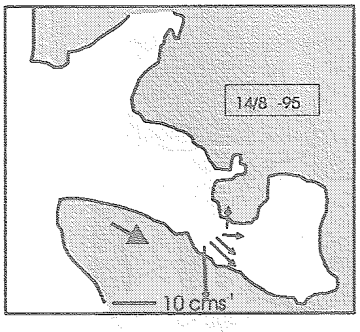


Fig. 12. Drifter experiments performed during up-fjord wind. The heavy arrow represents the wind conditions during the mapping (1 cm = 5 ms^{-1}).

internal Kelvin wave generated by up-fjord wind propagating around Kongsfjorden, show the same characteristics; when reaching the junction of the fjords, it continues into Krossfjorden (Reitan, 1996). As calm winds for longer periods are rare events in the fjord system, it is likely that the flow conditions in general are rapidly changing. The inflow from Kongsfjorden to Krossfjorden are therefore not expected to be a persistent feature, it is more likely to originate under certain favourable conditions. The inflow from Kongsfjorden to Krossfjorden suggests that the local conditions in Kongsfjorden will influence the outer parts of Krossfjorden. A more comprehensive field program will be necessary to give

This document is provided by JAXA.

definitive support and eventually explanations to these phenomena. Kongsfjorden will also indirectly affect the conditions in Krossfjorden, as the Coriolis effect causes the outflow from Kongsfjorden to leave the fjord system at the right hand side of the common mouth (Fig. 8a), and thereby blocking the exchange of water between Krossfjorden and the shelf. On the other hand, the development of an anticyclonic eddy in the common mouth will probably enhance the exchange between Krossfjorden and the shelf and counteract the exchange between Kongsfjorden and the shelf (Fig. 8b and 11b), as the eddy will lead the surface waters from the shelf into Krossfjorden and block the outflow from Kongsfjorden. As this eddy is developed in the numerical simulations with different driving forces, it is expected to be a frequent, but not persistent feature also in nature.

Numerical simulations has revealed internal Kelvin waves generated by wind to propagate around Kongsfjorden (Reitan, 1996). More generally Svendsen (1995) showed that processes on the shelf might propagate far into wide fjords as internal Kelvin waves. Asplin *et al.* (1999) examined the non-local wind-driven fjord-coast advection in a broad fjord in western Norway. They found that the temporal current field associated with internal Kelvin waves generated at the coast may replace ~50% of the upper water layer in the fjord within 1-2 days. As Kongsfjorden is wide and open, it is likely that the shelf might influence the fjord. Some support to this can be found in the drifter experiments performed during calm conditions (Fig. 5), where both experiments show a weak inflow on the southern side of Kongsfjorden. This is probably an internal Kelvin wave propagating from the shelf into and, if not damped, around Kongsfjorden.

In a narrow fjord with strong stratification rotation can be relatively unimportant because the width of the fjord is substantially less than the internal Rossby radius. The classical assumption that the circulation in the fjord is hydraulically controlled in the mouth of the fjord may then be justified. Hydraulic-controlled circulation may also exist in parts of a fjord where there are narrow passages and/or sills, and it has been shown that the exchange in narrow, stratified fjords take place as a pressure driven, mainly two-layer circulation (Svendsen, 1977, 1981; Klinck *et al.*, 1981; Stigebrandt, 1990). If rotational dynamics were not important in this fjord system, the brackish current would not be confirmed to the right-hand side of the fjords, and it would not describe the semi-circle movement around Blomstrandhalvøyen and the junction between the fjords. However, as the width of the fjords are larger than the baroclinic Rossby radius, rotation become important. The investigation indeed showed that the rotational effect play a significant role controlling the upper layer circulation in this complex fjord system. This is consistent with results found in broad sub-arctic fjords (Svendsen, 1991; Cushman-Roisin *et al.*, 1994; Asplin, 1995; Svendsen, 1995; Leth, 1995; Asplin *et al.*, 1999). No attempt is made to describe the circulation and investigate the exchange in the deeper layers. This is an important aspect which should be done. Further investigations will procure, in addition to 3-D simulations, a comprehensive field program based on time series of current and hydrography in selected sections across the fjords and across the adjacent shelf area.

References

Aanderaa Instruments (1987): Operating manual for recording current meter model 7 and 8. Technical Description No 159. Aanderaa Instruments, Norway, December 1987.

This document is provided by JAXA.

Asplin, L. (1995): Examination of local circulation in a wide, stratified fjord including exchange of water with the adjacent ocean, due to constant local up-fjord wind. Ecology of Fjords and Coastal Waters; Proc. of the Mare Nor Symp. on the Ecology of Fjords and Coastal Waters, Tromsø, Norway, 5–9 December, 1994, ed. by H.R. Skjoldal *et al*. Amsterdam, Elsevier, 177–184.

Asplin, L., Svendsen, H. and Cushman-Roisin, B. (1995): Observations and numerical simulations of freshwater runoff from Målselva into Malangen. Report, Geophysical Institute, University of Bergen, 62 p.

Asplin, L., Salvanes, A.G.V. and Kristoffersen, J.B. (1999): Non-local wind-driven fjord-coast advection and its potential effect on pelagic organisms and fish recruitment. Fish. Oceanogr., **8**:4, 255–263.

Blumberg, A. F. and Mellor, G.L. (1987): A description of a three-dimensional coastal ocean circulation model. Three-dimensional Coastal Ocean Models, ed. by N. Heaps. Washington, D.C., Am. Geophys. Union, 1–16.

Cushman-Roisin, B., Asplin, L. and Svendsen, H. (1994): Upwelling in broad fjords. Cont. Shelf Res., **14**, 1701–1721.

Den Norske Los (1992): Norges sjøkartverk. 2 ed.

Dowdeswell, J.A. and Tranter, M. (1993): Turbid plumes derived from glacial meltwaters: dynamics, forcing factors and sedimentation. NERC Grant GR9/679 Final report, 30 p.

Eilertsen, H.C., Taasen, J.P. and Weslawski, J.M. (1989): Phytoplankton studies in the fjords of West Spitsbergen: physical environment and production in spring and summer. J. Plankton Res., **11**, 1245–1260.

Gill, A.E. (1982): Atmosphere-Ocean Dynamics. San Diego, Academic Press, 662 p.

Hagen, J.O. and Lefauconnier, B. (1993): Reconstructed runoff from the high Arctic basin Bayelva in Svalbard based on mass-balance measurements. SINTEF. Polar Hydrology Report from Research Meeting in Trondheim March 29–30, 1993, 25–38.

Hasle, G.R. and Heimdal, B.R. (1998): The net phytoplankton in Kongsfjorden, Svalbard, July 1988, with general remarks on species composition of arctic phytoplankton. Polar Res., **17**, 31–52.

Ingvaldsen, R. (1996): Ferskvannsdrevet sirkulasjon i en arktisk fjord. M.Sc. Thesis in physical oceanography. Geophysical Institute, University of Bergen, 133 p.

Klinck, J.M., O'Brien, J.J. and Svendsen, H. (1981): A simple model of fjord and coastal circulation interaction. J. Phys. Oceanogr., **11**, 1612–1626.

Lefauconnier, B., Hagen, J.O. and Rudant, J.P. (1994): Flow speed and calving rate of Kongsbreen glacier, Svalbard, using SPOT images. Polar Res., **13**, 59–65.

Leth, O.K. (1995): A study on the effect of local wind on the dynamics of the upper layer in the inner part of Malangen. Ecology of Fjords and Coastal Waters; Proc. of the Mare Nor Symp. on the Ecology of Fjords and Coastal Waters, Tromsø, Norway, 5–9 December, 1994, ed. by H.R. Skjoldal *et al*. Amsterdam, Elsevier, 185–194.

Lewis, E.L. and Perkin, R.G. (1982): Seasonal mixing processes in an Arctic fjord system. J. Phys. Oceanogr., **12**, 74–83.

Liestøl, O. (1988): The glaciers in the Kongsfjorden area. Spitsbergen. Nor. Geogr. Tidsskr., **42**, 231–238.

Martinsen, E.A. and Engedal, H. (1987): Implementation and testing of a lateral boundary scheme as an open boundary condition in a barotropic ocean model. Coastal Eng., **11**, 603–627.

Mellor, G.L. (1996): Users Guide for a Three-dimensional, Primitive Equation, Numerical Model. New Jersey, Princeton University, 39 p.

Proehl, J.A. and Rattray, M., Jr. (1984): Low-frequency response of wide deep estuaries to non-local atmospheric forcing. J. Phys. Oceanogr., **14**, 904–921.

Quadfasel, D., Rudels, B. and Kurz, K. (1988): Outflow of dense water from a Svalbard fjord into the Fram Strait. Deep-Sea Res., **35**, 1143–1150.

Reitan, M. Bø (1996): Vinddriven sirkulasjon i ein arktisk fjord. M.Sc. thesis in physical oceanography. Geophysical Institute, University of Bergen, 128 p.

Roberts, J. and Roberts, T.D. (1978): Use of Butterworth low-pass filter for oceanographic data. J. Geophys. Res., **83**, 5510–5514.

Schauer, U. and Fahrbach, E. (1999): A dense bottom water plume in the western Barents Sea: downstream modification and interannual variability. Deep-Sea Res., Part I, **46**, 2095–2108.

This document is provided by JAXA.

Stigebrandt, A. (1990): On the response of the horizontal mean vertical density distribution in a fjord to low-frequency density fluctuations in the coastal water. Tellus, **42A**, 605–614.

Svendsen, H. (1977): A Study of the Circulation in a Sill Fjord on the West Coast of Norway. Mar. Sci. Comm., **3**(2), 151–209.

Svendsen, H. (1981): A study of circulation and exchange processes in the Ryfylkefjords. P.hD. thesis, Geophysical Institute, University of Bergen.

Svendsen, H. (1991): Preliminary results from a hydrophysical investigation of Porsangerfjord, Altafjord and adjacent coastal waters, June–August 1990. Report, Geophysical Institute, University of Bergen.

Svendsen, H. (1995): Physical oceanography of coupled fjord-coast systems in northern Norway with special focus on frontal dynamics and tides. Ecology of Fjords and Coastal Waters; Proc. of the Mare Nor Symp. on the Ecology of Fjords and Coastal Waters, Tromsø, Norway, 5–9 December, 1994, ed. by H.R. Skjoldal *et al.* Amsterdam, Elsevier, 149–164.

Weslawski, J.M., Jankowski, A., Kwasniewski, S., Swerpel, S. and Ryg, M. (1991): Summer hydrology and zooplankton in two Svalbard fjords. Pol. Polar Res., **12**(3), 445–460.

Weslawski, J.M., Koszteyn, M., Zajackowski, J., Wiktor, J. and Kwasniewski, S. (1994): Fresh water in Svalbard fjord ecosystem. Ecology of Fjords and Coastal Waters; Proc. of the Mare Nor Symp. on the Ecology of Fjords and Coastal Waters, Tromsø, Norway, 5–9 December, 1994, ed. by H.R. Skjoldal *et al.* Amsterdam, Elsevier, 229–241.

(Received April 3, 2000; Revised manuscript accepted July 24, 2000)

This document is provided by JAXA.

This document is provided by JAXA.

Mem. Natl Inst. Polar Res., Spec. Issue, 54, 409–416, 2001

Scientific note

The Arctic sea ice biological communities in recent environmental changes

Igor A. Melnikov[1], Ludmila S. Zhitina[2] and Helena G. Kolosova[2]

[1]*P. P. Shirshov Institute of Oceanology, Russian Academy of Sciences, Moscow 117851, Russia*
[2]*Department of Hydrobiology, Moscow State University, Moscow 119899, Russia*

Abstract: Biological materials obtained at the former Soviet Union ice station "North Pole-22" (NP-22) within the Beaufort Gyre in 1975–1981 have shown that the multi-year ice and ice-water interface is a rich and diverse environment inhabited by large numbers of diatoms and invertebrates. Recent data from the ice camp SHEBA (Surface Heat Budget of the Arctic Ocean) from the Beaufort Gyre in 1997–1998, comparable to the NP-22 data, demonstrate the following changes: (i) populations of sea ice diatoms are now very scarce by numbers of species and abundance; (ii) fresh water green algae, previously abundant only on the upper sea ice surface or within the uppermost sea ice layers, now dominate the entire sea ice thickness; (iii) populations of invertebrate animals like nematodes, copepods, amphipods, and turbellarians previously common within the sea ice interior are now not found in the multi-year ice and newly formed sea ice; (iv) cryopelagic fauna associated with the bottom sea ice surface as well as the under-ice zooplankton are also now scarce by numbers of species and abundance. These changes in the composition and structure of the sea ice communities within the Beaufort Gyre may be explained by increased melting of the sea ice cover during the last decade, and subsequent changes to the physical makeup of the sea ice.

1. Introduction

The Arctic Ocean is one of the major components of the world's atmosphere-ocean system and within this ocean, sea ice is the key dominant environmental feature. This 2–4 m thick sea ice cover affects the magnitude of both heat and gas fluxes between the atmosphere and upper ocean and supports a unique and tightly coupled biological community—the sea ice ecosystem. Observations made in 1970–1980 have shown that in spite of interannual variability in environmental factors the physical structure, chemical compounds, species composition, and species distribution within the sea ice were stable and predictable from year to year across the Arctic Ocean. The Arctic Ocean sea-ice can therefore be considered an integral and stable ecological system (Melnikov, 1997).

Recent environmental changes in the Arctic Ocean during the last two decades have been widely discussed in the literature, with many models predicting a greenhouse gas-induced warming in polar regions associated with warming of the upper ocean and a substantial retreat of the sea ice cover (Walsh, 1991; McPhee *et al.*, 1998; Johannessen *et al.*, 1995, 1999; Vinnikov *et al.*, 1999). Analysis of the climate trends in the Arctic indicates

This document is provided by JAXA.

considerable warming over the landmasses of Eurasia and North America, particularly in winter and spring (Chapman and Walsh, 1993). Over the last three decades, trends toward higher temperatures have been up to 1.5℃ per decade (Weller, 1999). On results of recent research on Arctic climate oscillatory behavior, a standing surface level pressure oscillation over much of the northern hemisphere was shown to be associated with a sea ice anomaly propagating anticyclonically around the Arctic Ocean (Mysak and Venegas, 1998), the upper ocean and ice circulation (Carmack *et al.*, 1995; Morison *et al.*, 1998) and river discharge (Johnson *et al.*, 1999). Hydrographic data obtained during the last decade (*e.g.*, AOS 1994, SCICEX cruises, 1993–1997) have supplied intriguing evidence that Atlantic Water flows into the Arctic Ocean had been warmed relative to previous years and inflow had increased in volume by about 20% (Carmack *et al.*, 1995; Morison *et al.*, 1998). Warming relative to historical data and also freshening of the upper ocean were observed. A warm core of the Atlantic Water with temperatures of 0.5° to 1.7℃ was observed above the Lomonosov Ridge, and another less apparent warm core with temperature of 1℃ existed over Mendeleev Ridge. According to Carmack *et al.* (1995) and Morison *et al.* (1998), these data indicate a fundamental change in the circulation of the Arctic Ocean since the early 1990s.

Recent field and satellite-based observations show a rapid decrease in the Arctic Ocean sea ice extent during the past 46 years (Cavalieri *et al.*, 1997; Johannessen *et al.*, 1999; Vinnikov *et al.*, 1999). Satellite observations indicate a decrease in areal ice extent of nearly 3% per decade since the late 1970s, accelerating in the last decade (Cavalieri *et al.*, 1997). Johannessen *et al.* (1995) reported a reduction of the annual mean ice cover of the Arctic Ocean during 1978 to 1994. Using satellite-derived ice maps, they estimated a decrease of the total sea ice extent of 0.05×10^6 km^2/yr, of which 14% was due to reduction of the multi-year ice area. Reduction of the sea ice cover is very noticeable in the Canadian Basin of the Arctic Ocean. Rothrock *et al.* (1999) compared sea ice thickness data acquired by the Scientific Ice Expedition (SCICEX) in the mid-1990s with data from 1958 and 1976, finding a mean decrease of 1.3-m (around 40%) in ice thickness over the deep Arctic Ocean with greater decreases in the eastern and central Arctic than in the western Arctic.

During the period 1975–1981, the former Soviet Union's "North Pole-22" ice station (NP-22) drifted within the Beaufort Gyre in the Canadian Basin of the Arctic Ocean. Twenty-plus years later and also within the Beaufort Gyre, in 1997–1998, the USA National Science Foundation conducted the year-round experiment SHEBA (Surface Heat Budget of the Arctic Ocean) supported by the Canadian Coast Guard icebreaker Des Groseilliers (Perovich *et al.*, 1999). At both the NP-22 and SHEBA ice camps we made multi-disciplinary biological studies of the sea ice-water system including sea ice observations and observations of the upper ocean (Melnikov, 1997; Melnikov *et al.*, 2000; Sherr *et al.*, 2000). The main goal of this paper is to show how do the environmental changes observed recently in the Arctic Ocean impact the physical-chemical composition of the sea-ice and sea ice-associated biological communities.

2. Material and methods

This research is based on material collected during the winter at the ice camps NP-22 from January to April 1980 and SHEBA from October 1997 to March 1998 within the

This document is provided by JAXA.

Beaufort Gyre. The field observations sampling methods and laboratory procedures were similar in both expeditions, giving a good opportunity for comparison of data obtained within the Beaufort Gyre across two decades. At each location we took first-year (FY) and multi-year (MY) ice cores on pristine floes away from the influence of the camp, in order to monitor the physical, chemical, and biological characteristics of the ice. Cores were taken with a 120-mm internal diameter SIPRE-style corer through the entire ice column. The total ice core length was measured, the surface cleaned and the whole ice core divided into equal 10 or 20-cm parts. Each ice section was crushed into small pieces, put into plastic bottles and melted at room temperature. For comparison of results, at the SHEBA ice camp we did not melt ice in filtered sea water to keep the same procedure that was used at NP-22. Salinity, silicate, phosphate, and chlorophyll *a* concentrations were measured on subsamples of the melt water. Aliquots of samples were preserved for species identifications in 4% formalin and processed six months later in the P.P. Shirshov Institute of Oceanology laboratory by standard planktonology methods. See Melnikov (1997) for details of field and lab methods.

3. Results

3.1. Sea ice interior

3.1.1. Physical, chemical, and biological components

The total data set includes 18 MY cores (7 from NP-22 and 11 from SHEBA) and 16 FY ice cores (4 from NP-22 and 12 from SHEBA). Dates and positions of sea ice core samplings, mean and standard deviations of salinity, silicate and chlorophyll *a* concentration are summarized in Table 1. Mean SHEBA values of the MY ice salinity are about half those of NP-22, but the FY values are twice as high. The most curious feature of the SHEBA ice samples is very low concentrations of Si in the MY and FY sea ice, an order of magnitude less than at NP-22: 3.76 μM and 2.18 μM in the MY and FY ice at NP-22, and 0.40 μM and 0.28 μM at SHEBA, respectively. The main feature of chlorophyll *a* concentrations in the ice cores is the two-fold decrease in SHEBA multi-year ice compared to NP-22, and three-fold increased chlorophyll *a* concentrations in first-year ice.

3.1.2. Flora

We found a total of 102 species of ice algae, 76% at NP-22 and 23% at SHEBA. The similarity between species was only 8%. The prevalence of diatoms characterizes both MY and FY sea ice at NP-22 with 79 species compared to SHEBA with only 18 species (Table 2). Fresh water algae (mostly Chlorophyta) were detected only on the upper surface of ice at NP-22. The obvious predominance of fresh water algae compared with diatoms was the main peculiarity of the algal populations at SHEBA where fresh water algae were dominant and were distributed within both MY and FY ice interiors from top to bottom.

3.1.3. Fauna

The outstanding feature of the MY and FY sea ice populations is the absolute absence of interstitial fauna within the sea ice interior in the SHEBA ice samples compared with the consistently high numbers found in the NP-22 samples. Ten species including Protozoa, Foraminifera, Acarina, Nematoda, Turbellaria, Harpacticoida and Amphipoda, in both the MY and FY sea ice, were found at NP-22, whereas only one species of Foraminifera was found at SHEBA (Table 3). Notable was the abundance of the free-living nematode

This document is provided by JAXA.

Table 1. Summary of ice thickness, date of sampling position, physical and chemical variables of MY and FY ice cores at the NP-22 and SHEBA ice camps. Data are mean ± 1SD.

Core #	Thick (cm)	Sampling date	Latitude	Longitude	Salinity (‰)	Silicate (mM/l)	Chl *a* (mg/l)
			NP-22, multi-year ice				
1	404 (11)	15 Feb 80	77°53′N	153°49′E	2.02±1.69	6.1±2.11	0.45±0.44
2	350 (9)	11 Mar 80	78°17′N	153°35′E	2.42±1.43	2.6±0.53	0.23±0.18
3	163 (5)	31 Mar 80	78°21′N	153°07′E	5.60±2.14	3.51±4.05	0.18±0.22
4	199 (6)	01 Apr 80	78°22′N	153°01′E	5.07±0.48	2.21±0.43	0.09±0.01
5	162 (5)	04 Apr 80	78°22′N	152°30′E	5.52±0.86	3.93±0.5	0.06±0.04
6	339 (11)	18 Apr 80	78°35′N	151°52′E	3.17±0.56	3.2±1.33	0.61±0.34
7	211 (4)	20 Apr 80	78°39′N	151°48′E	4.86±4.21	4.68±2.39	0.24±0.18
				Mean:	4.09±1.62	3.76±1.62	0.35±0.20
			NP-22, first-year ice				
1	104 (3)	23 Jan 80	77°40′N	154°99′E	0.99±0.09	1.90±0.69	0.05±0.01
2	114 (4)	01 Feb 80	77°48′N	153°54′E	0.84±0.19	ND	ND
3	129 (4)	26 Feb 80	78°05′N	154°36′E	0.88±0.22	1.98±0.33	0.09±0.07
4	167 (4)	28 Feb 80	78°07′N	153°54′E	1.28±0.25	2.67±0.70	0.06±0.03
				Mean:	0.99±0.19	2.18±0.57	0.06±0.03
			SHEBA, multi-year ice				
1	244 (10)	27 Oct 97	75°17′N	143°31′W	ND	ND	0.12±0.08
2	235 (12)	12 Nov 97	76°09′N	146°26′W	1.43±0.96	0.12±0.16	0.24±0.19
3	185 (9)	28 Nov 97	75°07′N	147°33′W	1.67±1.08	0.16±0.14	0.09±0.15
4	216 (11)	10 Dec 97	75°44′N	150°25′W	2.16±1.36	ND	0.31±0.53
5	178 (9)	29 Dec 97	75°17′N	149°59′W	2.62±1.60	0.72±0.43	0.13±0.05
6	177 (9)	12 Jan 98	74°51′N	150°25′W	2.97±1.87	0.74±0.37	0.11±0.05
7	260 (13)	27 Jan 98	74°51′N	155°38′W	2.10±1.30	0.46±0.27	0.31±0.32
8	281 (14)	18 Feb 98	74°54′N	157°50′W	2.55±1.58	0.35±0.22	0.05±0.04
9	417 (21)	09 Mar 98	75°28′N	160°18′W	2.08±0.95	0.08±0.05	0.17±0.13
10	287 (15)	29 Apr 98	75°57′N	166°13′W	2.50±2.02	0.45±0.37	0.09±0.09
11	291 (14)	25 May 98	76°24′N	167°11′W	0.94±0.50	0.56±0.18	0.11±0.13
				Mean:	2.10±1.32	0.40±0.24	0.16±0.16
			SHEBA, first-year ice				
1	62 (6)	19 Oct 97	75°20′N	144°29′W	0.41±0.19	ND	0.20±0.07
2	66 (6)	27 Oct 97	75°17′N	143°31′W	0.58±0.32	ND	0.46±0.50
3	77 (7)	11 Nov 97	76°09′N	146°23′W	1.74±0.89	0.08±0.01	0.13±0.10
4	79 (8)	26 Nov 97	76°13′N	147°43′W	3.03±1.85	0.36±0.27	0.41±0.25
5	116 (6)	12 Dec 97	75°41′N	150°44′W	2.42±1.54	ND	0.14±0.09
6	95 (9)	27 Dec 97	77°17′N	149°57′W	2.86±1.56	0.44±0.26	0.10±0.11
7	137 (7)	11 Jan 98	74°53′N	150°12′W	2.86±1.62	0.45±0.19	0.05±0.02
8	150 (8)	24 Jan 98	74°38′N	153°25′W	3.42±1.99	0.14±0.05	0.06±0.04
9	132 (7)	16 Feb 98	74°53′N	157°50′W	3.31±1.58	0.11±0.03	0.13±0.07
10	171 (9)	09 Mar 98	75°28′N	160°18′W	3.39±1.75	0.05±0.03	0.12±0.08
11	142 (7)	29 Apr 98	75°57′N	166°13′W	ND	0.25±0.09	0.18±0.16
12	138 (7)	25 May 98	76°24′N	167°11′W	ND	0.67±0.28	0.20±0.16
				Mean:	2.4±1.33	0.28±0.13	0.18±0.13

ND–no data; number of ice sections in parenthesis.

Theristus melnikovi associated with the MY sea ice interior at NP-22; yet it was never detected at SHEBA.

This document is provided by JAXA.

Table 2. Number of algal species present within sea ice interior in samples collected from ice camps NP-22 (winter 1979–1980) and SHEBA (winter 1997–1998), Beaufort Gyre, Canadian Basin of the Arctic Ocean.

Taxon	NP-22	SHEBA
Bacillariophyta	79	18
Dinophyta	NO	5
Chrysophyta	NO	1
Chlorophyta	NO	1
Silicoflagellatae	5	1

NO–not observed.

Table 3. Number of fauna species associated with the sea ice interior in samples from the ice camps NP-22 (winter 1979–1980) and SHEBA (winter 1997–1998), Beaufort Gyre, Canadian Basin of the Arctic Ocean.

Taxon	NP-22	SHEBA
Protozoa	3	NO
Foraminifera	1	1
Acarina	1	NO
Nematoda	2	NO
Turbellaria	1	NO
Harpacticoida	1	NO
Amphipoda	1	NO

NO–not observed.

Table 4. Average concentrations of silicate (Si), dissolved oxygen (O_2) and chlorophyll a (Chl a) in the 0–30 m surface water from ice camps NP-22 (1975–1976) and SHEBA (1997–1998), Beaufort Gyre, Canadian Basin of the Arctic Ocean.

Ice camp	Si (μM)		O_2 (ml/l)		Chl a ($\mu g/l$)	
	winter	summer	winter	summer	winter	summer
SHEBA	4.75	8.0	8.94	9.35	0.067	0.34
NP-22	11.4	13.2	8.30	8.31	0.061	0.22

3.2. Sea ice/water interface

3.2.1. Chemical and biological components

The mean annual values of silicate concentrations (μM) in the 0–30 m water column at SHEBA are decreased about 60% in winter and about 40% in summer compared with NP-22 (Table 4). The SHEBA mean seasonal O_2 concentrations are increased by 8% in winter within 0–30 m comparable to NP-22 and 13% in summer. The NP-22 O_2 concentrations were seasonally stable and the SHEBA winter O_2 concentrations were similar, but the summer concentrations are 55% higher than summer values at NP-22. The annual chlorophyll *a* concentrations were 0.273 $\mu g/l$ at SHEBA, and 0.159 $\mu g/l$ at NP-22, respectively.

3.2.2. Flora

A total of 85 species were identified in samples collected at NP-22 and SHEBA from the bottom ice surface (Melnikov *et al.*, 2000) as shown in Table 5. The main features of the SHEBA and NP-22 algal populations associated with the bottom surface of ice are:

1) A decrease of diatom species from 46 or 96% of total algal populations (NP-22) to

This document is provided by JAXA.

Table 5. Number of algal species present in samples collected at the water/ice interface from ice camps NP-22 (winter 1979-1980) and SHEBA (winter 1997-1998), Beaufort Gyre, Canadian Basin of the Arctic Ocean.

Taxon	NP-22	SHEBA
Bacillariophyta	46	22
Dinophyta	1	19
Chrysophyta	NO	1
Chlorophyta	NO	1
Silicoflagellatae	1	1

NO-not observed.

22 or 51% (SHEBA);

2) A remarkable difference in species composition between two collections: only three species of diatoms (*Chaetoceros socialis*, *Cylindrotheca closterium*, *Thalassionema nitzschioides*), one species of dinoflagelate (*Dinophysis acuta*) and one silicoflagelate (*Dictyocha speculum* var. *octonarius*) were common for both algal communities; similarity between species from the SHEBA and NP-22 algal populations was only 8%;

3) A remarkable increase of Dinophyta in the SHEBA samples with 19 species compared to the NP-22 with only one species;

4) Extensive development of high-density aggregations of green algae Ulothrix implexa (Chlorophyta) at SHEBA. It is a very common brackish- water species (Lokhorst, 1978) and has not been reported before in the high marine Arctic.

Table 6. Number of fauna species associated with the bottom sea-ice surface in samples collected from the ice camps NP-22 (winter 1979-1980) and SHEBA (winter 1997-1998), Beaufort Gyre, Canadian Basin of the Arctic Ocean.

Taxon	NP-22	SHEBA
Protozoa	2	3
Hydrozoa	2	3
Syphonophora	1	1
Ctenophora	1	1
Turbellaria	NO	1
Nematoda	1	NO
Nemertini	1	1
Polychaeta	2	2
Ostracoda	1	1
Copepoda	17	17
Cyclopoida	6	5
Harpacticoida	4	3
Mysida	1	1
Isopoda	2	NO
Amphipoda	14	5
Euphausidaceae	1	1
Decapoda	2	NO
Gastropoda	2	2
Chaetognatha	2	2
Appendicularia	2	3

NO-not observed.

This document is provided by JAXA.

3.2.3. Fauna

At the bottom ice surface we identified 75 species, 64 from NP-22 and 52 from SHEBA. There were only 21 species or 37% of the total common to both ice camps (Melnikov *et al*., 2000). The most notable difference was observed in amphipods, with 14 species or 33% of total faunal species at NP-22 and only 5 species or 11% of total species at SHEBA. Other dominant cryopelagic fauna collected at NP-22 like the polychaete *Antinoella sarsi* were not observed at SHEBA. At the same time the numbers of gelatinous plankton species like appendicularians, medusas and benthic larvae were much higher at SHEBA that at NP-22 (Table 6).

4. Concluding remarks

Observations over the last two decades which showed noticeable changes within the sea ice biological communities in the Arctic Ocean are as follows:

- Sea ice diatoms at SHEBA were very scarce by numbers of species and abundance both in the multi-year and in the newly formed ice;
- Fresh water green algae previously developed only on the upper-ice surface and/or within the upper sea ice layers (NP-22) now dominated within the whole sea ice interior (SHEBA);
- Populations of invertebrate like nematodes, copepods, amphipods, and turbellarians previously found within the sea ice interior (NP-22) were not found in the multi-year and first-year sea ice at SHEBA;
- In the SHEBA samples, fauna associated with the bottom sea-ice surface were also scarce by numbers of species and abundance.

We interpret these data to suggest that remarkable environmental changes have occurred in the last two decades between samplings at the ice camps NP-22 (1975–1981) and SHEBA (1997–1998) in the Beaufort Gyre. The multi-year ice cover thickness has decreased from the average 3–5-m thick at NP-22 to 1.5–2-m at SHEBA, and this is correlated with a decrease in MY ice salinity. At the same time, surface Si concentrations decreased as the freshwater layer thickened and/or the density difference increased, reducing the reinjection of deeper dissolved Si into the surface layer where sea-ice diatoms could use it. This in turn resulted in a marked decrease in diatoms, an increase in freshwater species, and a decrease in primary production (in term of chlorophyll *a* concentration) within MY ice. Faunal diversity also decreased dramatically, probably resulting from a combination of decreased *in situ* primary production and a freshening of interstitial water in summer, eliminating stenohaline forms. Increases in chlorophyll *a* and oxygen content in the water-ice interface suggest that total primary production has increased, probably because decreasing ice and snow thickness has allowed more light to reach the water column, but this possible overall increase in Arctic Ocean productivity has decreased the relative importance of the multi-year ice community to total energy flow.

Acknowledgments

We would like to thank the Canadian Coast Guard officers and crew of the icebreaker Des Groseilliers for their outstanding help during the SHEBA Ice Camp drift, and the

This document is provided by JAXA.

logistical assistance of the Polar Continental Shelf Project of Canada. We wish to thank also all participants of the SHEBA/JOIS project, who assisted both in field and lab procedure work. Special thanks are due to John (Jumper) Bitters, Bill Bosworth, Bruce Elder, John Govoni, Andy Heiberg, Dean Stewart and Terry Tucker for the sea ice core sampling assistance, and Sandy Moor, Karen Thompson, Jim Watkins and Cathy Welch for the laboratory data processing. We would like also to thank Barry Sherr and Pat Wheeler (Oregon State University, USA), and Harold (Buster) Welch (Fresh Water Institute, Canada) for their kind offers to use their facilities. This work was supported by grant #99-05-64767 of the Russian Foundation for Basic Research.

References

Carmack, E.C., Macdonald, R.W., Perkin, R.G., McLaughlin, F.A. and Pearson, R.J. (1995): Evidence for warming of Atlantic water in the southern Canadian Basin of the Arctic Ocean: Results from the Larson-93 expedition. Geophys. Res. Lett., **22**, 1061–1064.

Cavalieri, D.J., Gloersen, P., Parkinson, C.L., Comiso, J.C. and Zwally, H.J. (1997): Observed hemisphere asymmetry in global sea ice changes. Science, **278**, 1104–1106.

Chapman, W.L. and Walsh, J.E. (1993): Recent variations of sea ice and air temperatures in high latitudes. Bull. Am. Meteorol. Soc., **74**, 33–47.

Johannessen, O.M., Miles, M. and Bjorno, R. (1995): The Arctic's shrinking sea ice. Nature, **376**, 126–127.

Johannessen, O.M., Shalina, E.V. and Miles, M. (1999): Satellite evidence for an Arctic sea ice cover in transformation. Science, **286**, 1937–1939.

Johnson, M.A., Proshutinsky, A.Y. and Polyakov, I.V. (1999): Atmospheric patterns forcing two regimes of Arctic circulation: a return to anticyclone conditions? Geophys. Res. Lett., **26**, 1621–1624.

Lokhorst, G.M. (1978): Taxonomic studies on the marine and brackish-water species on Ulothrix (Ulotricales, Chlorophyceae) in Western Europe. Blumea, **24**, 191–299.

McPhee, M.G., Stanton, T.P., Morison, J.H. and Martinson, D.G. (1998): Freshening of the upper ocean in the Arctic: Is perennial sea ice disappearing? Geophys. Res. Lett., **25**, 1729.

Melnikov, I.A. (1997): The Arctic Sea Ice Ecosystem. Amsterdam, Gordon and Breach Sci. Publ., 204 p.

Melnikov, I.A., Zhitina, L.S. and Kolosova, L.G. (2000): Reaction of marine ecosystems on the global changes in the Arctic: upper ocean. Hydrometeorological and Biogeochemical Research in the Arctic; Proceedings of the Arctic Regional Center, v.II, 68–80.

Morison, J.H., Steele, M. and Andersen, R. (1998): Hydrography of the upper Arctic Ocean measured from the nuclear submarine USS Pargo. Deep-Sea Res., **45**, 15–38.

Mysak, A.M. and Venegas, S.A. (1998): Decadal climate oscillations in the Arctic: A new feedback loop for atmosphere-ice-ocean interactions. Geophys. Res. Lett., **25**, 3607–3610.

Perovich, D.K. and 21 colleagues (1999): Year on ice gives climate insights. EOS: Trans., **80** (41).

Rothrock, D., Yu, Y. and Maykut, G. (1999): The thinning of the Arctic sea-ice cover. Geophys. Res. Lett., **26**, 3469–3472.

Sherr, B., Ashjian, C., Campbell, R., Melnikov, I., Sherr, E., Welch, H. and Wheeler, P. (2000): Annual cycle of biological activity in the central Arctic Ocean. Nature (in press).

Vinnikov, K.Y., Robok, A., Stouffer, R., Walsh, J., Parkinson, C., Cavalieri, D., Mitchell, J., Garrett, D. and Zakharov, V. (1999): Global warming and northern hemisphere sea ice extent. Science, **286**, 1934–1937.

Walsh, J. E. (1991): The Arctic as a bellwether. Nature, **352**, 19–20.

Weller, G. (1999): Climate change and its impacts on the Arctic environment. Report of the Marine Mammal Commission Workshop, Girdwood, Alaska, 15–17 February 1998, 7–14.

(Received May 17, 2000; Revised manuscript accepted November 1, 2000)

This document is provided by JAXA.

Mem. Natl Inst. Polar Res., Spec. Issue, 54, 417–421, 2001

Scientific note

Laboratory experiments on frazil ice formation with application to the Arctic marine environment

Andrei G. Zatsepin[1] and Pavel N. Golovin[2]

[1]*P.P. Shirshov Institute of Oceanology, Nakhimovsky pr., Moscow 117851, Russia*
[2]*Arctic and Antarctic Research Institute, Bering st., 38, St. Petersburg 199226, Russia*

Abstract: Laboratory experiments on the frazil ice formation in the upper low saline water layer cooled from below by a more saline water layer indicate that frazil ice production is maximal when both layers are in turbulent state of motion. It is argued, that a considerable amount of frazil ice may be formed in the contact zone between fresh river water and cold marine water in the Arctic shelf zone. Frazil ice production in the fresh/salt water contact zone should be suspected as an important source of sediment incorporation into the Arctic surface ice cover.

Frazil ice is one of the important sources of sea ice in polar seas. According to Martin (1981), Weeks and Ackley (1982) frazil ice is formed:

a) in regions of open waters, called leads and polynyas, during cold and windy weather;
b) adjacent to deep ice shelves and icebergs where water with a lower freezing point due to hydrostatic pressure may be transported toward the sea surface;
c) at the interface between two water masses of different salinities, both near their respective freezing points;
d) from the drainage of cold dense brine from sea ice into the underlying water.

The first mechanism has been frequently observed and studied under both natural and laboratory conditions (Reimnitz and Kempema, 1987; Ushio and Wakatsuchi, 1993). Obviously it is an important mechanism in both Arctic and Antarctic seas. The second mechanism is not typical under Arctic conditions, because of the absence of deep ice shelves and the presence of strong density stratification that prevents upwelling of deep waters to the surface. The third and fourth mechanisms are governed by the effects of double diffusion of heat and salt (Turner, 1973). While the last one influences only ice stalactites growth (Martin, 1981), the third one is expected to be widespread in most Arctic seas where a low saline upper water layer is maintained due to strong river runoff. In spite of many observations (Cherepanov, 1972; Timokhov, 1989), it is still a question, how intensive is the frazil ice production in the contact zone between fresh and salt water under natural conditions? Does it contribute significantly to Arctic ice production and what is its impact on the Arctic marine environment?

Typically, the temperature of the low saline, or fresh, river water during the cold season in the Arctic is close to the freezing point. Entering the ice-covered sea, fresh mwater spreads

This document is provided by JAXA.

over the surface of much colder saline water and a two-layer system with sharp density interface is formed.

Due to the influence of the molecular transfer properties (the molecular coefficient of the heat transfer is two orders higher than the coefficient of salt diffusivity), the heat exchange across such an interface may be much more effective compared to that of salt. Taking into account the approximately linear dependence of the freezing temperature of the sea water on salinity it is easy to consider that in such circumstances the upper fresh water layer should be supercooled from below. The rate of supercooling and thus, frazil ice formation strongly depends on the heat and salt fluxes across the density interface.

The laboratory experiments by Martin and Kauffman (1974) have shown that in the absence of mechanically generated turbulence the basic mechanism of heat and salt transfer between the fresh and salt water layers is double-diffusive convection in the "diffusive" mode. Because of the very large density step across the density interface, the stability parameter $R=b(S''-S')/a(T''-T')$ is more than 100 or even 200, where a and b are the coefficients of thermal and salt expansion of sea water, T', S' and T'', S''—the temperature and salinity of the upper and lower layers, respectively. It was show by McClimans *et al.* (1978) and Stigebrandt (1981) that in such cases the convection process is very weak. The rates of heat and salt transfer are close to molecular and typical rates of frazil ice formation under the most favourable conditions are not more than a few millimeters per day. This means that a slush ice layer with the thickness about few millimetres may be formed during one day. Moreover, freezing decreases with time due to the thickening of the density interface. Similar laboratory results and theoretical estimates were obtained by McClimans *et al.* (1978), Stigebrandt (1981) and Krylov, (1989). In natural conditions the density interface is usually thicker than in laboratory conditions, so, the rate of supercooling and frazil ice formation due to quasi-molecular heat exchange between the fresh and salt water layers in polar seas is expected to be negligible.

However, it was discovered in a laboratory experiment by Zatsepin and Krylov (1987) that the rate of frazil ice formation considerably increases if the contacting layers of fresh and salt water are turbulently stirred. Subsequently a laboratory investigation of the process of heat and salt exchange across a density interface between fresh and salt layers stirred by vertically oscillating grids was carried out at room temperature (Krylov and Zatsepin, 1992). It was found that moderate turbulent stirring of the layers greatly enhances the heat and salt fluxes between the layers, but still some difference in the effective coefficients of heat and salt exchange remains for the ranges of the main non-dimensional parameters investigated (typical for natural conditions). Estimates based on the experimental results have shown that the rate of freezing in the presence of turbulence in the contacting layers may range from a centimetre up to a meter per day. So, it may be two orders of magnitude greater than in the case of pure double diffusion and as high as in open leads and polynyas!

Later Voropayev *et al.* (1995) carried out an analogous experiment in a tank filled with two layers of water: fresh water at 0℃ in the upper layer and salty (35 psu) cold water at temperature −1.9℃. The tank was placed in a large walk-in freezer at a temperature near 0℃. The turbulence induced in both layers enhanced the transport of heat across the sharp pycnocline between the layers. As time progressed the pycnocline and lower boundary of the upper layer became supercooled and small crystals of frazil ice were rapidly formed in the supercooled zone. These buoyant crystals rose to the surface and with time a sheet of

This document is provided by JAXA.

slush ice was formed at the surface of the fresh water. The rate of frazil ice formation (the thickness of the slush frazil ice layer, formed in a unit time interval) was consistent with estimates by Krylov and Zatsepin (1992).

Recent field studies performed in the Transdrift-IV expedition near the delta of the Lena river in the Laptev Sea during the flood period (late May–mid of June) give new evidence of intensive frazil ice formation in the contact zone between the fresh river and cold saline water layers. Temperatures of both the upper quasi-fresh and lower saline layers were close (within 0.1℃) to the freezing point. CTD data have revealed the presence of supercooled water layers 0.05–1.5 m thick in the pycnocline between the layers. The supercooling value was as much as 0.8℃! Both layers were in a turbulent state of motion. Although the turbulence characteristics were not measured, they were estimated on the basis of semi-empirical turbulence theory (Phillips, 1977). Thus, we obtained an estimate of the integral lengthscale L of turbulence and its mean-square velocity scale U^* using the expressions $L=kH$, $U^*=kU$, where H is the thickness of the layer, U — the scale of the mean horizontal velocity in the layer and $k\sim0.1$ — the empirical coefficient. The thicknesses of the layers were estimated from the CTD data. The scale of mean horizontal velocity produced by the river flood in the upper layer was taken as $U'=10$–50 cm/s, while the scale of mean horizontal velocity $U''=2$–10 cm/s for the lower layer was taken as typical for tidal motion in the Laptev Sea. On the basis of semi-empirical formulas from laboratory studies of frazil ice formation, similarity analysis and *in situ* data, the possible rates of frazil ice formation in the river/sea water contact zone were estimated for different stages of the seasonal flood near the mouth region of the Lena river. The calculated thickness of the frazil ice layer changed from a few centimeters per day during the period prior to the flood up to more than meter per day during the flood peak. The average porosity of the slush frazil ice layer (the ratio of the mass of the ice crystals to the sum of ice crystals mass and the mass of water, trapped between them) was taken equal to 0.3 for these calculations.

Of course, the application of laboratory results for estimating rates of frazil ice formation under natural conditions can cause justified criticism. However, such high rates of frazil ice formation in the Laptev Sea fresh/sea water contact zone during the flood period do not necessarily contribute to the increase of surface ice thickness. For almost all of the CTD stations the temperature of the upper layer was slightly higher than the freezing point, so frazil ice rising from the pycnocline to the surface should be completely melted. But in winter historical hydrology data have shown, that for about 40% of the Laptev Sea area the upper layer temperature was equal or below the freezing point (Golovin *et al.*, 2000)! So, it is reasonable to suspect that frazil ice formed at the fresh/saline water contact zone may significantly contribute to the Arctic ice cover during the cold season.

However, there is direct evidence of intensive ice formation at the pycnocline level during the flood period in the Laptev Sea. At one of the stations near the Lena river delta a conglomerate of the frazil ice was found attached to a cable at the depth of the upper pycnocline part. Its weight was about 1.5–2 kg and its height — about 0.6 m. It consisted of transparent chaotically oriented crystals of frazil ice within which inclusions of sediments transported by river water were clearly seen. The cable in this case served both as a nucleus and a place where the frazil ice crystals were trapped.

The frazil ice formation mechanism plays a significant role in sediment transport to the surface of both fast and drifting ice. Laboratory experiments have shown (Reimintz *et al.*,

This document is provided by JAXA.

1993) that the concentration of sediments in frazil ice may be much higher than the concentration of suspended sediments in river water. The enrichment of frazil ice by sediments is achieved due to the scavenging action by frazil ice flocs through mechanical trapping of both biological and terrigenous matter suspended in the water. This fact was experimentally recorded during the Transdrift-IV expedition. The concentration of the suspended matter in the frazil ice agglomeration attached to the cable was 60 times higher than in river water (Golovin *et al.*, 1999).

During production, growth and rising through the water column, frazil ice entraps sediments transported by river water. When rising to the surface, frazil ice crystals can be incorporated into the surface ice layer if the temperature of the upper fresh layer is equal to or below the freezing point. This condition is generally fulfilled in cold season, so the frazil ice production in the fresh/salt water contact zone should be suspected as one of the important sources of sediment incorporation into the Arctic ice cover. It may significantly contribute to the long-range transport of sediments in the Transpolar Ice Drift (Golovin *et al.*, 2000).

Acknowledgments

This work was partly supported by the Russian Ministry of Science and Technology and by the German Ministry of Education, Science Research and Technology.

References

Cherepanov, N.V. (1972): Systematic of crystal ice structures in the Arctic. Probl. Arktiki Antarkt., **40**, 78–83 (in Russian).

Golovin, P.N., Dmitrenko, I.A., Kassens, H. and Holemann, J.A. (1999): Frazil ice formation during the spring flood and its role in transport of sediments to the ice cover. Land-ocean Systems in the Siberian Arctic, ed. by H. Kassens *et al.* Berlin, Springer, 125–140.

Golovin, P.N., Dmitrenko, I.A., Kassens, H. and Holemann, J.A. (2000): Frazil ice formation along the upper boundary of the seasonal pycnocline and its role in glacial marine sedimentation in Arctic seas (using the Laptev Sea as an example). Dokl. Earth Sci., MAIK Nauka, **370**, 237–242 (in Russian).

Krylov A.D. (1992): On double-diffusive underwater freezing. Vestn. Mosk. Univ., **3**(30), 92–94 (in Russian).

Krylov A.D. and Zatsepin A.G. (1992): Frazil ice formation due to difference in heat and salt exchange across a density interface. J. Mar. Syst., **3**, 497–506.

Martin, S. (1981): Frazil ice in rivers and oceans. Ann. Rev. Fluid Mech., **13**, 379–397.

Martin, S. and Kauffman, P. (1974): Evolution of the under ice melt ponds, or double diffusion at the freezing point. J. Fluid Mech., **64**, 507–527.

McClimans, T.A., Steen, C.E. and Kjeldgaard, G. (1978): Ice formation in fresh water cooled by a more saline sublayer. Proc. IAMR. Symp. Ice Problems, **2**, 331–336.

Phillips, O.M. (1977): The Dynamics of the Upper Ocean. Cambridge University Press, 380 p.

Reimnitz, E. and Kempema, E.W. (1987): Field observations of slush ice generated during freeze-up in Arctic coastal waters. Mar. Geol., **77**, 219–231.

Reimnitz, E., Clayton, J.R., Kempema, E.W., Payne, J.R. and Weber, W.S. (1993): Interaction of rising frazil with suspended particles: tank experiments with applications to nature. Cold Reg. Sci. Technol., **21**, 117–135.

Stigebrandt, A. (1981): On the rate of ice formation in water cooled by a more saline sublayer. Tellus, **33**, 604–609.

Timokhov, L.A., ed. (1989): Vertical Structure and Dynamics of the Sub-ice Layer of the Ocean.

This document is provided by JAXA.

Leningrad, Gidrometeoizdat, 141 p. (in Russian).
Turner, J.S. (1973): Buoyancy Effects in Fluids. Cambridge Univ. Press, 367 p.
Ushio, S. and Wakatsuchi, M. (1993): A laboratory study on supercooling and frazil ice production processes in winter coastal polynyas. J. Geophys. Res., **98**, 20321–20328.
Voropaev, S.I., Fernando, H. and Mitchell, L. (1995): On the rate of frazil ice formation in polar regions in the presence of turbulence. J. Phys. Oceanogr., **25**, 1441–1450.
Weeks, W. and Ackley, S. (1982): The growth, structure, and properties of sea ice. CRREL, Monogr., **82-1**, 130 p.
Zatsepin, A.G. and Krylov, A.D. (1987): Underwater ice formation due to double-diffusion of heat and salt. Proc. III Congr. of Soviet Oceanogr., Phys. and Chem. of the Ocean, Polar and Regional Studies, Leningrad, 65–66 (in Russian).

(Received June 7, 2000; Revised manuscript accepted August 8, 2000)

This document is provided by JAXA.

This document is provided by JAXA.

Mem. Natl Inst. Polar Res., Spec. Issue, 54, 423-428, 2001

Scientific note

Stable isotope compositions of arctic copepods in the Greenland Sea in winter

Hiroshi Sasaki, Daisuke Kawai and Megumi Sato

Department of Biotechnology, Senshu University of Ishinomaki, Ishinomaki 986-8580

Abstract: Natural abundances of stable isotopes ($\delta^{13}C$ and $\delta^{15}N$) were measured in copepods collected in the Greenland Sea in January 1999. Standing stocks of zooplankton dominated by copepods in the upper 200 m varied among 12 stations and marked zooplankton increases at 4 stations (>10 mg-dry weight m^{-3}) were observed around the marginal ice zone, although surface chlorophyll *a* concentrations at all stations were nearly zero. The isotopic compositions of copepods varied in the ranges of $-22.2‰ \sim -20.6‰$ in $\delta^{13}C$ and of 8.2‰–12.2‰ in $\delta^{15}N$, which were comparable with those collected in other polar waters. The enrichment factors (difference in $\delta^{15}N$ between copepods and POM) of about 3.2 suggest possible linkage between winter copepods and winter POM without algal populations.

1. Introduction

Information on the life of pelagic zooplankton, including copepods, in arctic and subarctic waters during winter has been limited, particularly for populations inhabiting seasonally ice-covered and marginal ice zones (MIZ). In the Antarctic Ocean, a considerable amount of calanoid and harpacticoid copepods were observed under the fast ice in Lützow-Holm Bay during winter (*e.g.* Tanimura *et al.*, 1984, 1996). Many Antarctic krill (*Euphausia superba*) were also collected using a light-trap under the fast ice in austral winter (Kawaguchi *et al.*, 1986). Nishino and Kawamura (1994) examined the foregut contents of Antarctic krill collected in the South Georgia area in winter to evaluate feeding habits related to overwintering strategy and emphasized their possible carnivorous feedings during winter.

The natural abundance of C and N stable isotopes can be useful in examining sources of these elements to consumers (*e.g.* Wada *et al.*, 1987). These isotope ratios in animals are generally related to those in their diets (DeNiro and Epstein, 1981). The stable nitrogen isotopic ratio ($\delta^{15}N$) of consumers is systematically heavier than those of their diets (Minagawa and Wada, 1984; Wada and Hattori, 1991). There have been some reports of stable isotope measurements from polar marine food web studies. Geographic gradients in stable carbon isotope ratios ($\delta^{13}C$) of arctic zooplankton have been observed in the Bering, Chukchi and Beaufort Seas (Dunton *et al.*, 1989; Saupe *et al.*, 1989). Causes of these geographic variations might be a consequence of the intrusion of different water masses including ^{13}C-depleted carbon (Dunton *et al.*, 1989; Saupe *et al.*, 1989). Frazer (1996)

This document is provided by JAXA.

reported that larval krill (*E. superba*) collected around the Antarctic Peninsula in early winter were depleted in ^{15}N (< 1‰), primarily because of their herbivorous feeding on ice-associated food sources. Although the reported isotope values were quite variable, these data provide primary information on the lives of arctic and antarctic zooplankton in winter. Further investigations will have to focus on the overwintering mechanisms of these animals.

We present here preliminary data on $\delta^{15}N$ and $\delta^{13}C$ values of arctic copepods collected in the Greenland Sea in January 1999, and evaluate the use of these values as indicators of copepod food sources during winter.

2. Materials and methods

Samples were collected from 12 stations located in the Greenland Sea and southwest Barents Sea in January 1999 during the R/V Ivan Petrov Cruise. Zooplankton samples were obtained using a NORPAC net (North Pacific Standard net; 180 cm in length and 0.3 mm in mesh size) in the upper 200 m of the water column. Each sample was preserved with formalin and divided into two aliquots, one for dry weight measurements (60℃, 12 hours) and the other for stable isotope determinations and microscopic observations. The present study does not consider the microscopic observations of zooplankton. Routine oceanographic surveys were made using a CTD/RMS for water temperature and salinity measurements, and water sampling. One liter of seawater was filtered through a GF/F glass fiber filter for determinations of chlorophyll pigments.

Copepods were recovered from net-collected samples and were washed of detritus before analysis. Since most copepods were smaller than 4 mm long, approximately same sized-individuals were pooled to obtain sufficient material for isotopic analysis. One sample consisted of at least 5 individuals (350 μg to 2 mg in dry weight). Each sample with copepods was exposed to chloroform methanol solution for removing lipids and was dried in an aluminum dish at 60℃ for 12 hours. They were used for determinations of carbon and nitrogen stable isotopic compositions using an ANCA/GSL mass spectrometer (Europa Scientific Ltd). Results were expressed as conventional $\delta^{13}C$ or $\delta^{15}N$ values, where the ratio of the sample is compared to that of a standard,

$$\delta X(‰) = \{(R_{\text{sample}}/R_{\text{standard}}) - 1\} \times 1000.$$

X is ^{13}C or ^{15}N and R is $^{13}C/^{12}C$ or $^{15}N/^{14}N$. Standards were calibrated by PDB and atmospheric nitrogen. L-alanine ($\delta^{13}C = -21.5‰$, $\delta^{15}N = -5.3‰$) was used as a running standard for isotopic measurements. The reproducibility for one standard deviation was $\pm 0.1‰$ for $\delta^{13}C$ and $\pm 0.3‰$ for $\delta^{15}N$, respectively.

3. Results and discussion

Surface water temperature was warmer than 5℃ in the southwest Barents Sea located north of Norway (Sts. 1, 2, 3 and 4) and lower than 0℃ in the area west of Spitsbergen (Sts. 11, 8 and N4), where the sea surface was partly covered with ice (Table 1). The MIZ and packed ice zones were characterized by low salinity water (< 34.5 psu) (Table 1). All chlorophyll *a* concentrations observed in the upper 100 m were less than 0.01 mg m^{-3} (Table 1), indicating scarcely distributed phytoplankton as well as ice-associated algae

This document is provided by JAXA.

Table 1. Location, temperature and salinity of surface water, concentrations of chlorophyll a (0–100 m), and averaged zooplankton standing stocks (0–200 m). Stable carbon and nitrogen values of copepods collected in the upper 200 m layers. Numbers in parenthesis indicates standard deviation.

Station	Latitude (N)	Longitude (E)	Temp. (°C)	Sal. (PSU)	Chlorophyll *a* (mg m^{-3})	Zooplankton (mg m^{-3})	$\delta^{13}C$ (‰)	$\delta^{15}N$ (‰)
St. 1	71:00	17:59	6.21	34.52	<0.01	4.71	−22.2	11.9
St. 2	72:00	17:59	6.36	35.11	<0.01	0.12	−21.6	12.2
St. 3	72:59	17:59	6.2	35.15	<0.01	1.31	−21.5	9.4
St. 4	73:59	17:59	5.72	35.15	<0.01	8.28	−20.6	9.9
St. 5	74:59	17:59	1.31	34.83	<0.01	6.42	−20.8	11.0
St. X5	76:59	12:49	4.6	35.12	<0.01	9.25	−20.6	10.7
St. 11	78:00	2:29	−1.63	34.26	<0.01	5.15	−21.6	9.2
St. 10	78:58	0:27	3.4	34.87	<0.01	15.81	−21.5	8.2
St. 8	79:00	4:58	−1.77	33.84	<0.01	8.58	−21.7	8.8
St. N4	79:59	0:00	−1.69	34.16	<0.01	32.23	−21.4	9.0
St. N2	80:00	4:58	2.44	35	<0.01	14.23	−21.0	9.8
St. X10	80:57	4:11	0.84	34.96	<0.01	12.06	−21.4	9.5
Mean						9.85	−21.3	9.9
Std						(8.49)	(0.5)	(1.3)

derived from floating ice in this region in winter.

Averaged zooplankton standing stocks in the upper 200 m water column were relatively lower in the sea north of Norway (< 5 mg m^{-3}) compared with those in coastal areas west of Spitsbergen (> 5 mg mm^{-3}). In the northern-most stations around the MIZ (Sts. 10, N4, N2 and X10), marked increases of zooplankton were observed (> 10 mg m^{-3}). Collected zooplankton were dominated by calanoid copepods. The meso-zooplankton (> 180 μm in length) standing stocks in late summer and early fall varied interannually in the range of 1.5 to 20 g-dry weight m^{-2} in the Barents Sea (Skjoldal *et al.*, 1987). The largest zooplankton standing stock of this study obtained at St. N4 (32.23 mg m^{-3}) can be calculated as a depth-integrated value (0–200 m) of 3.16 g-dry weight m^{-2}, which was comparable with those found in summer-fall periods (Skjoldal *et al.*, 1987). Copepods were abundant in the winter Greenland Sea, although the concentration varied among stations.

The isotopic compositions of copepods collected in the present study varied in the range of −22.2‰~−20.6‰ in $\delta^{13}C$ values and of 8.2‰–12.2‰ in $\delta^{15}N$ values (Table 1). The $\delta^{13}C$ data were primarily comparable with those ranging from −22.8‰ to −20.9‰ collected in the northern Bering, Chukchi and western Alaskan Beaufort Seas during June–October (Saupe *et al.*, 1989). However, copepods sampled in the eastern Alaskan Beaufort and Canadian Beaufort Seas in June–October were relatively depleted in ^{13}C (−26.7‰~−24.6‰) (Saupe *et al.*, 1989). These variations were probably caused by recycling of ^{13}C-depleted carbon associated with the intrusion of upwelled waters in the southeastern Beaufort Sea (Dunton *et al.*, 1989; Saupe *et al.*, 1989). The geographical variation in $\delta^{13}C$ values seems to be more pronounced than the seasonal difference in $\delta^{13}C$ values. The relatively small geographic variation of $\delta^{13}C$ values obtained in this study (Table 1) indicated that there was less evidence for different carbon sources to copepods. Goericke

This document is provided by JAXA.

and Fry (1994) showed that $\delta^{13}C$ values of POM (particulate organic matter dominated by phytoplankton) using historical data vary weakly with temperature in the world ocean, although large deviations were observed, especially at high latitude, primarily due to disequilibrium of CO_2 concentrations in the atmosphere and surface waters. No marked relationship between $\delta^{13}C$ values and surface water temperature was recognized within the relatively restricted sea areas of the present study (Table 1).

Although little is known about isotopic compositions of arctic copepods in winter, $\delta^{15}N$ values of *Calanus* spp. (11.4±0.1‰) collected in the western Beaufort Sea in February (Dunton *et al.*, 1989) generally agreed with those from the present Norwegian coastal stations (Sts. 1 and 2, Table 1). Hobson *et al.* (1996) collected many animal samples including copepods in the Northeast Water (NEW) polynya off northeast Greenland in June-July and used their isotope data to evaluate linkages between pelagic and benthic ecosystems. Based on the $\delta^{15}N$ enrichment factor (difference in $\delta^{15}N$ between prey and predator) of +3.8‰ (Hobson and Welch, 1992), they suggested the existence a direct pathway from POM with less ice algae to two dominant calanoid species (*Calanus hyperboreus* and *C. gracilis*) having $\delta^{15}N$ values in the range of 7 to 9‰ (Hobson *et al.*, 1996). It was supported by the comparison of $\delta^{13}C$ values between POM (*ca.* −28‰) and ice algae (*ca.* −18.5‰), the last of which were more enriched than those of copepod grazers (*ca.* −22.5‰) (Hobson *et al.*, 1996).

Comparative POM isotope data collected during the present cruise (Sato *et al.*, in preparation) were variable but were depleted in ^{15}N (6.7±1.6‰) relative to those of copepods (9.9±1.3‰, Table 1). An enrichment factor was also reported by Wada and Hattori (1991) as 3.4±1.1‰. If the enrichment factors (Wada and Hattori, 1991; Hobson and Welch, 1992) can be applied to copepods in the Greenland Sea, the present enrichment value of +3.2 seemed to be the linkage between winter copepods and winter POM. No marked occurrence of phytoplankton (Table 1) and microheterotrophs (unpublished data) was found in sea water where zooplankton abundance increased. Thus these copepods might possibly be detritivorous.

Frazer (1996) reported isotopic compositions of larval krill (*Euphausia superba*) collected in winter along the west coast of the Antarctic Peninsula. The krill larvae in winter were generally enriched in ^{13}C (>−27‰) and depleted in ^{15}N (<1‰) relative to those in summer months (Frazer, 1996). Frazer (1996) also showed that the isotopic compositions of larval krill in early winter ($\delta^{13}C$: −24.9‰±0.9, $\delta^{15}N$: 2.7±0.2) did not differ from those in late winter ($\delta^{13}C$: −24.7±0.9, $\delta^{15}N$: 3.3±0.7), while the compositions of POM sampled in early winter ($\delta^{13}C$: −20.9±0.0, $\delta^{15}N$: −1.0±0.1) significantly differed from those in late winter ($\delta^{13}C$: −32.0±1.4, $\delta^{15}N$: 6.35±0.1) (Frazer, 1996). This suggested that seasonal shifts in isotopic compositions of larval krill did not result from changes in their diets and they could be primarily herbivorous prior to winter (Frazer, 1996). In contrast, foregut contents of krill collected in the South Georgia area during austral winter consisted of various fragments of crustacean zooplankton observed by detailed microscopic studies, indicating the existence of alternative carnivorous or detritivorous feeding modes (Nishino and Kawamura, 1994).

Our results show the possible utility of stable carbon and nitrogen isotope ratios in ecological studies on copepods. Although mechanisms that can alter isotopic compositions of copepods other than diets and overwintering behavior of arctic copepods in winter

This document is provided by JAXA.

remain uncertain because of insufficient data available, the enrichment value in $\delta^{15}N$ obtained in this study suggested the possibility of alternative detritivorous feeding of copepods during winter. Further information on isotopic variations of copepods and their food sources can provide insight into understanding and interpreting the feeding ecology related to overwintering strategies of arctic copepods.

Acknowledgments

We are grateful to Dr. H. Itoh for giving us the opportunity for this research, and also to the captain and crew of the R/V Ivan Petrov for their help on board. Thanks are extended to Ms. S. Yamamoto for providing us water samples collected in the Greenland Sea. This work was supported by the Ministry of Science and Education, Japan (No. 10041216).

References

DeNiro, M.J. and Epstein, S. (1981): Influence of diet on the distribution of nitrogen isotopes in animals. Geochim. Cosmochim. Acta., **45**, 341–351.

Dunton, K.H., Saupe, S.M., Golikov, A.N., Schell, D.M. and Schonberg, S.V. (1989): Trophic relationships and isotopic gradients among arctic and subarctic marine fauna. Mar. Ecol. Prog. Ser., **56**, 89–97.

Frazer, T.K. (1996): Stable isotope composition ($\delta^{13}C$, $\delta^{15}N$) of larval krill, *Euphausia superba*, and two of its potential food sources in winter. J. Plankton Res., **18**, 1412–1426.

Goericke, R. and Fry, B. (1994): Variations of marine plankton $\delta^{13}C$ with latitude, temperature, and dissolved CO_2 in the world ocean. Global Biogeochem. Cycles, **8**, 85–90.

Hobson, K.A. and Welch, H.E. (1992): Determination of trophic relationships within a high Arctic marine food web using $\delta^{13}C$ and $\delta^{15}N$ analysis. Mar. Ecol. Prog. Ser., **84**, 9–18.

Hobson, K.A., Ambrose, W.G., Jr. and Renaud, P.E. (1996): Sources of primary production, benthic-pelagic coupling, and trophic relationships within the Northeast Water Polynya: insights from $\delta^{13}C$ and $\delta^{15}N$ analysis. Mar. Ecol. Prog. Ser., **128**, 1–10.

Kawaguchi, K., Ishikawa, S. and Matsuda, O. (1986): The overwintering strategy of Antarctic krill (*Euphausia superba*) under the coastal fast ice off the Ongul Islands in Lützow-Holm Bay, Antarctica. Mem. Natl Inst. Polar Res., Spec. Issue, **44**, 67–85.

Minagawa, M. and Wada, E. (1984): Stepwise enrichment of ^{15}N along food chains: Further evidence and the relation between $\delta^{15}N$ and animal age. Deep-Sea Res., **48**, 1135–1140.

Nishino, Y. and Kawamura, A. (1994): Winter gut contents of Antarctic krill (*Euphausia superba* Dana) collected in the South Georgia area. Proc. NIPR Symp. Polar Biol., **7**, 82–90.

Saupe, S.M., Schell, D.M. and Griffiths, W.B. (1989): Carbon-isotope ratio gradients in western arctic zooplankton. Mar. Biol., **103**, 427–432.

Skjoldal, H.R., Hassel, A., Rey, F. and Loeng, H. (1987): Spring phytoplankton development and zooplankton reproduction in the central Barents Sea in the period 1979–1984. The Effect of Oceanographic Conditions on Distribution and Population Dynamics of Commercial Fish Stocks in the Barents Sea; Proc. 3rd Soviet-Norwegian Symp., ed. by H. Loeng. Bergen, Inst. Mar. Res., 59–90.

Tanimura, A., Fukuchi, M. and Ohtsuka, H. (1984): Occurrence and age composition of *Paralabidocera antarctica* (Calanoida, Copepoda) under the fast ice near Syowa Station, Antarctica. Mem. Natl Inst. Polar Res., Spec. Issue, **32**, 81–86.

Tanimura, A., Hoshiai, T. and Fukuchi, M. (1996): The life cycle strategy of the ice-associated copepod, *Paralabidocera antarctica* (Calanoida, Copepoda), at Syowa Station, Antarctica. Antarct. Sci., **8**, 257–266.

Wada, E., Terazaki, M., Kabaya, Y. and Nemoto, T. (1987): ^{15}N and ^{13}C abundances in the Antarctic

This document is provided by JAXA.

Ocean with emphasis on the biogeochemical structure of the food web. Deep-Sea Res., 34, 829–841.
Wada, E. and Hattori, A. (1991): Nitrogen in the Sea: Forms, Abundances and Rate Processes. Boca Raton, CRC Press, 208 p.

(Received April 17, 2000; Revised manuscript accepted August 1, 2000)

This document is provided by JAXA.

Mem. Natl Inst. Polar Res., Spec. Issue, 54, 429–436, 2001

Scientific note

Personal ultraviolet-B dosimetry at Koldewey-Station by using an electronic dosimeter ELUV-14

Saad El Naggar, Hartwig Gernandt, Nicole Spelten and Andrew Klaas

Alfred-Wegener-Institute for Polar and Marine Research (AWI), Columbus-Str., D-27568 Bremerhaven, Germany

Abstract: Personal exposure of ultraviolet-B irradiance (UV-B) was measured by small portable dosimeter (ELUV-14) at Koldewey-Station in Ny-Ålesund, from May 15 to August 15, 1999. While ten persons carried those dosimeters global irradiance was simultaneously measured by a UV-B spectral radiometer. The highest erythemal weighted global UV-B dose was 2200 J/m^2 recorded on June 8, 1999. The personal related maximum value was about 345 J/m^2 on May 25, 1999. This correponds to approximately 23% of the global dose recorded at the same day.

1. Introduction

Due to the ozone depletion during the last decades (*e.g.*, WMO, 1995; Bojkov *et al.*, 1990, 1995), increased concern has been given to the changes in the ultraviolet-B (UV-B) solar radiation reaching the earth surface (*e.g.*, Booth and Mardonich, 1994; Karsten *et al.*, 1999; Krzyscin, 2000; Seckmeyer *et al.*, 1995; McKenzie *et al.*, 1991). Since 1994 a personal dosimetry programme has been performed at Neumayer-Station (70°39′S; 08°15′W) to quantify the impacts of the UV-B radiation on human beings in Antarctica. During the summer season 1999, these studies were extended to Koldewey Station (78°56′N; 11°57′E) to quantify the range of personal related doses at Arctic latitudes for the first time.

Personal UV-B doses were measured with the dosimeter ELUV-14 (El Naggar *et al.*, 1995) from May 15 to August 15, 1999. Ten persons carried dosimeters as badges during outdoor activities. Simultaneously, global UV-B irradiance was continuously measured by a UV-B spectral radiometer (Groß, 1998; Groß *et al.*, 1998, 2001) and by a horizontally mounted dosimeter ELUV-14.

The obtained irradiance data were used to determine the global and the individual UV-B doses. Further evalution was focused on assessing a risk factor for Koldewey-Station by comparison of the measured irradiance to a reference. The reference here is set to be the maximum irradiance reaching the earth surface at sea level at a solar elevation of 90° measured at the Equator on June 8, 1998 (23°N; 17.75°W) using the same instrumentation.

2. Instrumentation and data processing

The UV-B spectral radiometer consists of a Bentham DM 150 double monochromator. A photon counting Micro-Channel Plate (MCP) is used as array detector. The MCP

This document is provided by JAXA.

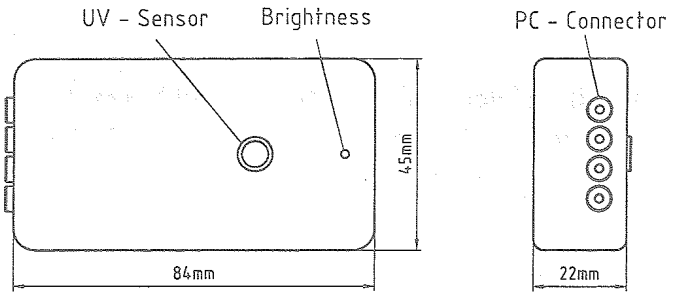


Fig. 1. A drawing of the ELUV-14 dosimeter illustrating size and position of sensors.

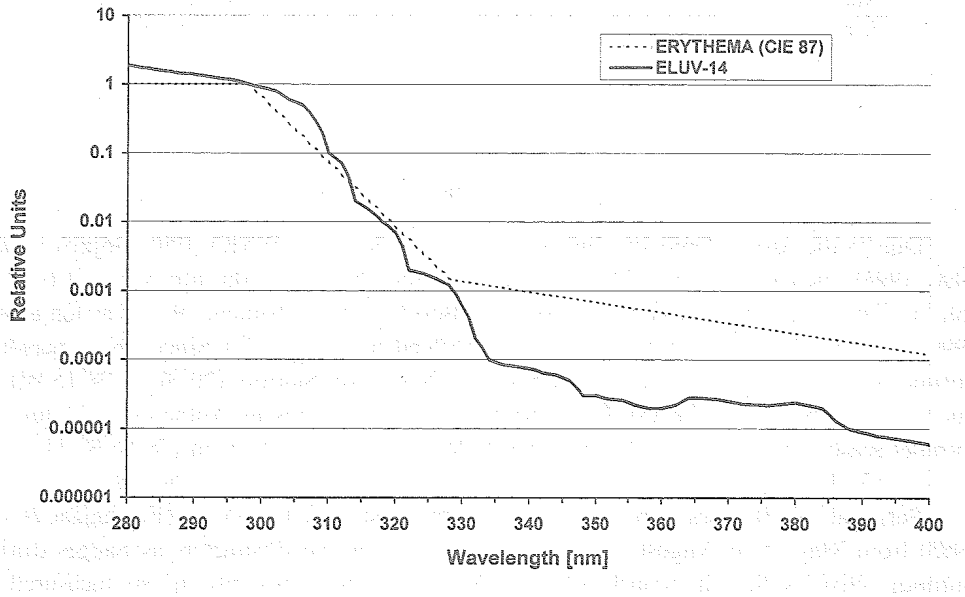


Fig. 2. Spectral sensitivity of the ELUV-14 dosimeter (solid line) and the standard erythemal spectra CIE 87 (dashed line).

consists of 32 channels. UV-B spectra are recorded in the wavelength range between 285 nm and 323 nm every 5 min. These irradiance data were used to calculate the unweighted, ELUV-14 and erythemal weighted global UV-B irradiances and doses. The ELUV-14 is a small robust waterproof 3-channel datalogger equipped with a special UV-B sensor, a Pt-100 temperature sensor, and a silicon photodiode as brightness sensor. It was designed as a personal outdoor dosimeter of size $82 \times 45 \times 22$ mm and a weight of 95 g including the lithium battery (Fig. 1). The UV-B sensor had a relative spectral sensitivity similar to the standard erythemal spectrum (McKinlay *et al.*, 1987). In Fig. 2 the spectral sensitivities are compared to relative units for the ELUV-14 dosimeter and the standard spectral erythemal response. Because of the good coincidence in the spectral range between 280 nm and 330

This document is provided by JAXA.

Table 1. Technical data of the UV-B dosimeter ELUV-14.

UV-weighted irradiance:	The dosimeter provides an UV-B irradiance weighted by ELUV-14 response function in mW/m^2. The ratio between by ELUV-14 measured irradiance and the erythemal weighted irradiance, derived from high resolution spectra (integrated from 290 - 322 nm) varies between **1.2** and **1.6** and is mainly a function of solar elevation and ozone.
Spectral range:	240...380 nm
Sensor sensitivity (max. at 280 nm):	3 $\mu W/m^2$ (typ.)
Measuring range: (normal): (extended):	$0 \sim 160$ mW/m^2 (typ.) $0 \sim 3.1$ W/m^2 (typ.)
Accuracy:	5%
Visible irradiance:	
Spectral range:	530...1020 nm
Sensor sensitivity (max. at 280 nm):	170 $\mu W/m^2$ (typ.)
Measuring range:	20 W/m^2 (typ.)
Temperature:	
Sensor:	PT-100
Range:	-55 °C...+50 °C
Resolution:	0.05 K
Accuracy:	0.5 K
Common parameters:	
Basic Sampling Rate (BSR):	programmable; 1..250 min, in 1 min steps for all input channels
Individual sampling rate:	1..250 min for each channel
Storage capacity:	512 KB
Autonomous operatio:	30 days (BSR = 1 min for all channels)
Battery:	Lithium, 2/3AA
Operation temperature:	- 40 °C .. +50 °C
Storage temperature:	-55 °C .. +70 °C
Size:	84*45*22 mm
Weight including battery	95 g
Housing:	PVC , waterproof
Data out:	ASCII, Microsoft EXCEL compatible
PC interface (with adaptor):	serial (RS-232)

nm, the ELUV-14 dosimeter can be used for erythemal weighted dosimetry.

The basic sampling rate is one minute and could be set up to 255 min. The storage capacity at a sampling rate of 1 min is about 30 days using a Flash Eprom Memory. System settings and data read out are controlled by a PC program running under MS Windows and using an RS-232 serial ASCII-spreadsheet data transfer. A special adaptor connects the dosimeter to the PC. Technical data of the ELUV-14 dosimeter are given in Table 1.

During the Arctic campaign, UV-B spectral radiometer and ELUV-14 data were permanently recorded.

The high resolution spectral radiometer data were used to derive weighted UV-B-irradiances by weighting the spectral data by the corresponding response function (ELUV-14, erythema) and integrating in the spectral range between 290 and 322 nm. Those

This document is provided by JAXA.

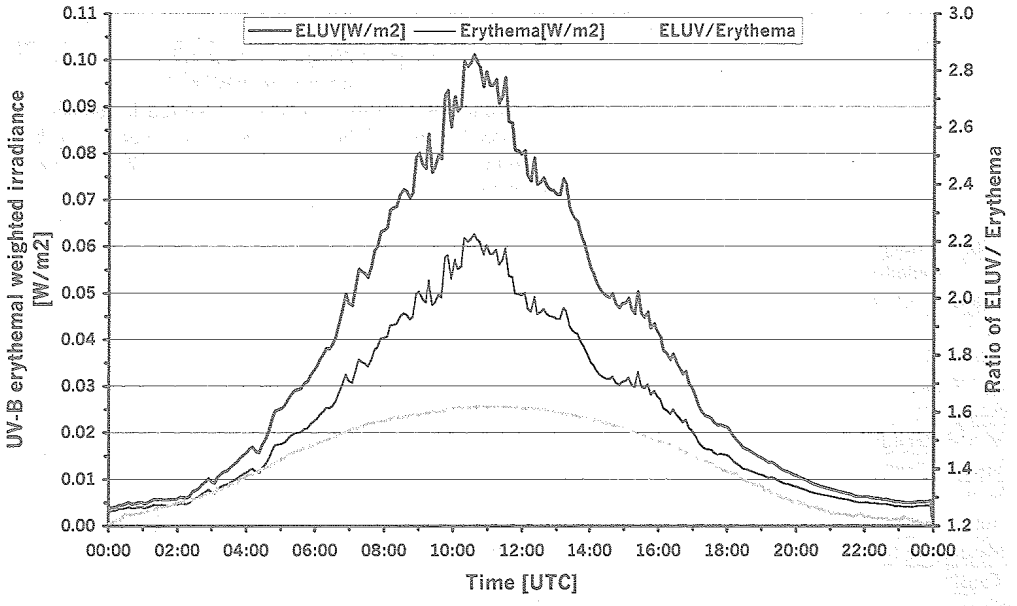


Fig. 3. Diurnal variation of ELUV-14 (bold line) and erythemal (thin line) weighted UV-B irradiances derived from spectral radiometer data recorded at Koldewey-Station on June 8, 1999. The ratio ELUV-14/Erythema (lower curve) is the transformation function between both weighted irradiances for this day.

weighted irradiances were used to calibrate the dosimeter.

The ELUV-14 weighted irradiance derived from spectrometer data in mW/m^2 was compared to the by ELUV-14 dosimeter directly measured irradiance at the same time and location. The ratio of those two irradiances yields the constant calibration factor of the dosimeter. The maximum relative error is about 5%.

Due to the fact that the spectral response of the dosimeter and that of the erythema are only similar but not equal (Fig. 2), a deviation between both weighted irradiances of the same day is expected. Comparison of both weighted irradiances derived from spectral data yields the transformation function between both weighted irradiances. This was calculated for each day. As an example, this comparison and the transformation function are shown in Fig. 3 for June 8, 1999. The ratio of the irradiances varies between 1.2 and 1.6 and is mainly a function of solar elevation and ozone.

The transformation of by ELUV-14 directly measured irradiance (ELUV-14 weighted) to the erythemal weighted irradiance was retrieved in post-processing according the derived transformation function of the same day.

The comparison shows that the small mobile ELUV-14 dosimeter is able to measure the erythemal weighted UV-B irradiances in good agreement with the spectral radiometer. Ozone data were obtained from the TOMS-data center (TOMS data, 1999) and used to study the impact of ozone column density on the erythemal weighted irradiance at Koldewey-Station.

Personal exposure of UV-B were recorded using 10 individual ELUV-14. The integrat-

This document is provided by JAXA.

ed UV-B irradiance, date, and time were recorded every minute. Daily erythemal weighted UV-B irradiance were retrieved by summing up the irradiance values after weighting by the corresponding transformation function.

3. Results and discussion

Figure 4 shows the record of unweighted and erythemal weighted daily global UV-B dose measured by the spectral radiometer at Koldewey-Station during the campaign. The large variability is mainly caused by the meteorological conditions, like cloud coverage, snow, and rain. In order to assess the impact of atmospheric ozone, the ratio between unweighted and erythemal weighted daily global UV-B dose was calculated and compared with the ozone column densities (DU) in Fig. 5. The ratio varies between 27 and 39 and is fairly well correlated to the corresponding daily ozone column densities. However, the original values of unweighted and weighted UV-B global doses are not correlated to ozone as can be seen by comparing Fig. 5 and Fig. 4. Only the ratio is significantly controlled by the variability of atmospheric ozone. This is explained by the effect of cloud coverage and snow as mentioned bevor.

Figure 4 shows that the maximum of daily UV-B dose was measured at Koldewey-Station on June 8, 1999. The diurnal variations of the erythemal weighted irradiances obtained by the spectral radiometer and by ELUV-14 for this case are shown in Fig. 3.

The maximum unweighted global UV-B irradiance was 1.6 W/m^2 and the corresponding maximum of erythemal weighted irradiance was 60 mW/m^2. The weighted UV-B dose for this day was 2200 J/m^2. The ozone column density was 312 DU.

In order to assess these doses recorded at Arctic latitudes, similar measurements performed at tropical latitudes are used as a reference. These data were obtained using the

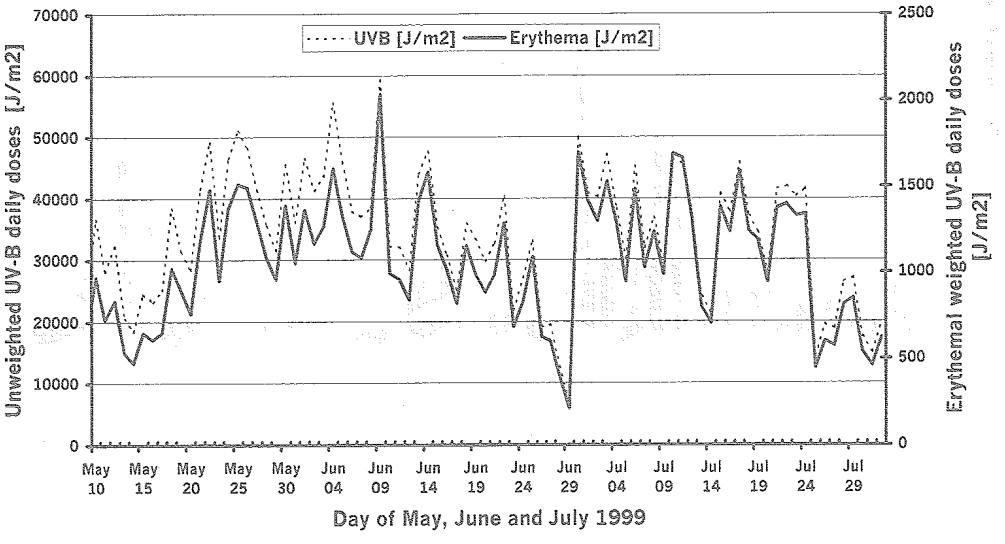


Fig. 4. Daily unweighted (dashed line) and erythemal weighted (solid line) global doses as recorded at Koldewey-Station from May to August, 1999.

This document is provided by JAXA.

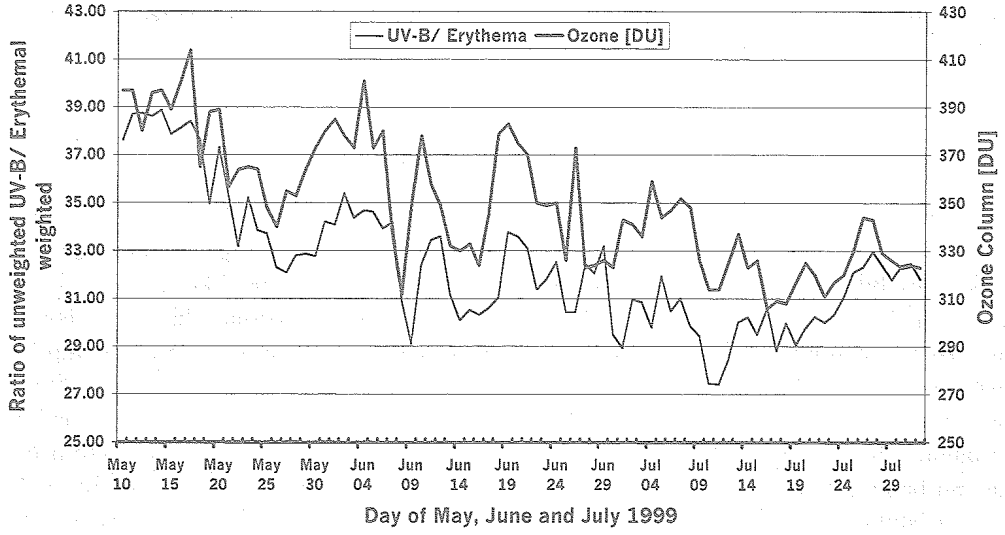


Fig. 5. Ratio of daily unweighted to erythemal weighted global UV-B doses (thin line) and ozone column densities recorded at Koldewey-Station from May to August, 1999.

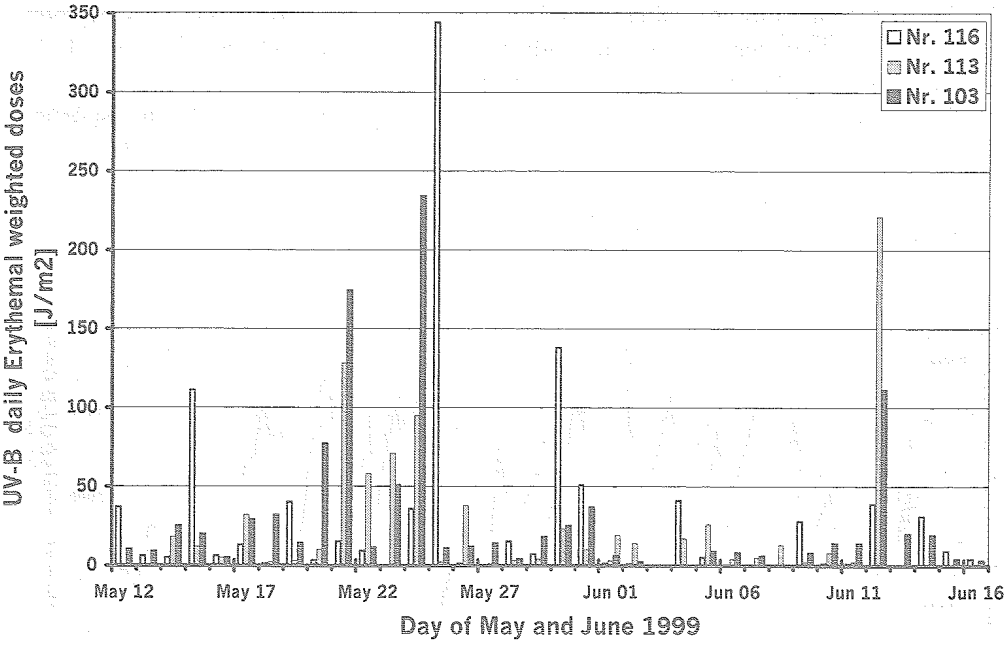


Fig. 6. Personal UV-B doses obtained for three persons at Koldewey-Station from May to June, 1999.

same instrumentation during voyages of the German research vessel "Polarstern" between Bremerhaven and Cape Town. Near the equator (23°N; 17.75°W) on June 8, 1998 the UV-B

This document is provided by JAXA.

irradiance was 4.5 W/m^2 at a solar elevation of 90° and a comparable ozone column density of 310 DU. The corresponding erythemal weighted irradiance was 250 mW/m^2 and the erythemal daily weighted dose reached about 4500 J/m^2 for clear sky conditions. This comparison shows that at the Arctic Koldewey-Station, the maximum irradiance was only 22% of the corresponding equatorial value. However the corresponding daily dose reaches values up to 45%. This higher fraction of the daily dose might be due to longer lasting sunlit conditions during the polar day.

In Fig. 6 three examples for daily personal UV-B doses are shown. The inter-diurnal variability mainly depends on outdoor activities. Thus no correlation to the variation of global doses exists. The recorded maximum of personal dose was about 345 J/m^2 on May 24, 1999. This corresponds to only about 23% of the global dose of this day.

4. Conclusion

The ELUV-14 personal dosimeter provides reliable data of erythemal weighted UV-B doses. The relative values can be easily calibrated by comparison with spectral radiometer measurements.

At Koldewey-Station, the maximum erythemal weighted UV-B irradiance is only 22% of the equatorial values, but the daily doses might reach up to 45% because of the longer lasting polar day.

The maximum recorded personal dose was about 23% of the global dose for the same day.

Acknowledgments

Thanks are due to all volunteers at Koldewey-Station who participated in the programme. The authors are also grateful to Dr. H. Tüg and Dr. Ch. Groß for evaluation and provision of the UV-B spectral radiometer data.

The UV-B spectral radiometer was developed at Alfred-Wegener-Institute for Polar and Marine Research (AWI). The electronic ELUV-14 dosimeter was developed in co-operation between AWI, ESYS GmbH, Berlin, and Institut für Fügetechnik und Werkstoffprüfung (IFW), Jena, Germany.

References

Bojkov, R.D., Bishop, L., Hill, Reinsel, G.C. and Tiao, G.C. (1990): A statistical trend analysis of revised Dobson total ozone data over the Northern Hemisphere. J. Geophys. Res., **95**, 9785–9807.

Bojkov, R.D., Bishop, L. and Fioletov, V.E. (1995): Total ozone trends from qualit-controlled ground-based data (1964–1994). J. Geophys. Res., **100**, 867–876.

Booth, C.R. and Mardonich, S. (1994): Radiation amplification factors: Improved formulation accounts for large increases in ultraviolet radiation associated with Antarctic ozone depletion. Ultraviolet Radiation in Antarctica: Measurements and Biological Effects, ed. by C.S. Weiler and P.A. Penhale. Washington, D.C., Am. Geophys. Union, 39–42 (Antarct. Res. Ser., Vol. 62).

El Naggar, S., Gustat, H., Magister, H. and Rochlintzer, R. (1995): An electronic personal UV-B-doisimeter. J. Photochem. Photobiol. B: Biol., **31**, 83–86.

Groß, C. (1998): Evaluierung des Array-Spektralradiometers des AWI. The 1997 status of solar UV spectroradiometry in Germany: Results from the National Intercomparison of UV Spectro-

This document is provided by JAXA.

radiometers, Garmisch-Partenkirchen, Germany, Schriftenreihe des Frauenhofer Instituts, Atmospärische Umweltforschung, 83–88.

Groß, C., Tüg, H. and Hanken, T. (1998): UV-B radiation measurements at Koldewey-Station. The Arctic and Global Change: Proc Fourth Ny-Ålesund Seminar, Ravello, Italy, 1998, ed. by R Casacchia *et al*. 51–54.

Groß, C., Tüg, H. and Schrems, O. (2001): Three years spectral resolved UV-measurements at Koldewey-Station (1997–1999). Mem. Natl Inst. Polar Res., Spec. Issue, **54**, 113–123.

Karsten, U., Bischof, K., Hanelt, D., Tüg, H. and Wiencke, C. (1999): The effect of UV radiation on photosynthesis and UV-absorbing substances in the endemic Arctic macroalga *Develaraea ramentacea* (Rhodophyta). Physiol. Plant., **105**, 58–66.

Krzyscin, Janusz W. (2000): Total ozone influence on the surface UV-B radiation in the late spring-summer 1963–1997: An analysis of multiple timescales. J. Geophys. Res., **105**, 4993–5000.

McKenzie, R.L., Matthews, W.A. and Johnston, P.V. (1991): The relationship between erythemal UV and ozon, derived from spectral irradiance measurements. Geophys. Res. Lett., **18**, 2269–2272.

McKinlay, A.F. and Diffey, B.L. (1987): A reference action spectrum for ultraviolet induced erythema in humans skin. CIE Res. Note, CIE J., **6/1**, 17–22.

Seckmeyer, G., Mayer, B., Bernard, G., McKenzie, R.L., Johnston, P.V., Kotkamp, M., Booth, C.R., Lucas, T.B., Mestechkina, T., Roy, C.R., Gies, H.P. and Tomlinson, D. (1995): Geographical differences in the UV measured by intercompared spectroradiometers. Geophys. Res. Lett., **22**, 1889–1892.

TOMS data (1999): http://jwocky.gsfc.nasa.gov/teacher/ozone_overhead.html

WMO (1995): Scientific Assessment of Ozone Depletion: 1944. Global Ozone Research and Monitoring Project, World Meteorological Organization, Report No. 37.

(Received May 31, 2000; Revised manuscript accepted September 18, 2000)

This document is provided by JAXA.

Mem. Natl Inst. Polar Res., Spec. Issue, 54, 437–443, 2001

Scientific paper

Arctic hot and CO_2 springs: Natural models of impact of climate change on terrestrial ecosystems

Dmitri G. Zamolodchikov[1] and Dmitri V. Karelin[2]

[1]*Forest Ecology and Production Center of Russian Academy of Sciences, Moscow 117418, Novocheremushkinskaya, 69, Russia*
[2]*Biological department of Moscow State University, Moscow 119899, Vorobyevy gory, Russia*

Abstract: The main purpose of this research was to investigate the carbon cycle in tundra ecosystems in the vicinity of hot springs as natural models of Global Warming and elevated atmosphere CO_2. Empirical data on ecosystem CO_2 fluxes, plant photosynthesis and respiration, vegetation and soil composition were obtained during field expeditions on the Chukotskiy Peninsula (Russia) in 1997 (Chaplino hot springs, 64°26′N, 172°30′W) and 1998 (Ioni hot and CO_2 springs, 65°48′N, 173°22′W). It was found that the influence of naturally increased temperature on carbon exchange considerably depends on the ecosystem type. Under elevated soil temperatures wet sedge ecosystems tend to increase their production, plant biomass, and, to some extent, soil carbon storage. Both species composition and carbon cycle parameters in more drained shrub ecosystems are less sensitive to elevated temperature in the immediate vicinity of the hot springs. Natural CO_2 enrichment of canopy air near the hot springs promotes reduction of photosynthetic efficiency in the studied plant species.

1. Introduction

A growing set of problems connected with the increase of greenhouse gases in the atmosphere and global warming requires further acceleration of investigations of carbon cycling in the biosphere. Long-term decadal to age-long effects of global change are now in focus. How will primary production and respiration change, what are the anticipated trends in ecosystem carbon stocks, and could natural ecosystems effectively compensate for a climate change event? A wide range of scientific approaches is required to answer these questions. One possible way is to study hot and CO_2-springs as a natural model of global change. Since the early nineties this research field has grown rapidly. Studies were carried out in different biomes (Koch, 1993; Körner and Miglietta, 1994, and others), though with a lack of data on northern ecosystems (Cook *et al.*, 1998). Within the tundra biome area, the Chukotskiy Peninsula in the Far East of Russia is known to be the richest in geothermal springs. The goal of the present study is to compare the carbon stocks and fluxes in hot springs-affected tundra ecosystems with adjacent permafrost ecosystems as controls.

This document is provided by JAXA.

2. Methods

Areas with hot spring surface activity are located only in the eastern part of the Chukotskiy Peninsula. Two summer expeditions were conducted to study hot springs: in 1997 (Chaplino, 64°26′N, 172°30′W) and 1998 (Ioni lake, 65°48′N, 173°22′W). The recorded surface water temperatures in the springs was as great as +90℃. The permanent geothermal heating causes elevated temperature in soil horizons. The temperature was as much as +30℃ in the upper 10 cm, higher deeper layers. Some of the Ioni springs have 24% carbon dioxide dissolved in surface water, which results in CO_2 concentration up to 600 ppm in the adjacent air.

Sampling plots were situated in typical tundra habitats on permafrost (control) and in the ecosystems affected by hot springs with no permafrost. In addition, we distinguished wet sedge and mesic shrub habitats. Four different sites were established in 1997 (temperature-affected sedge and shrub sites, and control sedge and shrub sites) and 5 in 1998 (the same sites and CO_2/temperature-affected sedge site in addition). The vegetation in the sedge sites located near hot springs was composed of *Carex cryptocarpa,* whereas *C. aquatilis* and *C. lugens* dominated at the control sites. The temperature-affected and control shrub sites were characterized by similar shrub species composition (*Betula exilis, Salix pulhra, S. chamissonis, S. reticulata*). The sedge species composition at these sites was different.

A portable infrared CO_2-analyzer "Li-Cor 6200" and the ecosystem closed chamber method (Vourlitis *et al*., 1993) were applied to measure net ecosystem carbon flux (NF) and gross respiration (GR). CO_2 flux measured under natural illumination was taken to be an estimate of net ecosystem flux, whereas the rate of CO_2 flux in the darkened chamber served as a measure of gross respiration. Gross primary production (GPP) was calculated as a difference between these two fluxes. We used acrylic chambers 42×42 cm base and 30 cm height, transparent to photosynthetically active radiation. Seasonal carbon fluxes were calculated for 34-day periods, when the living phytomass reserves were maximal. A more detailed description of the measuring technique is given by Zamolodchikov *et al*. (2000).

Photosynthesis and respiration of the dominant plant species were determined using standard leaf cuvettes. Gas exchange measurements of plant leaves were started under ambient CO_2 concentration and canopy temperature. During these measurements the average CO_2 concentration in the leaf cuvette was about 340 ppm in all studied species with exception for *Carex cryptocarpa* at the CO_2-enriched site (351 ppm).

The above-ground plant biomass was harvested on completion of the seasonal carbon flux measurements. Soil carbon reserves in the ecosystems were estimated using original data on thickness of soil horizons, bulk density and carbon content in soil samples.

Leaf photosynthesis response to photosynthetically active radiation (PAR) was approximated using the classical two parametrical hyperbolic formula by Monsi and Saeki (1953). Leaf respiration response to air temperature was described by two parametrical exponential equations (Lloyd and Taylor, 1994). The parameters of the equations were estimated using non-linear regression fitting.

This document is provided by JAXA.

3. Results and discussion

Before discussing the results of carbon flux measurements, it is important to characterize the principal ecological differences between the studied ecosystems. The mean seasonal air temperature in the canopy did not differ significantly in the control and hot springs ecosystems ($P=0.2$), averaging 10℃. Mean seasonal soil temperature at the depth of 10 cm was about 5℃ at the control sites and 13℃ at the temperature-affected sites ($P<0.01$). Both CO_2 and temperature-affected sites demonstrated maximum soil temperature at depth 10 cm (25℃). Thus, the geothermal influence resulted in increased soil temperature, but did not lead to noticeable changes in the canopy air temperature. The sedge sites had significantly greater ($P=0.03$) average volumetric soil moisture in the upper 10 cm (74%), compared to the shrub ecosystems (57%). The average seasonal water table was also higher in the sedge habitats. The carbon dioxide concentration above the plant canopy in the CO_2-enriched ecosystem fluctuated from 390 to 450 ppm, depending on wind speed and direction. The mean seasonal increase of canopy air CO_2 concentration in this ecosystem over the other habitats was 36 ppm.

Figure 1 summarizes seasonal GPP and GR rates in the sedge and shrub ecosystems averaged for both seasons (CO_2-enriched sedge site is not included). It can be seen that the wet sedge ecosystems increased their production ($R=0.91$) and respiration ($R=0.85$) rates under elevated temperature, whereas the drier shrub ecosystems did not show any clear trends ($R=0.07 \div 0.35$). In other words, the response of plant carbon exchange to elevated soil temperature depends on the ecosystem type. These trends in carbon fluxes are similar

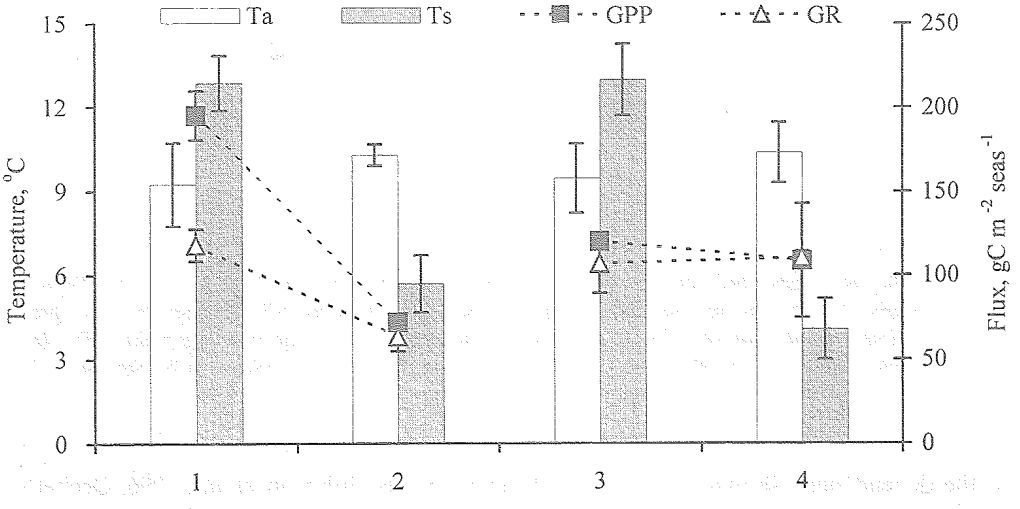


Fig. 1. Mean seasonal values of gross primary production (GPP), gross ecosystem respiration (GR), air temperature in a canopy (Ta) and soil temperature at the depth of 10 cm (Ts) in the studied ecosystems. The ecosystems are (1) wet geothermal with sedge dominance, (2) wet control with sedge dominance, (3) mesic geothermal with shrub dominance, and (4) mesic control with shrub dominance. Data are means ± standard errors.

This document is provided by JAXA.

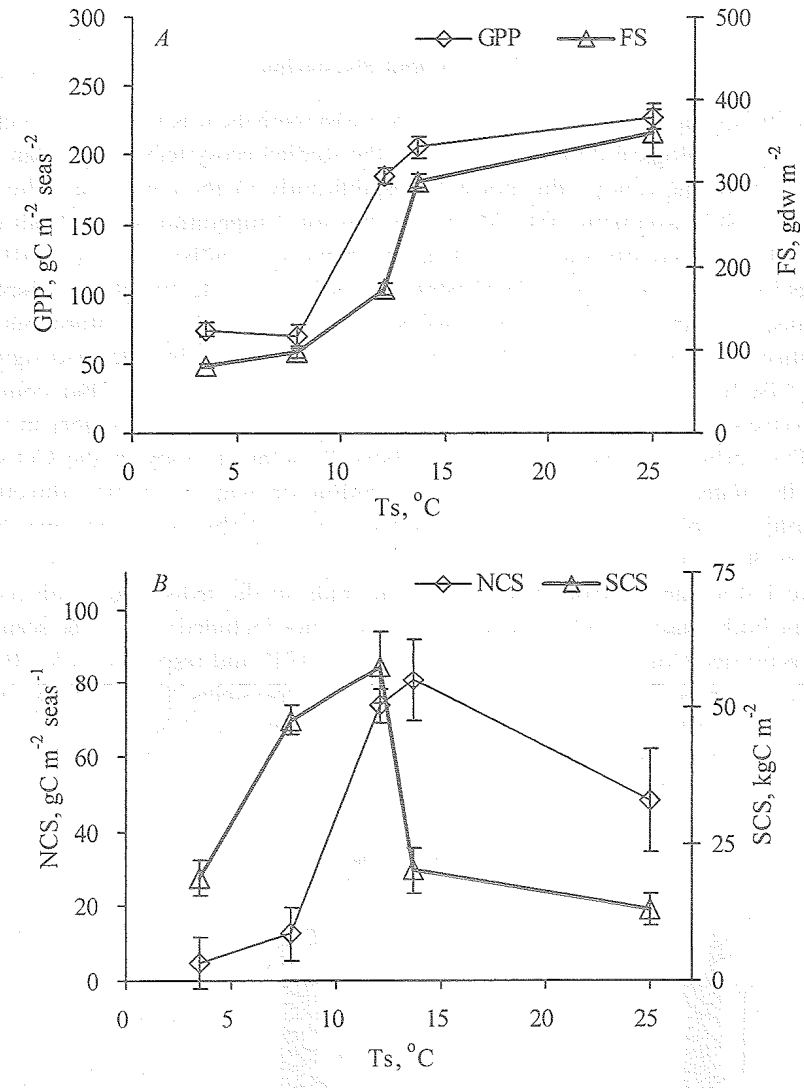


Fig. 2. The relationship between mean seasonal soil temperature at the depth of 10 cm (Ts) and carbon/phytomass parameters in different sedge ecosystems. The parameters are gross primary production rate (GPP, left axis, A), storage of foliage of vascular plants (FS, right axis, A), net carbon sink (NCS, left axis, B), and soil carbon storage (SCS, right axis, B). Each of the data points represents individual site. Data are means ± standard errors.

to the dependencies shown in manipulation experiments (Johnson *et al.*, 1996; Oechel *et al.*, 1998). The rates of GR and GPP CO_2 fluxes in the shrub permafrost habitats are significantly higher compared to the sedge control sites, whereas the reverse takes place in the geothermal ecosystems.

Figure 2 shows the responses of GPP, net carbon flux, foliage biomass of vascular plants, and soil carbon storage to soil temperature in the sedge ecosystems, including the

This document is provided by JAXA.

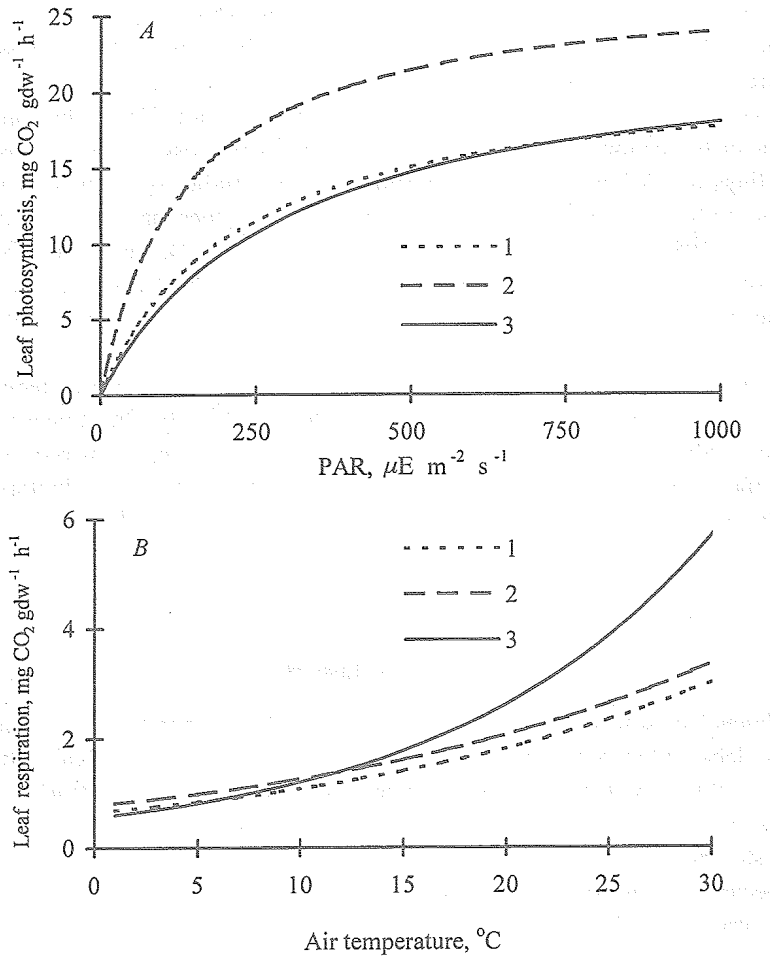


Fig. 3. Leaf photosynthetic response to ambient PAR (A) and leaf respiration response to air temperature (B) of Carex cryptocarpa *(geothermal site with naturally elevated CO_2 and soil temperature, (1); geothermal site with naturally elevated soil temperature, (2)) and* C. lugens *(control site, (3)). Measurements of all plants were made in similiar CO_2 conditions (340–350 ppm). Values of R^2 in non-linear approximations were estimated at 0.89–0.98 for leaf photosynthesis and 0.86–0.87 for leaf respiration ($n=54 \div 57$).*

CO_2-enriched site. One can see that the increase in soil temperature stimulates the growth of foliage biomass ($R=0.92$). The rates of production ($R=0.93$) and respiration ($R=0.95$) are both well correlated with the biomass. However, foliage biomass in the shrub ecosystems does not depend on soil temperature ($R=0.27$).

Most of the carbon in the studied ecosystems is stored in the underground components. Within a 3–12℃ range of average summer soil temperatures at depth 10 cm, the soil carbon storage is greater in the wet ecosystems under higher temperatures. However, it is smaller in ecosystems under temperatures higher than 12℃ (Fig. 2B). Hence, we may consider this soil temperature as optimal for carbon storage in wet ecosystems. Differences in soil carbon

This document is provided by JAXA.

storage agree with measured seasonal net carbon fluxes, which also decrease under higher temperatures. The soil carbon storage at the control shrub site was 1.6 times less than in the temperature-affected shrub ecosystem (1997).

The respiration characteristics of *C. cryptocarpa* were not affected by long-term CO_2 enrichment in the canopy, whereas the efficiency of its photosynthesis decreased (Fig. 3). These findings are consistent with the results of other studies on long-term natural CO_2 enrichment both in the vicinity of hot springs and in experiments (Cook *et al.*, 1998; Hilbert *et al.*, 1987; Oberbauer *et al.*, 1986; Oechel *et al.*, 1994; Tissue and Oechel, 1987). The observed increase in GPP at the CO_2- and temperature-affected site (Fig. 2A) is due to the significant increment of green above-ground plant biomass, which, in turn, is mostly related to the elevated soil temperature.

The respiration response of the control sedge species (*C. lugens*) to temperature rise was steeper then that of geothermal species *C. cryptocarpa* (Fig. 3). The same was characteristic of other studied plant species: the originally arctic species were less economical under higher temperatures in comparison with *C. cryptocarpa.* Long-term adaptation of these species (*Betula exilis, Salix chamissonis, S. pulhra, Empetrum hermafroditum*) is not accompanied by considerable changes in respiration; instead, these species increase their photosynthetic efficiency.

4. Conclusions

- The influence of soil temperature on carbon exchange parameters of tundra ecosystems strongly depends on ecosystem type (species composition, hydrological pattern, etc.).
- There is a tendency in wet sedge ecosystem under elevated soil temperature for increase of gross primary production, above-ground plant biomass and, to some extent, soil carbon storage.
- Both species composition and carbon cycle parameters in more drained shrub ecosystems are less reactive to elevated temperature.
- CO_2 enrichment in a canopy reduces the photosynthetic efficiency of the studied plant species.

Acknowledgments

This research was supported by the Research Institute of Innovative Technologies for the Earth (Japan) "Effects of elevated CO_2 and temperature on carbon fluxes and plant photosynthesis in tundra ecosystems". We are grateful to the Management of the Nature and Ethnic Reserve "Beringia" (Anadyr) for providing access to the research sites and A.I. Ivaschenko (Moscow State University, Moscow) for field assistance.

References

Cook, A.C., Tissue, D.T., Roberts, S.W. and Oechel, W.C. (1998): Effects of elevated CO_2 from natural CO_2 springs on *Nardus stricta:* photosynthesis, biochemistry, growth and phenology. Plant, Cell Environ., **21**, 417–425.

Hilbert, D.W., Prudhomme, T.I. and Oechel, W.C. (1987): Response of tussock tundra to elevated carbon dioxide regimens: analysis of ecosystem CO_2 flux through nonlinear modeling. Oecologia, **72**,

This document is provided by JAXA.

466–472.
Johnson, L.C., Shaver, G.R., Giblin, A.E., Nadelhoffer, K.J., Rastetter, E.R., Laundre, J.A. and Murray, G.L. (1996): Effects of drainage and temperature on carbon balance of tussock tundra microcosms. Oecologia, **108**, 737–748.
Koch, G.W. (1993): The use of natural situations of CO_2 enrichment in studies of vegetation responses to increasing atmospheric CO_2. Design and Execution of Experiments on CO_2 Enrichment, ed by E.D. Schultze and H.A. Mooney. Luxembourg, Office for Official Publications of the European Communities, 381–391.
Körner, C. and Miglietta, F. (1994): Long term effects of naturally elevated CO_2 on Mediterranean grassland and forest trees. Oecologia, **99**, 343–351.
Lloyd, J. and Taylor, J.A. (1994): On temperature dependence of soil respiration. Funct. Ecol., **8**, 315–323.
Monsi, M. and Saeki, T. (1953): Uber den Lichtfactor in den Pflanzengessellschaften und seine Bedeutung fur die Stoffproduction. Jpn. J. Bot., **14**, 22–56.
Oberbauer, S.F., Sionit, N., Hastings, S.J. and Oechel, W.C. (1986): Effects of CO_2 enrichment and nutrition on growth, photosynthesis, and nutrient concentration of Alaskan tundra plant species. Can. J. Bot., **64**, 2993–2998.
Oechel, W.C., Cowles, S., Grulke, N., Hastings, S.J., Lawrence, B., Prudhomme, T., Riechers, G., Stain, B., Tissue, D. and Vourlitis, G. (1994): Transient nature of CO_2 fertilization in Arctic tundra. Lett. Nature, **371**, 500–503.
Oechel, W.C., Vourlitis, G.L., Hastings, S.J., Ault, R.P. and Bryant, P. (1998): The effects of water table manipulation and elevated temperature on the net CO_2 flux of wet sedge tundra ecosystems. Global Change Biol., **4**, 77–90.
Tissue, D.T. and Oechel, W.C. (1987): Response of *Eriophorum vaginatum* to elevated CO_2 and temperature in the Alaskan tussock tundra. Ecology, **68**, 401–410.
Vourlitis, G.L., Oechel, W.C., Hastings, S.J. and Jenkins, M.A. (1993): A system for measuring *in situ* CO_2 and CH_4 flux from unmanaged ecosystems: An arctic example. Funct. Ecol., **7**, 360–379.
Zamolodchikov, D., Karelin, D. and Ivaschenko, A. (2000): Sensitivity of tundra carbon balance to ambient temperature. Water, Air Soil Pollut., **119**, 157–169.

(Received March 28, 2000; Revised manuscript accepted November 13, 2000)

This document is provided by JAXA.

This document is provided by JAXA.

Mem. Natl Inst. Polar Res., Spec. Issue, 54, 445–466, 2001

Scientific paper

Tundra plant responses to experimental and natural temperature changes

Ulf Molau[1]

[1]*Botanical Institute, Göteborg University, Box 461, SE 405 30 Göteborg, Sweden (e-mail: ulf.molau@systbot.gu.se) (http://www.systbot.gu.se/research/latnja/latnja.html)*

Abstract: The present five-year study of tundra plant responses to temperature variation is the first longer-term study emanating from the International Tundra Experiment (ITEX). Fieldwork was carried out at the Latnjajaure Field Station in a subarctic-alpine environment in northern Swedish Lapland during 1993–97. Five species were studied: *Cassiope tetragona*, *Dryas octopetala*, *Eriophorum vaginatum*, *Polygonum viviparum* (four years only), and *Ranunculus nivalis*. Experimental warming was established by using standardized open-top chambers (OTCs) according to the ITEX protocol. Assessed response variables include phenology, growth, and reproduction. All species responded positively to experimental warming by an accelerated flowering phenology and by increased propagule weight. In vegetative growth all species except the evergreen *C. tetragona* increased significantly in the warming treatment. After three years some long-term effects have built up, particularly in reproductive effort, *e.g.*, an increase in ovule number per flower. Summer climate was very variable during the study period, and the target species responded much stronger to the warming treatment in the coldest than in the warmest years. The importance of long-term studies in tundra ecosystems is highlighted.

1. Introduction

Arctic and alpine plants are known to be particularly sensitive to climate change and atmospheric nutrient deposition, both being components of Global Change (*e.g.*, Chapin *et al.*, 1995; Callaghan *et al.*, 1996; Henry and Molau, 1997; Molau and Alatalo, 1998; Alatalo and Molau, 2000). Among the climatic variables, ground surface temperature is the most powerful determinant of tundra plant responses in the Low Arctic, whereas precipitation increases in importance in the High Arctic (Wookey *et al.*, 1993; Henry and Molau, 1997; Molau, 1997a). After snowmelt, the temperature at the ground surface is determined by a combination of variables, *e.g.*, albedo, global solar radiation, airmass temperature, soil moisture, and permafrost.

Thanks to its susceptibility to Climate Change and relative simplicity of the ecosystem, the tundra may serve as an "early warning system" and is the optimal study system for experimental simulation of climatic variables in accordance with the prognoses for the next century (Callaghan *et al.*, 1996). Surface temperature manipulations, simulating one major component of Climate Change in arctic and alpine tundra, have been the main method in

This document is provided by JAXA.

the International Tundra Experiment (ITEX) initiated in 1990 (Henry and Molau, 1997). The aim of the research program is to study the responses of tundra plants to temperature enhancement. A set of circumpolar species was selected as study organisms (Molau and Mølgaard, 1996; Murray, 1997), representing all the major life forms in the tundra. For each species, selected response variables for growth and reproduction were provided in the ITEX Manual (Molau, 1993a; Molau and Mølgaard, 1996). At present, ITEX comprises research parties operating at thirty different field stations in thirteen countries. The first collection of results was recently published as a separate issue of Global Change Biology (vol. 3, 1997, Suppl. 1; see Henry and Molau, 1997, for review). This gathering of sixteen, mostly multisite, species-oriented studies covered short-term responses to experimental warming, *i.e.*, two or three growing seasons. This effort was followed up by a meta-analysis of the results from the ITEX stations during a workshop at the NCEAS computing facility in Santa Barbara, CA (Arft *et al.*, 1999).

In the present study, I present extended data sets for five of the "ITEX species" (*sensu* Murray, 1997) from one of the keystone sites in ITEX, the Latnjajaure Field Station in northern Swedish Lapland (subarctic-alpine). Five-year records on phenology, growth, and reproduction are provided for *Cassiope tetragona*, *Dryas octopetala*, *Eriophorum vaginatum*, and *Ranunculus nivalis*, and a four-year data set for *Polygonum viviparum*. In addition there is an nine-year record on flowering frequency in *E. vaginatum* (1992–2000). The aim of the study is to present more long-term data sets, which are rare in ecological field experiments in arctic and alpine environments, and to compare the results with the short-term results previously reported from ITEX (Henry and Molau, 1997; Arft *et al.*, 1999). The following questions are addressed: (1) How do the short-term (1–3 yr) results hold in the longer term?, (2) Are there other responses becoming visible only in the longer term records?, (3) Which climatic variables are the determinants of plant responses in the unmanipulated plots?, and (4) Can generalizations be made for responses of entire life forms or functional types of vascular tundra plants?

2. Materials and methods

2.1. Field site and plant communities

The fieldwork was conducted in northernmost Sweden at the Latnjajaure Field Station (LFS) in the valley of Latnjavagge, 68°21′N, 18°29′E, at 1000 m elevation. LFS belongs to the Abisko Scientific Research Station, run by the Royal Swedish Academy of Sciences. My research group from the Göteborg University has been operating at LFS since 1990. In 1990 and 1991, meteorological data were recorded only throughout the growing seasons, but from early spring 1992 a year-round automatic climate station has provided a continuous data set.

The valley is covered by snow for most of the year, and the climate is characterized by cool summers and relatively mild, snow-rich winters (annual minimum ranging from −27.3 to −21.7℃), with a mean annual temperature of −2.0 to −2.7℃ (data from 1993–97). Annual precipitation ranges from 605 mm (1996) to 990 mm (1993); the mean for 1990–97 was 808 mm. July is the warmest month with a mean temperature ranging from +5.4℃ (1992) to +9.9℃ (1997).

The vegetation in the valley comprises a wide range of communities of various species

This document is provided by JAXA.

richness. The soils of these ecosystems vary from dry to wet and from siliceous and acidic (pH=4) to calcareous and circumneutral (pH=6; Björk, 2000). Even though the geographical situation is subarctic-alpine (or "arcto-alpine"), the vegetation of the area is representative of the latitudinal Low Arctic, with *Cassiope tetragona*, *Dryas octopetala*, and *Carex bigelowii* among the dominant species (see Molau and Alatalo, 1998).

2.2. Meteorological methods

The LFS is equipped with an automatic climate station in continuous operation since April 1992. The central unit of the system is a Delta-T^{TR} data logger, accommodating data from thirteen different channels, including wind velocity and direction, air temperature, global radiation, and soil temperatures at various depths. The temperature sensors, recording hourly means, maxima, and minima are installed in a standard Stevenson Screen, in shelter at 2 m above ground. The data logger records data for all channels every minute and stores data as hourly means, maxima, and minima. In the summer season, a manual weather station is in operation according to the SMHI (Sveriges Meteorologiska och Hydrologiska Institut) standards, read daily at 0700 and 1900 hours Normal Time.

2.3. The plant species

Cassiope tetragona (Ericaceae) is a circum-arctic perennial dwarf-shrub in which the leaves remain photosynthetic for about five years. They are not shed after senescence, but remain on the shoot, allowing for retrospective growth analysis back at least 25 years in time (Callaghan *et al.*, 1989; Havström *et al.*, 1993). Vegetative reproduction occurs by layering (radiating ramets rooting while still attached to the maternal plant), except in dry heaths where individuals remain dense and well delimited. In all ITEX at Latnjajaure, four plants per plot were used (see below) in the studies. In the case of *C. tetragona*, the identified individual "plants" are dense tufts (10–40 cm diam.) of stems belonging to the same ramet, but within a plot all four "plants" may belong to the same genet, even though physiological integration was broken long ago. A population genetic study employing the RAPD method indicates that there are often 2–3 genotypes within each plot (Molau, unpubl. data), and morphological markers (*e.g.*, pedicel coloration) show the same spatial scale of variation. The plot means used in this study are thus likely to represent more than one genotype in most cases. Pollination mediated by bumblebees is infrequent, and the species seems to rely upon selfing for its reproductive success (Molau, 1993b). The dry capsules contain 3–400 tiny seeds each. At snowmelt in the early summer they are all dehisced, their seeds dispersed, but the actual process has remained enigmatic until recently. Fruit maturation is extremely late in this species, and a massive seed release in the month of September was recorded for the first time in 1997 (Molau, unpubl. data). In all other years, capsule dehiscence was not observed albeit awaited; snow accumulation started too early at least in 1993 and 1994. In most years, therefore, seed release takes place under the winter snow pack and dispersal is then very local, *i.e.*, within a meter or less. Dispersal away from the site of seed formation is thus a rare event.

Dryas octopetala (Rosaceae) is a trailing, semi-evergreen (ranging from wintergreen to truly evergreen) dwarf-shrub, the individual leaves of which remain photosynthetic for 1–2 years at our site. As in the former species, vegetative spread by layering is the dominant mode of dispersal within the local communities. Small flies pollinate the white flowers with

This document is provided by JAXA.

yellow anthers. Reproductive effort in terms of flower number produced per clone varies greatly among years (reflecting last year's climate), and so does reproductive success in terms of seed set (reflecting the present year's climate). The plumed seeds are wind-dispersed. Seed germinability is linearly correlated with seed mass (Welker *et al.*, 1997).

Eriophorum vaginatum (Cyperaceae), the arctic cottongrass, is a wintergreen sedge with monocarpic tillers. Individual leaves remain green for a little more than one year (Mark *et al.*, 1985; Shaver and Laundre, 1997; Wallberg, 1997; this study). Unlike most other species of the genus, *E. vaginatum* is a phalanx strategist, forming dense tussocks that may reach considerable age. Thanks to its superficial root system, it thrives on very shallow soils on top of an anaerobic layer as in boreal peat bogs or (in the tundra) in areas with permafrost and a shallow active layer. The circumpolar tussock tundra community dominated by *E. vaginatum*, covers more than 900000 km^2 in the Low Arctic (Bliss and Matveyeva, 1992). At Latnjajaure there is about 2 ha of this plant community, but despite the restricted patch size it is highly typical, developed in a flat area of local permafrost at the outlet of the lake. Flowering in *E. vaginatum* varies greatly among years and events of masting are highly synchronized over large regions within the Arctic (Shaver *et al.*, 1986; Molau and Shaver, 1997). Flowering takes place soon after snowmelt; the prefloration time is only 3–15 d at Latnjajaure. The blackish flowering spikes are born close to the ground surface and efficiently intercept incoming radiation, thereby being relatively independent of the ambient air temperature (Molau and Rosander, 1995). Subsequent elongation of the culm prior to seed dispersal reflects the level of ovule fertilization (reproductive success); culms of unfertilized inflorescences will not elongate at all, and the degree of culm elongation is therefore a good measure of fertilization rate (Molau and Shaver, 1997). The plumed seeds are efficiently wind dispersed; seed weight is linearly correlated with germinability (Molau and Shaver, 1997).

Polygonum viviparum (Polygonaceae) is a perennial herb with a short ascending rhizome, lacking horizontal rhizomes. This species is abundant in the dry, mesic, and moist meadows at Latnjajaure, but occurs, although more sparsely, in acidic heaths as well. Vegetative dispersal is nevertheless abundant in this species, brought about by asexually produced bulbils replacing most (sometimes all) of the flowers. Flowers occur only in the top section of the spike, but are usually not functional in terms of sexual reproduction. Despite high genetic variability within populations at Latnjajaure, only female flowers have been found (Bauert, 1996; Molau, pers. obs.). This is the normal condition in *P. vivparum*, but sexually reproducing populations with hermaphrodite flowers are known from the Central European Alps (Bauert, 1993). Seed production has never been recorded at Latnjajaure. A very long preformation lag phase (four years), from initiation to final development and maturation, of leaves and inflorescences was recently reported by Diggle (1997) from the Colorado Alpine.

Ranunculus nivalis (Ranunculaceae), the snow buttercup, is another perennial herb with small, spatially well-defined individuals. They have a short ascending rhizome and lack vegetative dispersal by horizontal rhizomes. *Ranunculus nivalis* is known as one of the species having the shortest prefloration time in the tundra; often the time lag from snowmelt to flowering is only a few days (Molau, 1997b). The yellow flowers are pollinated by small flies, and even if the species has some potential for self-pollination (Molau, 1993b) it is mainly outbreeding. The nutlets are green and photosynthetic during the process of

This document is provided by JAXA.

maturation (Molau, 1997b). *Ranunculus nivalis* is a characteristic plant in moist and wet alpine meadows with a good snow protection, and it is also found in nutrient-rich, less extreme snowbeds.

Several other species have been studied at Latnjajaure by other members of the research group, viz., *Carex bigelowii* (Stenström and Jónsdóttir, 1997), *Salix herbacea* (Jones *et al.*, 1997), *Saxifraga oppositifolia* (Stenström *et al.*, 1997), and *Silene acaulis* (Alatalo and Totland, 1997).

2.4. Measurements

Passive heating in the ITEX setup at Latnjajaure was achieved by using standard open-top chambers (OTCs; Fig. 1; Molau, 1993a; Molau and Mølgaard, 1996; Marion *et al.*, 1997). The hexagonal OTCs have a basal diameter of 1 m and are made of 3 mm thick polycarbonate plastic. They were installed at snowmelt in late May 1993 and have been permanently out in the field since then. The OTCs increase the ground surface temperature by 1.5–3℃, depending on vegetation cover and soil moisture (see Marion *et al.*, 1997, for review). For all species in this study, I have used 5 OTCs paired with 5 l-m^2 control plots, one for each OTC. In each plot (OTC or control) 4 individual plants were marked and monitored. The plant closest to the center of each quarter of a plot was chosen. For all subsequent comparisons and tests, only plot means of these four tagged plants were used. The design of the experiments and analyses follows Johnstone *et al.* (1996).

The variables measured can be grouped as qualitative and quantitative. Qualitative variables include mainly phenological measures, *e.g.*, time of snowmelt, prefloration time, postfloration time (days from flowering to seed dispersal), and time of leaf senescence or abscission. Quantitative variables encompass growth variables (*e.g.*, leaf size and shoot height) as well as reproductive ones, in terms of reproductive effort (RE; *e.g.*, flower number, ovule number) and reproductive success (RS; *e.g.*, seed number, seed weight). For each of the study species, the actual response variables were identified in the ITEX Manual (Molau and Edlund, 1996). Phenological data were recorded daily during the fieldwork in 1993–97. Growth responses were normally assessed by using some measure of leaf size. In

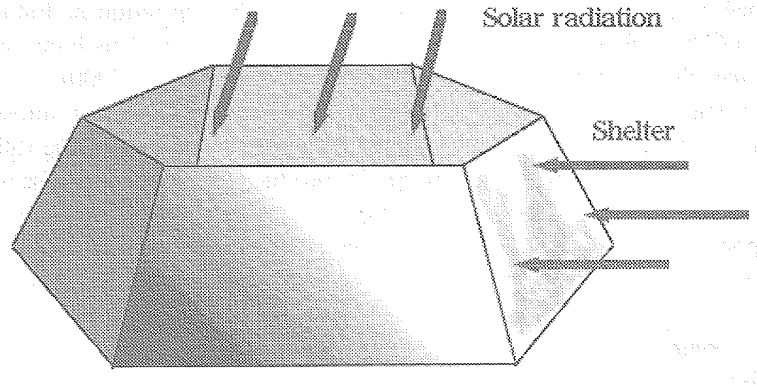


Fig. 1. A standard ITEX hexagonal open-top chamber (OTC). In the Latnjajaure set of OTCs, all panels are 60 cm wide at base and 40 cm high; the inclination of the walls is 73°.

This document is provided by JAXA.

C. tetragona, however, annual shoot increments were measured. Main shoots of each of the tagged "plants" were harvested in August 1997, and later analyzed under a stereo lens. This measuring method is more accurate than the non-destructive field measures reported in Molau (1997b); consequently, there are some discrepancies in the figures between the two studies, even though the interannual variation shows similar trends.

Quantitative variables were scored once a year at appropriate times. Seeds or bulbils were harvested at the time of maturation and stored in paper bags at room temperature; they were later weighed individually in the autumn of the year of harvest on a microgram Mettler AT80 balance at the Botanical Institute, Göteborg University. If available, 20 seeds or bulbils per ramet were weighed. In total over 1993–97, 2418 *D. octopetala*, 3058 *Eriophorum vaginatum*, and 3141 *R. nivalis* nutlets were individually weighed, as well as 2419 *P. viviparum* bulbils.

The statistical analyses were carried out with the StatView 5.0 and SuperANOVA software packages for the Macintosh. Only plot means were employed in the analyses and no transformations were needed to attain normality in the variables analyzed. When ANOVA models have been applied, they are designed according to the "two-way ANOVA without replication" (Sokal and Rohlf, 1981). Treatment (OTC and control) and year are both fixed effects (Sokal and Rohlf, 1981; Johnstone *et al.*, 1996). There is no interaction between time and the individuals as the responses of the individual plants are parallel through time (Sokal and Rohlf, 1981).

3. Results

3.1. Climatic variation among years

The climate during the summers of 1993–97 differed widely (Table 1). In the five-year study period, the 1995 summer was unusually cold and wet. The summer of 1997 was, on the other hand, the warmest on record in the northern Swedish mountains during the century as to mean temperature (SMHI, 1997), and the month of August in 1996 was even further above the record (SMHI, 1996). These two years in conjunction represent a "extreme event", in this part of Fennoscandia unique during the last century, and perhaps since the onset of the Little Ice Age in Scandinavia some 400 years ago. The impact of these two good summers in conjunction was easily visualized in the vegetation at Latnjajaure: the dwarf birch (*Betula nana*) was sprouting vigorously and increased its biomass by 17% in unmanipulated plots between 1995 and 1997 (Alatalo and Molau, 2000).

The among-year variability in climate is huge, and has a clear impact on seed maturation. In cold summers (*e.g.*, 1992 and 1995) hardly any species in the valley set seed, whereas in the warm summers almost any species produced a full seed complement (Molau and Larsson, 2000). This among-year variability is a normal stress component in the tundra, but the importance of "extreme events" has previously not been emphasized enough (but see Robinson *et al.*, 1998).

3.2. Plant responses

3.2.1. *Cassiope tetragona*

The white arctic heather, *C. tetragona*, showed no response in shoot increments (annual growth increments, AGIs) to the temperature treatment (Fig. 2; Table 2; two-way

This document is provided by JAXA.

Table 1. The climate at Latnjajaure during the summers of 1993–97. Data from the standardized ITEX climate station. TDD = Thawing Degree Days (temperature sum above 0°C).

Time of season Variable	Year				
	1993	1994	1995	1996	1997
May					
Mean temperature (°C)	−0.06	−2.19	−1.69	−2.19	−1.56
Maximum temperature (°C)	+11.0	+9.5	+9.6	+8.4	+7.1
Minimum temperature (°C)	−7.4	−12.6	−14.3	−14.9	−8.8
TDD	52.4	16.2	40.9	23.3	20.7
Precipitation (mm)	80.0	32.1	40.1	14.3	30.1
Global radiation (MJ/m²)	612	669	661	698	632
June					
Mean temperature (°C)	+1.60	+2.73	+4.36	+3.21	+5.26
Maximum temperature (°C)	+12.0	+12.6	+13.2	+11.3	+17.0
Minimum temperature (°C)	−5.5	−3.8	−0.9	−3.0	−5.7
TDD	65.3	79.2	131.1	98.4	165.4
Precipitation (mm)	60.1	30.1	44.7	91.2	6.2
Global radiation (MJ/m²)	572	557	534	519	663
July					
Mean temperature (°C)	+8.46	+7.61	+5.93	+7.37	+9.92
Maximum temperature (°C)	+18.1	+20.3	+18.3	+15.2	+20.5
Minimum temperature (°C)	+2.0	−1.6	−1.6	−0.3	+0.7
TDD	262.4	236.1	184.5	228.3	307.5
Precipitation (mm)	63.6	56.7	81.4	42.8	38.7
Global radiation (MJ/m²)	510	506	460	477	612
August					
Mean temperature (°C)	+6.57	+7.56	+5.28	+9.91	+8.88
Maximum temperature (°C)	+14.4	+21.1	+17.4	+19.1	+19.7
Minimum temperature (°C)	−0.6	−3.2	−1.5	+0.9	+0.4
TDD	203.6	236.3	163.9	307.1	275.2
Precipitation (mm)	63.3	38.9	142.0	66.7	54.2
Global radiation (MJ/m²)	277	372	310	376	345
Summer (June–August)					
Mean temperature (°C)	+5.54	+5.97	+5.19	+6.83	+8.02
Maximum temperature (°C)	+18.1	+21.1	+18.3	+19.1	+20.5
TDD sum	531.3	551.6	479.5	633.8	748.1
Total precipitation (mm)	187.0	125.7	268.1	200.7	99.1
Global radiation sum (MJ/m²)	1359	1435	1304	1372	1620

ANOVA, $F_{1,44}=0.006$, $p=0.99$). On the other hand, it showed significant among-year variation in shoot increments ($F_{4,44}=21.77$, $p<0.0001$), regardless of treatment, which must be induced by interannual variation in some environmental variable(s) other than temperature itself (*cf*. Molau, 1997b; Kudo *et al*., 1999). There were no significant correlations with the preceding summer's climate as to the responses in shoot increment and reproduction in the control plots.

The number of flowers per monitored plant varied greatly among years in the control

This document is provided by JAXA.

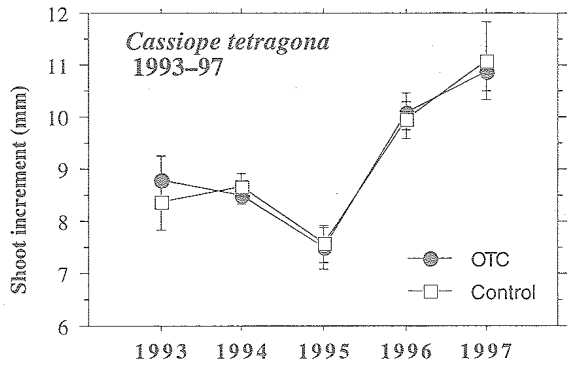


Fig. 2. Variation in the average length (±SE) of annual shoot increments of Cassiope tetragona *in OTCs and controls at Latnjajaure in 1993–97.*

Table 2. Summary table. Means of response variables for the study plant species at Latnjajaure 1993–97 (1994–97 for P. viviparum*). Data are given as mean±SE. The number of years of observation equals 5 in all species except* P. viviparum *(4 years). Data sources are annual means across all five plots within each of the two treatments (control and experimental warming). RS, reproductive success, is calculated as bulbil number for* P. viviparum, *fruit:flower ratio for* C. tetragona, *and seed:ovule ratio in the other species. The vegetative growth variables are species-specific (see text). The year of implementation (1993) is omitted from the thaw dates (i.e., data from 4 years are provided for all species with regard to this variable). Day numbers: 1 June=152, 1 July=182, 1 August=213.*

Species	Treatment	Thaw date (day no.)	Prefloration time (d)	Reproductive success	Propagule weight (mg)	Vegetative growth
Cassiope tetragona	control	154.4±5.7	32.6±1.5	0.44±0.06	3.83±0.79	9.12±0.32
	OTC	151.0±4.6	28.4±1.4	0.48±0.03	5.59±0.68	9.14±0.29
Dryas octopetala	control	142.7±4.2	50.0±2.8	0.28±0.07	0.34±0.04	17.1±0.3
	OTC	139.5±3.5	37.5±1.3	0.32±0.06	0.41±0.04	20.9±0.4
Eriophorum vaginatum	control	154.9±3.5	9.8±0.6	0.13±0.02	0.54±0.03	158±11
	OTC	153.3±4.4	6.4±0.5	0.10±0.02	0.86±0.02	200±29
Polygonum viviparum	control	142.7±4.2	56.7±2.1	20.8±1.9	1.12±0.05	423±13
	OTC	139.5±3.5	54.2±2.2	24.4±2.1	1.24±0.06	554±24
Ranunculus nivalis	control	154.9±2.0	14.1±1.3	0.28±0.03	0.41±0.02	16.9±0.5
	OTC	151.0±2.5	13.5±1.4	0.22±0.03	0.50±0.02	22.0±0.5

plots, from an average of 3.6 in 1996 to 54.1 in 1994; this variation corresponds well in magnitude to that reported from Ellesmere Island in the Canadian High Arctic by Johnstone and Henry (1997). In the Ellesmere data set there was a significant positive correlation between flower number per shoot and July TDD the year prior to flowering (Pearson product-moment correlation, $r=0.891$, $p<0.01$; Johnstone and Henry, 1997); this r-value is only slightly higher than in my data set from Latnjajaure ($r=0.809$, adjusted $r^2=0.540$, $p=0.0972$, $n=5$ control plot means).

The warming treatment accelerated the prefloration time (thawing–flowering) by 13%, from the grand average of 32.6 d in controls ($n=25$ plot means) to 28.4 d in OTCs ($n=23$). The difference between controls and treatment was highly significant in a two-way

This document is provided by JAXA.

ANOVA ($F_{1,44}=11.80$, $p=0.0014$), although the among-year variation was even larger ($F_{4,44}=20.94$, $p<0.0001$).

Reproductive success is difficult to measure in *Cassiope tetragona*. Capsule dehiscence takes place late in the season, and most years probably under the snow. During our extensive fieldwork at Latnjajaure, I observed massive capsule dehiscence only once, namely on the 12 of September in 1997. The 1997 summer was the warmest on record since our monitoring started in 1990. With no ripe, dehiscing fruits to deal with, the weight of entire, near-maturity fruits from OTCs and control plots were compared in 1995, revealing a near-significant ($p=0.055$) weight increase by the warming treatment (Molau, 1997b).

3.2.2. *Dryas octopetala*

The mountain avens, *D. octopetala*, showed positive responses to temperature amelioration in all variables measured. Like in all other species investigated, phenology was significantly accelerated; in this case plants in OTCs showed a prefloration time on average 12.5 d shorter than in untreated plots (Table 2; Appendix), the difference highly significant in a two-way ANOVA ($F_{1,44}=35.28$, $p<0.0001$). However, also the among-year difference was significant ($F_{4,44}=8.95$, $p<0.0001$), the treatment effect being smallest in the warmest year (1997).

Reproductive effort (number of ovules produced in 1994-97) did not differ significantly between treatments (two-way ANOVA, $F_{1,32}=2.60$, $p=0.117$) or among years ($F_{3,32}=1.87$, $p=0.154$). Reproductive success in terms of fertilization level (seed:ovule ratio) was normally lower in the OTCs than in the controls (Table 2; Appendix), probably due to pollination shortage in the chambers (the species is poorly self-pollinating; Molau, 1993b). The lower pollination level was also manifested in longer flower duration in the OTCs when compared to control plots in a two-way ANOVA ($F_{1,34}=26.09$, $p<0.0001$), with no significant difference among years ($F_{3,34}=2.70$, $p=0.061$). With regard to seed weight, however, *D. octopetala* responded as most tundra plants to temperature enhancement: seeds from plants in OTCs were heavier than in the control plots, at least in cold years; the treatment effect was only near-significant in a two-way ANOVA ($F_{1,39}=3.09$, $p=0.089$) but strongly significant among years ($F_{3,39}=15.88$, $p<0.0001$). In the cold summer of 1995, seeds in OTCs ended up more than three times heavier than in the control plots (Fisher's Protected LSD, $p<0.001$). Seed weight in controls was significantly positively correlated with temperature, especially in terms of TDD (thawing degree days, Pearson product-moment correlation, $r=0.997$, $p<0.0001$). The average seed weight in unmanipulated plants in 1995 (0.12 mg) is below the 0.15 mg level for any germination potential (*cf.* Welker *et al.*, 1997).

With regard to vegetative growth, leaf size increased significantly with enhanced temperature (two-way ANOVA, $F_{1,44}=69.47$, $p<0.0001$), but the effect also differed among the years ($F_{4,44}=3.54$, $p=0.014$); see Fig. 3. In control plots, leaf length showed the highest correlation with TDD of the preceding summer (Pearson product-moment correlation, $r=0.935$, $p=0.016$, $n=5$ years).

3.2.3. *Eriophorum vaginatum*

The arctic cottongrass, *E. vaginatum*, belongs to the vernal flora (Molau, 1993b) and has a very short prefloration time, on average 9.8 d (Table 2). Phenology was significantly

This document is provided by JAXA.

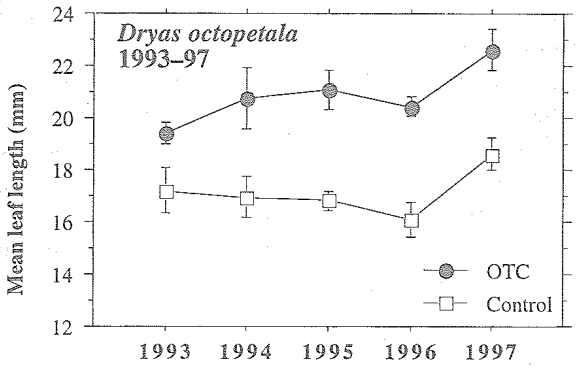


Fig. 3. Variation in the average length (±SE) of leaves of Dryas octopetala *in OTCs and controls at Latnjajaure in 1993–97.*

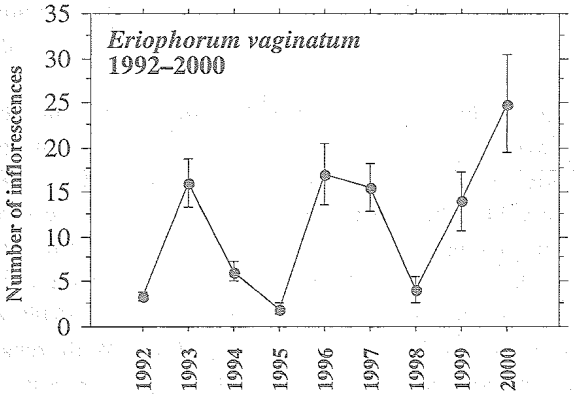


Fig. 4. Mean number (±SE) of inflorescences in twenty unmanipulated Eriophorum vaginatum *tussocks monitored at Latnjajaure in 1992–2000.*

accelerated in the enhanced temperature treatment, and the average prefloration time was reduced even more, to 6.4 d, a highly significant difference (two-way ANOVA, $F_{1,44}=25.59$, $p<0.0001$). Also the among-year variation in prefloration was significant ($F_{4,44}=7.76$, $p<0.0001$; see Appendix).

None of the two components of reproductive effort, the number of inflorescences per tussock and the number of ovules per inflorescence, differed significantly between treated and untreated plants. The nine-year monitoring of flowering (inflorescences per tussock) at Latnjajaure 1992–2000 revealed a huge interannual variation (Fig. 4), and all tussocks in the *ca.* 2 ha stand of *E. vaginatum* tussock tundra at the site seem to be highly synchronized (as they are in the north Alaskan tussock tundra, *cf.* Molau and Shaver, 1997, and references therein). This synchronous interannual variation was significant also in the tussocks included in the ITEX plots ($F_{4,42}=11.21$, $p<0.0001$). The flowering rate at Latnjajaure seems to be best correlated with TDD the summer three years prior to actual flowering, but the data set still is to small to allow proper testing and modeling. The good flowering years

This document is provided by JAXA.

of 1993, 1996, 1997, 1999, and 2000 correspond with the warmest summers at Latnjajaure during the 90'ies with a three-year delay, particularly with regard to summer TDD (summer TDD of 1990 was also high: 686.4). The years of minimum flowering in Fig. 4, 1995 and 1998, correspond to cold summers with a three-year delay as well (summer TDD in 1992: 518.8; in 1995: 479.5).

In addition, a late thawing induced a postponement of the final development of some tillers, as the number of inflorescences per tussock was negatively correlated with thawing date of the present year (linear regression, $r^2=0.268$, $p<0.0001$, $n=50$). The among-year variation in ovule number per inflorescence (two-way ANOVA, $F_{4,42}=5.74$, $p=0.0009$) was best correlated with the summer TDD one year back in time.

Reproductive success was generally reduced in the OTCs, an obvious chamber effect in this wind-pollinated species, although the level varied greatly among years (Table 2; Appendix). The variation in the percentage of fruiting inflorescences showed a significant dependence on inflorescence density (linear regression, $r^2=0.155$, $p=0.0052$, $n=48$), the main determinant of *E. vaginatum* pollen density in the air. Seed weight (Table 2; Appendix), on the other hand, was significantly higher in the experimentally warmed tussocks (two-way ANOVA, $F_{1,36}=93.83$, $p<0.0001$), and there was also a significant among-year variation ($F_{4,38}=5.31$, $p=0.0017$) where the experimentally induced relative increase in seed weight was largest in the coldest years (see Appendix). Culm elongation was measured only in 1993, but this response variable was then abandoned as it was shown to be linearly correlated to reproductive success in terms of seed:ovule ratio (Molau and Shaver, 1997).

From the monitoring of all individual leaves of one tiller per tussock in 1994–96, the maximum standing crop of green parts of leaves (corresponding to photosynthetic area) per season was calculated (Table 2; Appendix). The average for tussocks in the warming treatment over the years was 26% higher than in control plants, a significant treatment effect (two-way ANOVA, $F_{1,26}=9.92$, $p=0.0041$), whereas the interannual differences were insignificant ($F_{2,26}=0.31$, $p=0.74$). Also the maximum length of the longest leaf per tiller and season was higher in the OTCs (96.2±3.8 mm [mean±SE], $n=15$ plot means) than in the controls (83.07±2.3, $n=15$); here not only the treatment effect was significant ($F_{1,26}=11.20$, $p=0.0025$) but also the variation among years ($F_{2,26}=5.21$, $p=0.0125$). The number of leaves produced per tiller and season did not differ between OTCs and controls ($F_{1,26}=1.08$, $p=0.31$), but the leaves tended to remain green longer in the controls (412±65 d [mean±SD], $n=19$) than in the OTCs (400±36 d, $n=19$) although the difference was not significant in a *t*-test (DF=35, $p=0.49$). Leaf elongation rate in early summer was higher in the OTCs than in the controls, but so was also the senescence rate in late August (Fig. 5; *cf.* Wallberg, 1997).

3.2.4. *Polygonum viviparum*

The alpine bistort, *P. viviparum* (=*Bistorta vivipara*), was studied in the same plots as *D. octopetala* during 1994–97. The four-year monitoring revealed no significant acceleration of phenology in terms of prefloration in the warming treatment compared to controls (two-way ANOVA, $F_{1,35}=1.18$, $p=0.2856$), but this is the most late-flowering species of all five in the study and may respond to other cues as well.

With regard to reproductive effort, the proportion of flowers and asexually produced

This document is provided by JAXA.

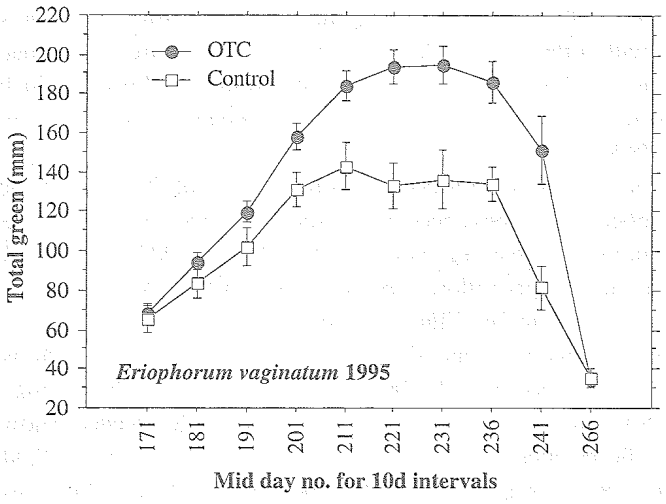


Fig. 5. Mean total length (±SD) of green (photosynthetically active) leaf tissue of forty monitored Eriophorum vaginatum *tillers in OTCs and controls at Latnjajaure in the summer of 1995.*

bulbils varied significantly among years ($F_{3,26}=6,53$, $p=0.0013$). The proportion of flowers was highest in the warmest year (1997; 0.209), but otherwise the pattern of variation was not consistent with any climatic variable of the same season. However, flower number in control plots showed a significant correlation to the temperature sum (TDD) of the preceding summer (linear regression, $r^2=0.925$, $p<0.0490$, $n=20$). It should be noted that the genotypes in our area produce unisexual female flowers only; reproduction is brought about only by bulbils (cloning). The number of bulbils per plant varied significantly among years ($F_{3,35}=9.24$, $p<0.0001$); the number also tended to be higher in plants in the OTCs than in controls (Table 2; Appendix), but this difference was not statistically significant ($F_{1,35}=2.66$, $p=0.11$). Bulbil weight was also higher in the OTCs, but as in the case of bulbil number this difference was non-significant ($F_{1,35}=2.71$, $p=0.11$), masked by the stronger interannual variation ($F_{3,35}=3.51$, $p=0.0252$). When the two measures are combined as "bulbil yield", the total weight of the bulbils produced on an inflorescence, the treatment effect is also significant ($F_{1,35}=7.32$, $p=0.0105$).

The results from Latnjajaure were compared with a recent study of the same species from the central Norwegian ITEX site at Finse (Totland and Nyhlén, 1998; Table 3) over the same four-year period (1994–97). Flower number and bulbil number both showed slightly higher figures in the Finse material, but with overlapping ranges. Bulbil weight, however, differed strongly between the two sites, the Latnja figures being almost twice as high as at Finse. For all three variables, the OTC figures were higher than the corresponding controls at both sites, respectively.

The two measures of vegetative growth, height of the shoot and area of the largest leaf (Table 2; Appendix), both showed a significant increase in the warming experiment, the difference being more pronounced in leaf area (Fig. 6; $F_{1,35}=21.95$, $p<0.0001$) than in shoot height ($F_{1,35}=5.14$, $p=0.0296$). The among-year difference was significant for shoot height ($F_{3,35}=5.20$, $p=0.0043$) but not for leaf area ($F_{3,35}=0.67$, $p=0.57$). Leaf area was measured

This document is provided by JAXA.

Table 3. Comparison of mean values of components of reproductive effort in Polygonum viviparum *at two ITEX sites: in northern Sweden (Latnjajaure; this study) and central Norway (Finse; Totland and Nyhlén, 1998).*

Variable	Site	Treatment	Mean±SE
Flower number	Latnjajaure	Control	2.75±0.58
	Latnjajaure	OTC	3.78±1.03
	Finse	Control	3.15±1.15
	Finse	OTC	5.28±2.22
Bulbil number	Latnjajaure	Control	20.8±1.9
	Latnjajaure	OTC	24.4±2.1
	Finse	Control	23.0±2.6
	Finse	OTC	26.3±3.0
Bulbil weigth (mg)	Latnjajaure	Control	1.12±0.05
	Latnjajaure	OTC	1.24±0.06
	Finse	Control	0.60±0.06
	Finse	OTC	0.85±0.11

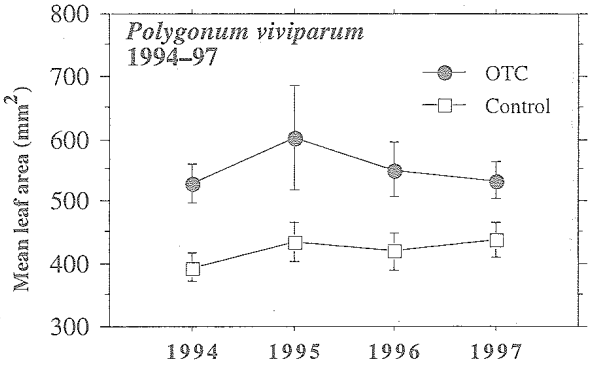


Fig. 6. Variation in leaf area (±SE) of Polygonum viviparum *in OTCs and controls at Latnjajaure in 1994–97.*

according to Wookey *et al.* (1993), using an algorithm taking leaf length and width into account.

3.2.5. *Ranunculus nivalis*

The snow buttercup, *R. nivalis*, belongs to the vernal flora of the valley (Molau, 1993b), as manifested by its short prefloration time (on average 14.1 d in control plots; Table 2). The small decrease in prefloration time seen in the warming treatment was far from significant (two-way ANOVA, $F_{1,44}=0.15$, $p=0.70$), whereas there was a significant among-year component to the variation ($F_{4,44}=7.35$, $p<0.0001$). Postfloration time showed the same picture: slightly faster in the OTCs (36.3±1.9 d, mean±SE, $n=23$) than in the controls (37.7±2.2 d, $n=23$), with no significant treatment effect ($F_{1,42}=1.46$, $p=0.23$) but a significant among-year component ($F_{4,42}=27.83$, $p<0.0001$).

The best measure of reproductive success in this species, viz. ovule number, increased steadily in the OTCs during the first three years of treatment, after which it leveled out

This document is provided by JAXA.

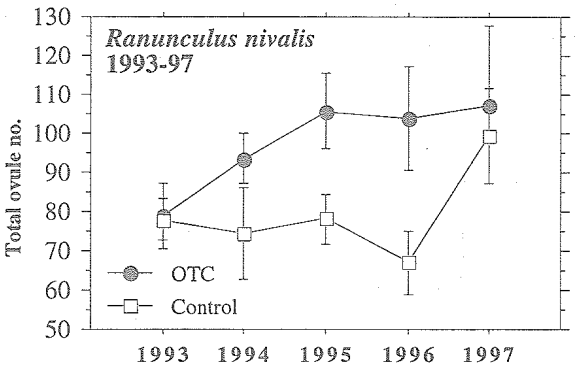


Fig. 7. Variation in the average ovule number (±SE) in flowers of Ranunculus nivalis *in OTCs and controls at Latnjajaure in 1993-97.*

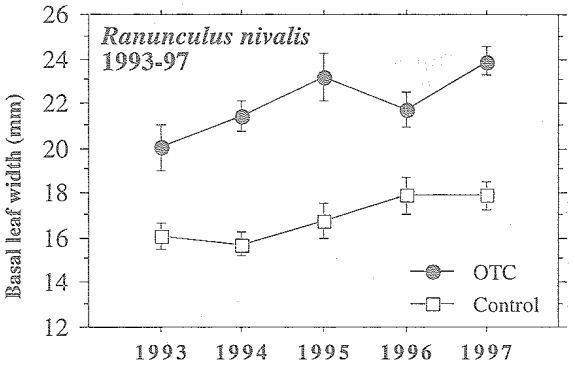


Fig. 8. Variation in the average width (±SE) of basal leaves of Ranunculus nivalis *in OTCs and controls at Latnjajaure in 1993-97.*

(Fig. 7). In the control plots the average ovule number varied considerably among years, mainly in response to the climate of the preceding year (linear regression on TDD one year prior to flowering, $r^2=0.947$, $p=0.0024$, $n=25$). After the experiment implementation season of 1993, ovule number remained steadily higher in OTCs than in controls, although there was a marked raise in the controls to almost OTC level following the warm August in 1996 (Fig. 7).

As in the other species in this study, propagule weight increased significantly in the warming treatment (Table 2; Appendix). *Ranunculus nivalis* nutlets were significantly heavier in the OTCs than in the controls (two-way ANOVA, $F_{1,42}=14.11$, $p<0.0001$), and the among-year variance component was highly significant as well ($F_{4,42}=6.09$, $p=0.0006$). Relative reproductive success in terms of seed:ovule ratio did not differ significantly between treatments ($F_{1,42}=2.14$, $p=0.15$) but among years ($F_{4,42}=4.21$, $p=0.0059$).

The most relevant measure of vegetative growth in *R. nivalis*, viz. basal leaf width (see Molau and Edlund, 1996), showed consistently much higher values in the warmed plots than in the controls (Fig. 8; Table 2; Appendix; two-way ANOVA, $F_{1,44}=72.14$, $p<0.0001$)

This document is provided by JAXA.

whereas the among-year component was barely significant ($F_{4,44}=2.73$, $p=0.0405$). The other growth measure recorded during the ITEX process at Latnjajaure, viz. inflorescence height at maturity, showed the same pattern of variation (OTCs 17.4±0.8 cm, controls 12.1 ±0.7 cm [means±SE]; between treatments $F_{1,42}=36.18$, $p<0.0001$; among years $F_{4,42}=4.37$, $p=0.0048$), but this measure seems to be biased as it covaries with reproductive success: in the control plots, a linear regression showed a significant dependence of shoot height on reproductive success in terms of seed:ovule ratio ($r^2=0.321$, $p=0.0029$, $n=23$; compare *E. vaginatum* above).

A final remark is relevant here: in the wet sedge community where *R. nivalis* has been studied, other species (particularly *Carex lachenalii*, *Calamagrostis stricta*, *Poa arctica*, and *Sphangum warnstorfii*) have responded much more vigorously to the warming treatment. The target species *R. nivalis* is now suffering from competitive exclusion, and is rapidly decreasing in numbers of genets, which are reduced by *ca.* 50% since the implementation in 1993 (Molau, unpubl. data).

4. Discussion

4.1. Climatic impact variation in time and space

The present study highlights the tundra plants' responsiveness to climatic variability. Even though tundra plants are extremely long-lived and well adapted to environmental fluctuations (Molau, 1993b, and references therein), they do respond vigorously to the among-year variation in climatic variables, particularly temperature (best measured as TDD), growing season length, global radiation, and precipitation. The warming experiment adopted in ITEX is a rather mild perturbation, as the variation in summer temperatures among years exceeds the treatment effect achieved by the OTCs (see Table 1).

However, the climatic cues differ in importance among life forms (functional types), species, and—not least important—even among populations within species according to the position of the study site in that particular species' distributional range in geographic and environmental space (see multisite reports, *e.g.*, Havström *et al.*, 1993; Graglia *et al.*, 1997; Henry and Molau, 1997, and references therein; Arft *et al.*, 1999). Hence, shoot increment in *Cassiope tetragona* responded strongly to interannual temperature variation in the High Arctic and in the high alpine zone in the Subarctic, whereas this response variable was not affected by climate but rather by nutrient availability at a tree-line site near Abisko in northern Sweden (Havström *et al.*, 1993). The Latnjajaure site (subarctic, mid-alpine) lies in between these extremes, probably close to the climatic optimum of *C. tetragona*. In the present five-year study there was no significant increase in shoot increment in the warming treatment, but a significant difference among the years. Precipitation is not limiting here, as it may be in the High Arctic (*cf.* Wookey *et al.*, 1993). Instead, the key factor must be sought among other environmental variables, such as growing season length (earliness of thaw) and radiation. The OTCs alter the precipitation and radiation climate only marginally (Marion *et al.*, 1997). The Ellesmere Island study (Johnstone and Henry, 1997) showed a high correlation between growth and TDD but did not report on radiation climate. However, the number of leaves per annual shoot increment is reported to have a better correlation with temperature (Havström *et al.*, 1993), a quantitative response variable that was not utilized in my study. As pointed out by S. Jonasson (*in litt.*) my data set for

This document is provided by JAXA.

shoot increments in both controls and manipulated plants shows a potential correlation with July mean temperatures, although not significant ($p=0.129$), but this does still not explain the significant lack of differentiation between responses in controls and OTCs. The lack of response to experimental warming is still enigmatic, but parallels that of evergreen *Saxifraga oppositifolia* at the same and other sites (Stenström *et al*., 1997). Recently, Kudo *et al*. (1999) showed that thawing date and growing season length are important cues for the vegetative performance in *C. tetragona* along a natural snow-cover gradient at Latnjajaure.

Here, it should be stressed that this is not a generalization that holds true for the entire "functional type" of evergreen dwarf-shrubs; species like *Empetrum hermaphroditum* and *Vaccinium vitis-idaea*, both mainly boreal in their distribution and with their climatic tolerance limit at the Latnjajaure site, respond vigorously to the warming treatment there (Alatalo and Molau, 2000, see also Graglia *et al*., 1997). Other "arctic specialists" among the evergreen dwarf-shrubs, however, appear to respond in the same manner as *C. tetragona*, *e.g*., *Saxifraga oppositifolia* (Stenström *et al*., 1997) and *Diapensia lapponica* (Molau, 1996; Kudo *et al*., 1999).

4.2. Growth and reproduction

With regard to vegetative growth, the plant's responses are usually conspicuous already during the first season of treatment, even though leaf preformation requires long time in some species, *e.g*., up to four years in *Polygonum viviparum* (Diggle, 1997). In the latter case, even a five-year study is far too short to generate any reliable analysis of correlation between climate and plant performance in terms of numbers of modules (*i.e*., leaves) produced, even though their size is usually determined by the climate of the summer of final development.

The picture is even more complex with regard to reproductive structures. Inflorescences are preformed at least one year prior to their final development in most tundra plants (Sørensen, 1941; Molau, 1993b, and references therein), and in some cases the reproductive effort is determined by the summer climate 3–4 years prior to actual flowering (*e.g*., *Eriophorum vaginatum*, Molau and Shaver, 1997; *Polygonum viviparum*, Diggle, 1997). Here, short-term studies including two or three field seasons will fail to demonstrate any adequate relationships, and even the present longer-term study gives little room for hypothesis testing.

In many, perhaps most, of the tundra vascular plant species, successful reproduction is a more rare event than we have anticipated. My five-year study clearly shows that successful reproduction in tundra plants is rather episodic, as the study period involved everything from very cold summers (1995; hardly any seed set in most plant species in the area) to extremely warm ones (1996, 1997; massive seed output in all species). The importance of extreme climatic events in the tundra has been under-estimated until quite recently. It is becoming increasingly evident that just a few subsequent years of aberrant climate may substantially change plant performance (Callaghan *et al*., 1996; Robinson *et al*., 1998; Alatalo and Molau, 2000), thereby influencing species' maintenance in their habitats as well as their overall productivity. Change in stature (from decumbent to ascending) in, *e.g*., deciduous shrubs such as the dwarf birch (*Betula nana*), may feed back directly to the local climate in terms of reduced albedo, affecting the radiation balance of the area.

Previous studies show that seed weight did not differ significantly between rather

This document is provided by JAXA.

remote ITEX sites in either *Dryas octopetala* (Latnjajaure and Niwot Ridge, Colorado; Welker *et al.*, 1997) or *Eriophorum vaginatum* (Latnjajaure and Toolik Lake, Alaska; Molau and Shaver, 1997). However, bulbil weight in *Polygonum viviparum* was almost twice as high at Latnjajaure than at the Norwegian Finse site, both within the Scandes Mountains. Despite the existing genetical variation within populations of *P. viviparum* demonstrated by Bauert (1993, 1996), most of the variation in characters like propagule weight should be expected to be contributed by differences among populations in a mainly asexually reproducing species (*cf.* Molau and Prentice, 1992, and references therein).

4.3. Response rate

The tundra plant short-term responses to experimental warming (reported in Henry and Molau, 1997, and references therein; Arft *et al.*, 1999) hold true also in the somewhat longer term. In addition, some responses build up through the years, such as the increase in ovule number per flower or inflorescence. Such longer-term responses at the plant level take at least three years to become evident and statistically validated. Responses to warming at the community level require even longer time periods of study (*e.g.*, Chapin *et al.*, 1995; Molau and Alatalo, 1998; Alatalo and Molau, 2000).

Some responses were rather instant, indicative of changes that might take place in a changing climate. In particular, propagule weight increased already the first season of treatment in all study species. From the data set it is evident that a poor summer like that of 1995 does not inflict much seed production, whereas summers like those of 1996 and 1997 may very well be the most important ones in an individual plant's life time when reproductive output is concerned.

4.4. Forecast

The "truly" arctic and alpine evergreen dwarf-shrubs are the most vulnerable to climate warming, whereas graminoids and herbs have the best capability to cope with rapid changes in the environment in the short term. Deciduous shrubs, like the mid-alpine dwarf form of *Betula nana*, seems to be slower starters but winners in the long run if facing temperature increase; these processes are seen in the community level experiments at Latnjajaure after 3–4 years of study (Molau and Alatalo, 1998; Alatalo and Molau, 2000). It should also be underpinned that the plants dealt with in the ITEX program are all "arctic specialists"; species with a mainly boreal distribution and with their upper distributional limits in the Low Arctic or the mid alpine zone, may respond quite differently to the imposed environmental cues (Graglia *et al.*, 1997; Kudo *et al.*, 1999). The observed response spectra in the handful of species studied cannot immediately be applied to entire plant life forms or "functional types", even though some general trends may be identified (see Henry and Molau, 1997; Arft *et al.*, 1999). In the Low Arctic as well as in alpine environments, a shift in balance among the resident plant life forms towards a dominance by deciduous dwarf-shrubs is to be expected in a warmer climate. The immigration of alien species from lower vegetation zones is an even slower process (Callaghan *et al.*, 1996; Molau and Alatalo, 1998).

Short-term growth responses assessed during the first two or three years of an ITEX survey provide a solid starting-point picture of the responses of individual plant species to climate change, even though tuning of the responses in a competitive environment requires

This document is provided by JAXA.

much longer data sets. Reproductive responses require longer-term studies, but in most cases five-year terms seem sufficient. Secondary, indirect responses like those brought about by plant-plant competition, however, need longer study periods and another scale of observation. With the ongoing activities within ITEX and related projects we will hopefully acquire a much better understanding of long-term changes in the tundra within the next decade.

Acknowledgments

This study was carried out thanks to substantial grants from the Swedish Natural Sciences Research Council (NFR; B-AA/BU 08424), the Kempe Foundation, the Swedish Agency for Nature Protection, and a starting grant from the Swedish Society for Nature Conservation. I thank the following field assistants for their work during the 1993–97 field sessions: Juha Alatalo, Sünne Burmeister, Elizabeth Cooper, Karsten Hagmann, Annika Jägerbrand, Olga Khitun, Petra Kiiskinen, Karin Lindblad, Eva Nilsson, Urban Nordenhäll, Henrik Pärn, Priitta Pöyhtäri, Satu Räsänen, Anna Stenström, and Tomás Zicha. I thank Bente Eriksen, Ingibjörg Svala Jónsdóttir, and Sven Jonasson for critical reading of earlier drafts of this paper. Special thanks are due to Vivian Aldén, among other things responsible for all weighing of propagules at the laboratory. I would also like to thank the Abisko Natural Sciences Research Station (ANS) and its staff for help and hospitality.

References

Alatalo, J.M. and Molau, U. (2000): Responses of subarctic-alpine plant communities to simulated environmental change: biomass and reproduction. submitted to Global Change Biol.

Alatalo, J.M. and Totland, Ø. (1997): Response to simulated climatic change in an alpine and subarctic pollen-risk strategist, *Silene acaulis*. Global Change Biol., **3 (Suppl. 1)**, 74–79.

Arft, A.M. and 28 colleagues (1999): Response patterns of arctic plant species to experimental warming. Ecol. Monogr., **69**, 491–511.

Bauert, M.R. (1993): Vivipary in *Polygonum viviparum*: an adaptation to cold climate? Nord. J. Bot., **13**, 473–480.

Bauert, M.R. (1996): Genetic diversity and ecotypic differentiation in arctic and alpine populations of *Polygonum viviparum*. Arct. Alp. Res., **28**, 190–195.

Björk, R. (2000): Soil properties and plant community types at Latnjajaure. B.Sc. thesis, Botanical Institute, Göteborg University, 16 p.

Bliss, L.C. and Matveyeva, N.V. (1992): Circumpolar arctic vegetation. Arctic Ecosystems in a Changing Climate: An Ecophysiological Perspective, ed. by F.S. Chapin III *et al*. New York, Academic Press, 59–89.

Callaghan, T.V., Carlsson, B.Å. and Tyler, N.J.C. (1989): Historical records of climate-related growth in *Cassiope tetragona* from the Arctic. J. Ecol., **77**, 823–827.

Callaghan, T.V., Maxwell, B., Molau, U., Oechel, W.C. and Panikov, N.S. (1996): Terrestrial ecosystems and feedbacks on climate change. Arctic Systems: Natural Environments, Human Actions, Nonlinear Processes, ed. by J. Lloyd Wright and C.W. Sheehan. Oslo, IASC, 68–82.

Chapin, F.S.III, Shaver, G.R., Giblin, A.E., Nadelhoffer, K.J. and Laundre, J.A. (1995): Responses of arctic tundra to experimental and observed changes in climate. Ecology, **76**, 694–711.

Diggle, P.K. (1997): Extreme preformation in alpine *Polygonum viviparum*: an architectural and developmental analysis. Am. J. Bot., **84**, 154–169.

Graglia, E., Jonasson, S., Michelsen, A. and Schmidt, I.K. (1997): Effects of shading, nutrient application and warming on leaf growth and shoot densities of dwarf shrubs in two arctic-alpine plant communities. Ecoscience, **4**, 191–198.

This document is provided by JAXA.

Havström, M., Callaghan, T.V. and Jonasson, S. (1993): Differential growth responses of *Cassiope tetragona*, an arctic dwarf-shrub, to environmental perturbations among three contrasting high- and subarctic sites. Oikos, **66**, 389–402.

Henry, G.H.R. and Molau, U. (1997): Tundra plants and climate change: the International Tundra Experiment (ITEX). Global Change Biol., **3 (Suppl. 1)**, 1–9.

Johnstone, J.F. and Henry, G.H.R. (1997): Retrospective analysis of growth and reproduction in *Cassiope tetragona* and relations to climate in the Canadian High Arctic. Arct. Alp. Res., **29**, 459–469.

Johnstone, J.F., Molau, U. and Marion, G.M. (1996): Experimental design and statistical analysis in ITEX. ITEX Manual, 2nd ed., ed. by U. Molau and P. Mølgaard. Copenhagen, Danish Polar Centre, 46–48.

Jones, M.H., Bay, C. and Nordenhäll, U. (1997): Effects of experimental warming on arctic willows (*Salix* spp.): a comparison of responses from the Canadian High Arctic, Alaskan Arctic, and Swedish Subarctic. Global Change Biol., **3 (Suppl. 1)**, 55–60.

Kudo, G., Nordenhäll, U. and Molau, U. (1999): Effects of snow-melt timing on leaf traits, leaf production and shoot growth of alpine plants: comparisons along a snow-melt gradient in northern Sweden. Ecoscience, **6**, 439–450.

Marion, G.M., Henry, G.H.R., Freckman, D.W., Johnstone, J., Jones, G., Jones, M.H., Lévesque, E., Molau, U., Mølgaard, P., Parsons, A.N., Svoboda, J. and Virginia, R.A. (1997): Open-top designs for manipulating field temperatures in high-latitude ecosystems. Global Change Biol., **3 (Suppl. 1)**, 20–32.

Mark. A.F., Fetcher, N., Shaver, G.R. and Chapin, F.S.III. (1985): Estimated ages of mature tussocks of cotton sedge, *Eriophorum vaginatum*, along a latitudinal gradient in central Alaska. Arct. Alp. Res., **17**, 1–5.

Molau, U., ed. (1993a): ITEX Manual. Copenhagen, Danish Polar Centre.

Molau, U. (1993b): Relationships between flowering phenology and life history strategies in tundra plants. Arct. Alp. Res., **25**, 391–402.

Molau, U. (1996): Climatic impacts on flowering, growth, and vigour in an arctic-alpine cushion plant, *Diapensia lapponica*, under different snow cover regimes. Ecol. Bull., **45**, 210–219.

Molau, U. (1997a): Phenology and reproductive success in arctic plants: susceptibility to climate change. Global Change and Arctic Terrestrial Ecosystems, ed. by W.C. Oechel *et al*. New York, Springer-Verlag, 153–170.

Molau, U. (1997b): Responses to natural climatic variation and experimental warming in two tundra plant species with contrasting life forms: *Cassiope tetragona* and *Ranunculus nivalis*. Global Change Biol., **3 (Suppl. 1)**, 97–107.

Molau, U. and Alatalo, J.M. (1998): Responses of subarctic-alpine plant communities to simulated environmental change: biodiversity of bryophytes, lichens, and vascular plants. Ambio, **27**, 322–329.

Molau, U. and Edlund, S. (1996): Plant response variables. ITEX Manual, 2nd ed., ed. by U. Molau and P. Mølgaard. Copenhagen, Danish Polar Centre, 23–32.

Molau, U. and Larsson, E.-L. (2000): Seed rain and seed bank along an alpine altitudinal gradient in Swedish Lapland. Can. J. Bot., **78**, 728–747.

Molau, U. and Mølgaard, P., ed. (1996): ITEX Manual, 2nd ed. Copenhagen, Danish Polar Centre.

Molau, U. and Prentice, H.C. (1992): Reproductive system and population structure in three arctic *Saxifraga* species. J. Ecol., **80**, 149–161.

Molau, U. and Rosander, T. (1995): The Arctic Tundra in a Changing Climate. Medieteknik©, Göteborg University, video presentation, 38 min.

Molau, U. and Shaver, G.R. (1997): Controls on seed production and seed germinability in *Eriophorum vaginatum*. Global Change Biol., **3 (Suppl. 1)**, 80–88.

Murray, D.F. (1997): Systematics of the ITEX species. Global Change Biol., **3 (Suppl. 1)**, 10–19.

Robinson, C.H, Wookey, P.A., Lee, J.A., Callaghan, T.V. and Press, M.C. (1998): Plant community responses to simulated environmental change at a high arctic polar semi-desert. Ecology, **79**, 856–866.

Shaver, G.R. and Laundre, J.A. (1997): Exsertion, elongation, and senescence of leaves of *Eriophorum*

This document is provided by JAXA.

vaginatum and *Carex bigelowii* in Northern Alaska. Global Change Biol., **3 (Suppl. 1)**, 146–157.

Shaver, G.R., Fetcher, N. and Chapin, F.S.III. (1986): Growth and flowering in *Eriophorum vaginatum*: annual and latitudinal variation. Ecology, **76**, 1524–1535.

SMHI (1996): Väder och vatten. Augusti 1996. SMHI, Norrköping (in Swedish).

SMHI (1997): Väder och vatten. Augusti 1997. SMHI, Norrköping (in Swedish).

Sokal, R.R. and Rohlf, F.J. (1981): Biometry, 2nd ed. New York, Freeman.

Sørensen, T. (1941): Temperature relations and phenology of the northeast Greenland flowering plants. Medd. Grønl., **125(9)**, 1–305+Pl. 1–15.

Stenström, A. and Jónsdóttir, I.S. (1997): Responses of the clonal sedge, *Carex bigelowii*, to two seasons of simulated climate change. Global Change Biol., **3 (Suppl. 1)**, 89–96.

Stenström, M., Gügerli, F. and Henry, G.H.R. (1997): Response of *Saxifraga oppositifolia* L. to simulated climate change at three contrasting latitudes. Global Change Biol., **3 (Suppl. 1)**, 44–54.

Totland, Ø. and Nyhlén, J. (1998): Assessment of the effects of environmental change on the performance and density *Bistorta vivipara*: the use of multivariate analysis and experimental manipulation. J. Ecol., **86**, 989–998.

Wallberg, L. (1997): *Eriophorum vaginatum*: temperature impacts on leaf length and shoot initiation. B. Sc. thesis, Göteborg University, 10 p.

Welker, J.M., Molau, U., Parsons, A.N., Robinson, C.H. and Wookey, P.A. (1997): Responses of *Dryas octopetala* to ITEX environmental manipulations: a synthesis with circumpolar comparisons. Global Change Biol., **3 (Suppl. 1)**, 61–73.

Wookey, P.A., Parsons, A.N., Welker, J.M., Potter, J.A., Callaghan, T.V., Lee, J.A. and Press, M.C. (1993): Comparative responses of phenology and reproductive development to simulated environmental change in sub-arctic and high arctic plants. Oikos, **67**, 490–502.

(Received April 3, 2000; Revised manuscript accepted September 1, 2000)

This document is provided by JAXA.

Appendix

Annual means of plant response variables at Latnjajaure 1993–97 in controls and open-top chambers (OTCs). Values are given as plot means±SE; $n=5$ for each year and treatment. Each value is the mean of data from four individual plants in each plot. Thawing dates for 1993 are not analyzed for OTCs (given within brackets) as they were implemented at thawing and consequently had no impact on thawing time that year; they were, however, used for calculating prefloration time as the warming experiment started out as the OTCs were put out.

a. *Cassiope tetragona*

Year	Treatment	Thawing date (day no.)	Prefloration time (d)	Flower duration (d)	Fruit : flower ratio	Fruit weight (mg)[1]	Annual growth increment (mm)
1993	Control	135.6±1.6	43.0±1.0	12.7±1.2	0.63±0.06		8.37±0.52
1993	OTC	(135.6±1.6)	36.6±2.0	11.2±1.6	0.53±0.05		8.78±0.47
1994	Control	155.1±5.1	31.4±1.4	9.5±0.2	0.54±0.14		8.66±0.28
1994	OTC	150.4±4.9	31.8±3.4	6.7±1.9	0.44±0.06		8.51±0.16
1995	Control	168.4±5.4	27.7±2.7	9.1±1.8	0.18±0.09	3.83±0.79	7.58±0.36
1995	OTC	163.1±5.0	25.9±1.6	12.4±2.8	0.41±0.11	5.59±0.68	7.48±0.38
1996	Control	153.5±1.8	34.9±3.5	13.6±3.9	0.55±0.20		9.94±0.35
1996	OTC	149.6±1.3	28.4±0.8	11.2±1.4	0.58±0.05		10.10±0.36
1997	Control	140.7±0.6	26.8±1.1	12.6±0.9	0.33±0.13		11.07±0.76
1997	OTC	140.8±0.8	19.4±1.1	12.2±2.1	0.46±0.07		10.86±0.36

[1]Fruit weight measured only in 1995 (see Molau, 1997b).

b. *Dryas octopetala*

Year	Treatment	Thawing date (day no.)	Prefloration time (d)	Flower duration (d)[1]	Seed : ovule ratio[2]	Seed weight (mg)	Leaf length (mm)
1993	Control	137.4±1.5	47.5±1.2	9.7±0.6		0.22±0.04	17.2±0.9
1993	OTC	(137.4±1.5)	42.9±1.5	10.1±0.3		0.21±0.05	19.5±0.4
1994	Control	133.2±2.0	65.2±2.1	8.6±1.2	0.26±0.08	0.28±0.04	17.0±0.8
1994	OTC	133.2±2.0	36.8±1.8	11.4±0.2	0.22±0.09	0.36±0.10	20.8±1.1
1995	Control	152.5±1.8	48.1±2.2	7.8±0.5	0.11±0.11	0.12±0.01	16.8±0.4
1995	OTC	147.0±4.2	35.0±2.7	12.7±1.1	0.52±0.17	0.40±0.09	21.1±0.8
1996	Control	145.8±4.0	55.7±4.3	10.1±0.4	0.48±0.20	0.47±0.02	16.1±0.6
1996	OTC	144.0±4.1	40.8±3.8	13.7±1.0	0.31±0.09	0.46±0.08	20.5±0.4
1997	Control	139.2±1.9	33.6±2.0		0.34±0.09	0.61±0.03	18.6±0.6
1997	OTC	133.8±2.3	32.3±1.8		0.22±0.06	0.61±0.05	22.6±0.8

[1]Flower duration not recorded in 1997.
[2]Seed:ovule ratio not calculated in 1993 due to lack of seed set in marked plants.

This document is provided by JAXA.

c. *Eriophorum vaginatum*

Year	Treatment	Thawing date (day no.)	Prefloration time (d)	Postfloration time (d)	Seed : ovule ratio	Seed weight (mg)	Total green length (mm)[1]
1993	Control	142.2±0.7	13.2±1.0	60.1±1.1	0.13±0.02	0.52±0.02	
1993	OTC	(142.2±0.7)	9.5±0.3	54.6±1.2	0.09±0.02	0.80±0.03	
1994	Control	160.2±0.6	9.6±0.9	61.0±3.0	0.05±0.02	0.69±0.07	164.3± 8.7
1994	OTC	159.7±0.3	7.0±0.2	51.9±2.2	0.08±0.02	0.86±0.02	207.3±12.8
1995	Control	161.0±1.3	9.7±1.9	69.0±2.1	0.08±0.01	0.30±0.03	143.9±12.9
1995	OTC	160.5±1.1	5.8±1.4	72.5±1.3	0.06±0.02	0.79±0.07	202.2±14.6
1996	Control	152.1±0.9	9.9±0.5	66.1±1.1	0.09±0.01	0.58±0.03	166.6±29.4
1996	OTC	151.4±0.6	4.4±0.4	64.0±2.2	0.20±0.04	0.85±0.03	190.7±12.6
1997	Control	146.2±2.6	6.6±0.7	40.5±0.9	0.30±0.04	0.54±0.04	
1997	OTC	141.6±1.6	5.2±1.4	35.2±2.9	0.04±0.02	1.03±0.04	

[1]Tillers monitored at 5–10 day intervals in the summers of 1994–1996; maximum value of the season used.

d. *Polygonum viviparum*

Year	Treatment	Thawing date (day no.)	Prefloration time (d)	Bulbil no.	Bulbil weight (mg)	Shoot height (cm)	Leaf area (cm^2)
1994	Control	133.2±2.0	62.9±2.6	11.9±1.5	0.99±0.14	9.39±0.64	3.65±0.23
1994	OTC	133.6±1.6	57.6±3.6	13.8±1.6	0.99±0.06	10.64±0.29	5.30±0.31
1995	Control	152.5±1.8	52.6±2.7	23.7±2.9	1.14±0.05	11.80±1.03	4.35±0.30
1995	OTC	147.0±4.2	50.0±1.1	30.7±3.0	1.24±0.11	13.00±0.99	6.01±0.83
1996	Control	145.8±4.0	63.5±6.8	24.4±3.8	1.13±0.05	11.07±0.74	4.21±0.30
1996	OTC	144.0±4.1	53.9±7.5	27.2±3.1	1.44±0.14	11.97±0.59	5.51±0.43
1997	Control	133.8±1.6	51.7±3.3	23.4±3.8	1.23±0.13	11.64±0.35	4.40±0.27
1997	OTC	133.8±2.3	54.3±4.4	25.7±4.4	1.28±0.08	12.49±0.42	5.34±0.29

e. *Ranunculus nivalis*[1]

Year	Treatment	Thawing date (day no.)	Prefloration time (d)	Postfloration time (d)	Seed : ovule ratio	Nutlet weight (mg)	Basal leaf width (mm)
1993	Control[2]	190.6±5.6	6.4±1.9	24.7±2.5	0.27±0.06	0.32±0.04	16.2±0.3
1993	OTC	(190.6±5.6)	5.5±1.6	22.5±1.5	0.31±0.08	0.41±0.07	20.0±1.0
1994	Control	159.2±1.5	14.0±1.4	35.6±2.0	0.14±0.08	0.39±0.05	15.8±0.8
1994	OTC	154.4±3.6	13.8±3.1	40.4±1.3	0.06±0.02	0.49±0.06	21.5±0.9
1995	Control	155.9±0.6	16.1±2.5	47.1±0.6	0.29±0.06	0.38±0.02	16.8±1.1
1995	OTC	153.8±1.7	16.3±3.4	39.4±3.6	0.27±0.02	0.47±0.03	23.2±0.9
1996	Control	154.8±1.3	20.5±3.1	49.0±5.5	0.23±0.08	0.44±0.04	18.0±1.5
1996	OTC	152.0±1.8	15.7±1.7	46.5±2.1	0.27±0.01	0.58±0.03	21.7±0.9
1997	Control	149.6±2.2	13.6±2.0	33.9±1.0	0.43±0.04	0.51±0.01	17.9±1.0
1997	OTC	143.8±5.3	16.3±3.2	32.6±2.4	0.19±0.04	0.55±0.03	23.9±0.8

[1]A few figures for 1993–95 are slightly changed since the report in Molau (1997b); this revision is a result of revisitation of rain-damaged or poorly written field protocols. The deviations are minor and do not affect the analysis results.

[2]Note unusual late thawing in 1993, due to the abnormal winter snow depth (≥3 m at the site in March).

This document is provided by JAXA.

Mem. Natl Inst. Polar Res., Spec. Issue, 54, 467-478, 2001

Scientific note

Pattern of seedling emergence of alpine plants: Comparisons between fellfield and snowbed habitats

Yoshiko Shimono and Gaku Kudo

Graduate School of Environmental Earth Science, Hokkaido University, Sapporo 060-0810

Abstract: We observed the germination pattern of alpine plants at a fellfield (three species) and a snowbed (four species) in relation to environmental differences between the habitats. Emergence patterns of seedlings varied among species within each habitat, especially at the fellfield, which has a relatively long growing season. At the fellfield, the peak of seedling emergence occurred early in the growing season for *Potentilla matsumurae*, mid-season for *Patrinia sivirica*, and late season for *Bupleurum ranunculoides*. At the snowbed, germination of *Peucedanum multivittatum* started immediately after snowmelt, germination of *P. matsumurae* and *Primula cuneifolia* were concentrated in early July, and germination of *Arnica unalaschcensis* was common in mid-July in 1998. Species which produced large seeds tended to have a short period for seedling growth, while species which produced small seeds tended to continue seedling growth as long as they could. Temperature requirements for germination of *P. matsumurae* differed between the habitats. Seeds in the snowbed population needed a warmer temperature regime for germination than seeds in the fellfield population. These results indicate that germination traits may differ between habitats even within the same species.

1. Introduction

Because the young seedling stage is most sensitive to various environmental stresses for establishment of most plants, timing of seed germination crucially affects subsequent survivorship of seedlings under seasonal climates where growing conditions fluctuate throughout the year (Baskin and Baskin, 1979; Kachi and Hirose, 1990; Marks and Prince, 1981; Maruta, 1976). Various factors are related to the timing of seed germination: *e.g.* life form (Baskin and Baskin, 1988), seed size (Gross, 1984; Stanton, 1985), and environmental conditions such as water availability (Swagel *et al.*, 1997) and winter severity (Meyer *et al.*, 1995; Meyer and Monsen, 1991). It has been reported that the germination pattern varies among co-occurring species within a moist grassland community in a warm temperate region (Masuda and Washitani, 1990). This means that there are several choices of germination schedules for plants under conditions of relatively long growing season.

Arctic and alpine environments are characterized by short growing season (Billings and Mooney, 1968; Bliss, 1971), where current year seedlings must rapidly grow to larger than a certain critical size for survival during winter (Maruta, 1983, 1994). Therefore, variation of seed germination timing among co-occurring species may be much smaller

This document is provided by JAXA.

there than in temperate environments.

Generally, growing conditions in alpine environments are not uniform but heterogeneous even within a local area. This is mainly caused by differences in the time of snowmelt (Billings, 1974; Miller, 1982). Fellfields and snowbeds are contrasting habitat types within the alpine ecosystem. Fellfields are located on ridges or around mountaintops, snowbeds on leeward slopes. Little snow accumulation at fellfields results in freezing soil during winter, frost in spring, and soil drought in the growing season. On the other hand, thick snow cover at snowbeds protects soil and plants from freezing and frost, and lingering snow provides water in summer. Because of such differences in soil conditions, factors that threaten seedling establishment should differ between the habitats.

In alpine environments, soil drought and needle ice activity are considered to be the most important environmental stresses for seedling establishment during the first growing season (Bliss, 1971). This is especially applicable to fellfield plants. At snowbeds, plants are not exposed from snow cover until the middle of the season when frost is not common, and water supply from lingering snow and developed organic soil retain soil moisture throughout the growing season. On the other hand, the growing season is extremely short due to the lateness of snowmelt. Therefore, germination of snowbed plants should occur as early as possible after snowmelt so that seedlings can extend the growing period until winter. At fellfields, simultaneous germination in early season may result in complete failure in seedling establishment due to spring frost or unexpected snowfall. On the other hand, germination too late in the season may cause insufficient growth, which makes it difficult to overwinter. Furthermore, drought stress may prevent seedling establishment through the summer season. Therefore, a scattered germination pattern thorughout the growing season may be adaptive for risk dispersal at fellfields.

We observed germination patterns of several alpine plant species at a fellfield and a snowbed. The purpose of this study is to confirm whether there is any variation of germination timing among co-occurring species within habitats, and whether expected patterns of seedling emergence occur between the habitats, by comparing germination timing and survival during a summer season in the field.

2. Materials and methods

2.1. Study sites

This study was conducted at a fellfield and a snowbed situated in the central part of the Taisetsu Mountains (43°13′-45′N, 142°32′-143°19′E), Hokkaido, northern Japan. The sites are located 1500 m apart from each other.

The fellfield site is located on a terrace at 1700 m above sea level. There is little snow accumulation during winter due to strong wind, and ground temperatures sometimes fall to −15℃ in winter. Dwarf shrubs such as *Empetrum nigrum* var. *japonicum*, *Diapensia lapponica* ssp. *obovata*, *Loiseleuria procumbens*, and *Bryanthus gmelinii* dominate, lichens (mainly *Cladonia* and *Cetraria* species) commonly cover the ground. Because of poor vegetation cover, the soil surface temperature becomes extremely high on fine days even in early spring, but frost can occur unexpectedly. Soil moisture is generally low throughout the summer due to less-organic gravelly soil (Y. Shimono, unpublished data).

The snowbed site is located on a southeast-facing slope at 1880 m a.s.l. Because of

This document is provided by JAXA.

thick snow cover, the soil surface temperature remains constant at 0℃ during winter. Snow usually disappears sometime in July. Dwarf shrubs such as *Phyllodoce caerulea*, *P. aleutica*, and *Sieversia pentapetala*, and herbs such as *Primula cuneifolia*, *Peucedanum multivittatum*, and *Veronica stelleri* var. *longistyla*, dominate there. Because of development of organic soil and dense plant cover at the snowbed, soil moisture remains moderate (Y. Shimono, unpublished data).

The time of snow disappearance was recorded in 1998 and 1999 at the snowbed, and soil surface temperature was recorded at one hour intervals by Optic StowAway (Onset Co., U.S.A.) from May to September in 1998 and 1999 at both sites. Precipitation and solar radiation accumulation at one-hour intervals were also recorded by automatic data loggers (KADEC UP, Kona Systems, Japan) during summer at the fellfield in 1998 and 1999.

2.2. Observation of seedling emergence

On 3 June 1998, six 100×100 cm quadrats were set on places where some seedlings just started to emerge at the fellfield. On 9 June 1998, six 40×40 cm quadrats were placed at the snowbed similarly. Thereafter, emergence and survival of current-year seedlings were recorded at 10-day intervals until 27 September 1998, and the species of each seedling was identified. The current-year seedlings were distinguished by the presence of cotyledons. Species of which more than 40 seedlings were observed at each site were used for analysis in this study. The temperature requirement for germination of each species was quantified by measuring mean soil surface temperature during 10 days before germination among cohorts observed at 10-day intervals.

Only seedlings of *Potentilla matsumurae*, one of the identified species, were observed commonly at both habitats. We continued the observation of *P. matsumurae* the next year by using the same quadrats to compare the effect of yearly fluctuation of snowmelt timing on germination patterns. Emergence and survival of current-year seedlings were recorded at 10-day intervals from 10 June to 28 August 1999 in the same quadrats.

2.3. Comparisons of seed size

It is known that variation of seed size influences germination rate (Stanton, 1984; Winn, 1985) and subsequent survivorship (Galen *et al.*, 1991; Maruta, 1994; Vera, 1997). To grasp seed size variations among observed species and other co-occuring species within each community, seed weights of dominant species (total 28 species, listed in Table 2) were measured at the fellfield and the snowbed. Fully mature seeds were collected from more than 20 individuals in each species at each habitat, dried at room temperature for about one month, and then seed weights without any attachments such as pappus were measured (20 replications).

3. Results

3.1. Environmental conditions

Timing of snowmelt at the snowbed fluctuated between the years. Spring of 1998 was characterized by very little snow and warm conditions which resulted in very early snowmelt. Snow disappeared on 8 June in 1998 at the snowbed, 42 days earlier than in 1999.

This document is provided by JAXA.

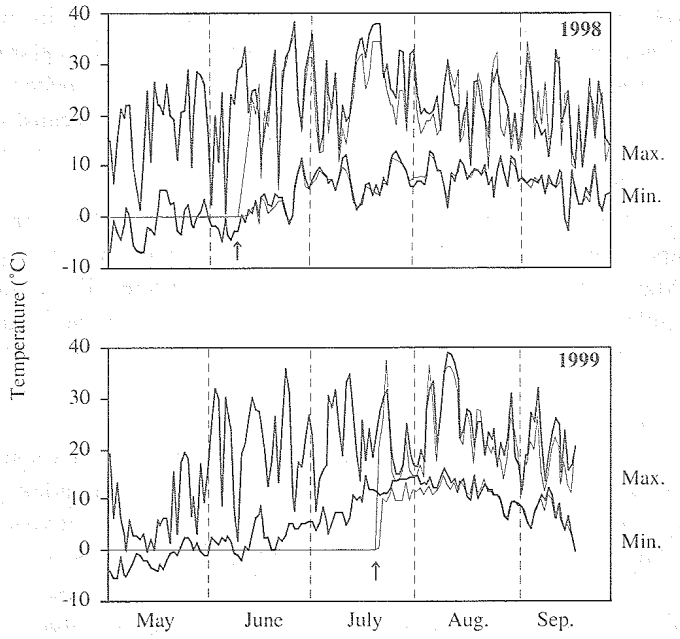


Fig. 1. Seasonal transition of daily maximum and minimum soil surface temperatures at the fellfield (thick lines) and the snowbed (thin lines). Arrows show the time of snowmelt at the snowbed. Until snowmelt, soil surface temperature remained at 0°C at the snowbed.

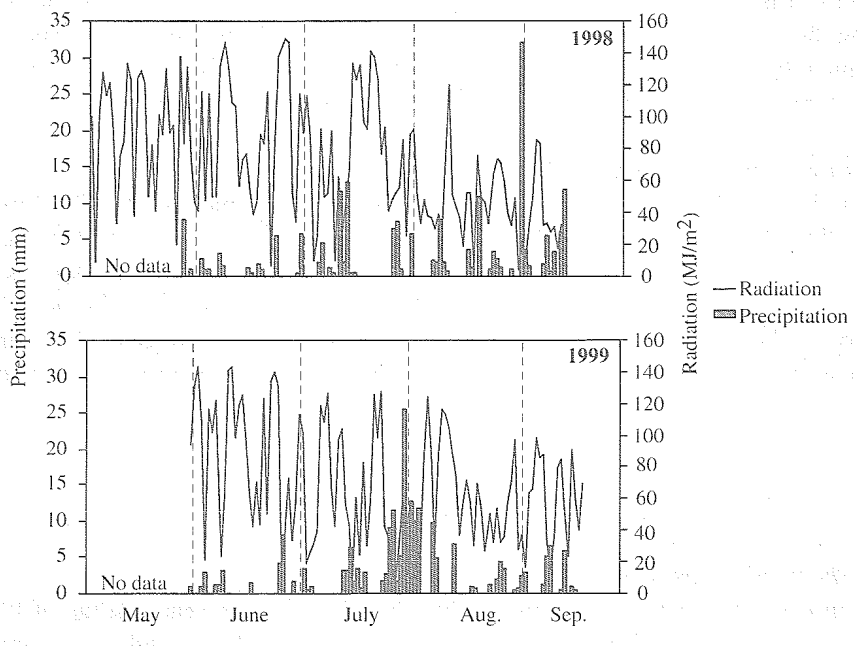


Fig. 2. Seasonal transition of daily accumulation of solar radiation and precipitation. Measurements were done at the fellfield in 1998 and 1999.

This document is provided by JAXA.

Soil surface temperature sometimes increased to more than 20℃ in May, but frost occurred nearly every night (Fig. 1). Soil surface temperature highly fluctuated in June when daily maximum temperature was sometimes higher than 30℃ on fine days, while daily minimum temperature sometimes decreased below zero at night. Because of little rainfall and strong solar radiation (Fig. 2), June corresponded to a dry season in this area. Starting in July, daily minimum temperature increased to more than 5℃. Daily maximum temperature at the snowbed was lower than that at the fellfield in both years (Fig. 2, Two group t-test, $P<.0001$, 1.4℃ difference in 1998 and 2.1℃ difference in 1999). Similarly, daily minimum temperature at the snowbed was slightly lower than that at the fellfield ($P<.001$, 0.3℃ difference in 1998 and 0.9℃ difference in 1999).

3.2. Patterns of seedling emergence in 1998

Among seedlings observed in the quadrats, three herbaceous species (*Potentilla matsumurae*, *Patrinia sibirica*, and *Bupleurum ranunculoides* var. *alpinum*) were identified as common species at the fellfield, and four herbaceous species (*Peucedanum multivittatum*, *Potentilla matsumurae*, *Arnica unalaschcensis* var. *tschonoskyi*, and *Primula cuneifolia* var. *cuneifolia*) at the snowbed (Table 1). Densities of current-year seedlings were higher at the snowbed (5016 seedlings/m^2) than at the fellfield (38 seedlings/m^2).

Emergence patterns of seedlings varied among the species at both habitats, especially at the fellfield (Fig. 3). At the fellfield, the peak of seedling emergence occurred in early growing season for *P. matsumurae*, mid-season for *P. sivirica*, and late season for *B. ranunculoides*. Because seed dispersal of these species occurred later than the peak emergence time of each species, current year seedlings were derived from overwintered seeds. At the snowbed, germination of *P. multivittatum* started immediately after snowmelt, and new emergence of seedlings stopped by the middle of July. Seedlings of *P. matsumurae* and *P. cuneifolia* showed similar emergence patterns. Germination of both species was concentrated at the beginning of July in 1998. Germination of *A. unalaschcensis* was common in

Table 1. Total number of seedlings observed in six quadrats, and survival rate during the first summer. Quadrate size was 100×100 cm at the fellfield and 40×40 cm at the snowbed.

	Total number of seedlings	Living seedlings at the end of summer	Survival rate
Fellfield			
Potentilla matsumurae (98)	63	44	0.70
(99)	24	20	0.83
Patrinia sibirica	56	31	0.55
Bupleurum ranunculoides	74	66	0.89
Other species	10		
Snowbed			
Potentilla matsumurae (98)	183	163	0.89
(99)	160	139	0.87
Primula cuneifolia	62	50	0.81
Peucedanum multivittatum	299	139	0.46
Arnica unalaschcensis	44	30	0.68
Other species	88		

This document is provided by JAXA.

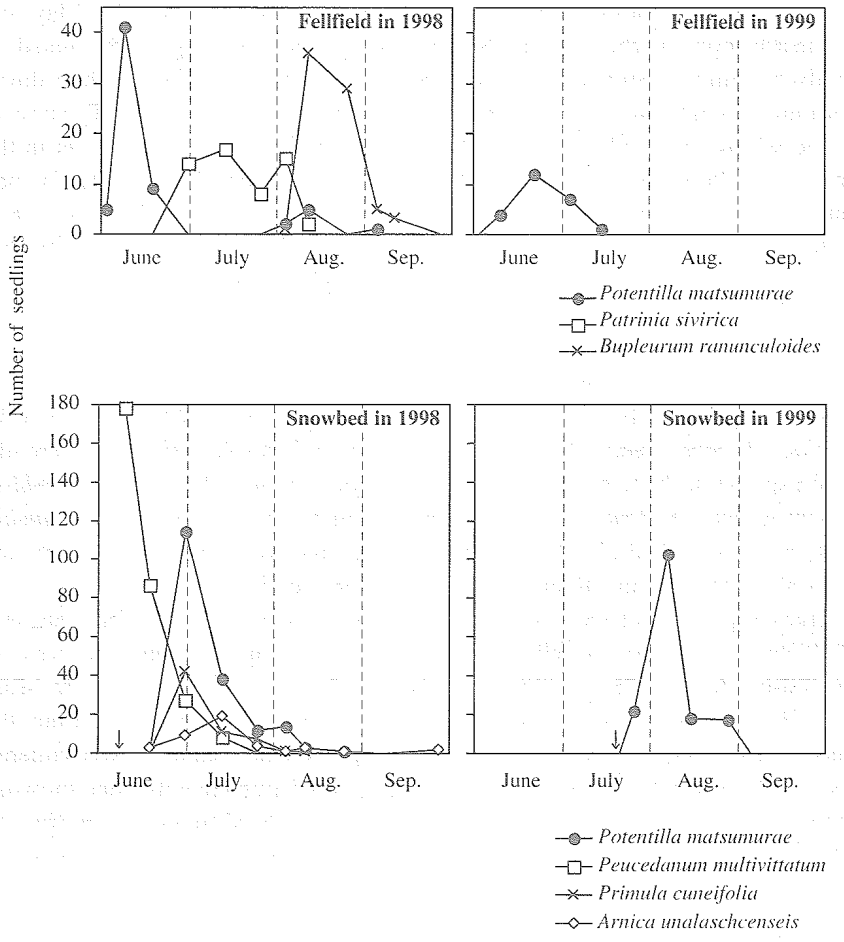


Fig. 3. The number of new seedlings of each species at the fellfield and the snowbed. In 1999, seedlings of Potentilla matsumurae *were observed. Arrows show the time of snowmelt at the snowbed.*

mid-July. All of these seedlings were derived from overwintered seeds.

Distributions of daily mean temperature just before seedling emergence showed that temperature demand for germination significantly differed among the species within each habitat (Fig. 4, Kruskal-Wallis $H=109.66$, $df=2$, $P<.0001$ at the fellfield, and $H=378.23$, $df=3$, $P<.0001$ at the snowbed). At the fellfield, *P. matsumurae* germinated at a significantly lower temperature, and *P. sivirica* needed higher temperature for germination than other species (Steel-Dwass multiple comparisons test for nonparametric analysis, $P<.01$). At the snowbed, *P. multivittatum* germinated at a significantly lower temperature than other species (Steel-Dwass multiple comparisons test for nonparametric analysis, $P<.01$).

Leaf senescence of *P. multivittatum* seedlings, the earliest emerging species, began in mid-August, while seedlings of other species retained green leaves until mid-September. The

This document is provided by JAXA.

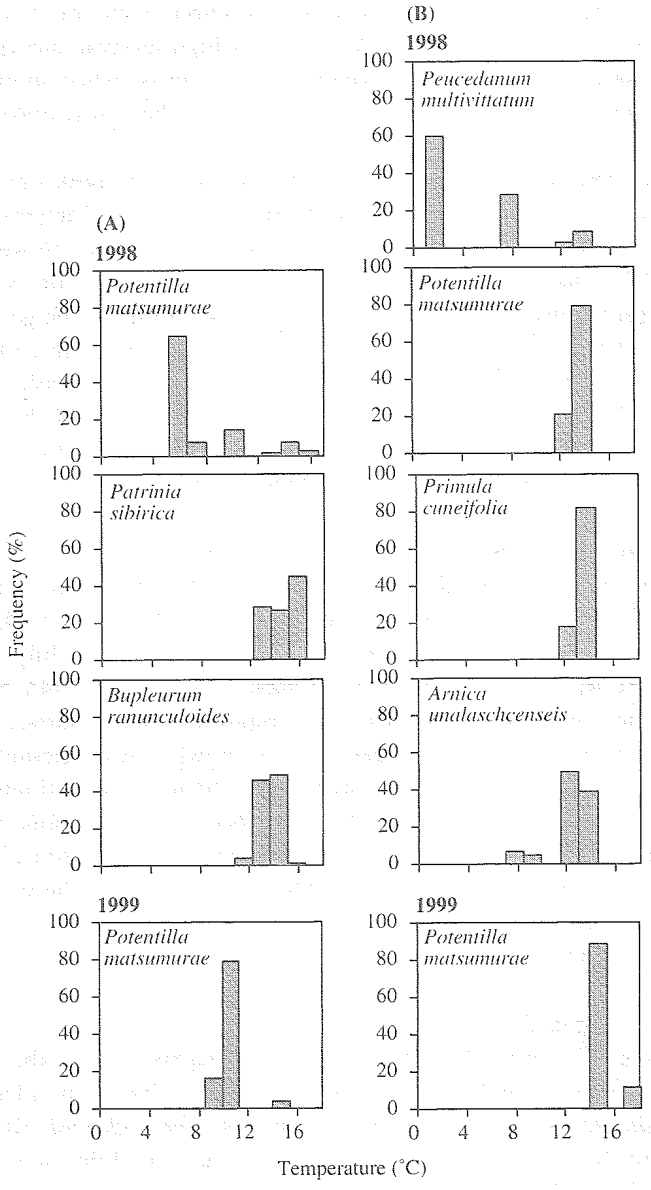


Fig. 4. Emergence of new seedlings with reference to the daily mean soil surface temperature during 10 days before germination of each species in both years at the fellfield (A) and the snowbed (B). When seedlings emerged within 10 days after snowmelt, mean temperature from snowmelt to emergence is used.

survival rate during the 1998 season was low in *P. sivirica* and *P. multivittatum* (Table 1). There was no rainfall during about 10 days in mid-July 1998 when *P. sivirica* germinated vigorously, therefore many seedlings seemed to die of desiccation. Two other species which germinated in months other than July at the fellfield showed high survival rates ranging

This document is provided by JAXA.

from 0.70 to 0.89. At the snowbed, there was little effect of no rainfall, therefore three species, though not *P. multivittatum*, showed relatively high survival rates ranging from 0.68 to 0.89. In the case of *P. multivittatum*, germination occurred when snowmelt water was supplied in the quadrate, therefore many seedlings were washed away outside the quadrates before rooting.

The growing period of each species was obtained from the peak time of germination to leaf senescence in late September (but mid-August for *P. multivittatum*). At the fellfield, seedlings of *P. matsumurae* had the longest growing period (about 16 weeks in 1998 and 14 weeks in 1999), and *B. ranunculoides* had the shortest growing period (6 weeks). *Patrinia sivirica* germinated vigorously for one month, so seedlings that germinated in early July had a 13-week growing period, and seedlings that germinated in early August had 8 weeks. At the snowbed, seedlings of *P. matsumurae* and *P. cuneifolia* had the longest growing period (about 13 weeks), and seedlings of *A. unalaschcensis* had 11 weeks. The growing period of *P. multivittatum* seedlings was the shortest (9 weeks). In 1999, lingering snow shortened the growing period of *P. matsumurae* to only 8 weeks.

3.3. Comparison of P. matsumurae germination between habitats and years

At the snowbed, *P. matsumurae* did not germinate until more than 10 days after snowmelt in 1998 when snow disappeared in early June; however, it took only one week after snowmelt to germinate in 1999 when snow disappeared in mid-July. Daily mean soil surface temperature was below 8℃ when snow melted in 1998, and 14℃ in 1999. Because no seeds germinated when the daily mean temperature of the soil surface was lower than 12℃ (Fig. 4), the time of seedling emergence at the snowbed was determined not only by snowmelt timing but also by seasonal temperature changes. Interestingly, fellfield seeds could germinate under cooler conditions than snowbed seeds, *i.e.*, about 5℃ in 1998, and 8℃ in 1999 (Fig. 4). Distribution of germination temperature significantly differed between the habitats (Kolmogorov-Smirnov test, $P<.0001$ in both years). The yearly difference in peak germination times between 1998 and 1999 was 10 days at the fellfield, whereas it was more than one month at the snowbed.

3.4. Seed weight of dominant species

Most alpine species produced small seeds. Seed weights of 10 of the 15 species at the fellfield and 12 of the 15 species at the snowbed were less than 1 mg (Table 2). Seeds of *P. sibirica*, *B. ranunculoides*, *P. multivittatum*, and *A. unalaschcensis* were larger than 1 mg. Especially, seeds of *P. multivittatum* were largest among alpine species. Seed sizes of *P. matsumurae* (0.3–0.5 mg) and *P. cuneifolia* (<0.2 mg) were relatively small.

4. Discussion

Although several species are compared in this study, patterns of seedling emergence varied among the species within habitats, especially at the fellfield, which has a relatively long growing season. Maruta (1994) reported that final seedling size at the end of the first growing season is correlated with seed size, and that large seedling size is advantageous for the winter survival of two *Polygonum* species growing in an alpine region. At the fellfield, *Potentilla matsumurae* germinated early in the growing season. Because of small seed size,

This document is provided by JAXA.

Table 2. List of species and habitats in which seed weights were measured. Mean value and SD of individual seed weight of each species are shown.

Family	Species	Habitat	Seed weight (mg)
Compositae	*Saussurea yanagisawae*	Fellfield	3.47±0.72
	Arnica unalaschcensis var. *tschonoskyi*	Snowbed	0.91±0.08
	Solidgo virga-aurea var. *leiocarpa*	Snowbed	0.68±0.03
Cyperaceae	*Carex stenanta* var. *taisetsuensis*	Fellfield	0.75±0.10
	Carex pyrenaica	Snowbed	0.61±0.03
Diapensiaceae	*Diapensia lapponica* ssp. *obovata*	Fellfield	0.061±0.002
Empetraceae	*Empetrum nigrum* var. *japonicum*	Fellfield	0.86±0.11
Ericaceae	*Arctous alpinus* var. *japonicus*	Fellfield	5.01±0.92
	Bryanthus gmelinii	Fellfield	0.016±0.001
	Loiseleuria procumbens	Fellfield	0.026±0.001
	Therorhodion camtschaticum	Fellfield	0.028±0.001
	Vaccinium uliginosum var. *alpinum*	Fellfield	0.20±0.01
	Vaccinium vitis-idaea	Fellfield	0.24±0.01
	Phyllodoce aleutica	Snowbed	0.016±0.001
	Rhododendron aureum	Snowbed	0.084±0.004
	Vaccinium ovalifolium	Snowbed	0.140±0.005
Gentianaceae	*Gentiana nipponica*	Snowbed	0.13±0.01
Primulaceae	*Primula cuneifolia* var. *cuneifolia*	Snowbed	0.11±0.01
Ranunculaceae	*Anemone narcissiflora* var. *nipponica*	Snowbed	6.47±1.21
Rosaceae	*Potentilla matsumurae*	Fellfield	0.46±0.09
		Snowbed	0.40±0.07
	Sieversia pentapetala	Snowbed	0.46±0.06
Scrophulariaceae	*Penstemon frutescens*	Fellfield	0.26±0.02
	Pedicularis chamissonis var. *japonica*	Snowbed	0.91±0.03
	Veronica stelleri var. *longisyla*	Snowbed	0.11±0.01
Umbelliferae	*Bupleurum ranunculoides* var. *alpinum*	Fellfield	1.87±0.15
	Tilingia ajanensis	Fellfield	2.06±0.07
		Snowbed	1.95±0.15
	Peucedanum multivittatum	Snowbed	5.60±0.93
Valerianaceae	*Patrinia sibirica*	Fellfield	2.02±0.11

P. matsumurae probably needs a long growing season to accumulate enough reserves before the onset of winter. However, June is the driest season, when daily ground temperature fluctuates intensely. Therefore, seedlings are required to tolerate both freezing temperature and drought stress in this period. The relatively high survival rate during the first summer of *P. matsumurae* (0.70) seems to be evidence of tolerance. On the other hand, *Patrinia sibirica* and *Bupleurum ranunculoides*, having relatively large seed sizes, germinated later than *P. matsumurae*, resulting in a shorter growing season. Due to larger amounts of storage in seeds, these seedlings may not need a long growing period to reach critical size during the first summer, in comparison with species having smaller seeds. In fellfields, later germination may be advantageous to escape frost damage and desiccation stress early in the season. The high survival rate of *B. ranunculoides* may reflect this advantage. Although the temperature requirement for germination was higher in *P. sibirica* than that in *B. ranunculoides*, as shown in Fig. 4, actual emergence of seedlings of *P. sibirica* was earlier than that of *B. ranunculoides* (Fig. 3). Other environmental factors than simple mean temperature, such as day length, may act as important stimuli for germination in these species. For

This document is provided by JAXA.

example, the germination of *Betula pubescens* was enhanced as the day length increased (Bewley and Black, 1982). In contrast, the germination of *Tsuga canadenses* was increased under the short day length condition (Stearns and Olsen, 1958).

At the snowbed, *Peucedanum multivittatum* showed simultaneous germination soon after snow disappearance. We observed that germination of *P. multivittatum* started soon after snowmelt, indicating that this species could germinate under very cool conditions, around 0℃ to 4℃. *P. matsumurae* and *Primula cuneifolia* did not germinate below 12℃, even when snowmelt occurred earlier than usual. Large seeds of *P. multivittatum* are hard to trap in the soil (Chambers *et al*., 1991), and remain on the soil surface where water content reduces quickly (Maruta, 1976). The soil surface absorbs snowmelt water soon after snowmelt. Therefore, very quick germination after snowmelt may be important for seedling establishment of *P. multivittatum*. A previous study reported that most tundra species require nearly water-saturated soils for germination and seedling establishment (Oberbauer and Miller, 1982).

Because *P. multivittatum* stopped growing by mid-August, the leaf life-span of *P. multivittatum* was shortest among the species at the snowbed. If leaf senescence of this species is determined by stimulus of day length or cool temperature, seedlings occurring in late snowmelt years would have an extremely short growing period. Large amounts of resource storage in seeds would make such a life cycle possible. Also, *Arnica unalaschcensis*, having relatively large seeds, tended to germinate slowly, resulting in a short growing season. Therefore, species having larger seeds can get along with a relatively short growing period even in snowbed environments, in comparison with species having smaller seeds. Masuda and Washitani (1990) also reported that interspecific variation of emergence timing seemed to be associated with mean seed weight among the species, *i.e.,* larger seeds tended to emerge later than smaller seeds.

Germination temperature requirements of *P. matsumurae* varied between the habitats. These results indicated that physiological traits of germination in this species may differ between the fellfield and snowbed populations. Snowbed seeds could not germinate when daily mean temperature of soil surface was lower than 12℃. At the snowbed, snow usually disappears in July when mean temperature is more than 10℃, therefore, populations at the snowbed may not have the ability to germinate under cooler conditions than 10℃.

Species specific patterns of emergence at the fellfield varied more than that at the snowbed. At the fellfield, the growing period for plant growth is about 4 months from June to September in every year. On the other hand, the growing period at the snowbed fluctuated unpredictably from about 4 months in 1998 to 2 months in 1999, depending on the snowmelt timing. Germination timing of *P. matsumurae* fluctuated between the years, especially at the snowbed. In fact, the growing period of *P. matsumurae* at the snowbed in 1999 was almost the same as that of *B. ranunculoides*, which was late germination species at the fellfield. Thus, variations of snowmelt timing strongly determined the actual timing of germination of snowbed plants.

Although many species showed concentrated germination patterns with narrow ranges, germination of *P. sivirica* lasted constantly beyond one month at the fellfield. In addition, most seedlings of *P. matsumurae* at the fellfield emerged in June, but some seedlings also emerged in August. We hypothesize that simultaneous germination immediately after snowmelt would be an advantage for seedling establishment in snowbeds, and scattered

This document is provided by JAXA.

germination through the growing season would be an advantage in fellfields. As we expected, snowbed species showed simultaneous germination after snowmelt, and fellfield species which emerged early in the growing period, when environmental conditions fluctuated considerably, may have a wider range of germination timing. Measurements of overwintering survival pattern are necessary to confirm whether such differences in emergence patterns are advantageous.

This study indicates that germination patterns vary among species within a community even in an alpine environment having a short growing season, and such variation partly reflects the variation of seed size. Although we compared only herbaceous species in this study, alpine shrubs such as *Loiseleuria procumbens*, *Bryanthus gmelinii*, *Phyllodoce caerulea*, and *P. aleutica* are important component species at this site, which produces very small seeds ranging from 0.01 to 0.02 mg. The germination timing of these species is an interesting subject for further study.

Acknowledgments

We would like to thank T. Kohyama, S. Tsuyuzaki, and H. Fukuda for their valuable suggestions in planning and discussion. S. Suzuki and T. Kasagi provided assistance and advice. This study was partly supported by a Japan Ministry of Education, Science and Culture Grant-in Aid (#10740355) to G. Kudo.

References

Baskin, C.C. and Baskin, J.M. (1988): Germination ecophysiology of herbaceous plant species in a temperate region. Am. J. Bot., **75**, 286–305.

Baskin, J.M. and Baskin, C.M. (1979): Studies on the autecology and population biology of the weedy monocarpic perennial, *Pastinaca sativa*. J. Ecol., **67**, 601–610.

Bewley, J.D. and Black, M. (1982): Physiology and Biochemistry of Seeds in Relation to Germination, Vol. 2. Berlin, Springer-Verlag.

Billings, W.D. (1974): Adaptations and origins of alpine plants. Arct. Alp. Res., **6**, 129–142.

Billings, W.D. and Mooney, H.A. (1968): The ecology of arctic and alpine plants. Biol. Rev., **43**, 481–529.

Bliss, L.C. (1971): Arctic and alpine plant life cycles. Ann. Rev. Ecol. Syst., **2**, 405–438.

Chambers, J.C., Macmahon, J.A. and Haefner, J.H. (1991): Seed entrapment in alpine ecosystems: effects of soil particle size and diaspore morphology. Ecology, **72**, 1668–1677.

Galen, C. and Stanton, M.L. (1991): Consequences of emergence phenology for reproductive success in *Ranunculus adoneus* (Ranunculaceae). Am. J. Bot., **78**, 978–988.

Gross, K.L. (1984): Effects of seed size and growth form on seedling establishment of six monocarpic perennial plants. J. Ecol., **72**, 369–387.

Kachi, N. and Hirose, T. (1990): Optimal time of seedling emergence in a dune-population of *Oenothera glazioviana*. Ecol. Res., **5**, 143–152.

Marks, M. and Prince, S. (1981): Influence of germination date on survival and fecundity in wild lettuce *Lactuca serriola*. Oikos, **36**, 326–330.

Maruta, E. (1976): Seedling establishment of *Polygonum cuspidatum* on Mt. Fuji. Jpn. J. Ecol., **26**, 101–105.

Maruta, E. (1983): Growth and survival of current-year seedlings of *Polygonum cuspidatum* at the upper distribution limit on Mt. Fuji. Oecologia, **60**, 316–320.

Maruta, E. (1994): Seedling establishment of *Polygonum cuspidatum* and *Polygonum weyrichii* var. alpinum at high altitudes of Mt Fuji. Ecol. Res., **9**, 205–213.

Masuda, M. and Washitani, I. (1990): A comparative ecology of the seasonal schedules for 'reproduction

This document is provided by JAXA.

by seeds' in a moist tall grassland community. Func. Ecol., **4**, 169–182.
Meyer, S.E. and Monsen, S.B. (1991): Habitat-correlated variation in mountain big sagebush (*Artemisia tridentata* ssp. *vaseyana*) seed germination pattern. Ecology, **72**, 739–742.
Meyer, S.E., Kitchen, S.G. and Carlson, S.L. (1995): Seed germination timing patterns in intermountain *Penstemon* (Scrophulariaceae). Am. J. Bot., **82**, 377–389.
Miller, P.C. (1982): Environmental and vegetational variation across a snow accumulation area in montane tundra in central Alaska. Holarct. Ecol., **5**, 85–98.
Oberbauer, S. and Miller, P.C. (1982): Effect of water potential on seed germination. Holarct. Ecol., **5**, 218–220.
Stanton, M.L. (1984): Seed variation in wild radish: effect of seed size on components of seedling and adult fitness. Ecology, **65**, 1105–1112.
Stanton, M.L. (1985): Seed size and emergence time within a stand of wild radish (*Raphanus raphanistrum* L.): the establishment of a fitness hierarchy. Oecologia, **67**, 524–531
Stearns, F. and Olson, J. (1958): Interactions of photoperiod and temperature affecting seed germination in *Tsuga canadensis*. Am. J. Bot., **45**, 53–58.
Swagel, E.N., Bernhard, A. Van H. and Ellmore, G.S. (1997): Substrate water potential constraints on germination of the strangler fig *Ficus aurea* (Moraceae). Am. J. Bot., **84**, 716–722.
Vera, M.L. (1997): Effects of altitude and seed size on germination and seedling survival of heathland plants in north Spain. Plant Ecol., **133**, 101–106.
Winn, A.A. (1985): Effects of seed size and microsite on seedling emergence of *Prunella vulgaris* in four habitats. J. Ecol., **73**, 831–840.

(Received May 2, 2000; Revised manuscript accepted July 11, 2000)

This document is provided by JAXA.

Mem. Natl Inst. Polar Res., Spec. Issue, 54, 479-486, 2001

Scientific paper

Ecological notes on the heath community on Mt. Ebeko, Paramushir Island, northern Kuriles

Susumu Okitsu[1], Yoshinori Minami[2] and Sergei Yu. Grishin[3]

[1]*Faculty of Horticulture, Chiba University, 648 Matsudo, Matsudo 271-8510*
(E-mail: okitsu@midori.h.chiba-u.ac.jp)
[2]*Faculty of Agriculture, Tamagawa University, Tamagawa Gakuen 6-chome, Machida-shi, Tokyo 194-8610*
[3]*Institute of Biology and Pedology, Russian Academy of Sciences, Vladivostok 690022, Russia*

Abstract: Although the northern Kuriles provide ecologically interesting issues on plant communities owing to their phytogeographical position between Hokkaido with its rich flora and Kamchatka with its poor flora, and to repeated volcanism of the islands, ecological studies of the plant communities in this area still remain insufficient. In 1997 we had an opportunity to visit the east slope of Mt. Ebeko, Paramushir Island, northern Kuriles. This paper documents the vertical distribution of the heath community on the east slope of the mountain at altitudes between 30 m to 650 m. Ecological characteristics of the community are discussed with reference to the effects of volcanic activities of the mountain. The dominant plants of the community were dwarf shrubs, forming a treeless heath community that covers the whole east slope. They included *Calamagrostis purpurascens*, *Loiseleuria procumbens*, *Empetrum nigrum* and *Arcterica nana*, forming a heath community in species composition and physiognomy. The heath community of Mt. Ebeko developed under a highly oceanic climate. Plots at lower altitudes consist of a higher number of species including lots uncommon species appearing only at lower altitudes and more common species, while the plots at higher altitudes consisted of a smaller number of species, with only common species. Such decrease of the number of species per plot toward higher altitude might be due to the effect of repeated volcanic activity of Mt. Ebeko. The treeless dwarf shrub vegetation of Mt. Ebeko resembles the wind exposed dwarf scrubs on Mt. Taisetsu, Hokkaido in dominant species and physiognomy.

1. Introduction

The northern Kuriles include the major Islands Alaid, Shumshu, Paramushir and Onekotan, corresponding floristically to the Northern Kurile Region *sensu* Barkalov (1998, 2000). Floristically they are located between the rich Japanese floral region and the comparatively poor Kamchatka floral region (Hultén, 1933). Climatically they belong to a highly oceanic sector of the subarctic zone, having a few climatic relevant areas in the Northern Hemisphere (Tuhkanen, 1984). Additionally, three major islands, Alaid, Paramushir and Onekotan, have active volcanoes. The plant communities of the islands are expected to show interesting ecological characteristics related to volcanic activities as well

This document is provided by JAXA.

as their floristic position and highly oceanic climate.

However, after World War II the northern Kuriles were closed to Japanese botanists. Botanical studies by Russian botanists in the area after World War II are also not abundant (*cf*. Takahashi, 1996). Formerly Kudo (1922) provided an overview of the plant communities and an enumeration of the plants of Paramushir Island. Tatewaki (1934) reported on the flora of the northern Kuriles, and he further noted (Tatewaki, 1944) the dominant species and the distribution of major plant communities of Paramushir and Shumshu Islands. Tatewaki (1957) completed the description of floristic composition and distribution of plants on the Kurile Islands, reviewing the botanical studies before World War II. After World War II Russian botanists started botanical studies on the Kurile Islands (Vorobiev, 1956, 1963; Chernyaeva, 1976). Recently Barkalov (1980, 1981, 1984, 1998, 2000) intensively revealed the flora of the northern Kuriles. Japanese botanists have also recently published notes on the plants of the northern Kuriles (Takahashi and Kuwahara, 1998; Okitsu, 1999, 2000). However, despite these studies, ecological studies of the plant communities in this area remain insufficient.

In 1997 we had an opportunity to visit Paramushir Island, northern Kuriles, and conducted a field survey on the distribution of the plants on the east slope of Mt. Ebeko. This paper records the heath community on the east slope of Mt. Ebeko, Paramushir Island, and notes some ecological characteristics of the community with reference to the volcanic activities of the mountain.

Nomenclature follows Voroshilov (1982).

2. Study area

2.1. Location and physiography

The field survey was conducted on the east slope of Mt. Ebeko, Paramushir Island, northern Kuriles.

The Kurile Islands form a chain of volcanic islands connecting easternmost Hokkaido and the southernmost point of Kamchatka in a northeasterly direction, from 43°36′ to 50°57′N, and 145°24′ to 156°35′E. The Kurile Islands separate the Sea of Okhotsk from the Pacific Ocean (Fig. 1, right).

Paramushir Island is in the northernmost group of the Kurile Islands, *ca*. 70 km southwest of the southernmost point of Kamchatka (Fig. 1, right), with two more islands close to it, Shumshu to the northeast and Alaid to the northwest. Paramushir Island consists of two volcanic chains running north to south with altitudes around 900 and 1500 m at the mountain tops. The highest point of the island is 1816 m in altitude (Mt. Chikura) at the northern end of the southern volcanic chain (Fig. 1, left).

Mt. Ebeko (1136 m altitude) is located in the northern part of the volcanic chains of Paramushir Island, situated 10 km southwest of Severo-Kuril'sk city (Fig. 1, left). This mountain is an active volcano, which has erupted repeatedly recently (Menailov, 1992). Lava flows and ash deposits cover the east slope of the mountain, forming a monotonous topography gentle and smooth with an inclination of 10–15°.

2.2. Climate

Tatewaki (1957) provided reliable climatic data on Paramushir Island (data from

This document is provided by JAXA.

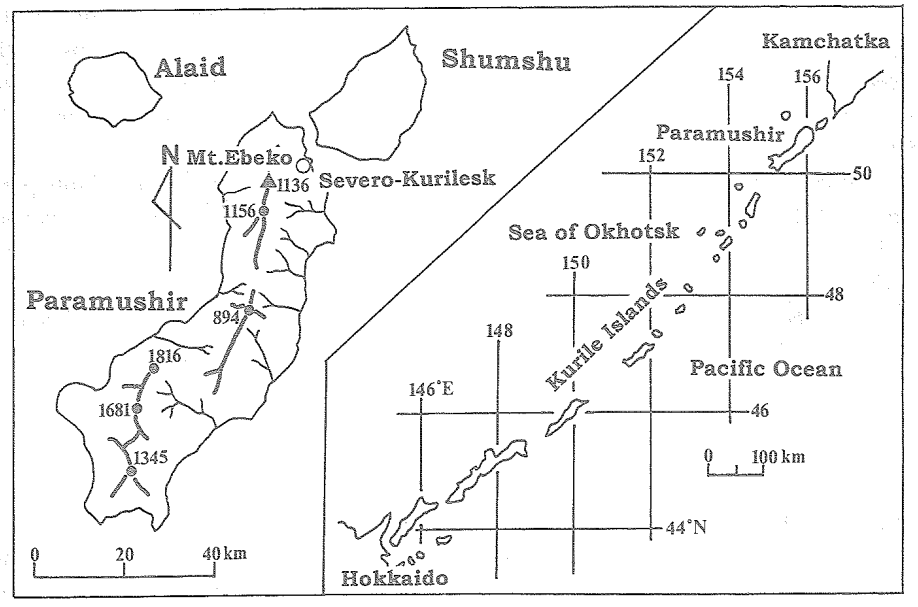


Fig. 1. Location of the Kurile Islands between easternmost Hokkaido and the southernmost point of Kamchatka, and that of Paramushir Island (right). Location of Mt. Ebeko on Paramushir Island (left). The figures on Paramushir Island show altitudes (m a.s.l.) at mountain tops.

Suribachi meteorological station, southeast coast of the island, 50°11′N and 155°45′E, 11 m altitude, 1936–1940). Annual mean temperature on the island is 2.3℃, the mean temperature of the warmest month (August) 11.0℃, and that of the coldest month (January) −4.6℃. The Warmth Index (WI: a summation of mean monthly temperatures more than 5℃: Kira (1949), *cf.* Hämet-Ahti *et al.* (1974)) comes to 16.9℃•month. Annual mean relative humidity is 84.8% with very small fluctuations during the year, and mean annual precipitation amounts to 1376 mm. Those two climatic parameters indicate a very humid climate. Paramushir Island experiences a highly oceanic climate, as Tuhkanen (1984) pointed out, having very few climatically relevant regions in the Northern Hemisphere (Tuhkanen, 1984).

2.3. Vegetation

Three major altitudinal vegetation belts occupy the east slope of Mt. Ebeko: a belt from the lowermost part of the slope to altitude 350 m, altitudes between 350 m to 650 m, and from 650 m upward.

In the lowermost belt up to the altitude 350 m, *Alnus crispa* (Ait.) Pursh (=*A. maximowiczii* Call.) thickets dominate (Kudo, 1922). *Pinus pumila* (Pall.) Regel thickets cover less area mixed with *Alnus crispa* thickets as a subordinate element (Tatewaki, 1944). This belt is characterized by the *Alnus crispa* thickets. The most prominent feature of the vegetation not only of this belt but also of Paramushir Island on the whole is principally the lack of forests such as *Betula ermanii* Cham., *Picea jezoensis* (Sieb. et Zucc.) Carr. and

This document is provided by JAXA.

Larix gmelinii (Rupr.) Rupr. (Kudo, 1922; Tatewaki, 1957). Only *Salix udensis* Trautv. et Mey. (=*S. sachalinensis* Fr. Schmidt) forms small patches of forests along streams, reaching the height of *ca.* 10 m (Kudo, 1922; Tatewaki, 1944, 1957). In this zone the heath community occurs only sporadically on exposed slopes among *Alnus crispa* and *Pinus pumila* thickets.

In the belt from 350 m to 650 m altitude, dwarf shrubs and herbaceous plants prevail, forming a heath community belt. The dominant plants include *Calamagrostis purpurascens* R.Br., *Loiseleuria procumbens* (L.) Desv., *Empetrum nigrum* L. *sensu lato* and *Arcterica nana* (Maxim.) Makino.

In the uppermost belt from 650 m upward, the vegetation become scarce with sporadic occurrence of *Saxifraga merkii* Fisch, *Luzula arcuata* (Wahl.) Sw. and *Calamagrostis purpurascens* R. Br. owing probably to present volcanic activity.

3. Methods

The field survey was concentrated on the east slope of Mt. Ebeko from the lower part of the slope at 30 m altitude up to 650 m altitude; on the slope from 650 m upward vegetation cover becomes very scarce. Heath community dwarf shrubs and herbaceous plants were exclusively surveyed, because they occupy the widest altitudinal range on the slope covering altitudes from 30 m to 650 m, dominating the physiognomy of the slope.

In all 107 lie on the slope at altitudes from 30 to 650 m. Micro-topographically the plots were located on the straight, flat slopes, having similar conditions. The plot size was generally 2×2 m^2. In each plot, the species which occurred were recorded.

4. Results and discussion

4.1. Plant occurrence and ecological characteristics of the community

The total number of species in the area surveyed was 58 (Table 1). Thirteen of 58 species (22%) occur with relatively high frequency of more than 40% (43 plots); *Calamagrostis purpurascens*, *Loiseleuria procumbens*, *Empetrum nigrum*, *Arcterica nana*, *Geum calthifolium*, *Salix arctica*, *Cnidium ajanense*, *Phyllodoce aleutica* and *Cassiope lycopodioides*, *Solidago decurrens*, *Rhododendron aureum*, *Rhododendron camtschaticum* and *Agrostis flaccida*. These species can be regarded as common species. In contrast, 38 of 58 species (66%) occurred sporadically with low frequency of less than 10%. The species composition of the plant community on the east slope of Mt. Ebeko consists of a small number (13 of 58) of common species associated with many sporadic ones.

The common thirteen species of the community include eight dwarf shrubs and five herbaceous plants. Physiognomically the dwarf shrubs dominated all over the plots surveyed. The plant community of the study area can be regarded as a heath community represented primarily by dwarf shrubs in terms of the species composition and physiognomy. This heath community is essentially treeless. Kudo (1922) and Tatewaki (1957, 1958) pointed out that heath is the most important type of community in the central and northern Kuriles. Tuhkanen (1984) also considered the treeless heath in this area to be the representative vegetation of the highly oceanic sector of northern and middle boreal subzone of eastern Eurasia including the Kurile Islands. Thus the dwarf shrub community or heath

This document is provided by JAXA.

Table 1. Frequency occurrence (%) of plant species in four different altitudinal ranges on the east slope of Mt. Ebeko, Paramushir Island, northern Kuriles.

Altitudinal range (m)	0–399	400–499	500–599	600–650	Total
Number of plots	21	24	42	20	107
Total number of species	50	27	26	20	58
Mean number of species per plot	12.4	10.5	9.2	8.4	10.0
Calamagrostis purpurascens R.Br.	38	100	76	80	75
Loiseleuria procumbens (L.) Desv.	57	96	67	75	73
Empetrum nigrum L.	48	92	71	70	71
Arcterica nana (Maxim.) Makino	38	79	62	75	64
Geum calthifolium Menz.	48	54	57	85	60
Salix arctica Pall.	43	33	79	40	54
Cnidium ajanense (Regel et Til.) Drude	43	58	57	50	53
Phyllodoce aleutica (Spreng.) Heller	62	42	55	35	50
Cassiope lycopodioides (Pall.) D.Don	19	38	57	80	50
Solidago decurrens Lour.	71	42	57	15	49
Rhododendron aureum Georgi	38	54	50	30	45
Rhododendron camtschaticum Pall.	52	50	50	20	45
Agrostis flaccida Hack.	67	29	43	25	41
Carex koraginensis Meinsh.	14	33	21	65	31
Oxytropis revoluta Ledeb.	29	71	19	–	29
Vaccinium uliginosum L.	48	50	7	–	23
Saussurea riederi Herd.	10	38	21	15	22
Pedicularis chamissonis Stev.	48	17	–	–	13
Deschampsia flexuosa (L.) Nees	–	17	19	–	11
Spiraea betulifolia Pall.	24	4	–	25	10
Geranium erianthum DC.	29	17	–	–	9
Cassiope stelleriana (Pall.) DC.	–	–	21	5	9
Calamagrostis purpurea (Trin.) Trin.	38	8	–	–	9
Geum pentapetalum (L.) Makino	33	4	–	–	8
Anaphalis margaritacea (L.) Clarke	33	–	–	–	7
Viola biflora L.	29	–	2	–	7
Penstemon frutescens Lamb.	5	4	–	20	6
Maianthemum kamtschaticum (Cham.) Nakai	24	4	–	–	6
Cirsium kamtschaticum Ledeb. ex DC.	19	4	–	–	5
Vaccinium vitis-idaea L.	19	–	–	–	4
Sibbaldia procumbens L.	19	–	–	–	4
Rubus arcticus L.	19	–	–	–	4
Aruncus dioicus (Walt.) Fern.	19	–	–	–	4
Trisetum spicatum (L.) K.Richt	–	–	7	5	4
Lycopodium alpinum L.	5	13	–	–	4
Rumex acetosella L.	19	–	–	–	4
Pedicularis verticillata L.	14	–	–	–	3
Trientalis europaea L.	10	–	2	–	3
Veronica stelleri Pall. ex Link	14	–	–	–	3
Bryanthus gmelinii D.Don	–	–	–	15	3
Cerastium fischerianum Ser.	14	–	–	–	3
Primula cuneifolia Ledeb.	–	–	7	–	3
Fritilaria camtschatcensis (L.) Ker-Gawl.	5	–	2	–	2
Sorbus sambucifolia (Cham. et Schlecht) M.Roem	10	–	–	–	2
Artemisia unalaskensis Rydb.	10	–	–	–	2
Luzula oligantha Sam.	10	–	–	–	2
Senecio cannabifolius Less.	10	–	–	–	2
Juncus beringensis Buchenau	–	–	5	–	2
Lonicera caerulea L.	5	–	–	–	1
Swertia tetrapetala Pall.	5	–	–	–	1
Veratrum oxysepalum Turcz.	5	–	–	–	1
Picris hieracioides L.	5	–	–	–	1
Rosa rugosa Thunb.	5	–	–	–	1
Ixeris dentata (Thunb.) Nakai	5	–	–	–	1
Saxifraga sachalinensis Fr.Schmidt	–	–	2	–	1
Saxifraga merckii Fisch.	–	–	–	5	1
Deschampsia caespitosa (L.) Beauv.	5	–	–	–	1
Viola langsdorffii Fisch. ex Ging	5	–	–	–	1

This document is provided by JAXA.

community of Mt. Ebeko corresponds well with the treeless heaths described by Tatewaki (1958) and Tuhkanen (1984).

Hämet-Ahti and Ahti (1969) stated that the occurrence of treeless boreal heaths is closely related to the distribution of alder forests, and that the lowlands of Iceland, the Aleutian Islands and the Kurile Islands are referred to as boreal heath sections rather than to the arctic. Hämet-Ahti (1981) additionally stressed that treeless heaths occur exclusively along the most oceanic coastal areas of the boreal zone. The heath community of Mt. Ebeko is a type of plant community related to a highly oceanic climate in the northern boreal subzone.

4.2. Vertical distribution of plants and the effect of volcanism on it

The total number of species in an altitudinal range decreased from lower to higher altitude, from 50 to 20 (Table 1). The mean number of species per plot in each altitudinal range also decreased from lower to higher altitude, from 12.4 to 8.4 (Table 1). The thirteen common species showed no clear altitudinal dependence. The higher number of species (*e.g. Oxtropis revolta*, *Vaccinium uliginosum* and *Pedicularis chammisonis*) per plot at lower altitude consisted of many sporadic species appearing only at lower altitude as well as the common species (Table 1). The plots in the lowest altitudinal range contained many sporadic species with frequency less than 10%. The species at higher altitude were almost entirely common species.

The decreasing number of species toward higher altitude can be partly explained by the effect of repeated volcanism. The community at higher altitudes remains at an earlier stage of succession. The relatively low number of species (58) and the scarce vegetation cover on upper slopes (650 m upward) supports this hypothesis.

Okitsu (1987) pointed out that on active volcanoes of Hokkaido, timberline is lower than on dormant volcanoes and non-volcanic mountains, and that *Pinus pumila* thickets and associated dwarf shrub community occupy non-forested areas on such mountains. This finding can explain the effect of volcanic activity of Mt. Ebeko on the decreasing number of species toward higher altitude.

Another issue relating to the effect of volcanic activity on a plant community is admixture of species in different habitats. The heath community on Mt. Ebeko contains species in different habitats; species on wind-exposed slopes are *Calamagrostis purpurascens*, *Loiseleuria procumbens*, *Arctoerica nana*, *Salix arctica* and *Cassiope lycopodioides*, while those in snow bed habitats are *Geum calthifolium*, *Cindium ajanense*, *Phyllodoce aleutica* and *Solidago decurrens*. There is no clear species segregation at high altitude, suggesting that repeated volcanism effectively aborts any development of habitat segregation. The plots at lowermost altitudes contain many species which only occur there. Examples are *Vaccinium vitis-idaea*, *Sibbaldia procumbens*, *Rubus arctics*, *Rumex acetosella*, *Pedicularis verticillata*. This species occurrence suggests less frequent effect of volcanism on the lower part of the mountain.

The insufficiency of time for maturation of the heath community causes some species to occur only sporadically with no clear altitudinal tendency. Examples of such species include *Spiraea betulifolia*, *Cassiope stelleriana*, *Penstemon frutescens*, *Lycopodium alpinum* and *Bryanthus gmelinii*. Those species appeared at higher altitude rather than lower altitude.

This document is provided by JAXA.

4.3. Comparison between wind exposed dwarf shrubs on Mt. Taisetsu and the heath community on Mt. Ebeko

On top of Mt. Taisetsu, central Hokkaido, Japan, treeless vegetation similar to that on Mt. Ebeko, wind exposed dwarf shrubs (Okitsu, 1987, 1999), appears. It is ecologically worthwhile to compare them.

The dominant species among wind exposed dwarf shrubs on Mt. Taisetsu are *Diapensia ovobata* (Fr. Schmidt) Nakai, *Arctous alpina* (L.) Niedz., *Loiseleuria procumbens*, *Empetrum nigrum*, *Arcterica nana*, *Vaccinium vitis-idaea*, *Vaccinium uliginosum* and *Rhododendron aureum* (Okitsu, 1999). Five of those eight species (except *Diapensia ovobata*, *Arctous alpina* and *Vaccinium vitis-idaea*) are also the dominant species of the dwarf shrub vegetation on Mt. Ebeko (Table 1). This indicates that the wind exposed dwarf shrub vegetation on Mt. Ebeko is similar to that on Mt. Taisetsu. Floristically, only six of 58 species listed in Table 1 are absent from Mt. Taisetsu; *Salix arctica*, *Solidago decurrens*, *Carex koraginensis*, *Oxytropis revolta* and *Artemisia unalaskensis* (*cf.* Tatewaki and Samejima, 1959). This floristic comparison also supports the similarity between the heath community on Mt. Ebeko and wind exposed shrubs on Mt. Taisetsu.

Acknowledgments

We thank Drs.V.V. Yakubov and V.P. Verkholat (Institute of Biology and Pedology, Vladivostok), and Dr. M. Imazu (Chiba University) for their field assistance and companionship, and also Prof. Dr. Ken Sato of Hokkai Gakuen University, Sapporo for helpful comments on the manuscript.

References

Barkalov, V.Yu. (1980): New species of vascular plants for the Kuril Islands. Bot. Zh., **65**, 1802–1808 (in Russian).

Barkalov, V.Yu. (1981): New and rare species of vascular plants from the Islands of Shumushu and Paramushir. Bull. Main Bot. Gard. Acad. Sci. USSR, **120**, 37–41 (in Russian).

Barkalov, V.Yu. (1984): New and rare species of vascular plants from the Kurile Islands. Bot. Zh., **69**, 1685–1690 (in Russian).

Barkalov, V.Yu. (1998): Flora of the Kurile Islands. Summary of the Dissertation of the Fulfillment of the Doctor of Biological Science. Vladivostok, 45 p. (in Russian).

Barkalov, V.Yu. (2000): Phytogeography of the Kurile Islands. Nat. Hist. Res., Spec. Issue, **7**, 1–14.

Chernyaeva, A.M. (1976): Flora of the Onekotan Island. Bull. Main Bot. Gard. Acad. Sci. USSR, **87**, 21–29 (in Russian).

Hämet-Ahti, L. (1981): The boreal zone and its biotic subdivision. Fennia, **159**, 69–75.

Hämet-Ahti, L. and Ahti, T. (1969): The homologies of the Fennoscandian mountain and coastal birch forests in Eurasia and North America. Vegetatio, **19**, 208–219.

Hämet-Ahti, L., Ahti, T. and Koponen, T. (1974): A scheme of vegetation zones for Japan and adjacent regions. Ann. Bot. Fenn., **11**, 59–88.

Hultén, E. (1933): Studies on the origin and distribution of the flora in the Kurile Islands. Bot. Not., **1933**, 325–345.

Kira, T. (1949): Forest zones in Japan. Ringyo Kaisetsu Shiriizu 17 (Guide to the Forestry Series 17). Sapporo, Nihon Ringyo Kyokai, 36 p. (in Japanese).

Kudo, Y. (1922): Flora of the Island of Paramushir. J. Coll. Agr. Hokkaido Imp. Univ., Sapporo, **IX. Pt. 2**, 23–183.

Menailov, I.A. (1992): Activity of Ebeko volcano (Kuriles) in 1987–1991, the character of eruptions,

This document is provided by JAXA.

features of products and potential hazard for the town of Severo-Kurilsk. Volcanol. Seismol., **1992, No. 5-6**, 21-33 (in Russian).
Okitsu, S. (1987): *Pinus pumila* zone. Vegetation of Hokkaido, ed. by K. Ito. Sapporo, Hokudai Tosho Kankôkai, 129-167 (in Japanese).
Okitsu, S. (1999): Phytogeography of the vegetation of Mt. Taisetsu, central Hokkaido, northern Japan. Actinia, **12**, 103-112 (in Japanese).
Okitsu, S. (2000): Ecological phytogeography of the *Pinus pumila* zone of Japan. Natural History of the Alpine Plants, ed. by G. Kudo. Sapporo, Hokudai Tosho Kankôkai, 37-49 (in Japanese).
Takahashi, H. (1996): Material for phytogeography of vascular plants in the Kuril Islands. Acta Phytotax. Geobot., **47**, 271-283 (in Japanese).
Takahashi, H. and Kuwahara, Y. (1998): Notes on *Ruppia occidentalis* S. Watson from Atlasova (Alaid), the Northern Kurils. Acta Phytotax. Geobot., **49**, 193-204 (in Japanese).
Tatewaki, M. (1934): Vascular plants of the northern Kuriles. Bull. Biogeogr. Soc. Jpn., **4**, 257-334.
Tatewaki, M. (1944): Vegetation of the district around the Paramushir Strait. Report of the Scientific Investigation in the Kurile Islands, ed. by Hoppô Sôgô Bunka Kenkyukai, 13-51 (in Japanese).
Tatewaki, M. (1957): Geobotanical studies on the Kurile Islands. Acta Horti Gotob., **21**, 43-123.
Tatewaki, M. (1958): Forest ecology of the islands of the North Pacific Ocean. J. Fac. Agr. Hokkaido Univ., **50**, 371-486 with 30 plates.
Tatewaki, M. and Samejima, J. (1959): Alpine plants of the Central Mountain District, Hokkaido, Japan. Bot. Inst. Fac. Agr. Hokkaido Univ., Sapporo, 70 p. (in Japanese).
Tuhkanen, S. (1984): A circumboreal system of climatic-phytogeographical regions. Acta Bot. Fenn., **127**, 1-50.
Vorobiev, D.P. (1956): Material of the flora of the Kuril Islands. Trans. Far East Branch Acad. Sci. USSR. Ser. Bot. **3(5)**, 3-79 (in Russian).
Vorobiev, D.P. (1963): Vegetation of the Kuril Islands. Nauka, 93 p. (in Russian).
Voroshilov, V.N. (1982): Key to Plants of the Soviet Far East. Nauka, 672 p. (in Russian).

(Received March 31, 2000; Revised manuscript accepted September 18, 2000)

This document is provided by JAXA.

Mem. Natl Inst. Polar Res., Spec. Issue, 54, 487–493, 2001

Scientific paper

Occurrence of bryophytes on Paramushir Island, northern Kuriles, Far East Russia

Yoshinori Minami[1], Susumu Okitsu[2], Hiroshi Kanda[3], Valentina Ya. Cherdantseva[4] and Sergei Yu. Grishin[4]

[1]*Faculty of Agriculture, Tamagawa University, Tamagawa Gakuen 6-chome, Machida-shi, Tokyo 194-8610*
[2]*Faculty of Horticulture, Chiba University, 648 Matsudo, Matsudo 271-8510*
[3]*National Institute of Polar Research, Kaga 1-chome, Itabashi-ku, Tokyo 173-8515*
[4]*Institute of Biology and Pedology, Russian Academy of Sciences, Vladivostok 690022, Russia*

Abstract: Some differences in species composition between the region facing the Okhotsk Sea and Pacific Ocean on northern Paramushir Island (Ост. Парамушир, lat. 51°N, long. 157°E), northern Kuriles, in far eastern Russia, and also the vertical distribution of bryophytes in vegetation dominated by creeping pine *Pinus pumila* and dwarf heath on the flank of Mt. Ebeko are reported. In the northern Kuriles, research on vegetation was difficult due to political circumstances after World War II. The northern Kuriles occupy a very important position as the halfway point at the vegetation zone, which extends from northern Japan (Hokkaido) to the Aleutian Islands and Bering Strait. Although the northern Kuriles are situated in the lower latitudes of the subarctic zone, dwarf shrub heath and alpine tundra vegetation are distributed at relatively low altitudes on mountain slopes. Most species observed on this island are distributed in boreal or alpine tundra vegetation, owing to shortage of insolation because many cloudy days with fog and drizzle in the growing season (maritime climate) influence the plant growth condition in this area.

1. Introduction

Bryophytes in understory vegetation play an extremely important role in the control of the moisture change and protection of the soil surface against erosion. In addition, they contain the dominant species of the understory in shrub or dwarf heath vegetation in the northern region (Longton, 1992). Bryophytes growing in such areas are also very important plants in understanding the vegetation dynamics, *e.g.* succession after a disturbance (Longton, 1992). Ecosystems under severe environmental conditions in arctic and subarctic regions are easily modified by climatic change caused by global atmospheric warming originating in increasing human activities (Oechel and Vourlitis, 1994).

Little knowledge, however, is available about the direct or indirect influence of changes in environment on vegetation in the northern regions. Furthermore, accurate information about distributions of species and vegetation types in those regions, especially in the Far East region of Russia, is also limited. Here, we report some differences in species composition between the region facing the Okhotsk Sea and that facing the Pacific Ocean

This document is provided by JAXA.

on northern Paramushir Island, northern Kuriles, in far eastern Russia, and also report the vertical distribution of bryophytes in vegetation dominated by creeping pine *Pinus pumila* and dwarf heath on the flank of Mt. Ebeko.

2. Details of the study area

2.1. Studies of bryophyte flora in northern Kuriles

After World War II, the northern Kuriles were closed to botanists. Even Russian botanists were restricted from entering this area for research. One bryological study of this area had been published before World War II by Horikawa (1933). Fourteen species of bryophytes were collected in this region. After World War II, a number of floristic studies on bryophytes were published in the Kurile Islands (Abramova, 1960; Vasiljeva, 1960; Bardunov and Cherdantseva, 1984; Cherdantseva and Osipov, 1998), but in the northern Kuriles there are only the two reports by Noguchi (1967) and Cherdantseva (1986). Furthermore, there is insufficient information on the ecological-phytogeographical aspects of plants in this area.

2.2. Study sites

The northern Kurile area is an important intermediate point between Northern Japan (Hokkaido) and the Aleutian Islands and north-eastern Siberia facing Bering Strait. There are many young volcanoes on these islands. This is an ecologically very interesting region where the various stages of primary succession after disturbance by an eruption are observed.

Paramushir Island (Ост. Парамушир, lat. 51°N, long. 157°E, Fig. 1) is the largest of the northern Kuriles. It covers more than 2000 km^2 in area, with mountainous terrain, formed by glaciation and volcanism. Mountains generally reach 500-1000 m above sea level. Three active volcanoes (Ebeko, Chikurachki and Fuss Peak) and many dormant volcanoes are combined in several large mountain chains.

The Ebeko volcanic group was formed about 2400 years ago. Three volcanoes that formed recently are very active, but the amount of erupted material is relatively small. Volcanologists have counted 35 horizontal layers of volcanic tephra, including those of Alaid, Chikurachki and Fuss Peak volcanoes, in the soil profile at the foot of Mt. Ebeko (Melekestsev *et al.*, 1993). Recent eruptions were in 1934-1935, 1963-1964, 1967, 1969 and 1987-1990. Vast lava fields, of age about 2000 years, are situated on the east and west slopes of Mt. Ebeko. Other slopes are covered by older volcaniclastic material, metamorphosed by intensive and long volcanic activity (by gases and thermal water). Vast deposits of lava comprise the east foot of Mt. Ebeko, where the modern town of Severo-Kuril'sk is situated.

Chikurachki volcano is situated on the south-western part of the island. It is an active stratovolcano, formed by lava flows and pyroclastics (bombs and lapilli). A huge eruption occurred in 1853, and about 1 km^3 of volcaniclastic material was erupted. The pyroclastics cover the ground to a depth of 25 cm at a distance of about 25 km (Gorshkov, 1967). Taking into account the most recent data on Kamchatka (Braitseva *et al.*, 1997), it was the largest eruption of the 19th century in the Kuriles-Kamchatka region. A few eruptions have taken place in this century (1958, 1961, 1964, 1973), the latest in 1986, with 0.1 km^3 of volcaniclastic material (Ovsyannikov and Muravyev, 1992).

This document is provided by JAXA.

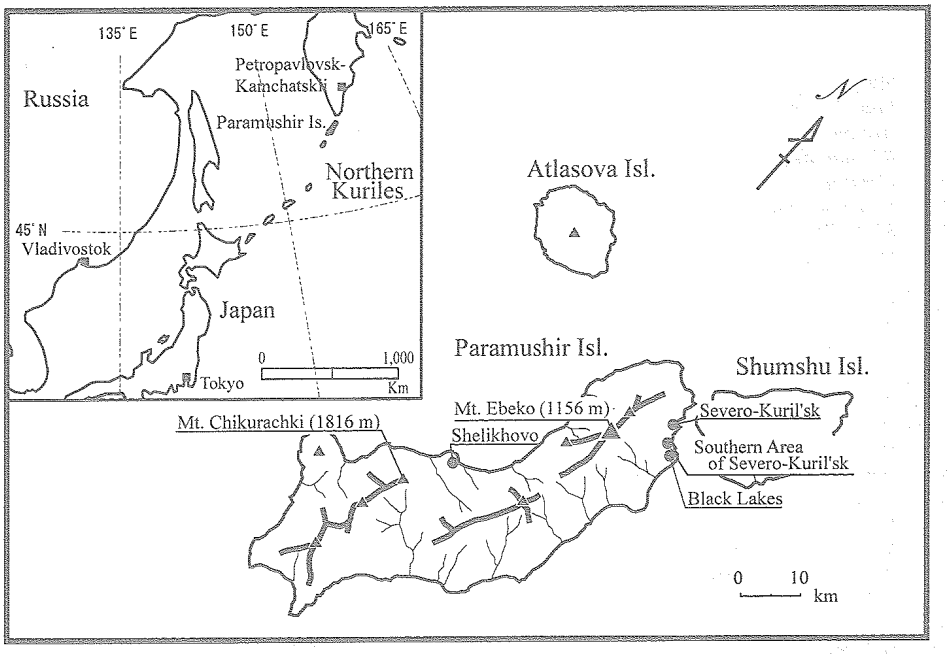


Fig. 1. Location of Paramushir Island, northern Kuriles, and the study sites.

The climate of the northern Kuriles is very severe, with a cold vegetation period. This condition does not allow forest to form. There is a large amount of precipitation, especially snow. Snow cover may reach a depth of 5 m on the east slope of Mt. Ebeko, and more than 20 m in deep river valleys. As a result, snow patches may persist for many years, even near sea level.

The northern Kuriles belong to the marine sector of the subarctic zone climatically (Grishin, 1995). Although the northern Kuriles are situated at lower latitude than the subarctic zone, dwarf shrub heath or alpine tundra vegetation is distributed from relatively low altitude on mountain slopes. A shortage of insolation owing to many cloudy days with fog and drizzle in the growing season influences the plant growth condition in this area (Cherdantseva, 1998). Kira's Warmth Index around the northern Kuriles is extremely low, reaching below 15℃·month (Grishin, 1995). Therefore, the predominant tree species in this region are creeping or shrub types, *e.g. Pinus pumila* and *Alnus crispa*.

The four study sites on this island were Black Lakes, southern area of Severo-Kuril'sk (expressed hereafter as Southern Area), City of Severo-Kuril'sk (expressed hereafter as City), and Shelikhovo (Fig. 1). We also set study sites on the flank of Mt. Ebeko on the northern part of this island, at altitudes from 370–650 m.

3. Results and discussion

3.1. Species composition observed on Paramushir Island

The bryophyte compositions sampled from the four study sites are shown in Table 1.

This document is provided by JAXA.

Table 1. Composition table of the main bryophytes on Paramushir Island.

	Study site / Species	Black lakes	Southern area	City	Shelikhobo	Mt. Ebeko
M*	*Polytrichum juniperinum*	II	I	–	I	I
M	*Arctoa fuluvella*	–	I	I	I	I
M	*Rhytidiadelphus subpinnatus*	II	I	–	–	I
M	*Ceratodon purpureus*	II	–	–	I	I
M	*Sanionia uncinata*	II	I	–	–	–
M	*Rhytidiadelphus calvescens*	II	II	–	–	–
M	*Dicranum hamulosum*	II	I	–	–	–
M	*Plagiomnium acutum*	II	–	–	I	–
M	*Brachythecium populeum*	II	–	–	–	I
M	*Pleurozium schreberi*	–	I	–	–	I
M	*Philonotis fontana*	–	I	–	II	–
M	*Dicranum majus*	–	I	–	I	–
M	*Polytrichum piliferum*	–	I	–	–	I
M	*Dicranoweisia crispula*	–	–	II	–	I
M	*Ditrichum heteromallum*	–	–	II	–	III
M	*Pohlia wahlenbergii*	–	–	II	I	–
M	*Aulacomnium palustre*	–	–	–	I	I
M	*Bryum* sp.	–	–	–	I	I
M	*Racomitrium heterostichum*	–	–	–	I	I
M	*Racomitrium canescens*	–	–	–	I	I
M	*Polytrichum formosum*	II	–	–	–	–
M	*Plagiothecium cavifolium*	–	I	–	–	–
M	*Herzogiella turfacea*	–	–	II	–	–
M	*Andreaea nivalis*	–	–	II	–	–
M	*Philonotis* sp.	–	–	II	–	–
M	*Pogonatum dentatum*	–	–	II	–	–
M	*Mnium stellare*	–	–	II	–	–
M	*Amblystegium juratzkanum*	–	–	II	–	–
M	*Dicranum viride*	–	–	II	–	–
M	*Cyrtomnium hymenophyllum*	–	–	–	I	–
M	*Dicranum fuscescens*	–	–	–	I	–
M	*Amblystegium varium*	–	–	–	I	–
M	*Amblystegium serpens*	–	–	–	I	–
M	*Calliergon cordifolium*	–	–	–	I	–
M	*Calliergon richardsonii*	–	–	–	I	–
M	*Bryum schlecheri*	–	–	–	I	–
M	*Funaria hygrometrica*	–	–	–	I	–
H**	*Diplophyllium* sp.	–	–	–	I	–
M	*Grimmia olympica*	–	–	–	–	IV
M	*Kiaeria starkei*	–	–	–	–	II
M	*Kiaeria falcata*	–	–	–	–	I
M	*Pohlia nutans*	–	–	–	–	I
M	*Oligotrichum aligerum*	–	–	–	–	I
M	*Pogonatum urnigerum*	–	–	–	–	I
M	*Pogonatum sphaerothecium*	–	–	–	–	I
M	*Polytrichastrum alpinum*	–	–	–	–	I
M	*Polytrichum norvegicum*	–	–	–	–	I
M	*Cratoneurella uncinifolia*	–	–	–	–	I
M	*Atrichum* sp.	–	–	–	–	I
M	*Fissidens* sp.	–	–	–	–	I
M	*Orthotrichum* sp.	–	–	–	–	I
M	*Pohlia* sp.	–	–	–	–	I
H	*Jungermannia* sp.	–	–	–	–	I
M	*Dicranum* sp.	–	–	–	–	I

Roman numerals show frequency: V, 100–80%; IV, 80–60%; III, 60–40%; II, 40–20%; I, 20–1%.
*: M, Moss.
**: H, Hepatics.

This document is provided by JAXA.

The bryophyte nomenclature follows Ignatov and Afonina (1992). Most species observed on this island are distributed in boreal or alpine tundra vegetation (Cherdantseva and Osipov, 1998; Czernyadjeva, 1995). Half of the species reported by Horikawa (1933) were found on Paramushir Island in this research. *Rhitidiadelphus calvescens* and *Sanionia uncinata* were characteristics species in both the Black Lakes and Southern Area. The bryophyte flora in both sites was very similar, because both sites are closely situated. The bryophyte composition in City, however, was considerably different, although City was adjacent to the other two sites. Artificial environmental factors may influence the distribution of bryophytes. The bryophyte flora in Shelikhobo and Mt. Ebeko was also similar to each other. As Shelikhobo is situated on the northern side of Mt. Chikurachki, this area is affected by volcanic activity. Therefore, the bryophyte species composition is similar that on Mt. Ebeko. Species which were distributed only either Shelikhobo or Mt. Ebeko were also observed. In Shelikhobo facing the Okhotsk Sea (Fig. 1), we found some species distributed mainly in wet conditions. These species could not be found on Mt. Ebeko. Mt. Ebeko is a volcano, so species growing on volcanic soil or rocks are observed, *e.g. Grimmia olympica, Kiaeria starkei, etc.*

The northern Kuriles occupies a very important position as the halfway point of the vegetation zone, which occupies the chain of the volcanic islands connecting the Aleutian Islands and Bering Strait from Hokkaido. Most species observed on Paramushir Island have a wide distribution range from Kamchatka peninsula (Cherdantseva and Osipov, 1998; Czernyadjeva, 1995) to Hokkaido (Iwatsuki and Inoue, 1972).

Table 2. Vertical distribution of bryophytes on the flank of MT. Ebeko

Species	Altitude (m)	250	300	370	400	450	500	550	620
M	*Grimmia olympica*								
M	*Kiaeria starkei*								
M	*Ditrichum heteromallum*								
M	*Racomitrium fasciculare*								
M	*Kiaeria falcata*								
M	*Pohlia nutans*								
M	*Racomitrium heterostichum*								
M	*Polytrichum juniperinum*								
M	*Dicranum scoparium*								
M	*Arctoa fuluvella*								
H	*Jungermannia* sp.								
H	*Hepaticae* sp.								
M	*Cratoneurella uncinifolia*								
M	*Pogonatum sphaerothecium*								
M	*Polytrichum norvegicum*								
M	*Polytrichum piriferum*								
M	*Atrichum* sp.								
M	*Fissidens* sp.								
M	*Oligotrichum aligerum*								
M	*Orthotrichum* sp.								
M	*Pogonatum urnigerum*								

Solid lines show frequent distribution and dotted lines show rare distribution of each species with altitude.

This document is provided by JAXA.

3.2. Vertical distribution of bryophytes on Mt. Ebeko

Mt. Ebeko is situated on the northern part of Paramushir Island (Fig. 1). *Pinus pumila* is the predominant tree species, with *Empetrum nigrum* and *Rhododendron aureum* on the flank of Mt. Ebeko. There are many windy sites on the slopes. Dwarf shrub heath vegetation is found at alt. 400 m asl. *Grimmia olympica*, *Kiaeria starkei* and *K. falcata* with scrub *Pinus pumila* were observed in volcanic substrata.

The distribution of the main bryophyte species from alt. 370 to 650 m on the flank of Mt. Ebeko is shown in Table 2. Dwarf shrub heath and alpine tundra develop at all of these elevations. The distribution of most bryophyte species is restricted to certain elevations, except for a few species adapted to quite unstable and oligotrophic conditions, *e.g.* *Grimmia olympica*, *Kiaeria starkei* and *Ditrichum heteromallum*.

Generally, high-alpine and arctic ecosystems are mostly oligotrophic. Indigenous plants demonstrate strategies based on resource uptake and efficiency of resource usage rather than resource availability (Shaver and Chapin, 1980). Similar environmental condition can be found when snow melt streams flow onto landslide scar on volcanic lands. Many young volcanoes sprinkled over the northern Kurile Islands, and the ground surface on flanks of mountains, show quite unstable and oligotrophic conditions because of accumulation of volcanic ash and gravel. Mt. Ebeko has also such a ground condition produced by the volcanic materials, so the bryophyte composition is represented by distinctive species (such as *Grimmia olympica* or *Kiaeria starkei*), especially on flanks at higher altitude.

Acknowledgments

We thank Dr. V. P. Verkholat, Dr. V. V. Yakubov (Institute of Biology and Pedology, Vladivostok), and Dr. M. Imazu (Chiba University) for their cooperation in the field research.

References

Abramova, A.L. (1960): About mosses of Kurile Islands. Mater. po Prirodnym Resursam Kamchatki i Kuril'skikh Ostrovov, ed. by A.V. Stostenko and D.P. Vorobjev. Magadan, 85–97 (in Russian).

Bardunov, L.V. and Cherdantseva, V.Ya. (1984): Contributions to flora leafy mosses of the Southern Kurile Islands. Sistematiko-Floristicheskie Issledovaniya Sporovykh Rastenij Dal'nego Vostoka, ed. by V.Ya. Cherdantseva *et al.* Vladivostok, 34–53 (in Russian).

Braitseva, O.A., Melekestcev, I.V., Ponomaryeva, V.V., Sulerzhitskiy, L.D. and Pevzner, M.M. (1997): Geochronology and parameters of largest explosive eruptions at Kamchatka during the last 10000 years. Rossiiskaya Nauka: Vystoyat i Vozroditsya. Moscow, Nauka, 237–244 (in Russian).

Cherdantseva, V.Ya. (1986): On bryoflora at the northern Kurile archipelago. Flora i Sistematika Sporovykh Rastenij Dal'nego Vostoka, ed. by L.N. Vassiljeva *et al.* Vladivostok, 156–162 (in Russian).

Cherdantseva, V.Ya. (1998): A review of mosses in the south of the Russian Far East. Chenia, **5**, 205–215.

Cherdantseva, V.Ya. and Osipov, S.V. (1998): On the moss (Musci) flora of Kamchatka Peninsula. Bot. Zh., **83**, 85–92 (in Russian).

Czernyadjeva, I.V. (1995): On the moss flora of the Kamchatka Peninsula. Bot. Zh., **80**, 61–74 (in Russian with English summary).

This document is provided by JAXA.

Gorshkov, G.S. (1967): Volcanism of Kuril Islands Arc. Moscow, Nauka, 288 p. (in Russian).
Grishin, S.Yu. (1995): The boreal forests of north-eastern Eurasia. Vegetatio, **121**, 11–21.
Horikawa, Y. (1933): The bryological flora of the Northern Kuriles Islands. Bull. Biogeogr. Soc. Jpn., **4**, 335–337.
Ignatov, M.S. and Afonina, O.M. (1992): Check list of mosses of the former USSR. Arctoa, **1**, 1–85.
Iwatsuki, Z. and Inoue, H. (1972): Bryophytes of the Hidaka Mountains, Hokkaido, Northern Japan. J. Hattori Bot. Lab., **36**, 533–546.
Longton, R.E. (1992): The role of bryophytes and lichens in terrestrial ecosystems. Bryophytes and Lichens in a Changing Environment, ed. by J.W. Bates and A.M. Farmer. New York, Oxford University Press, 32–76.
Melekestsev, I.V., Dvigalo, V.N. and Kiryanov, V.Yu. (1993): Ebeko volcano (Kuril Islands): The history of eruptive activity and future volcanic danger. Vulkanol. Seismol., **3**, 69–81 (in Russian).
Noguchi, A. (1967): A small collection of bryophytes made by Dr. S. Bergman in the Kuriles. J. Jpn. Bot., **42**, 85–89.
Oechel, W.C. and Vourlitis, G.L. (1994): The effects of climate change on land-atmosphere feedbacks in arctic tundra regions. Trends Ecol. Evol., **9**, 324–329.
Ovsyannikov, A.A. and Muravyev, Ya.D. (1992): Eruption of Chikurachki volcano in 1986 yr. Vulkanol. Seismol., **5–6**, 3–20 (in Russian).
Shaver, G.R. and Chapin, F.S., III. (1980): Response to fertilization by various plant growth forms in Alaskan tundra: Nutrient accumulation and growth. Ecology, **61**, 662–675.
Vasiljeva, L.N. (1960): On the flora Sphagnum of the Kurile Islands. Mater. po Prirodnym Resursam Kamchatki i Kuril'skikh Ostrovov, ed. by A.V. Stoshenko and D.P. Vorobjev. Magadan, 99–100 (in Russian).

(Received April 25, 2000; Revised manuscript accepted July 21, 2000)

This document is provided by JAXA.

This document is provided by JAXA.

Mem. Natl Inst. Polar Res., Spec. Issue, 54, 495–505, 2001

Scientific paper

Biological characteristics of dark colored material (cryoconite) on Canadian Arctic glaciers (Devon and Penny ice caps)

Nozomu Takeuchi[1], Shiro Kohshima[2], Kumiko Goto-Azuma[3] and Roy M. Koerner[4]

[1]*Frontier Observational Research System for Global Change, International Arctic Research Center, University of Alaska Fairbanks, 930 Koyukuk Dr., P.O. Box 757335, Fairbanks AK 99775-7335, U.S.A.*
[2]*Biological Laboratory, Faculty of Bioscience and Biotechnology, Tokyo Institute of Technology, Ookayama 2-chome, Meguro-ku, Tokyo 152-8551*
[3]*National Institute of Polar Research, Kaga 1-chome, Itabashi-ku, Tokyo 173-8515*
[4]*Terrain Sciences Division, Geological Survey of Canada, 601 Booth St., Ottawa, Ontario, K1A 0E8, Canada.*

Abstract: Biological characteristics of dark colored material (cryoconite) collected from Canadian Arctic glaciers (Devon and Penny ice caps) are described. The cryoconite consists of mineral particles and organic matter. The amount of organic matter was 0.8–13.8% dry weight. Seven taxa of snow algae (Chlorophyta and Cyanophyta) were observed in the cryoconite. The mineral particles, the algae, the bacteria, and amorphous organic matter formed small dark colored granules (cryoconite granules). The size of the granules was approximately 0.4 mm in diameter. Microscopy of the granules revealed that the granules contain bacteria with mucus like substance, and that the surface of the granules was covered with filamentous blue-green algae. These observations suggest that the granules are formed by algal and bacterial activity on the glaciers, and that the cryoconite includes a large amount of biological products. The amount of the cryoconite per unit area on the glacier surface was generally small (mean 48 g m^{-2} in dry weight). In contrast, a large amount of the cryoconite was deposited at the bottom of cryoconite holes. The small amount of cryoconite on the glacier surface means that the effect of the cryoconite on albedo reduction of the glacier surface is small.

1. Introduction

Impurities in snow and ice, such as airborne particles, have been shown to affect the solar heat-intake to glaciers, sea ice and seasonal snow cover (*e.g.*, Warren and Wiscombe, 1980; Warren, 1982). Dark colored material on snow and ice can reduce surface albedo and thus could accelerate melting. Therefore, albedo-reducing material with snow and ice may significantly affect the cryosphere extent in the world.

Dark colored material on the glacier surface was first named cryoconite by the Arctic explorer N. E. Nordenskjöld (1875). Recent studies have revealed that cryoconite on some glaciers contains a large amount of algae and bacteria (Gerdel and Drouet, 1960; Wharton *et al.*, 1981, 1985; Kohshima, 1987, 1989). This suggests that these microbes play important roles in the formation process of albedo-reducing material on glaciers. Since living algae

This document is provided by JAXA.

and some microbes have been reported on snow and ice in various parts of the world (Kol, 1942, 1968, 1969; Kol and Peterson, 1976; Ling and Seppelt, 1993; Yoshimura *et al.*, 1997), formation of cryoconite by biological activity may be a common phenomenon on glaciers globally. In the Arctic region, several studies of cryoconite have been done (*e.g.*, Adams, 1966; Charlesworth, 1957; Gribbon, 1979). Although these studies have revealed the components of cryoconite, the precise structure and formation process of cryoconite are still not well known.

This study aims to clarify biological characteristics of cryoconite on Canadian Arctic glaciers (Devon ice cap and Penny ice cap). The composition, structure, and amount of cryoconite on the glacier surface are described. Based on detailed observations of cryoconite, the processes of its formation, and its effect on albedo reduction of the glacier surface, are discussed.

2. Field description and methods

Glacier surface material (cryoconite) was collected in the ablation areas of the Devon ice cap (April 1997) and the Penny ice cap (May 1997) in Nunavut, Canada (Fig. 1). On Devon ice cap, sampling was done at three sites (site A–C) of a valley outlet glacier (the Sverdrup Glacier) on the northwest part of the ice cap. The equilibrium line of the mass balance of the ice cap is at 1200 m a.s.l. (Koerner and Lundgaard, 1995). On Penny ice cap, sampling was done at five separate sites (site D–H), on Coronation Glacier on the east and on Greenshield Glacier on the west. The glacier surface of all of the sampling sites was covered with a 10–40 cm thick snow and was completely frozen during the period when samples were collected. After the snow on the glacier surface was removed, ice including cryoconite was collected on the surface and on the bottoms of cryoconite holes with an ice chisel. The collected samples were melted in plastic bags and were preserved as 3% formalin solution in 100-m*l* clean polyethylene bottles. They were transported to Japan for analysis.

The organic matter in the cryoconite was measured by the following method. After the samples were dried (65℃, 24 hour) and weighed, they were burned for 1 hour at 1000℃ in an electric furnace. The percentage of weight reduction by this manipulation was measured.

The structure of the cryoconite was observed with an optical microscope, a fluorescent microscope (Nikon Optiphoto 2), and a scanning electron microscope (FE-SEM, S-800, HITACHI Co.). DAPI (4'6-diamidino-2-phenylindole) straining was used for bacteria observation with the fluorescence microscope. For scanning electron microscopy, the cryoconite was dried with a critical-point dryer (HC-80, HITACHI Co.), and was coated with carbon and Pt-Pd.

To observe the inner structure of the cryoconite, thin sections were made. The samples were dehydrated in a series of ethanol and acetone (50%, 70%, 80%, 100%, 100% of ethanol, and 100%, 100% of acetone), and then embedded in polyester resin. The embedded sample was ground by a grinder with abrasive to a thin section (approximately 0.1 mm thick). The section samples were observed with an optical microscope.

This document is provided by JAXA.

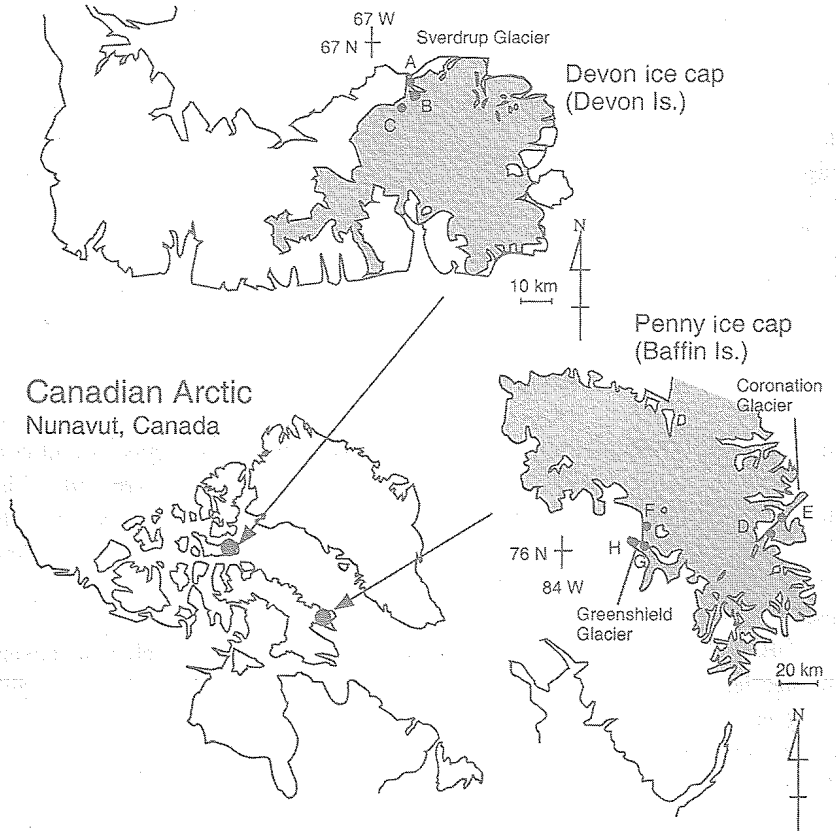


Fig. 1. Maps of Devon and Penny ice caps in the Canadian Arctic. Sampling sites (A–H) are shown in each map.

3. Results and discussion

3.1. Composition and structure of the cryoconite

The cryoconite consisted of mineral particles and organic matter. Table 1 shows the percentage of organic matter (dry weight) in the cryoconite collected at each sampling site. The mean percentage of the organic matter was 8.9% (it ranged from 0.8 to 13.8%). The mineral particles included in the cryoconite are transparent or brown colored. The size of the mineral particles ranged from 30 to 330 μm.

Algae were contained in the cryoconite. The following three species of green algae (Chlorophyrta) and four species of blue-green algae (Cyanophyta or Cyanobacteria, they are referred to here as blue-green algae for simplicity) were observed.

Green algae (Chlorophyta):

Ancylonema nordenskioldii Berggren (Fig. 2a)

Filaments straight or slightly curved, consisting of 1–8 cells. Cells cylindrical with truncate or rounded apices, 23 ± 5.9 μm in length, and 9.4 ± 0.9 μm in width (mean

This document is provided by JAXA.

Table 1. Percentage of organic matter and mean diameter of cryoconite granules of Canadian Arctic glaciers. The locations of sites A to H are shown in Fig. 1.

	Devon ice cap			Penny ice cap					
Site	A	B	C	D	E	F	G	H	Mean
Altitude (m)	1065	700	300	790	670	960	660	450	
Percentage of organic matter (%)	4.8	10.5	10.4	13.8	11.2	13.8	6.2	0.8	8.9
Size range of the granules (min-max μm)	160 -840	90 -1340	160 -1020	170 -1720	190 -1090	140 -660	170 -860	90 -530	
Mean size of the granules (μm)	330	410	430	620	530	330	380	240	440

$\pm$standard error (SE), sample number (n)=25). Cytoplasm homogeneous and containing reddish pigment. Chloroplasts, bright green, and parietal with one pyrenoid. This species dominated the total algal biomass at sites G and H. This species has been reported from many glaciers in Greenland, Arctic sea ice surface, Himalaya, and Alaska (Gerdel and Drout, 1960; Melnikov, 1997; Yoshimura *et al.*, 1997; Kol, 1942)

Trochiscia sp. (Fig. 2b)

Cells spherical 12$\pm$2.8 μm in diameter (mean$\pm$SE, n=16). Cell wall covered with numerous slender spines, each up to 5 μm long. Chloroplasts one to several, bright green with one pyrenoid.

Cylindrocystis sp. (Fig. 2c)

Cells cylindrical with rounded apices, 1 to 2 times longer than the width, 35$\pm$1.4 in length, and 15$\pm$0.4 μm wide (mean$\pm$SE, n=9). Chloroplasts usually two, with one pyrenoid.

Blue-green algae (Cyanophyta or Cyanobacteria):

Calothrix parietina Thuret (Fig. 2d)

Filaments brown, sinuous, often branched, cylindrical, long-tapering at the upper end, and 9.3$\pm$1.6 μm in wide (mean$\pm$SE, n=11). Trichome blue-green or brownish, cylindrical. Heterocysts brownish and spherical. This species dominated the total algal biomass at sites A, B, C, D, and F. This species has been reported in the cryoconite of Greenland (Gerdel and Drout, 1960)

Oscillatoriacean alga 1 (Fig. 2e),

Trichome blue-green and 1.6$\pm$0.3 μm in wide (mean$\pm$SE, n=9).

Oscillatoriacean alga 2 (Fig. 2f),

Trichome blue-green and 5.6$\pm$1.2 μm in wide (mean$\pm$SE, n=5).

Chroococcacean alga,

Cells blue-green, spherical, and 3.1$\pm$1.1 μm in diameter (mean$\pm$SE, n=16).

The algae, mineral particles, and amorphous organic matter were formed into small dark-colored granules (Fig. 3, cryoconite granules). The granules were shaped almost spherical. Their sizes ranged from 0.1 to 1.7 mm in diameter (mean: 0.4 mm, Table 1). The granules were observed at all of the study sites. The thin section of the granule shows that

This document is provided by JAXA.



Fig. 2. Algae observed in cryoconite of Canadian Arctic glaciers. (Scale bar = 20 μm). A Chroococcacen alga, which was also observed in the cryoconite, is not shown in this figure.

many brown or transparent mineral particles 0.1–0.5 mm in diameter were included inside the granule and that amorphous black or brown matter (organic matter) occupied the surfaces and gaps of mineral particles of the granule (Fig. 4).

Figure 5 shows a granule observed with a florescent microscope. The surface of the granule was densely covered with Oscillatoriacean (filamentous) and Chroococcacean (coccid) algae (Fig. 5a, red colored parts). Observations with DAPI straining revealed that there were many bacteria around the blue-green algae (Fig. 5b). Figure 6 shows the granule

This document is provided by JAXA.

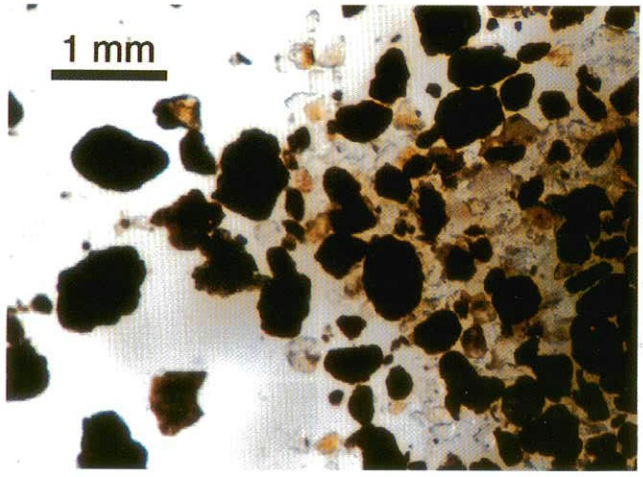


Fig. 3. Dark colored granules (cryoconite granules) in cryoconite of Canadian Arctic glaciers.

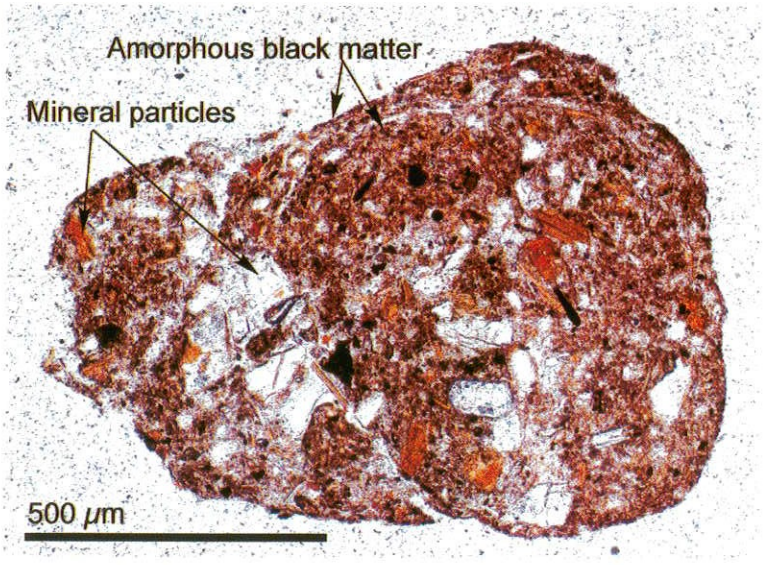


Fig. 4. Thin-section of a cryoconite granule (Devon ice cap, site C).

observed with a scanning electron microscope. The surface of the granule was entangled by the filamentous blue-green algae (Fig. 6a). In some granules, several cells of *Trochiscia* sp. (Green algae) are observed inside the granule (Fig. 6b, c). A large number of bacteria were observed in the granules and were often covered with a mucus-like substance (Fig. 6d).

These observations suggest that the granules are formed by algal and bacterial activity. The spherical shape of the granules is likely to be maintained by entanglement of

This document is provided by JAXA.

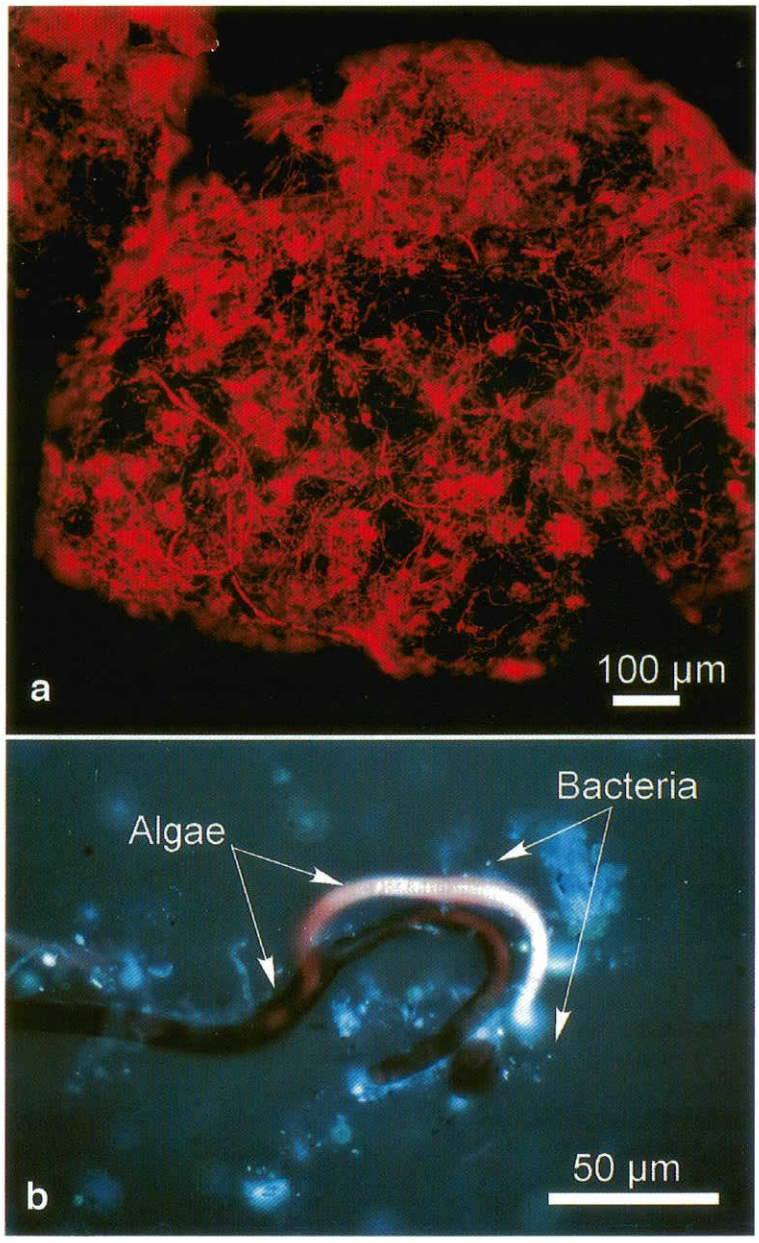


Fig. 5. The cryoconite granule observed with a fluorescent microscope. a: The surface of the granule is covered with filamentous blue-green algae (red: algae with pigment fluorescent). b: Bacteria were observed around algae. (blue: DAPI strained bacteria, brown or pink: algae with pigment fluorescent)

This document is provided by JAXA.

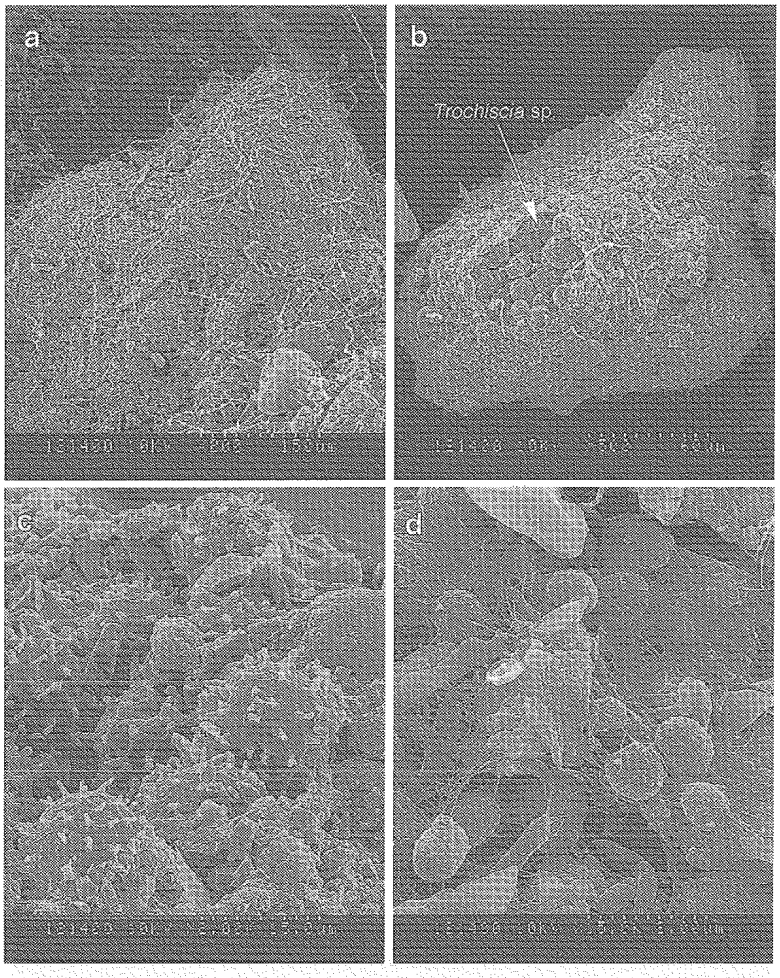


*Fig. 6. The cryoconite granule observed with a scanning electron microscope. a: The granule surface with filamentous blue-green algae (Devon), b: the surface of the granule (Penny), c: Algae buried in the granule (*Trochiscia *sp.), d: bacteria with mucus like substance in the cryoconite granule (Penny).*

filamentous blue-green algae and by adhesion of mucus-like organic matter. The size of the granule may enlarge due to growth of filamentous algae. The mucus-like organic matter may be a product of bacterial decomposition of old algae and other organic particles trapped in the granules, and/or a product of blue-green algae which have been reported by Ohtani *et al.* (1991), and by Cameron and Devaney (1970). Thus, the granule seems to be a microbial complex capable of contemporaneous photosynthesis and decomposition. This granule structure is similar to the cryoconite reported from Himalayan and Tibetan glaciers (Kohshima, 1987, 1989), suggesting that the granules are structures commonly found on glaciers globally.

This document is provided by JAXA.

3.2. *Amount of cryoconite on the glacier surface*

The amount of cryoconite per unit area on the glacier surface was generally small (0.22–26 g m^{-2} in dry weight, Table 2) except at site H (347 g m^{-2}). The large amount at site H is probably due to a large supply of wind-borne mineral particles (0.8% of organic matter only), since site H is close to the left bank margin of the glacier (approximately 100 m from the sampling site).

Table 2. Amount of cryoconite per unit area on the surfaces of Canadian Arctic glaciers.

	Devon ice cap			Penny ice cap					
Site	A	B	C	D	E	F	G	H	Mean
Altitude (m a.s.l)	1065	700	300	790	670	960	660	450	
Suface ice (g m^{-2})	0.91	0.22	3.3	0.69	1.0	1.7	26	350	48
Cryoconite hole (g m^{-2})	2800	2300	2100	1400	1400	1800	2700	4400	2359

In contrast with the small amount of cryoconite on the glacier surface, a large amount of cryoconite was deposited at the bottoms of cryoconite holes (Table 2). Cryoconite holes were observed at all sampling sites. Diameters and depths of the holes ranged from 1.0 cm to 20 cm, and from 10 to 30 cm, respectively. The cryoconite was deposited to approximately 3 mm thickness at the bottoms of the holes. Based on the density of cryoconite (dry weight per unit volume), the amount per unit area at the hole bottom (3 mm thickness) can be obtained at each sampling site (Table 2). The cryoconite amount in the holes is 1400–4400 g m^{-2} (mean: 2359 g m^{-2}). This amount is approximately 50 times larger than on the glacier surface.

The small amount on the glacier surface indicates that the effect of the cryoconite on albedo reduction of the glacier surface is small. Albedo of the summer surface at 300 m elevation of the Sverdrup Glacier on Devon ice cap has been reported to be 40–50% (Keeler, 1964). This albedo is consistent with the albedo of clean ice (Paterson, 1994). In contrast, a large cryoconite amount (50–900 g m^{-2}) has been reported on the surface of a Himalayan glacier (Takeuchi *et al.*, 2000). The albedo of the Himalayan glacier surface is remarkably reduced by the cryoconite (10–30%, Kohshima *et al.*, 1993). The mean amount of cryoconite on the Himalayan glacier is approximately 6 times larger than that on Arctic glaciers (300 *versus* 48 g m^{-2}). This fact indicates that the effect of the cryoconite on albedo reduction is much smaller on Arctic glaciers compared with on a Himalayan glacier.

Since the cryoconite of both the Arctic and Himalayan glaciers is dominated by dark colored granules, the cryoconite amount difference between the glaciers may be due to conditions of granule formation. The composition and structure of the granules strongly suggest that the granules are formed by algal and bacterial activity on the glaciers. Therefore, physical and/or chemical conditions affecting the algal and bacterial activity may be responsible for formation of the granules. The small cryoconite amount on Arctic glaciers may be due to lower biological activity there. Cryoconite holes, which contain a large amount of cryoconite, may be the only suitable place for cryoconite formation on Arctic glaciers. As Wharton *et al.* (1985) suggested, the cryoconite at the bottoms of the holes also would have an albedo effect on glacier ablation. However, the effect is likely to be much less than that of cryoconite on the glacier surface, because the cryoconite holes

This document is provided by JAXA.

found on the glacier surface were small in area, estimated at only 6.9% (Penny) and 3.2% (Devon) of the study area. Although it is still unclear which factors affect biological activity and how the cryoconite amount on the glacier surface is determined, biological activity may play an important role in cryoconite formation and albedo reduction of the glacier surface.

Acknowledgments

The field work was carried out during the period of an ice-core drilling project in 1997 by the Geological Survey of Canada and the Nagaoka Institute of Snow and Ice Studies. We thank all of the members of the ice-core drilling project for their help in the field work. We also would like to thank the Polar Continental Shelf Project for logistic support. We appreciate suggestions on the manuscript by two anonymous reviewers. The field work was partly supported by a grant for Promotion of Surveys and Research in Earth Science and Technologies and Ocean Development of the Science and Technology Agency of Japan.

References

Adams, W.P. (1966): Ablation and run-off on the White Glacier, Axel Heiberg Island, Canadian Arctic Archipelago. Axcel Heiberg Island Research Reports, Glaciology No.1, McGill University, Montreal.

Cameron, R.E. and Devaney, J.R. (1970): Antarctic soil algal crust: Scanning electron and optical microscope study. Trans. Am. Microsc. Soc., **89**, 264–273.

Charlesworth, J.K. (1957): The Quaternary Era 1. London. Edward Arnold, 1700 p.

Gerdel, R.W. and Drouet, F. (1960): The cryoconite of the Thule Area, Greenland. Trans. Am. Microsc. Soc., **79**, 256–272.

Gribbon, P.W.F. (1979): Cryoconite holes on Sermikavasak, West Greenland. J. Glaciol., **22**, 177–181.

Keeler, C.S. (1964): Relationship between climate, ablation, and run-off on the Sverdrup Glacier, 1963, Devon Island, N.W.T. Arct. Inst. North Am., Res. Pap., **27**, 1–80.

Koerner, R.M. and Lundgaard, L. (1995): Glaciers and Global Warming. Geogr. Phys. Quaternaire, **49**, 429–434.

Kohshima, S. (1987): Formation of dirt layers and surface dust by micro-plant growth in Yala (Dakpatsen) Glacier, Nepal Himalayas. Bull. Glacier Res., **5**, 63–68.

Kohshima, S. (1989): Glaciological importance of micro-organisms in the surface mud-like materials and dirt layer particles of the Chongce Ice Cap and Gozha glacier, West Kunlun Mountains, China. Bull. Glacier Res., **7**, 59–66.

Kohshima, S., Seko, K. and Yoshimura, Y. (1993): Biotic acceleration of glacier melting in Yala Glacier, Langtang region, Nepal Himalaya. Snow and Glacier Hydrology: Proceedings of the International Symposium held at Kathmandu Nepal, November 1992, ed. by G.J. Young. Wallingford, IAHS, 309–316 (IAHS Publ. **218**).

Kol, E. (1942): The snow and ice algae of Alaska. Smithson. Misc. Collect., **101**, 1–36.

Kol, E. (1968): Kryobiologie. Biologie und Limnologie des Schnees und Eises. I. Kryovegetation. Die Binnengewsser. Vol. 24, ed. by A. Thienemann, (founder), H.-J. Elster, W. Ohle, and E. Stuttgart. Schweizerbart'sche, Verlagsbuchhandlung, 216 p.

Kol, E. (1969): The red snow of Greenland. II. Acta Bot. Acad. Sci. Hung., **15** (3–4), 281–289.

Kol, E. and Peterson, J.A. (1976): Cryociology. The Equatorial Glaciers of New Guinea, Results of the 1971–1973 Australian Universities' Expeditions to Irian Jaya: Survey, Glaciology, Meteorology, Biology and Paleoenvironments, ed. by G.S. Hope *et al.* Rotterdam, Balkema, 81–91.

Ling, H.U. and Seppelt, R.D. (1993): Snow algae of the Windmill Island, continental Antarctica. 2. Chloromonas rubroleosa sp. nov. (Volvocales, Chlrophyta), an alga of red snow. Eur. J. Phycol., **28**, 77–84.

Melnikov, I.A. (1997): The Arctic Sea Ice Ecosystem. Amsterdam, Gordon and Breach Sci. Publ., 204 p.

This document is provided by JAXA.

Nordenskjöld, N.E. (1875): Cryoconite found 1870, July 19th–25th, on the inland ice, east of Auleitsivik Fjord, Disco Bay, Greenland. Geol. Mag., Decade 2, **2**, 157–162.
Ohtani, S., Akiyama, M. and Kanda, H. (1991): Analysis of Antarctic soil algae by the direct observation using the contact slide method. Nankyoku Shiryô (Antarct. Rec.), **35**, 285–295.
Paterson, W.S.B. (1994): The Physics of Glaciers. 3rd ed. Oxford, Elsevier, 480 p.
Takeuchi, N., Kohshima, S., Yoshimura, Y., Seko, K. and Fujita, K. (2000): Characteristics of cryoconite holes on a Himalayan glacier, Yala Glacier Central Nepal. Bull. Glaciol. Res., **17**, 51–59.
Warren, S.G. (1982): Optical properties of snow. Rev. Geophys. Space Phys., **20**, 67–89.
Warren, S.G. and Wiscombe, W.J. (1980): A model for the spectral albedo of snow. II: Snow containing atmospheric aerosols. J. Atoms. Sci., **37**, 2734–2745.
Wharton, R.A., Vinyard, B.C., Parker, G.M., Simmons, G.M., Jr. and Seaburg, K.G. (1981): Algae in cryoconite holes on Canada Glacier in Southern Victoria Land, Antarctica. Phycologia, **20**, 208–211.
Wharton, R.A., McKay, C.P., Simmons, G.M. and Parker, B.C. (1985): Cryoconite holes on glaciers. BioScience, **35**, 449–503.
Yoshimura, Y., Kohshima, S. and Ohtani, S. (1997): A community of snow algae on a Himalayan glacier: Change of algal biomass and community structure with altitude. Arct. Alp. Res., **29**, 126–137.

(Received April 4, 2000; Revised manuscript accepted August 11, 2000)

This document is provided by JAXA.

This document is provided by JAXA.

Mem. Natl Inst. Polar Res., Spec. Issue, 54, 507–513, 2001

Scientific paper

Ecological role of fungal infections of moss carpet in Svalbard

Tamotsu Hoshino[1], Motoaki Tojo[2], Hiroshi Kanda[3] and Anne Marte Tronsmo[4]

[1]*Bioscience and Chemistry Division, Hokkaido National Industrial Research Institute, 2-1, 2-jo, 17-chome, Tsukisamu-higashi, Toyohira-ku, Sapporo 062-8517*
[2]*Graduate School of Agriculture and Biological Sciences, Osaka Prefecture University, 1-1, Gakuen-cho, Sakai 599-8531*
[3]*National Institute of Polar Research, Kaga 1-chome, Itabashi-ku, Tokyo 173-8515*
[4]*The Norwegian Crop Research Institute, Fellesbygget, N-1432, Ås, Norway*

Abstract: Moss vegetation plays an important role as a producer in the early stages of primary succession in the Arctic. Some fungi actively attack mosses growing in polar regions. We observed the ecological impact of phytopathogenic fungi in Barentsburg, Longyearbyen and Ny-Ålesund in Svalbard. Many fungal infections were seen in some kinds of moss colonies (*Aulacomnium palustre, Sanionia uncinata, Straminergon stramineum* and *Tomenthypnum nitens*), and pathogenic fungi formed moribund patches in the moss carpet. Higher plants and other mosses had invaded in those moribund moss patches. These findings suggest that phytopathogenic fungi play an important role in the pattern of succession in Arctic terrestrial ecosystems.

1. Introduction

Moss vegetation plays an important role in primary succession in polar regions. Moss colonies also offer habitats for terrestrial invertebrates such as insects, ticks and nematodes. Therefore, moss communities are a key part of the terrestrial ecosystems in polar regions (Longton, 1997). Microorganisms, especially fungi in polar regions, are well known for their formation of mycorrhizae, basidiolichen and decomposers (Laursen and Chmielewski, 1982). In addition, some fungi have been reported to actively attack mosses growing in the Arctic, including Jan Mayen in the Greenland Sea (Wilson, 1951), Ellesmere Island in northern Canada (Longton, 1973), and Svalbard in the Barents Sea (Ridley *et al*., 1979; Hoshino *et al*., 1999); and in Antarctica, in the South Sandwich Islands, South Orkney Islands (Longton, 1973) and on Cape Bird, Victoria Land (Greenfield, 1983).

Wilson (1951) studied infections of *Rhacomitrium* carpet on Jan Mayen Island and reported that the moss disease was caused by an unidentified basidomycete. *Pythium ultimum* var. *ultimum* (Hoshino *et al*., 1999) and *Pythium* sp. (Tojo *et al*., unpublished results) cause parasitic disease in *Sanionia uncinata* in Svalbard. On the other hand, *Thyronectria antarctica* var. *hyperantarctica*, an undetermined plectomycete (Hawksworth, 1973; Longton, 1973), *Coleroa turfosorum*, *Bryosphaeria megaspora*, *Epibryon chorisodontii* (Fenton, 1983) and *Rhyzopus* sp. (Greenfield, 1983), which may cause parasitic disease in mosses, have been isolated from various regions of the Antarctic Zone.

This document is provided by JAXA.

Therefore, fungi also play another ecological role in polar regions, since some fungi may cause not only disintegration of dead moss shoots but also infection in moss colonies. However, there have been very few ecological studies on moss pathogenic fungi in the Arctic and Antarctic regions. In this study, we aim to elucidate the ecological characteristics of moss pathogenic fungi in the Arctic.

2. Materials and methods

2.1. Isolation of fungi from moss colonies

Moribund moss shoots were collected to isolate parasitic fungi in Barentsburg (78°N, 14°E), Longyearbyen (78°N, 15°E) and Ny-Ålesund (79°N, 12°E) on Svalbard in June and August, 1999.

Fungi were isolated at sampling sites. We collected *ca.* 2000 shoots respectively from 5 dead and 2 healthy moss colonies at each site. Collected dead and healthy moss shoots were untied and rinsed twice with sterilized water. Each shoot was cut up into 1 cm pieces. Fifty dead and 20 healthy moss shoots from each site were immediately placed on potato dextrose agar (PDA, Difco) plates. Fungi growing on moss shoots were cultivated at room temperature (*ca.* 15–20℃) for 2–5 days. Single fungal colonies were selected from each plate and subcultured on PDA slants.

2.2. Morphology

Isolates were pre-grown on corn meal agar (CMA, Difco) plates at 15℃, and agar discs 7 mm in diameter were taken from actively growing colony margins and inoculated onto CMA plates. Cultures were incubated for 7 to 30 days at 15℃ for morphological observation. The morphological characteristics examined were: dimensions of hyphal swelling, and width of the main hyphae. The isolates were also grown on grass blades for 3 to 7 days at 5 and 15℃ to determine zoospore production (Martin, 1992). At least 30 hyphal swellings were examined for each isolate for all characteristics.

2.3. Growth temperature

Mycelial discs 5 mm in diameter were cut from the margin of an actively growing fungal colony in subcultured PDA plates, transferred to the centers of PDA plates (9 cm in diameter), and inoculated at 9 different temperatures from 0 to 40℃, in duplicate. After 1, 2 and 3 days following inoculation, the colony diameters were determined. The linear mycelial growth rate per day was calculated after the initial lag period.

3. Results and discussion

3.1. Fungal infection pattern

Moss carpets of *Sanionia uncinata* (Hedw.) Loeske [=*Drepanocladus uncinatus* (Hedw.) Warnst.] predominated in Barentsburg, Longyearbyen and Ny-Ålesund. Moribund moss colonies were sometimes found in the moss carpets after the snow bed had melted in wet or submerged areas (Fig. 1A). Especially, many fungal infections were distributed at bases of cliff where there were snowdrifts during spring. Fungal infections were seen in irregular patches along a snow melt stream or forming a circular pattern

This document is provided by JAXA.

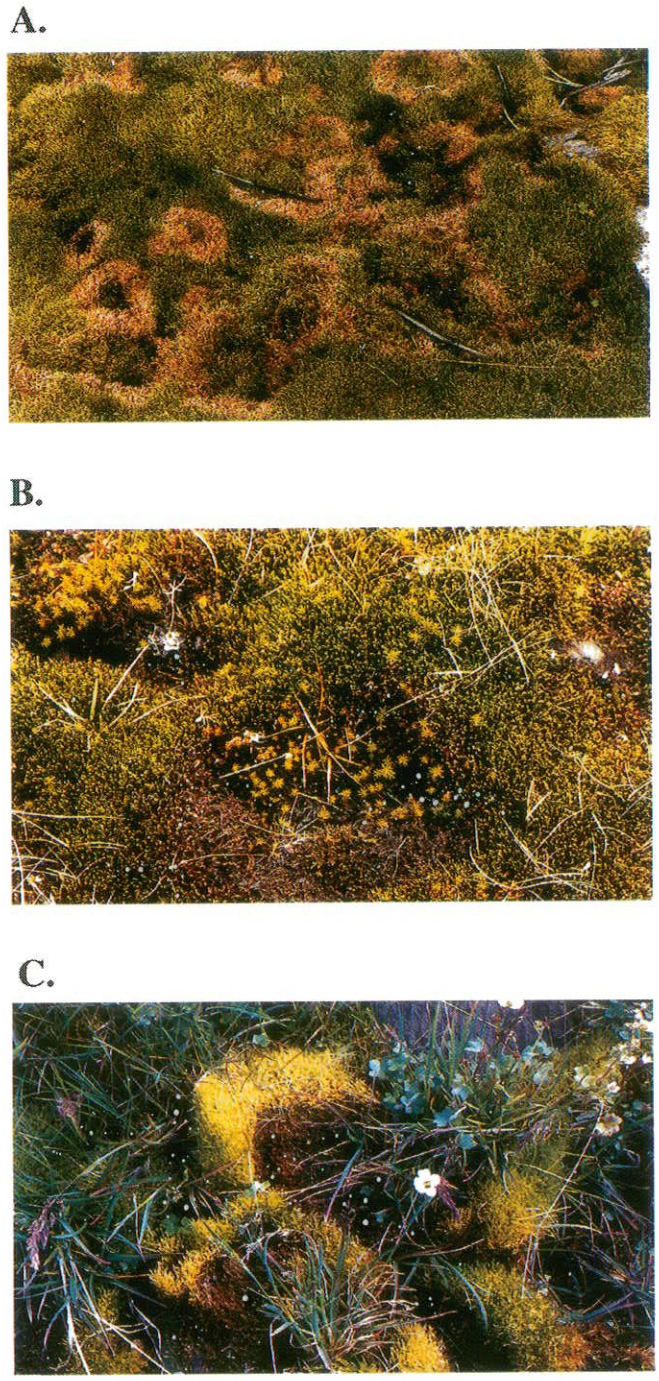


Fig. 1. Fungal infections in Sanionia uncinata *in Svalbard. A: Fungal infections in Ny-Ålesund. B and C: Fungal infections in Barentsburg.*

This document is provided by JAXA.

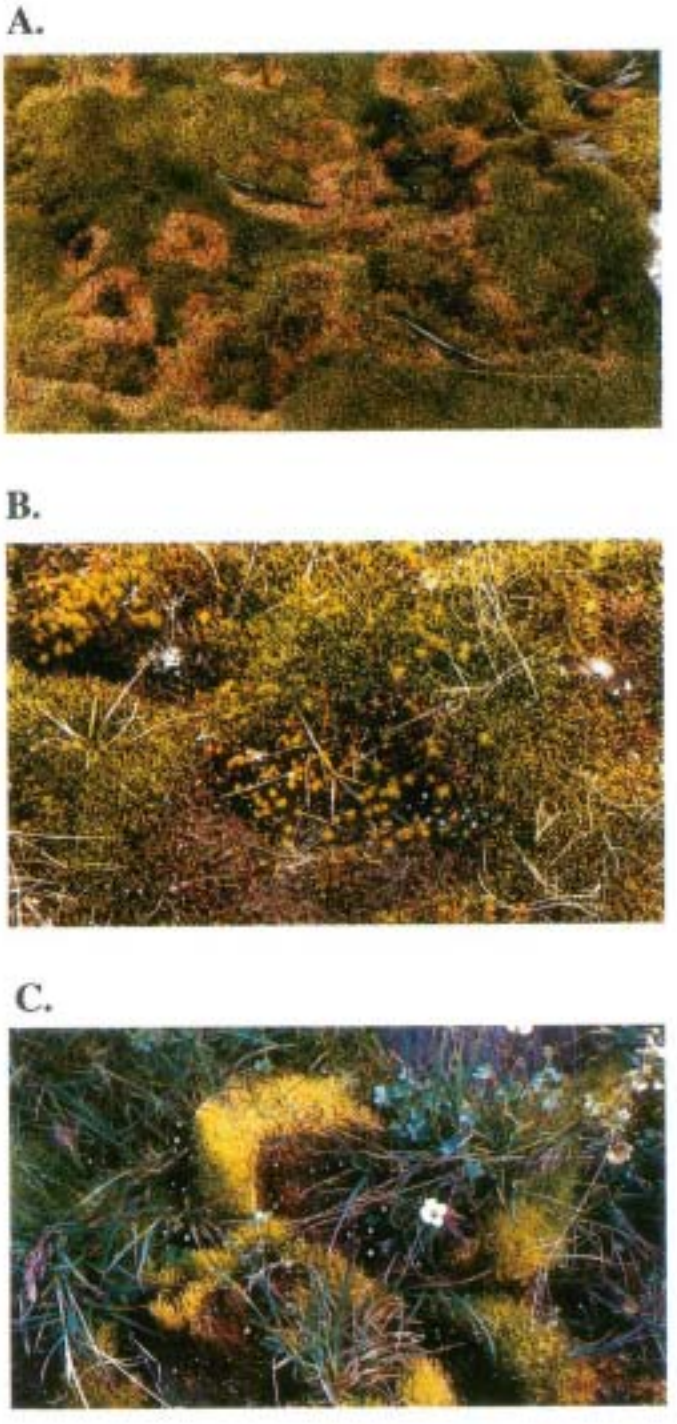


Fig. 1. Fungal infections in Saniona uncinata *in Svalbard. A: Fungal infections in Ny-Ålesund. B and C: Fungal infections in Barentsburg.*

This document is provided by JAXA.

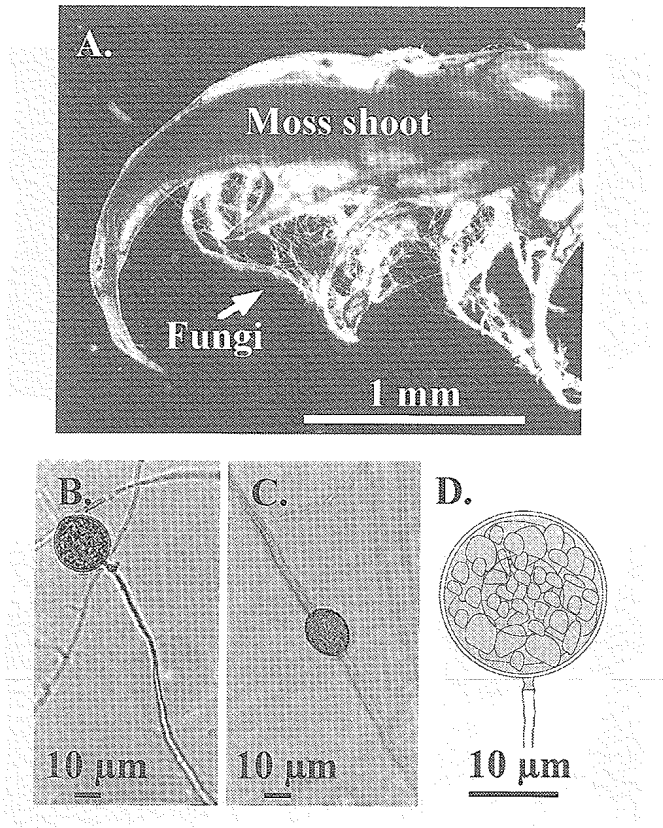


Fig. 2. Mycological characteristics of moss pathogenic fungi from Svalbard. A: Microscopically observation of fungal infected moss shoot. Terminal (B) and intercalary (C) hyphal swellings in CMA plates. D: Illustrated terminal hyphal swelling.

(Hoshino *et al.*, 1999). Mycelia on moss shoots were visible to the naked eye immediately after thawing (Fig. 2A). In Antarctica, many fungal infections in *S. uncinata* and *Polytrichum juniperinum* have been observed in moss vegetation near the seashore (Hoshino *et al.*, unpublished results). However, we could not find any obvious disease in moss along the coasts of Barentsburg, Longyearbyen and Ny-Ålesund.

Ridley *et al.* (1979) reported a large number of concentric bands in dead moss in Reindalen, Svalbard, although the host moss was not described in their brief report. They reported that there were many concentric fungal rings in the Arctic moss, one of the rings reaching 1 m in diameter. However, we observed only irregular patches and small circular patterns of fungal infections. A similar infection pattern was reported on Ellesmere Island and in Antarctica (Longton, 1973). We also found a regrowth of moss shoots in center of fungal infections in Ny-Ålesund (Fig. 1A). On the other hand, in relatively warmer areas, Barentsburg and Longyearbyen, we did not observe such regrowth. Many saprophytic microorganisms invaded and to grew in fungal infections in Barentsburg and Longyearbyen. Therefore, moss shoots in fungal infections were destroyed by the fungal decomposition process.

This document is provided by JAXA.

3.2. Mycological characteristics of pathogenic fungi

All isolates from dead moss shoots from Barentsburg, Longyearbyen and Ny-Ålesund produced only non-sexual organs, hyphal swellings in CMA plates and grass blades (Fig. 2B–D: all of them were lacking in oogonia production). In addition, isolates did not produce zoospores in artificial condition. However, all isolates from dead moss shoots in Svalbard could not grow in CMA plates containing 5 μM metalaxyl (specific growth inhibitor of *Pythium*, data not shown). Hyphal swellings of isolates from Svalbard were terminal globose and sometimes formed intercalary (Fig. 2B and C). Diameters of hyphal swellings were 20–25 μm. Hyphal swellings had outer wall like chlamydospores (Fig. 2B and D). Similar morphological characteristics were reported from the *Pythium* sp. from Alaska (Hamm *et al.*, 1988). Morphological comparisons between these characteristics and reference data from Van der Plaats-Niterink (1981) indicate that the isolate was the *Pythium* sp. HS group. Previously, *Pythium* spp. were isolated in Alaska (Hamm *et al.*, 1988), Devon Island (Booth and Barrett, 1971), Kola peninsula in Russian Arctic (Petrov, 1983), Finnmark in northern Norway (Hoshino *et al.*, 2000) and Svalbard (Gaertner, 1954).

3.3. Ecological characteristics of moss pathogenic fungi

Our previous report (Hoshino *et al.*, 1999) showed that the host plant of *Pythium* spp. was *S. uncinata* in Longyearbyen and Ny-Ålesund. In this report, we found fungal infection patches in other moss species such as *Aulacomnium palustre* (Hedw.) Schwaegr., *Straminergon stramineum* (Brid.) Hedenaes and *Tomenthypnum nitens* (Hedw.) Loeske in Barentsburg. Parasitic fungus, *Pythium* sp. HS group was isolated from all species of moribund mosses. However, we could not obtain *Pythium* sp. from healthy moss shoots. Therefore, it is thought that this parasitic fungus has low host specificity.

The *Pythium* HS group isolated from plants collected in temperate zone countries, has been shown to be parasitic with strong pathogenic activity in many cultured plants (Van der Plaats-Niterink, 1981), but there have been no reports of this fungus having pathogenic activity in mosses. However, Arctic isolates killed artificially inoculated shoots of *S. uncinata* (Hoshino *et al.*, unpublished results). Agricultural activity in Svalbard is very low (a few greenhouse and farm lands are in two Russian settlements), and moss is one of

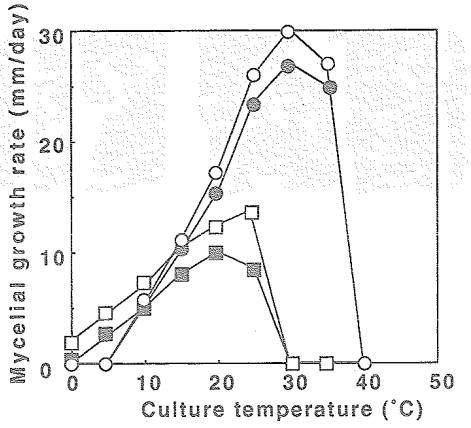


Fig. 3. Effects of culture temperature on mycelial growth of Arctic and temperate zone isolates, Pythium *HS group. Temperate isolates (94Pyl-4: ○, 94Rh-1: ●) were isolated from Yamanashi Prefecture in Japan. Arctic isolates were isolated from Barentsburg (□) and Longyearbyen (■).*

This document is provided by JAXA.

the dominant vegetation plants. Therefore, these Arctic isolates probably gained a wide range of parasitic activity to adapt to the environmental conditions of the high Arctic.

The morphological characteristics of Arctic isolates corresponded to those of temperate isolates. However, Arctic isolate showed a different response to temperature (Fig. 3). They grew at 0℃ but the temperate isolates did not grow at 0℃ (same conditions as those under snow cover). The optimal growth temperature of Arctic isolates is 20–25℃ and that of temperate isolates is 30℃. On the other hand, the mycelial growth rate of isolates from Svalbard, compared with that of isolates from the temperate zone, was very low at temperatures above 10℃. These results suggest that the Arctic isolates have evolved as "specialists" with a narrow temperature range and high adaptation to the cold climate in Svalbard.

3.4. Ecological role of pathogenic fungi

Pathogenic fungi have invaded in a moss carpet and formed patches after several years. Host moss shoots were destroyed in the center parts of fungal infections. We often found some higher plants (*Deschampsia* spp., *Poa* spp. and etc.) or other mosses (*Bryum* spp., *Polytrichum* spp. and etc.) in those moribund moss patches (Fig. 1B and C). Thus, the invasion of phytopathogenic fungi in a moss carpet is thought to lead the formation of pathogenic patches as "open spaces" where other plants easily colonize. Figure 4 shows our hypothesis concerning the development of moribund moss colonies and the ecological role of phytopathogenic fungi in the Arctic. The formation of pathogenic patches might be the

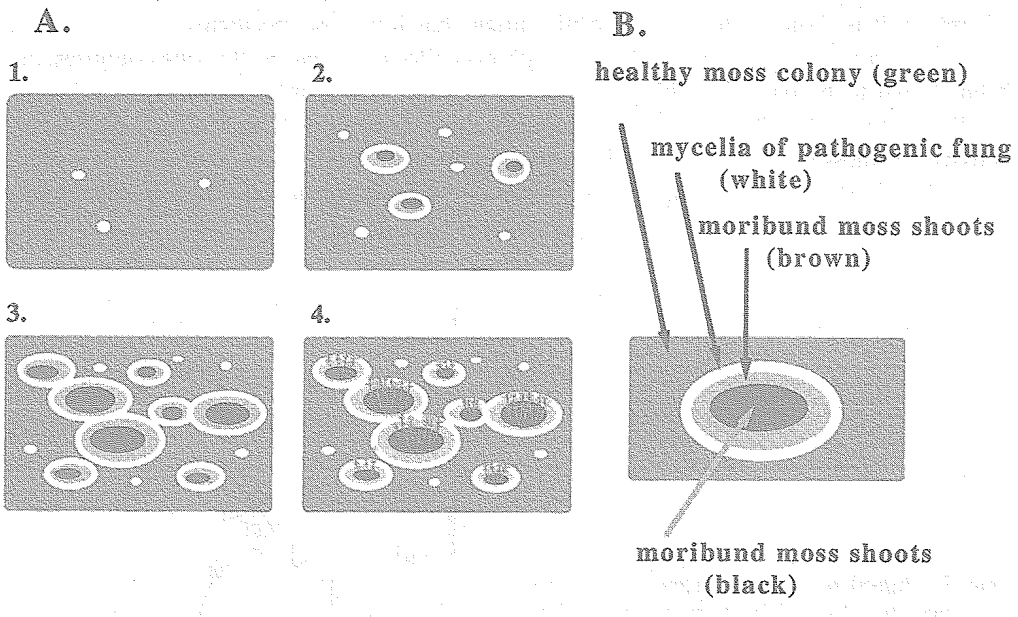


Fig. 4. The hypothesis of ecological impact of moss pathogenic fungi. A: Disease development of moss blight. 1: The invasion of pathogenic fungi in stable moss colony. 2: The spread of fungal infections. 3: The spread of moribund area. 4: the invasion of other plants. B: Morphology of fungal infection.

This document is provided by JAXA.

first step in changes in the patterns in plant communities in polar regions. Previous theories of the succession and colonization of polar plants have focused on plant-environmental or plant-plant interactions. Our observations offer a new concept of the colonization of polar plants.

Acknowledgments

This research project was financially supported by a grants from Ministry of International Trade and Industry (Japan) and a fellowship from The Research Council of Norway. We are indebted to Mr. Takeshi Ueno (The Graduate University for Advanced Studies) for technological support in the collection of moribund moss colonies in Ny-Ålesund, Svalbard.

References

Booth, T. and Barrett, P. (1971): Occurrence and distribution of zoosporic fungi from Devon Island, Canadian Eastern Arctic. Can. J. Bot., **49**, 359–369.

Fenton, J.H.C. (1983): Concentric fungal rings in Antarctic moss communities. Trans. Br. Mycol. Soc., **80**, 413–420.

Gaertner, A. (1954): Über das vorkommen niederer Erdphycomyceten in Afrika, Schweden und an einigen mitteleuropäischen Standorten. Arch. Mikrobiol., **21**, 4–56.

Greenfield, L. (1983): Thermophilic fungi and actinomycetes from Mt. Erebus and a fungus pathogenic to Bryum antarctium at Cape Bird. N.Z. Antarct. Rec., **4**, 10–11.

Hamm, P.B., Hansen, E.M., Hennon, P.E. and Shaw, C.G. (1988): *Pythium* species from forest and muskeg areas of southeast Alaska. Trans. Br. Mycol. Soc., **91**, 385–388.

Hawksworth, D.L. (1973): *Thyronectria antarctica* (Speg.) Seeler var. *hyperantarctica* D. Hawksw. var. nov. Br. Antarct. Surv. Bull., **32**, 51–53.

Hoshino, T., Tojo, M., Okada, G., Kanda, H., Ohgiya, S. and Ishizaki, K. (1999): A filamentous fungus, *Pythium ultimum* Trow var, *ultimum*, isolated from moribund moss colonies from Svalbard, Northern Islands of Norway. Polar Biol., **12**, 68–75.

Hoshino, T., Tojo, M. and Tronsmo, A.M. (2000): Pythium Blight of moss colonies (*Sanionia uncinata*) in Finnmark. Polarflokken, **24**, 161–164.

Laursen, G. and Chmielewski, M. (1982): The ecological significance of soil fungi in Arctic tundra. Arctic and Alpine Mycology, ed by G.L. Laursen and J.F. Ammirati. Seattle, University of Washington Press, 432–492.

Longton, R.E. (1973): The occurrence of radial infection patterns in colonies of polar bryophytes. Br. Antarct. Surv. Bull., **32**, 41–49.

Longton, R.E (1997): The role of bryophytes and lichens in polar ecosystems. Ecology of Arctic Environments, ed. by S.J. Woodin and M. Marquiss. Oxford, Blackwell, 69–96.

Martin, F.M. (1992): *Pythium*. Methods for Research on Soilborne Phytopathogenic Fungi, ed. by L.L. Sigleton *et al*. St. Paul, APS Press, 39–49.

Petrov, V.F. (1983): Pathogenic microflora of root growth in perennial grasses in Khibiny. Bull. Appl. Bot. Genet. Plant Breed., **82**, 45 (in Russian with English summary).

Ridley, M., Gillow, C., Perkins, D. and Ogilvie, J. (1979): Oxford University expeditions to Svalbard 1978. Bull. Oxf. Univ. Explor. Club. New Series, Commem. Vol., 29–79.

Van der Plaats-Niterink, A.J. (1981): Monograph of the genus *Pythium*. Stud. Mycol., **21**, 1–241.

Wilson, J.W. (1951): Observations on concentric 'fairy rings' in Arctic moss mat. J. Ecol., **39**, 407–416.

(Received March 23, 2000; Revised manuscript accepted November 13, 2000)

This document is provided by JAXA.

This document is provided by JAXA.

Program of Second International Symposium on Environmental Research in the Arctic and Fifth Ny-Ålesund Scientific Seminar, 23-25 February 2000, Tokyo

Session I: Overview of the Environmental Research in the Arctic (1)

1. NIPR Arctic Environment Research in 1990-1999. Y. Fujii.
2. Observations of the Arctic troposphere and lower stratosphere with the SOUSY Svalbard radar. J. Röttger.
3. Climate Change and its Impacts on the Arctic. G. Weller.
4. Greenland Summit Environment Observatory . A. Ohmura.
5. Circum-Arctic ice core records from small ice caps: a different view on Holocene climate. R.M. Koerner.
6. Chinese First Expedition to the Arctic Ocean. Z. Dong and W. Qin.
7. Greenland Sea in Winter. H. Ito and co-authors.
8. The International North Water Polynya Study (NOW) : an Early Synthesis. L. Fortier, M. Fortier, M. Fukuchi, Y. Gratton, L. Legenere and T. Odate.
9. Greenhouse gas fluxes in winter and thawing period at Arctic tundra Ecosystem. Y. Harazono, N. Ohta, A. Miyata, K. Nakamoto, R. Zulueta and W.C. Oechel.
10. Persistent organic pollutants in Arctic animals in the Barents Sea area and at Svalbard; levels and effects. G.W. Gabrielsen.
11. Global Change impacts on terrestrial plant communities: long-term studies in the northern Scandes. U. Molau.

Session II: Overview of the Environmental Research in the Arctic (2)

12. Activity and Development of Scientific Community Ny-Ålesund. K.J. Holmén.
13. What is needed in order to achieve a full scale environmental monitoring station in Ny-Ålesund? P. Prestrud.
14. Recent contributions to long-term atmospheric studies at Koldewey-Station. H. Gernandt and R.Neuber.

Session III: Upper Atmosphere Environment

15. Climatic mesospheric cooling: the importance of long time-series of ionospheric soundings. C.M. Hall.
16. Geomagnetically Conjugate Auroras between Iceland and Syowa Station. N. Sato.
17. Response of the Thermosphere to High-Latitude Energy Inputs. S. Maeda and H. Fujiwara.
18. Sounding rockets from SvalRak. I.K. Nyheim.
19. SS-520-2 Rocket Experiment Plan. T. Mukai and Y. Inatani.
20. Observations of the Arctic mesosphere and D-region with the EISCAT Svalbard radar and the SOUSY Svalbard radar. J. Röttger.
21. Noctilucent cloud observations with CCD cameras in both northern and southern hemispheres during 1997-1999 . T. Sugiyama, G. Witt, N. Ueno, B.Z.O. Gjede, R.M. Mac-Mahon, S. Nikolashkin, G.A. Gavrilyeva and P. Ammosov.
22. Gravity waves simulated by a high-resolution GCM. K. Sato, T. Kumakura and M. Takahashi.
23. A study on the polar atmospheric tide by the EISCAT and cooperative observation network: comparisons with observation and theory. T. Aso.

Session IV: Atmosphere Environment (1)

24. Ground based, balloon and aircraft measurements of greenhouse gases in the Arctic. S. Aoki, S. Morimoto, G. Hashida, M. Shiobara, T. Yamanouchi, S. Sugawara, T. Machida, H. Honda, K. Kawamura, S. Yoshimura and T. Nakazawa.
25. Ten years of Carbon Dioxide monitoring on Zeppelinfjellet (78°54'N, 11°53'E). K.J. Holmén and V. Bazhanov.
26. Global quality control for long-lived trace gas measurements. R. Francey, M. Groening, K. Holmén, K-R. Kim, J. Miller, P. Tans and N. Trivett.

Session V: Atmospheric Environment (2)

27. Forthcoming Arctic field campaign ASTAR 2000 (Arctic Study of Tropospheric Aerosol and Radiation). T. Yamanouchi and A. Herber.
28. Aerosol measurements at Ny-Ålesund/Spitsbergen and its possible climate impact. A. Herber, A. Rinke, R. Neuber, M. Fortmann, R. Schumacher, L.W. Thomason, M. Kriews, J. Notholt, T. Albrecht, T. Yamanouchi, M. Shiobara, K. Dethloff and H. Gernandt.
29. Arctic stratospheric aerosols -PSCs and background sulfate particles-. Y. Iwasaka, T. Shibata, H. Adachi, M. Watanabe, T. Sakai, K. Hara, Y. Inomata, M. Fujiwara, M. Hayashi and K. Shiraishi.
30. Chemical composition of total deposition samples from Spitsbergen. M. Kriews, I. Stölting and O. Schrems.
31. Measurement of atmospheric pollution in the Siberian Arctic. T. Fukasawa, S. Ohta, K. Enomoto, N. Murao, S. Yamagata, T. Shimizu and V.N. Makarov.
32. Preliminary measurements of CH_4 emission at a burnt forest in West Siberia. T. Nakano, M. Fukuda, M. Utsumi and G. Inoue.
33. Radiative forcing due to anthropogenic activities. F. Stordal and G. Myhre.

This document is provided by JAXA.

34. Natural variability of the surface spectral and total albedo in Svalbard. J.B. Orbek and S. Claes.
35. Three years spectral resolved UV measurements at Koldewey-Station. Ch.Groβ, H. Tüg and O. Schrems.
36. Estimation of tropospheric Water Vapor content using a network of GPS receivers in Ny-Ålesund. A. Rius, G. Ruffini and L. Cucurull.
37. In-situ measurement for a polar low over the Norwegian Sea. Y. Asuma, Y. Fukuda, K. Kikuchi, M. Shiobara, M. Wada and G.W. Kent Moore.
38. Feasibility Study on Scientific Balloon Experiment at Ny-Ålesund. H. Honda, N. Izutsu and N. Yajima.

Poster Session I:

101. Announcement of an EU research program at Ny-Ålesund: The NItrogen Cycle and Effects on the oxidation of atmospheric trace species at high latitudes (NICE). H.J. Beine, R. Sparapni and I. Allegrini.
102. Temporal variations of atmospheric CO_2 concentration and its carbon isotope in Ny-Ålesund, Svalbard. S. Morimoto, S. Aoki, s. Yoshimura and T. Yamanouchi.
103. An intercomparison campaign of ozone and temperature measurements in the Arctic (NAOMI-98, Ny-Ålesund/Spitsbergen). R. Neuber, G. Beyerle, P. von der Gathen, P. Wahl, A. Dahl, M. Gross, Th. McGee, U. Klein and W. Steinbrecht.
104. Ozone loss rates determined with Match. A. Schulz, M. Rex, N.R.P. Harris, G.O. Braathen, E. Kyrö, E. Reimer, R. Alfier, I. Kilbane-Dawe, M. Allaart, M. Alpers, B.R. Bojkov, J. Cisneros, H. Claude, E. Cuevas, J. Davies, H. DeBacker, H. Dier, V. Dorokhov, G. Fast, B, Johnson, B. Kois, E. Kosmidis, Z. Litynska, I.S. Mikkelsen, M. Molyneux, G. Murphy, H. Nakane, F. O'Connor, C. Parrondo, P. Skrivankova, C. Varotsos, C. Vialle, P. Viatte, V. Yushkov, C. Zerefos and P. von der Gathen.
105. Surface energy and radiation balances in the Kongsfjorden area. T. Georgiadis, M. Nardino, F. Calzolari, V. Levizzani and R. Pirazzini.
106. Field reflectance data on different snow covers at Ny-Ålesund. R. Casacchia, F. Lauta, R. Salvatori, S. Ghergo, J.B. Ørbæk, A. Cagnati and M. Valt.
107. Large cloud drops rimed on snow crystals observed at Ny-Ålesund, Svalbard, Arctic. H. Konishi and M. Wada.
108. Spectral reflectance of melting snow in a high Arctic watershed on Svalbard: Some implications for optical satellite remote sensing studies. J.G. Winther, S. Gerland, J.B. Ørbæk, B. Ivanov, A. Blanco and J. Boike.
109. Glaciological observation on Pioner Ice Cap, Severnaya Zemlya in 1996. S. Takahashi, S. Matoba, A. Takahashi, O. Watanabe and L. Savatugin.
110. Leaching of chemical compositions in the snowpack at the dome of Austfonna ice cap, Svalbard. Y. Iizuka, M. Igarashi, K. Watanabe, K. Kamiyama and O. Watanabe.
111. The geochemical phenomenon - Local geochemical fields in the glacier. V.N.Makarov.
112. Regional characteristics of chemical constituents in surface snow, arctic cryosphere . O. Watanabe, H. Motoyama, K. Kamiyama, M. Igarashi, K. Goto-Azuma, Y. Fujii, Y. Iizuka, S. Matoba and H. Narita.
113. Chemical analysis of the shallow ice core and surface snow samples from North Greenland. M. Igarashi, M. Tagami, H. Motoyama, M. Takata, O. Watanabe, H. Narita, H. Shoji, J.P. Steffensen and H.B. Clausen.
114. On the detailed density profile of NGRIP-S1 shallow ice cores from Greenland. H. Narita, H. Shoji, H.B. Clausen and S.J. Johansen.
115. The North Water Polynya study : preliminary hydrographic results. Y. Gratton, H. Melling R.G. Ingram and R.F. Marsden.
116. Bio-optical characteristics in northern Baffin Bay. H. Sasaki, S. Saito, T. Hirawake and P. Larouche.
117. Pico and nanophyt oplankt on Dist ribution in the North Water (76°- 79°N) as estimated by flow cytometry. S. Demers, B. Mostajir, J.N. Bouchard F. Vidussi, C. Vasseur and M. Fukuchi.
118. Species composition, biomass and photosynthetic activity of the bottom ice algae in the North Water Polynya during the springtime. M. Gosselin, C. Nozais and C. Michel.
119. Physiological study on photosynthetic pigments of phytoplankton in the North Water Polynya. Y. Hayashi, Y. Kashino, Y. Suzuki, T. Odate and S. Kudoh.
120. Feeding activities of Arctic copepods in the NOW Polynya.. H. Hattori, N. Kobahashi, M. Sanpei and K. Takahashi.
121. Respiration and excretion rates of Calanus hyperboreus, C. glacialis and Metridia longa in relation to environmental conditions at North Water Polynya during autumn. K. Takahashi, K. Takahashi and S. Taguchi.
122. Observation of downward particle flux in the North Water Polynnya. M. Fukuchi, M. Sampei, H. Sasaki, Y. Kashino, S. Kudoh and B. Hargrave.
123. Vegetation and soil relationships in the recently deglaciated terrains in Ny-Ålesund, Svalbard. S. Kojima and N. Wada.
124. Flora and vegetation of deglaciated area in Ny-Ålesund, Svalbard. H. Kanda, S. Imura, Y. Minami and S. Kojima.
125. Arctic Polygonum viviparum; Growth and reproduction in relation to preformation. S. Nishitani, T. Masuzawa, G. Gabrielsen, N. Misato, H. Kanda and J. Ishidsu.
126. Comparisons of germination pattern and seeding survival of Potentilla matsumurae (Rosaceae) between alpine fellfield and snowbed habitats. Y. Shimono and G. Kudo.

This document is provided by JAXA.

127. Variations in reproductive characteristics of two sympatric alpine shrubs, Phyllodoce caerulea and Phyllodoce aleutica along a snowmelt gradient. T. Kasagi and G. Kudo.
128. Ecological role of fungal infections of moss carpet in Svalbard. T. Hoshino, M. Tojo, H. Kanda and A.M. Tronsmo.
129. Occurrence of plants in northern Kuriles, a highly oceanic sector of the subarctic zone. I. Notes on distribution of bryophytes. Y. Minami, S. Okitsu, V.Ya. Cherdantseva and S.Yu. Grishin.
130. Occurrences of plants in northern Kuriles, a highly oceanic sector of the subarctic zone. II. Distribution of dwarf shrubs and herbaceous plants on Mt. Ebeko, Paramushir Island. S. Okitsu, Y. Minami and S.Yu. Grishin.
801. New persistent organic pollutants of concern. Ivan C. Burkow.

Poster Session II:
201. A new aurora spectrograph for collaborative observation with EISCAT Svalbard radar. S. Okano, M. Taguchi, T. Aso and M. Ejiri.
202. Interhemispheric conjugacy of auroral poleward expansion observed by conjugate imaging riometers at ~ 67°and 75° ~ 77° invariant latitude. H. Yamagishi, Y. Fujita, N. Sato, M. Nishino, P. Stauning and L. Ruiyuan.
203. Conjugate imaging riometer observations at Polar Cusp/Cap Stations. M. Nishino, H. Yamagishi, N. Sato, L. Ruiyuan, P. Stauning and J.A. Holtet.
204. Haze layers and their characteristics observed over Spitsbergen during the AAMP 1998 campaign. M. Shiobara, S. Yamagata, M. Watanabe, T. Shibata, R. Neuber, G. Beyerle, R. Schumacher, A. Herber, P. Rairoux and D. Nagel.
205. Aircraft observation of carbonyl sulfide (COS) over mid-high latitude of Northern Hemisphere during AAMP98. Y. Inomata, K. Matsunaga, S. Sugawara, S. Morimoto, Y. Iwasaka, K. Osada, M. Watanabe and M. Shiobara.
206. Black carbon and common ionic species in the Arctic atmospheric aerosol. K. Eleftheriadis, S. Nyeki, K. Tørseth and I. Colbeck.
207. Event-induced aerosol sampling at Spitsbergen. M. Kriews, I. Stölting and O.Schrems.
208. The production of HONO in Arctic aerosols. H.J. Beine, F. Valentini, A. Ianniello, R. Sparapani and I. Allegrini.
209. The possible influence of local pollution sources on chemical compound measurements at Zeppelin: Using SODAR to identify flow pattern. H.J. Beine and S. Argentini.
210. Detailed stratigraphy analysis of a NGRIP shallow ice core using laser tomograph system. M. Takata, Y. Fujii, O. Watanabe, H. Shoji and N. Azuma.
211. Vertical distribution of heavy metals in Vestfonna, Svalbard ice core. S. Matoba, A.E. Eroglu, H. Motoyama, Y. Fujii, O. Watanabe and M. Nishikawa.
212. Contrastive anthropogenic acidification in Arctic and Antarctic cores. Y. Fujii, K. Kamiyama, F. Nishio, H. Shoji, K. Goto-Azuma, M. Kohno and O. Watanabe.
213. Preliminary results from 289 m ice core on Austfonna ice cap, Svalbard . O. Watanabe, H. Motoyama, M. Igarashi, K. Goto-Azuma, T. Nagasaki, L. Karlof and E. Isaksson.
214. Asynchronism of glacier fluctuations in the Arctic and in the Alps at the end of 20 century. T. Khromova and L. Chernova.
215. Climate Changes and its impact on Northern Eurasia Glaciers reduction by the scenarios of the former climates. M. Ananicheva, N. Davidovich and Y. Kononov.
216. Status report on the GPS Positioning at Ny-Ålesund, Svalbard in 1994. M. Kanao and M. Wada.
217. The determination of the "invariant point" of the VLBI antenna in Ny-Ålesund. P. Tomasi, M. Rioja and P. Sarti.
219. Climatic and biological forcing of the vertical flux of biogenic particles under first-year ice in the Canadian Arctic in spring. M. Fortier, L. Fortier and L. Legendre.
220. Observations of CO_2 partial pressure, total inorganic carbon and nutrients in the Greenland Sea in winter season. S. Yoshimura, S. Aoki, T. Nakazawa, S. Morimoto, G. Hashida, S. Ushio and H. Ito.
221. Oxygen isotope hydrography in Northeastern Greenland Sea in January 1999. M. Yamamoto, S. Tsunogai and N. Tanaka.
222. Seasonal difference in stable isotope compositions of arctic copepods. H. Sasaki, D. Kawai, H. Suzuki, M. Sato and M. Fukuchi.
223. The most important plankton grazers in Kongsfjorden, Ny-Ålesund. Spatial distribution patterns of three Calanus species in an Arctic glacial fjord. S. Kwasniewski, S.F. Petersen, H. Hop and G. Pedersen.
224. Reproductive strategies of the bearded seal, Erignathus Barbatus. S.M. Van Parijs, K.M. Kovacs and C. Lydersen.
225. Soil respiration in relation to primary succession in Ny-Ålesund Svalbard. H. Koizumi, Y. Bekku, A. Kume, T. Nakatsubo, T. Masuzawa and H. Kanda.
226. Ecosystem Carbon Cycle on a Glacier Foreland in Ny-Ålesund, Svalbard. T. Nakatsubo, Y. Bekku, M. Uchida, H. Kanda and H. Koizumi.
227. Primary production of mosses in Ny-Ålesund, Svalbard. M. Uchida, Y. Bekku, T. Nakatsubo, T. Ueno, H. Kanda and H. Koizumi.
228. Structure and functional role of moss colony, Sanionia uncinata in different water environments. T. Ueno, Y. Bekku, S. Imura and H. Kanda.
229. Photosynthetic and water relational characteristics in two co-occurring Polygonum species at a scoria desert in an

This document is provided by JAXA.

alpine timber line of Mt. Fuji. T. Nakano, A. Tanaka, T. Ohtsuka, Y. Abe, H. Tanabe, Y. Sato, C. Sakano and Y. Yamamura.

230. Biological characteristics of dark colored material in Canadian High Arctic glaciers. N. Takeuchi, S. Kohshima, K. Goto-Azuma and R.M. Koerner.
231. UV-B-Personal-related dosimetry at Koldewey-Station by using an electronic Dosimeter ELUV-14. S.E.Naggar.
901. Opportunities for European Research Collaboration under the Ny-Ålesund Large Scale Facility Program 2000 – 2002. J.B. Orbek.

Session VI: Glaciological Environment (1)

39. Atmospheric Teleconnection between Japan and the Saint Elias Mountains, Yukon. G. Holdsworth.
40. Gas diffusion in polar firn and its application to atmospheric composition history and paleothermometry. J. Chappellaz.
41. Determination of ice flow velocity in Svalbard from ERS-1 interferometric observations. B. Lefauconnier, D. Massonnet and G. Anker.
42. Effects on spectral reflectance from snow ageing. J.G. Winther and S. Gerland.
43. In-situ snowpack temperature monitoring at an Arctic tundra site: A comparison of manual and automatic measurements. S. Gerland and J.G. Winther.
44. Polythermal glaciers in Northern Scandinavia - an important source of paleo environmental records. P. Holmlund.
45. An ice core record from Lomonsovfonna, Svalbard: viewing the isotopic, chemical and structural data between 1920-1997 in relation to instrumental records. E. Isaksson, V. Pohjola, J. O'Dwyer, T. Jauhiainen, J. Moore, J-F. Ponglot, R. Vaikmåe, R.S.W. van de Wal, H.A.J. Meijer and J.O. Hagen.
46. Sedimentary environment of the glaciers in the northern part of Svalbard recorded in ice cores. O. Watanabe, H. Narita, S. Takahashi, N. Kameda, K. Kamiyama, H. Motoyama, M. Miyahara, S. Matoba, A. Furukawa, T. Shiraiwa, K. Azuma, M. Igarashi, Y. Fujii, E. Isaksson, S. Arkhipov and O. Hagen.
47. Ice-core chemistry variation on Penny Ice Cap, Baffin Island, Canadian Arctic over the last two centuries. K. Goto-Azuma, R.M. Koerner and D.A. Fisher.
48. The North-GRIP deep drilling project in Greenland. S.J. Johnsen, D.D. Jensen, N. Gundestrup and O. Watanabe.
49. Evolution of White Glacier, Canada, in $2xCO_2$ climate, a numerical model study. O.Albrecht.

Session VII: Glaciological Environment (2)

50. Ocean tides and loading in the Arctic. M.S. Bos and T.F. Baker.
51. Inversion of global tide gauge data for present-day ice load changes. H.P. Plag.
52. Continuous gravity observation at Ny-Ålesund, Svalbard with a superconducting gravimeter CT#039. T. Sato, K. Asari, H.P. Plag, H. Digre and K. Kaminuma.

Session VIII: Marine Environment

53. Arctic Ocean Change and Consequences to Biodiversity: A Perspective. E. Carmack.
54. Seasonal cycle of carbon export in the Nordic Seas. P. Wassmann.
55. Physical and chemical indicators of changes in the Barents Sea ecosystem in the second half of the 20th century. O.V. Titov.
56. Wind and freshwater driven circulation in an Arctic fjord system. R. Ingvaldsen, M.B. Reitan, H. Svendsen and L. Asplin.
57. The arctic sea ice ecosystem controlling by global warming. I.A. Melnikov, L.S. Zhitina and E.G.Kolosova.
58. High latitude air-sea-ice interaction: The atmospheric forcing of deep ocean convection. G.W.Kent Moore.
59. Thermohaline structures observed in the Greenland - Barents Sea, January 1999. M. Naya and H. Nagashima.
60. Laboratory experiments on frazil ice formation and thermohaline convection with applications to the Arctic marine environment. A.G. Zatsepin, V.L. Didkovskii, S.N. Dikarev, S.N. Poyarkov and P.N. Golovin.
61. Temporal change of phytoplankton distribution in the North Water Polynya. T. Odate, T. Hirawake, S. Kudoh and M. Fukuchi.
62. Organic Carbon Mineralization by new Types of Psychrophilic Sulfate-Reducing Bacteria in Permanently Cold Sediments off the Coast of Svalbard. C. Knoblauch, K. Sahm, J. Sagemann, K. Ravenschlag and B.B. Jørgensen.

Session IX: Terrestrial Ecosystems

63. Algal primary succession on newly deglaciated Arctic moraine, Ny-Ålesund, Svalbard. J. Elster, K. Kubeckova, J. Kastovsky and H. Kanda.
64. Response of microbial biomass in arctic soil to artificial warming by using Open top chamber. Y. Bekku and H. Kanda.
65. The long-term influence of elevated temperature on biological production and carbon cycle in Arctic terrestrial ecosystems. D.G. Zamolodchikov and D.V. Karelin.
66. Plant speciation and phylogeography in the North Atlantic region. C. Brochmann.

This document is provided by JAXA.

AUTHOR INDEX

Ananicheva, Maria 183
Anker, Geir 279
Aoki, Shuhji 71
Aso, Takehiko 43
Asplin, Lars 393

Baker, T. F. 291
Barber, D. 343
Beyerle, G. 65
Bezgreshnov, A.M. 193
Bos, M. S. 291

Calzolari, Francescopiero 125
Carmack, Eddy 365
Cherdantseva, Valentina Ya. 487
Claes, Stefan 125
Colbeck, I. 91

Dahl, A. 65
Davidovich, Natalia 183
Dong, Zhaoqian 331

El Naggar, Saad 429
Eleftheriadis, K. 91

Fortier, L. 343
Fortier, M. 343
Francey, Roger 81
Fujii, Yoshiyuki 209
Fukuchi, M. 343

Gabrielsen, Geir Wing 349
Georgiadis, Teodoro 125
Gerland, Sebastian 193, 261
Gernandt, Hartwig 49, 429
Golovin, Pavel N. 417
Goto-Azuma, Kumiko 227, 253, 495
Gratton, Y. 343
Grishin, Sergei Yu. 479, 487
Groening, Manfred 81
Gross, M. 65
Groß, Christian 113

Hall, C. M. 21
Hargrave, B. 343
Henriksen, Espen O. 349
Herber, Andreas 101
Holdsworth, Gerald 161
Holmén, Kim 81
Holtet, Jan A. 29
Honda, Hideyuki 133
Hoshino, Tamotsu 507

Igarashi, Makoto 169, 227, 253
Ingvaldsen, Randi 393
Isaksson, Elisabeth 253
Ito, Hajime 337
Ivanov, B. 193
Izutsu, Naoki 133

Jüttner, Hans-Ulrich 301

Kameda, Takao 209, 227
Kamiyama, Kokichi 169, 209, 227, 243
Kanda, Hiroshi 487, 507
Karelin, Dmitri V. 437
Karlöf, Lars 253
Kawai, Daisuke 423
Kim, Krung-Ryul 81
Klaas, Andrew 429
Klein, U. 65
Koerner, Roy M. 203, 495
Kohshima, Shiro 495
Kolosova, Helena G. 409
Kononov, Yuriy 183
Kudo, Gaku 467

Lefauconnier, Bernard 279
Legendre, L. 343
Levizzani, Vincenzo 125
Liu, Ruiyuan 29

Makarov, V. N. 271
Massonnet, Didier 279
Matoba, Sumito. 227
McGee, Th. 65
McLaughlin, Fiona 365
Melnikov, Igor A. 409
Miller, John 81
Minami, Yoshinori 479, 487
Miyahara, Morihiro 253
Molau, Ulf 445
Morimoto, Shinji 71
Motoyama, Hideaki 227, 243, 253
Murata, Yozo 29
Myhre, G. 107

Nagasaki, Tomoharu 253
Nardino, Marianna 125
Narita, Hideki 209, 227
Neuber, R. 49, 65
Nishino, Masanori 29
Nishio, Fumihiko 209
Nyeki, S. 91

This document is provided by JAXA.

Odate, T. 343
Ohmura, Atsumu 153
Okitsu, Susumu 479, 487

Pirazzini, Roberta 125
Plag, Hans-Peter 301

Qin, Weijia 331

Reitan, Marit Bø 393
Rioja, Maria 319
Röttger, Jürgen 1, 9

Sand, Knut 261
Sarti, Pierguido 319
Sasaki, Hiroshi 423
Sato, Megumi 423
Sato, Natsuo 29
Schrems, Otto 113
Shimono, Yoshiko 467
Shoji, Hitoshi 209, 221
Spelten, Nicole 429
Stauning, Peter 29
Steinbrecht, W. 65
Stordal, F. 107
Svendsen, Harald 393

Takeuchi, Nozomu 495
Tans, Pieter 81
Tojo, Motoaki 507
Tomasi, Paolo 319
Trivett, Neil 81
Tronsmo, Anne Marte 507
Tørseth, K. 91
Tüg, Helmut 113

Von der Gathen, P. 49, 65

Wahl, P. 65
Wassmann, Paul 377
Watanabe, Okitsugu 169, 209, 221, 227, 243, 253
Weller, Gunter 143
Winther, Jan-Gunnar 193, 261

Yajima, Nobuyuki 133
Yamagishi, Hisao 29
Yamanouchi, Takashi 71, 101

Zachek, A.S. 193
Zamolodchikov, Dmitri G. 437
Zatsepin, Andrei G. 417
Zhitina, Ludmila S. 409

Ørbæk, Jon Børre 125, 193

This document is provided by JAXA.

MEMOIRS OF NATIONAL INSTITUTE OF POLAR RESEARCH
(Nos. 1–2: Japanese Antarctic Research Expedition Scientific Reports)

Special Issue

No. 1. Nagata, T. ed.: Proceedings of the Symposium on Pacific-Antarctic Sciences. 275 p. February 1967
No. 2. Murayama, M. ed.: Report of the Japanese Traverse Syowa-South Pole 1968–1969. 279 p. March 1971
No. 3. Nagata, T. ed.: Proceedings of Antarctica Review Meeting. 83 p. March 1974
No. 4. Torii, T. ed.: Geochemical and geophysical studies of Dry Valleys, Victoria Land in Antarctica. 89 p. February 1975
No. 5. Nagata, T. ed.: Yamato meteorites collected in Antarctica in 1969. 110 p. August 1975
No. 6. Nagata, T. ed.: Proceedings of IAGA Meeting on Unmanned Observations in Antarctica. 100 p. August 1976
No. 7. Ishida, T. ed.: Glaciological studies in Mizuho Plateau, East Antarctica, 1969-1975. 274 p. January 1978
No. 8. Nagata, T. ed.: Proceedings of the Second Symposium on Yamato Meteorites. 267 p. February 1978
No. 9. Nagata, T. ed.: Proceedings of the Second Symposium on Rocket Experiments in Antarctica. 91 p. October 1978
No. 10. Kusunoki, K. and Suzuki, Y. ed.: Ice-coring project at Mizuho Station, East Antarctica, 1970–1975. 172 p. December 1978
No. 11. Matsuda, T. and Hoshiai, T. ed.: Proceedings of the Symposium on Terrestrial Ecosystem in the Syowa Station Area. 152 p. February 1978
No. 12. Nagata, T. ed.: Proceedings of the Third Symposium on Antarctic Meteorites. 282 p. February 1978
No. 13. Nagata, T. ed.: Proceedings of the Seminar III on Dry Valley Drilling Project, 1978. 245 p. September 1979
No. 14. Nagata, T. ed.: Proceedings of the First Symposium on Antarctic Geosciences, 1978. 229 p. October 1979
No. 15. Nagata, T. ed.: Proceedings of the Fourth Symposium on Antarctic Meteorites. 293 p. December 1979
No. 16. Hirasawa, T. ed.: IMS in Antarctica; Collected Antarctic Research Papers presented to the First International Symposium on IMS in Melbourne, November 27–December 1, 1979. 144 p. September 1980
No. 17. Nagata, T. ed.: Proceedings of the Fifth Symposium on Antarctic Meteorites. 317 p. December 1980
No. 18. Nagata, T. ed.: Proceedings of the Third Symposium on Coordinated Observations of the Ionosphere and the Magnetosphere in the Polar Regions. 502 p. March 1981
No. 19. Kusunoki, K. ed.: Proceedings of the Third Symposium on Polar Meteorology and Glaciology. 324 p. October 1981
No. 20. Nagata, T. ed.: Proceedings of the Sixth Symposium on Antarctic Meteorites. 415 p. December 1981
No. 21. Nagata, T. ed.: Proceedings of the Second Symposium on Antarctic Geosciences, 1980. 171 p. March 1982
No. 22. Nagata, T. ed.: Proceedings of the Fourth Symposium on Coordinated Observations of the Ionosphere and the Magnetosphere in the Polar Regions. 287 p. September 1982
No. 23. Hoshiai, T. and Naito, Y. : Proceedings of the Fifth Symposium on Antarctic Biology. 128 p. October 1982
No. 24. Kusunoki, K. ed.: Proceedings of the Fourth Symposium on Polar Meteorology and Glaciology. 326 p. December 1982
No. 25. Nagata, T. ed.: Proceedings of the Seventh Symposium on Antarctic Meteorites. 343 p. December 1982
No. 26. Nagata, T. ed.: Proceedings of the Fifth Symposium on Coordinated Observations of the Ionosphere and the Magnetosphere in the Polar Regions. 201 p. March 1983
No. 27. Nemoto, T. and Matsuda, T. ed.: Proceedings of the BIOMASS Colloquium in 1982. 147 p. July 1983
No. 28. Nagata, T. ed.: Proceedings of the Third Symposium on Antarctic Geosciences, 1982. 289 p. October 1983
No. 29. Kusunoki, K. ed.: Proceedings of the Fifth Symposium on Polar Meteorology and Glaciology. 227 p. November 1983
No. 30. Nagata, T. ed.: Proceedings of the Eighth Symposium on Antarctic Meteorites. 457 p. December 1983

This document is provided by JAXA.

No. 31. Nagata, T. ed.: Proceedings of the Sixth Symposium on Coordinated Observations of the Ionosphere and the Magnetosphere in the Polar Regions. 179 p. July 1984
No. 32. Hoshiai, T. and Fukuchi, M. ed.: Proceedings of the Sixth Symposium on Polar Biology. 169 p. August 1984
No. 33. Nagata, T. ed.: Proceedings of the Fourth Symposium on Antarctic Geosciences, 1983. 240 p. September 1984
No. 34. Kusunoki, K. ed.: Proceedings of the Sixth Symposium on Polar Meteorology and Glaciology. 241 p. December 1984
No. 35. Nagata, T. ed.: Proceedings of the Ninth Symposium on Antarctic Meteorites. 326 p. December 1984
No. 36. Nagata, T. and Sato, N. ed.: Proceedings of the Seventh Symposium on Coordinated Observations of the Ionosphere and the Magnetosphere in the Polar Regions. 353 p. July 1985
No. 37. Yoshida, Y. ed.: Proceedings of the Fifth Symposium on Antarctic Geosciences, 1984. 225 p. September 1985
No. 38. Nagata, T. ed.: Energetics and Dynamics of the Middle and the Upper Atmosphere at High Southern Latitudes: Collected Papers presented to the SCAR Workshop at Bremerhaven, September 25-28, 1984. 164 p. December 1985
No. 39. Kawaguchi, S. ed.: Proceedings of the Seventh Symposium on Polar Meteorology and Glaciology. 252 p. December 1985
No. 40. Hoshiai, T., Nemoto, T. and Naito, Y. ed.: Proceedings of the Seventh Symposium on Polar Biology. 497 p. February 1986
No. 41. Yanai, K., Takeda, H. and Shimoyama, A. ed.: Proceedings of the Tenth Symposium on Antarctic Meteorites, 1985. 393 p. July 1984
No. 42. Sato, N. ed.: Proceedings of the Eighth Symposium on Coordinated Observations of the Ionosphere and the Magnetosphere in the Polar Regions, 1985. 154 p. August 1986
No. 43. Yoshida, Y. ed.: Proceedings of the Sixth Symposium on Antarctic Geosciences, 1985. 165 p. September 1986
No. 44. Hoshiai, T. and Ohyama, Y. ed.: Proceedings of the Eighth Symposium on Polar Biology, 1985. 260 p. December 1986
No. 45. Kawaguchi, S. and Watanabe, O. ed.: Proceedings of the Eighth Symposium on Polar Meteorology and Glaciology, 1985. 111 p. December 1986
No. 46. Yanai, K. ed.: Proceedings of the Eleventh Symposium on Antarctic Meteorites, 1986. 282 p. March 1987
No. 47. Ejiri, M. ed.: Proceedings of the Ninth Symposium on Coordinated Observations of the Ionosphere and the Magnetosphere in the Polar Regions, 1986. 224 p. March 1987
No. 48. Sato, N. ed.: Proceedings of the Nagata Symposium on Geomagnetically Conjugate Studies and the Workshop on Antarctic Middle and Upper Atmosphere Physics. 325 p. August 1987
No. 49. Watanabe, O. ed.: Ice Drilling Technology; Proceedings of the Fourth International Workshop on Ice Drilling Technology, Tokyo, April 20–23, 1993. 408 p. March 1994
No. 50. Berkman, P. A. and Yoshida, Y. ed.: Holocene environmental changes in Antarctic coastal areas; Proceedings of International Workshop held at the National Institute of Polar Research, Tokyo, October 20–22, 1993. 107 p. August 1994
No. 51. Watanabe, O. ed.: Proceedings of the International Symposium on Environmental Research in the Arctic 19–21 July 1995, Tokyo. 398 p. December 1996
No. 52. Fukuchi, M. ed.: Proceedings of the International Symposium on Environmental Research in the Antarctic 3–4 December 1996, Tokyo. 254 p. July 1998
No. 53. Motoyoshi, Y. and Shiraishi, K. ed.: Origin and evolution of continents; Proceedings of the International Symposium "Origin and Evolution of Continents", 13–14 October 1997, Tokyo. 230 p. December 1998

This document is provided by JAXA.

Acknowledgments to Referees

Ageta, Y. (Nagoya U.)
Aoki, S. (Tohoku U.)
Aoki, T. (MRI)
Aso, T. (NIPR)
Bos, M. (Proudman Oceanographic Laboratory)
Deguchi, H. (Hiroshima U.)
Elster, J. (Acad. Sci. Czech Repub. Sect. Plant Ecol.)
Enomoto, H. (Kitami Inst. Tech.)
Foppiano, A. J. (U. Concepcion)
Fujii, Y. (NIPR)
Gernandt, H. (AWI)
Goto-Azuma, K. (NIPR)
Hall, C. (U. Tromsø)
Hara, K. (NIPR)
Herber, A. (AWI)
Higuchi, K. (MSC)
Higuchi, M. (National Science Museum)
Hirasawa, N. (NIPR)
Hobson, K.A. (Canadian Wildlife Service)
Holmén K. J. (Stockholm U.)
Igarashi, M. (NIPR)
Imura, S. (NIPR)
Isaksson, E. (NP)
Ito, H. (NIPR)
Kameda, T. (Kitami Inst. Tech.)
Kamiyama, K. (NIPR)
Kanao, M. (NIPR)
Kikuchi, T. (CRL)
Kimura, H. (Gifu U.)
Kodama, Y. (Hokkaido U.)
Kohno, M. (NIPR)
Kojima, S. (Tokyo Woman's Christian U.)
Kudoh, S. (NIPR)
Mannouji, N. (JMA)
Masuzawa, T. (Shizuoka U.)
Matsumoto, K. (NAO)
Melnikov, I. A. (P. P. Shirshov Inst. Oceanol.)
Morimoto, S. (NIPR)
Motoyama, H. (NIPR)
Nagashima, H. (Tokyo Suisan U.)
Nakada, M. (Kyusyu U.)
Nakao, M. (Nagoya U.)
Nakatsubo, T. (Hiroshima U.)
Oechel, W. C. (San Diego State U.)
Ohmura, A. (ETH)
Ohshima, K. I. (Hokkaido U.)
Ohtani, S. (Shimane U.)
Okano, S. (Tohoku U.)
Ozawa, T. (NIPR)
Röttger, J. (Max-Planck-Institut)
Sasaki, H. (Senshu U. Ishinomaki)
Sato, Ken (Hokkai-Gakuen U.)
Sato, Kaoru (NIPR)
Sato, Katsufumi (NIPR)
Shibata, T. (Nagoya U.)
Shibuya, K. (NIPR)
Shiraiwa, T. (Hokkaido U.)
Shoji, H. (Kitami Inst. Tech.)
Suzuki, K. (Shinshu U.)
Svendsen, H. (U. Bergen)
Svoboda, J. (U. Toronto)
Taguchi, S. (Soka U.)
Takahashi, H. (Hokkaido U.)
Takahashi, S. (Kitami Inst. Tech.)
Takenaka, A. (NIES)
Takeshita, S. (NIPR)
Titov, O. V. (Polar Res. Inst. Marine Fish. Oceanogr.)
Wassmann, P. (U. Tromsø)
Watanabe, K. (Nagoya U.)
Weller, G. (U. Alaska)
Yamagata, S. (Hokkaido U.)
Yamanouchi, T. (NIPR)
Ørbæk, J. B. (NP)

This document is provided by JAXA.

This document is provided by JAXA.